Urban Geometry: The Effect of Height Diversity and Buildings Configuration on Thermal Performance and Cooling Load at Urban Scale. A Case Study in Dubai / UAE

ألهندسة ألحضرية : تأثير ألتباين في ألارتفاعات وتكوين ألمباني على ألاداء ألحراري وحمل ألتبريد على ألمستوى ألحضري . دراسة في دبي / ألامارات ألعربية ألمتحدة

By

SUNDUS LUAY SHAREEF

A thesis submitted in fulfilment

of the requirements for the degree of

DOCTOR OF PHILOSOPHY IN ARCHITECTURE AND

SUSTAINABLE BUILT ENVIRONMENT

at

The British University in Dubai

Professor Bassam Abu Hijleh
May 2018

Urban Geometry: The Effect of Height Diversity and Buildings Configuration on Thermal Performance and Cooling Load at Urban Scale. A Case Study in Dubai /UAE

ألهندسة ألحضرية : تأثير ألتباين في ألارتفاعات وتكوين ألمباني على ألاداء ألحراري وحمل ألتبريد على ألمستوى ألحضري. دراسة في دبي / ألامارات ألعربية ألمتحدة

by

Sundus Luay Shareef

A thesis submitted to the Faculty of Engineering

in fulfilment of the requirements for the degree of

Doctor of Philosophy in Architecture and Sustainable Built Environment

at

The British University in Dubai

May 2018

Thesis Supervisor
Professor: Bassam Abu-Hijleh

Approved for award:

_____   _____

Name   Name
Designation   Designation

_____   _____

Name   Name
Designation   Designation
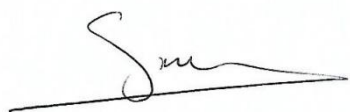
Date: _____

DECLARATION

I warrant that the content of this research is the direct result of my own work and that any use made in it of published or unpublished copyright material falls within the limits permitted by international copyright conventions.

I understand that a copy of my research will be deposited in the University Library for permanent retention.

I hereby agree that the material mentioned above for which I am author and copyright holder may be copied and distributed by The British University in Dubai for the purposes of research, private study or education and that The British University in Dubai may recover from purchasers the costs incurred in such copying and distribution, where appropriate.

I understand that The British University in Dubai may make a digital copy available in the institutional repository.

I understand that I may apply to the University to retain the right to withhold or to restrict access to my thesis for a period which shall not normally exceed four calendar years from the congregation at which the degree is conferred, the length of the period to be specified in the application, together with the precise reasons for making that application.

_____
Signature of the student

COPYRIGHT AND INFORMATION TO USERS

The author whose copyright is declared on the title page of the work has granted to the British University in Dubai the right to lend his/her research work to users of its library and to make partial or single copies for educational and research use.

The author has also granted permission to the University to keep or make a digital copy for similar use and for the purpose of preservation of the work digitally.

Multiple copying of this work for scholarly purposes may be granted by either the author, the Registrar or the Dean of Engineering only.

Copying for financial gain shall only be allowed with the author's express permission.

Any use of this work in whole or in part shall respect the moral rights of the author to be acknowledged and to reflect in good faith and without detriment the meaning of the content, and the original authorship.

Abstract

Urban geometry and buildings morphology are important factors that affect both thermal behaviour of the spatial environment as well as a building's energy performance. This research aims to explore the effect of the urban block with different building configurations on energy performance at the urban level. For this aim, a literature review was conducted to identify the previous and recent studies relevant to this research topic. It has been proven that the compactness element is a key urban geometry variable that controls the desired thermal performance of the built environment in hot climates. However, the previous studies have primarily focused on traditional methods of increasing the shading effect, such as by increasing buildings height / canyon width H/W ratio to provide the required compactness for desired solar access and energy saving target.

This research attempts to provide alternative methods to achieving the required compactness and increase the shading effect by adapting building height variations and configurations in urban block design. As observed in the previous literature, the energy consumption assessment and the strategies that can be adopted to reduce this consumption are generally implemented and evaluated on the scale of individual buildings. Therefore, further investigation of both the diversity in building heights and the effect of this on the energy performance, and the evaluation of the energy consumption at the urban scale is required to fill the gap identified in previous literatures.

This study utilised two software packages to simulate a base case urban configuration and evaluate this case against the proposed suggested scenarios of different configurations. The proposed scenarios depending on the urban configuration sustainable strategies were implemented and simulated to find the effect of adopting these strategies on the building's total energy performance within the case study area, i.e., the Dubai / UAE local context and weather characteristics. Three groups with 56 proposed scenarios were simulated, where in different ratios of building height variation were implemented in the first two groups, and different building configurations were adopted for the third group. The research found that a significant variation in building height reduces the cooling load more than a gradual height variation, and consequently offers more energy saving. The variation along the short direction of the urban block has a greater positive effect and the saving in cooling energy consumption reaches 4.6 %. The significant variation in building height along the short axis of the urban block provides more shading to the canyons and the adjacent buildings compared to the base case.

This over shading reduces the air temperature by 1.1 $^\circ$C within the canyon and directly reduces the conduction heat gain through the buildings envelop. This is in addition to the other effect represented by reducing the direct solar access to the building surfaces and decreases the solar energy gained by the buildings envelop through direct radiation. Furthermore, building orientation plays a significant role in the thermal performance of the urban block, and it contributes to the total cooling load energy saving of the urban block by 6.6 % at the peak time of cooling demand. Moreover, the research found that the variation in building heights will increase the wind velocity by up to 23 %, and this improvement in air flow affects the outdoor air temperature positively. This positive effect of the height variation on the outdoor air temperature of the urban canyons reduces the conduction heat gain through the buildings envelop by 4 %, and consequently reduces the energy required for cooling purpose.

In addition, the alternative arrangement of the buildings within the block is another geometrical variable that affects the thermal performance of the built environment. It has been found that the alternative, or stagger arrangement, provides more shading effect on both canyon and building surfaces. However, this arrangement reduces the wind speed due to the obstruction created by the buildings mass and decreases the air velocity in the canyons. On the other hand, this type of configuration improves the distribution of the air around the buildings block and consequently enhances the outdoor thermal comfort around most of the buildings within the urban block. The reduction of 1.9 $^\circ$C in outdoor air temperature, and 4.9 % in cooling load is achieved by increasing the H/W ratio of the main canyons from 0.96 to 1.2. Therefore, designing the urban block with a significant diversity in building heights, or gradual height variation will have the potential of a shading effect and wind speed increase to enhance the thermal performance of the urban block.

Finally, adopting the rectangular shape of the urban block, creating diversity in building heights and alternative building morphology are some of passive urban design strategies that can be followed for the optimised urban block configuration, with high efficient morphology and less environmental impact. This prototype is recommended for the new urban development in the UAE and other areas of the same climate zone.

الملخص

الهندسه الحضريه وتركيب المباني هما من العوامل المهمه التي تؤثر في الاداء الحراري للبيئه المكانيه. هذه الدراسه تهدف الى اكتشاف تأثير مجموعه من المباني في اشكال مختلفه من التصميم والتركيب الحضري على الاده الكلي للطاقه على المقياس حضري. لتحقيق هذا الهدف تم دراسه ومراجعه معظم الدراسات والبحوث المنشوره والتي تعنى بنفس اختصاص هذا البحث. بالاضافه الى ذللك تم تحديد متغيرات التصميم الحضري والاستراتيجيات المتبعه للوصول الى التصميم المستدام. في هذه الدراسه يتم اتباع الاستراتيجيات الرئيسيه للتصميم المستدام لتحسن التصاميم الحاليه بأتجاه تصميم حضري لمجمع مباني اكثر استدامه, افل استهلاكا للطاقه واقل تأأثيرا سلبيا على المحيط.

هذه الدراسه استخدمت مجمع المباني في التصميم الحضري لاكتشاف اكثر من نموذج او تصميم على الطاقه التي يستهلكها التصميم المفترض في مناطق الطقس الحار . لقد ثبت ان عامل التقارب بين المباني هو احد المفاتيح الرئيسيه للسيطره على الاداء الحراري البيئه المبنيه . الدراسات السابقه ركزت بشكل عام على تحقيق التقارب بين المباني بالاعتماد على دراسه الطريقه التقليديه لتحقيق هذا التقارب وهي زيادة ارتفاع الابنيه نسبة لعرض الرواق لتقليل الاشعاع الواصل من الشمس وبالتالي تقليل الطاقه المطلوبه للتبريد.

هذا البحث عمل على دراسه طريقه بديله لتحقيق التقارب او توفير الظل المطلوب بين المباني وذللك بأعتماد التباين بين ارتفاع المباني في مجمع واحد من الابنيه. الاختلاف بين ارتفاعات الابنيه في المجمع الواحد تم تقييمه لنفس المساحه المبنيه وبالاحتفاظ بنفس العرض للرواق بين المباني. اضافه الى هذا, اظهرت الدراسات السابقه ان التقييم لأداء الطاقه كان يتم اعتماده نسبة الى المبنى الواحد بشكل منفصل. المزيد من الدراسه والبحث للتأثير المتكامل لمجموعه الابنيه ضمن المساحه المحدده على الطاقه المستهلكه ودراسة الارتفاعات المختلفه للابنيه سيحقق سد الفجوه الموجوده واضافه جديده للدراسات السابقه.

النظريه التي اعتمدها هذا البحث هي استخدام برامج الكمبيوتر لأجراء محاكاه لأداء النماذج المفترضه لتصميم المباني ومقارنتها بنموذج اساسي , وتم تحديد المتغيرات للتصاميم المفترضه والتي تمثل متغيرات الهندسه الحضريه . نتجت عن المتغيرات المتبعه للهندسه الحضريه 56 نموذج مفترض تم اختبارها بأرتفاعات مختلفه وتتنظيم مختلف للمباني. كما تم تحديد نواتج عمليه المحاكاة والتي تشمل العوامل الخارجيه للمناخ المحلي. تم اعتماد عوامل الطقس الحار والتي تعود لمدينة دبي , الامارات العربيه المتحده كأساس لتشغيل برامج الكمبيوتر ولأجراء عمليه المحاكاة. نواتج المحاكاة شملت : تأثير الظل, درجة الحراره, سرعة الرياح , والرطوبه النسبيه.لقد تم استخدام اثنان من برامج الكمبيوتر , االاول عمل على ايجاد التغيرات في العوامل المناخيه المحيطه بالابنيه وفقا للمتغيرات في الهندسه الحضريه التي طبقت على كل نموذج مفترض. اما البرنامج الثاني فقد استخدمت فيه نواتج البرنامج الاول كمدخلات لأيجاد التغيرات في الأداء الحراري للمباني و الطاقه التي تستهلكها المباني لاغراض التبريد.

من اهم النتائج التي وصل اليها البحث أن لأختلاف الارتفاعات بين الابينيه ضمن المجمع الواحد تأثيرا ملحوظا على عوامل المناخ الخارجي المحيط وبالتالي على مجمل الطاقه المستهلكه في المجمع .فقد وجد ان تطبيق التباين بين ارتفاعات المباني على المحور القصير للمجمع وبفارق ملحوظ سيقلل من الطاقه المطلوبه للتبريد مقارنة بتطبيق الارتفاع المتدرج وباتالي سيوفر طاقه بمقدار 4.6 % مقارنة بالنموذج الاساسي .

السبب في ذللك يعود الى ان التباين الملحوظ في الارتفاع سيعمل على توفير ظل اكبر لكل من الرواق الخارجي المحيط بالابنيه من جهه , و سطوح وجدران الابنيه من جهه اخرى مما سيعمل على تقليل الطاقه اللازمه للتبريد. تحسن الاداء الحراري سيكون من جانبين: الاول تقليل درجة الحراره المحيطه بالأبنيه وبالتالي تقليل الحراره المنتقله من الخارج الى الداخل عن طريق التوصيل . والثاني تقليل الاشعاع المباشر على سطوح وجدران الابنيه مماقل الحراره المباشره المكتسبه عن طريق الاشعاع, فالحراره الخارجيه في هذا النوذج تقل بمقدار 1.1 درجه مئويه مقارنه بالنموذج الاصلي.

من جانب اخر اثبت هذا البحث اهميه الاتجاه في توفير الطاقه بالنسبه لمجمع المباني وان الأتجاه المناسب يمكن ان يوفر بما يصل الى % 6.6 من الطاقه المطلوبه للتبريد. اضافه الى ماسبق اثبتت هذه الدراسه ان التباين في ارتفاعات المباني يحسن ويزيد من سرعه الرياح بمقدار يصل الى % 23 مماينعكس ايجابيا على زيادة معامل الحمل الحراري , ويحسن الاداء الحراري الخارجي في ذات الوقت.

اما بالنسبه الى تركيب المباني ضمن المجمع الواحد فقد وجد ان الترتيب المتناوب يوفر ظلا اكبر ويؤثر ايجابيا على الاداء الحراري للرواق والمباني على حد سواء. وبالمقابل هذا الترتيب للمباني سيقلل من سرعة الرياح في الرواق الرئيسي , لأن المباني ستعمل على صد الرياح وتقليل سرعتها بشكل ملحوظ مقارنة بالنموذج الاصلي.من جانب اخر الترتيب المتناوب للابنيه سيعمل على تحسين حركة الهواء حول معظم الابنيه ضمن المجمع مما سينعكس ايجابيا على تحسين الاداء الحراري الخارجي والداخلي للابنيه المحيطه. الترتيب المتناوب للابنيه سيقلل من درجه الحراره الخارجيه مقارنة بالنموذج الاصلي بمقدار 1.9 درجه مئويه, ومن الطاقه اللازمه للتبريد بمقدار يصل الى % 4.9 وذللك بزيادة نسبة الارتفاع الى عرض الرواق من 0.96 الى 1.2 . لذلك فأن التصميم الحضري لمجمع المباني الذي يعتمد التباين الملحوظ او المتدرج في الارتفاعات سيمكن من زيادة كفاءة التظليل وتحسين الاداء الحراري للابنيه على المستوى الحضري. واخيرا فأن اعتماد الشكل المستطيل في التصميم الحضري لمجمع المباني , التباين في الارتفاعات , الترتيب المتناوب للابنيه هي من المتغيرات التي يمكن اعتمادها في الهندسه الحضريه للوصول الى تصميم اكثر كفاءة في استهلاك الطاقه , والذي يمكن ان يعتمد كنموذج في مخططات التطوير الحضري في دولة الامارات العربيه المتحدة و في المناطق ذات الخصائص المناخيه المشابهه.

Acknowledgment

I am very grateful to *Allah* for granting me guidance, patience, strength and health to accomplish this work.

The challenges that I have passed for being the first graduate in the 'Architecture and Sustainable Built Environment' Programme, and with all difficulties that I have faced in this research, I would like to thank everyone who has encouraged and supported me at different stages during the years of this research.

First and foremost, I'm greatly indebted to the director of study and my supervisor Prof. Bassam Abu-Hijleh, who has supported me throughout this research with his knowledge, patience and inspiration. Special appreciation is also dedicated to Prof. Steve Sharples from the University of Sheffield, School of Architecture for his advice and valuable notes throughout the research main stages. I would also like to thank the second supervisor Dr. Hanan Taleb, Dr. Riad Saraiji and all the faculty members at the British University in Dubai for their support, and I would like to extend my thanks to all individuals, administration, IT and library staff.

Last but not least, I am thankful to the British University in Dubai for providing this opportunity of postgraduate studies, and I would like to express my full respect and gratitude to Prof. Abdullah Alshamsi the vice chancellor of the British University in Dubai for his support and efforts in the creation and development of a high quality research-led university.

Finally, my great and deep gratefulness to my parents and family for their understanding, patience and unbounded support during the difficult phases of this work. To my beloved son, thank you.

<div align="right">Sundus Luay Shareef 2018</div>

Table of Contents

List of Figures

List of Tables

List of Acronyms

(H/W)	Aspect ratio (Height /Width)
(ABL)	Atmospheric Boundary Layer
(CFD)	Computational Fluid Dynamics
(DEM)	Digital Elevation Model
(DM)	Dubai Municipality
(GIS)	Geographic Information System
(GHG)	Green House Gases
(GCC)	Gulf Cooperation Council
(HTB2)	Heat Transfer through Building
(IES-VE)	Integrated Environmental Solutions-Virtual Environment
(LCTs)	Land Cover Types
(LCRI)	Low Carbon Research Institute
(Tmrt)	Main Radian Temperature
(MRT)	Mean Radiant Temperature
(PMV)	Predicted Mean Vote
(SVF)	Sky View Factor
(3D)	Three- dimensional Model
(2D)	Two- dimensional Model
(UBL)	Urban Boundary Layer
(UCL)	Urban Canopy Layer
(UHI)	Urban Heat Island
(USHI)	Urban Surface Heat Island
(WSA)	Welsh School of Architecture

Chapter 1

Introduction

1.0 Introduction

1.1 Sustainability and the Built Environment Background

By 2030 and according to United Nations (UN) statistics presented in the ' UN Climate Change Conference Paris, 2015' , five billion people will live in urban and developed areas. This number will represent 61% of the world's population in 2030. These statistics bring into consideration the extent of the urbanisation effect on nature and the climate. Previous studies have proved the effect of urbanisation on increasing air temperature when compared with non-urbanised areas (Ignatiusa, Wonga and Jusuf, 2015). Cities represent a number of communities and neighbourhoods where people can work, live and access entertainment. Day by day cities offer tremendous opportunities for community, employment, education, excitement and interest. For all of these reasons, cities have become attractive areas for living. On the other hand, cities create problems of congestion, noise and pollution, but most people do not have the choice to recognise and assess the trade-offs. Being able to analyse and determine the best balance of urban benefits and environmental quality allows policy-makers the opportunity to plan these cities and how to establish the highest level of benefit.

Living in towns and low-density cities has some advantages, but people may prefer living in compact and dense cities as long as there is an equilibrium between the development elements; built areas and open spaces, private and public transportation, and usage of natural and artificial resources. A city, district, community, neighbourhood and a complex can all be considered as systems of interdependent components. The major variables or components that affect the design of any development are urban form, transport, landscape area, building design, waste management, as well as energy and water supply (Stanley, 2014). The best sustainable design involves the equilibrium between these components, and in order to make cities more suitable for people and serve for generations, all of the mentioned components are

required for a viable city, and should be involved and operated smoothly within the design or system equation. In the Arabian Gulf region, cities have expanded rapidly within a short time period. This expansion has combined with the application of the latest and smart innovations in planning, design, construction and transportation sectors. Therefore, these cities have unique and special characteristics compared to other world cities and provide the opportunity to adopt the latest planning and design theories.

On the other hand, it is obvious that city growth becomes a key issue in the global problems of climate change, global warming, greenhouse gas emissions and depleting natural resources. Therefore, many studies and publications have explored the relationship between the sustainability levels required to be achieved and the urban planning of any development. Many of these studies concentrated on the main urban design factors, such as urban form, building design, liveability, land use and transportation system in order to analyse, evaluate and develop the sustainability level of cities and developments (Shamsuddin, Abu Hassan and Bilyamin, 2012; Badland et al., 2014; Stanley, 2014; Dempsey, Brown and Bramley, 2015). However, some of these researchers studied the sustainability on an urban scale from the aspect of resource conservation and pollution reduction.

Furthermore, it has been widely recognised that the built environment has a direct effect on people's health, happiness and consequently on their productivity (Kent and Thompson, 2014). Thus, the major role of the sustainable urban design is to optimise the urban development's form in order reduce the potential negative impacts on people's health, enhance resource efficiency and improve productivity at the same time.

Sustainability was defined by different official proclamations, according to the UN it is 'meeting the needs of the present without compromising the ability of future generations to meet their own needs' (UN, 1987).

The United States Environmental Protection Agency (EPA) defined sustainability as what we need for our survival from surrounding natural environments, either directly or indirectly. Furthermore, it creates a kind of harmony and maintains this between humans and nature (EPA, 2008).Sustainability itself has different definitions, but in general 'sustainable system or process can be continued indefinitely, without depleting any of the materials or energy resources required to keep it running' (Wright, 2011).

Simply put, it is living the present while taking the future into consideration, in terms of resources conservation and nature preservation. The UN World Summit (New York, 2005) stated that the 'Sustainability' as a concept has three pillars 'Economy, Society and Environment'. Environmentally, sustainability is concerned with the developments and the impact of human activities on the environment or nature, and the sustainable environment is the environment with a lower negative impact and high resources efficiency.

Economically, the sustainable outcome is the amount that can be consumed during the time period at a continuous use until the end of the period (Basiago, 1999). The Sustainability concept has changed the traditional economic assumption that the supply of natural resources is unlimited (Hicks, 1946).

The new concept of economic sustainability has replaced this theory with the attitude of allocating the resources efficiently, stating that economic sustainability is the ability to support the defined target of economic production (Goodland, 1995).

Socially, sustainability is about enhancing peoples' lives and wellbeing. The term 'Neighbourhood' or 'Community' refers to a number of residential units and the related facilities that serve the resident's needs (Kearns and Parkinson, 2001). Malekia et al. (2015) stated that; liveable, sustainable neighbourhoods are one of the determining and essential factors for developing sustainable environments.

The sustainable neighbourhood is a neighbourhood that integrates the three sustainability pillars 'Environment, Economy and Society'. From the social aspect, providing the required open areas, landscaped area, playground and community facilities will encourage the sociality and people communications. From the economic aspect, those sustainable neighbourhoods that provide all the services and facilities will create liveable, healthy independent communities that will have a positive effect on the individuals and the whole society (Badland, 2014). However, 'The Sustainable Urban Design' provides a high level of sustainability and efficiency in terms of major urban design dimensions, such as liveability, land use, transportations, buildings design, landscaped areas and environmental performance.

1.2 Climate Change

Observing the geological history of the earth's climate shows that climate change takes place over millions of years, and the abrupt reorientations of the Earth's climate foreshadowing the way the climate responds to present human activity (Trevor, 2009). The United Nations Framework Convention on Climate Change (UNFCC 1992) defined 'Climate change' as 'natural climate variation observed over comparable time periods, directly or indirectly attributed to human activity that alters the composition of the global atmosphere'. The scientific facts surrounding climate change were illustrated by Trevor (2009) as the burning of oil, coal and gas, causing a significant rise in atmospheric carbon dioxide and nitrogen oxides.

The impact of climate change on the planet 'Earth' is important for governments, decision-makers, journalists, editors, corporate leaders, and industry stakeholders. Furthermore, it is necessary for all interested people who wish for a balanced, scientific and honest reflection on this issue to address this major global problem.

Figure1.1 shows the CO_2 emission of world countries,, the figure shows moderate to high carbon footprint averages in tons per capita in most Arab countries, and the GCC countries are shown to be high CO_2 emitters.

CO2 emissions (metric tons per capita)

■	< 0.22
■	0.22 ; 0.69
■	0.69 ; 1.42
■	1.42 ; 2.41
■	2.41 ; 4.54
■	4.54 ; 6.68
■	6.68 ; 9.26
■	> 9.26

Source : The World Bank - 2011
Copyright © Actualitix.com All rights reserved
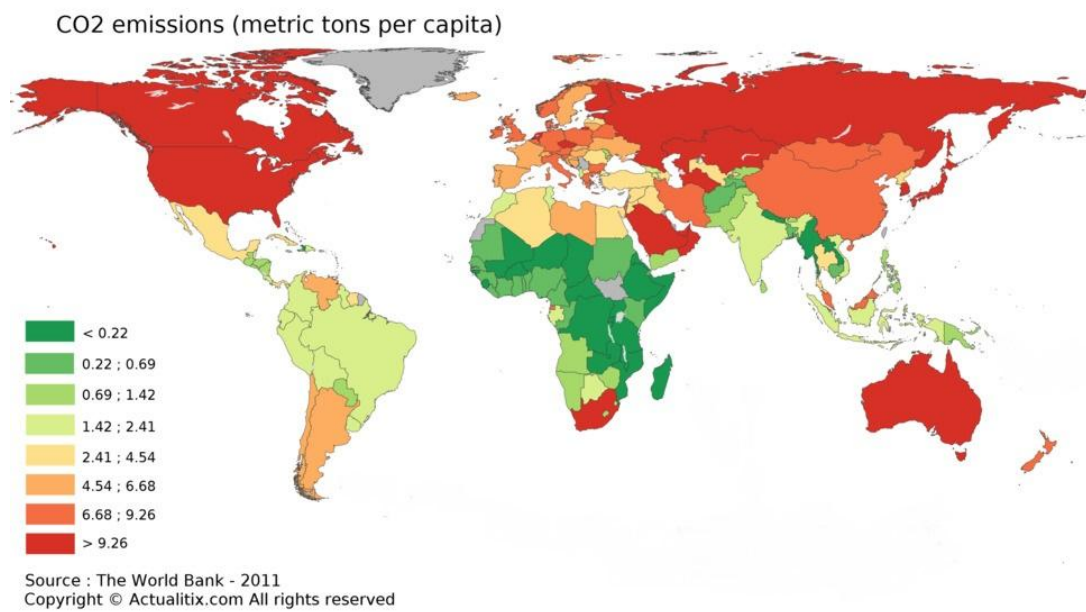
Figure1.1: World CO_2 Emission (World Bank, 2011)

These values represent a major environmental challenge, particularly for Gulf countries. However, according to the International Energy Agency IEA (2012) Sudan, Tunisia and Morocco produce lower carbon emission averages when compared with the world's average(see Figure 1.2).

In order to reach the target of carbon dioxide reduction, we must reduce the dependence on fossil fuels and move towards more sustainable and clean forms of energy, as energy is strongly connected to climate change problems. On the other hand, it is crucial to find alternative and new design solutions for reducing energy consumption. In addition to adopting and increasing the use of the natural resources, such as solar access and potential wind power in designing our new cities and developments.
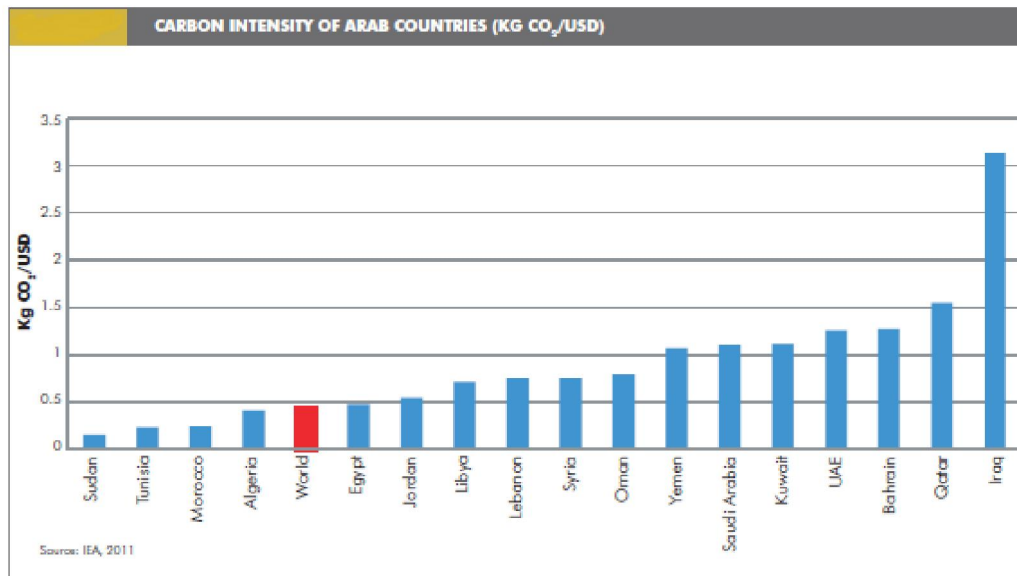
Figure 1.2: CO$_2$ averages of Arab countries (IEA, 2012)

1.3 Pollution and Global Warming

Cities and urban environment pollution is caused by different factors; density and transport within cities, human activities, construction and buildings' effects on nature and landscape areas, atmospheric pollution by CO$_2$ emissions and noise pollution (Kent andThompson,2014). Pollution influences human health and well-being and can make cities uneasy places to live. Greenhouse Gases (GHG) averages is one of the air pollution indicators most used. Greenhouse Gases Emissions refers to all gases that trap heat in the atmosphere; the main greenhouse gases in the atmosphere are; Carbon dioxide (CO$_2$), Methane (CH$_4$),and Nitrous oxide (N$_2$O). These gases are the main reason for global warming, depleting the ozone layer and climate change (Karl and Trenberth, 2003). GHG are emitted through various fossil fuel burning processes. The fossil fuels (coal, natural gas and oil) are burnt for heating, solid waste burning, trees and wood products, the decay of organic waste in municipal solid waste landfills, chemical reactions and manufacturing operations are some resources of GHG (NASA, 1998).

Furthermore, the building and construction industry, transportation, agriculture and industry are the major recourses of these gases. Global warming, Urban Heat Island (UHI) and the increase in global air temperature is a result of the GHG emission effect. Figure 1.3 shows the prediction of increase in global air temperature within the next 100 years.
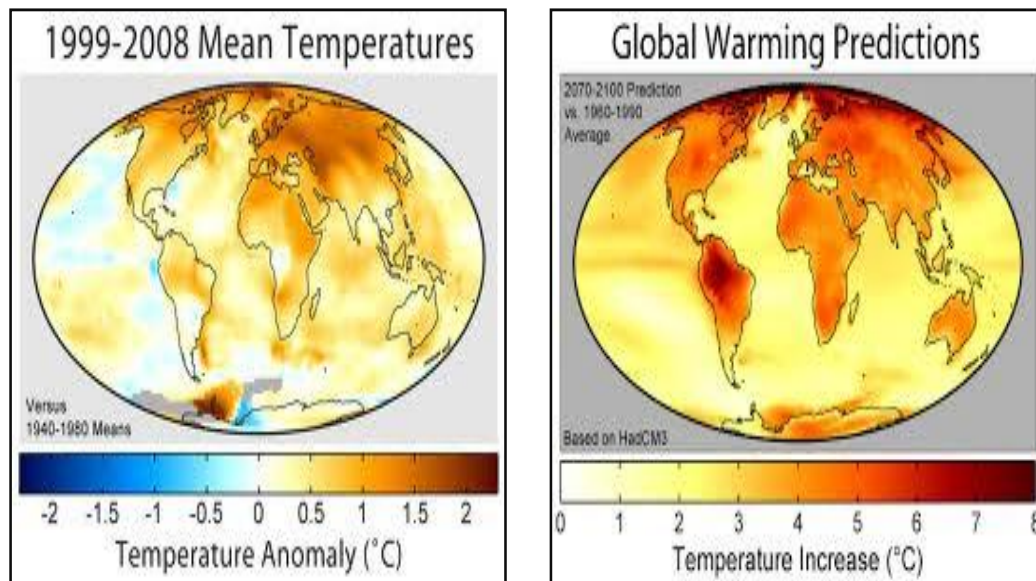
Figure 1.3: NASA, GISS Surface Temperature Analysis (NASA, 2013)

Buildings design, transportation systems and open areas significantly affect the sustainability of the urban level. Figure1.4 shows that buildings contribute to the CO_2 emissions by 43 % while the transportation share is 32 % (U.S. Pew, 2013). Therefore, cities should be designed in a way that minimise the GHG averages and pollution percentages. The new cities should be designed to keep their inhabitants healthy, secure and happy. For this aim cities must become greener and robust with a stable ecosystem. Our built environment at the present time suffers enough and an integrated approach is urgently needed. Successful solutions depend on understanding the relationship between the involved sustainability elements; environmental, historical, social, and economic. The solutions should start from the individual building to the block, neighbourhood, district, city, region and up towards the globe.

Building contribution to CO₂ emissions

Transportation 32%

Buildings 43%

Industry 25%

Residential 21%

Commercial 17%

Industrial 5%

Source: Pew Center on Global Climate Change
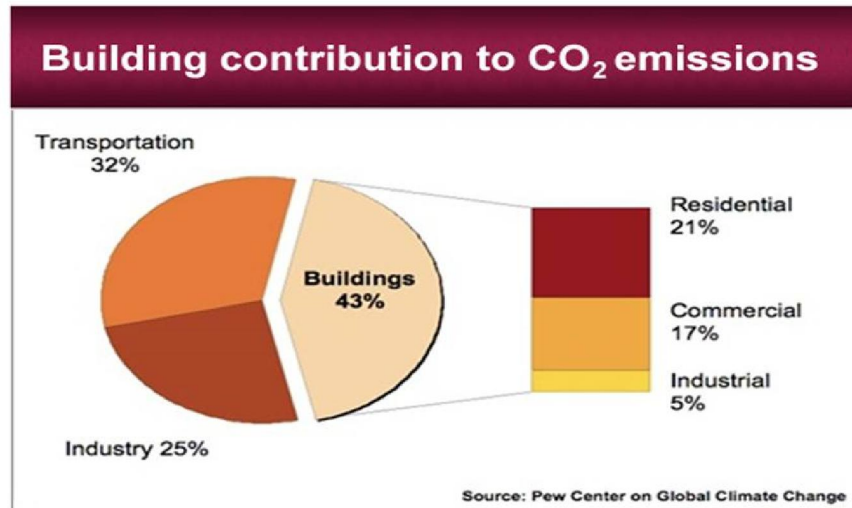
(U.S Pew Research Center, 2013)

Figure 1.4: Buildings and transportation contribution to CO2 emissions (Pew Center, 2013)

1.4 Urban Planning and Design

Urban Design is the process required to shape development projects, neighbourhoods, communities, districts and cities. Urban planning is integrating all the elements involved in the built environment. Urban design is a matter of creating the relationship between people and spaces, i.e., the management of public functions and spaces. Urban design requires a wide knowledge of most sciences, planning, engineering, social, economy, management and computer programs. The key elements of urban planning include open and landscaped areas, land use, transportation systems, building patterns and design, street patterns, water and energy efficiency, waste management, and the use of renewable resources. Each one of these elements is of significant effect on the sustainability of urban design.

1.4.1 Sustainable Urban Design

Sustainable urban design is an accumulation of the number of elements that form the sustainable master plan covering sustainable buildings design, sustainable transportation systems, efficiency in resources use,, liveable urban space, land use diversity, sustainable parks, and optimised buildings configuration for a lower environmental impact (Trancik,

1986; Dias, Curwell and Bichard, 2014; Lo, 2016; Chao and Liu, 2016). Integrating the mentioned factors forms the 'Sustainable Master Plan'. The sustainable master plan is significant to people's well-being, it is directly affects people's lifestyles, time, health, effort, and welfare. Transit solutions, resources conservation, as well as indoor and outdoor environments represent some urban design factors that have a direct effect on people's daily lives. Sustainability on the urban level could be achieved through understating the sustainability three pillars and the interface between them: environment, economy and social. Urban area includes residential, commercial and industrial buildings. In addition to the open and green spaces, road networks, and water sheds. All these compensates of the urban designs should be designed in a way that provides vitality and comfort to improve people's lifestyles. The sustainability or efficiency in energy use is one of the most important factors that affects the sustainability level of the built environment.

This efficiency can be obtained in different ways. One of these ways is by increasing the dependence on the use of solar energy for heating, cooling and lighting. In addition of optimising the building design and the urban form for lower energy consumption. Therefore, it is the responsibility of the urban designer or planner to adopt all the passive and active design strategies that maximise the urban design efficiency or sustainability (Yuan and Ng, 2014; Whang and Kim, 2014; Li, Quan and Yang, 2016). However, the biggest challenge for the urban planner is to improve and optimise the relationship between the three major elements in urban design concept; density, movement and recourses. Apart from this is, it is useful in finding the best and optimised design for the urban block, neighbourhood, distract and city plan. Therefore, the appropriate, passive design is one of the solutions that can be adopted to achieve the sustainable design. The economic and social factors have their effect on the equation as well. Therefore, the optimised sustainable design targets to solve this equation and reach the balance in the sustainability three poles on urban level.

1.4.2 Liveable Environment

Creating a liveable environment is one of the sustainable urban design principles, and the level of urban liveability could be considerably important in achieving sustainability in the urban environment. The urban sustainability can be obtained by creating a liveable community, neighbourhood and city. Urban liveability covers a number of factors, it is a multi-dimensional construct that includes accessibility, number of public parks and open spaces, walkability, transportation planning, urban density and land use diversity, all of which are design elements that could be improved to achieve high levels of liveability and sustainability. Wheeler (2001) and Balsas (2004) stated that it is difficult to define and measure the concept of urban liveability, but Lynch (1998) set some principles for liveability measurement, such as safety, equity and continuity. Moreover, Oberlink (2006) added accessibility and inclusiveness to the previously mentioned indicators.

Furthermore, many of the liveability dimensions are linked to ecosystem factors, including the effects of the urban microclimate, quality of the landscape, vegetation and greenery. Lennard (2008) mentioned walkability as one of the liveability measurements, and expressed how increasing walkability would positively affect the liveability and sustainability through reducing the dependents on transportations which leads to a reduction in noise and air pollution as well. In the same context, Vine, Buys and Aird (2012) stated that increasing the residential density is one of the policies that is adopted in Brisbane, Australia to decrease car dependence and increase the residents' walkability.

Badland (2014) showed that providing some facilities and liveability indicators in neighbourhoods will have a positive effect on residents' health and wellbeing (Figure 1.5).
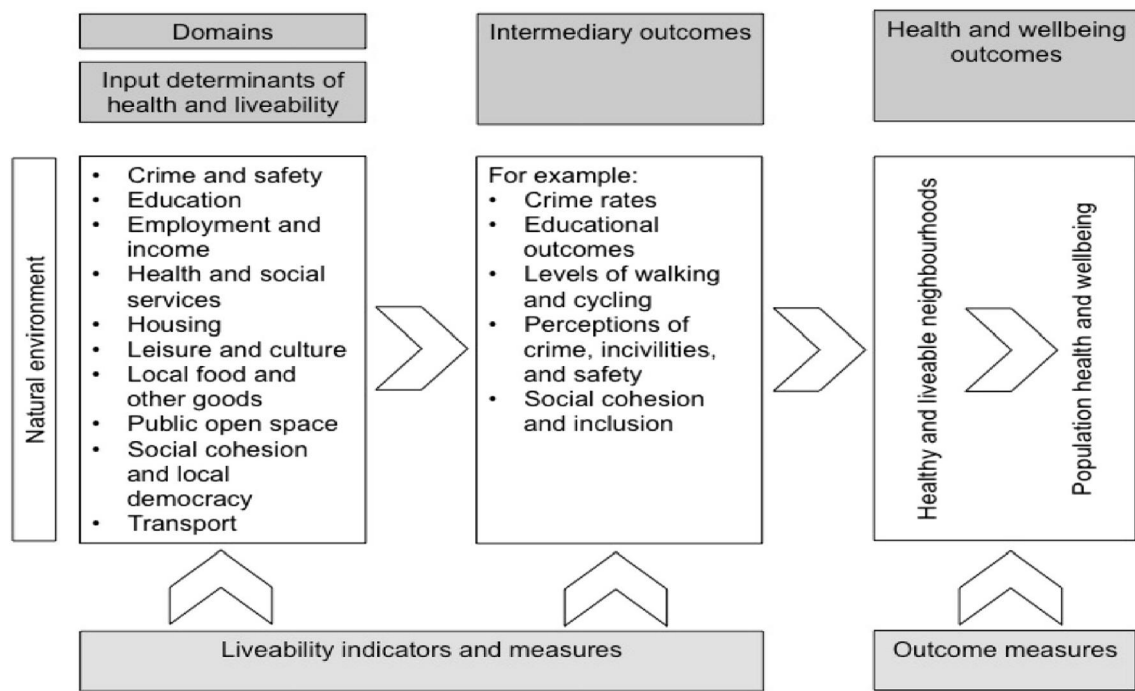
Figure 1.5: Pathway of liveability for wellbeing outcomes (Badland et al., 2014)

However, studying urban liveability and the effect of urban design on people's health, wellbeing and productivity is in progress all the time. The effect of the urban parks on the built environment sustainability and liveability was addressed by many studies. Parks and open and landscaped areas are urban design elements that play a significant role in providing a liveable outdoor environment (Guzman and Harrell, 2014). Landscaped areas and open spaces has a crucial influence in city sustainability. The positive effect of greenery and urban parks on outdoor and indoor environments has been explored and proved in many studies. Furthermore, the materials used for landscaped and open areas, streets and urban parks has an influence impact on thermal performance of the built environment (Tooming, 1996; Crook and Forster, 2014).

Figure 1.6 the shows the difference between the well-connected landscape network to the city centre and the wildlife landscape within the urban area (Ritchie and Thomas, 2010).

12

Liveable outdoor environment and sustainable outdoor urban design consequently affects the indoor environment and thermal performance of individual buildings (Johar et al., 2015; Lenzholzer et al., 2015).

Figure 1.6: Landscape planning for urban areas (Ritchie and Thomas, 2010)

1.5 Climatic Urban Design

Climatic Urban Design is a passive design strategy that can be adopted to produce a sustainable urban design or sustainable master plan. Sunlight access and fresh air circulation are important factors for any urban designer and should be considered in planning the sustainable master plan. Optimising the maximum benefit of natural resources of solar gain, fresh air and natural light is one of the major targets in any sustainable design. Even though, designing according to these factors is highly affected by the development location and local climatic conditions. In the cold climates, designing for the maximum solar gain is a target for successful and sustainable design, while the desire of the maximum solar gain is less in the hot, humid locations(Berger et al., 2014; Yuan and Ng, 2014; Djukic, Vukmirovic and Stankovic, 2016). However, achieving the balance between the desired solar gain and the maximum benefit from daylight is one of the challenges in urban planning and design.

Moreover, the comfort index which represents the numerical values of outdoor air temperature and humidity that measure the comfort or discomfort, is one of the parameters that indicates the level of sustainability in urban design, and it is the urban planner's responsibility to create a comfortable, balanced built environment (Oke, 1987; Givoni, 1998; McGrath, 2013; Yuan and Ng, 2014). Zoning codes and urban design regulations are generally established to control the over shading effect of buildings on each other, and to secure fair access of sunlight and natural air for each building in any complex or neighbourhood.

1.6 Urban Form and Urban Design Elements

Urban design covers a number of elements that form the urban design or urban master plan. These elements cover: buildings design, land use, transportation system, urban canyon design, parks and open spaces (Dempsey, Brown and Bramley, 2012; Guhathakurta and Williams, 2015). The integration of the mentioned urban design elements produces the urban form. The urban form represents the structure of the urbanisation and reflects the proximity and the density of the urban area (Lo, 2016). It covers street patterns, building patterns and design, as well as land use patterns. The nature and physical characteristics of the urban form directly affects the energy performance of the development starting from the neighbourhood, community, district and the city. However, Badland et al. (2014)highlighted the impact of the urban form on health outcomes, and the effect of urban form on energy performance and CO_2 emissions is explored and proved in many studies (Yuan and Ng, 2014; Guhathakurta and Williams, 2015; Fang, Wang and Li,2015; Zhang, Guindon, and Sun, 2016).

1.6.1 Buildings Design and Geometry

Buildings geometry and design is one of the major elements that contribute to urban design and planning, buildings design covers a number of variables, namely building shape, height,

orientation, glazing percentage and building materials. Previous studies have proved the effect of building design elements on both outdoor and indoor thermal performance of the built environment (Negendahl and Nielsen, 2015; Leiteet et al., 2015; Cruzet et al., 2016). Hemsath, Alagheband and Bandhosseini (2014) reported the effect of optimising building geometry as one design factor critical in the early design stages on enhancing the building's energy performance. The studies addressed a number of buildings design variables to find their effect on indoor energy consumption. Gomes et al. (2015)studied the effect of building organisation within a complex and explored the effects of different organisation plans on building energy performance. On the other hand, Abohela, Hamza and Dudek (2013) investigated the effect of building roof shape on the air flow and wind speed, and how this variable affects indoor thermal performance and energy consumption. Moreover, building facade materials, insulations, construction materials and the effect of the U-Value have a major impact on indoor energy performance, and this fact is presented in many studies (Alsemaa et al., 2016; Robati, 2017).

1.6.2 The Urban Canyon

The 'Urban Canyon' is an urban design and planning element that could be adopted to achieve the maximum benefits from natural resources and creating the desired comfortable environment. The urban canyon is defined by Oke (1978) as a geometric abstraction of urban space that creates a spatial environment. It could be a street, a yard, a garden, a boulevard, a walkway or a driveway (Syrios and Hunt, 2008). The Urban Canyon describes the height/width ratio (H/W) of the space between two or more adjacent buildings within the complex or neighbourhood. The Urban Canyon orientation has a significant effect on the urban microclimate condition and thermal comfort within the canyon space (Arnfield, 1990; Todhunter, 1990; Shishegar, 2013; Yang, Qian and Lau, 2013).

Johansson (2006) stated that the urban canyon can be categorised into three types according to the H/W ratio:, 1) shallow canyon, 2) uniform canyon, and 3) deep canyon (Figure 1.7).
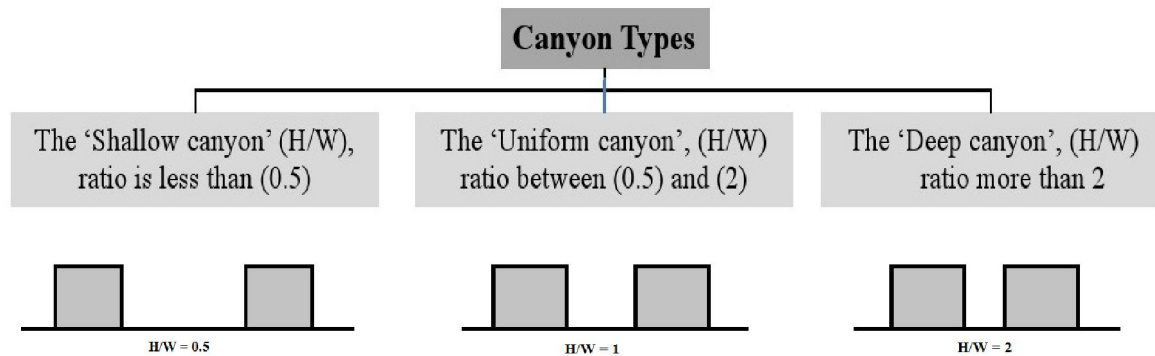
Figure 1.7: Canyon three types (Johansson, 2006)

1.6.3 Buildings and Canyon Design Indicators

1.6.3.1 Buildings Height to Canyon Width H/W Ratio

The height/width H/W ratio is one of the 'Canyon' parameters. It is the height of one or more than one adjacent buildings over the canyon width; also known as the 'Aspect ratio'. The aspect ratio was adopted in many studies to express the canyon geometry and to evaluate variation in buildings organisation and configuration (Shishegar, 2013; Lee, Jusuf and Wong, 2013; Yang, Qian and Lau, 2013; Ng and Chau, 2014).H/W ratio is an expression of the compactness and density of the urban form. A high H/W ratio reflects the high density of the developed area (Andreou, 2014). Generally, a high H/W ratio has a positive effect of creating the desired outdoor thermal comfort in hot climate regions. On the other hand, H/W affects another urban design factor that should be taken into consideration, such as viewshed and daylight access. However, the viewshed is the amount of the geographical area that can be observed from a specific point, high H/W and increasing the compactness of the urban block or the community reduces the viewshed factor.

1.6.3.2 Sky View Factor (SVF)

The Sky View Factor (SVF) represents the amount of possible observed sky from one point. It indicates the available sky for scattering of daylight and solar radiation, therefore, it can be used for evaluating daylight and heat exchange parameters (Gal, Lindberg and Unger, 2009). Furthermore, SVF is an urban indicator that represents building height, proximity and morphology. It is used to explore and assess the urban geometry and buildings configuration effect on urban microclimate parameters. The importance of using and calculating the SVF appears in changes that occur in solar irradiation in the urban canyon space. These changes in solar radiation affect the thermal performance and energy calculations of the buildings around the canyon. Therefore, the SVF is a crucial factor in energy consumption at the urban level (Oke, 1987). It is used in studies that are concerned with the mitigation of urban phenomena, such as Urban Heat Island UHI (Unger, 2004). Figure 1.8 shows the effect of the SVF of horizontal and convoluted surfaces. On the horizontal surface, the short wave is reflected without any obstruction. On the other hand, the convoluted shape increases the short wave received and decreases the long wave reflection. This will modify the surface heat flux consequently because of the emitted radiation (Oke, 1987).
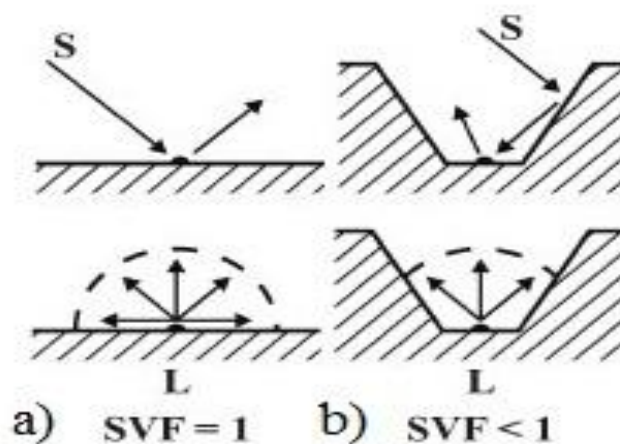
Figure 1.8: Comparison of SVF for horizontal and convoluted surfaces (Oke, 1987)

SVF can be measured using the 'Fisheye' instrument (Figure 1.9). Moreover, some computer simulation software such as 'ENVI-MET' calculates the SVF as an outcome parameter from modelling the urban geometry. A higher SVF indicates that a higher amount of the sky can be viewed from the measured point (Chen and Ng, 2011).
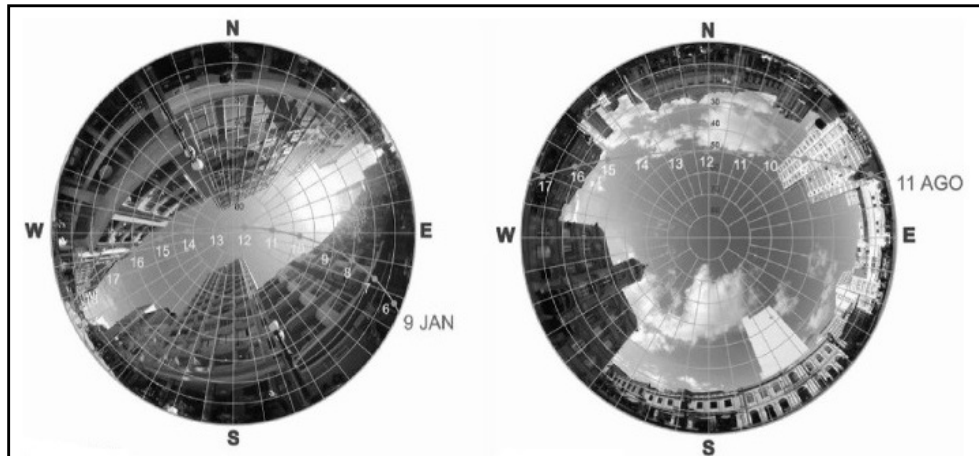
Figure 1.9: The Fisheye image for low (left) and high (right) Sky View Factor
(Kruger, Minella and Rasia, 2010)

The range of SVF value is between 0 and 1. The 1 SFV gives an indication of no obstruction to the sky in the measured point, while the 0 SVF corresponds to a point without any view access to the sky. According to the field measurement study conducted by Kruger, Minella and Rasia (2010),a deep canyon with a H/W ratio of more than 1 has a SVF of less than 0.3. An SVF can be used in urban geometry and canyon studies as an alternative expression to the H/W ratio, as the SVF expresses the relationship between the canyon width and the variation in building heights.

Furthermore, the SVF is adopted and simulated using the 'Geographical Information System (GIS)' computer software to find the effect of urban geometry on the UHI and dynamic wind speed and direction (Chen and Edward, 2011).

1.6.3.3 Gross Floor Area (GFA) or Built-up Area (BUA)

The 'Gross Floor Area (GFA)' or the 'Built-up Area (BUA)'represents the amount of the built area on the specific site or plot, and the GFA ratio or the BUA ratio represents the total built-up area over the plot area. The BUA is an indicator that expresses building configuration within the complex, it both affects and is affected by the other urban geometry indicators, such as SVF and H/W ratio. For example, the SVF is small when the H/W ratio is high and the BUA is also high, respectively (Pont and Haupt, 2004; Cheng, 2009; Cheng and Steemers, 2010; Salat, 2011; Ignatius, Wong and Jusuf, 2015). On the other hand, the 'Floor area Ratio (FAR)' is a factor that can be multiplied by the plot area to find the allowable Built-up BUA or GFA for each plot. Hence, the FAR controls the compactness of the built-up area, and it is normally indicated in the development codes and regulations to control the allowable built-up area and story number on each plot (Figure 1.10).
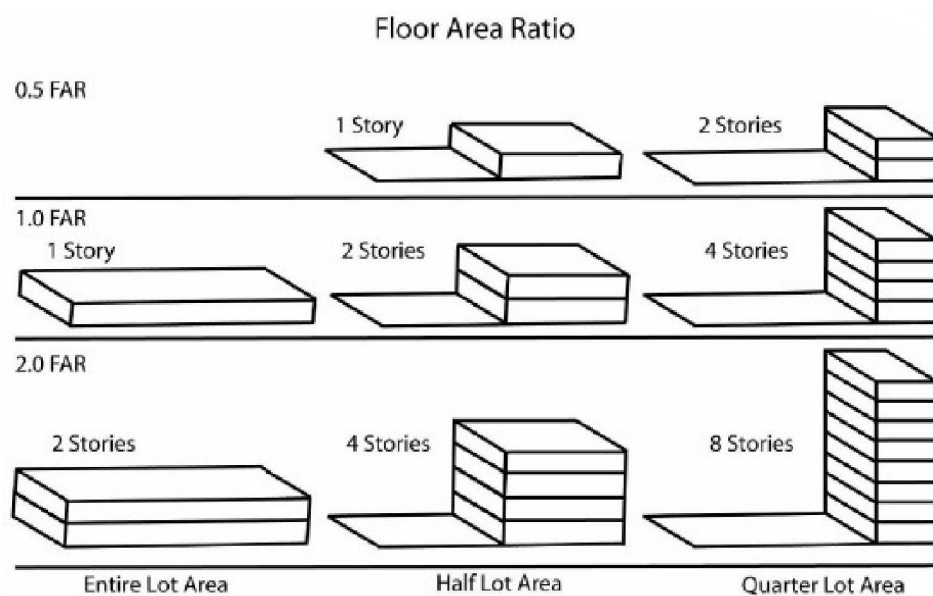
Figure 1.10: The floor area ratio for the same plot area and the compactness in built-up area (WordPress, 2011)

However, the BUA calculations varied between the development codes or the urban design regulations, some codes exclude specific areas from the total BUA, such as the areas of basements, external balconies, elevator shafts and mechanical ducts (Business Bay Development Code, 2005; Jumeriah Village Development Code, 2006).

1.7 Dubai / UAE Urban Planning and Design

Observation and investigation in Dubai urban planning design and according to interviews with Dubai municipality urban planning department engineers, shows that the new urban planning of the liner city tends towards planning and constructing clustered communities and neighbourhoods to form cities within cities or a 'Clustered City' (DM, 2015). Figure 1.11shows different types of urban form. Dubai, as a new city, represents an example of the clustered city. Porter (1990) stated that the cluster includes a number of elements or buildings that grow together. This type of urban planning and development is followed to avoid sprawl or the uncontrolled urbanisation.
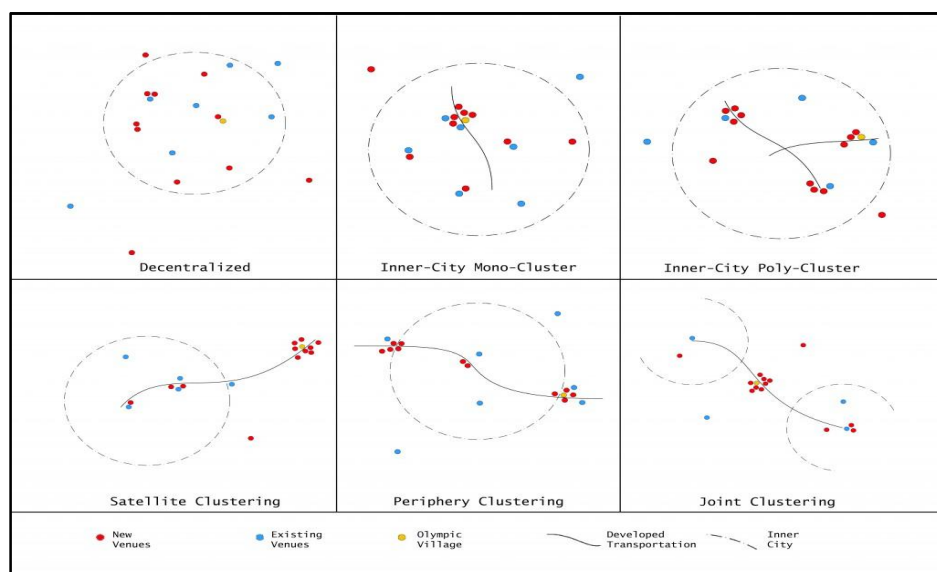
Figure 1.11: Types of urban planning and form (City Forms, 2015)

Figure 1.12 shows an example of Dubai's clusters, cities or districts. Furthermore, it ensures the implementation of high standards in planning, design and throughout the construction process. It provides the opportunity to apply the new practices and adopt urban design elements determined to achieve the sustainable urban design. Each community or neighbourhood is (or should be) constructed according to specific urban codes and regulations. These codes and regulations are mainly issued by the master developer of the district, and should be implemented by the consultants, contractors, and subcontractors of the project. According to the Dubai Master Plan (2020), which was launched by Dubai Municipality (DM) (February, 2012), only 20 % of the total area of the city is constructed and covered with urban fabric.

Twenty percent of the undeveloped land which is under the commitment of the strategy behind the Dubai Master Plan is under planning and construction, while the off shore manmade islands represents 23% of Dubai's total area and it is partially constructed (DM, 2016).
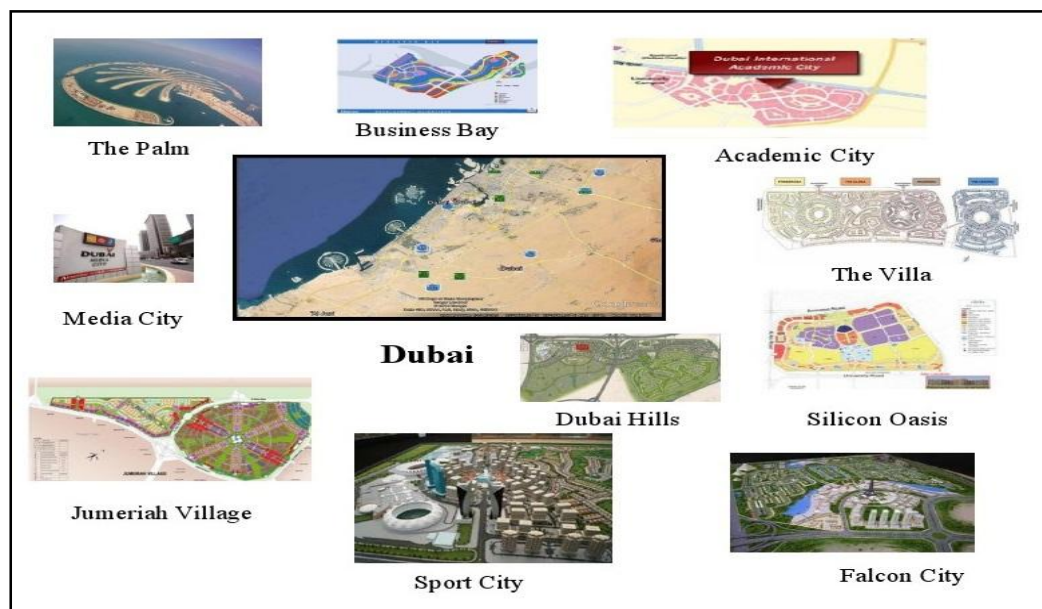
Figure 1.12: Example of Dubai's clusters, cities and districts (Author, 2018)

In this context, in 2011 the Dubai municipality (DM) began the implementation of green building regulations and specifications on building scales with the cooperation of authorities, master developers and all the construction stakeholders, in order to achieve the highest international standards with local conditions. The Dubai Green Building Regulations Practice Guide was developed to provide a guidance for each of the regulations applied in the building lifecycle, including design, construction, operation /maintenance, and deconstruction, to ensure the desired and the positive outcome for the three pillars of the sustainability; environmental, economic and social. As part of this and in complying with the vision of extending and developing the city towards being one of the world's most sustainable cities, this research explores the opportunity of optimising buildings morphology and configuration on the urban scale towards more sustainable design with high standards in terms of energy conservation and pollution reduction, and to achieve high levels of air quality, outdoor comfort and the desired sustainable environment.

1.7.1 Urban Planning Codes and Mid-Rise Buildings

Each city or district in Dubai is planned and constructed according to the district urban planning code. The code or regulation of each area or city contains the city's master plan, land use, types and heights of the buildings. The code also contains the specifications of each type of building with all architecture and facade design and materials. Residential mid-rise buildings can be seen in most of these codes, but the configuration of this type, height and orientation is different from one code to another. Figure 1.13shows an example of the master plan and the availability of mid-rise buildings in two districts in Dubai 'Jumeriah Village' and 'Downtown Jebel Ali', the two districts are still under construction and the opportunity of implementing the revision on the regulation code is still available. This study will analyse residential mid-rise buildings in order to find the best configuration of this type of building that can help to achieve minimum energy consumption.

This should reflect positively on carbon emissions and outdoor microclimate quality. This aim comes to comply with the national and global target of reducing carbon emission and footprint and creating a liveable, sustainable environment.
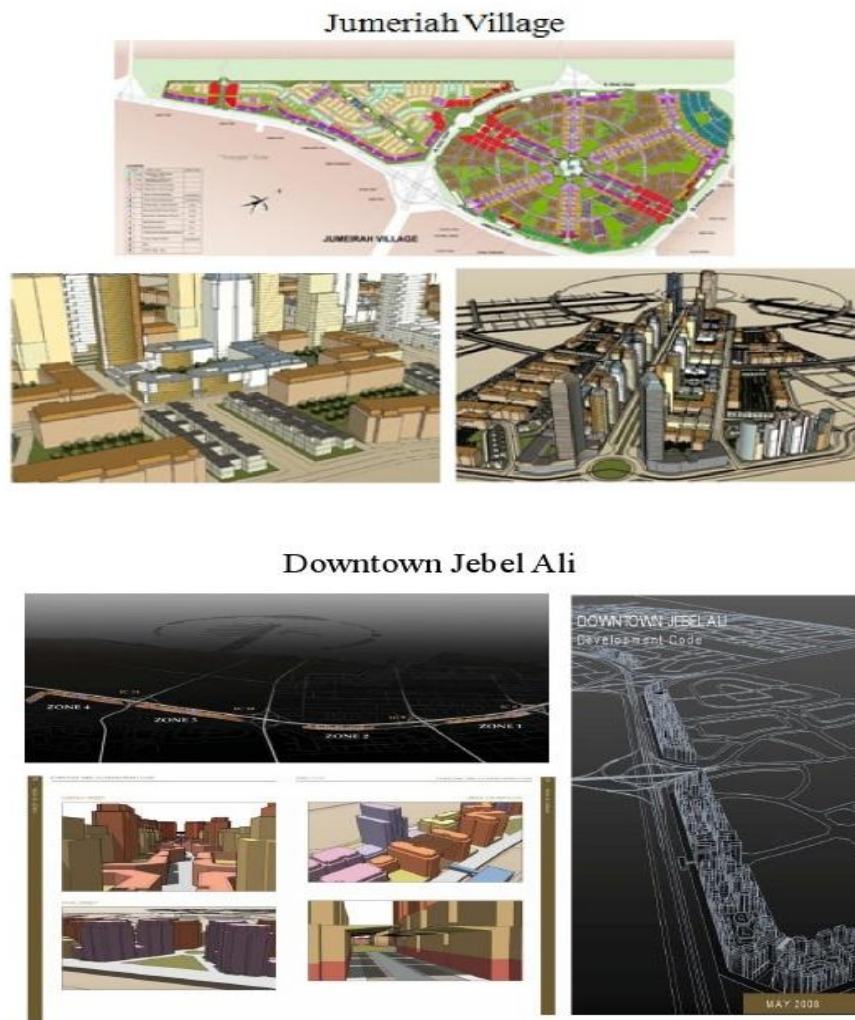
Figure 1.13: 'Jumeriah Village' and 'Downtown Jebel Ali', two district planning codes in Dubai (Author, 2018)

1.8 The Significance of the Study

The previous studies illustrated and proved the importance of including the micro climate and weather data in early design stages. The major microclimate data, such as, solar radiation, air temperature averages and prevailing wind has to be considered by the urban planner in the

concept design to achieve the sustainable master plan (Wong, Jusuf and Tan, 2011; Ebrahimabadi, Nilsson and Johansson, 2015; Darwish, Ragheb and Ahmed, 2016).However, the climatic design aims to achieve a sustainable urban design according to the location on the earth and the local context of a specific area or region. However, in this research the literature review method of the study is conducted to investigate the previous studies related to urban planning and to explore the urban configuration effect of the built environment. Previously, most of these studies adopted numerical models to present and simulate urban environmental performance, and to find the effect of the urban geometry on the microclimate parameters, specifically air temperature and wind speed. The use of the computer software to simulate and evaluate the built environment microclimate performance has started recently with a limited number of software. The recent progress in computer software encourages the researchers for further investigation to achieve sustainability and resources efficiency by adopting the climatic design. However, the effect of urban geometry and configuration on outdoor thermal performance, and the reflection of this performance on a building's energy consumption still needs more investigation. Furthermore, a few number of published studies explored the effect of urban design and configuration within the local context of the UAE, and according to the weather characteristics of this region. This study and further research with similar concept would be important to support the continuous development in UAE cities, as the published studies that explored the sustainability on urban level in the UAE in general, and Dubai in particular, is extremely rare.

This research will adopt computer software to simulate, analyse and evaluate the urban configuration, and to identify the effect of urban geometry variables on outdoor microclimate parameters and indoor energy consumption. However, this study will adopt the 'canyon' as one of the urban configuration elements, and a developed model of different configurations to find the effect of urban variables on the environmental parameters.

Furthermore, it seeks to achieve the best configuration that enhances the thermal performance of the urban canyon, and affects urban liveability positively.

The effect of urban geometry will be studied by analysing the building configurations impact on outdoor thermal performance parameters including solar radiation and shading effect, air temperature, humidity, wind speed and air movement. For this aim, this research will adopt the developed urban block model and the simulation software according to the UAE local context and weather characteristics. The effect of urban design elements were illustrated in a number of previous publications, as will be demonstrated in the next chapter. Still, some urban geometry variables, such as building height diversity and urban block configuration required more investigation in order to find the effect of these variables on the outdoor and indoor thermal performance within the local context.

Therefore, the contribution of this study could be delivered by identifying the effects of building geometry and configuration on microclimate parameters and reflecting this effect on a building's energy performance. Furthermore, within the local context and according to the Dubai Municipality Urban Plan, Dubai is committed to construct 20 % of the nonurban area. This provides the opportunity to apply the optimised configuration on a wide range through the codes and regulations implemented by Dubai Municipality (DM) and the Master Developers. Furthermore, this study is important as it is aligned with the '2015 Dubai Strategic Plan' of developing sustainable communities and developments towards the '2021 Dubai Urban Master Plan'. The study comes to and comply with the vision of His Highness Sheikh Mohammed bin Rashid Al Maktoum, the UAE Vice President, Prime Minister and Ruler of Dubai, for promoting Dubai as an iconic, global, green and sustainable city (WAM, 2016). This research will focus on optimising buildings and canyon geometry towards a high level of sustainable performance in terms of outdoor microclimate conditions and indoor energy consumption.

Climate change and environmental concerns are at the top priorities of the UAE and Dubai agenda, and conducting this research will offer valuable results that could be taken into consideration by the urban planning and construction sectors. Furthermore, the results of this study will contribute to the 'Supreme Energy Council' and the UAE target of reducing energy consumption and CO_2 emission by 16 % by 2021 (DEWA, 2016), and it will encourage the emirate's attitude towards creating sustainable neighbourhoods and developments. Moreover, the findings of this research can be generalised to other world regions with the same weather characteristics and climatic conditions.

1.9 The Research Questions

The questions to be addressed by this research are:

1.   What is the effect of buildings configuration and height diversity on the urban microclimate in terms of shading, air temperature, humidity, air movement and wind speed?

2. What is the effect of buildings / canyon configuration and orientation on outdoor thermal performance according to Dubai / UAE weather characteristics?

3. What is the integrated effect of the changes in urban geometry and the surrounding microclimate on energy consumption covering cooling load of buildings within the same block or complex?

4. What are the best urban configurations that optimise the cooling load of the urban block or complex of buildings?

1.10 Research Aim and Objectives

This research will explore the optimisation of urban geometry and buildings configuration effect on energy performance at the urban level in Dubai and the broader UAE. The research aims to adopt the potential of urban planning to reduce energy consumption on the urban scale. For this aim and to answer the research questions the following objectives are indicated:

1. Urban geometry elements covering buildings / canyon variables and indicators will be identified.

2. The major microclimate parameters will be explored namely; air temperature, shading, humidity, and wind speed.

3. Case study area will be selected to obtain the physical dimensions.

5. Proposed scenarios for investigating the selected urban geometry variables will be developed to be evaluated against a base case.

6. The effect of buildings' geometry variables on the listed microclimate parameters will be investigated using an appropriate method.

7. The effect of the variation in the microclimate parameters on reducing the cooling load will be analyzed and discussed.

8. The best urban configurations in terms of improving the outdoor microclimate parameters and reducing the indoor cooling load will be recommended.

However, the previous findings related to the urban geometry variables and the effect of these variables on canyon microclimate parameters and building energy consumption will be illustrated in detail in the next chapter. The literature review, Chapter 2 will illustrate the previous and recent findings related to urban configuration and urban geometry design.

1.11 The Research Focus and Limitations

This research focuses on a number of urban geometry variables and their effect on outdoor microclimate and indoor thermal performance. It will be conducted on Dubai / UAE climate conditions, and the results can cover the locations with the same climate characteristics. The study does not explore the effect of other climate zones.

The research will focus on the residential buildings group, other types of buildings such as; offices, commercial, industrial, educational, etc. can be adopted in future studies. The residential buildings or the dwellings in this study will include one prototype; the mid-rise buildings. High rise, low rise, and the unlimited towers will not be included in the scope of this study work.

1.12 The Research Framework

This research will pass through four phases, each phase will be covered in one or more than one chapter of this study. Figure 1.14shows a brief on this study's four phases.

Phase One

In the first phase of this study the literature review method of the study will be conducted, and an overview of the built environment elements will be explored.

Furthermore, urban geometry variables and microclimate parameters will be identified. The latest publications and findings related to urban configuration and energy performance will be

illustrated. In addition, exploring the sustainable urban and buildings design strategies for optimising urban geometry towards enhancing urban microclimate and buildings energy performance. In this phase the research questions, aim and objectives will be illustrated. Furthermore, the research variables will be selected. This phase will be covered in the first two chapters of this study.

Phase Two

In phase two, the previous methodologies related to urban geometry and microclimate investigation will be explored. The most followed methodologies in urban studies will be presented in detail.

In this phase the methodology that will be followed to achieve the research aim and objectives will be selected. Moreover, the case study area will be selected and described, and an urban block of buildings will be indicated for data collection. The collected data will cover physical buildings and block design and dimensions. Furthermore, the microclimate data collected will be used for method validation.

The case study area will be modelled and simulated, and the method will be validated against the field collected data. Moreover, the suggested strategies for optimising the urban geometry will be implemented in the developed proposed scenarios. The suggested scenarios will be based on the base case and newly developed scenarios with a variation in the variables of urban geometry and building design. The variation will adopt the sustainable design strategies that were proved in previous literature and publications. This phase will be covered in chapters three and four.

Phase Three

Phase three of this study will address the suggested scenarios of revising and optimising urban geometry variables. This phase will be covered in chapters five, six and seven. The suggested scenarios will adopt the climatic urban design strategies mentioned in the literature review chapter. The selected methodology will be implemented. Furthermore, the results of the comparison between the base case and the suggested scenarios will be illustrated, analysed and discussed in this phase. The results will cover the effect of variation in the urban geometry variables, on the outdoor microclimate parameters. The microclimate outcome data to the indoor environment will be integrated. This integration aims to find the impact of the changes that occur in microclimate parameters on the indoor energy performance. Moreover, the best configurations that enhance the outdoor microclimate parameters and reduce the indoor energy consumption will be presented.

Phase Four

In phase four of this study, the conclusion as a final outcome of this study will be presented. This phase will be included in the last chapter of the study, chapter eight. Furthermore, general recommendations based on the analysed results will be suggested.

The recommendation will present the best configurations that enhance the outdoor thermal performance and reduce indoor energy consumption. The optimised buildings configuration and urban block design for minimum energy consumption will be recommended. Finally, the future studies and a recommendation for further investigation in this research study area will be presented.
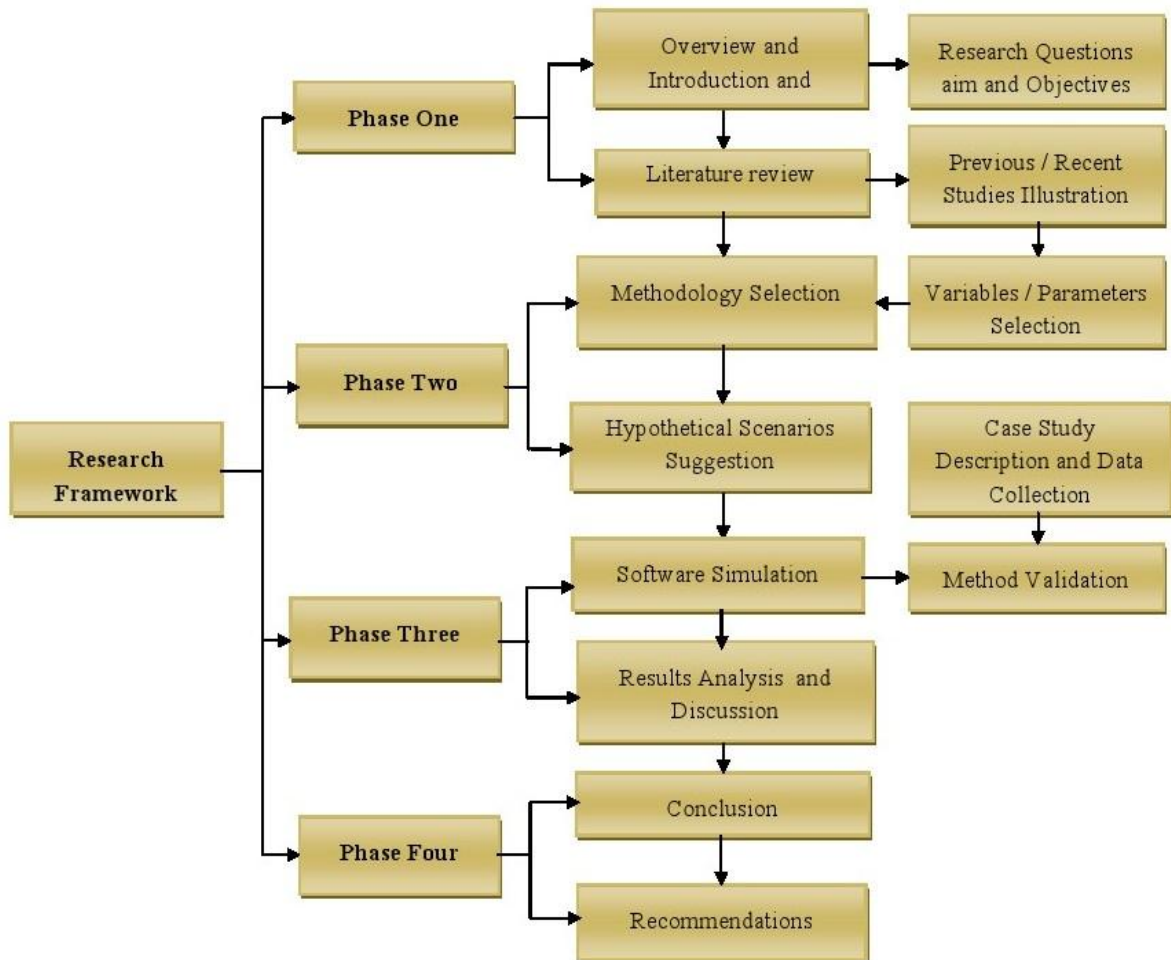
Figure 1.14: The Framework of the Research (Author, 2018)

Chapter 2

Literature Review

2.0 Literature Review

2.1 The Microclimate and the Built Environment

The atmosphere of the earth is divided into four layers excluding the 'Exosphere' layer. The closest layer to the earth is the 'Troposphere' layer (Figure 14). The troposphere extends 12 km-20 km from the earth's surface into the atmosphere. Microclimate conditions is a part of the earth's Troposphere layer called the Atmospheric Boundary Layer (ABL) (Danielson, Levin, and Abrams, 2003). Figure 2.1 shows the altitude of the four atmospheric layers; Troposphere, Stratosphere, Mesosphere, and Thermosphere (UCAR, 2016).
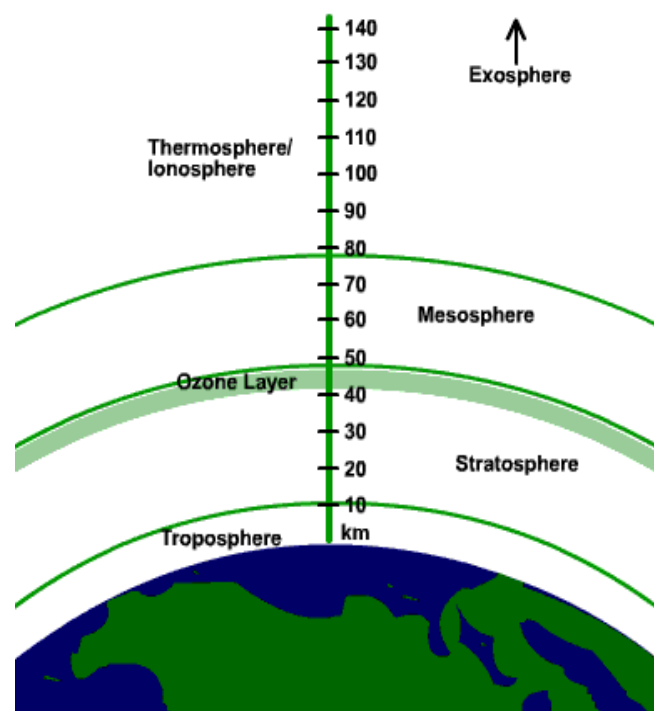
Figure 2.1: Atmosphere layers (UCAR 2016)

The Atmospheric Boundary Layer (ABL) extends from the earth's surface to a range of 200 m-500 m above the ground surface level (Szokolay, 2008).

The first 100m of the ABL is most affected by the changes in the earth's surface (Garratt, 1994; Kaimal and Finnigan, 1994). This layer can be divided into two sub layers: Urban Boundary Layer UBL and Urban Canopy Layer UCL. Figure 2.2 shows the boundary of each layer within the ABL.

The UBL is above the average height of the buildings, while the UCL is the layer in the space between the buildings. The UCL microclimate is affected by the morphology, shape and roughness of the developments (Oke, 2002). Most of the built environment research is concerned with the UCL as it has the most significant effect on the thermal performance of the built environment (Marciotto et al., 2010; Pichierri et al., 2012).

However, the microclimate is the climatic conditions of the UBL and the UCL of the built environment. Microclimate represents the climatic parameters of a local division from the larger area (Oke, 2002). It can be the climatic conditions of a small area, such as the canyon between the buildings, or it can also represent the climatic conditions of a larger area, such as a city that has different climatic conditions to the surrounding area (Erell et al., 2011).
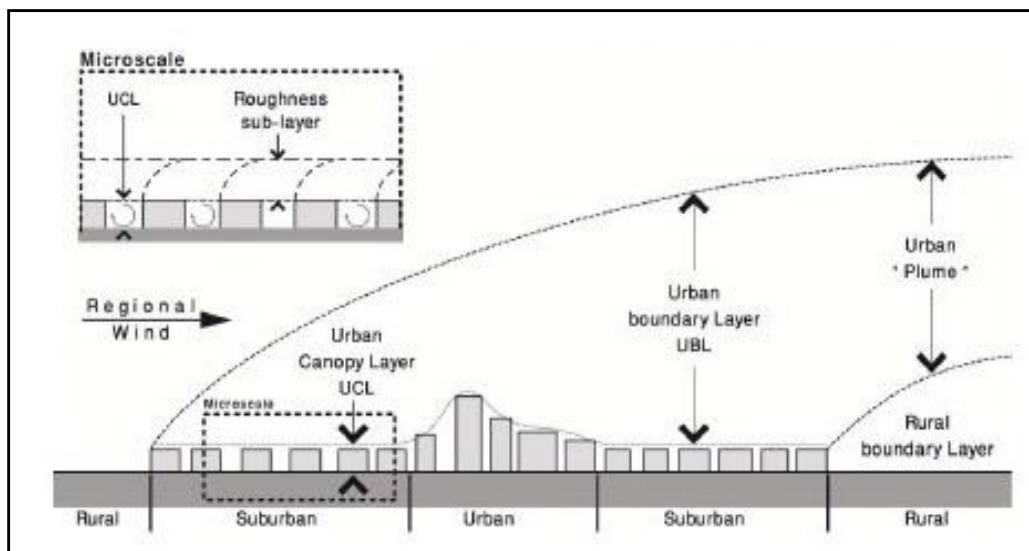
Figure 2.2: Scheme of the UBL and the UCL of the developments (Oke, 2002)

Generally, the microclimate major parameters include air temperature, solar radiation, humidity and wind speed. The interaction between the urban geometry and the microclimate conditions have a significant effect on the thermal performance of outdoor and indoor environments. It is still difficult to predict every single factor that contributes to the microclimate conditions of the built environment. It is found that some phenomena such as the Urban Heat Island UHI are important factors that affect climatic conditions, both on a local and global scale (Saitoh et al., 1996; Unger et al., 2010; Peng et al., 2011). The UHI was explored and illustrated in previous literature in order to find the reasons behind these phenomena, and its impact on climatic conditions. In addition, this literature also sought to find solutions to reduce and mitigate its negative effect on the built environment.

2.2 Urban Heat Island UHI

The Urban Heat Island UHI is one of the most effective phenomena in global warming and climate change. Zhao (2011) stated that the UHI contributes to climate warming, contributing about 30% of its effect. The UHI represents the area where the temperature is higher than the surrounding and rural area. It is an urban phenomenon which has both outdoor and indoor environmental impacts. Generally, the UHI is caused by the solar radiation absorbed by the structures in developed areas (Park, 2007). Therefore, the main reason behind the UHI is the modification of the natural land by developments, and urbanisation, which act as the main causes of this phenomena (Park, 2007). Sustainable urban design can have a direct impact on reducing the effect of the UHI on the surrounding environment. Increasing the indoor energy consumption is one of the serious negative impacts of this phenomena (Rizwan, Dennis and Liu, 2008).

Previous studies showed the importance of urban geometry and design in reducing the effect of this phenomena on microclimate conditions (Ichinose, Matsumoto and Kataoka, 2008). Che-Ani et al. (2009) highlighted the factors that affect the UHI in two ways:

1) Micro climate factors (wind speed and behaviour, humidity and cloud layer), and 2) Urban geometry factors(urban pattern, density, built-up area, Sky View Factor (SVF) and urban materials).

Figure 2.3 shows the main resources that generate the UHI including the controllable and uncontrollable variables. Population growth and air pollution are among the controllable resources of the UHI, while wind speed, diurnal conditions and seasons are determined as uncontrollable variables. The figure also shows the urban design variables that affect this phenomenon, such as building materials used, SVF and the landscaped green areas (Rizwan et al., 2008).
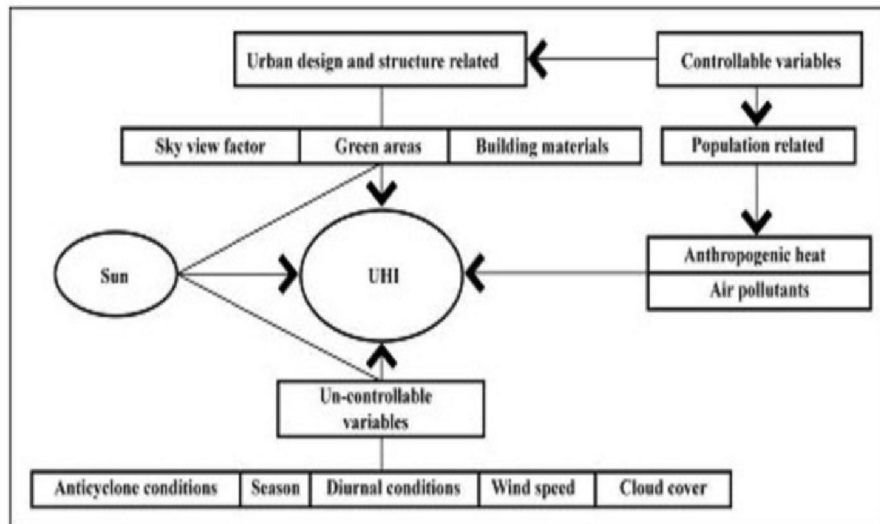
Figure 2.3: Resources of generating UHI(Rizwan et al., 2008)

2.2.1 Types of Urban Heat Island UHI

The UHI is divided into two types: a) Urban Surface Heat Island (USHI), and b) Atmospheric Urban Heat Island (AUHI) which represents the UHI within the urban space. The USHI is the average temperature on the horizontal surfaces such as roofs of buildings, outdoor equipment and canyon pavements. It is a diurnal phenomenon that is affected by the sun's position and the surface material (Peng et al., 2011). The USHI is measured by using the remote sensing

data collected from satellite sensors (Weng et al., 2004). Figure 2.4 shows the USHI according to the Land Cover Types (LCTs) in Shijiazhuang, China (Liu et al., 2015).

The Landsat satellite image presents the surface temperature according to land types (urbanisation types) on four different dates. The other type is the UHI within the atmospheric boundary layer which can be divided into two types depending on the atmospheric layer.

The first one is the UHI within the UBL above the building's average height. The air temperature of this layer is affected by the interaction with the roughness of the building's roof. The second type of the UHI is the one within the Canopy Layer Heat Island (CLHI),which represents the area within the urban space between the buildings or the canyon space (Oke, 1976).
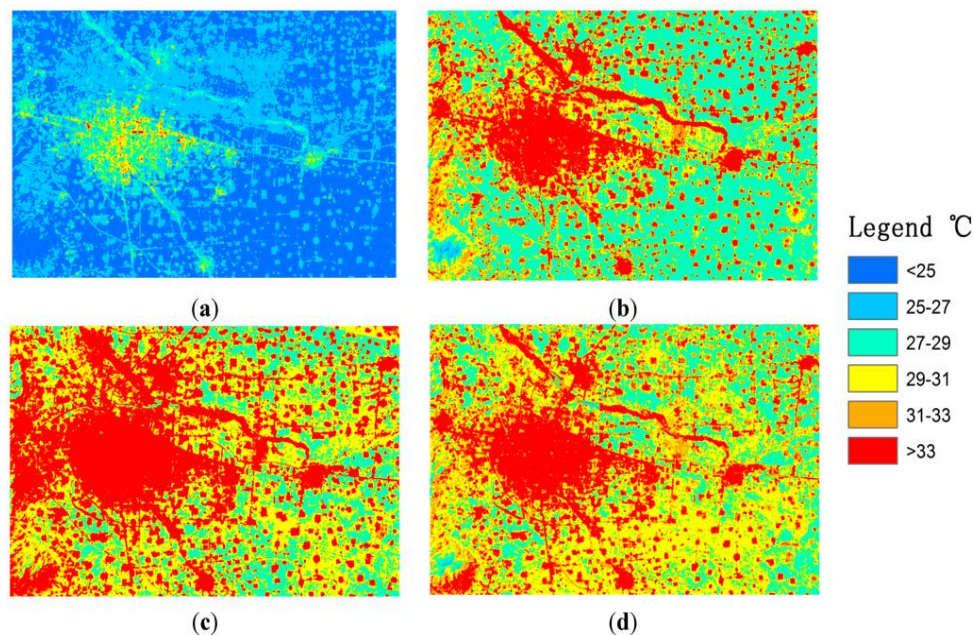
Figure 2.4: Landsat image of (USHI) in Shijiazhuang, China on (a) 5 September 2006;(b) 23 August 2007; (c) 12 August 2009; and (d) 15 August 2010(Liu et al., 2015)

The Canopy Layer Heat Island (CLHI)is the part of the high temperature air within the urban canyon space. It extends from the canyon ground to the average height of the buildings. It depends on the building's geometry, canyon height to width ratio, percentage of greenery and canyon material (Oke, 1976). The CLHI generally measured by weather measuring tools used in fixed stations at ground level. The effect of the UHI on microclimate conditions will be

explored in the next section as well as exploring its effect on indoor thermal performance and energy consumption.

2.2.2 The Effect of the Urban Heat Island UHI

According to the United States Environmental Protection Agency(US EPA, 2008), the effect of the UHI is felt in an increase in the developed area's air temperature compared to the rural surrounding area air temperature of between 1ºC - 3ºC during the day. This increase of air temperature will consequently increase electricity demand by 1.5 % -2 %. Accordingly, GHG emission and air pollution will be increased. For large cities this increase in electricity load will be elaborated in a 5 % -10 % increase in consumption in order to cover the effect of the UHI on a larger scale. The UHI is affected by the day and night time, figure 2.5 shows that day air temperature is higher than the night air temperature. The variation between surface temperature and air temperature at night is less compared to this variation in the day time. This result reflects the fact that during the day time the developed surfaces absorb the solar radiation more than reflecting this radiation, while at night time the surfaces release this heat and the balance between the surface and air temperature at night occurs (US EPA, 2008).
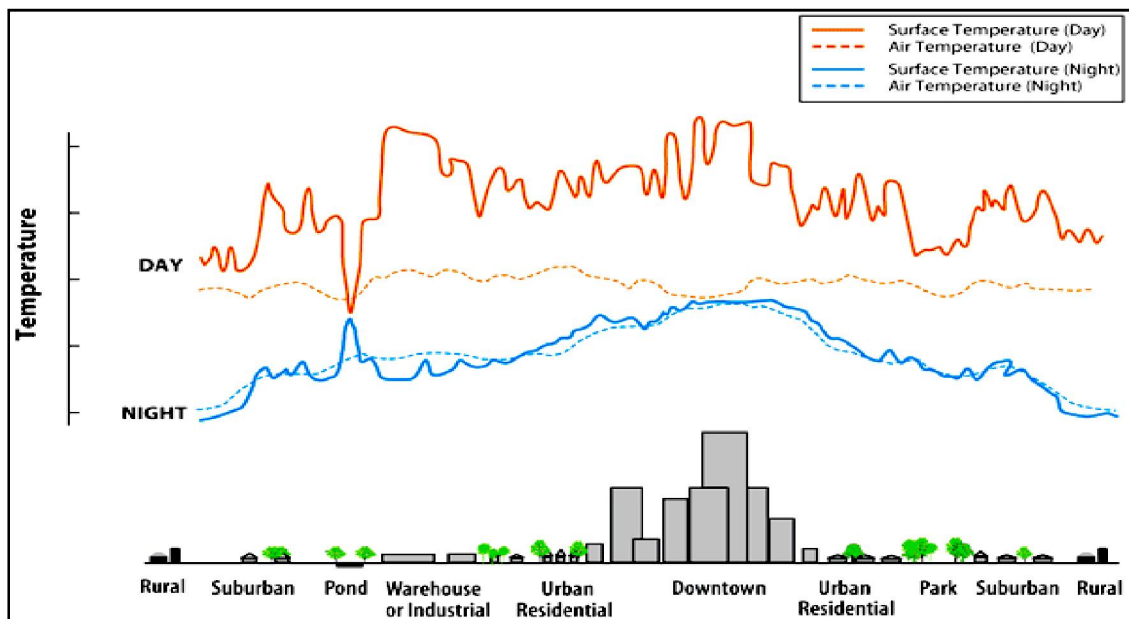
Figure 2.5: Diurnal attitude of the UHI (US EPA, 2008)

On the other hand, Wanphen and Nagano (2009) found that the variation in air temperature within the urban context can reach 5°C - 15°C because of the pockets of small islands. However, the impact of the UHI is different according to the location of the area and weather conditions. Hirano and Fujita (2012) conducted a field measurement study to find the effect of UHI in Tokyo, Japan. The researchers stated that UHI is an accumulation of high temperature areas, and it has a more positive effect by reducing heating consumption in winter, compared to the negative effect of increasing cooling consumption in summer. The researchers proved that the area function and the building group are another determined factors in evaluating the effect of UHI. In spite of the positive effect of reducing energy consumption in the winter, the authors did not recommend stopping the effort of mitigating the UHI and its impact on the global environment. In the same context Kolokotroni, Zhang and Watkins (2006) explored the effect of UHI on cooling and heating load in London, UK. The researchers found that the UHI causes an increase in cooling load by 25 %, and a decrease in heating load by 22% compared with the load in rural areas (Figure 2.6). This type of result proves that the effect of UHI on energy consumption is varied according to the site location on earth, and weather conditions of the area.
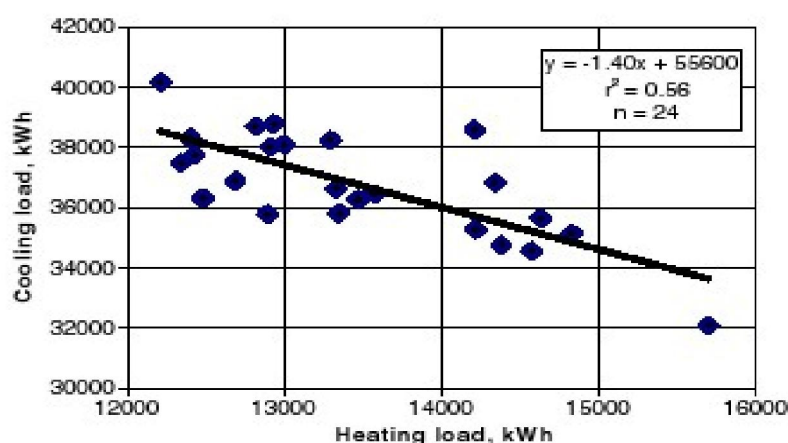
Figure 2.6: The effect of UHI in London on cooling and heating load
(Kolokotroni, Zhang and Watkins, 2006)

2.2.3 Strategies for Mitigating the Effect of UHI

A number of strategies can be adopted for UHI mitigation. These strategies cover the landscaped vegetation areas, and surfaces materials (Takebayashi and Moriyama, 2012). Trees and green areas play an important role in reducing the effect of UHI. These features provide the shading required to protect the surface from irradiation, in addition to the evapotranspiration cooling effect for urban areas. Green roofs also have the same effect. Furthermore, increasing the effective albedo for streets, roofs and walls surfaces will provide surfaces with high reflection and less absorption (Taha, 2013). On the other hand, as illustrated in the first chapter, the most influential factor behind the UHI phenomenon is the GHG(Trevor, 2009). The main reason behind the increase in GHG averages is the increase of energy demand and consumption(Zhang and Huang, 2014). Reducing the dependence on the fossil fuel energy and the use of clean energy will reduce the UHI effect. Moreover, optimising the urban and buildings design, and implementing passive design strategies has a significant role in reducing energy consumption, and consequently, reducing the UHI effect(Unger, 2010). Han, Taylor and Pisello (2015) in their published paper studied the effect of retro reflective building facade material on the building surface temperature and the UHI. The authors selected the city of Miami to conduct their research. They found that a retro reflective facade has a positive effect on reducing both building envelope temperature on indoor level, and UHI on outdoor level.

2.3 Canyon and Thermal Mass Exchange

Energy balance in the canyon is affected by the canyon elements including, walls, ground surface and other objects within the canyon space. The main factors that have the major influence in canyon energy balance are H/W ratio, orientation and materials.

The fact of the heat exchange between the canyon elements and air within the canyon space has been proven in many studies (Nunez and Oke, 1977).

Ali-Toudert and Mayer (2006) proved the significant influence of the thermal mass exchange within the canyon on both outdoor and indoor space. Erell et. al (2011) presented the equation that controls the thermal mass exchange within the canyon space;

$Q = Ks + Kt + Kr + Ls + Lt + Le$ Eq.(2.1)

Where Q is the total net radiations, (Ks)represents the short wave solar radiations comes from the sky, and (Kt) is the short radiation that defuses from the surrounding surfaces, (Kr) is the same radiation that is reflected from the canyon surface. (Ls) refers to the long wave radiation comes from the sky, while (Lt) and (Le)refers to the same radiation emitted and reflected by the canyon surface, and should be calculated to find the energy balance in any canyon. Figure 2.7 shows the direct shortwave radiation, the reflected long wave, and the emitted radiation by the canyon surfaces (Erell et al., 2011).
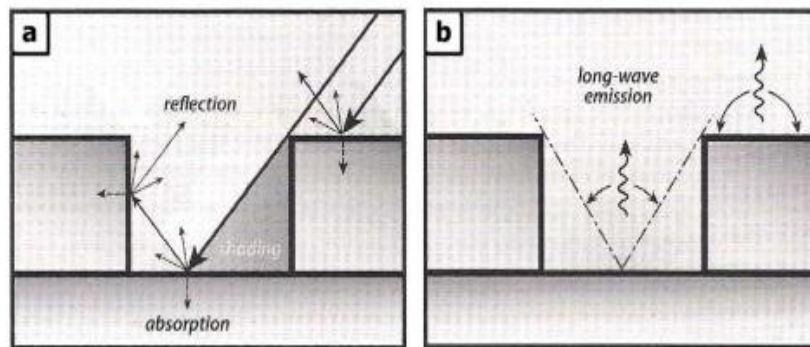
Figure 2.7: The long and shortwave radiation in the canyon space (Erell et al., 2011)

Figure 2.8 presents the effect of canyon orientation on the energy flux density, in a north - south oriented canyon, and compare this between east and west facing walls from one side, and top to bottom space of the canyon from the other side. However, 60 % of the incoming energy through radiation is released as a sensible heat, and 10 % is the latent heat that is

reflected from the ground, while the remaining 30 % is heat absorbed by canyon surface material (Nunez and Oke, 1977).
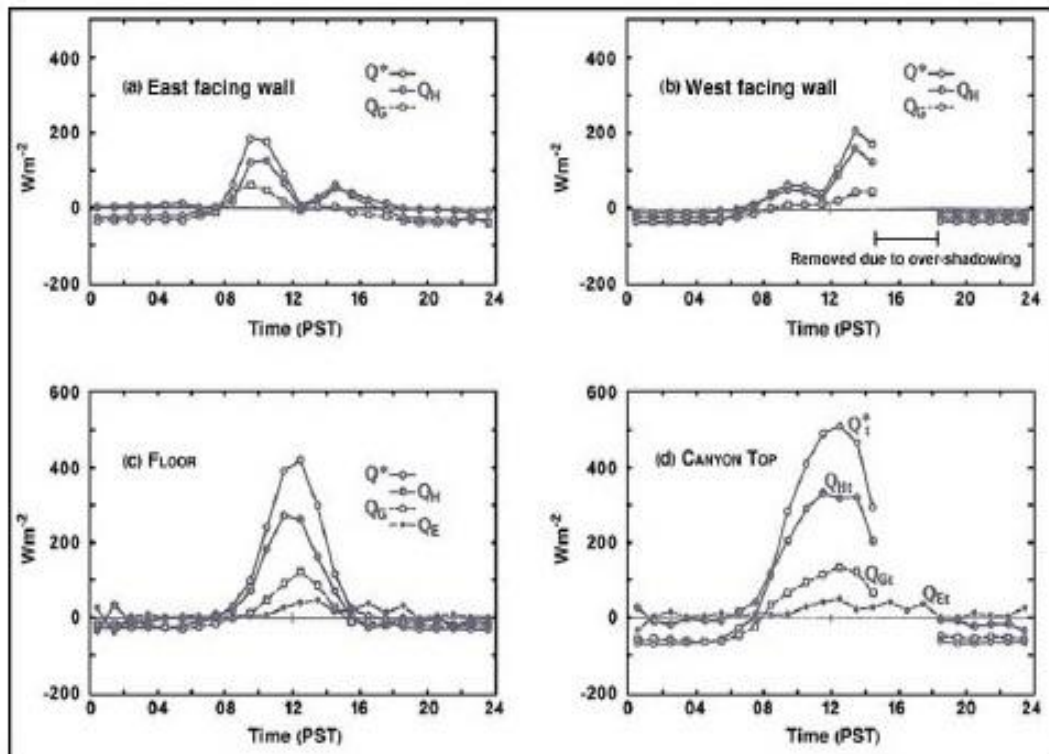
Figure 2.8: Diurnal energy flux in canyon with H/W ratio=1;(a) east facing wall, (b) west facing wall, (c) canyon ground, and (d) canyon top(Nunez and Oke,1977)

Another study proved that a deep canyon with the high aspect ratio traps more heat than the shallow canyon (Pearlmutter et al., 2005). In a canyon with high H/W ratio the air temperature at the top of the canyon decreases while the stored temperature in the canyon surface increases (Marciotto et al., 2010). A shallow canyon with a low H/W ratio has a larger exposed surface to the short and long wave sun radiation, this will consequently affect the amount of heat gain and the canyon surface temperature. The short wave affects the canyon space directly by convention or it is absorbed and sorted as gained heat in the canyon surface and transferred by conduction to the inner space of the buildings. Hence, the radiation effect and the canyon heat gain highly depend on the H/W which is consequently affects the surface temperature of the canyon.

Moreover, Arnfield and Grimmond (1998) and Pearlmutter et al. (2005) reported the effect of the wind flow as another significant factor that influences the air temperature and energy balance of the canyon, this effect will be illustrated in detail in the next section.

2.3.1 Canyon Air Flow and Wind Velocity

Prior to illustrating the wind speed and air flow in the canyon space, the wind regime and wind pattern of the urban area will be explored. Previous studies proved the effect of urbanised area on the wind regime due to the effect of the structures on shaping the natural landscape. These changes in wind flow pattern are generally observed within the ABL. This layer extends from the ground surface to 200-500m above the ground as mentioned in the first section of this chapter. The urbanised area creates an obstruction and a roughness that affects the wind speed and pattern. The topology of the structured land increases the roughness factor of the urban area compared to the non-urban area. Figure 2.9 shows how the types of land topology reduces the incoming 20mph wind speed depending on the height of the buildings. Wind speed is reduced to 5.7mph within a tall buildings and urbanised area, while it is 9.5mph in the housing and landscaped area, and 14.9 mph in the open areas (Rlsenergy, 2012).
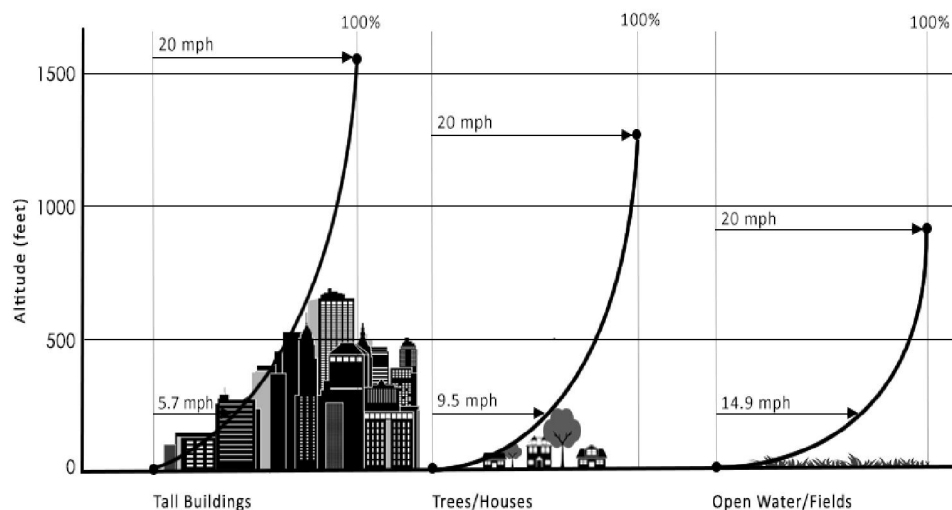
Figure 2.9: Gradient wind speed velocity (Rlsenergy, 2012)

The roughness that is created by the urban structures is the major factor that affects wind regime and velocity and it is the crucial factor between the developed and natural landscape.

Beaufort (1805) developed a wind scale to express and describe wind velocity. This scale identifies and classifies wind speed and wind type on a scale between 1-64 knots. Furthermore, the scale shows the appearance and the effect of each wind speed and its type on the land and water (Table 2.1).

Table 2.1: Beaufort Wind Scale Developed in 1805 by Sir Francis Beaufort, U.K. Royal Navy

Beaufort wind scale	Mean Wind Speed		Limits of wind speed		Wind descriptive terms	Probable wave height in metres*	Probable maximum wave height in metres*	Seastate	Sea descriptive terms
	Knots	m/s	Knots	m/s					
0	0	0	<1	0–0.2	Calm	-	-	0	Calm (glassy)
1	2	0.8	1–3	0.3–1.5	Light air	0.1	0.1	1	Calm (rippled)
2	5	2.4	4–6	1.6–3.3	Light breeze	0.2	0.3	2	Smooth (wavelets)
3	9	4.3	7–10	3.4–5.4	Gentle breeze	0.6	1.0	3	Slight
4	13	6.7	11–16	5.5–7.9	Moderate breeze	1.0	1.5	3–4	Slight–Moderate
5	19	9.3	17–21	8.0–10.7	Fresh breeze	2.0	2.5	4	Moderate
6	24	12.3	22–27	10.8–13.8	Strong breeze	3.0	4.0	5	Rough
7	30	15.5	28–33	13.9–17.1	Near gale	4.0	5.5	5–6	Rough–Very rough
8	37	18.9	34–40	17.2–20.7	Gale	5.5	7.5	6–7	Very rough–High
9	44	22.6	41–47	20.8–24.4	Severe gale	7.0	10.0	7	High
10	52	26.4	48–55	24.5–28.4	Storm	9.0	12.5	8	Very High
11	60	30.5	56–63	28.5–32.6	Violent storm	11.5	16.0	8	Very High
12	-	-	64+	32.7+	Hurricane	14+	-	9	Phenomenal

Understanding the changes in wind speed and pattern within the urban area generally, and canyon space particularly, is very important in thermal mass exchange studies. Many studies explored and proved the significant effect of wind speed on both outdoor thermal comfort and indoor air temperature. However, canyon fabric and surface material are elements that affect the canyon air flow behaviour (Offerle, 2007; Li, 2012), as well as the canyon surface

material, the crucial factor that controls the air flow behaviour in the canyon is the H/W ratio. The numerical study published by Andrea (2014) shows the Computation Fluid Dynamics (CFD) in the canyon of three different H/W ratios: 0.5,1, and 2. The three ratios represent the three types of canyon respectively: shallow, uniform and deep canyon (Figure 2.10).

The figure shows how air velocity varies between the three types of canyon, the blue colour represents low velocity and the red colour represents high velocity. It is clear that air velocity is decreased with the increase of H/W from 0.5 to 2 in figure 2.11 a, b, and c.
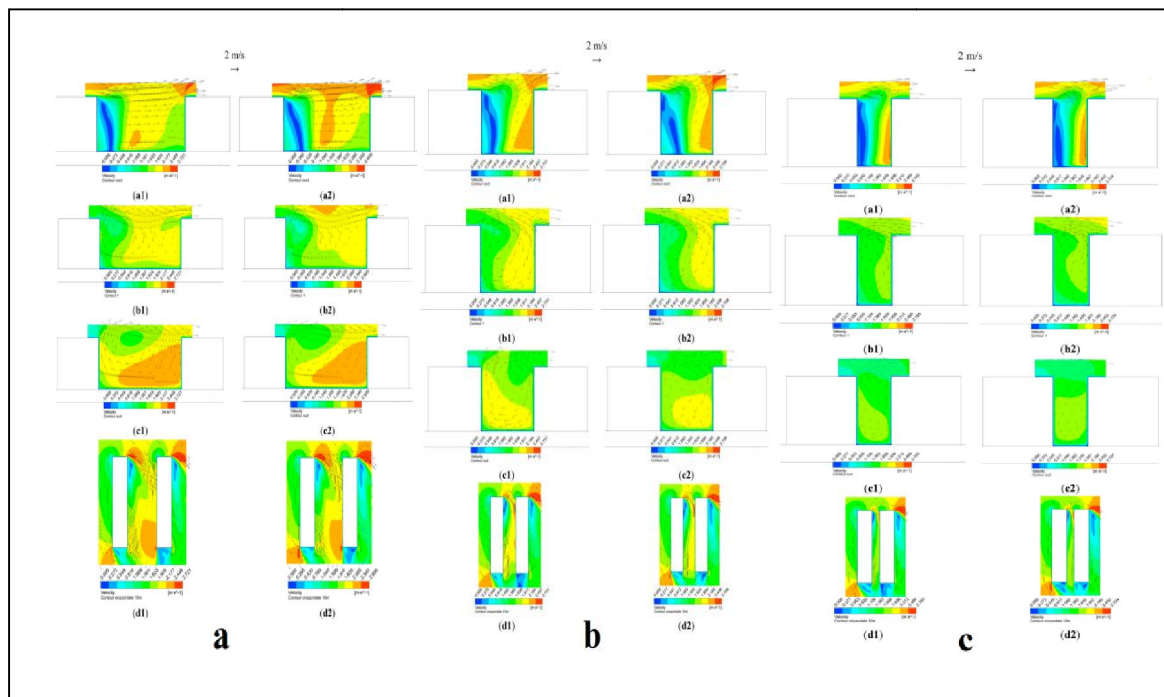
Figure 2.10: Air velocity comparison between the three types of canyon with H/W ratio of; a=0.5, b=1,c=2 (Andrea, 2014)

Furthermore, the behaviour of the secondary flow that is formed in the canyon space as a result of the primary flow over the building's roof is illustrated by Erell et al. (2011). Figure 2.11 shows the canyon secondary flow pattern according to primary flow over the building's roof in the four wind directions. The parallel winds with the canyon orientation is the most affective wind in the canyon space (Figure 2.11 b).

Generally, the perpendicular wind on canyon orientation forms a vortex in the canyon spaces, the number of vortex increases in the angled canyon orientation with respect to wind direction, further increase in vortex is observed in the deep canyon (Figure 2.11 a, c and d).
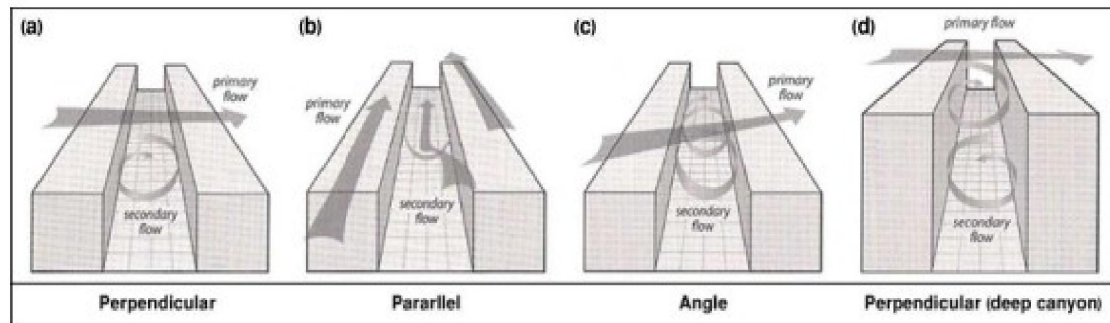
Figure 2.11: The secondary flow in the canyon according to four wind directions (Erell et al., 2011)

However, the 'Lee vortexes' are formed in the uniform canyons as a result of the primary perpendicular wind flow over the canyon roof, and these vortexes affected by the canyon surface temperature. Figure 2.12 shows how the vortex changes according to the high temperature surfaces in the canyon space, as the vortex behaviour changes to cool the hot surfaces (Xie et al., 2005; Erell et al., 2011).

Furthermore, Littlefair et al. (2000) presented the air flow and thermal behaviour in the canyon of the low to high aspect ratio. The researchers highlighted the canyon air flow performance and variation by comparing canyons with H/W ratio between 0.3 and 1.
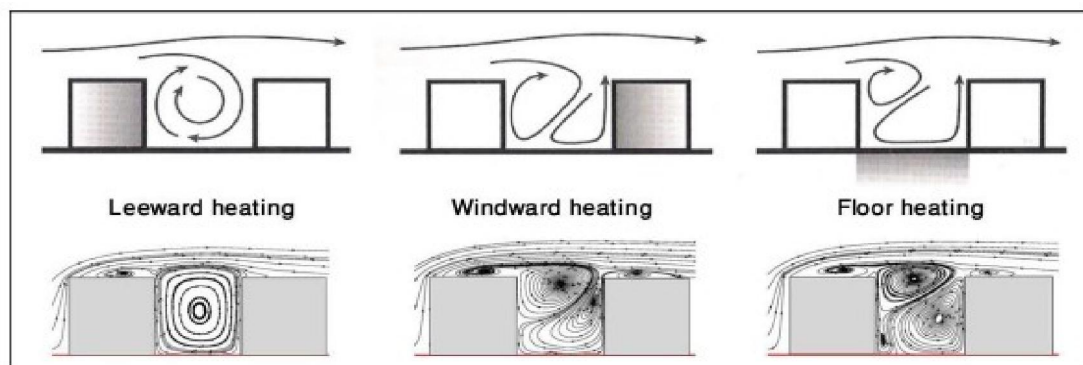
Figure 2.12: The effect of the surface temperature on the 'Lee vortexes' in the canyon space
(Erell et al., 2011)

For the low aspect ratio less than 0.3, a great amount of outdoor air takes place and provides an effective access to air flow, and the air does not recycle too much (Figure 2.13 a).

For the second or medium H/W ratio between 0.3 and 1 the canyon is getting narrower, the air mass drops and the vortex forms (Figure 2.13 b). In this ratio and in spite of reducing the incoming air, the mixing of the air in the internal space of the canyon is very efficient for heat dispersion and enhancing the outdoor thermal comfort. On the other hand, for the high aspect ratio or H/W of more than 1, both of the previous situations occurs, the air mass drops and recirculation dramatically happens (Figure 2.13 c).
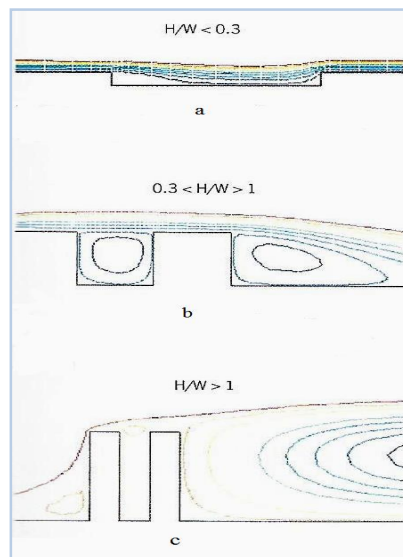
Figure 2.13: The streamline of the three case of aspect ratio; a) H/W < 0.3,b) 0.3 <H/W < 1.0, and c) H/W > 1.0 (Littlefair et al., 2000)

The vortex moved to the top of the canyon and the air does not reach inside the canyon because of the high H/W ratio. Therefore, both affect the heat traps inside the canyon, and the air temperature increases in the deep canyons with high H/W ratio.

2.3.2 Canyon Air Temperature Distribution

The effect of solar radiation and wind flow on the canyon can be reflected in the variation in air temperature within the canyon space. Nakamura and Oke(1988) were the pioneers in conducting a numerical study to find the effect of the mentioned micro climate factors on

canyon air temperature. The researchers studied the variation in air temperature in a uniform canyon with H/W ratio almost equal to 1.

The study was conducted in Tokyo, Japan in an east-west orientation canyon. The data were collected at the roof level in addition to the 63controlling points within the canyon as shown in figure 2.14.
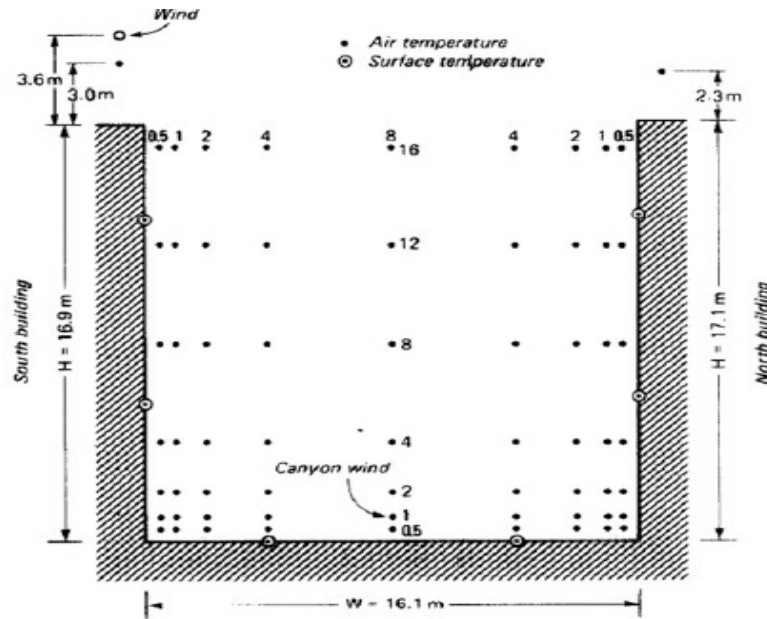
Figure 2.14: The data collection points in the uniform canyon H/W ratio = 1.06
(Nakamura and Oke, 1988)

The researchers found that the wind speed at the bottom reduced by 2/3 compared to wind velocity at the roof. With respect to the air temperature a slight variation of less than 1°C were observed between the roof air temperature and the temperature within the canyon.

On the other hand, the floor surface temperature is higher than the temperature in the centre of the canyon space. This increase may reaches2°C during the daytime due to the effect of direct solar radiation. This finding of the variation in temperature between the canyon space and the canyon floor surface is supported in later studies conducted on uniform canyon (Taesler, 1980; Niachou et al., 2008).

2.3.3 Canyon Surface Albedo

The surface albedo is the measure of a surface solar reflection (Mirzaei and Haghighat, 2010). It is one of the most effective parameters in variation between the surface and the surrounding air temperature (Nazarian and Kleissl, 2015). Surface albedo depends on surface material. Figure 2.15 shows that the light surface reflects more solar radiation compared with dark surfaces, and high albedo represents high reflection. The albedo percentages for some construction and pavement materials are presented in figure 2.16.
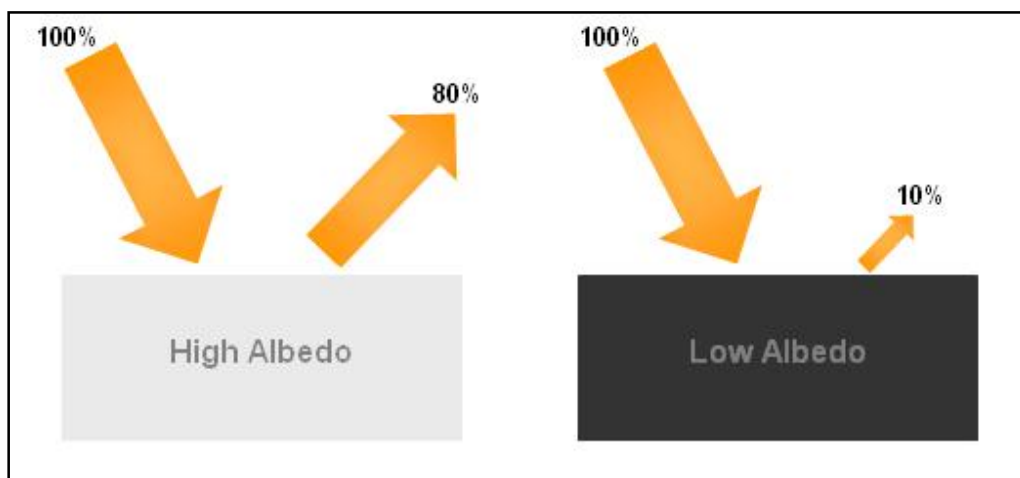
Figure 2.15: Light surface with high albedo compared with dark surfaces with low albedo
(US EPA, 2012)

The earth average albedo is 0.30, as 30 % of the sun radiation is reflected by the earth's surface. Urban albedo is the measure of reflectively of an urban surface, it is the ability of the urban canyon to reflect solar radiation. The UHI phenomenon is highly affected by the urban surface albedo, it is affected by settlements that generate, absorb, reflect and trap the heat (EPA, 2012). Nazarian and Kleissl (2015) conducted a study to find the effect of the canyon surface albedo on building wall temperature. The researchers found that replacing asphalt with concrete decreases the canyon surface temperature. The concrete albedo is 15 % - 20 % and it is higher than the asphalt albedo with a percentage of 5 % - 10 %, therefore, the concrete reflects more radiation than the asphalt. On the other hand, the building wall temperature increased as a result of the reflected radiation from canyon surface.

Material	Albedo (%)
White asphalt shingles	21
Black asphalt shingles	5
White granular-surface bitumen	26
Red clay tile	33
Red concrete tile	18
Unpainted concrete tile	25
White concrete tile	73
Galvanized steel (unpainted)	61
Aluminum	61
Siliconized white polyester over metal	59
Polyvinylidene fluoride (PVDF) white over metal	67

Figure 2.16: Construction materials albedo (Lawrence Berkeley National Laboratory, 2015)

2.4 The Effect of Urban Geometry on Microclimate Parameters

Microclimate and outdoor thermal comfort are highly affected by urban geometry and buildings configuration, and the microclimate around a building is a significant factor in building energy performance, it represents the exchanging relationship between one building and its neighbouring buildings or a building and the surrounding natural environment.

A literature review as a method of study is conducted to identify the recent and previous studies related to the urban geometry and its effect on the built environment. The effect of urban geometry and design on the built environment can be evaluated through a number of micro climate parameters. Many studies have examined air temperature as an environmental parameter that express the variation in urban design variables, such as building configuration, building external material and street surface albedo. The most related studies and publications on urban planning and design shows that building configuration, canyon H/W, building / canyon orientation and materials are the most urban parameters relevant and

responsible for the microclimatic changes around a building (Todhunter, 1990; Arnfield and Mills, 1994).

These parameters directly affect the, solar access, air temperature, airflow and speed at the pedestrian level, and consequently the urban microclimate (Nakamura and Oke, 1988; Arnfield and Mills, 1994). Nazarian and Kleissl (2015) studied two of the urban design variables: surface material and building geometrical design, the researchers used the 'ANSYS/FLUENT 14.5' software for adopting 'Computational Fluid Dynamics (CFD)' simulation in order to find out the effect of these two design factors on urban street environment. The researchers examined the effect of ground surface materials, including concrete and asphalt, on a number of environmental parameters. For this aim, the researchers developed a model for urban configuration to be simulated; the model has a fixed height and length blocks dimensions equals to (D=1) and used it to estimate the outdoor comfort in the street 'canyon'. The authors used the weather condition of Southern California on a clear summer day and validated the results against the actual field measurements of air temperature and wind speed (Figure 2.17).
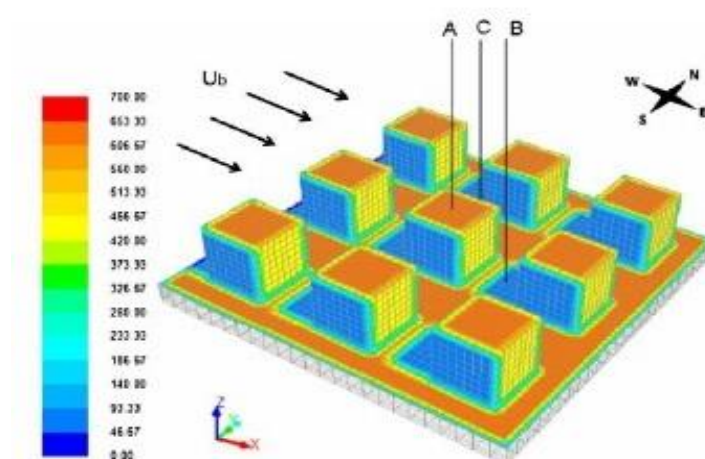
Figure 2.17: The 3D developed model and the solar heat flux in W/m² (Nazarian and Kleissl, 2015)

The researchers explored the effect of urban geometry by simulating four scenarios with respect to H/W or aspect ratio in order to find the effect of urban density on the mentioned outdoor environmental parameters of air temperature and wind speed. The researchers claimed that a number of studies adopted the ANSYS/FLUENT (CFD) to simulate the turbulence of air flow on the street scale but these studies did not investigate the effect of three dimensional mass on air flow movement, and the changes in air turbulence that could be caused by constructing this mass or development. The researchers examined the effect of four simulated cases of H/W aspect ratio on the alter configuration and the movement of air flow of each case, and they illustrated the variation in diurnal temperature for the building's outdoor wall and ground according to air movement variation. The researchers concluded that a high H/W ratio causes a small vortex and decreases the wind velocity which reduces the buildings adjacent ground, wall and roof temperature, and this reduction in air temperature is varied according to ground and wall materials. Furthermore, many studies explored the thermal performance of the built environment and the effect of urban developments on urban spatial environment.

A recent publication that studied the effect of urban geometry factors on the environmental parameters of the built environment is a study published by Andreou (2014).The researcher presented the urban geometry effect in the Mediterranean area. The researcher studied the effect of some urban parameters, such as urban geometry, street pattern and orientation on solar access and shading. The author compared between two locations, traditional and contemporary areas in Greece, and selected the canyon to study the effect of urban variables. This included street orientation and building H/W ratio and analysed the effect of these factors on the buildings' solar gains.

The two selected sites in Greece represent a contemporary and traditional pattern in the city, the researcher conducted a comparison between these two sites, both sites have the same street axis orientation but they are varied in H/W ratio. The traditional site has a higher H/W ratio which is between 4 and 2, compared with 0.9 to 0.7 in the contemporary site, and both sites have the same latitude of 37°N. Andreou (2014) also identified the weather of this area as high solar intensity weather where shading is desired during summer while a limited level of solar access and solar gain is preferred in winter. The Autodesk Ecotect software was used in this study for case study simulation, and the researcher justified the use of this software as it is successful in simulating the shading and solar access on an urban level. Further to the shading assessment and analysis that were obtained from the use of the software, the results were compared to the thermal field measurement data collected by the researcher. The simulation was conducted according to four directions of street orientation further to the variation in H/W ratio varied between high and low ratio in the two selected sites. The author's results showed that in summer, the traditional configuration with a high H/W ratio and dense pattern performed more positively than the contemporary one with the respect of environmental comfort. Figure 2.18 shows the comparison of shading percentages between the two H/W ratio; a higher H/W of 3.0 provides more shading percentages than the lower one at 0.6 (Andreou, 2014). Furthermore, the researcher studied the effect of trees on the solar access and shading on outdoor space, and proved a significant effect of this urban variable on the urban microclimate. The researcher stated that the finding of this study is important as it provides a formulation guideline for urban designers in the same region and the same weather characteristics.
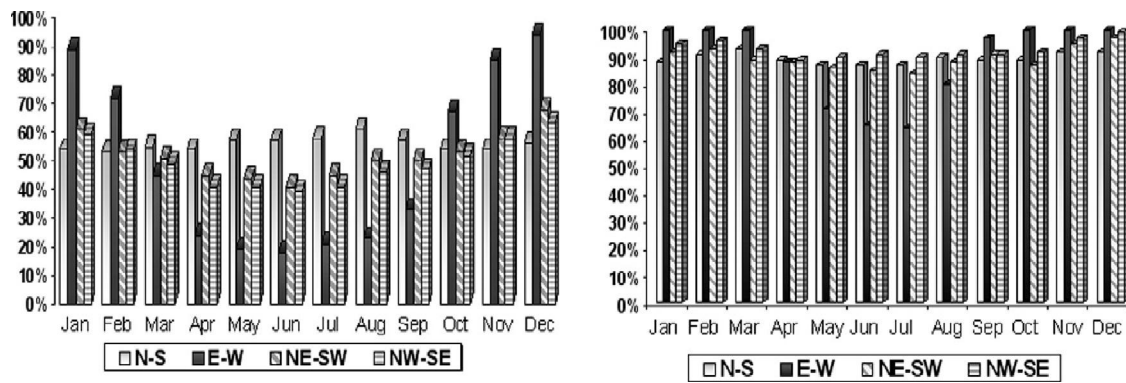
Figure 2.18: Shading percentages of the horizontal surface of streets on N-S, E-W, NE-SW and NW-SE axis, with H/W ratio of 0.6 (left), and 3.0 (right) (Andreou, 2014)

Djukic, Vukmirovic and Stankovic (2015) analysed and compared two suggested proposals for developing the central area of Leskovac, Serbia. The researchers evaluated the two proposals against the existing design. They conducted a computer software simulation on four different times on one summer day. Simulating the existing case shows that there is a significant deference in microclimate parameters between the vegetated and non-vegetated areas, and the difference between these areas reached 3°C in air temperature. Furthermore, the area covered with trees is less in air temperature by 0.5°C -0.6°C than the area covered with grass. Simulating the suggested scenarios shows that the difference in air temperature between these two scenarios was less than 0.5°C. Therefore, the researchers suggested a 'Solution scenario' to develop and enhance the suggested proposals (Figure 2.19). The 'Solution scenario' kept the diagonal street of the existing case and more vegetation were suggested along the northwest side of the park, further to a suggestion of paving the main part of the square area with reflective material instead of asphalt, adding water features, covering the rest of the area with grass and increase the number of trees.
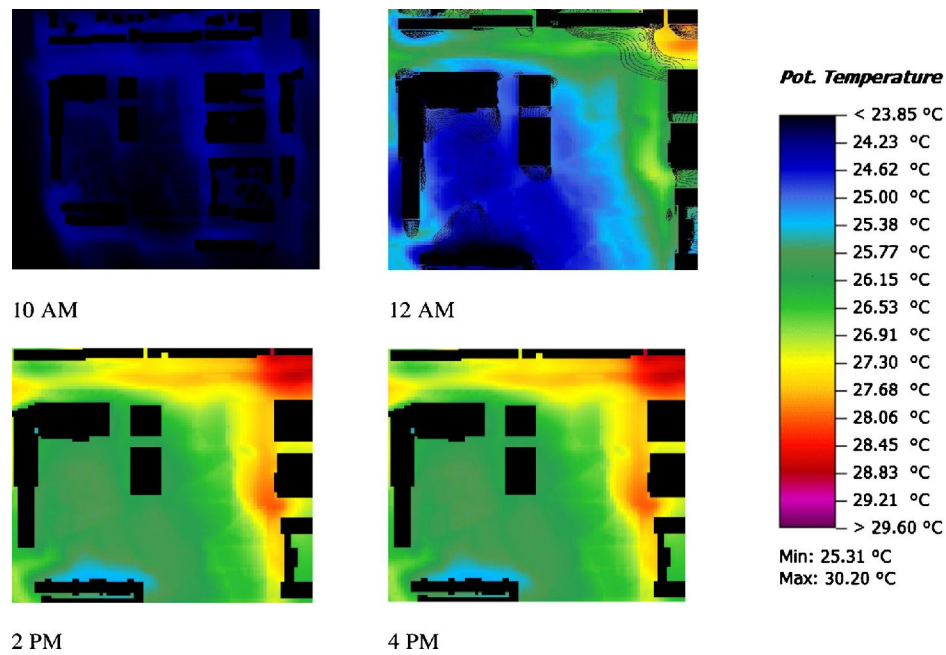
Figure 2.19: Air temperature simulation of existing case study

(Djukic, Vukmirovic and Stankovic, 2015)

The study compare the air temperature collected from the five receptor points as field measurements with the simulation results of the solution scenario, and the results show that the average temperature reduction between the existing case and the solution scenario varied between 0.3-1.5°C during the four simulation periods of the selected simulation day.

These findings highlight the significant effect of vegetation, paving or cladding material, and water features on urban microclimate. In another study, the H/W ratio of urban morphology was adopted by Schulte, Tan and Venkatram (2015) to develop a model for reducing the emissions caused by transportation, the researchers examined the effect of the relationship between building heights and street widths to develop their model using the comparison between two cities; Hanover, Germany and Los Angeles, USA to find how the dense pattern can reduce the emissions caused by transportation. On the other hand, the effect of the urban canyon geometry on the airflow and microclimate in Morocco was explored through a study carried out by Johansson (2006).

The researcher adopted the field measurements data over 1.5 years and selected both types of canyon as a case study area; the deep and the shallow canyon with an aspect ratio of 9.7 and 0.6, respectively. The researcher concluded that wind speed, as one of the microclimate parameters, is around 0.4 m/s in the deep canyon which is considered more stable and slower when compared with the wind in a shallow canyon of 0.7 m/s. The research found that the deep canyons in Morocco provide more preferable microclimates in the two main seasons, summer and winter. On the other hand, a large number of studies adopted and developed models to evaluate the effect of developments on the surrounding environment, and the surface albedo temperature is the most evaluated parameter in most of these studies. Yang and Li (2015) used a three-dimensional numerical models to study the urban surface temperature and the role of the horizontal surfaces in urban albedo averages, the researchers used the SVF as an alternative to the H/W ratio to represent the urban geometry configurations. The researchers found a linear relationship between the SVF of horizontal surfaces and urban albedo averages (Figure 2.20). Aida (1982) was one of the first researchers who studied the effect of the urban geometry on the surface solar absorption using the experimental method, the researcher adopted concrete blocks to simulate the urban canyon.
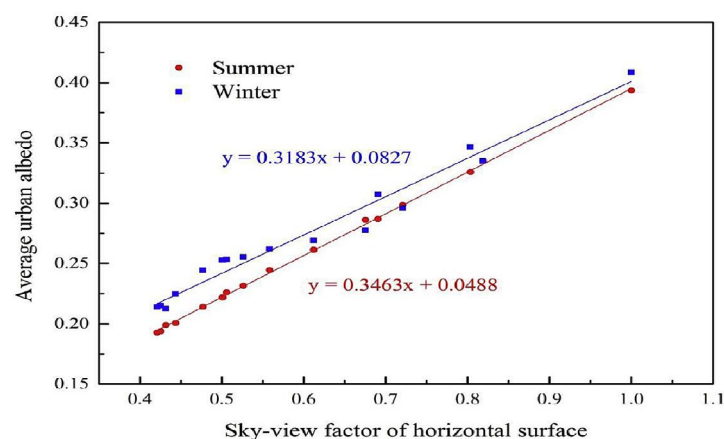
Figure 2.20: The relationship between SVF and the urban albedo(Yang and Li,2015)

On the other hand, Boutet (1987) explored the effect of five primary building shapes on urban air movement and illustrated the cubic shape effect on air flow within the complex. The author stated that buildings being angled to the air direction decreases the air velocity by 50 % - 60 % (Figure 2.21).
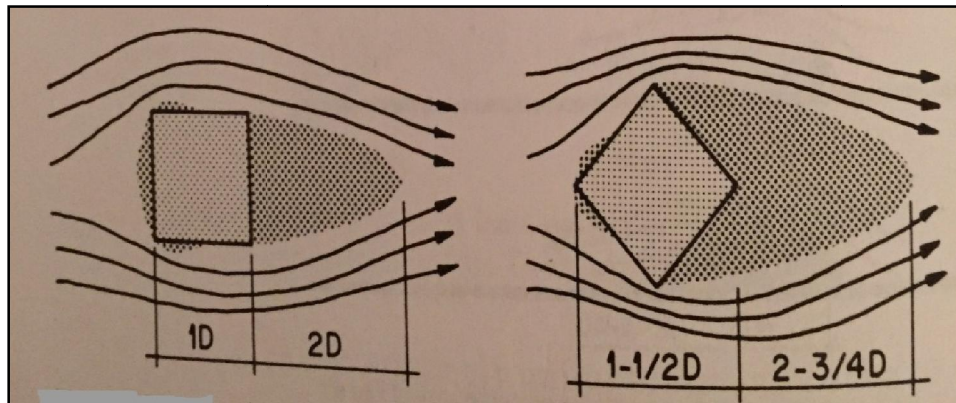
Figure 2.21: The effect of cubic shape orientation on air flow (Boutet, 1987)

Moreover, the researcher highlighted the effect of two building configurations on air flow and movement and claimed that arranging the buildings alternately will enhance the potential of the air flow around most of the buildings within the complex (Figure 2.22).
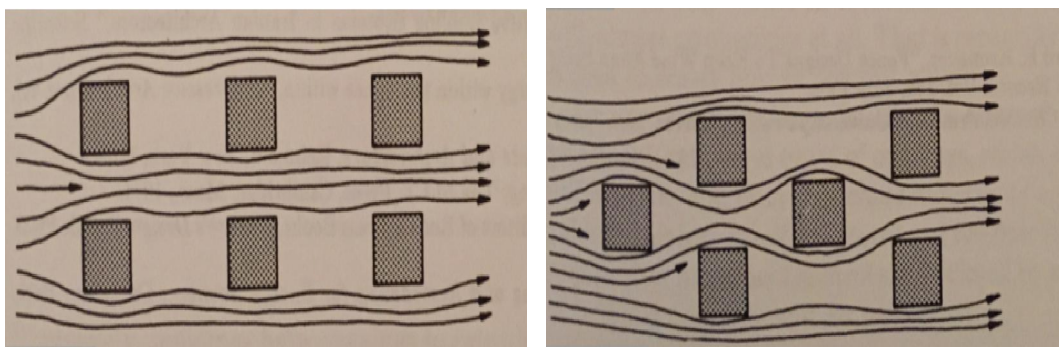
a) Linearly buildings arrangement   b) Alternating buildings arrangement

Figure 2.22: The air flow effect on tow of building configurations (Boutet, 1987)

Block density and building design have a significant effect on urban design sustainability, and it is proved that the dense form has a significant effect on energy conservation. The challenge of the urban designer is to find the most optimised configuration to achieve the desired energy conservation without neglecting other design factors, such as viewshed and urban ventilation. The viewshed is one of the urban design factors that should be taken into consideration when planning according to climatic and other urban design factors.

The viewshed represents the geographical area that can be viewed from specific locations excluding the points that are located behind any obstruction, such as buildings. Sander and Manson (2007) studied the viewshed calculation using the 'Geographic Information System (GIS)' and 'Digital Elevation Model (DEM)' data to evaluate the viewshed of a specific region in Minnesota, USA, and they found that generalisation of a uniform height will serve better for some land use to achieve the desired viewshed.

On the other hand, Lehmann (2010) studied the effect of the compact form on energy conservation and found that the most compact form is the most sustainable form, which could be represented by the vertical form of mid-rise and high-rise buildings. Moreover, the researcher presented the most promising model in terms of solar gain and heat conservation, the researcher took into consideration the optimum land use required for the same number of units, and proved that the six floors   mid-rise buildings are the most preferred form for energy conservation, but the author reached this result in specific weather conditions and generalising this result needs more research and investigation according to the other locations of studied areas (Figure 2.23).

The relationship between the main microclimate parameters, such as air temperature, wind speed, and relative humidity has been addressed in many studies. The relationship between the outdoor air temperature and the relative humidity has been explored by Giannopoulou et al. (2014). The researchers conducted a survey and data analysis to collect the data of the two parameters from 26 stations in Athena, Greece, and they highlighted the inverse relationship between the air temperature and the relative humidity.
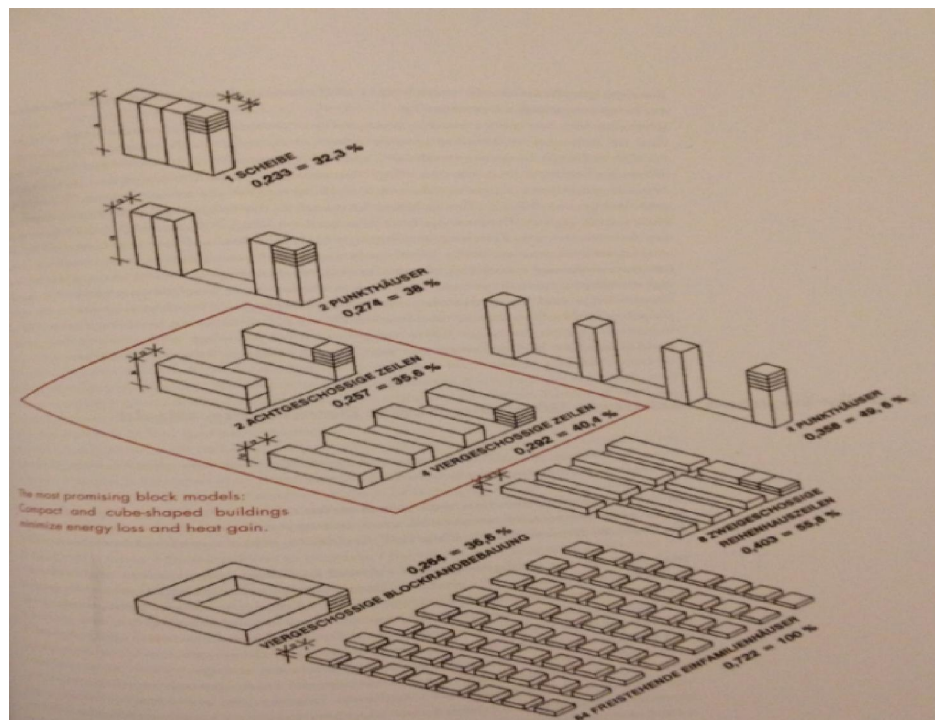
Figure 2.23: The most promised and sustainable composition(Lehmann, 2010)

Furthermore, the researchers found that the highest air temperature was recorded in the western station, while the lowest air temperature was recorded in the northern station (Figure 2.24).
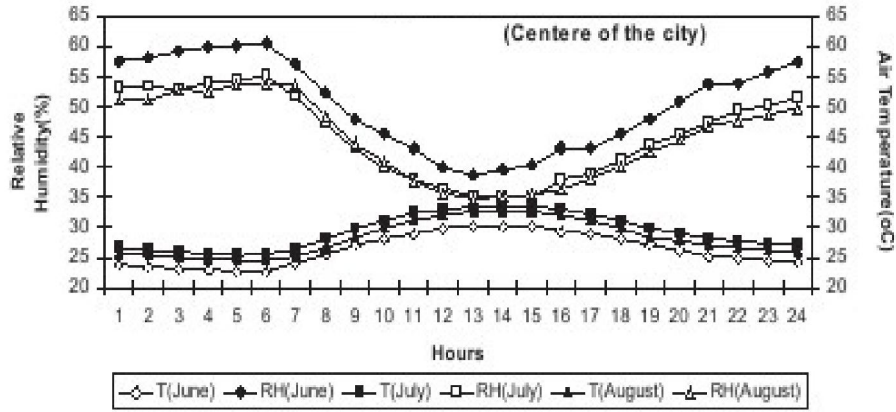
a) Centre station
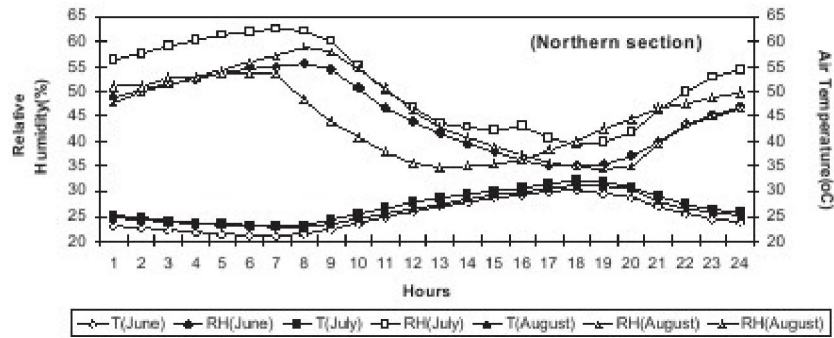
b) Northern station
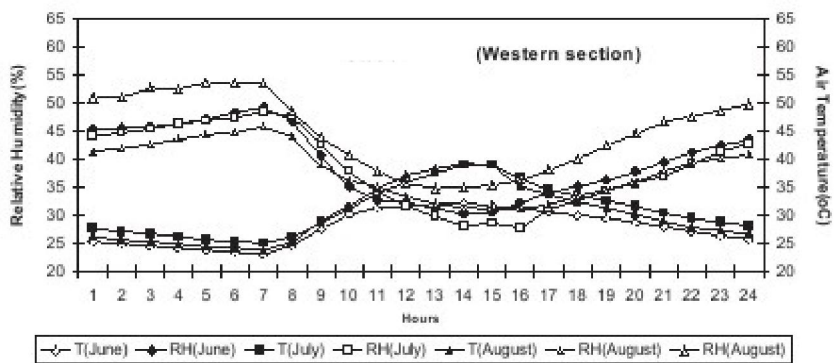
c) Western station

Figure 2.24: The relation between the outdoor air temperature and the relative humidity(Giannopoulou et al., 2014)

Furthermore, a field measurement study conducted by Irulegi, Serra and Hernandez (2017) to find the relation between the air temperature and relative humidity in Mediterranean climatic zone, San Sebastian, Spain. Figure 2.25 below shows the inverse relationship between the two microclimate parameters.

26/04/2016		
Outdoor		
TIME	Tº	HR
1:00	9.7	83
2:00	10	83
3:00	9.9	83
4:00	9.9	82
5:00	9.6	82
6:00	9.4	83
7:00	9.9	80
8:00	11.2	73
9:00	12.2	67
10:00	12.7	63
11:00	13.3	63
12:00	13.3	65
13:00	14.1	63
14:00	14.2	61
15:00	13.8	66
16:00	12.7	72
17:00	12.7	73
18:00	12.7	72
19:00	12.4	73
20:00	12.1	72
21:00	12.1	73
22:00	12.1	73
23:00	11.8	76
0:00	11.4	80

Figure 2.25: The outdoor air temperature and relative humidity file measurement in the Mediterranean zone, Spain (Irulegi, Serra and Hernández, 2017)

However, the relationship between the wind speed and the relative humidity was explored in an experimental study conducted by Lee and Lau (2016). The researchers highlighted the effect of the wind flow and relative humidity on heat transfer, and they presented the inverse relationship between wind velocity and relative humidity. This relationship affects the heat transfer coefficient positively by enhancing heat transfer. Table 2.1 shows the empirical data collected from the laboratory experiment.

Table 2.2: The experimental data for the relationship between the relative humidity and the wind velocity (Lee and Lau, 2016).

Average maximum velocity of positive and negative ionic wind at different levels of relative humidity

Relative humidity (%)	Positive ionic wind		
	Supplied voltage (kV)	Average maximum velocity (m/s)	Location of maximum velocity along the vertical axis (mm from reference point)
30	9	1.14	2.5
40		1.08	2.5
50		1.10	5
60		0.40	7.5
70		0.60	10
30	10	1.71	0
40		1.11	0
50		1.52	2.5
60		1.42	2.5
70		0.88	10
30	11	1.83	0
40		1.8	0
50		1.83	2.5
60		1.83	5
70		1.05	10
30	12	1.93	0
40		2.06	0
50		1.91	0
60		1.37	5
70		1.17	7.5

2.5 Building Physics and Outdoor Microclimate Parameters

The physics laws explain the exchange effect between the microclimate parameters behaviors and impact on the buildings within the urban block. The buildings impact on the wind speed or the effect of the buildings in windward direction have been explored by the "British Research Station at Garston", an experimental study was conducted in order to find the effect of tall building among low buildings on wind flow. It has been found that when the airstream hits the tall building it is divided in to two parts , one moved at the top of the buildings, and the other at the bottom. The positive effect of the pressure in front of the building and the negative pressure behind the building, allows to move the air from the positive pressure area to negative pressure area (Figure 2.26).

The flow in front of the tall building forms a large vortex , the vortex occurred on both sides of the tall buildings accelerates the air and increases the wind velocity at the ground level.
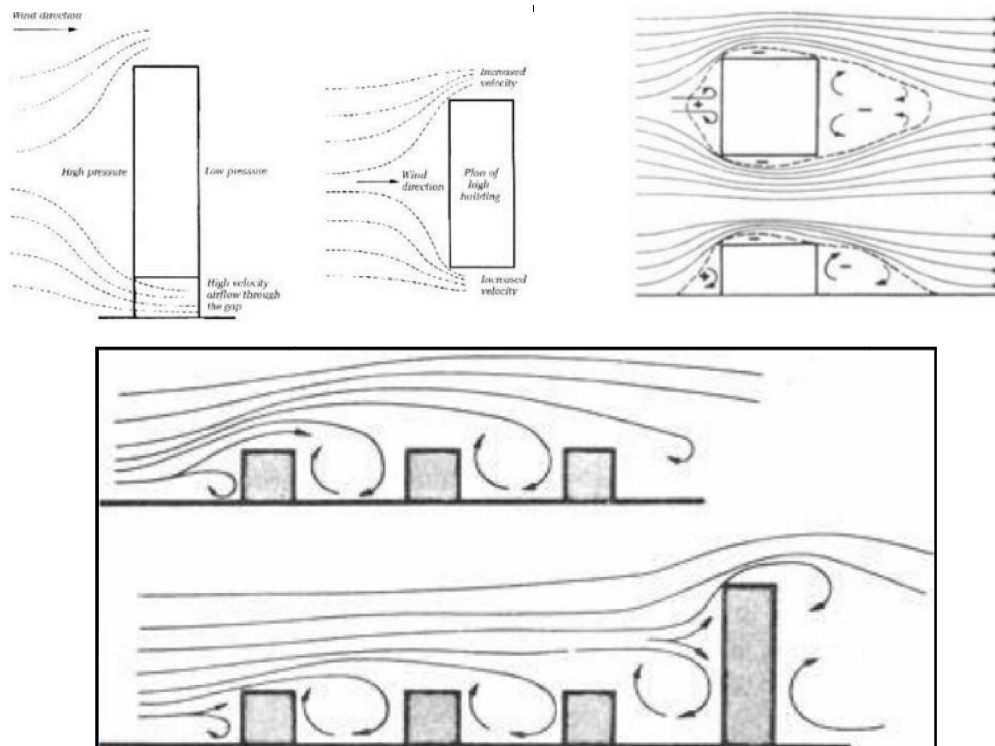
Figure 2.26: The effect of tall building in between short buildings
(The British Research Station at Garston, 2016)

This performance of the tall building as an obstacle in windward direction can be explained by 'Bernoulli Equation' for energy conservation. The equation interpret the increase in wind velocity and the reduction in air temperature in the negative pressure area to conserve the energy of the fluid.

The influence of building geometry on the wind velocity and the 'Convective Heat Transfer Coefficient CHTC' was presented by Montazeri et.al (2015). The researchers studied the effect of the ratio between building' height and building' width on the CHTC . The researchers investigated three ratios of buildings dimensions H > W, H = W, and H < W by studying the effect of different wind velocity and Reynolds number for turbulence and laminar flow.

The authors stated that by increasing the height of the buildings , the wind speed increased near the buildings surfaces. The wind velocity became at the maximum at the top of the building and the minimum at the bottom where the horseshow vortex forms (Figure 2.27). Accordingly, the maximum CHTC occurs at the top of the buildings, while the CHTC observed to be less in the lower part of the building. This reduction in the CHTC at the bottom of the building is related to the small vortex effect in this area, and the increase in the residence time of air. Increasing the residence time of the air in the bottom area reduces the difference in temperature between this air and the building surface.

The reduction in the air temperature difference between the surface and the surrounding air consequently reduces the heat flux and the CHTC. On the other hand , in the case of H < W, the building performs as wind block or obstacle in the windward, and increasing the width of the building results in reduction in wind speed and CHTC. This is mainly related to the effect of the width on blocking the wind speed and the time of the air remaining near the surfaces and becomes with a higher temperature . The reduction in the variation between the air temperature and the surfaces temperature results in to a reduction in CHTC (Figure 2.28).

For the ratio of H = W, the wind distribution found to be normal and the increase of the CHTC is the highest at the top of the buildings (Figure 2.29). Therefore, the CHTC increases with the increase in wind velocity and the reduction in CHTC is related to the reduction in wind velocity.
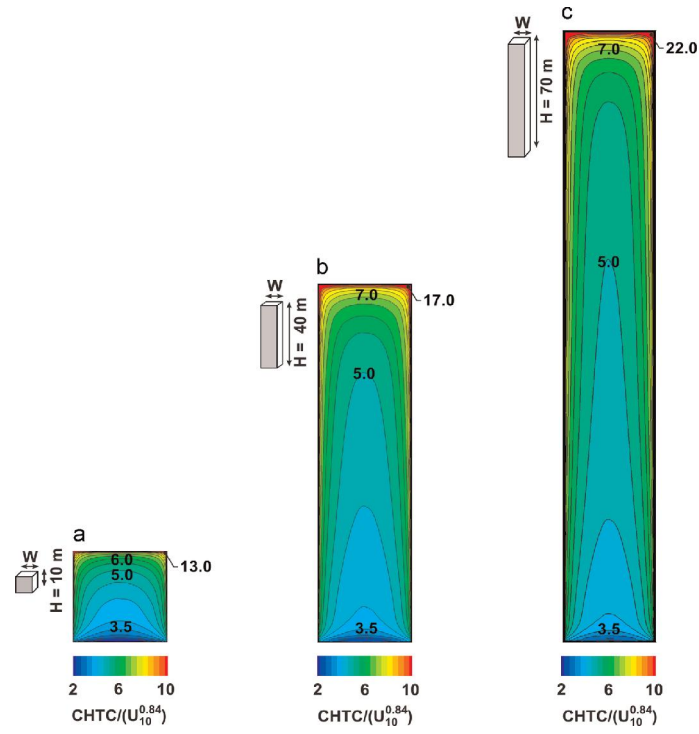
Figure 2.27 : Distribution of wind speed a cross the building surface for H > W;

a) H = 10 m, (b) H = 40 m, and (c) H = 70 m
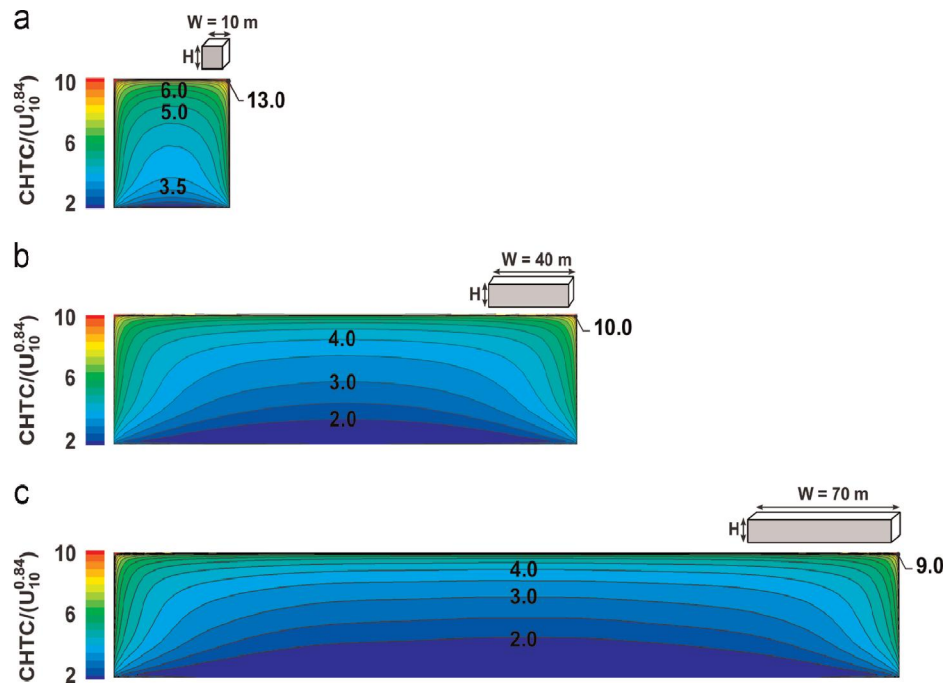
Figure 2.28: Distribution of wind speed a cross the building surface for H < W;

a) H = 10 m, (b) H = 40 m, and (c) H = 70 m
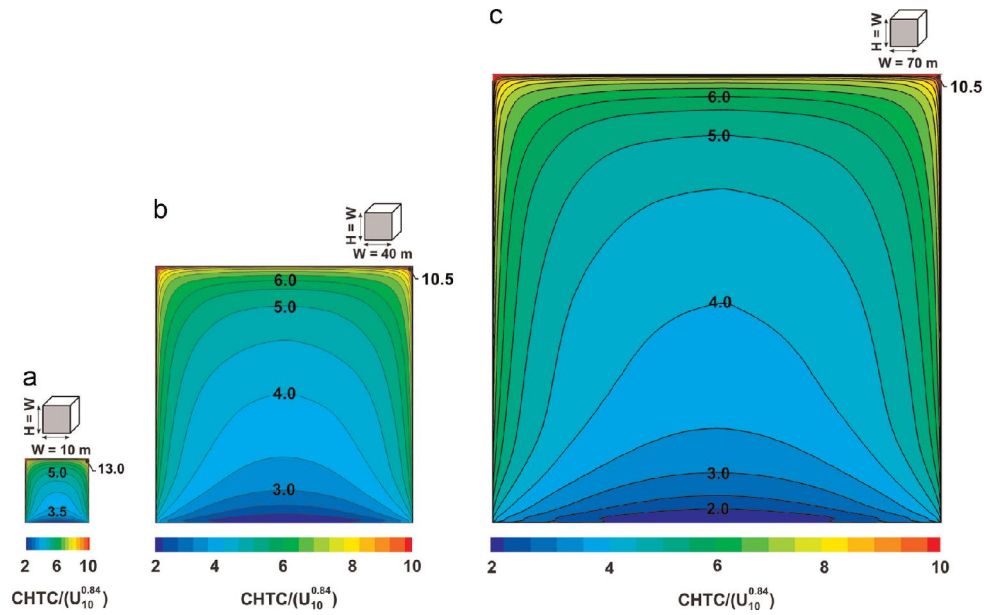
Figure 2.29 : Distribution of wind speed a cross the building surface for H = W;

a) H = W =10 m, (b) H = W = 40 m, and (c) H = W = 70 m

2.6 Ventilation and Air Quality in the Urban Canyon

Canyon ventilation and air quality are determined factors in urban liveability, designing for liveable and walkable streets required to provide a desired level of canyon ventilation with an acceptable wind speed, and controlling the air quality on the urban level is a liveable, sustainable urban design requirement. Air pollution is an environmental problem that requires further research and study. Kwak et al. (2014) examined the effect of wind speed on air quality with respect to pollution caused by NO_2 and O_3 concentration. The researchers conducted their study in a canyon of high-rise buildings area in Seoul, Korea. The researchers used and integrated model based on 'Computational Fluid Dynamics (CFD)' taking into consideration the mobile and vehicle emissions. The authors proved the considerable impact of high-rise buildings geometry and vehicle emissions on air pollution and NO_2, O_3 concentrations in the $1km^2$ simulated environment.

Ng and Chau (2013) highlighted the effect of buildings configuration, permeability and building ground floor setbacks on people and air pollution exposure in isolated urban canyons

in Honk Kong. The researchers found that neither building separation nor building ground floor setbacks have a significant effect on air pollution exposure, and they compared the building setbacks with the perverting wind direction and proved that the perverting wind has a major effect. Moreover, the researchers adopted and analysed different scenarios and found that the discrepancy in effect between the parallel and the perpendicular wind is very small.

Kruger, Minella, and Rasia (2010) used the Envi-met software to explore the effect of wind speed on air pollution in the canyon. The researchers simulated four scenarios of wind direction and speed in order to find the effect of each scenario on NO_2 concentration. The researchers found that the peak of NO_2 concentration is occurred by the transportations. The NO_2 concentration and the pollution diffusion were calculated depending on models and equations that were developed in previous studies. The results were analysed and evaluated according to the traffic status during the day to find the values and the peak hours of NO_2concentration and air pollution.

2.7 Energy Performance of the Built Environment

Urban design elements, such as urban form and configuration, land use, open and landscaped areas, road planning and transportation systems have a significant effect on the thermal performance of the built environment (Wong et al., 2011; Zanon and Verones, 2012; Wang and Kexin, 2013; Yeo, Yoon and Yee, 2013). Thermal performance of the built environment covers two levels; 1) outdoor thermal performance, and 2) indoor thermal performance. The outdoor thermal performance directly influences indoor thermal performance. The surrounding microclimate is the significant factor in this relationship (Figure 2.30). The indoor thermal performance controls and indicates the energy consumption of the building. Building energy consumption covers the energy use for lighting, ventilation, cooling and heating load. On the other hand, thermal performance and energy consumption of the built environment affects the averages and the CO_2 emissions footprint. It is difficult to obtain an

accurate analysis of building energy performance without taking into consideration the surrounding environment. Analysing, evaluating and optimising the buildings energy performance within the whole complex, provides the opportunity to create a sustainable built environment with the preferable outdoor microclimate.

Consequently, this will be reflected to the indoor energy performance positively. However, it is important to integrate the energy performance of each building within the block in order to find out the full image of the block energy performance. This will provide the opportunity to adopt urban planning to reduce energy consumption on a large scale at an early design stage.

Energy performance of the built environment has been explored in many studies, the significant influence of energy consumption and carbon emissions on the sustainability of the built environment presented in a paper by Zhang and Huang (2014). The researchers conducted a numerical study to measure the carbon emissions over an eight-year dataset between (2000) and (2008) in Shenzhen, China. They conducted their study to analyse the impact of the observed increase in carbon emissions over this period.

The model for the low-carbon city in terms of adopting smart transportation strategies and sustainable urban planning was developed in China by Wang and Kexin (2013). However, the Italian case studies by Zanon and Verones (2012). The researchers integrated energy consumption with spatial planning in an innovative method.

The researchers shifted the energy conservation from building scale to territorial scale. In the same meaning, Statistics Database (DB) and Geographic Information System (GIS) software, were used by Yeo, Yoon and Yee (2013) to develop a module forecasting energy demand on urban level.

```
                    ┌─────────────────────┐
                    │   Urban Geometry    │
                    └─────────────────────┘
                              │
                              ▼
                    ┌─────────────────────┐
                    │    Urban Density    │
                    │                     │
                    │ Buildings Morphology│
                    │                     │
                    │  H/W ratio and SVF  │
                    │                     │
                    │    Built Up Area    │
                    │                     │
                    │ Parks and Open Areas│
                    │                     │
                    │Buildings Pattern and│
                    │      Design         │
                    └─────────────────────┘
                              │
                              ▼
                    ┌─────────────────────┐
                    │Thermal Performance on│
                    │     Urban Level     │
                    └─────────────────────┘
```
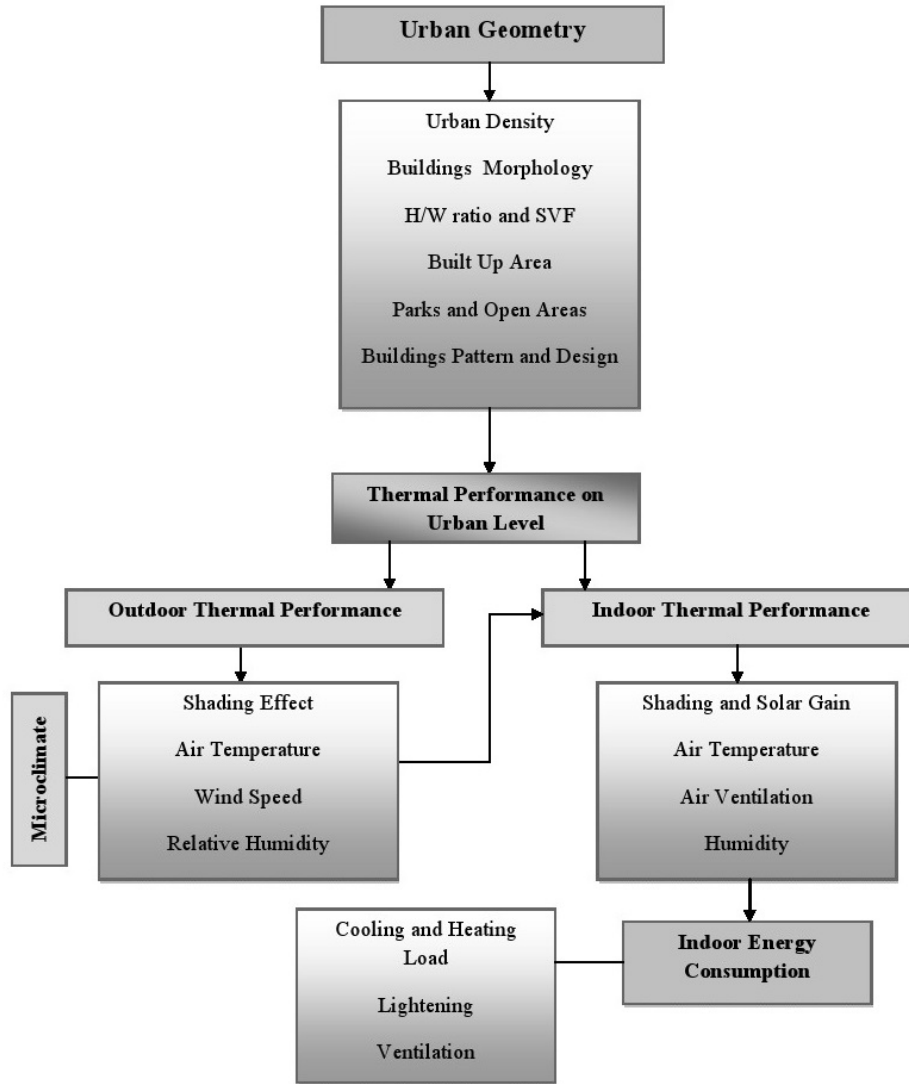
Figure 2.30: The effect of urban geometry on indoor thermal performance and energy consumption through the outdoor microclimate parameters (Author, 2016)

On the other hand, Al Znafer (2014) studied the effect of SVF on outdoor thermal comfort and indoor energy consumption of an individual building in Al Riyadh city, Saudi Arabia. The researcher conducted an empirical research and collected outdoor metrological and geometrical data. The researcher found a strong linear correlation between the SVF and the outdoor comfort at the pedestrian level from one side, and the SVF with energy consumption of dwelling buildings on the other side (Figure 2.31).
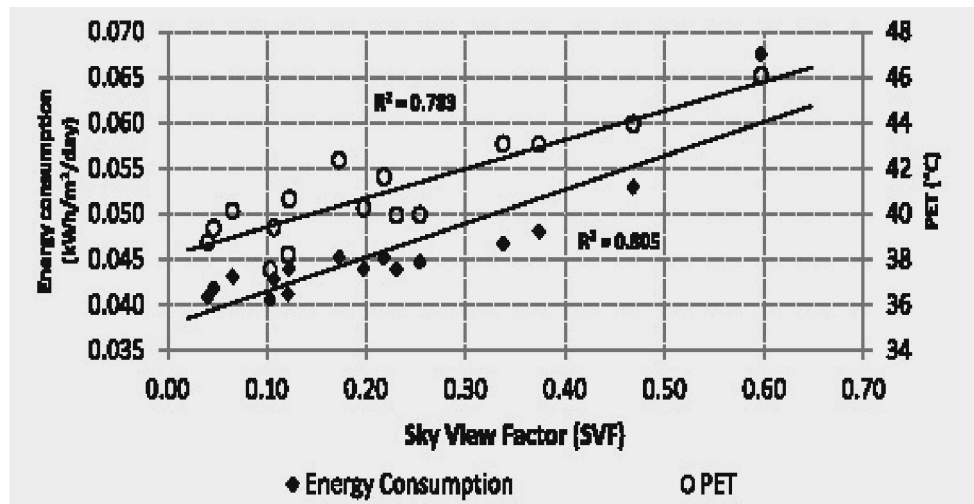
Figure 2.31: The SVF liner relation with energy consumption and thermal comfort
(Al Znafer, 2014)

Investigating and evaluating energy consumption on a large scale still needs more research and study. The use of the software provides a good opportunity to reflect the effect of outdoor microclimate parameters on indoor energy consumption. Nevertheless, most of the software concord with each performance separately, including outdoor and indoor. This required an integrated method of study between the two types of software to identify the energy consumption on a large scale.

2.8 The Effect of Urban Geometry on Building Energy Consumption

Urban and building geometry is one of the urban planning factors that has a significant effect on the outdoor thermal performance of the built environment, as well as the indoor energy consumption (Tuhus-Dubrow and Krarti, 2010; Ignatiusa, Wonga and Jusuf, 2015). Many studies have addressed the influence of urban geometry and building morphology on the thermal performance of the 'canyon' as it represents one of the urban geometry elements.

However, limited studies were carried out to investigate the effect of urban geometry on energy consumption at the urban scale. Stromann-Andersen and Sattrup (2011) carried out a

study to identify the effect of the canyon orientation and the H/W ratio on indoor energy consumption.

The researchers found that urban canyon design has an impact on energy consumption on the residential buildings and office buildings by 19 % and 30 %, respectively. However, the researchers conducted their study in a cold climate area in Copenhagen, Denmark, and included the heating and lighting load into energy consumption calculations. Furthermore, optimising some of the urban geometry factors, such as building shape for more efficiency in energy use, has been explored in many studies (Depecker et al., 2001; Tuhus-Dubrow and Krarti, 2010).

A study conducted by Yang Lin (2013) aimed to optimise energy consumption of the buildings on a large scale in Taipei. The researcher applied building passive design strategies, and found that building material, glazing, air conditioning setting temperature, shading devices and building orientation have a significant influence on the reducing energy consumption of the individual buildings. The researcher adopted the bottom to top method to calculate the energy consumption at a large scale. However, this study did not include the effect of the buildings within the block on each other on energy consumption at the block scale.

One recent study explored the effect of urban geometry on building energy consumption at the urban scale; this research carried out by Al Znafer (2014). The researcher explored the effect of canyon H/W ratio on building energy consumption in Al Riyadh, Saudi, Arabia. The researcher explored the effect of canyon H/W ratio on microclimate parameters and outdoor urban comfort. Furthermore, the researcher investigated four orientations of the urban canyon and their effect on outdoor thermal performance and indoor energy consumption.

The researcher found that a high H/W ratio provides more energy saving at the indoor level. Moreover, a NE-SW canyon orientation shows less energy consumption for the all examined H/W ratio (Figure2.32).
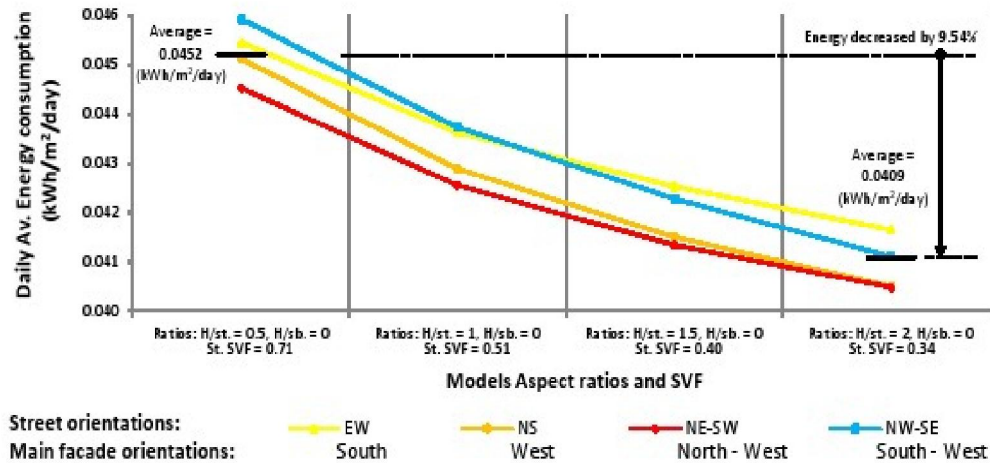
Figure 2.32:The daily average energy consumption of the building group with respect to four canyon H/W ratios and orientations E-W, N-S, NE-SW, and NW-SE (Al Znafer, 2014)

On the other hand, the NW-SE orientation of the canyon shows the highest energy consumption, particularly in a low H/W ratio as the obstruction to the sun is less (Figure 2.26). Moreover, the figure shows a progressive decrease in energy consumption between the H/W of 0.5 and 2.0, and SVF between 0.71 and 0.34, this decrease reaches a maximum of 9.5 % in the buildings within the deep canyon.

2.8.1 Cooling Plant Load and Energy Saving

The cooling load in general refers to the load or the energy required to release the heat from the space, it reflects the building heat gain. This load covers sensible and latent cooling load. The sensible load calculation depends on the dry bulb temperature of the building, while latent load depends on the wet blub temperature.

Both loads are needed to calculate the design and select the Heating, Ventilation and Air Conditioning (HVAC) system of the building (Cummings, 2012). In a dry climate the calculation of the sensible load is an important factor for estimating the cooling load. In a hot humid climate the latent load also affects the HVAC system selection as it depends on the wet bulb temperatures.

The worst case for both outdoor blub temperature is required to calculate the cooling sensible and latent load, and to design a HVAC system that maintains the desirable indoor air temperature (Sabzi, 2015).

Mahboob et al. (2014) studied the impact of buildings density on cooling load in Dubai, UAE. The researcher explored the impact of a number of internal and external heat gain elements on the cooling load in the hot climate conditions of Dubai, UAE. However, in the UAE, which represents shot, humid climate around 70 % of the energy consumed is for building space conditioning (Mahboob et al., 2014). The researchers compared the cooling load of low-rise and high-rise individual buildings, and they found that the urban density has an inverse impact on cooling load. The cooling load decreases as the buildings density increases. Moreover, the researchers investigated the effect of the insulation material on reducing the heat gained by the building envelope, and consequently reducing the cooling load. Furthermore, the researchers found that building density and proper shading devices can reduce the cooling load by 20 % - 30 %.

Afshari, Nikolopoulou and Martin (2013) investigated the effect of building retrofits on total energy consumption in a study carried out in Abu Dhabi, UAE. The researches illustrated the energy consumption of a case study building in Abu Dhabi and found that the most influenced parameter on cooling load consumption is the outdoor air temperature.

Figure 2.33 shows the effect of air temperature compared to the direct solar effect and humidity on cooling load consumption.

Furthermore, the researchers reported that the cooling load contributes to more than 60 % of the total energy consumption of the typical case study building in Abu Dhabi, UAE. Therefore, reducing the outdoor air temperature is the main target to reduce the load required for cooling and accordingly the total energy consumption.
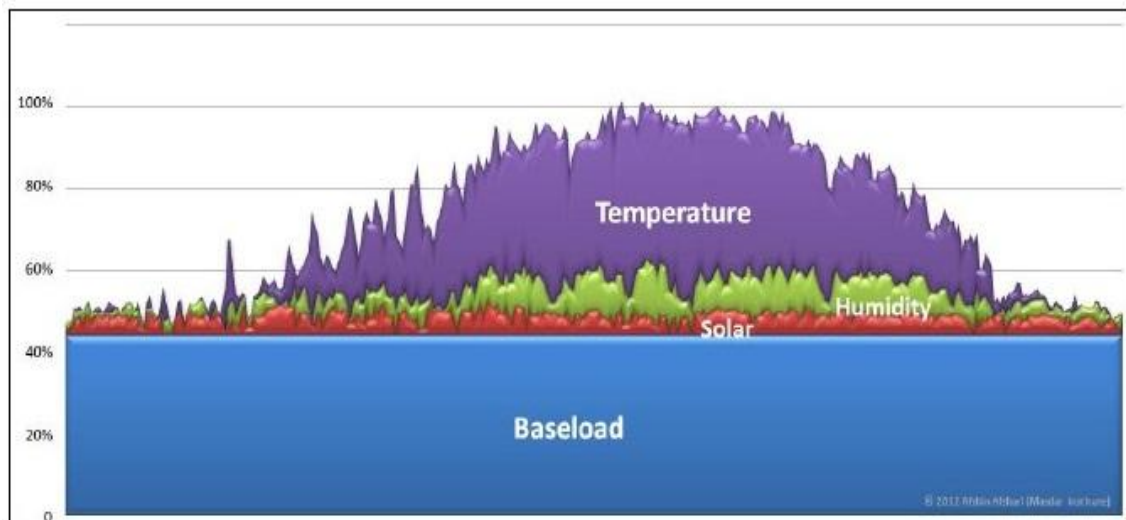
Figure 2.33:The contribution of air temperature compared to direct solar gain and humidity in cooling load consumption in Abu Dhabi, UAE (Afshari, Nikolopoulou and Martin, 2013)

The air temperature can be expressed by the dry bulb and wet bulb temperatures; both temperatures play a major role in designing the HVAC system of the buildings. The dry bulb temperature is the real temperature of the air and it indicates the real amount of heat in the air and is measured by degrees Celsius (°C), Fahrenheit (°F) or Kelvin (°K), while the wet bulb temperature is the lowest temperature that can be reached by evaporating water into the air. The wet bulb temperature is a function of the relative humidity, and when the air is saturated the dry and wet temperatures are equal.

Relative humidity is a measure of the actual amount of water carried by the air compared to the maximum amount of water vapor the air can carry. It gives an indication on the saturation of the air as a percentage. The relative humidity is inversely related to the air's dry bulb temperature. Figure 2.34 shows the general relationship between both parameters.

However, when the humidity is high, the system should work harder to remove the humidity from the indoor space and creates a comfortable space. For a humid climate such as Dubai, the desirable wind speed to create natural cooling is in the range of 0.53 m/s - 3.04 m/s.

The relative humidity has a significant effect on the comfort zone parameters. For 60 % relative humidity the rage specified for the air temperature is 31 °C, 32.5 °C, or 34 °C at wind velocity of 1.5 m/s, 3m/s, or 6 m/s. At 40 % relative humidity the air temperature could be higher to reach to 33 °C, 35 °C, or 37 °C for the same wind velocity respectively (Sallal and Al-Rais, 2011).
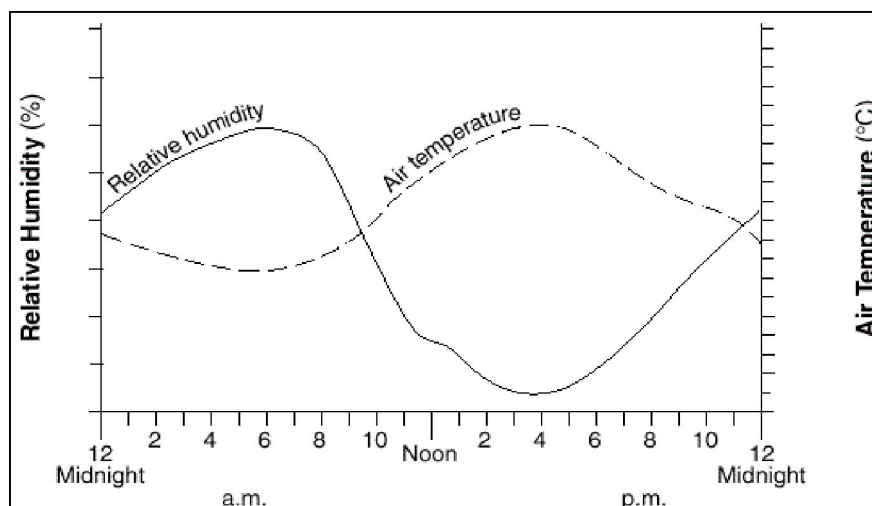
Figure 2.34: The inverse relationship between the air's dry bulb temperature and relative humidity (Quora, 2016)

The importance of the relative humidity or the ambient wet bulb temperature appears in it is effect on the latent heat or latent load. The latent load is the load that affects the design and the size of the cooling tower. It is the load responsible to keep the indoor humidity level at a comfortable level of 55 %. However, the cooling load tower design is affected by the water flow rate, the inlet water temperature and the outlet water temperature plus the ambient wet bulb temperature. Therefore, the wet bulb temperature directly affects the size and the selection of the cooling tower, as the cooling tower provides a water temperature that is higher than the wet bulb temperature by 5°C -7°C.

The cooling load has to be increased as the water temperature increases and every location has it is design temperature for the cooling tower. On the other hand, the wet bulb temperature is always between the dry bulb temperature and the dew point. The dew point is the point when the air is 100 % saturated, when the wet bulb is low this means that the air is dry and can hold more water vapor. In the same concept, when the relative humidity is low the dew point is below the dry air temperature, and when the relative humidity is high the dew point temperature is close to the dry air temperature (Figure 2.35).
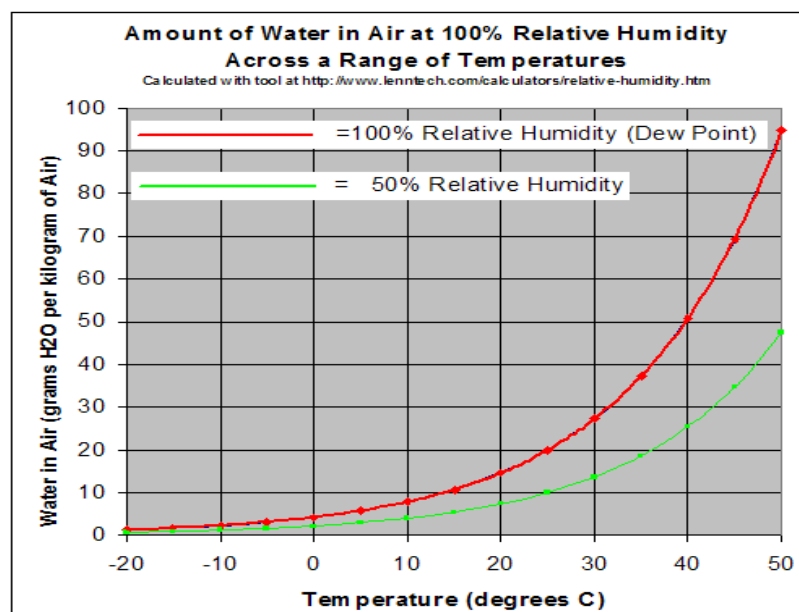
Figure 2.35:The relation between the relative humidity and the dew point (Quora, 2016)

2.9 The UAE Urban Environment Researches and Studies

Locally, a limited number of studies related to buildings geometry and configuration impact on environmental sustainability have been undertaken. The effect of the UHI on air temperature in Dubai, UAE was explored in the research published by Taleb and Abu-Hijleh (2012). This study compared two urban morphologies, the organic and structured urbanisation, in order to find the effect of each structure on outdoor air temperature.

The researchers adopted the Envi-met software to evaluate three large areas in the city; the first organic configuration area is represented by 'Al Bastakiya' the traditional area in the city, and the two structured developments are represented by proposed orthogonal and volume-ortho configurations.

The researchers discussed the results according to the SVF of each configuration by simulating various wind speeds, and they concluded that among the three configurations the organic morphology has the most positive effect on outdoor comfort and air temperature in the city (Figure2.36).
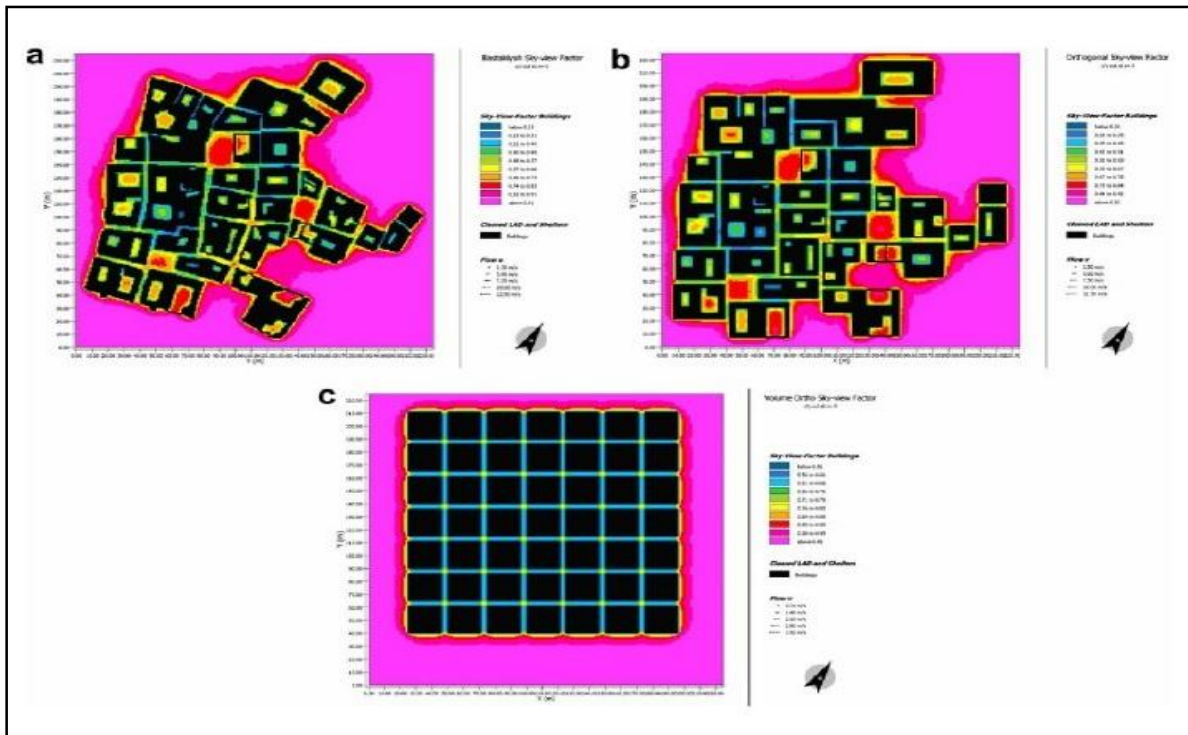
Figure 2.36: The three urban configurations - organic and two structured configuration
(Taleb and Abu-Hijleh, 2012)

The effect of the urban canyon on microclimate parameters and outdoor passive cooling strategies in Dubai was investigated and published in a paper by Al-Sallal and Al-Rais (2012).The researchers simulate two models of urban wind, laminar and turbulence using the Computational Fluid Dynamics (CFD) model, and they evaluated the thermal comfort on a pedestrian level. The researchers found that the wide canyon with an aspect ratio H/W of 1.75 provides a more comfortable microclimate with respect to wind velocity, while the wind speed increased in open areas, such as parking areas. Moreover, the researchers found that most of the simulated locations with an aspect ratio of between 0.67 and 2.0 had a light to gentle wind speed.

Simulating the narrow streets of the traditional areas shows that the street width of 4m or less can increase wind speed passing through the street or the canyon; this result can be used to enhance the passive cooling in the canyon and offers a better passive cooling performance.

On the other hand, achieving a more sustainable urban design in hot, humid climates was the aim of the paper published by Taleb and Musleh (2014), a case study location in Dubai was adopted for the research and a number of urban design parameters were evaluated through different scenarios. The researchers aimed to find the potential of adopting the parametric urban design tools and three software packages: Grasshopper, Galapagos Gas and ANSYS/ FLUENT (CFD) to achieve a more sustainable design., The researchers proved that the parametric design methodology achieved a 1 % - 8 % reduction in solar energy evaluation experiments.

2.10 The Urban Canyon in Hot Climate

The design of an urban canyon in a hot climate can be used to modify the effect of solar access and enhance the prevailing wind effect on the canyon environment. Bakarman and Chang (2015) explored the effect of two types of canyon: 1) deep canyon with a H/W equal to 2.2 and 2) shallow canyon with a H/W ratio equal to 0.4. The researchers selected Al Riyadh city, Saudi Arabia to conduct their research as a hot and, arid climate. The deep canyon was represented in a traditional case study area, while the modern case study area was the example of the shallow canyon (Figure 2.37).

The researchers conducted a numerical study and field measurement to identify the effect of both types of canyon on the formation of UHI. They concluded that for a low H/W ratio of a shallow canyon the UHI increased. Furthermore, the ambient air temperature in both canyon types, deep and shallow, is higher by 5 % and 15 %, respectively, when compared with the surrounding rural areas.

Figure 2.37: Canyon aerial and street views of (a) deep, old canyon, and (b) shallow, modern canyon (Bakarman and Chang, 2015)

Another study explored the effect of canyon geometry on climatic parameters in a hot and humid climate. The study conducted by Kruger, Minella, and Rasia (2010) proved the direct relationship between the morphology and the variation in microclimate. The researchers followed two approaches, field measurement and software simulation, to evaluate the effect of urban geometry on microclimate in Curitiba, Brazil. The climatic conditions of the city represent the subtropical hot and humid climate.

The researchers adopted the SVF to be an indicator of urban geometry variation and to study the effect of this variation on air temperature. The researchers used the SVF to represent the variation in urban geometry of the case study street. The researchers conducted their study in a pedestrian street located in the city's downtown area. The street is a combination of houses, mid-rise and high-rise buildings. The researchers conducted a field measurement to collect the environmental parameters, namely, air temperature, humidity and wind speed. They indicated monitoring points along the case study street to take the SVF of 18 monitoring points using a 'Fisheye image' instrument.

The researchers concluded that a higher SVFs cores less in the comfort parameters as the obstruction of the sun on hot days is very limited. Furthermore, they proved the linear relation between SVF and the outdoor air temperature. Figure 2.38 shows the correlated results of the linear relationship between the SVF and Mean Radiant Temperature (MRT), and the same effect of the SVF on the UHI.
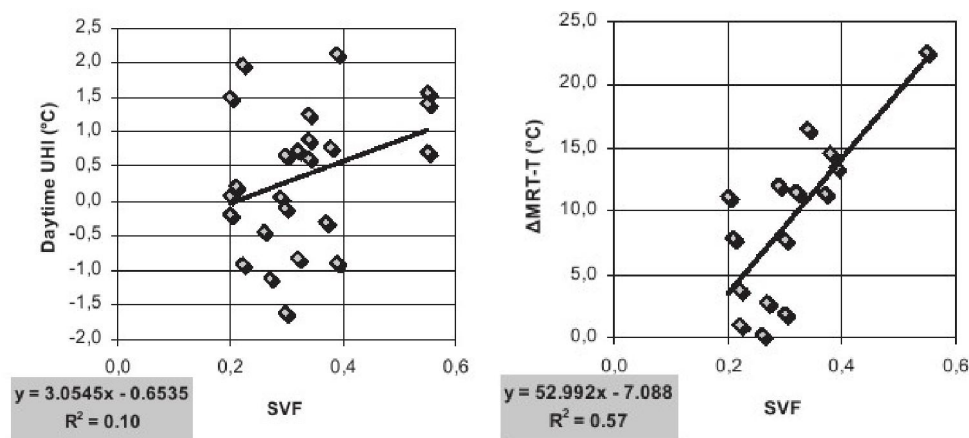
Figure 2.38: The relationship between SVF and a) daytime UHI, b) mean radiance temperature
(Kruger, Minella, and Rasia, 2010)

Furthermore, a study conducted by Al Znafer (2014) explored the canyon geometry in a hot and arid climate. The researcher investigated the effect of H/W ratio and height / setback ratio on climatic parameters in Al Riyadh city, Saudi, Arabia. The research examined the effect of canyon orientation on the micro climate parameters. The researcher conducted the study in two directions. Firstly, the researcher collected field measurement data to evaluate and assess the microclimate parameters in two types of canyon, the deep and the shallow canyon. The researcher found that the deep canyon has an average air temperature higher than the shallow canyon with 3 $^\circ$ C in the early morning.

Other than that, the air temperature of both canyons is close during the day until the afternoon; by the night the temperature of the deep canyon is warmer again (Figure 2.39).
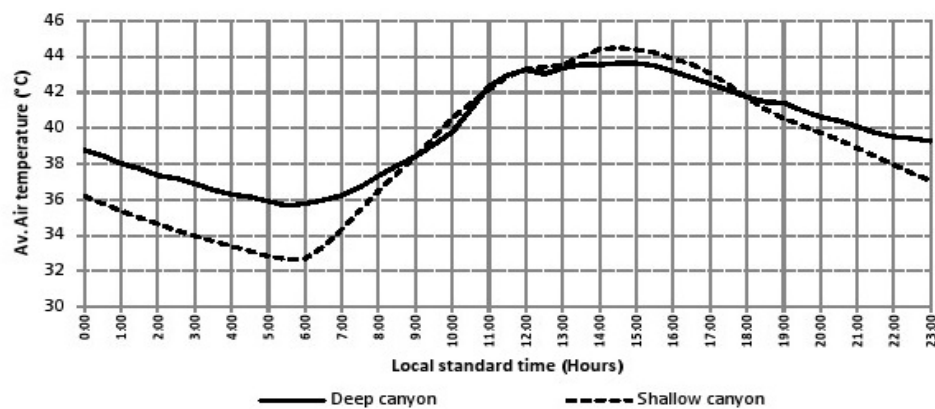
Figure 2.39: Average air temperature within the deep and shallow canyons (Al Znafer, 2014)

The second direction of the study consists on simulating proposed scenarios of four H/W ratios; (0.5,1.0,1.5, and 2.0) to find their effect on canyon microclimate parameters. The parameters observed included Mean Radiant Temperature (Tmrt), humidity and wind velocity (Figure 2.40).
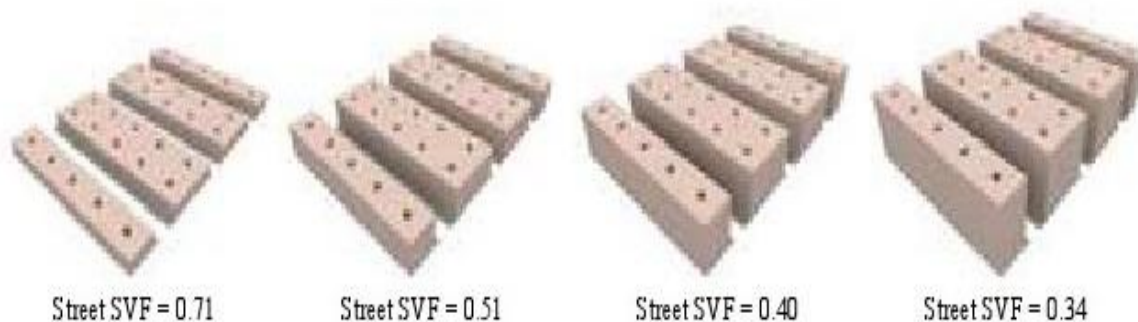
Figure 2.40: Proposed configurations with four H/W ratios; (0.5, 1.0, 1.5, and 2.0) (Al Znafer, 2014)

The researcher used the ENVI-MET software to simulate the canyon effect on outdoor microclimate parameters. The H/W is evaluated by indicating the SVF as it is the parameter that is calculated by the ENVI-Met software.

Figure 2.41 shows that the average air temperature in a deep canyon with a H/W ratio = 2.0 is lower than the average air temperature in shallow canyon with the lowest H/W ratio of 0.5.
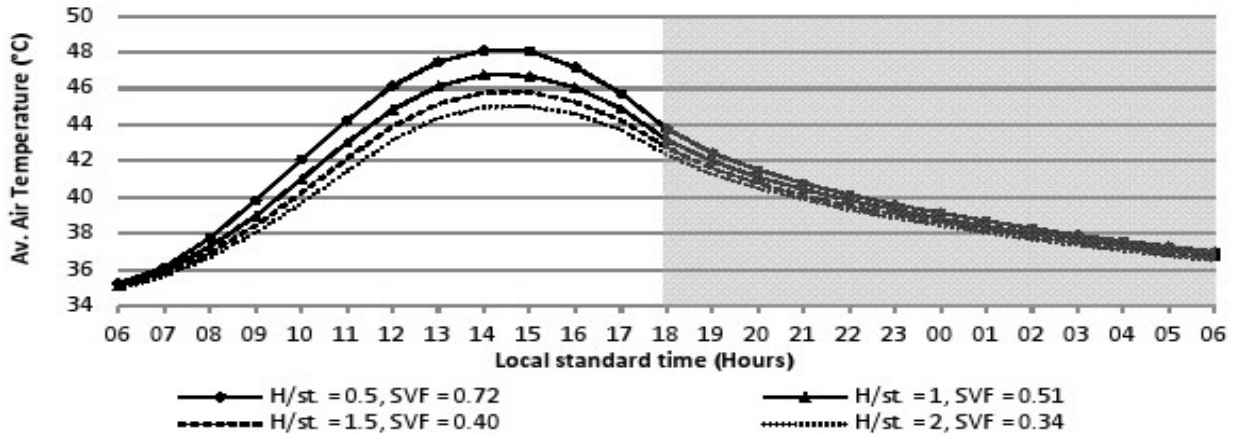
Figure 2.41: Average air temperature in the canyons at 1.2m and H/W ratio = 0.5, 1.0, 1.5,and 2.0 (Al Znafer, 2014)

Furthermore, the researcher studied the Tmrt for the same H/W ratios at four canyon orientations: E-W, N-S, NE-SW, and NW-SE. The researcher found that the canyon that extended along the E-W was warmer than the canyons that extended along the other directions. The hours of espouser to the sun is higher in this canyon, and the duration of extreme Tmrt was about ten hours, as shown in figure 2.42.
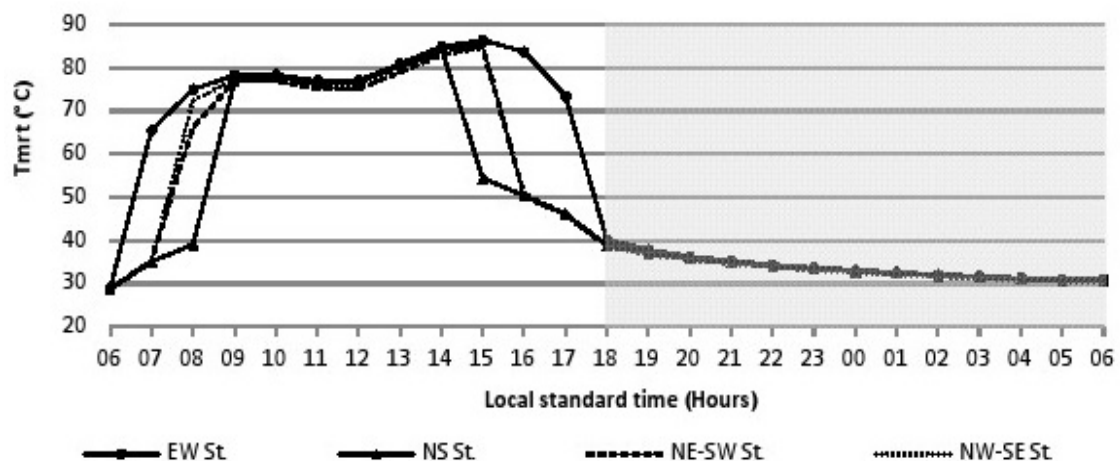
Figure 2.42: Diurnal Tmrt of H/W=0.5 for s canyon in four orientations(Al Znafer, 2014)

However, the deep canyon with a H/W ratio = 2.0 with the E-W orientation shows similar extreme Tmrt attitude, as the extreme Tmrt, with sun exposure lasting for about ten hours also (Figure 2.43).

On the other hand, the duration of the extreme Tmrt depends on the canyon type or H/W ratio. Figure 2.37 shows a H/W ratio for the deep canon of 2.0. For this canyon, and with N-S orientation, the extreme Tmrt duration is only one hour (11:00am-12:00pm). For the other orientations, there is a similarity in extreme Tmrt attitude, but there is a shifting in time. However, for the NW-SE orientation extreme Tmrt duration is three hours, and it is longer than the duration of the NE-SW orientation.
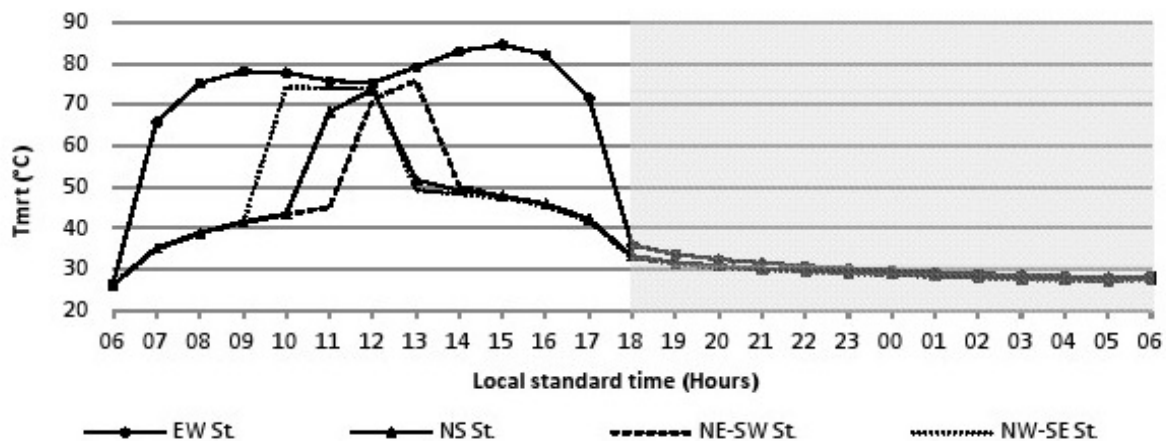
Figure 2.43:Diurnal Tmrt of H/W= 2.0 for canyon in four orientations (Al Znafer, 2014)

Furthermore, the researcher studied the effect of the four H/W ratio and the four canyon orientations on wind velocity in the canyon. The NW-SE canyon orientation shows the highest averages of wind velocity as this is the prevailing wind direct.

In contrast, the NE-SW orientation shows the minimum averages of velocity as the prevailing wind is perpendicular to canyon orientation (Figure 2.44).

Moreover, the averages of wind speeds reduce progressively from the shallow to the deep canyon by approximately 20 % (Figure 2.44).
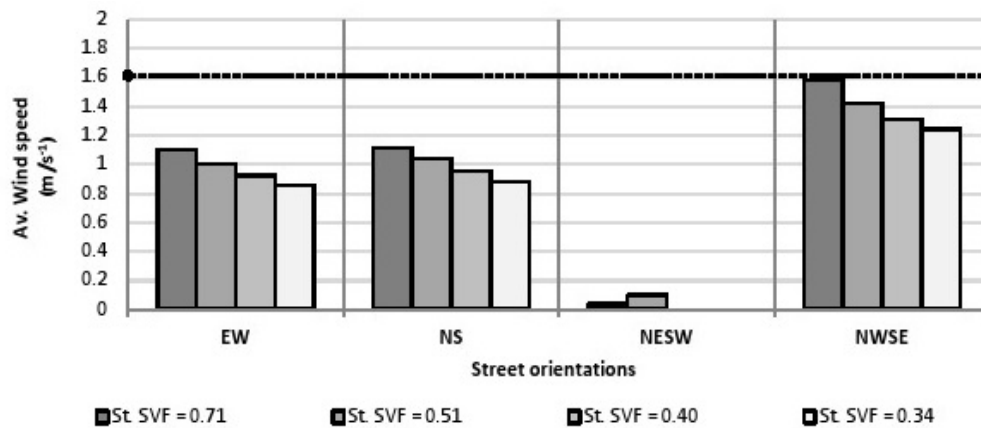
Figure 2.44: The variation of wind speed in the canyon of the four studied H/W ratios and in four orientations (Al Znafer, 2014)

2.11 Climatic Urban Design Strategies

The climatic urban design strategies are based on adopting climate and natural resources to create the desired thermal performance in the built environment. Previous literature and studies proved that urban geometry variables, such as canyon' orientation, buildings and canyon H/W ratio, and buildings configuration are key factors in climatic urban design. These factors play a significant role in creating the preferable and comfortable microclimate at the pedestrian level, in addition of their effect on energy and thermal performance of the settlements. The main micro climate factors targeted by urban designers pursuing a pleasant microclimate are: 1) solar effect, and 2) wind effect. As illustrated in the literature review chapter of this study, historical and previous researchers explored the effect of each of these two climatic factors ,and adopted these main factors to enhance and optimise the urban geometry design towards a more efficient design.

2.11.1 Solar Effect

Designing according to the desired solar effect and solar gain is different from one site to another depending to the location on the earth. In this study the weather characteristics of the case study area is categorised as hot and arid weather most of the year.

For this type of weather, reducing the solar effect should be the major target for the architect or urban planner. This reduction in solar gain will be reflected positively on the built environment. It will help to mitigate the effect of the UHI and reduce the energy consumption on urban level. Reducing the solar effect on urban level can be obtained through adopting urban geometry variables. It has been proved that the best orientation for reducing solar effect in a hot climate is extending the length of the buildings along the E-W axis (Shashua and Hoffman, 2003). Todhunter (1990) highlighted that this orientation will reduce the solar gain in summer months as less area is oriented towards the south direction. Figure 2.45 shows that the S-N direction is exposed to the highest amount of sun radiation, and the E-W direction will protect the largest area of the buildings from sun radiation.
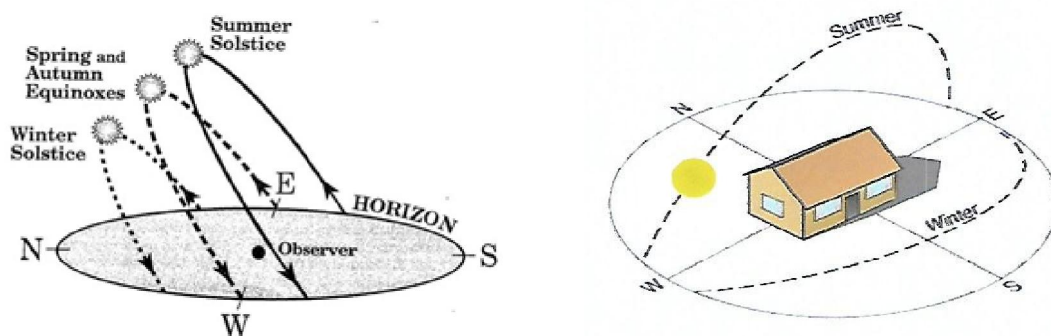
Figure 2.45:Sun path and best solar orientation for less solar gain in summer (Eco-who,2015)

The amount of the solar radiation received by the surfaces depends on the latitude. This amount is significant in the latitudes between 20°-40°, and the impact in summer is more significant than winter in this location of the earth (Arnfield, 1990). The urban geometry is very import in this location to form and control solar irradiation effects.

Arnfield (1990) investigated the effect of the H/W ratio and two orientations on the amount of the solar received by the canyon ground and building walls. The researcher conducted a numerical study for all earth latitudes, and six H/W ratios of 0.25. 0.5, 1.0, 2.0, 3.0 and 4.0 (Figure 2.46).
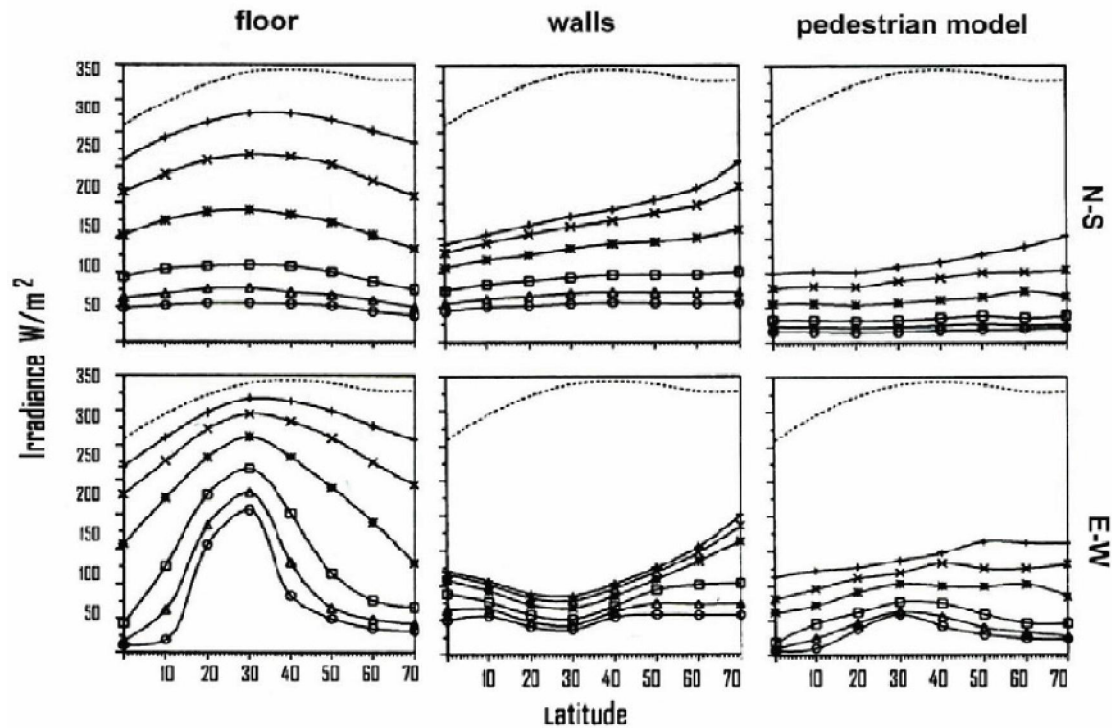
Figure 2.46: Canyon surfaces solar irradiation in two orientations and six H/W ratios
(0.25+, 0.5x, 1*, 2□,3Δ and4○) (Arnfield, 1990)

The researcher found that the ground receives more solar radiation than the walls in a low H/W ratio. Furthermore, the orientation affects the amount of solar radiation received by walls more than the ground. In summer it is more efficient to orient the building wall along the E-W axis in order to protect the wall from the exposure (Figure 2.46).

However, Toudert and Mayer (2004) found that exact E-W orientation provides less shading for the canyon in a hot and arid climate.

This will affect the indoor thermal performance by increasing the absorbed solar energy. The researchers stated that orienting the block of buildings with an angle along NW-SE or NE-SW is better for the desired shading for the buildings. The NE-SW orientation increases the solar exposure during the morning, while the NW-SE orientation increases the exposure to the afternoon radiation (Toudert and Mayer 2004). Furthermore, the diversity in buildings height within an urban canyon plays an important role in increasing the shading effect.

The effect of diversity in buildings height for creating comfortable outdoor environments was proved by Edward (2010). The researcher explored the benefits of the height diversity in a dense and compact form. The author presented the 'Environmental Diversity Map'.

This map shows the effect of height diversity on three of the microclimate parameters: temperature, shading and wind (Figure 2.47).
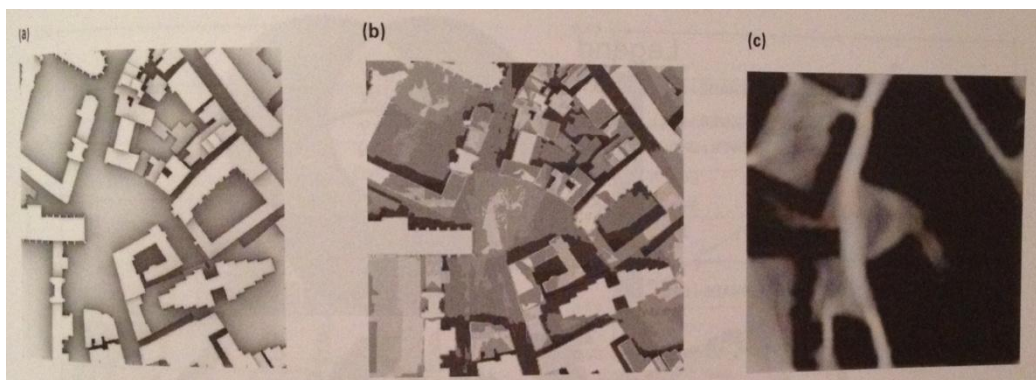
Figure 2.47: The 'Environmental Diversity Map', the effect of the three parameters: a) temperature, b) shading and c) wind (Edward 2010)

Furthermore, the dense or compact configuration of buildings pattern provides the desired protection from the solar radiation. Previous studies proved the effect of the organic and dense patterns on creating the desired outdoor thermal comfort in a hot climate. Andreou (2014) highlighted the effect of the traditional compacted form in creating the desired shading in a Mediterranean city.

The researcher compared two locations, traditional and contemporary areas, in Greece. The researcher found that the compacted traditional pattern provides more desired outdoor shading comparing with the contemporary area (Figure 2.48). Furthermore, the author illustrated that street pattern, buildings configuration and latitude are some of the factors that contribute to the canyon solar access.
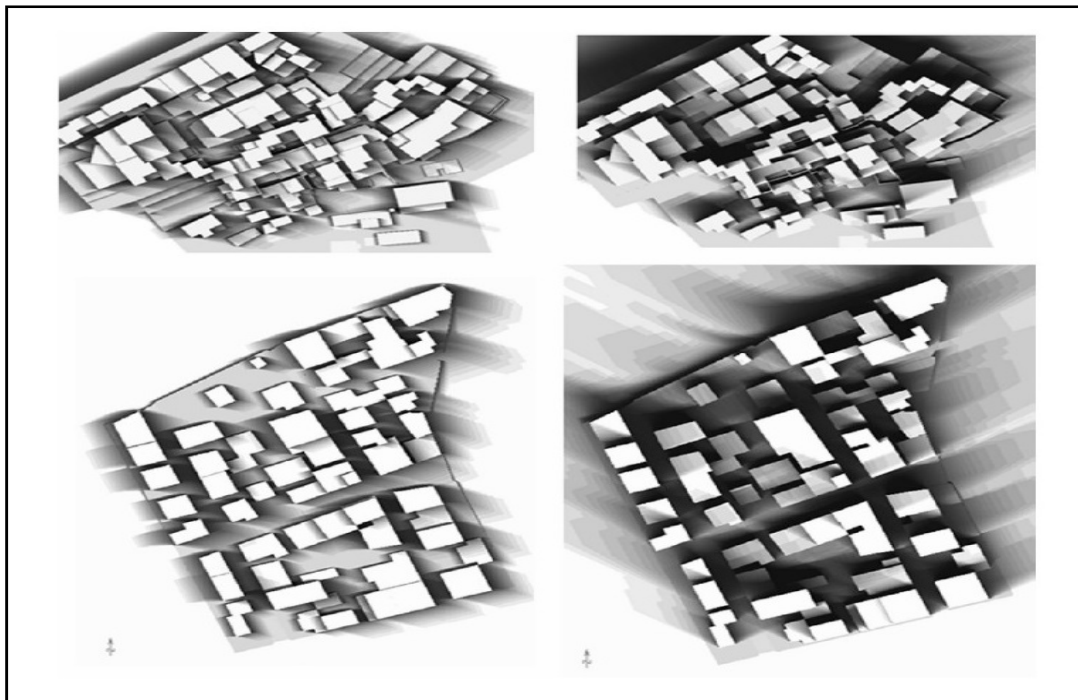
Figure 2.48: The shading effect on traditional area (up) and contemporary (down) in summer and winter (Andreou, 2014)

2.11.2 Wind Effect

The impact of the urban geometry parameters on prevailing wind and air behaviour have been addressed in many studies. The airflow and air quality within the canyon are determining factors that affect the outdoor thermal comfort and human health (Yang and Li, 2011). The formation of the airflow by adopting urban geometry variables plays a significant role in mitigating the UHI. Thus, urban geometry and canyon design, are key factors in using the potential wind and designing a desired microclimate for the built environment.

The airflow behaviour in the canyon can be studied through the effect of the two layers of the urban space. The Urban Boundary Layer (UBL), which is above the buildings height, and the Urban Canopy Layer (UCL), which represents the space within the canyon between the buildings. The UCL represents the pedestrian level of the canyon and it is isolated or blocked by the above UBL (Oke, 1988). The air flow is slow in UCL by the effect of the obstruction objects with the canyon, such as buildings, trees, transportation vehicles.

On the other side, the air flow with the UBL layer is stronger and it is affected by the canyon orientation and the H/W ratio (Oke, 1988). The orientation of the canyon is a very important element in climatic urban design. The wind effect can be adopted to reduce the canyon air temperature and UHI consequently. Ali-Toudert (2006) proved that a canyon extending along a N-S direction is more efficient in releasing heat comparing with the E-W direction. Cao, Li and Meng(2015) explored the effect of the canyon orientation on the air velocity and UHI. The researcher studied eight angles of canyon orientation in Guangzhou, China. The researchers concluded that for a specific location on the earth, a canyon should be designed with a specific angle to increase the wind speed (Figure 2.49). The increase in wind speed will consequently reduce the average temperature and the UHI effect in the canyon (Figure 2.50). Furthermore, the H/W ratio plays a significant role in forming the air flow within the canyon. The airflow within the canyon can be categorised into three types: 1) isolated roughness flow, 2) the weak influence flow, and 3) the skimming flow (Oke, 1988). The canyon geometry and the H/W ratio are the influencing factors in transition between these types of flow (Figure 2.51).
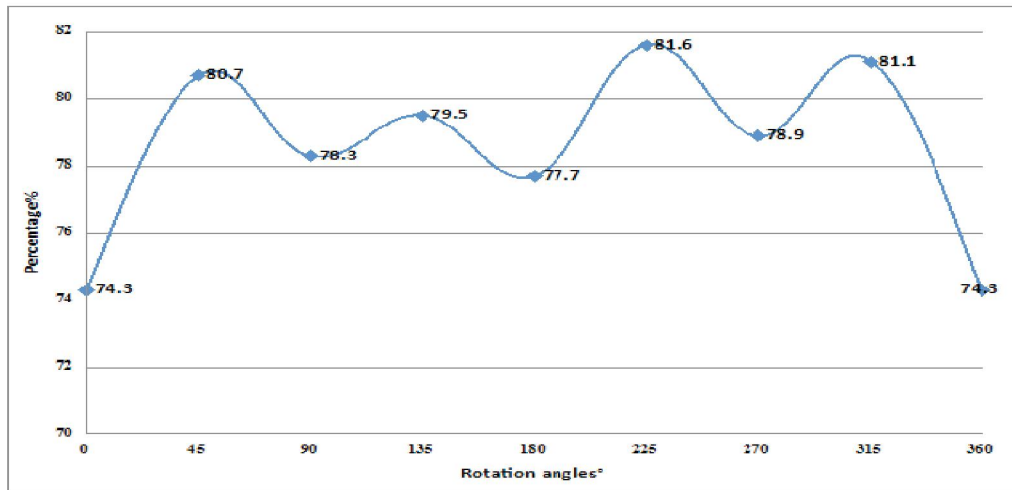
Figure 2.49:The relationship between the air velocity and canyon angles (Cao, Li and Meng, 2015)
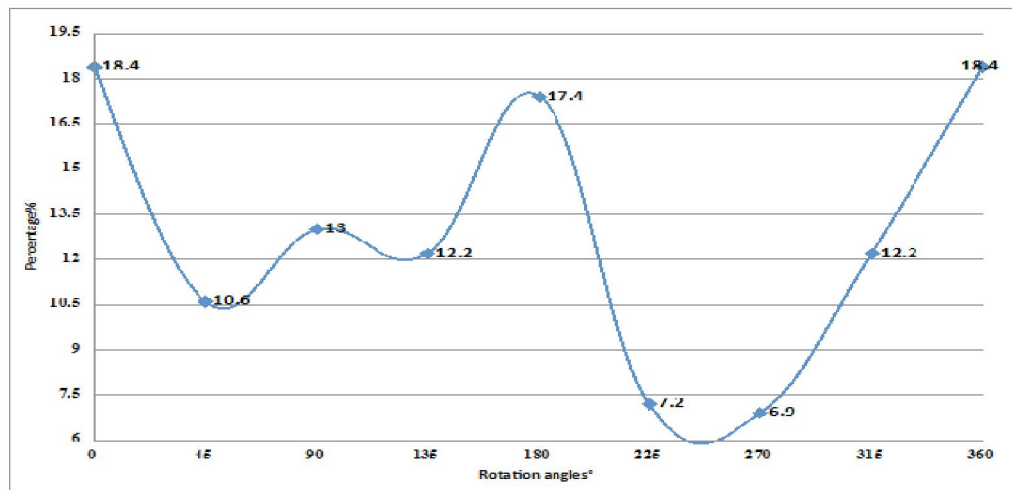
Figure 2.50: The percentage of urban heat island UHI intensity and canyon angles

(Cao, Li and Meng, 2015)

In the uniform or shallow canyon, the isolated flow takes place between the buildings. Increasing the H/W ratio will cause a vortex circulation in the space between the buildings, and the airflow will be slower in the deep canyon. Further increase in H/W ratio creates more vortex and leads to the skimming flow (Figure 2.51).

In the same context, Priyadarsini and Wong (2005) proved the effect of building height diversity on the canyon microclimate, particularly, on airflow and wind speed parameters.

The researchers found that placing any block of high-rise buildings within mid-rise buildings will increase and enhance the air movement and velocity within the canyon. They also found that this change in air movement will enhance the air temperature within the canyon, and by placing more than one high-rise building the wind velocity can be increased by 90 % and the air temperature can be decreased by 1°C (Figure 2.52). A separate research was conducted to identify methods to enhance the street or canyon sustainability conducted by (Chan et al., 2001).The researchers proved that the variation in building heights can provide better ventilation, and can enhance the urban microclimate, but they recommended that the H/W ratio should not exceed five in order to keep the microclimate within preferable levels.
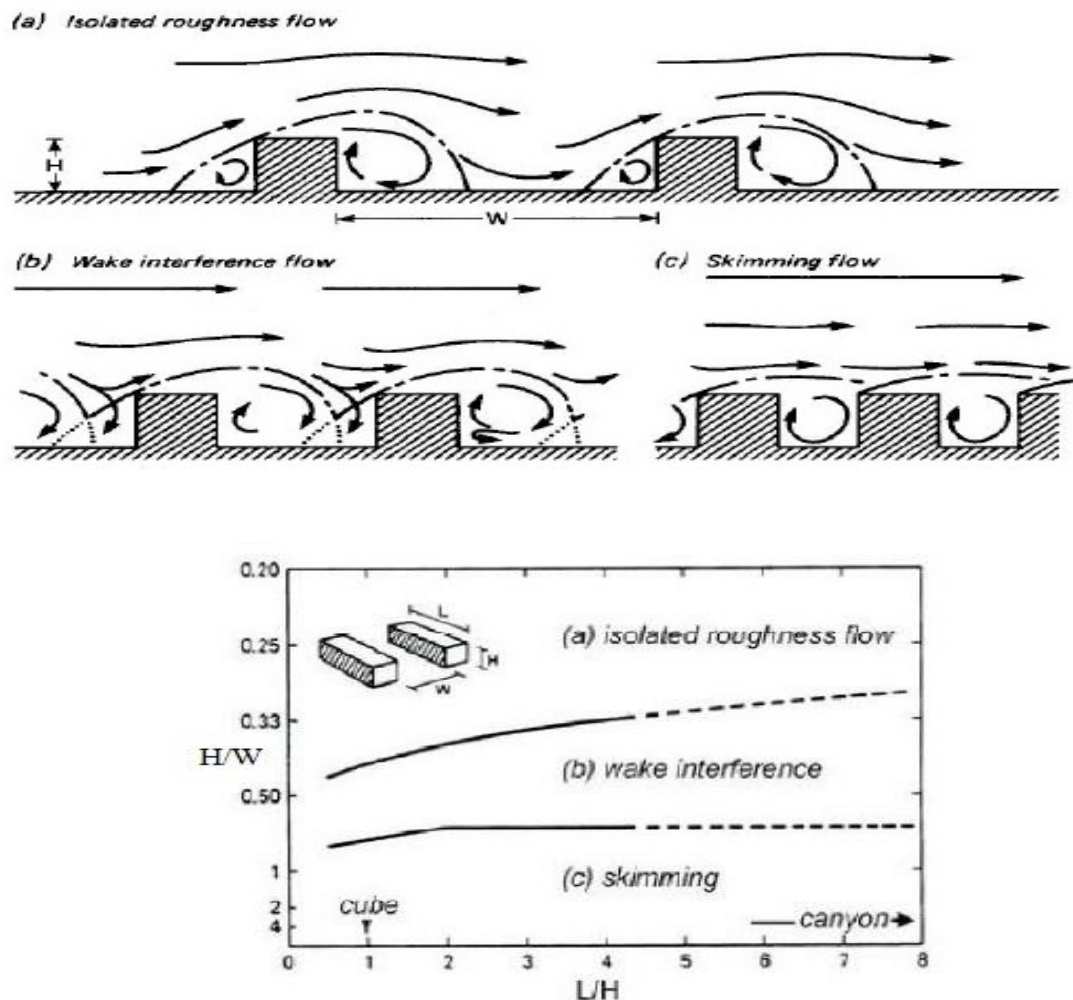
Figure 2.51: The effect of canyon H/W ratio and the three types of air flow within the UBL
(Oke, 1988)

Furthermore, Yang, Qian and Lau (2013) studied the urban form effect on wind velocity and the canyon ventilation in Shanghai, China. The researchers conducted their study on ten high-rise residential areas and concluded that increasing the SVF by 10 % would increase wind velocity by 7% - 8%. Moreover, the researchers stated the importance of a diverse wind instead of a uniform wind for people's outdoor comfort and activities.
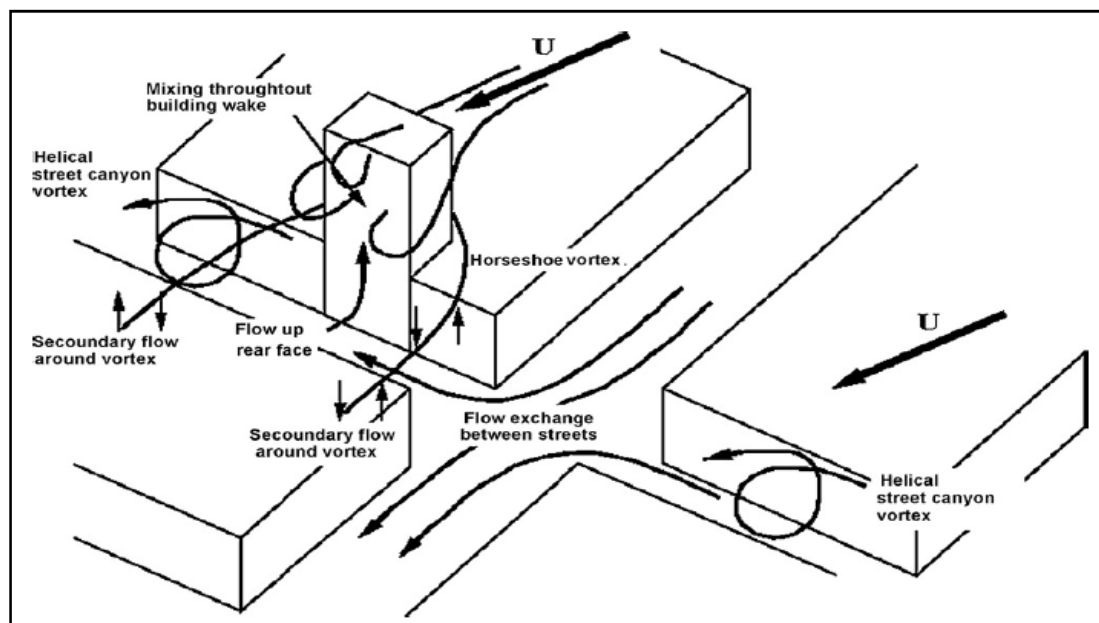
Figure 2.52: The effect of high-rise block within midrise blocks on enhancing air movement
(Priyadarsini and Wong, 2005)

The buildings configuration has been explored in a number of studies in order to find the effect of buildings arrangement on wind speed and airflow behaviour in the canyon. Santamouris (1999) found that arranging buildings in a grid configuration and creating parallel, strait canyons, will promote the airflow within the canyon (Figure 2.53).

Moreover, the researches claimed that rearranging the buildings with a winding configuration is suitable for hot or cold stressful climates. This configuration decreases the speed of the wind and reduces the air velocity within the canyon (Figure 2.53).
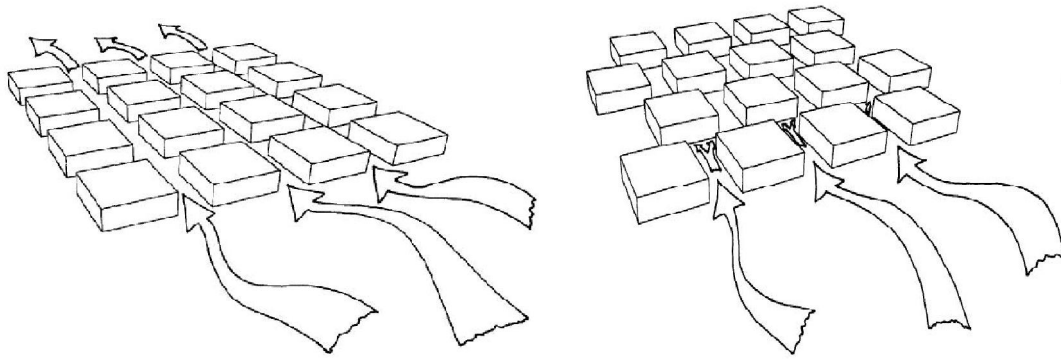
Figure 2.53: Airflow in the parallel and strait buildings configuration (Santamouris, 1999)

However, the prevailing wind can be adopted to enhance the thermal performance of the built environment on both the outdoor and indoor levels. The effect of canyon geometry and buildings configuration on potential of wind speed requires more investigation. Recently, the progress in simulation software provides a good opportunity for this type of researchers.

2.12 Summary of the Previous literatures on Urban Geometry and Gap Identification

A literature review as a method of study was conducted at the beginning of this research. Reviewing previous literatures shows that most of the studies related to urban geometry concentrated on the effect of the urban geometry elements on the outdoor thermal performance. However, recent studies have adopted computer simulation software in order to identify the effect of urban geometry variables on micro climate microclimate parameters. The most geometrical variables that have been studied include canyon orientation and H/W ratio. Moreover, most of these studies have explored the effect of the uniform canyon.

The uniform canyon with different aspect ratios is the most studied variable, as illustrated in this chapter. The variation in the buildings height within the complex has not been addressed or explored in detail; this gap has been identified according to the literature review. The height diversity is one of the urban geometry variables that needs more investigation. Furthermore, few studies have explored the effect of microclimate parameters on indoor thermal performance and energy consumption at the urban level. Most of the previous studies explored the energy consumption of individual buildings.

Therefore, this study attempts to fill this gap by exploring the effect of urban geometry variables, particularly buildings height diversity in the urban block, on microclimate parameters. Moreover, this research aims to integrate this effect to evaluate and optimise the whole block energy consumption. Furthermore, very limited studies have explored the effect of urban block configuration and buildings morphology on indoor energy consumption in general and cooling load in particular. On the other hand, a buildings alternative or stagger arrangement is one of the urban geometry variables that has not been addressed or simulated using the software method of study. However, the diversity in buildings height, buildings staggered arrangement and their effect on indoor cooling load were not addressed by any of the reviewed and recent studies. This research attempts to fill this gap and identify the effect of the buildings height diversity and alternative configuration on indoor energy consumption at the urban scale.

2.13 Urban Geometry and the Research Selected Variables

Urban geometry covers a number of variables, and the previous literatures illustrated the most important variables of urban geometry covers: building's H/W ratio, buildings /canyon orientation and buildings shape and geometry, in addition to buildings and canyon surface materials (Andreou and Axarli,2012; Andreou, 2013; Qingyuan and Yu, 2014; Crook and Forster, 2014; Ai and Mak, 2015).

The previous studies explored the influence of different urban geometry and design variables on both outdoor urban microclimates and indoor thermal performance. The effect of passive design strategies has been explored and adopted to enhance the thermal performance of the built environment by a number of researchers (Yang Lie, 2013; Qingyuan and Yu, 2014; Whang and Kim, 2014). However, previous studies have focused on the effect of street or canyon design and orientation on outdoor thermal comfort and microclimate parameters (Andreou and Axarli, 2012;Andreou, 2013; Ai and Mak, 2015). On the other hand, many researchers studied the effect of buildings and urban surface materials on the built environment (Tooming, 1996; Crook and Forster, 2014). In this research three of the building and urban geometry variables will be explored in order to identify their effect on the urban microclimate of a complex. Additionally, the research will seek to identify the reflection of this effect on buildings energy consumption and cooling plant load at urban level.

The selected building and canyon design variables are:

1) Buildings / canyon orientation

 2) Buildings' height diversity

3) Buildings' configuration.

Furthermore, the Built-up BUA and SVF, as urban geometry indicators, will be adopted to evaluate the base case and the variation between the suggested proposed scenarios, to compare the findings of this study with previous literature results.

Chapter 3

Methodology

3.0 Methodology

3.1 Introduction

Urban geometry and buildings configuration have a significant impact on urban microclimate buildings energy performance. In the literature review chapter of this research the factors that affect the urban microclimate behaviour were explored, and the affected microclimate parameters were illustrated. In this chapter the methodologies followed for analysing the effect of the urban geometry on outdoor microclimate and energy performance of the built environment will be illustrated. The most proper method to conduct this research will be selected. In additional to the literature review as a widely used and common method of research, other approaches and methods will be used to model, analyse, and evaluate the impact of the urban geometry on the built environment depending on the scale of the studied area.

Generally, in urban design and planning studies, the use of the case study and simulation approach is the most widely followed method to conduct the urban studies, various types of computer software simulation were used in previous literatures and publications for this aim. Some of the computer software that were used for urban microclimate and energy consumption studies include City Cad, Integrated Environmental Solution-Virtual Environment (IES-VE), ECOTECT, Virvil Plugins, Design Builder-Energy Plus, ANSYS/FLUENT and ENVI-MET. These software programs were used to simulate the relation between the urban design factors ,and the microclimate environmental parameters by adopting the case study method (Bruse, 1999; Ozkeresteci et al., 2003; Muhaisen and Gadi, 2006; Kruger, Minella and Rasia, 2010; Stromann-Andersen and Sattrup, 2011; Al-Masri and Abu-Hijleh, 2012; Taleb and Abu-Hijleh, 2012; Gill et al., 2013; Taleb, 2014; Djukic, Vukmirovic and Stankovic, 2015).

On the other hand, the quantitative method of research has traditionally been used to investigate any phenomena using the statistical technique of developing a mathematical model or formula. It is mainly employed on a large set of empirical or numerical data to identify the relationship between the studied phenomena and a mathematical expression. Recently, many urban studies have integrated quantitative data, such as Digital Elevation Model (DEM) with the simulation approach by using various types of software. The aim of this integration is to evaluate and represent the microclimate and environmental parameters on a large scale. An example of this approach is the use of DEM and Geographical Information System (GIS) in order to generate the climatic map or mapping the distribution of the CO_2 concentration in a specific region. Chen and Edward Ng (2011) adopted the quantitative DEM data and the GIS software in order to generate a Climatic map. Moreover, the researchers approached the case study qualitative method by using the Kowloon Peninsula in the southern territory of Hong Kong for their study. The researchers used the geographical building database to characterise two widely discussed urban aspects: wind dynamic and the effect of the UHI. Furthermore, some studies adopted the quantitative method and empirical data to develop a mathematical model that represent the relationship between the urban design factors and the environmental parameters (Ruiz-Arias et al., 2009; Tarekegn et al., 2010).

3.2 The Most Employed Methodologies in Urban Planning Studies

3.2.1 Case study

Previous literature shows that the case study as a method for studying and exploring the effect of the built environment on the urban level is adopted in many published studies. Some studies selected a case study using a simple grid to be analysed in terms of environmental parameters (Ratti et al., 2005; Taleghani et al., 2014; Quan et al., 2014).

Other researchers indicate a specific location to conduct their study. Stromann-Andersen and Sattrup (2011) adopted the case study method for comparing two study areas with different H/W ratios in Copenhagen (Figure 3.1). The scale and the location of the case study is varied according to the research aims and objectives (Djukic, Vukmirovic and Stankovic, 2015). Taleghani et al. (2013) compared six types of block typologies in the Netherlands to study the effect of the court on energy efficiency. Mavrogianni et al. (2010) selected 15 dwelling archetypes in an area of London to evaluate the energy performance in dwelling, house group (Kavgic, 2010).
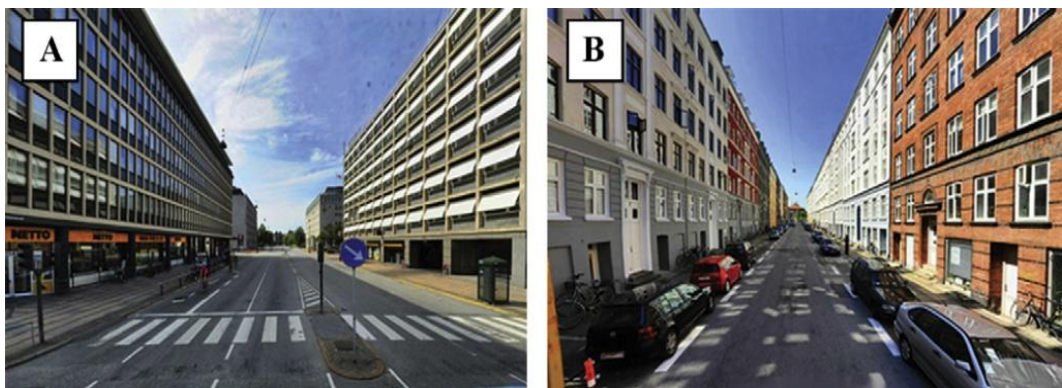
Figure 3.1: Contemporary urban case study, Copenhagen(a) H/W ratio 0.8(b) H/W ratio 1.25(Stromann-Andersen, 2011)

3.2.2 Observation and Field Measurements

Field measurements is one of the most followed empirical methods that is used to explore the effect of the buildings configuration on the built environment, as proved in the previous literatures and studies; building height to street width ratio, buildings shape and orientation, and canyon orientation are significant factors that influence the environmental performance of the build environment (Yin Ng and Kwan Chau, 2013; Bady et al., 2008; Chan et al., 2003). The field measurements method was used by many researchers to collect data from the site of the selected case study. Murena and Vorraro (2003), Murena and Favale (2007) and Ghenu et al. (2008) used the field measurement approach to conduct their research and to explore the effect of the built environment on air pollution.

However, the time factor and the availability of the required instruments are some of the limitations of this method. Kruger, Minella and Rasia (2010) adopted this approach to collect the SVF from 18 monitoring points in Curitiba, Brazil. The researchers conducted comfort surveys and measured microclimatic data in order to evaluate urban comfort on the pedestrian level (Figure 3.2).
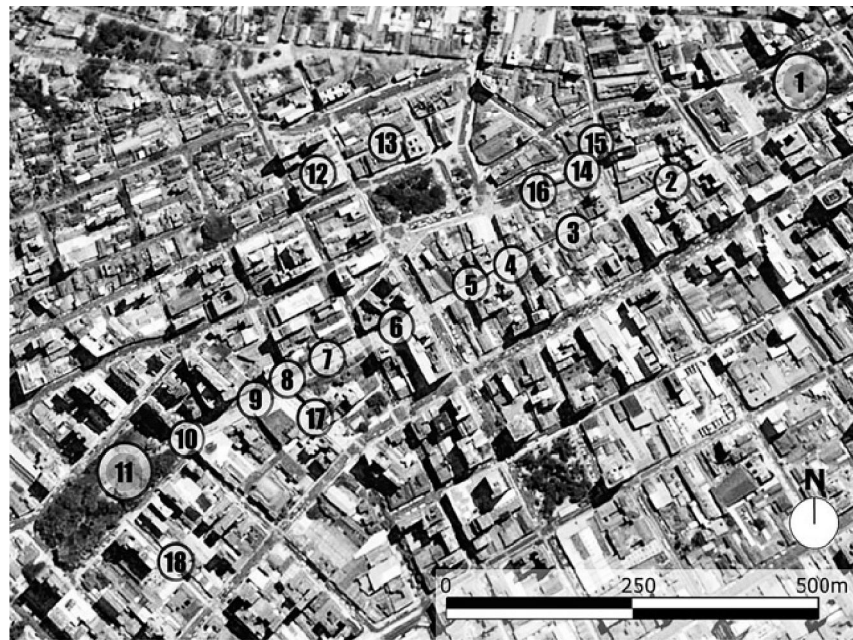
Table 1
Characteristics of the monitoring points.

Point	SVF	H[a]	W	H/W
2	0.2	30	18	1.7
3	0.32	19	18	1.1
4	0.34	[b]	[b]	—
5	0.22	28	18	1.6
6a	0.26	32	25	1.3
6b	0.27	32	25	1.3
7	0.39	20	25	0.8
8	0.37	[b]	[b]	—
9	0,29	33	30	1.1
10	0,30	32	30	1.1
13	0,21	21	9	2.3
14	0.55	[c]	[c]	—
16	0.38	[c]	[c]	—
17	0.21	29	18	1.6
18	0.3	20	18	1.1

[a] Estimated height, obtained from Rayman results from fisheye images.
[b] Street crossing.
[c] Square.

Figure 3.2: Field measurements and data collection from 18 monitoring points
(Kruger, Minella and Rasia, 2010)

3.2.3 The Computer Simulation Software

Recently, software simulation has been widely used in exploring and studying the thermal behaviour of the built environment, some of these software programs provide an accurate prediction of the microclimate and outdoor thermal behaviour, such as ENVI-Met, ANSYS-FLUENT and GIS. Other software programs provide more detail in presenting indoor energy performance, such as IES-VEIES-VE, ECOTECT, and Design Builder-Energy Plus.

In urban studies, computer software is generally used for modelling, simulating, analysing and evaluating the selected case study area or abase case and the proposed scenarios (Bruse, 1999; Ozkeresteci et al., 2003;Taleb and Abu-Hijleh, 2012; Andreou, 2014).

3.2.3.1 Outdoor Microclimate Simulation Software

The outdoor simulation software is generally used to simulate the outdoor geometrical and environmental variables, and to predict the urban microclimate parameters. This type of software used to provide the Computational Fluid Dynamics (CFD) simulation that allows the analysis of the microclimate changes according to any change in urban geometry or buildings configuration. A wide range of environmental parameters could be predicted using the outdoor simulation software, such as solar shading, solar gain, air temperature, air flow, wind speed, humidity and air pollution. Some of the most widely used software programs for outdoor simulation are ENVI-MET, City Cad, GIS, Urba Wind and ECOTECT (Bruse, 1999; Ozkeresteci et al., 2003; Kruger, Minella, and Rasia, 2010; Andreou, 2011; Taleb and Abu-Hijleh, 2012; Gill et al., 2013).

ENVI-MET is one of the most used software programs for CFD analysis, and microclimate parameters prediction. The accuracy and validity of the ENVI-MET program has been proved in many studies and publications (Bruse, 1999; Ozkeresteci et al., 2003; Gill et al., 2013). In additional to microclimate parameters, Kruger, Minella, and Rasia (2010)used the ENVI-MET software to simulate four scenarios of wind speed in order to identify the effect of each

scenario on NO_2 concentration. On the other hand, Chen and Ng (2011) used the GIS software to analyse and evaluate the effect of SVF on microclimate parameters in Honk Kong. The researchers adopted the 'Digital Elevation Model (DEM)' to generate a 'Climatic Map' that provides a virtual evaluation and supporting tool for urban planners and decision makers (Figure 3.3).
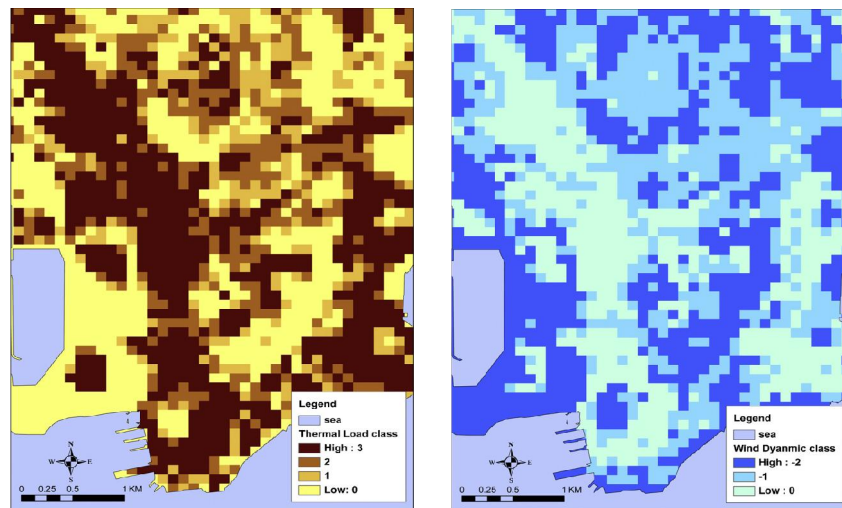
Figure 3.3: Thermal load distribution and wind map using DEM data and GIS (Chen and Ng, 2011)

However, most of the outdoor simulation software programs do not have the capability to analyse and predict indoor thermal performance parameters. In order to identify the influence of urban geometry variables on indoor energy performance, another type of software is required. The integration between the two types of the software has recently been used to identify the effect of outdoor microclimate parameters on indoor energy consumption (Yang et al., 2012; Berardi, 2016). Most of the previous studies used the field measurement and empirical data as an input data for simulating indoor energy performance and for predicting the effect of the outdoor microclimate (Sun and Augenbroe, 2014; Magli et al., 2014; Al Znafer, 2014).

Yang et al. (2012) integrated two simulation software programs, ENVI-MET and Energy Plus to conduct a quantitative analysis, and to identify the effect of the surrounding microclimate on the energy performance of individual building within a complex.

The researchers included effective microclimate factors, covering solar radiation, air temperature, humidity and wind speed, in their study to explore the effect of these factors on building energy consumption. Figure 3.4 shows the detailed method of integrating ENVI-MET and Energy Plus software.
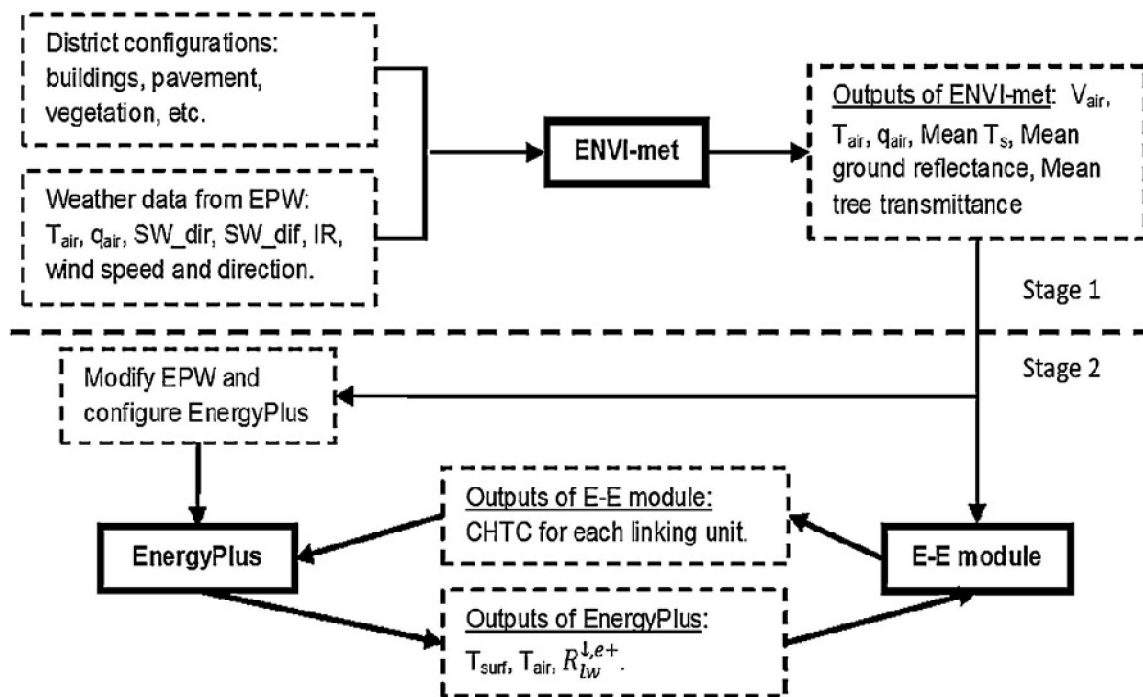
Figure 3.4: The method of coupling ENVI-MET and Energy Plus software (Yang et al., 2012)

3.2.3.2 Indoor Thermal Performance Simulation Software

Recently, software simulation has been widely used in studying the energy performance of the built environment (Stromann-Andersen and Sattrup, 2011; Taleb, 2014; Li, Quan and Yang, 2016). The Integrated Environmental Solution- Virtual Environment IES-VE, Designer Builder - Energy Plus, ECOTECT, are among the most widely used software programs for

indoor thermal performance studies. These software programs are generally used to obtain a wide variety of indoor thermal performance parameters, such as air temperature, solar gain, daylight analysis, humidity, CO2 emission, air ventilation, cooling and heating load (Muhaisen and Gadi, 2006; Stromann-Andersen and Sattrup, 2011; Al-Masri and Abu-Hijleh, 2012; Taleb, 2014). In the published paper that addressed the effect of courtyards in residential buildings in the UAE, Al-Masri and Abu-Hijleh (2012) used the IES-VE software to explore the variation in two environmental parameters: daylight factor and cooling load energy consumption. Furthermore, the researchers evaluated the effect of different types of glazing, wall thickness and insulation materials on these two parameters.

On the other hand, the paper published by Hammad and Abu-Hijleh (2010) illustrated the effect of using the external dynamic louvers on south, east and west facades in an office building in Abu Dhabi, UAE. The researchers explored there reduction in energy consumption of cooling and lighting energy consumption for each facade orientation and louvers option (Figures 3.5 a and b).
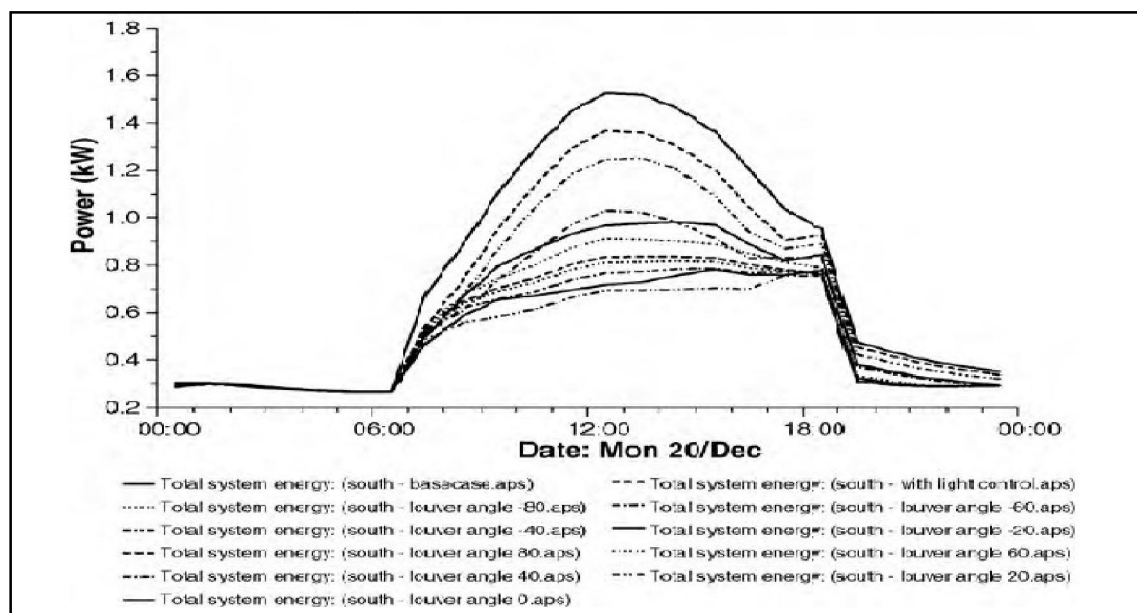
a) Cooling load consumption
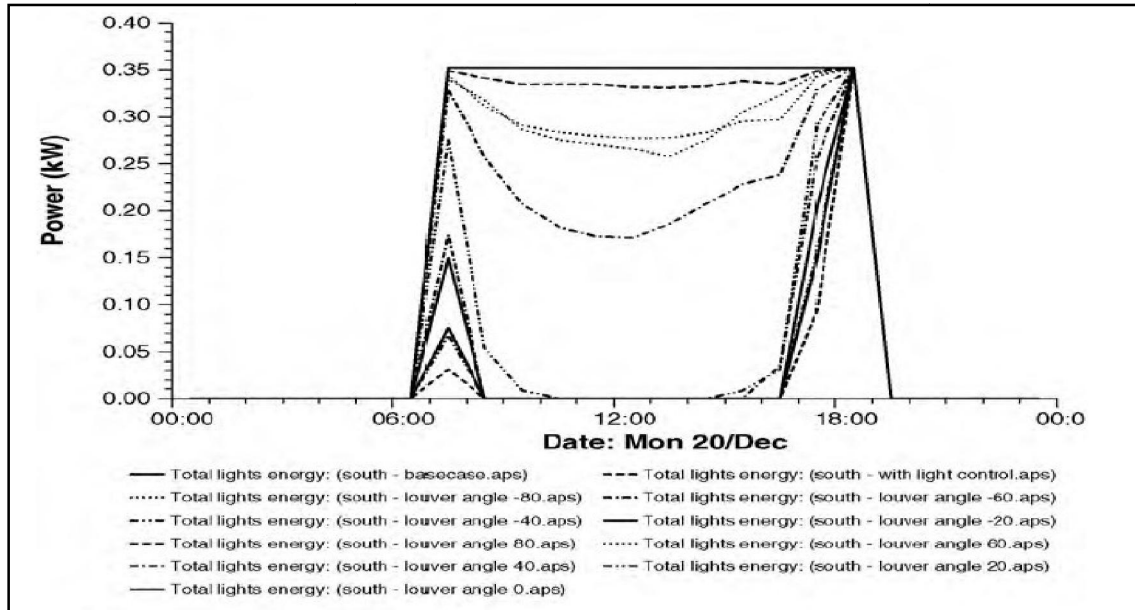
b) lighting consumption

Figure 3.5: IES simulation software and output parameters (Hammad and Abu-Hijleh, 2010)

In the same context, the effect of passive cooling strategies on residential villas in the UAE was explored in paper published by Taleb (2014). In this paper the IES-VE software was adopted to simulate the passive cooling strategies effect on three environmental parameters namely: air temperature, cooling load and energy consumption. Muhaisen and Gadi (2005) used the IES-VE software to investigate the effect of different proportions of the courtyard on solar gain and energy demand in Rome, Italy. The energy demand was expressed by heating and cooling load as one of the IES-VE software output parameters. Figure 3.6 shows the effect of ten courtyard ratios on cooling and heating load using IES-VE.

Further to that, the researchers adopted the Sun Cast application of the software to conduct a shading analysis for each proposed proportion of the courtyard in the two main seasons, summer and winter. Other than that, Stromann-Andersen and Sattrup (2014) used the software to study the effect of the dense area on solar gain and daylight factor using the Sun Cast and Radiance applications of the IES-VE software.
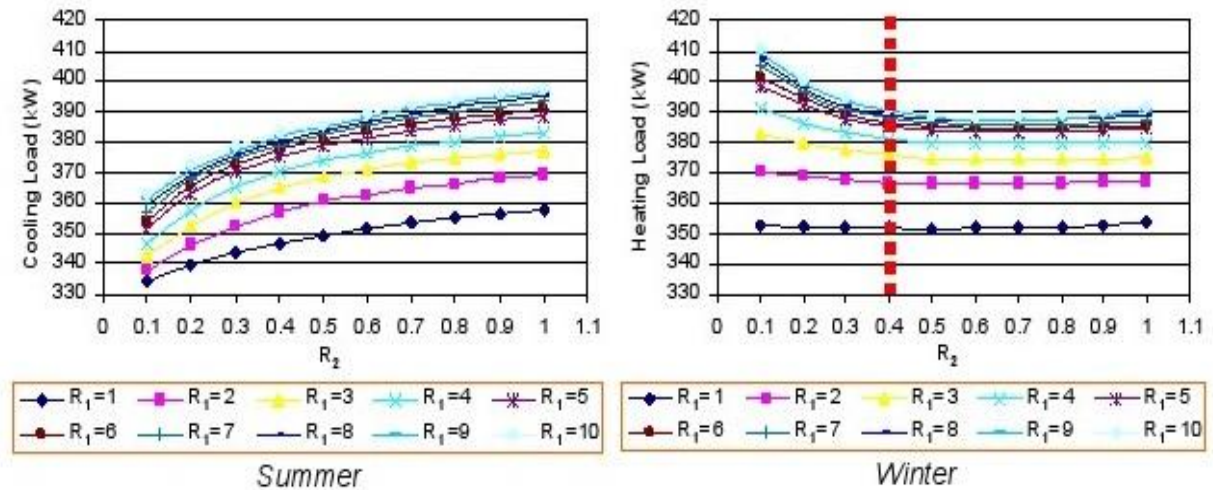
Figure 3.6: The effect of 10 courtyard ratios on cooling and heating load using IES-VE
(Muhaisen and Gadi, 2005)

The researchers explored the effect of these two factors on energy consumption of office buildings in Copenhagen, Denmark. However, ECOTECT software is another program that is used for simulating, analysing and evaluating the effect of building geometry. It provides a wide range of outdoor and indoor outcome parameters. The parameters cover shading effects, solar gain, air temperature, daylight analysis, CO_2 emission, cooling and heating load. In addition to providing a water usage estimation and analysis, and acoustic analysis. Figure 3.7shows the daylight factor analysis using ECOTECT software (Andreou, 2011).
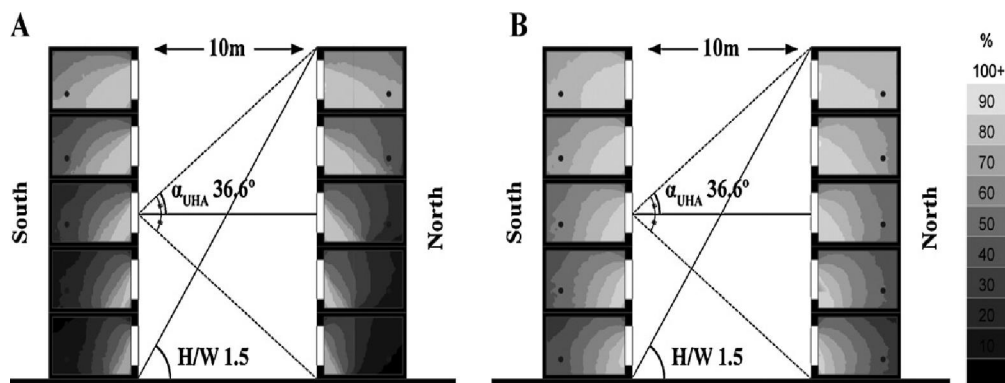
Figure 3.7: Daylight factor analysis in the canyon between office buildings for two working hours
a) 8am and b) 5pm (Andreou, 2011).

Energy Plus is another energy performance simulation software. The software is used to predict the indoor thermal performance parameters, such as air temperature, air ventilation, HVAC system, glare and luminance calculations. Berardi (2016) used field measurements and Energy Plus software in a study conducted in Toronto, Canada.

The research aimed to explore the effect of green roofs on buildings energy consumption. The collected data represents different types of green roof. The researcher used this data as an input data for running Energy Plus software, and predicting indoor thermal performance. The research concluded with the effect of each roof type on monthly and annual energy saving (Figure 3.8).
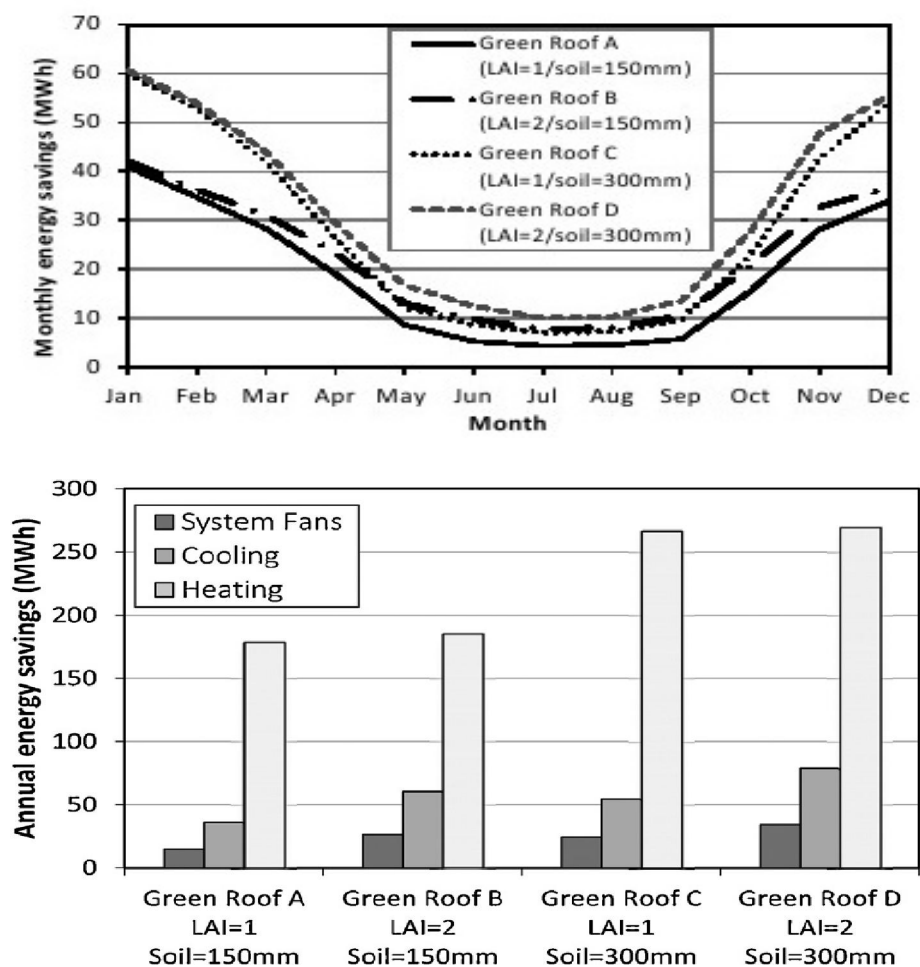
Figure 3.8: Monthly and annual energy saving for different types of green roofs using Energy Plus software (Berardi, 2016)

3.3 Methods of Exploring Energy Performance of Developments

To calculate and evaluate the energy performance on the urban scale, different methods have been used in previous studies. All of the applied methods are divided and categorised in to groups according to number of types, such as building functional type, floor area type and dwelling type, some of these buildings groups take the social aspect in to consideration like building household type, and some of the studies take the climate zone as a factor to indicate the buildings group. (Jones et al. 2001; Shimoda et al., 2004; Zhao et al., 2011).

Furthermore, the Bottom to Top method is one of the methods that is adopted to scale up the models from the building level to the block and district levels (Yang Lin, 2013; Li, 2015). The concept of the bottom to top method is calculating the energy performance of the selected building that represents a specific category, and then the overall energy performance or consumption can be obtained by gathering the calculation of all buildings in the same group (Kavgic, 2010). Compared with the Top to Bottom method, which is easier to apply as it requires less data, the bottom to top method is more advantageous when used in this research as it considers more detail, such as environmental parameters and urban design parameters including air temperature, wind speed, buildings geometry and building envelope materials (Swan and Ugursal, 2009). Other than that, some researchers go for more details in classifying the buildings according to the building occupant's behaviour, building envelope specification and thermal prosperities (Shimoda et al., 2004).

3.4 The Research Methodology Selection

The aim of this research is to explore the effect of urban geometry and buildings configuration on thermal performance at the urban level. In addition of identifying the optimised buildings configuration with the lowest energy consumption and negative environmental impact.

In order to achieve this aim, a number of objectives were listed in the first chapter of this study. The research objectives cover exploring urban geometry variables from one side and finding the effect of these variables on thermal performance of the built environment from the other side. The literature review method of study is conducted to explore the most followed methodologies for similar aim. The previous literatures showed the most methods used in exploring the effect of urban design on thermal performance of the built environment. However, the recent studies adopted the computer simulation software to explore the effect of urban geometry variables on micro climate microclimate parameters.

Furthermore, many studies adopted the computer simulation software to explore the energy performance at the buildings level. However, the case study method is one of the most widely used methods in urban studies, as illustrated in section 3.2 of this chapter.

Hence, this research will use a combination of three methods to achieve the research aim and to answer the research questions. The methods that will be adopted in this research are:

1) Literature review

2) Case study

3) Computer simulation software

The literature review method is conducted to explore and identify urban geometry variables and to identify the most effective variables on thermal performance of the built environment. This is in addition to identifying the micro climate microclimate parameters and exploring their effect on indoor thermal performance. Furthermore, the previous literature will be used to illustrate and highlight the historical and latest results in sustainable urban design and planning. Moreover, a case study area will be selected, and a block of buildings will be chosen. The selection of a case study area will be basically adopted for observation and physical dimension measurements. Furthermore, microclimate data will be collected for the

computer software validation. Moreover, a package of two computer simulation software programs will be used in this study, and the validity of the software will be evaluated against the actual field data. The software will be used for modelling, simulating and evaluating the base case and the suggested proposed scenarios. The selected package of software includes;

1) ENVI-MET software for outdoor Computational Fluid Dynamics (CFD) simulation

2) Integrated Environmental Solution Virtual Environment IES-VE) for indoor simulation

The suggested proposed scenarios aim to optimise buildings geometry and configuration to minimise the energy consumption at a large scale. The aim of using the ENVI-MET program is to identify the effect of the buildings configuration on outdoor microclimate parameters. The second software IES-VE will be used for indoor thermal performance. It will be used for indoor energy consumption simulation and evaluation. The reason behind selecting the two software is to reflect the effect of outdoor microclimate parameters on indoor energy performance. The capability and the limitations of each software will be illustrated in detail in this chapter. The urban geometry variables that will be studied include:

1) buildings / canyon orientation

2) buildings height diversity

3) buildings configuration

The effect of the mentioned urban geometry variables on canyon microclimate parameters will be studied and analysed. The outdoor outcome parameters will cover; 1) solar shading, 2) air temperature, 3) humidity and 4) wind speed. Furthermore, the effect of these parameters on indoor air temperature, cooling load and energy consumption of the buildings will be calculated. Figure 3.9 shows a scheme of the methods that will be followed in this research.
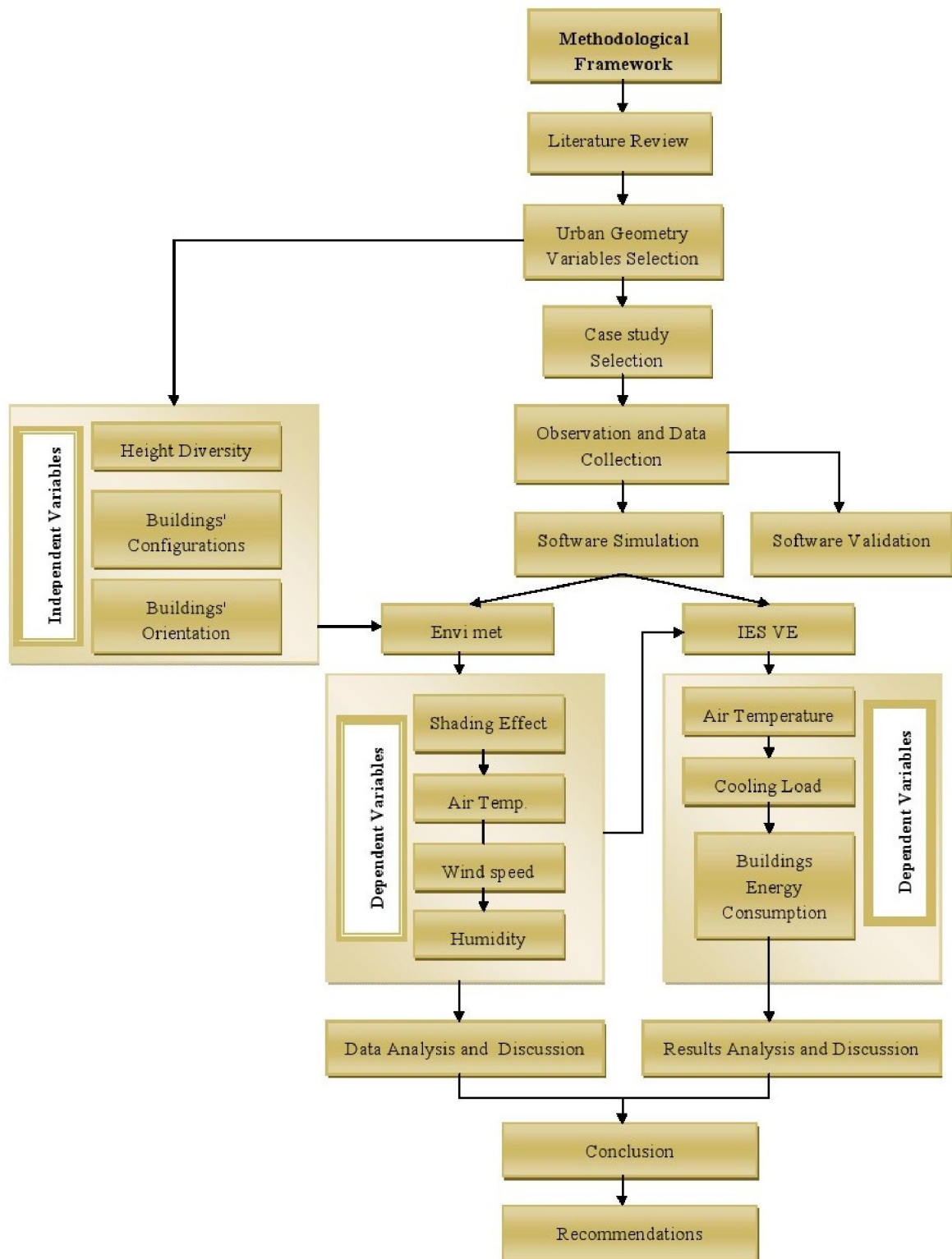
Figure 3.9 : The Research Methodological Framework (Author, 2018)

3.4.1 The Selected Case Study Description

The case study area is selected to collect the physical data required for developing an urban block model, which is in addition to the microclimate data required for the software validation. The selected case study area is located in Dubai, UAE, the weather data of Dubai International Airport will be the reference data for running the simulation software. The case study community is a part of the Emirates Hills development, which was constructed 10-12 years ago. The community consists of two phases of residential buildings (Figure 3.10).

Figure 3.10: Google Images of 'The Greens' case study area (Google, 2016)

The buildings were constructed according to Dubai Municipality (DM) regulations and specifications codes. However, the area was constructed before the implementation of green buildings regulations and specifications in Dubai (2008).The community consists of two clusters of mid-rise buildings. The mid-rise residential buildings are a combination of G+3 and G+6 buildings (Figure 3.11). Furthermore, the community includes a number of one level (ground floor) buildings, namely the community centre and the mosque.

Figure 3.11: The mid-rise residential buildings in The Greens (Author, 2016)

The total area of the first cluster is 90,110 square meters, and the second one is 112,550 square meters, according to the symmetry in buildings design within the cluster, and in order to reduce the simulation time. Furthermore, these dimensions apply to the limitation in grid dimensions and cells number of the ENVI-MET software. The simulation area will cover the canyon of 20m and the buildings on both sides. The total built-up area that will be simulated is 45,280 square meters, and the length of the canyon will be simulated as150m. The cluster or block of buildings chosen is from one functional group, the mid-rise residential buildings group. Selecting the buildings from one functional group will avoid any variation in data that will be used for indoor thermal performance simulation.

The case study will be used for field and physical measurements that reflects the actual buildings and canyon dimensions. In addition of obtaining buildings specifications and materials required for running simulation process. Furthermore, the case study area will be used for collecting an actual microclimate data that can be used for outdoor software validation.

3.4.2 The Computer Simulation Software Selection

The aim of this research is to find the effect of the urban geometry configuration on outdoor microclimate parameters and indoor energy consumption. For this aim two types of software will be used. For the first stage the ENVI-Met simulation software will be used to obtain the outcome of outdoor microclimate parameters. Then, the outcome microclimate parameters will be used as an input parameter for indoor energy consumption simulation software in the second stage.

In this stage the IES-VE program will be used for indoor energy consumption calculations (Figure 3.12). The reason behind using the two software is the limitation of each software in simulating both outdoor and indoor energy and thermal performance parameters. However, the limitation of each software will be presented in detail in the next sections. The outdoor thermal performance simulation software was selected for its accuracy and flexibility in simulated model area analysis, specifically the x-y dimensions of the model. In additional to the availability of the professional and science version in a reasonable price for educational use. Other outdoor thermal performance simulation software have some limitations regarding the boundary dimensions and the availability. For example, the ANSYS-FLUENT 14.5 is one of the more accurate software programs with a high flexibility in modelling tools, and it can provide a wide range of microclimate parameters as mentioned previously, but the boundary size is limited in the version that is available for educational use.

The Autodesk and ANSYS-FLUENT partner company provides the advanced version of the software for professional use specifically. Another software, such as the City Cad concerned more with sustainability in urban form covering some urban planning elements, such as land use, waste management, transportations system, and open areas for planning liveable communities.

The IES-VE software is selected for its wide range of indoor thermal performance and energy consumption parameters, in additional to its accuracy and the wide use in professional and actual case studies that adopted the IES-VE for energy use prediction and energy auditing (Colorado State University, Fitchburg State University, Fitchburg, Massachusetts, United States, 2013; IES-VE, 2017). Other energy performance software such as HTB2 and Heat Transfer through Building (HTB), were developed by Cardiff University for energy consumption evaluation. The software used for calculating the influence of the outdoor microclimate conditions through the building fabric, and it is generally used by the university students (Jones and Alexander, 1999). The software developed by Welsh School of Architecture (WAS) by integrating the Sketch Up software and produce the VirVil energy auditing software (Bassett et al., 2012).

On the other hand, the detailed simulation capabilities software Energy Plus is one of the most accurate software programs that is also used for indoor energy performance, but it requires a high level of user experience and a good level of knowledge in mechanical systems (Al Zanfer, 2014). From the above, the energy consumption evaluation software and the availability of these software are limited compared to the IES-VE, which is available for educational use with a detailed and wide range of tutorial resources, therefore, the IES-VE is the selected software for the indoor energy performance.
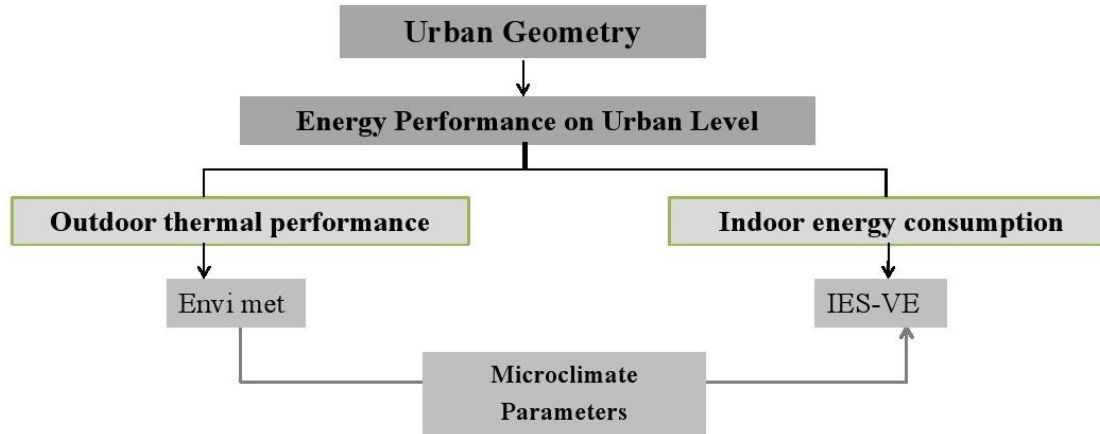
Figure 3.12: Software selection for the urban geometry and energy consumption simulation
(Author, 2108)

The following sections will illustrate the capability and the limitation of the two software programs that will be used in this research: 1) ENVI-Met and 2) Integrated Environmental Solution -Virtual Environment IES-VE. In addition of the selected grid size and dimensions for the base case and proposed scenarios.

3.4.2.1 The ENVI-Met 4.1 Microclimate Simulation Software

The ENVI-Met program is the selected software for outdoor thermal behavior prediction. ENVI-Met is a German production software developed by Bruse (1999) and the latest version ENVI-Met v.4.1 was released in November, 2016 (Bruse 2016). The software has been used for urban and microclimate studies by many researchers in order to predict the atmospheric changes within the UCL (Bruse, 1999; Johansson, 2006; Ali-Toudert and Mayer, 2007; Fahmy and Sharples, 2009; Meng et al., 2012). The ENVI-met software is a grid based, three-dimensional model in three versions or dimension sets: (100*100*40), (150*150*35), and (250*250*25). The range of each grid cell size is varied between 0.5m and 10m to provide high resolution with available boundary.

The resolution varied between 5 pixel /grid and100 pixel/grid in each version. The software adopts the finite element to calculate the CFD parameters in each grid point (x, y, z). It has been developed according to algorithms of the CFD equation package; the Navier-Stokes equations for wind flow, energy and momentum equations, and E-ε atmospheric flow turbulence equations. The heat flux and short-wave radiation at any point (x, y, z) is calculated based on the number of points exposed to the sun, in addition to the surface albedo and vegetation distribution. While the long-wave radiation is calculated at any point depending on the horizontal reflected long-wave, walls, and ground surfaces reflection. The software is basically developed to simulate the micro climate parameters in urban space covering; air flow, heat exchange, vapor exchange, vegetation effect, particles turbulence and dispersion. Moreover, the software allows distribution on a three-dimensional model microclimate urban parameters, covering heat flux, radiation, wind speed, and Predicted Mean Vote (PMV)(Peng and Jim, 2013). Further to that, it provides a daily profile for wide range of output parameters includes; air temperature, relative humidity, wind speed and direction, Mean Radiant Temperature (MRT), and CO_2 emission (Lahme and Bruse, 2003). Moreover, the software calculates the SVF as one of the geometric parameters for urban modelling. The software operation depends on setting the initial physical dimensions and climatic conditions of the simulated model covering; air temperature, wind speed, buildings specifications, soil prosperities and plant types. The setup of the software initial conditions is divided into two groups; 1) The physical morphology data covering model dimensions and position on earth, receptors position, plants position, and surfaces material distribution; 2) the micro climate data covers weather and microclimate parameters in addition to the simulation date and duration. The morphological data can be represented using the workspace area file, while all the microclimate conditions and micro climate data can be edited and saved in the configuration file.

Figure 3.13 shows the general input and output data flow through software processes in addition to the types of input and output files. The ENVI-Met is user friendly software, it doesn't need a wide knowledge in setting weather and initial conditions data. Furthermore, assigning and editing specification and materials in the 3D model is not complicated.
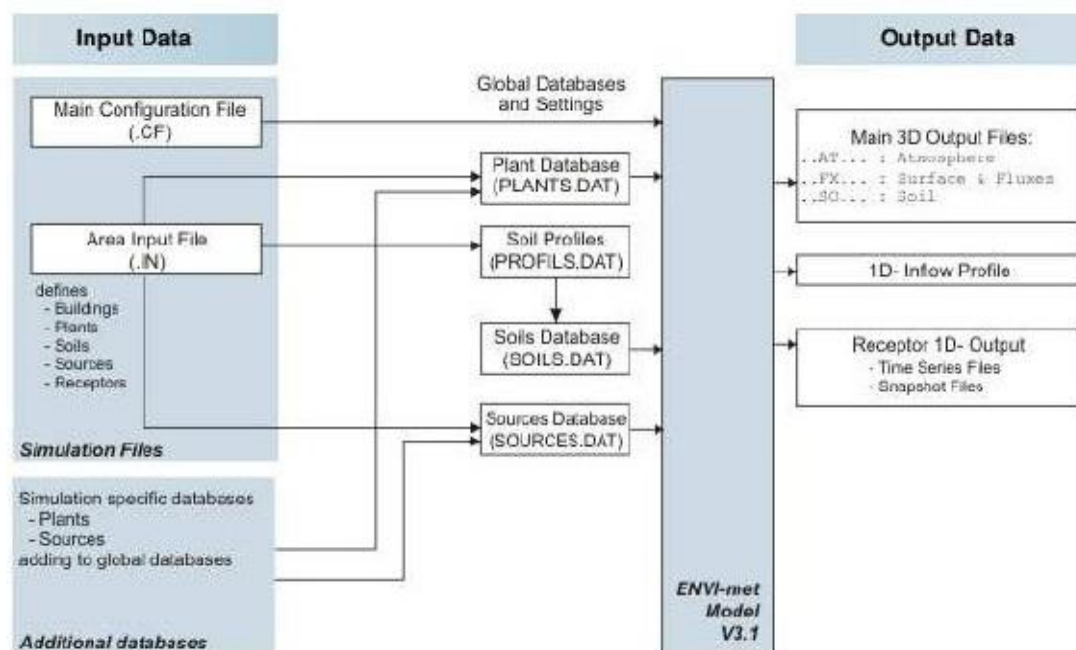
Figure 3.13: Input and output data flow in ENVI-Met 3.1 software (Bruse, 2004)

In term of output results, the Leonardo tool is the ENVI-Met visualisation tool that allows viewing the simulation results in two-dimensional (2D) and three-dimensional (3D) visual images. However, the validity of the software has been presented in a number of studies (Bruse, 1999; Gill et al., 2013).

Figure 3.14 shows the comparison between the measured and simulated data along 48 hours in a software validation process carried out by Gill et al. (2013). The figure shows the underestimation data reported by Al Zanfer (2014). However, the underestimation data can be avoided by increasing the simulation duration.
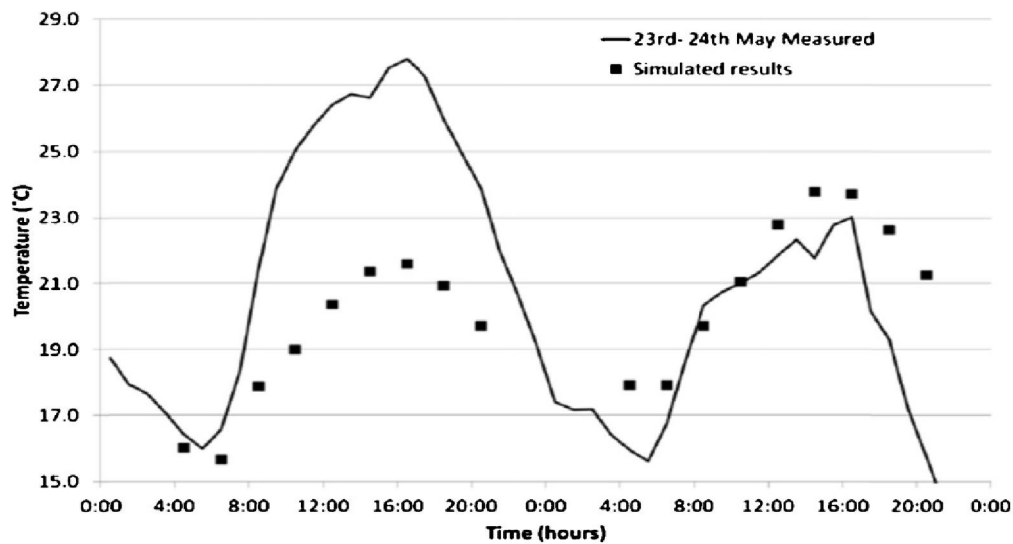
Figure 3.14: ENVI-Met v.3.0 validation, the measured and simulated air temperature along duration of 48 hours work (Gill et al., 2013)

In this research, the ENVI-Met 4.1 released in November 2016 is selected and will be used to predict the outdoor microclimate parameters, including: 1) air temperature, 2) wind flow, and 3) relative humidity, in addition to illustrating the SVF of the simulated models. The software will be used for predicting and analysing the microclimate parameters of the base case, further to predict the effect of the suggested scenarios on these parameters. The outcome data that will be obtained will be used as an input condition data for indoor thermal performance simulation software.

The IES-VE is the selected software program for simulating the indoor thermal performance It will be used to find the impact of the changes that occur in the microclimate parameters by buildings morphology on building energy performance. The latest version of the software ENVI-Met v.4.1 will be used in this research. In this version there is an enhancement in the use of specific tools, the interface and window arrangement. However, the ENVI-met v.4.1 will be used for analysing urban and outdoor microclimate parameters of the base case and to predict the effect of the suggested scenarios on these parameters.

The ENVI-Met 4.1 Software Limitations

Reviewing the previous studies that used the ENVI-Met software, and through the use of the software in this study, a number of limitations are indicated. The most prominent limitation indicated is the grid size limitation. The available version for student use is (100*100*40), while the advanced version Science and Professional the (150*150*35) and (250*250*25) simulation versions. The cell selected size is varied between 0.5m and 10m. The version selected for simulation controls the boundary of the selected model. This is one of the software limitations that controls the maximum urban area that can be simulated.

The second limitation is related to the maximum height of the simulated model. As increasing the version size in the x-y directions affects the size in the z direction, the maximum height that can be simulated is controlled by the available cells in the z direction and the developed model size depends on the selected version. Increasing the model size in the x-y directions requires reducing the height of the model in the z direction, and this is indicated as another limitation in the software. Furthermore, as there is no statistical data that proves the accuracy of the selected boundary, the applicability of running the simulation process can only be checked through the simulation report, the report mentions any error in the boundary dimensions before the simulation process. The challenge of selecting the appropriate grid size and model boundary was overcome by checking the setting of the model with different scale for x, y, z grid size, and these models were checked before running the simulation process. Verifying and checking the model shows different errors and comments, the print screen of the comment that were followed to reach to the most accurate and acceptable grid size specifically with the maximum height of the model is presented in the appendix. The third limitation related to the modelling tools capabilities. The software generally used for modelling strait line shapes, a curved line cannot be modelled as the software grid cell is fixed into a square shape only.

However, the model selected for this study does not contain any curved lines as it adopts the pavilion, grid configuration for the urban block. Furthermore, the use of the software tools through the modelling process does not have any options available in other modelling software, such as copy, cut, past and trim options. Moreover, the data extraction and generating graphs in ENVI-met needs to be developed. There is a lake in statistics presentation as the only way for data extraction is exporting the data to Excel file or spread sheet, therefore, this limitation was overcome by using the Microsoft Office software to illustrate the data as graphs and charts. Finally, the software provides a daily output results only, other option for monthly or annual simulation duration and data extraction from same simulation cycle is not applicable. Beside that and in spite of the advantages of its high resolution, the software takes a long time for simulation, as the time step dt= 2s, therefore, it takes more than 24 hours to run the simulation cycle depending on the device specifications. However, running the simulation processes requires the usage of laboratory devices for more than one day in order to simulate the 56 scenarios of this research.

3.4.2.2 IES-VE Software for Indoor Energy Performance Simulation

The third phase of this study is to find the effect of the base case study and the suggested scenarios on the energy performance of the urban block or complex. For this aim, the IES-VE software will be used. In this research the IES-VE software will be used for it is accuracy, capability, validity and the continuity in progressing to comply with marketing and academic requirements (Bruse, 2004; Gill et al., 2013). The IES-VE software is recently and widely used for simulating the indoor thermal performance of the buildings, the capability of the software allows to use different buildings configuration and materials. The software covers number of application, and each application generates a number of output parameters, Sun cast, Apache simulation, radiance and fluxpro are software applications that can be adopted to predict the buildings environmental performance.

Furthermore, the software generates a wide number of environmental parameters covers; indoor air temperature, solar gain, shading effect, external and internal conduction gain, relative humidity, comfort index, heating and cooling plant load, and so on.

However, in this research two IES-VE applications will be used: 1) Sun Cast application and 2) Apache application. The Sun Cast application will be run to simulate solar radiation and shading analysis using the same day used for the outdoor ENVI-Met simulation, the capability of IES-VE simulates the sun's path around the buildings at any specific time of the day. The 'Sun Cast' application is the solar / shading feature analysis in the IES-VE, it enables to view shading or solar energy on a 3D model, determine parameters for analysis – time period covers one year, and understand the intensity of the sun on the external building facade . The solar exposure simulates the direct shading only. In order to run the 'Sun Cast' simulation the parameters can be set for a specific period or one year analysis.

The Apache application will be used to find the total cooling plant load the of the block in the same selected simulation day. Figure 3.15 shows the initial data required to be set prior running the IES-SE simulation process.
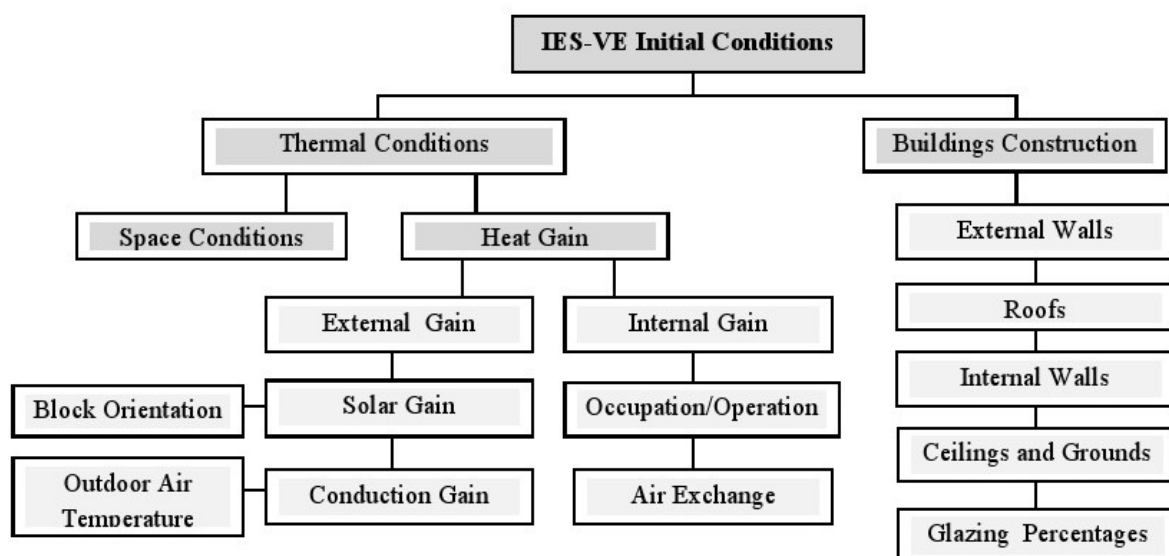
Figure 3.15: Flow chart of Initial conditions required for running the IES-VE software (Author, 2018)

In this research the base case of a building complex and the suggested proposed scenarios will be modelled in IES-VE using the same grid dimensions that is used in ENVI-Met. However, the hourly microclimate data results from using ENVI-Met software will be used as an initial input data in IES-VE. The data obtained from using the ENVI-Met will be exported to a spread sheet to show the microclimate data of each point with x and y coordinates.

The snapshot data generated from ENVI-Met will be edited as a design data in the weather file of the IES-VE software.

The IES-VE Software Limitations

The capability, validity and accuracy of the IES-VE software had been proved in number of publications. However, the limitation of the IES-VE indicated related to the software CFD capability. A wide range of weather data is built-in with the software covers all over the world, and simulating the weather conditions is selected according to the location or re-join of the study prior the simulation process. However, this built-in weather data generally adopted for the indoor thermal performance prediction for the model in any location and climate zone. The first and major limitation indicated in the IES-VE is the disability of the software to provide the variation in outdoor micro climate or microclimate data. Therefore, the observed shortage in the IES-VE software requires another software for CFD simulation that can provide the outdoor thermal performance parameters. In order to overcome this limitation, and to achieve the research objectives of assessing the effect of the variation in outdoor microclimate parameter on the indoor thermal performance, another simulation software was required for CFD analysis.

Hence, this was the reason behind using the ENVI-Met as an outdoor micro climate data simulation software. The ENVI-MET is used to answer this research questions related to the

effect of urban geometry on outdoor thermal performance and microclimate conditions at the first stage of the simulation processes.

The other limitation of the IES-VE software is the limitation in editing the desired microclimate data in terms of outdoor environmental parameters. However, some of this data can be edited to the weather file with limited conditions. The parameters that can be edited is the air temperature covering maximum and minimum dry bulb and wet bulb. Wind speed, relative humidity or outdoor pollution particles cannot be adjacent in the stored weather file. In this research this limitation was overcome by edition the maximum and minimum air temperature extracted from the ENVI-Met simulation software, and the humidity were represented by the wet bulb temperature. Nevertheless, the wind speed effect represented by the ENVI-Met CFD simulation software.

3.5 Procedures of linking ENVI-met to IES-VE Software Data

The data results from using ENVI-Met software will be used as a boundary condition to run the IES-VE simulation process. The generated data from the ENVI-Met represents the outdoor microclimate conditions for IES-VE indoor simulation software. The first stage is generating all outdoor microclimate data using the ENVI-Met software. The second stage is evaluating and analysing the results and find out the notable variation in microclimate data. The variation will be assessed according to the orientation and urban topology effect on outdoor microclimate parameters. The weather file in IES-VE not applicable to be edited, but outdoor design air temperature can be forced to replace the effect of the weather file conditions. This temperature will be extracted from the ENVI-Met simulation results.

The average of air temperature will be obtained from the nine receptors mentioned in ENVI-Met simulation procedure, and at a height of average building centroid from the ground level (Yang, 2012; Al Znafer, 2014).

The procedure of coupling ENVI-Met and IES-VE represents one-way coupling, no feedback data will be reversed to the ENVI-Met models. However, the initial conditions cover air temperature, wind speed and direction, relative humidity required to run the ENVI-Met simulation will be illustrated in the next sections. Furthermore, the hourly output metrological data of the simulation day 21st of June will be started at 5:00 am to 5:00 am on 22nd of June.

The maximum and minimum outdoor dry and wet bulb air temperature edited manually to the IES_VE weather file according to the extracted data of each configuration and orientation obtained from ENVI- Met. The IES-VE output result covers a number of indoor thermal parameters that reflect the effect of outdoor microclimate parameters on indoor thermal performance.

3.6 The Computer Software Validation

3.6.1 The Validation of the Outdoor Microclimate Simulation Software ENVI-Met

In order to validate the accuracy of the selected microclimate simulation software ENVI-Met v.4.1, a pilot study was conducted to collect the field microclimate data required to be compared with data generated as a simulation results. The pilot study was conducted in the selected case study location on 26th of February, 2017.The site located in Dubai, in The Greens compound of mid-rise buildings.

The chosen site consists of eight buildings as a combination of G+4 and G+7 buildings. The dimensions of the G+4 buildings are 25m*60m, and the dimensions of G+7 buildings are 25m*30m. The average height of each floor is 4m and the total height of each type of buildings is 20m and 32m, respectively. Figure 3.16 shows the selected area for software validation. The main street and canyon of the block is 20 m in width, while the setback between the buildings is 10m. Four types of plants were observed that forms the landscaped

and planting area in the setback canyon between the buildings. In addition of the few number of plants are distributed in the main canyon/ street between the buildings. Figure 3.17 shows the location of the measurement tool in the main canyon.

Figure 3.16:The canyon in the case study area for software validation(Author, 2108)

3.6.1.1 The Microclimate Measurement Tool and Data Collection

The tool that is used for the microclimate data measurements and collection is the 4-in-1 Environmental Meter-model 45170.This tool allows to measure four of the microclimate parameters at specific point. The parameters that can be measured using this tool covers: Air Temperature, Relative Humidity, Air flow and light level. The tool is an ergonomic pocket size housing, with a LCD simultaneous display of weather data (Figure 3.17). Furthermore, the tool allows to hold the displayed value and records the Min/Max readings. The range of the measured air temperature by this device is varied between 0° C - 50° C, while it can dedicate the wind velocity from 0.4m/s up to 30m/s. The accuracy of the device for air temperature and wind velocity is ±3% and ±1.2 ° C respectively. In this research, the data collected for the software validation covers the air temperature over12 hours. The data was collected from specific point in the chosen site at a level of 1.4m, and it is compared with

receptor data generated using the ENVI-Met v.4.1 at the same level using the ^{o}C unit (Figure 3.17).

Figure 3.17: The location and the tool used for microclimate data measurements (Author, 2108)

3.6.1.2 The Simulation Model, Process and Results

The indicated site was modelled using the ENVI-Met software v.4.1. The grid dimensions selected is 80*40*40 to represent the x,y,z dimensions of the model respectively. The cell size selected is x=5, y=5 and z=2. The weather file has been chosen from the built-in weather files that indicates the sun path and solar access of the location of Dubai, UAE. In addition to the block of the buildings mentioned previously, the site consists of four types of planets in general. The plants were represented by using the built-in vegetation types in the ENVI-Met v. 4.1 database. The first type is (AC) Acacia with a height of 2m and crown width of 3m. The second type is (PI) Pine Tree with a height of 4m and crown width of 5m. The (ZI) Zitrusbaum is the third type with a height of 4m and crown width of 3m. The fourth type is (A3) KL.Robinie with a height of 12 m and crown width of 7 m.

The initial setting data used for running the software covers location indication, air temperature, relative humidity, wind speed and direction. The initial temperature of starting the simulation process is 21°C, wind speed is 3m/s, and the relative humidity is 64 %.

Other values related to planet and soil specifications are kept according to the default data built in the software file database. The simulated model and the measured data is illustrated in detail in appendix A.1. The microclimate parameter selected for software validation is the air temperature, and one receptor is indicated in the model to represent the exact location of the site station. The data collected at level of 1.4 m over 12 hours of measurement starting from 7:00 am to 7:00 pm, with a records of air temperature at the beginning of each hour. The simulation starting time has been chosen is 4:00 am before the sunrise and continuo for 24h to avoid the underestimation data reported by previous studies (Emmanuel and Fernand, 2007). Figure 3.18 illustrates the calibration between the measured and simulated air temperature, and a good and strong correlation is found at the starting and ending of the simulation loop respectively. However, some variation has been observed at the peak time.
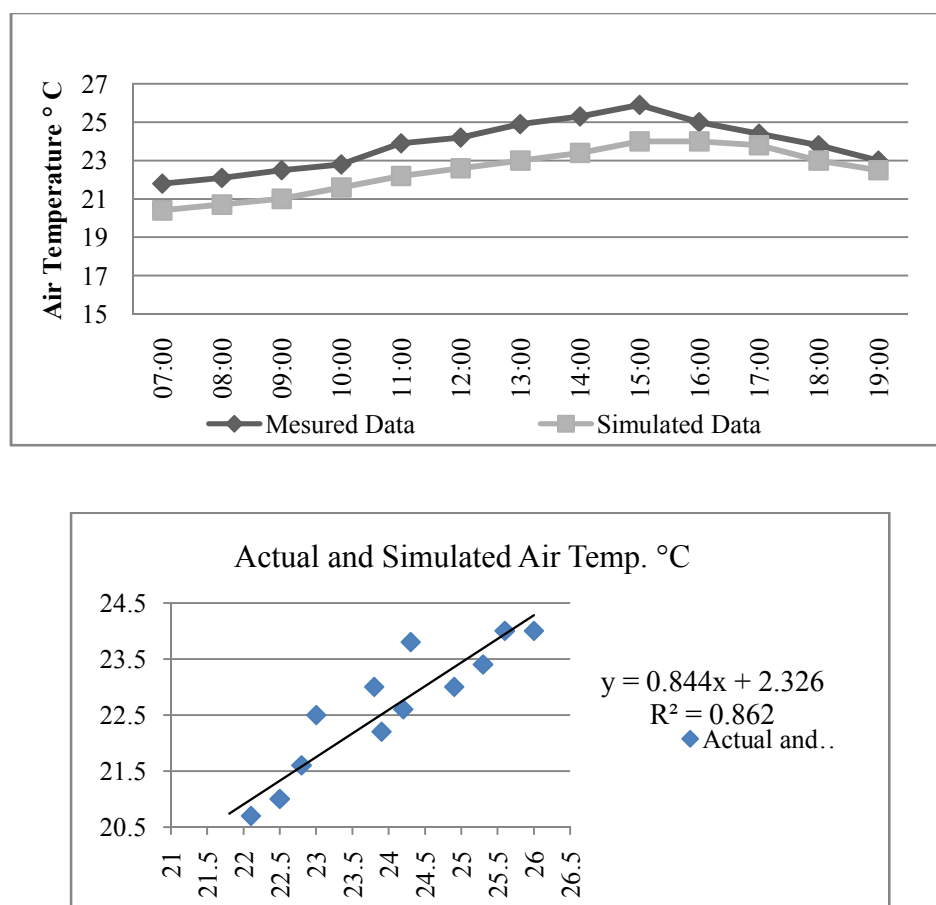
Figure 3.18: Measured and simulated data relation for ENVI-Met software validation on 26th of February (Author, 2018)

The variation in the data between 1:00 pm and 5:00 pm may related to the transportation effect on increasing the actual measured air temperature as this is the time of school bus drop off, and this residential area is occupied by families with 2-3 number of children in average.

Furthermore, the validity of the previous versions of the ENVI-Met software has been proven in many studies (Ali-Toudert, 2005; Meng et al., 2012; Al Znafer, 2014). Figure 3.19 shows the strong relation between the measured and the simulated data using the ENVI-Met 3.1 (Tseliou and Tsiros, 2016).
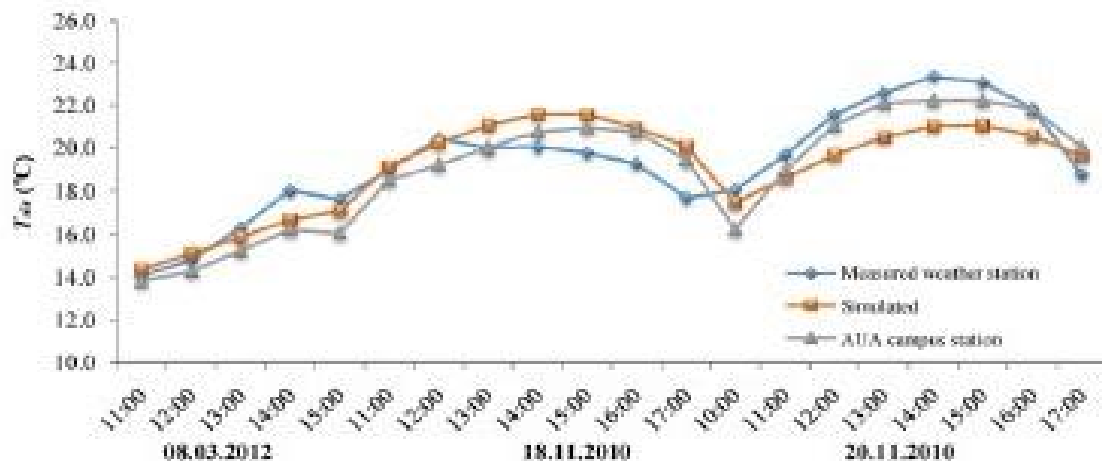
Figure 3.19: ENVI-Met v.3.1 validation (Tseliou and Tsiros, 2016)

3.6.2 The Validation of the Indoor Thermal Performance Software IES-VE

Many published studied proved the validation of the IES-SE software (Al-Masri and Abu-Hijleh, 2012; Taleb, 2014). However, the software has been validated in a previous study conducted to evaluate the indoor thermal performance for Al Waha nationhood in Dubai, UAE. The community consists of 206 semi-attached villas, the villas are designed in three types according to bedroom number: two, three and four. The facilities are very limited in the community covering swimming pool, playground area, landscape and hardscape (Figure 3.20).

Figure 3.20: The case study for data collection used in IES-VE software validation (Author, 2018)

3.6.2.1 Data collection and Validation Process

One villa of is selected for the software validation. The indoor air temperature of the villa for one day and 12 hours data is evaluated against the values obtained from modelling the villa using the IES-SE and running the simulation for the indoor thermal performance. The initial condition set for running the software covers, thermal and construction files.

The thermal file contains the internal gain including occupant and lighting gain, while in the construction file the material used in villa is adopted. The simulation has been run for one day 3rd of February 2015. However, no indoor air conditioning system was used during the measurements day.

Figure 3.21 shows the measured and simulated data for the mentioned day. The data measurements started at6:30am and continues for eighteen hours till 11:30 pm with a variation between the actual and simulated data. This variation is less in the afternoon when the highest air temperature degree was recorded. However, the highest variation observed is 3.3 %, the validity of the software is acceptable, and the software is valid when the variation between the measured data and the simulated data is less than 5% as highlighted by Rahman et al. (2008).
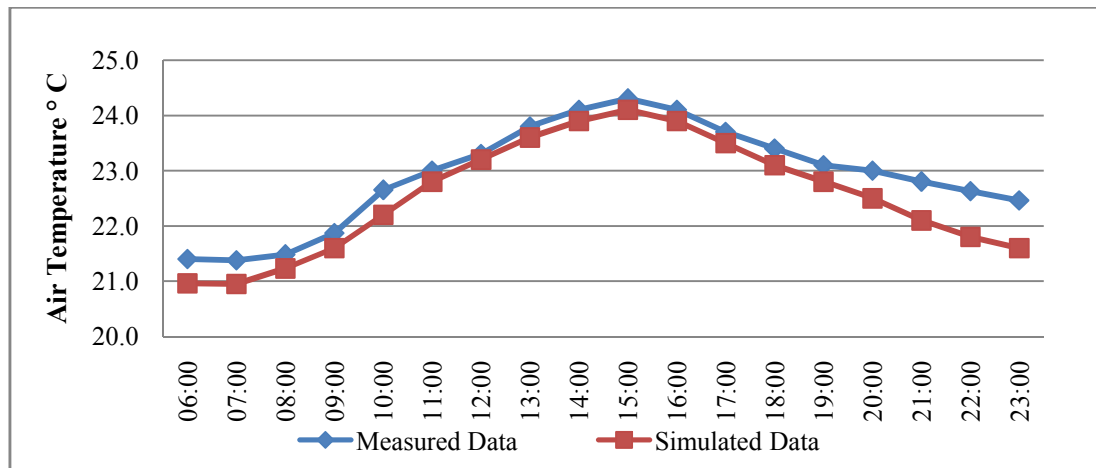
Figure 3.21: The measured and simulated data for IES-VE software validation on 3rd of February
(Author, 2018)

Furthermore, the validity of the IES-VE software against the actual data and the design builder software has been addressed by Taleb (2014), figure shoes the validation of the software along one-year actual data (Figure 3.22).
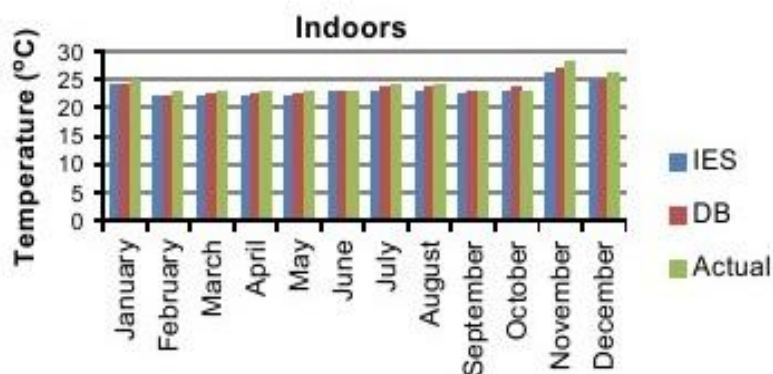
Figure 3.22: Validation of the IES-VE software against the actual data (Taleb, 2014)

3.7 The Developed Proposed Scenarios Climatic Strategies

The criteria behind developing the proposed scenarios follows the climatic urban design strategies mentioned in section 2.10 in the previous chapter. The previous studies stated the most effective urban geometry variables in enhancing microclimate parameters of the canyon space. The selected urban geometry variables for this study cover; 1) canyon orientation, 2) buildings' height diversity, and 3) buildings' configuration.

132

The climatic urban design strategies aim to reduce the effect of solar gain and to increase the effect of potential wind. For this aim the selected urban design variables for reducing solar gain are; the canyon orientation and the height diversity. In the suggested scenarios, the main canyons will be oriented in four directions as will be presented in detail in the next chapter. The E-W, NE-SW orientations will investigate the effect of the sun path and solar radiation on the urban block. The N-S and NW-SE orientations will explore the effect of the wind on the urban block thermal performance. Height diversity will be adopted to create the shading effect by simulating significant and gradual diversity in buildings height. Furthermore, and for increasing wind speed previous studies proved the effect of adopting the potential wind on enhancing the thermal performance of the built environment. Figure 3.23 presents the method of climatic design strategies that is followed to develop the proposed configuration of the three groups.
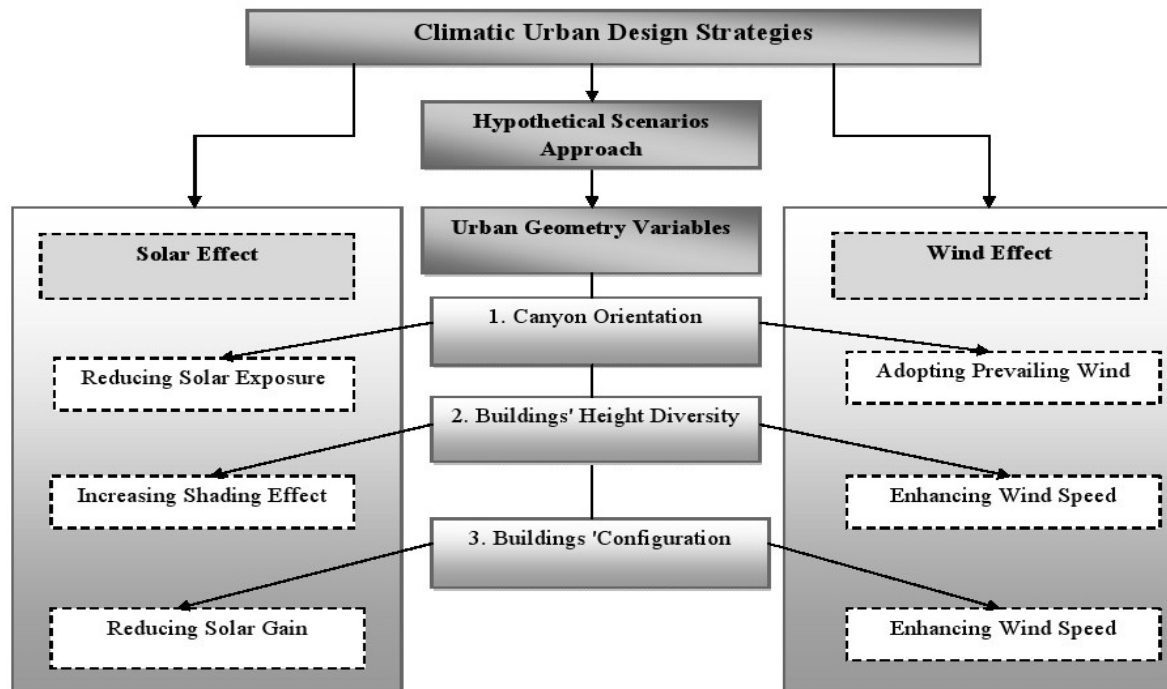
Figure 3.23: Climatic urban design strategies and proposed scenarios approach (Author, 2018)

The base case study simulation will be conducted on a complex or block of twenty-four residential buildings. Each building is 30m* 30m in floor area, with total height of G+5 or six floors, and according to the physical dimensions and measurements, the average selected height for each floor is 4m. The total built-up area of each building is 5,400 m² (900 * 6) m². The total built-up area of the model that will be simulated is 129,600 m² (5400 * 25) m².

The width of the main canyon between the buildings will be fixed to 25m, and the setback between two buildings is 15m. The simulation will cover different proposed scenarios for buildings heights and configurations. The fixed built-up will be used as an urban design indicator to compare the base case and the developed scenarios. The developed scenarios will be classified into three groups according to the selected urban geometry variables, each group will cover number of developed configuration.
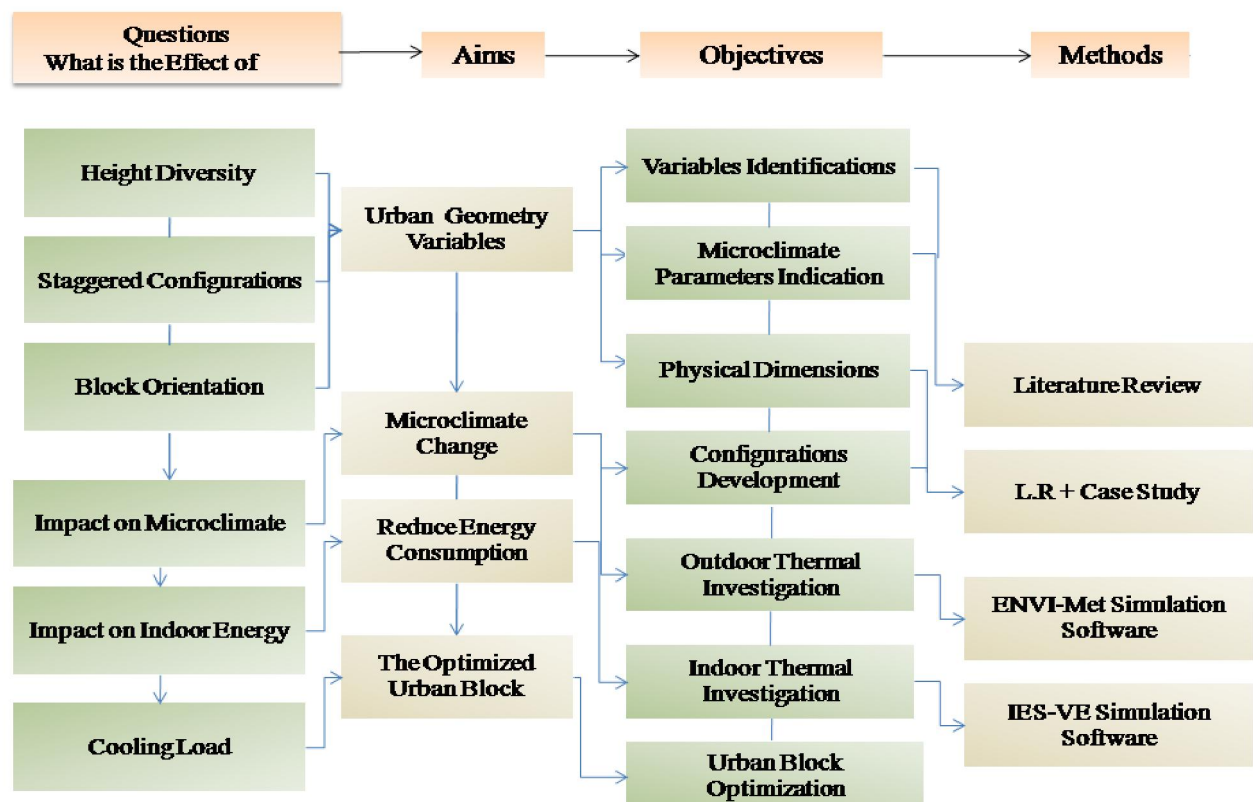
Figure 3.24: The research questions, aims, objectives and methodology mapping (Author, 2018)

Chapter 4

The Proposed Urban Block Configurations

4.0 The Proposed Urban Block Configurations

In this chapter, the basic methods and theories of sustainable urban form and block configuration will be illustrated. The methodological urban planning approach that is followed for generating the proposed scenarios will be explained in detail. The generated configurations will represent the contribution to the physical and spatial urban geometry and energy consumption of the buildings block as illustrated in the previous chapter. Furthermore, this chapter illustrates in detail the criteria that is followed in generate the proposed scenarios with respect to the urban planning and building regulation codes implemented in Dubai, UAE. The general dimensions that is related to canyon width and buildings height, further to the building standards and specifications, will be adopted. Finally, the chapter presents the proposed scenarios in groups, and explains in detail the variation between the base case and the developed scenarios, in addition to indicating the selected grid dimensions, and the initial conditions that will be used for running the simulation software.

4.1 Planning and Regulations for Sustainable Form

Urban and building planning regulations can be defined as employing the design theories and elements to achieve the sustainable form. As mentioned in the first chapter of this research, the sustainable form should provide the level of comfort required in terms of virtual, sound and thermal design. This will lead to providing the level of sustainability in the three poles; environmental, economic, and social. Therefore, integrating design elements and theories results to the desired sustainable geometry or configuration. This concept can be applied to city district, neighbourhood, community, complex and block planning.

Furthermore, the sustainable urban planning aims to achieve the better composition that provides the required outdoor comfort and indoor energy consumption. The reflection of this requirements can be noticed on the housing topologies.

However, it has been proved that the mid-rise buildings and the medium population housing provide higher level of sustainability (Marcus and Sarkissian, 1986; Heathcott, 2005; Fahmy and Sharples, 2009). This type of housing provides the opportunity to control environmental problems, in addition to providing the opportunity to adopt the climatic design strategies and manage the nature resources to create the desired indoor and outdoor environment. Therefore, the centralisation, compactness and management in planning midrise buildings and medium population housing offer more sustainable from than the low-rise and population housing. The controlling, centralisation and management in planning can be represented in the pattern planning; pattern planning is one of the planning strategies that can be adopted to achieve the sustainable form. Moreover, the pattern planning provides higher sustainable level in all design and construction stages. Figure 4.1 shows that the pattern planning can be applied in all design scales and phases; urban planning, building's facade and building fabric (Steemers, 2006).
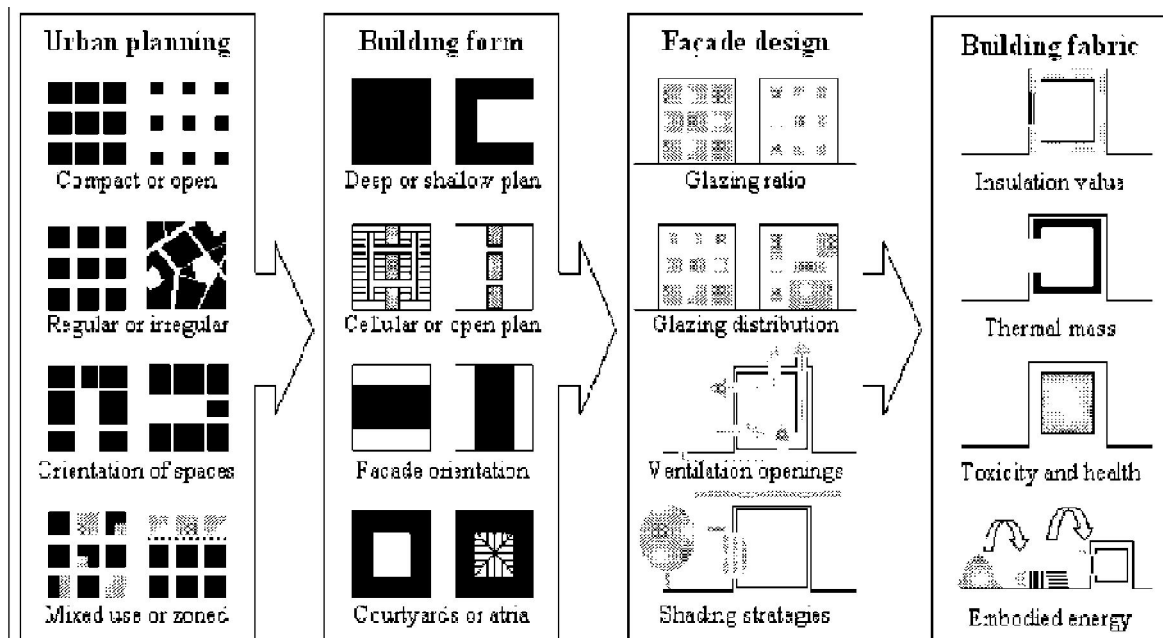
Figure 4.1: Pattern planning can be implemented from urban form to building fabric design (Steemers, 2006)

4.2 Cluster Planning and the Urban Compactness Elements

As mentioned in the previous section, pattern planning is one of the planning strategies that provides a high level of sustainability on planning and construction stages. Pattern planning, controlling, compactness and centralisation in planning can be represented in cluster planning. Previous studies proved the effect of the compact form on creating a comfort outdoor environment by reducing the exposure to sun access in hot arid climate locations (Neuman, 2005). On the other hand, the effect of the compacted form on other climatic parameters that control the outdoor climatic parameters should be taken into consideration. All outdoor micro climate parameters and natural resources, such as wind flow and ventilation, need can be included and adopted in cluster or block design (Johansson, 2006).

Exploring urban forms and configuration to find out the most sustainable form with respect to outdoor and indoor environment is one of this research aims. The compactness of any urban form can be achieved by planning for a high H/W ratio and accordingly a small SVF, in addition of providing a high BUA and floor area ratio FAR for any plot (Lehmann, 2010).

Keeping the BUA to the maximum allowed, is one of the developer targets, at the same time, planning for the desired outdoor comfort and minimum energy consumption is a major concern for the urban planner. This research investigating the potential of finding the best configuration or block of buildings that provides a minimum energy consumption compared to the other configurations. This will be explored on a block of buildings with a fixed BUA, and the height diversity and building configurations will be the urban design variables that will be employed for this aim, and this represent the guidelines that will be adopted to generate the proposed scenarios.

4.3 The Methodological Approach to the Development of the Proposed Scenarios

Developing the proposed scenarios utilised the urban configuration showed in figure 4.2 and presented by Martin and March (1972). The three basic urban forms presented in the figure are the Pavilion, the Court and the Street. In this study, the developed scenarios will be based on the Pavilion form. Moreover, the physical dimensions of the developed scenarios take in to consideration the physical dimensions observed and followed in Dubai urban planning codes and regulations.
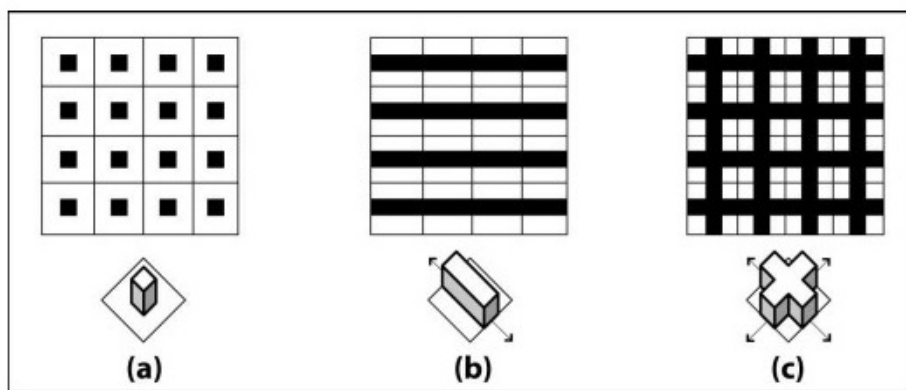
Figure 4.2: Buildings typology forms: (a) Pavilion, (b)Street, and (c) Court(Martin and March, 1972)

Martin and March (1972) presented the grid as an urban configuration generator; the same concept in urban planning was presented by Gropius (1966) at Harvard University. The grid as a planning concept can be found in block, neighbourhood and city planning. By presenting the three forms in figure 4.2, the authors simplified the complicated configurations of the real urban developments. The three types have been approached in many studies in urban topologies as an individual form or combined forms. Al Znafer (2014) employed the combination of the two forms, Street and Court, to express the urban configurations of old developments in Al Riyadh City. In this research the Pavilion form will be adopted to develop and study the urban topologies effect on the surrounding microclimate parameters. This form can be found in a number of existing compounds or communities in Dubai (Jumeriah Village Code, 2006), in addition to including this form in many regulation codes

for current and future developments (Business Bay Regulation Code, 2005; Jumeriah Village Code, 2006; Limitless, 2008). The dimensions of the developed configurations cover 1) building dimensions, and 2) canyon (street or alley) dimensions. Building, street, alley minimum and maximum urban dimensions are varied according to developed area and various development codes. The developed configurations dimensions are selected based on the observation of the case study and reviewing the building codes and regulations followed in Dubai, UAE. Figures 4.3 and 4.4 show an example of general urban dimensions mentioned in these codes. Figure 4.3 shows in detail the canyon dimensions presented in the development code of Downtown Jebel Ali. The main canyon (street) width in this code is varied between 23.5m and 25.7m (Limitless, 2008).
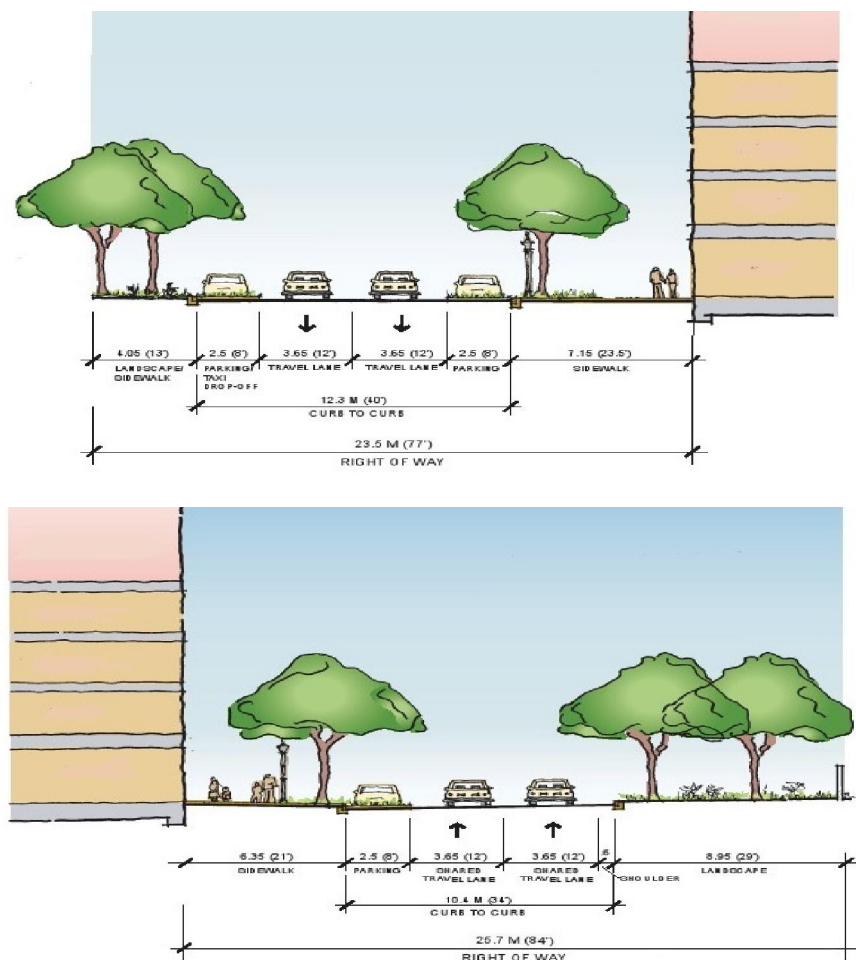
Figure 4.3: Example of canyon (street) dimensions in Dubai regulation Codes
(Downtown Jebel Ali regulation code, Limitless, 2008)

140

Figure 4.4 shows the alley or the setback between the two buildings. In the reviewed buildings and urban regulation codes, the setback is varied between 10m and 20m according to the use of this setback as a local street, driveway, alley, walkway or landscaped area.
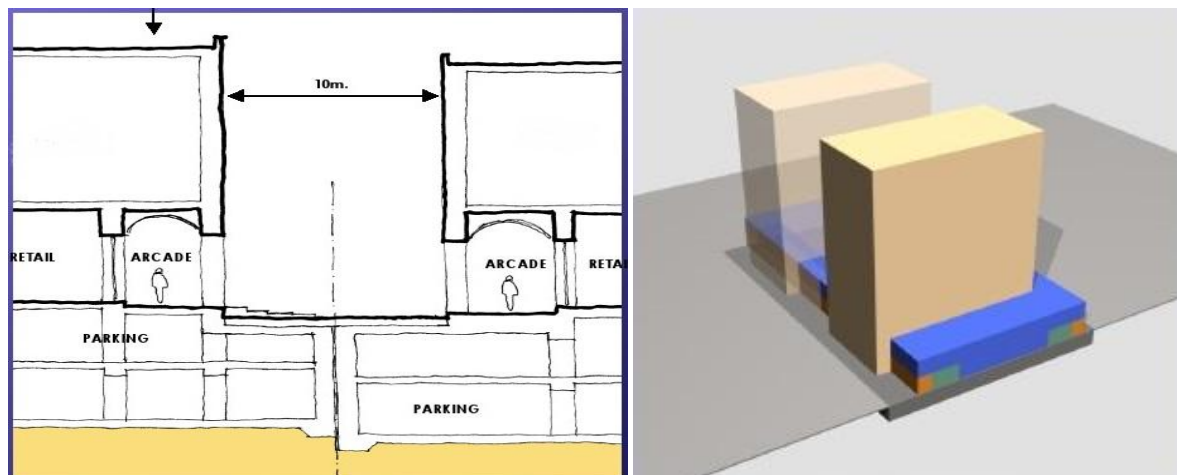
Figure 4.4: Example of alley (setback) width in Dubai regulation Codes
(Business Bay regulation code, Halcrow, 2005)

4.4 The Cluster Urban Form

The cluster form as defined in the introduction chapter of this research is a number of elements that are arranged and grow together (Porter, 1990). On the urban level, the cluster form provides the capability to adopt the climatic design strategies in order to achieve the optimised sustainable from with respect to resources efficiency. Moreover, the cluster form can be implemented to control the compactness of the urban form, it can be adopted in hot climate areas to increase the compactness and reduce the exposure to the solar radiation, in addition to providing a low-pressure outdoor area that can enhance the air movement, further to the use of these areas for greenery and water features for evaporative cooling (Golany, 1996). Therefore, the cluster form can enhance the sustainability on it is three levels, environmental, economic and social, hence, it is considered as the smart urban form (Swaid, 1992). However, this form can be implemented on all building categories: high, mid, and low-rise buildings.

The recent architectural and urban planning trend of constructing a prototype villa community is a good example of the cluster form in urban planning. Figure 4.5 presents two cluster forms in Dubai, UAE for low-rise and mid-rise buildings.

a) The Falcon City   b) Mirdif Hills

Figure 4.5: The cluster urban form in Dubai, UAE

4.5 The Development Criteria of the Proposed Groups

The development criteria of the proposed groups are based on developing a base case configuration and a number of proposed configurations. The base case will be represented in a complex or block of buildings with simple configuration and uniform height. The criteria behind the developed scenario are creating and evaluating diversity in buildings height and buildings configurations. The height diversity is going to be implemented in two directions: 1) height variation in the short axis direction, and 2) height variation in the long axis direction. On the other hand, buildings arrangement in the staggered configuration will be explored in different scenarios. Based on that, the developed scenarios will be classified into three groups in addition to the base case; the base will be simulated in four directions. Figure 4.6 illustrates the matrix of the proposed groups including the break - down simulation of the proposed scenarios in the four orientations.
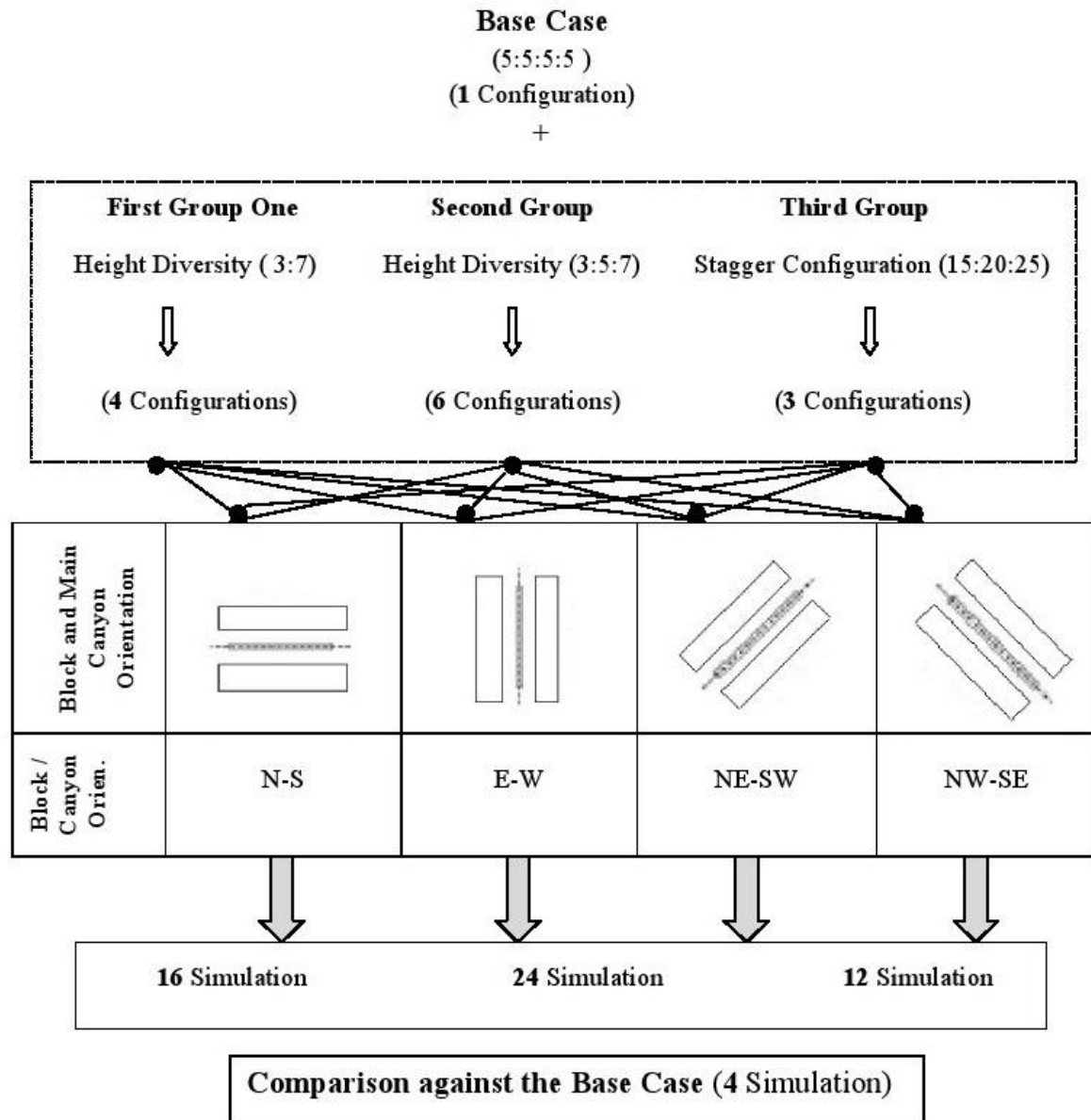
Figure 4.6: The matrix of the proposed groups showing the 56 proposed configurations
(Author, 2018)

The height variation in the short axis is represented in the first group, while the height variation in the long axis is represented in the second group. The third group will cover the staggered arrangement of buildings.

The first group consists of four scenarios according to the proposed variation in building height in the short axis of the block, while the second group consists of six scenarios according to the height variation in the long axis of the block.

The third group represents the variation in buildings configuration to form a staggered configuration, and this group consists of three configurations depending on the variation in width between the main canyons and the alleys. All configurations will be simulated in four orientations to result with 56 simulation model and result data sets.

4.6 The Physical Characteristics of the Proposed Configurations

The proposed block configurations are classified in to three groups depending on the variables that will be studied. Each group will consist of a number of scenarios or configurations. The simulation results of the suggested scenarios of each group will be compared to each other and to the base case. In the developed and examined scenarios, the adopted form the Pavilion has been placed in different configurations. However, general dimensions for plot area is adopted in order to evaluate the effect of the developed scenarios on the outdoor microclimate and indoor energy consumption. In the developed scenarios, the physical dimensions of the building and street width is adopted from the measurements collected from the case study that was used for the software validation.

In addition of using the urban regulation codes recommended dimensions. The dimensions of the plot selected for the proposed cluster or block is (400m*300m) with total plot area of 120,000 m^2. Therefore, the boundary dimensions of the selected grid for ENVI-Met simulation software will be (80*60) by assuming the cell size dx = 5, dy = 5, and dz = 2.

The height boundary dimension is varied according to the height of buildings, and it is assigned by the software as double the height of the highest building. This grid dimensions represent the total plot of the block and the boundary dimensions of the simulation model.

The buildings have uniform dimensions of (30m*30m), and the height of the buildings is varied according to the scenario or group configurations. Total building floor area or gross

floor area (GFA) for each building of the base case configuration and all configurations is 900m². The total BUA of the building according to the floor number is 5,400m² for each building in the base case. However, the total BUA of the urban block is 129,600m².

This BUA of the urban block represents the total BUA of the 24 buildings in all configurations of the three groups. The width of the main canyon (street) and the two side canyons is the same (25m) in all configurations of the first two groups, while the alleys width is fixed at15m. For the third group the canyon and alley width will be varied according each of the configuration settings.

Figure 4.7shows the plan, cross and longitudinal sections in x and y directions for the base case configuration. However, the same plan (top view) represents the first and the second group configurations. The sections (front and side view) will be varied according to the buildings height variation for each configuration in the two first groups.

Figure 4.8 presents the third group configurations, the plan or top view of each configuration is illustrated in figures 4.8 a, b and c for the three configurations of the third group. The details of each configuration and the width variation of the canyons and alleys will be explained in detail in the next chapter.
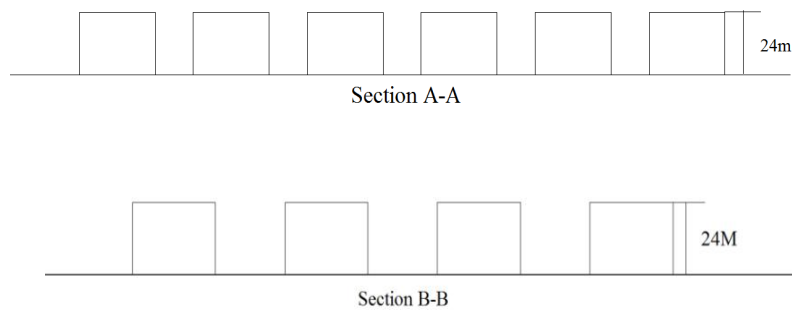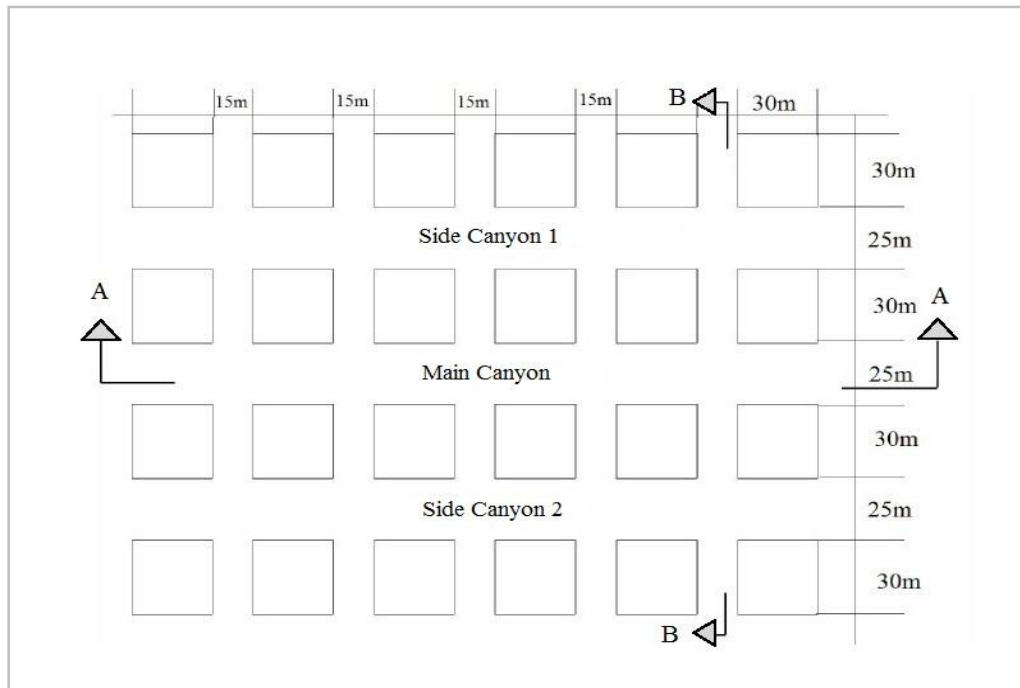
Figure 4.7: The plan and the two sections A-A and B-B along the long and short axis of the base case configuration (5:5:5:5) (Author, 2018)
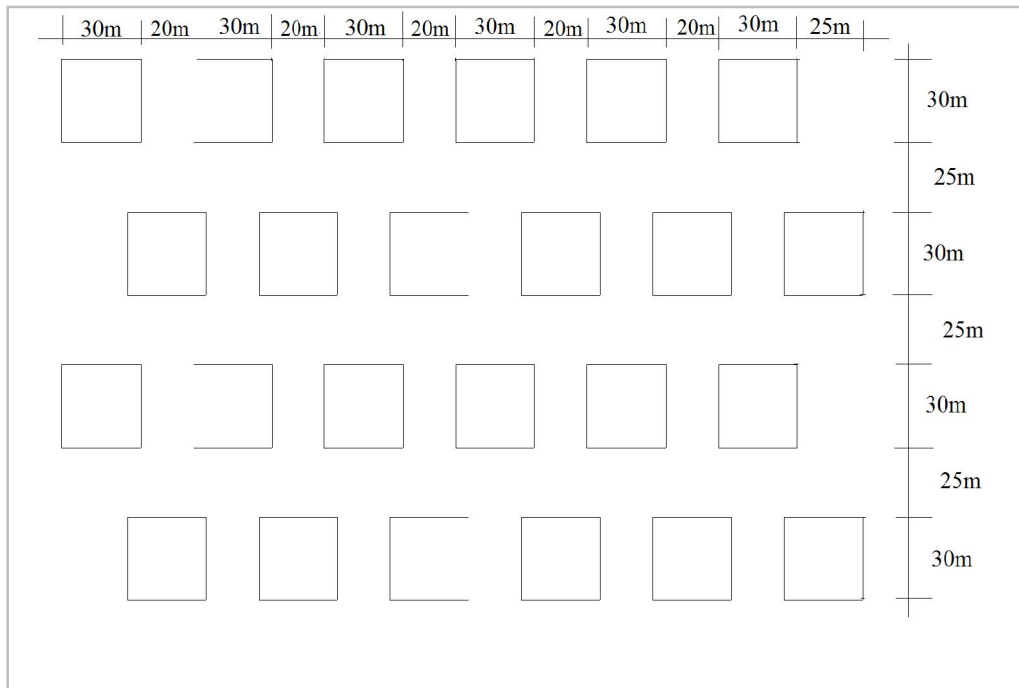
a) The top view of the first configuration in the third group, the uniform height 32m, main canyons width 25m, alleys width 20m G3-3.0 (25:20) (Author, 2018)
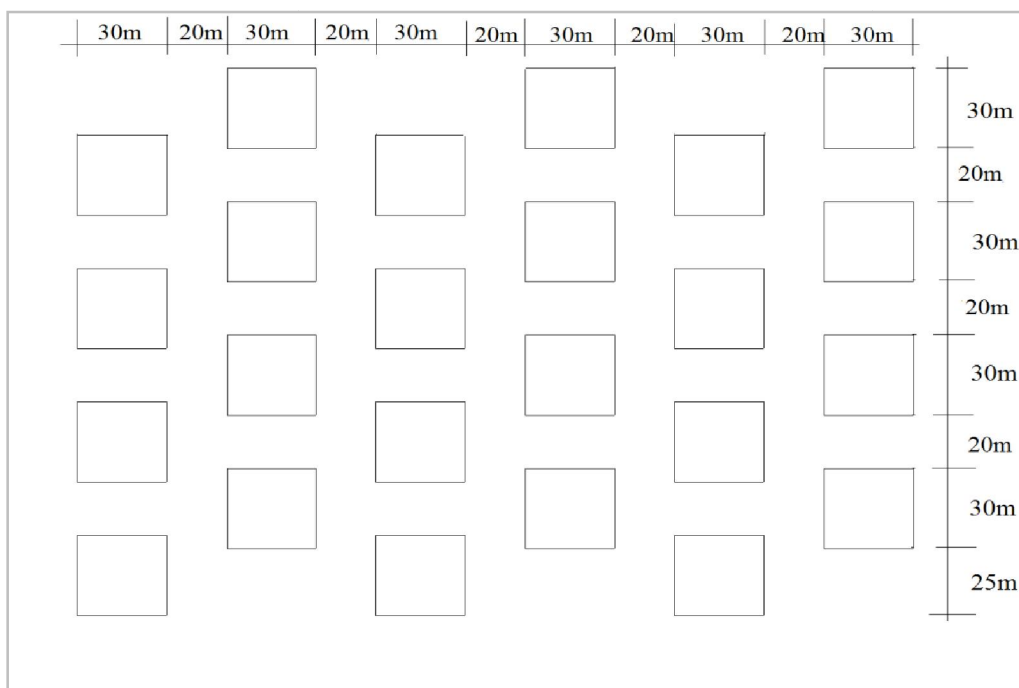
b) The top view of the second configuration in the third group, the uniform height 32m, main canyons width 20m, alleys width 20m G3-3.1 (20:20)
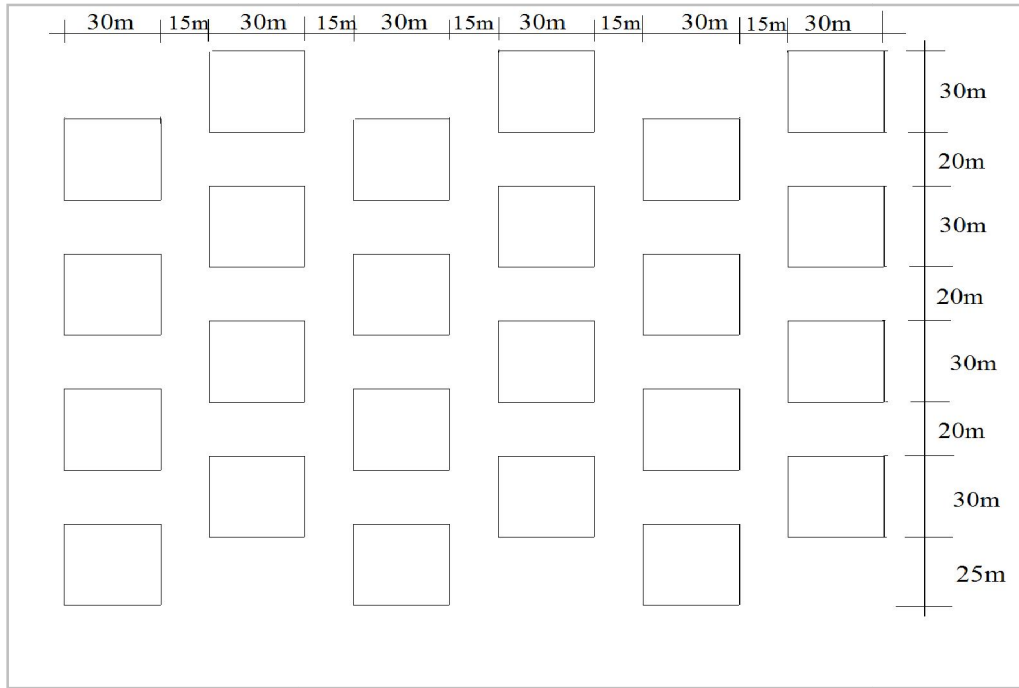
c) The top view of the third configuration in the third group, the uniform height 32m, main canyons width 20m, alleys width 15m G3-3.2 (20:15)

Figure 4.8: Plans of the third group three configurations (Author, 2018)

4.6.1 The Base Case Configuration

The base case represents the common and simple block of 24 buildings that forms the urban block. The buildings in this group are with one uniform height 24m as it is selected from the midrise buildings category, with a floor number G+5 and the average selected height of the floor is 4m.

The total built-up area of each building is 5400 m² and the total built-up area of the block is 129,600 m². The 24 buildings are placed in the Pavilion setting with one main canyon and two side canyons of 25m in width according to the data extracted from the urban planning codes followed in the UAE, Dubai. The vertical alleys or the setback between the buildings are with a width of 15m. Building materials and specifications extracted from the materials recommended in the green code and regulations issued by Dubai Municipality, and it will be illustrated in detail in the input data section for the simulation software.

The base case will provide a standard or the scale for comparing other groups and their different scenarios or configurations. Figure 4.9 illustrates the base case and the three groups of the simulated models and their descriptions.

4.6.2 The First Group Configurations

The first group is a configuration of 24 buildings that forms the urban block with a variation in buildings height. It represents building topologies and height variation along the short direction of the complex. The variation in building height is adopted and represented by the proportion of (3:7). Hence, two different height are implemented in this group; G+3 and G +7 with a buildings height of 16m and 32m, respectively. The total BUA for the whole block is kept as the same BUA of the general base case 129,600 m². This group consists of four different scenarios or configurations. The first scenario of this group is with a configuration of G1-1.0 (7:3:3:7) which represents the variation in height from higher to lower towards the centre of the block. The second configuration G1-1.1 (3:7:7:3) represents the block with fluctuated height for building arrangement, and the third configuration G1-1.2 (3:7:3:7) is developed by placing the highest buildings in the middle of the block. The fourth configuration G1-1.3 (3:3:7:7) adopting the variation in building height towards one direction from the lower to higher building. These four configurations will be simulated in four different ordinations: N-S,E-W, NE-SW, and NW-SE. Therefore, 12 models will represent this group and will be simulated in order to be compared with each other from one side, and with the base case from the other side. This comparison will be in terms of outdoor microclimate micro climate parameters and indoor cooling load consumption (Figure 4.9).

4.6.3 The Second Group Configurations

The second group represents building topology and height variation along the long axis of the block. The same configuration of the 24 buildings that forms the base case urban block is

selected with three different, gradual heights. The three heights with a floor number G+3, G+5, and G+7 and building heights of 16m, 24m, and 32m, respectively.

The first case of this group is G2-2.0 with proportions of (7:5:3:3:5:7). The other scenarios represent the height variation extending from the outer and inner directions of the block to form five more scenarios or models, namely: G2-2.1 (5:7:3:3:7:5), G2-2.2 (7:3:5:5:3:7), G2-2.3 (3:7:5:5:7:3), G2-2.4 (3:5:7:7:5:3), and G2-2.5 (5:3:7:7:3:5). Each model will be simulated in the four ordinations; N-S, E-W, NE-SW, and NW-SE to result in 24 different configuration and output datasets of the second proposed group (Figure 4.9).

4.6.4 The Third Group Configurations

The third group consists of three configurations. The criteria of developing this group is finding the effect of the stagger or alternative arrangement of the buildings on the canyon micro climate parameters. Similar to the base case and the two first groups, the block of the buildings in the third group contains 24 buildings with a uniform height of G+5 and 24m. Each configuration has the same total BUA of the base case with an area of 5,400 m² and 129,600 m² for the building and the block, respectively. The buildings will be arranged alternatively by placing the second row in the centre of the first row. Accordingly, the canyons width would be changed to achieve this arrangement. In the first configuration the alternative arrangement will be adopted in the long direction and the canyon width will be kept at25m, while the alleys width will be increased to 20m. In the second configuration the alternative arrangement will be in both directions of the block, hence, the canyons and the alley width will be the same width of 20m. The third configuration will represent the arrangement in the short direction, therefore, the alleys width will be the same as the base case 15m, and the canyons width will be reduced to 20m (Figure 4.9).

The Base Case Configuration
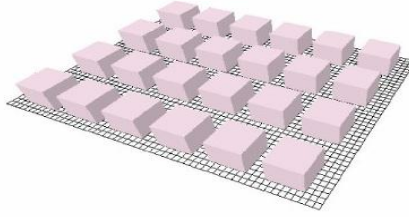
Base Case (5:5:5:5)

The First Group
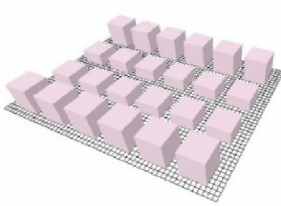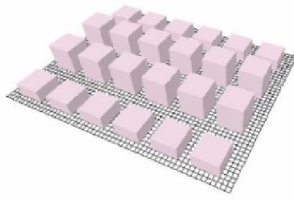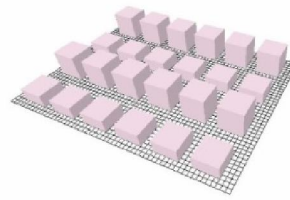
G1-1.0 (7:3:3:7)　　G1-1.1 (3:7:7:3)　　G1-1.2 (3:7:3:7)　　G1-1.3 (3:3:7:7)
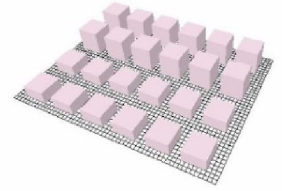
The Second Group
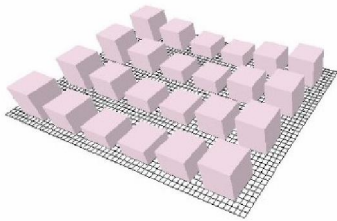
G 2-2.0 (7:5:3:3:5:7)　　G 2-2.1 (3:5:7:7:5:3)　　G 2-2.2 (5:7:3:3:7:5)
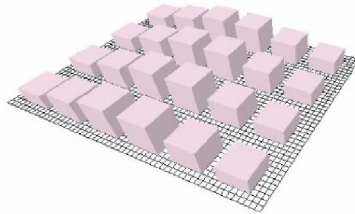
G 2-2.3 (7:3:5:5:3:7)　　G 2-2.4 (3:7:5:5:7:3)　　G 2-2.5(5:3:7:7:3:5)

G 3-3.0 (5:5:5:5)(25:20)   G 3-3.1(5:5:5:5)(20:20)   G 3-3.2 (5:5:5:5)(20:15)
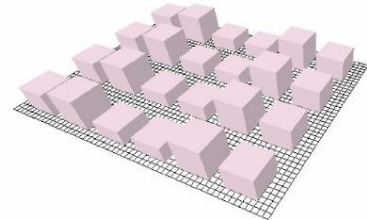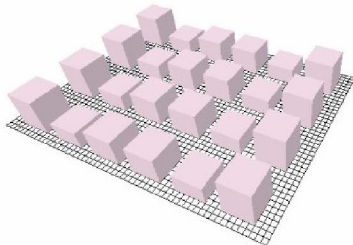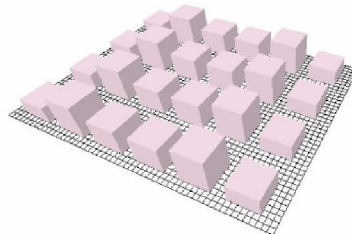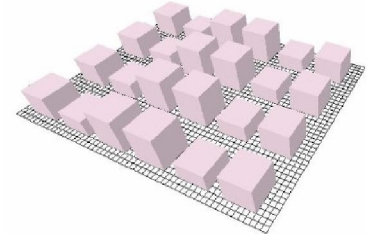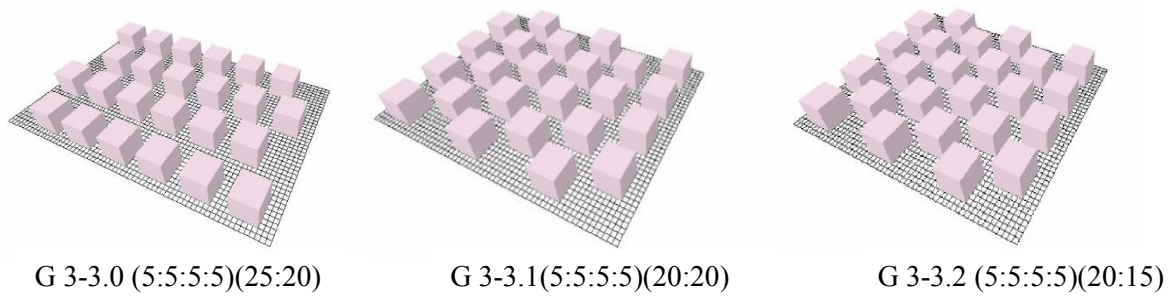
Figure 4.9: The base case and the three groups of the proposed configurations according to the studied variables; building height variation and alternative configurations

4.7 Initial Input Data for Simulation Process

4.7.1 Preliminary Studies, the Dubai, UAE Climate

Dubai is extended along the Arab Gulf in the north of the UAE. It is located on the 25°.25' N Latitude and 55°.33' E Longitude. Generally, the weather of the UAE is categorised as a hot desert or hot arid climate, but some references describe it as a tropical climate due to the high percentage of humidity (ESDAC, 2006) (Figure 4.10).
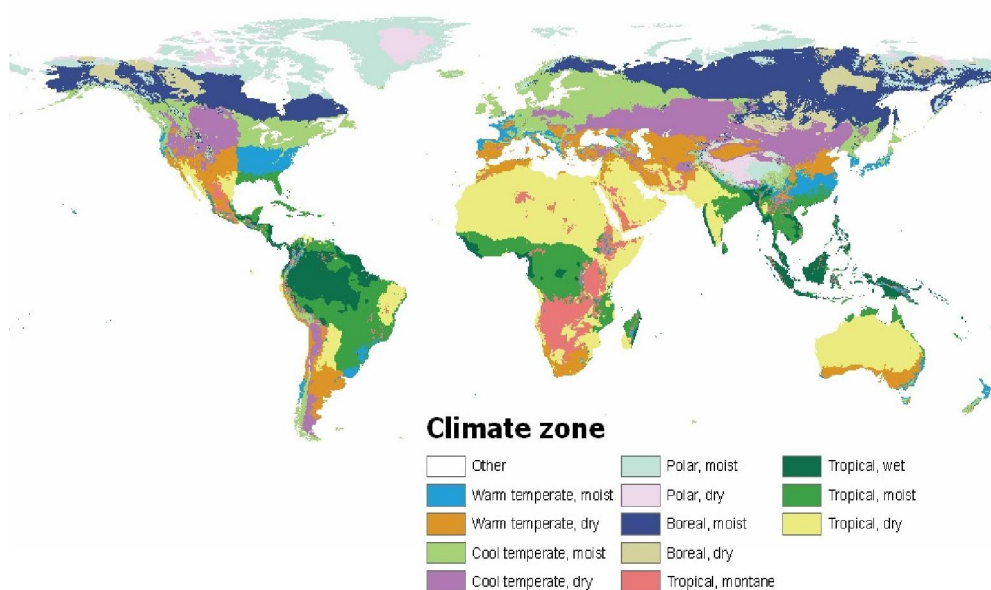
Figure 4.10: Earth Climatic Zones (European Soil Data Center ESDAC, 2006)

The weather in the UAE in general and in Dubai particular is sunny most days of the year. Figure 4.11shows the Sun Path in specific days over the year.
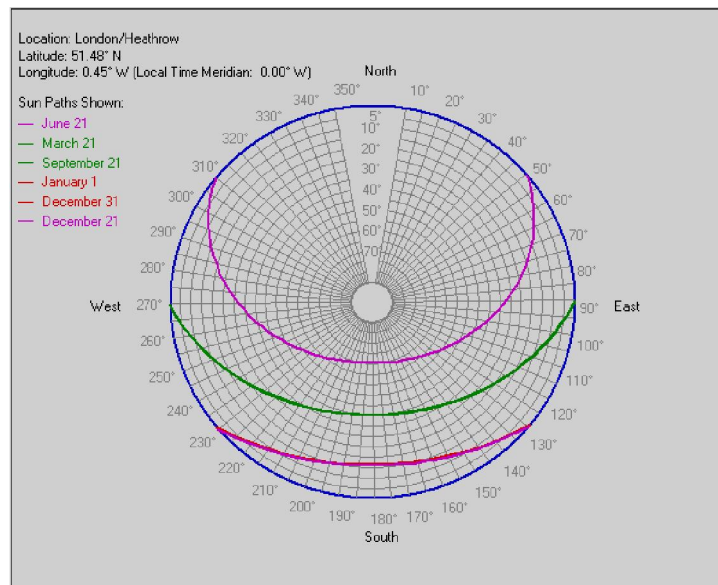
Figure 4.11: Sun Path during the year according to Dubai weather file (IES, 2016)

According to the location from the earth, the longest days in Dubai are20 and 21 of June with 13.42 hours of day time, while the shortest days are 20 and 21 of December with 10.34 hours of day time (Figure 4.12a). The earliest sunrise is on 9June at 5:27am, while the latest sunset is on 2July at 7:14 (Figure 4.12b). The black line in figure b shows the solar sunrise, solar noon and solar sunset over the year.
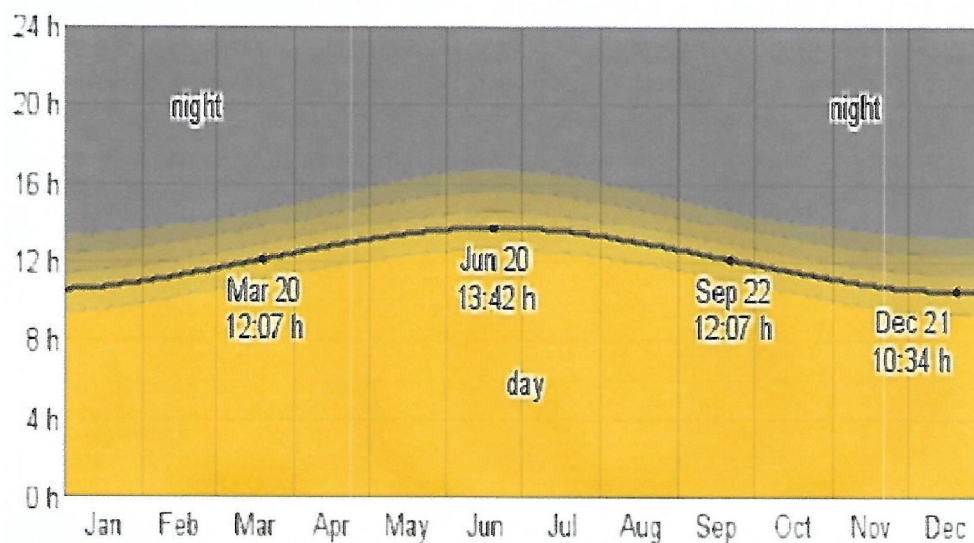
a) Daily Hours of Daylight and Twilight
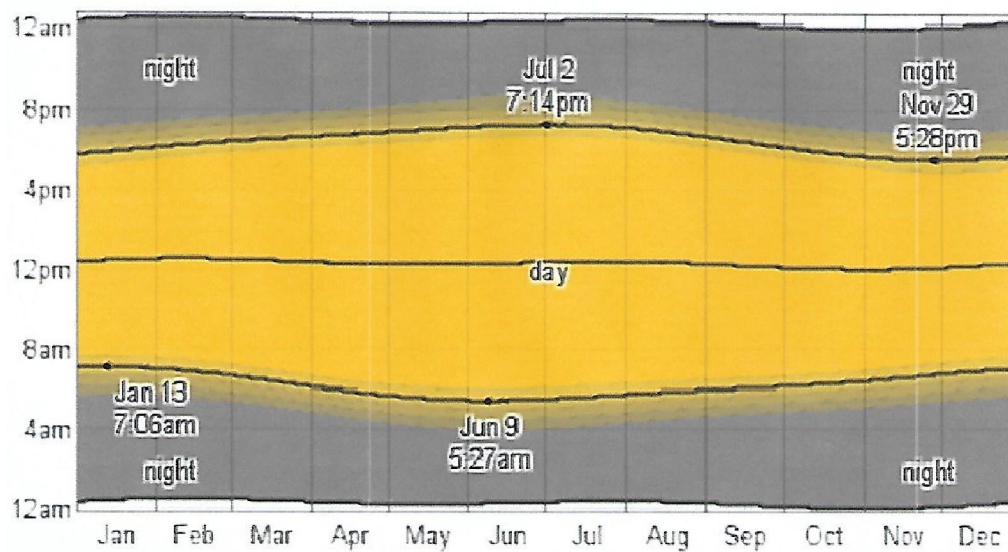
b) Daily Sunrise & Sunset with Twilight

Figure 4.12: Daily weather data in Dubai, UAE (Weather Spark, 2012)

According to Dubai Airport weather station records, the minimum and maximum summer air temperature is varied between 28 °C and 39 °C, respectively, with an average humidity between 66% am and 64% pm in August. While the average winter air temperature is between 14°C and 24°C in February with relative humidity of 81 % am and 63 % pm (Figure 4.13a and b).
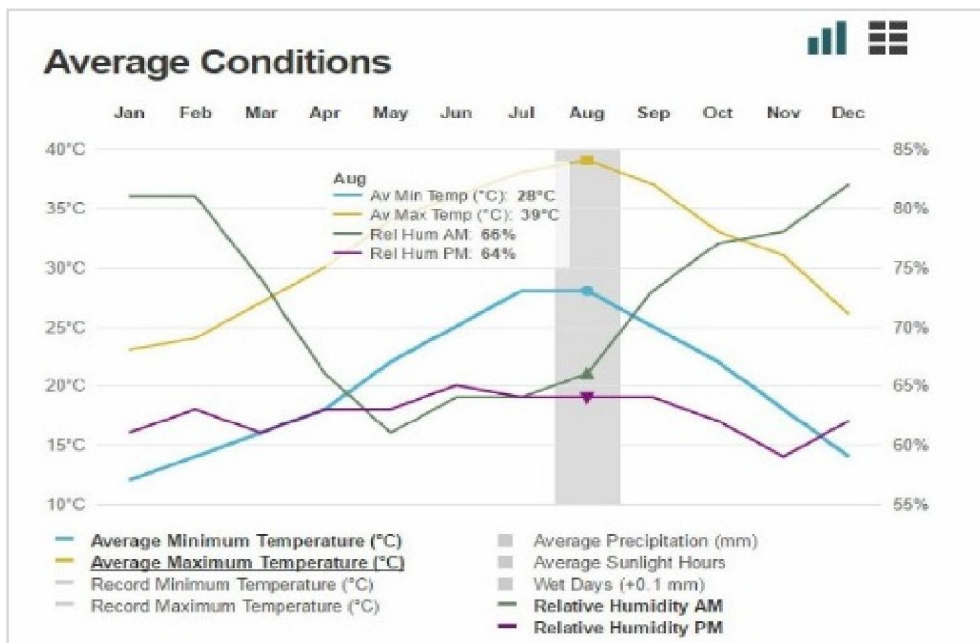
a) Dubai Airport Station summer average weather conditions
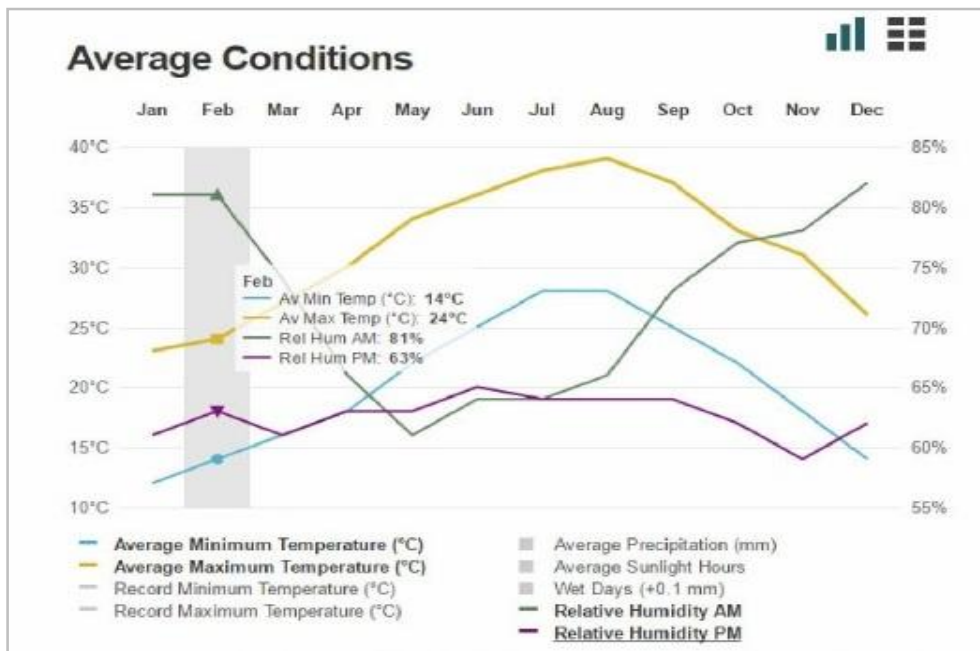
b) Dubai Airport Station winter average weather conditions

Figure 4.13: Dubai International Airport weather data (Helicon, 2011)

The Wind Rose of Dubai weather shows that the prevailing wind is the northwest wind with speeds that varied between 3 m/s - 9 m/s and it is rare that the wind speed rises above 12 m/s, although it has reached 15 m/s -20 m/s occasionally (Figure 4.14). However, early morning wind is calm with a slight south wind direction offshore. This wind turns to north-west after 10:00 am on shore. The south or north east wind occasionally blows from the desert, and sometimes it turns into a sandstorm and lasts for more than a few hours.
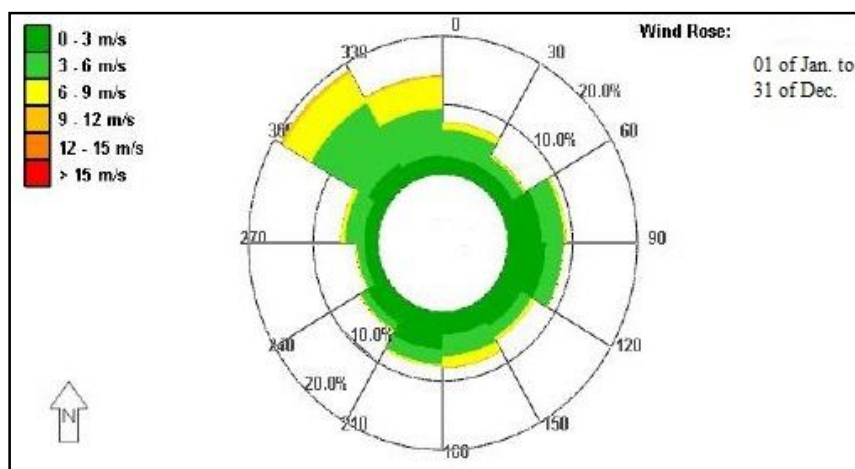
Figure 4.14: Prevailing wind in Dubai, Dubai Weather File (IES-VE, 2017)

Figure 4.15 shows that the average daily wind in Dubai is 4 m/s and the maximum wind speed reaches 7m/s, while the minimum wind speed is around 1m/s. The yearly parentages of the northwest wind is 17.6 % (Figure 4.16).
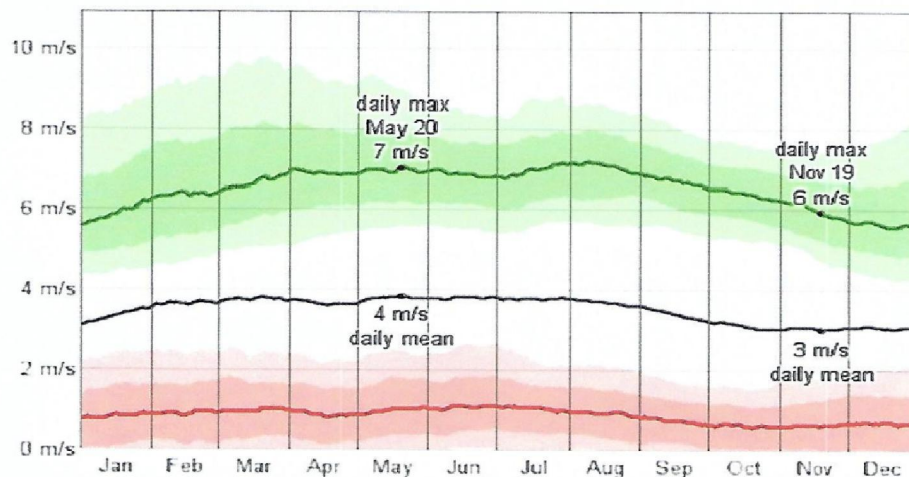
Figure 4.15: Wind speed daily averages in Dubai (Weather Spark, 2016)
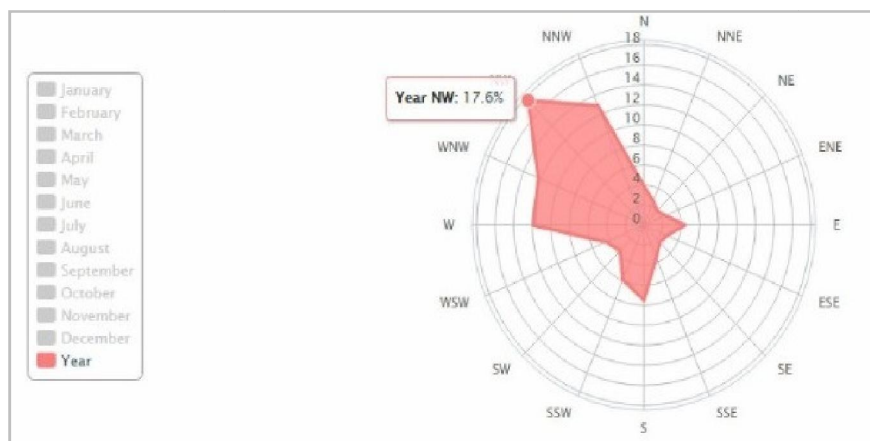
Figure 4.16: Prevailing wind direction and distribution in percentages(Wind Finder, 2017)

Planning and designing according to prevailing wind is a passive design element used to maximise the benefits of natural ventilation in early design stage. In this research the averages of the longest day 21th of June will be adopted as an initial conditions data for running the outdoor microclimate simulation software

4.7.2 Micro climate Initial Conditions for Outdoor Simulation Software ENVI-Met

In order find the effect of the selected variables and variation in the proposed scenarios, the ENVI-Met software will be used to find out this effect on the external microclimate parameters. Running the ENVI-Met software requires a number of physical and micro climate initial conditions. The software version will be used in this research is the latest version ENVI-Met 4.1 (2016/2017). The simulation process is available in three versions; (100*100*40), (150*150*35) and (250*250*25). The first version (100*100*40) will be used in this study as it is the most suitable version for the grid size of the models generated for the base case and the suggested scenarios of different configuration and height variation. In spite of that the grid size of the other two versions is bigger in x and y directions, the grid size in z direction is lower than the first version. Therefore, the first version is more flexible in simulating the variation in buildings height. The numerical results generated using ENVI-Met will cover one typical summer hot day according to Dubai weather, as the consumption is at maximum averages, while in winter period there is no demand related either to heating or to cooling load. The same simulation day will be used for the base case and all suggested scenarios. According to the selected number of building dimensions and the total modelled area, the size of the grid chosen is (80*60) to model the base case and the different scenarios with scale of (5m*5m*2m) for grid cell in (x,y,z) directions.

The material of the buildings in all scenarios will be fixed at the concrete block for walls and concrete slab for roofs, and the soil characteristic will be used is the ENVI-Met default soil data for all simulation process. The data will be collected at a height of 1.4m above the ground level which represents the pedestrian level, and the records will be averaged from the snapshoot of 9 receptor points in the middle of the canyons between the buildings of the proposed complex.

The ENVI-Met 4.1 software allows to indicate the location of the simulated model but the initial condition data should be edited in the simulation file for each project or scenario.

The Dubai, UAE location is selected as a study weather condition area, and the location of 25.25° N latitude, 55.33° E longitude is indicated, however, the initial conditions of weather data for running the simulation will be set. The setting data covers air temperature, humidity and wind direction and wind speed, and the simulation will cover 24 hours starting from 21st June at 5:00 am to 22nd June 4:59 pm. The initial conditions for running the software is adopted from the statistics and records weather data of Dubai Airport Weather Station (Helicon, 2016). The selected day for simulation process is 21stJune which represents the longest day in the year as presented in the methodology chapter. The simulation will cover 24 hours starting at 5:00 am before sunrise in order to maintain stable weather conditions for the core model and avoid any underestimation of the short wave radiation.

Figure 4.17 shows that the average of air temperature is 30.5°C, and relative humidity is 64.5 %, while the wind speed average at 10 m is 4 m/s (Figure 4.18).
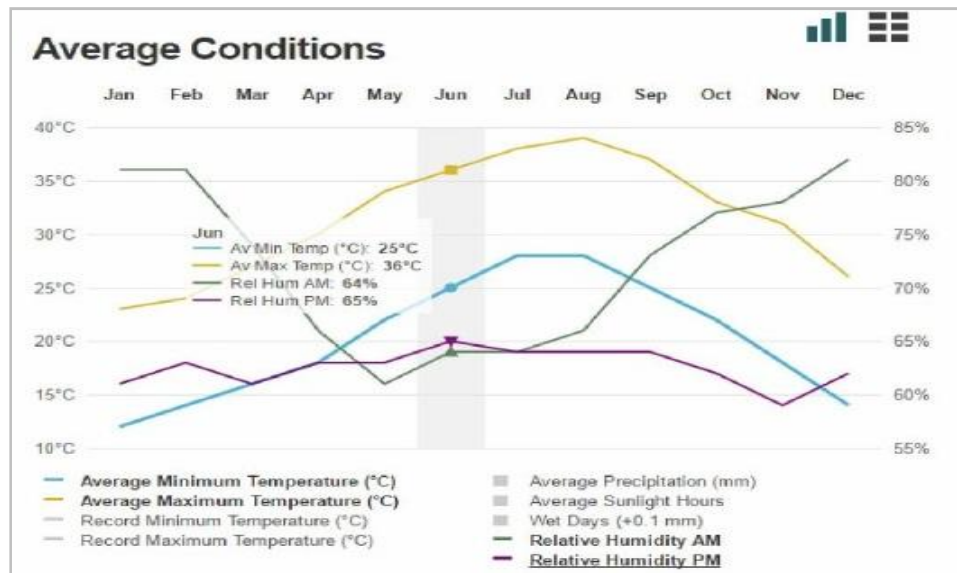
Figure 4.17: Air temperature and relative humidity averages in Dubai in June (Helicon, 2016)
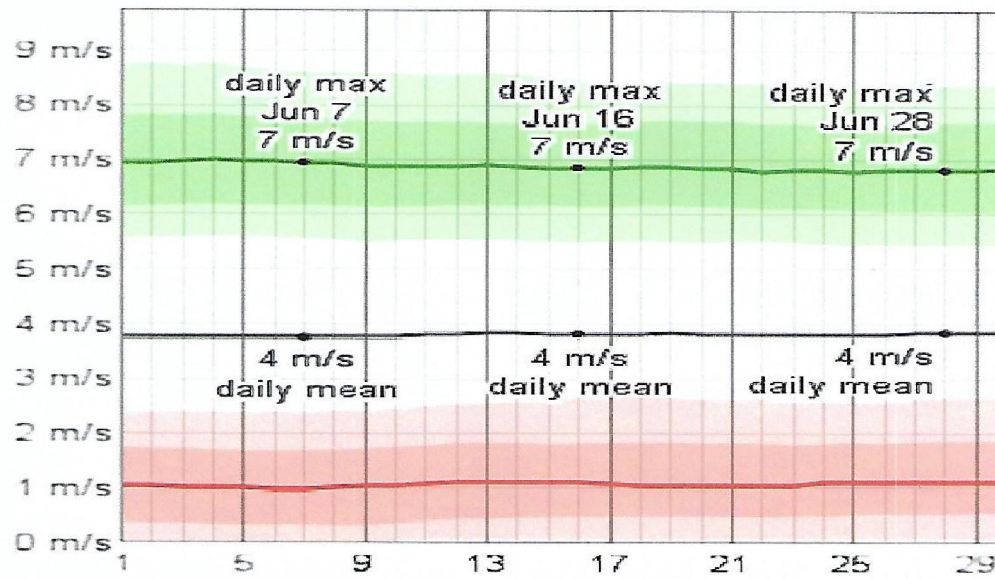
Figure 4.18:Wind speed averages in Dubai in June (Weather Spark, 2016)

Moreover, figure 4.19 shows that the prevailing wind in Dubai is of a North-West wind direction and represents 21.5 % of the total wind in June. The initial input microclimate conditions for running the simulation process using the ENVI-Met software is illustrated in Table 4.1.
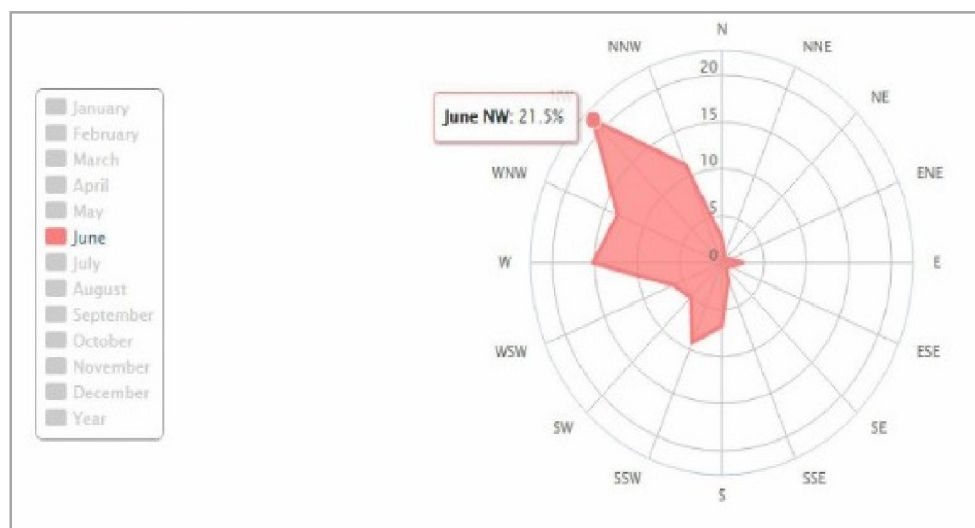
Figure 4.19: Prevailing North-West wind direction and distribution June in percentages
(Wind Finder, 2017)

Table 4.1: Initial Physical and micro climate input data in the typical configuration file in ENVI- Met 4.1.1

[**LOCATION**] ---

The Location on earth:	Longitude 55°.33' ; Latitude25°.25'
Climate Type:	Hot, Desert
Longitude Time Zone Definition:	GMT + 4

[**GRID**] ---

Grid boundary dimensions:	80*60
Cell size:	dx=5, dy=5, dz=2
Data collection at z:	1.4 m from the ground level

[**BUILDING FABRIC**] --

Building properties

Inside Temperature:	23°C
Heat Transmission Walls [W/m²K]:	0.43
Heat Transmission Roofs [W/m²K]:	0.25
Albedo Walls:	0.3
Albedo Roofs:	0.15

Building interior specifications;

Wall albedo:	0.2 (reflects 20% of incoming radiation)
Roof albedo:	0.3 (reflects 30% of incoming radiation)

INITIAL METEROLOGICAL DATA---

Start Simulation at Day:	21.06.2017
Start Simulation at Time:	05:00:00
Total Simulation Time:	24 h
Save Model State each:	30Min.
Model Resolution:	1:5
Wind Speed at 10 m above Ground:	4m/s
Roughness Length z0at Reference Point:	0.01
Initial Temperature Atmosphere:	33.5°C
Relative Humidity in 2m:	64.5%
Cloud Cover:	Clear sky

[**TURBULENCE**] --

Options Turbulence Model

Turbulence Closure ABL (0:diagn.,1:prognos.):	1.0
Turbulence Closure 3D Model (0:diag.,1:prog):	1.0
Upper Boundary for e-epsilon (0:clsd.,1:op.):	0.0

[**SOLARADJUSTENT FACTOR**] ---

Factor of shortwave adjustment (0.5 to 1.5 depending on sky clearness):	1.0

[CLOUDS COVER FRACTION OTKA] ---

(0-8 Completely Clear - Completely cloudy)
Fraction of HIGH clouds (x/8):   0.0
Fraction of MEDIUM clouds (x/8):   0.0
Fraction of LOW clouds (x/8):   0.0

[LBC-TYPES] --- ---
Types of Lateral Boundary Conditions
LBC for T and RH (1:open, 2:forced, 3:cyclic):   2.0
LBC for TKE (1:open, 2:forced, 3:cyclic):   2.0

The soil specifications and roughness values are kept as a default for the base case and all configurations and shown in table 4.2. This data was set for the base case all other configurations for running the simulation process. Furthermore, the micro climate output data extracted from ENVI-Met simulation represents an average of receptors data. In the base case and all other group configurations nine receptors are placed in the main and side canyons of the developed model (Figure 4.20).All the data will be collected at the level of 1.4m from the ground level at the receptors points (Figure 4.21).
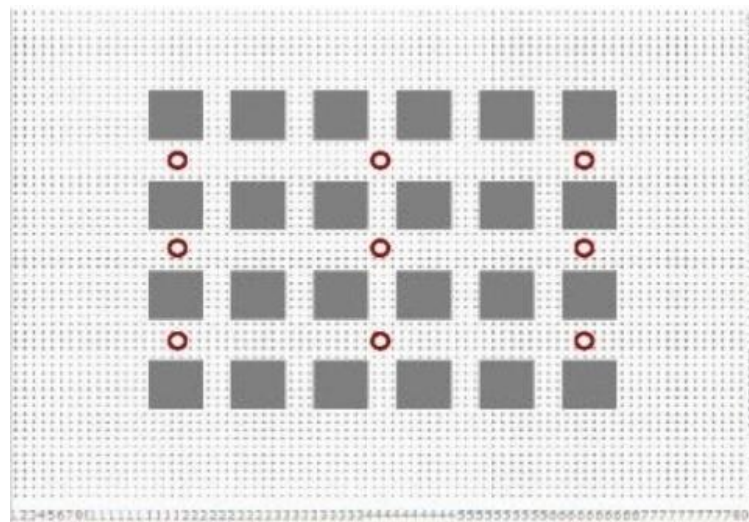
Figure 4.20: The location of the nine receptors in the general plan of the block configurations extracted from ENVI-Met 4.1 software (Author, 2018)

The microclimate parameters average values of these receptors will be plotted and discussed. Moreover, the average values for the output data will be integrated to the IES-VE as an input external microclimate conditions.
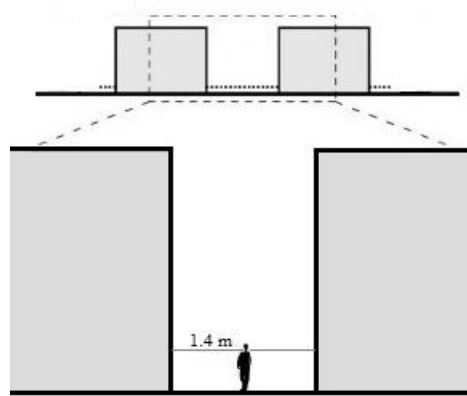
Figure 4.21: The selected height of 1.4m from the ground the for the extracted outdoor micro climate data (Author, 2018)

4.7.3 The Initial Conditions for the Indoor Thermal Performance Simulation Software IES-VE

The outdoor microclimate parameters obtained from ENVI-Met will be reflected on the indoor thermal performance of the urban block. The evaluation of the indoor thermal performance will cover; 1) solar gain, 2) conduction gain, and 3) cooling plant load. The cooling plant load calculations of each group configurations will be based on selecting the best configuration performance with respect to reducing the maximum outdoor air temperature. The best configuration will be a result of a comparison with other scenarios or configurations in the same group of different maximum air temperature averages. On the other hand, the best configuration will be evaluated against the base case configuration to find the variation in the indoor thermal performance and to find the energy saving through the variation in cooling load.

The solar gain covers the external and internal heat gains, the external solar gain reflects the effect of the exposure to the solar radiation of the sun, and the internal gain covers a number of variables and initial conditions that will be set in the IES-VE software prior to running the simulation process. The internal gain input data will be the same for the base case and all configurations. Hence, the variation in the output data of the solar gain extracted from the IES-VE software will reflect the variation in shading effect and external gain occurred by the variation in buildings height and configurations within the group. On the other hand, and as illustrated previously in literature review chapter, the cooling load includes the cooling sensible load and the cooling latent load. The cooling sensible load reflects and affected by the dry bulb temperature, whereas the cooling latent load depends on the wet bulb temperature. Therefore, the maximum dry bulb air temperature and the wet bulb air temperature extracted for the ENVI-Met simulation results will be the input micro climate data for the external heat gain in the IES-VE simulation process. Figure 4.22 illustrates the base case (G + 5) of the urban block presentation in the IES-VE software.
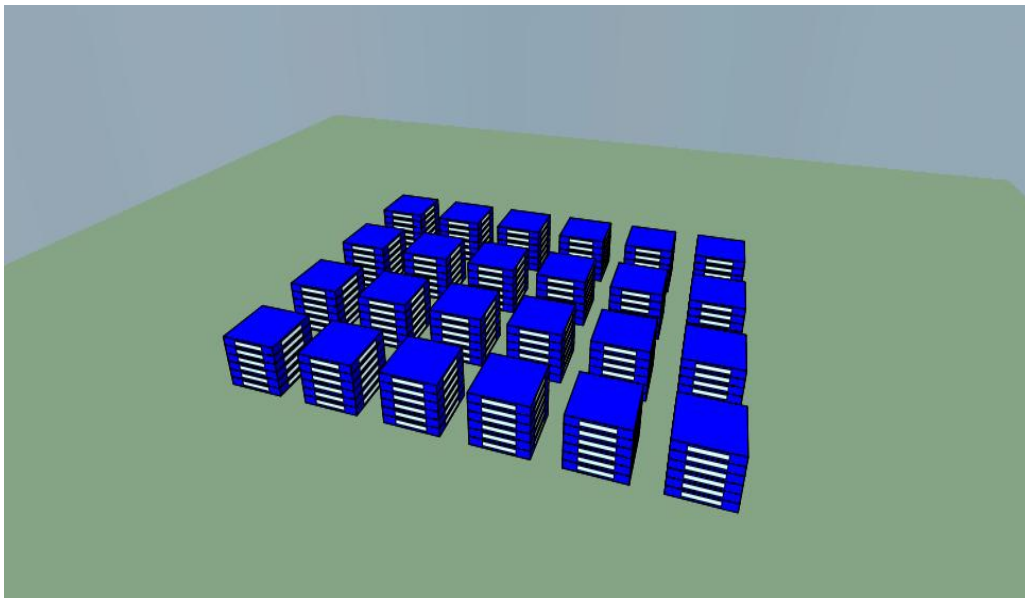
Figure 4.22: The base case configuration (G + 5) of the urban block presentation in the IES-VE (Author, 2018)

4.7.3.1 General Input Data for Indoor Thermal Performance Prediction Software IES-VE

The energy consumption of the residential buildings in hot climate is mainly dominated by the cooling load consumption. In this study location which categorised as a hot desert climate zone, buildings cooling strategies depends mainly on mechanical system which may be used continuously most days of the year. Therefore, the cooling plant load is selected to explore the effect of urban topology on energy consumption of the residential buildings. For this study, the cooling plant load is going to be estimated using the IES-VE software, and it will be designed to maintain an indoor air temperature of 23°C. The IES-VE simulation software offers a wide range of indoor environmental a thermal parameters with respect to building envelop and materials. In addition of taking the building operation and the occupation effect in to consideration, furthermore, the IES-VE offers a very good level of accuracy.

The input data required to run the IES-VE simulation process is divided into types; 1) the model physical data, and 2) thermal initial data. The model physical data covers the model dimensions and specifications including the building materials. The model of the base case and the proposed scenarios will be modelled in the IES-VE working space with all exact dimensions implemented in using the ENVI-Met software. With respect to the physical dimensions of the model, no variation occurred in the modelling procedure between the two software, the dimensions, coordinates and the cell size (scale) used is the same in both ENVI-Met and IES-VE software. The IES-VE provides a larger number of built-in weather file depending on the location of the earth, this weather file covers countries from all contents. The nearest built -in weather file to the location of this study is the same weather station data used to collect the average of micro climate data for ENVI-Met data input Dubai International Airport Station. However, the build-in weather file in the IES-VE does not allow to calculate any variation in the outdoor microclimate conditions caused by the effect of buildings topology.

Therefore, the outdoor microclimate data of the investigated models will be extracted from the ENVI- Met software and will be used for running the IES-VE software. One of the IES-VE limitation mentioned in the methodology chapter, is the limitation of the microclimate condition that can be inserted in the IES-VE.

The IES-VE allows editing of the design air temperature, dry bulb and wet bulb only, any variation in wind speed could not been added to the IES-VE weather files. On the other hand, the ENVI-Met software is well known in conducting the CFD simulation, therefore, the maximum air temperature extracted from the ENVI-Met is normally affected by the variation in wind speed. Furthermore, the data of the relative humidity extracted from the ENVI-Met is in the percentages.

The wet bulb air temperature was calculated using an application that calculates the wet bulb temperature using the dry bulb temperature and relative humidity. However, building materials and specifications will be indicated using Building Manager prior to running simulation process. The default file for building material covering walls, roofs, facade material can be used to indicate the required material specifications for the simulated models. The built-in specification and thermal conditions follows the ASHRAE load requirements. However, and with respect to the 'Sa'fat', the Dubai Green Building Evaluation System, the U- Value for the external wall is varied between 0.57 W/m² k for bronze and silver 'Sa'fat', and 0.42W/m² k for the golden and platinum 'Sa'fat', and for the roof the U-Value is 0.3 W/m² k. The buildings material specifications and the typical construction setting data for the simulated models is illustrated in detail in appendix B. Furthermore, and with respect to the indoor conditioning system setting conditions, the acceptable indoor air temperature for the hot desert climate is varied between 23 º C and 25 º C (Al-ajmi and Loveday, 2010). Moreover, building operation and occupation data should also be set prior to simulation

process. New thermal profile has been set in the Building Manager, this file contains the operation and thermal input data as illustrated in table 4.2.

The air temperature is set according to the default temperature suggested by the IES-VE according to the location to be 23 ^{o} C. Moreover, and according to ASHRAE (2007) the ventilation rate is generally varied between 1 for low contaminate air to 4 for high contaminate air, gasses and dangerous particles. In order to achieve an equilibrium pressure, the amount of the air leaving the space and entering the space must be the same, and the ventilation rate is set for the low contaminate air to be 1 ach (air change per hour). The actual amount of air change in a well mixed ventilation scenario will be 63.2 % after 1 hour and 1 ach (Bearg 1993). With respect to the urban block floor layout, number of apartments and occupants or people calculations. Each floor area is 900 m² , and it is consist of apartments with 180 m² floor area and two bedrooms. This result in 5 apartments in each floor, for the ground floor the number of apartments is 4 as the ground floor contains of some services and reception area.

According to ASHRAE (2009c) the calculation of the people number in the residence unit is the bedroom number plus one.

The calculation will be based on the base case block of 24 buildings (G +5) as the following:

Ground Floor = 4 apartments * 3 people = 12 people

Typical floor = 5 apartments * 3 people = 15 * 5 floors = 75 people

Total number of people in each building = 87

Total number of people in the urban block = 2,088

The number of 2000 people will be used for the proposed urban block residents

Table 4.2: The setting conditions in the typical thermal file in the IES-VE software for all configurations

----

[**LOCATION**] --

The Location on earth: Longitude55°.33' ;Latitude 25°.25'
Weather station: Dubai International Airport Station
Loads methodology: ASHRAE Loads

[**THERMAL CONDITIONS**] ---

Project daily profile: Continuously
Project weekly profile: Continuously
System to maintain cooling at: 23°C
The internal gain -florescent type consumption: 10 w/m²
The number of occupancy: 2000 people
The natural ventilation maximum flow: 1 ach
Maximum dry bulb temperature: Varied according to each configuration
Minimum dry bulb temperature: Varied according to each configuration
Wet bulb temperature at maximum dry bulb temperature: Varied and extracted
from the relative humidity of each configuration

Chapter 5

The Outdoor Thermal Performance of the Proposed

Configurations

5.0 The outdoor Thermal Performance of the Numerical Modelling

Running the simulation process of the base case and the proposed scenarios has generated a set of output microclimate data. The obtained results from ENVI-Met simulation software is divided in two types: 1) visualised maps as jpg format type, and 2) statistics data that is exported to Excel file format in order to be illustrated as graphs. In this chapter, the results of simulating the base case configuration and the proposed scenarios of each group will be illustrated. These results will be compared with the base case simulation results, in addition to comparing the results of each scenario within the same group with each other to find the best configuration. The microclimate parameters that will be covered during the results analysis are: air temperature, wind speed, and relative humidity. The microclimate data of the 21st. June, 2017 was adopted as an initial condition or boundary data . However , the comparison between the 2017 microclimate data and the average of the five years data is illustrated in appendix A2.

Furthermore, the SVF of the base case and the different proposed configurations will be illustrated to reflect the effect of the diversity in buildings height on the solar exposure of each configuration. Moreover, the energy consumption represented by the cooling load demand of the whole block will be simulated and investigated. The cooling load of the whole block will be calculated using the IES-VE software, and the base case block energy demand for cooling will be compared with the other proposed developed configurations.

The comparison will be evaluated according to the urban geometry variables variation covering: 1) height diversity, and 2) buildings topology. This comparison aims to find the effect of the changes in developed urban block configurations on the thermal performance of the indoor environment specifically cooling load energy demand.

5.1 The Base Case Configuration Simulation Results

The base case represents the configuration of the 24 building with a uniform height of G+5,and 24m as a total building height. Figure 5.1 shows the isometric (3D) view of the base case configuration. The main and the side canyons are with width of 25m, and the width of the alleys is 15m as shown in the configuration plan of the proposed block (Figure 5.2). This plan will be the general plan for the two proposed groups that will be explored in this study. Figure 5.3 illustrates the front and the side view of the base case configuration, the proportions of the buildings height in the base case is (5:5:5:5).

The buildings are placed in the Pavilion configuration, each building has a 30m*30m footprint and the total built-up area of the building is 5,400 m². The total built-up area of the whole block is 129,600 m². Nine receptors are indicated in the main and side canyons of the proposed block in order to find the average of the microclimate outdoor data of each configuration.
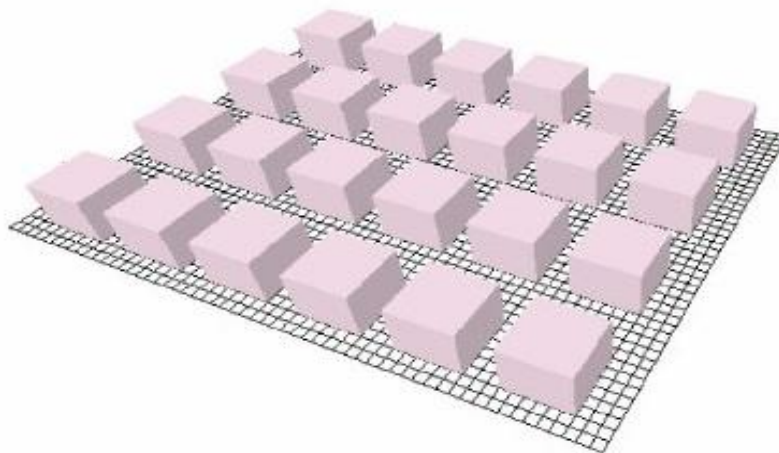
Figure 5.1: The isometric view for the (3D) model of the base case configuration
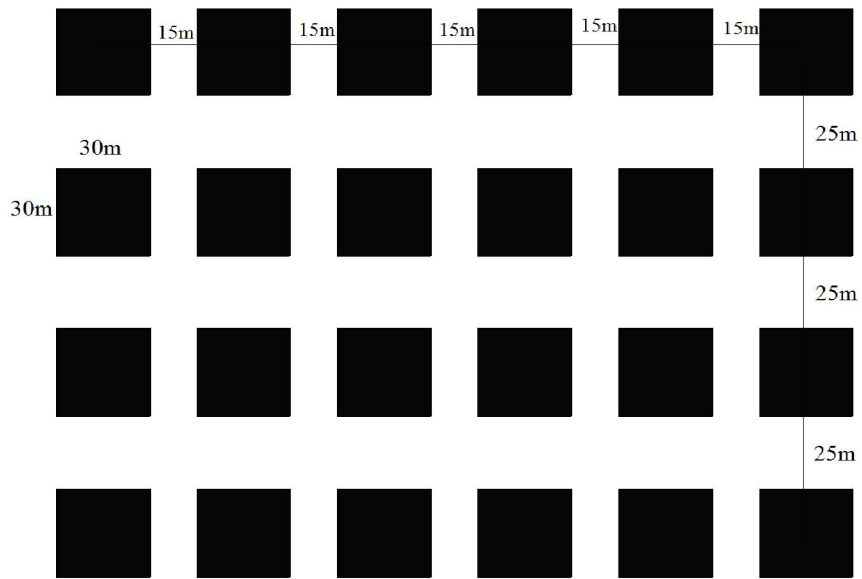
Figure 5.2: The general plan that represents the base case and the proposed scenarios configuration of the first and second groups

a) Front view
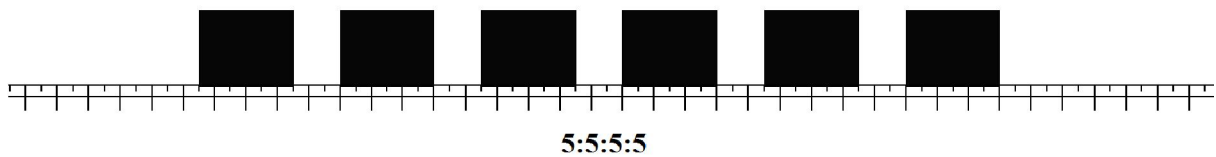
b) Side view

Figure 5.3: a) Front view (top) and b) side view (bottom) of the base case configuration that represents the short axis (top), and long axis (bottom) of the urban block

5.1.1 Sky View Factor

The sky view factor is the indicator that represents the amount of the sky that can be observed from specific point. It is another expression the impact of the H/W ratio but is more precise in reflecting the effect of H/W ratio in specific points with different locations along any canyon.

Figure5.4 shows the SVF in the main canyons and the alleys of the base case configuration. It is clear from the figure that there is a uniformity in the SVF in each canyon according to the same height for buildings and the same canyons width of this configuration. Although, the SVF near the edge of the complex is higher than the SVF of the points in the middle of the canyons. This shows that the fixed H/W ratio along any canyon does not necessarily or accurately reflect the amount of the canyon surface that is exposed to the sky or the sun. In this case, the H/W ratio of each canyon is 0.96, and each of the three canyons is an example of the uniform canyon. On the other hand, the alleys have a H/W ratio of 1.6. The average SVF of the base case is 0.45 (Figure 5.4).
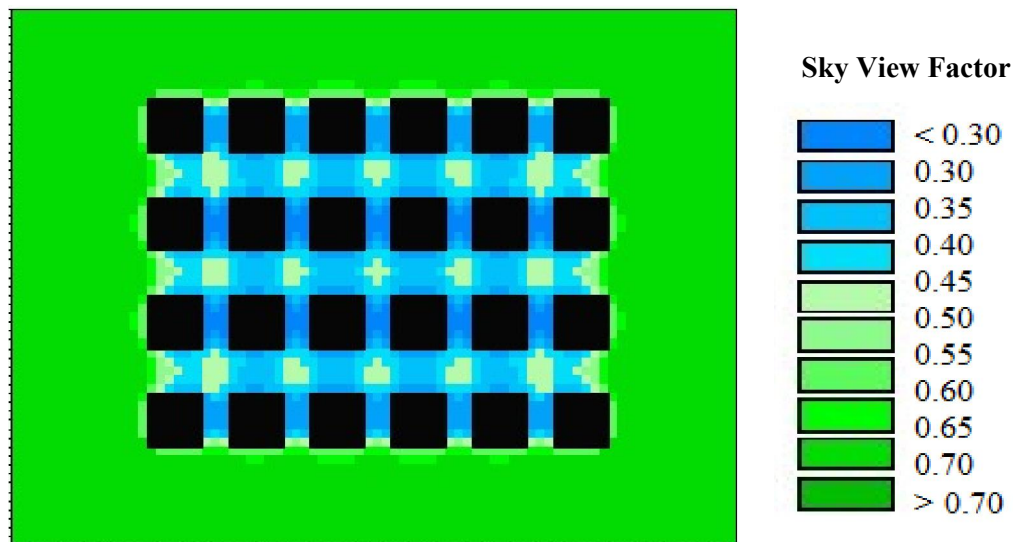
Figure 5.4: The Sky View Factor (SVF) of the base case (5:5:5:5:5) configuration

5.1.2 Air Temperature

The outdoor air temperature of the base case is evaluated according to the four orientations simulation using ENVI-Met software. The base case is simulated in the block orientations of; N-S,E-W, NE-SW, and NW-SE. The outdoor air temperature results of the base case model are generated and exported in to a spreadsheet. The average air temperature profile of the selected simulation day 21June in the four orientations is illustrated in figure 5.5. The figure shows the diurnal air temperature of the 24 hours in the four orientations. The figure shows that the air temperature of the model starts to increase after sunrise from 6.00 to reach the maximum at 15:00 in the four block orientations. The average maximum air temperature recorded in all orientations was at 15:00 with a maximum value of 37.6 $^{\circ}$C in the NE-SW block orientation. While the E-W and the N-S block orientations recorded slightly lower maximum air temperatures of 35.8 $^{\circ}$C and 35.8 $^{\circ}$C, respectively. Hence, the variation in air temperature between the highest maximum in NE-SW and the lowest maximum in N-S orientations is 1.8 $^{\circ}$C.
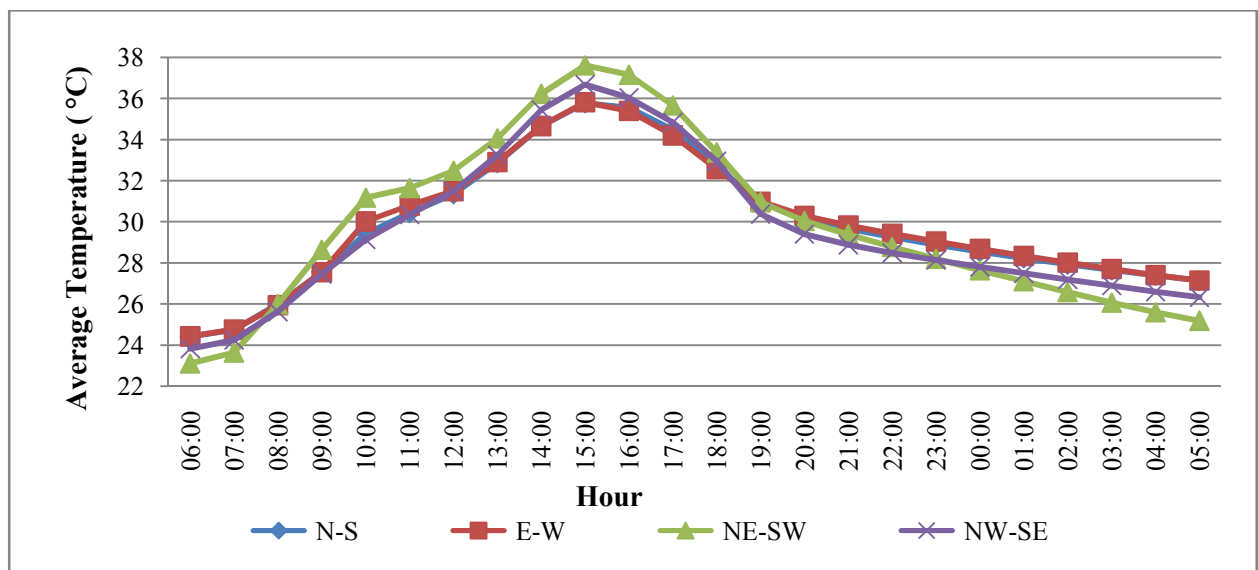
Figure 5.5: Hourly profile of the average air temperature on 21 June for the base case configuration in the four orientations: N-S, E-W, NE-SW, and NW-SE

5.1.3 Wind Speed

The initial wind speed used for simulating the base case was 4m/s according to the wind averages obtained from the data provided by Dubai Airport Weather Station. The results of the wind speed were generated by running the simulation process for the 24 hours on the same simulation day 21st June is presented in figure 5.6. The figure shows that in all orientations, the wind speed decreased slightly during the day. The NW-SE orientation recorded the highest maximum wind speed of 3.4 m/s. This direction is aligned with the N-W prevailing wind direction in the UAE. Similar to the air temperature results, the N-S and the E-W orientations show very close values of wind speed along the simulated day with maximum values around 2.4 m/s and minimum around 1.9 m/s. The variation between the highest maximum wind speed in NW-SE and the lowest maximum speed in N-S and E-W orientations is about 1m/s. On the other hand, the NE-SW orientation recorded wind speed values less than the NW-SE orientation with a maximum of 2.8 m/s.
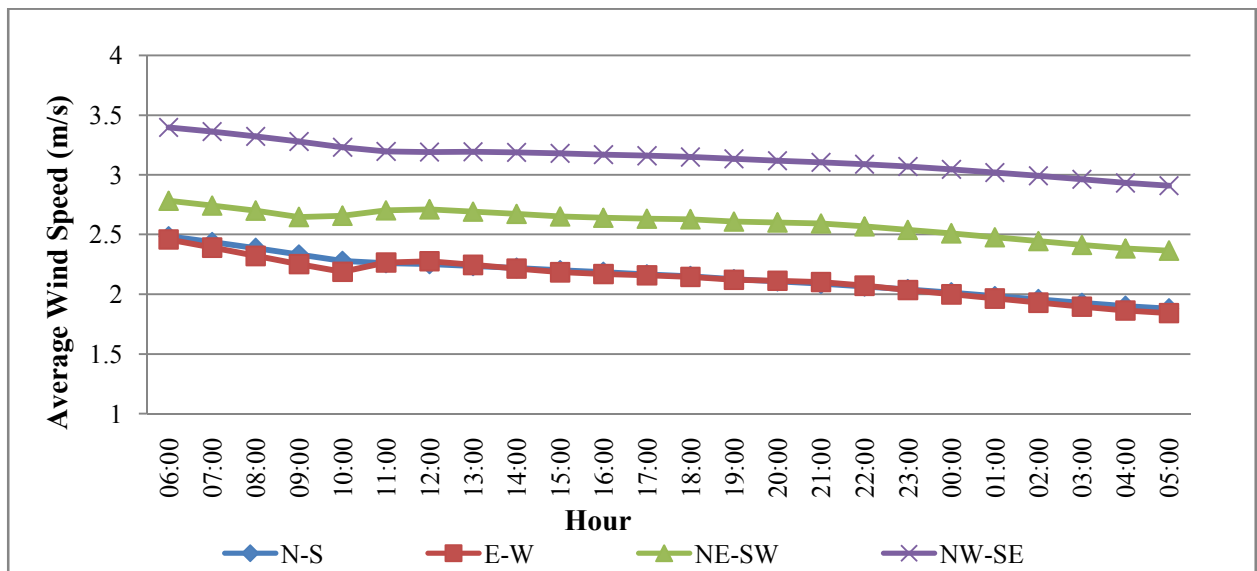
Figure 5.6: Hourly profile of the average wind speed for the base case configuration in the four orientations; N-S, E-W, NE-SW, and NW-SE

5.1.4 Relative Humidity

The relative humidity profile of the base case is presented in figure 5.7. The minimum relative humidity recorded at the same of the maximum air temperature to reflects the inverse relationship between the relative humidity attitude and air temperature performance of the base case configuration. However, the relative humidity in the early morning is at the maximum average, and it is the highest in the NE-SW orientation while the minimum is in the same orientation at 16:00 pm with a value of 37.8%.
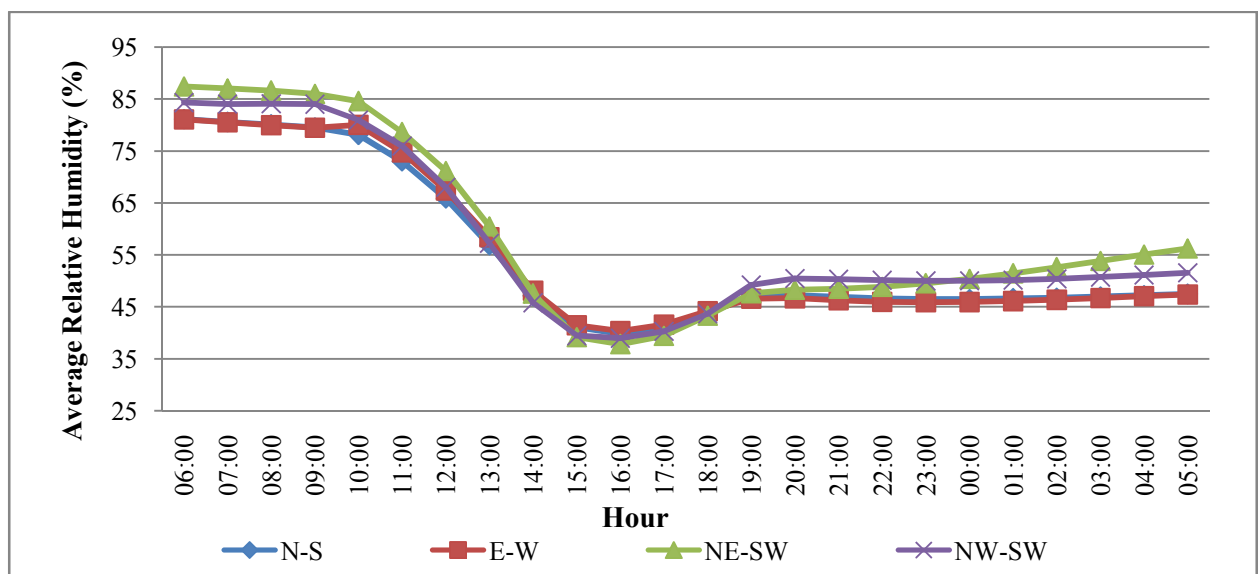
Figure 5.7: Hourly profile of the average relative humidity for the base case configuration in the four orientations; N-S, E-W, NE-SW, and NW-SE

5.2 The First Group of the Proposed Configurations

The first group of the proposed configurations represents the variation in buildings height with a proportion of 3:7 applied in the short axis of the urban block. This proportion of the mid-rise buildings is represented by floor number of; G+3 and G+7. The built-up area of each G+3 building is 3,600 m², and the BUA of each G+7 building is 7,200 m². The total BUA of the block in this group is 129,600 m², figure 5.8 presents the four configurations of the first group.
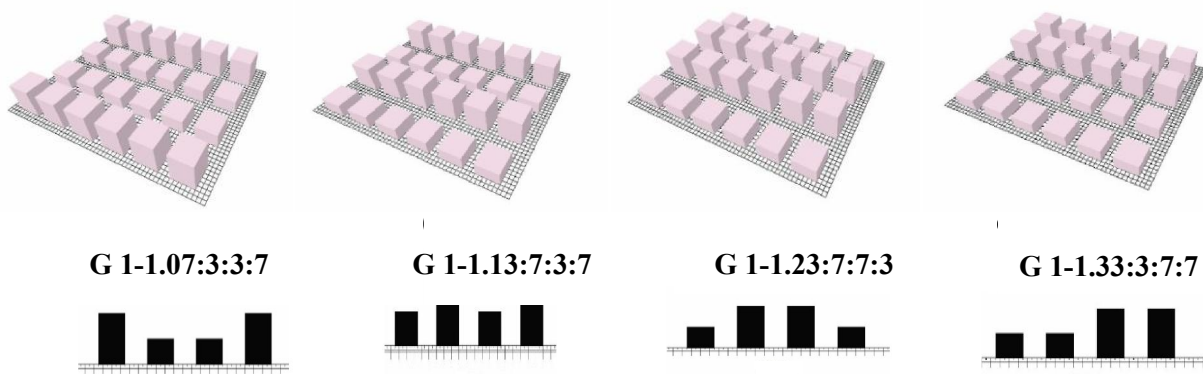
Figure 5.8: Isometric view of the first group of proposed configurations with buildings height proportion (3:7): G 1-1.0(7:3:3:7), G 1-1.1(3:7:3:7), G 1-1.2(3:7:7:3), and G 1-1.3(3:3:7:7)

This group consists of four scenarios or configurations, namely: G1-1.0, G1-1.1, G1-1.2, and G1-1.3 with proportions of; (7:3:3:7), (3:7:3:7), (3:7:7:3), and (3:3:7:7), respectively (Figure 5.8).The variation in buildings height in this group is implemented in the short axis of the block. The first configuration in this group is represented by the G1-1.0 (7:3:3:7) configuration with the height variation towards the inner axis of the block. The second configuration G1-1.1 (3:7:3:7) in the first group represents the fluctuation in buildings height with the same adopted proportion (3:7). The third configuration is developed by placing the highest buildings of G+7 in the middle of the block, while the lower buildings of G+3 are placed at the edges of the block, this scenario is G1-1.2 (3:7:7:3). The last configuration in this group is represented by the configuration G1-1.3(3:3:7:7). The buildings of G+3 and G+7 in this configuration are arranged according to height from lower to higher and each two adjacent rows contain the same buildings height.

The low buildings G+3 are placed in the first two rows while the higher buildings G+7 are placed in the rows behind and along the long axis. The SVF of each configuration, in addition to the microclimate parameters results will be illustrated in following sections.

The results of the first group will be illustrated for all configurations by comparing them with each other, and with the base case. The micro climate parameters to be covered are: 1) air temperature, 2) wind speed, and 3) relative humidity.

5.2.1 Sky View Factor

The variation in the sky view factor between the configurations of the first group and the base case is illustrated in figure 5.9. Comparing the first group configurations to the base case, the third configuration of the first group G1-1.2 (3:7:7:3) shows the lowest SVF average with a value of 0.40. This can be interpreted by the fact that the number of points exposed to the sky or the sun are less in this configuration compared to the other configurations, including the base case. However, the second configurationG1-1.1 (3:7:3:7) recorded a SVF similar to the base case, but the G1-1.3 (3:3:7:7:) third configuration had a slightly higher SVF of 0.46 compared to the base case.

On the other hand, the base case performs better with regards to the sun exposure than the first configuration G1-1.0 of proportion (7:3:3:7). The SVF of the first configuration is 0.50, and it is higher than the base case by 10 %.

However, it has been found that the SVF is not the only variable that affects the outdoor air temperature within the block, the orientation is the key factor that can control the outdoor microclimate parameters including the air temperature.

Base Case (5:5:5:5)

SVF = 0.45

G1-1.0 (7:3:3:7)

SVF = (0.50)

G1-1.1 (3:7:3:7)

SVF = (0.45)

G1-1.2 (3:7: 7:3)

SVF = (0.40)

G1-1.3 (3:3:7:7)

SVF = (0.43)
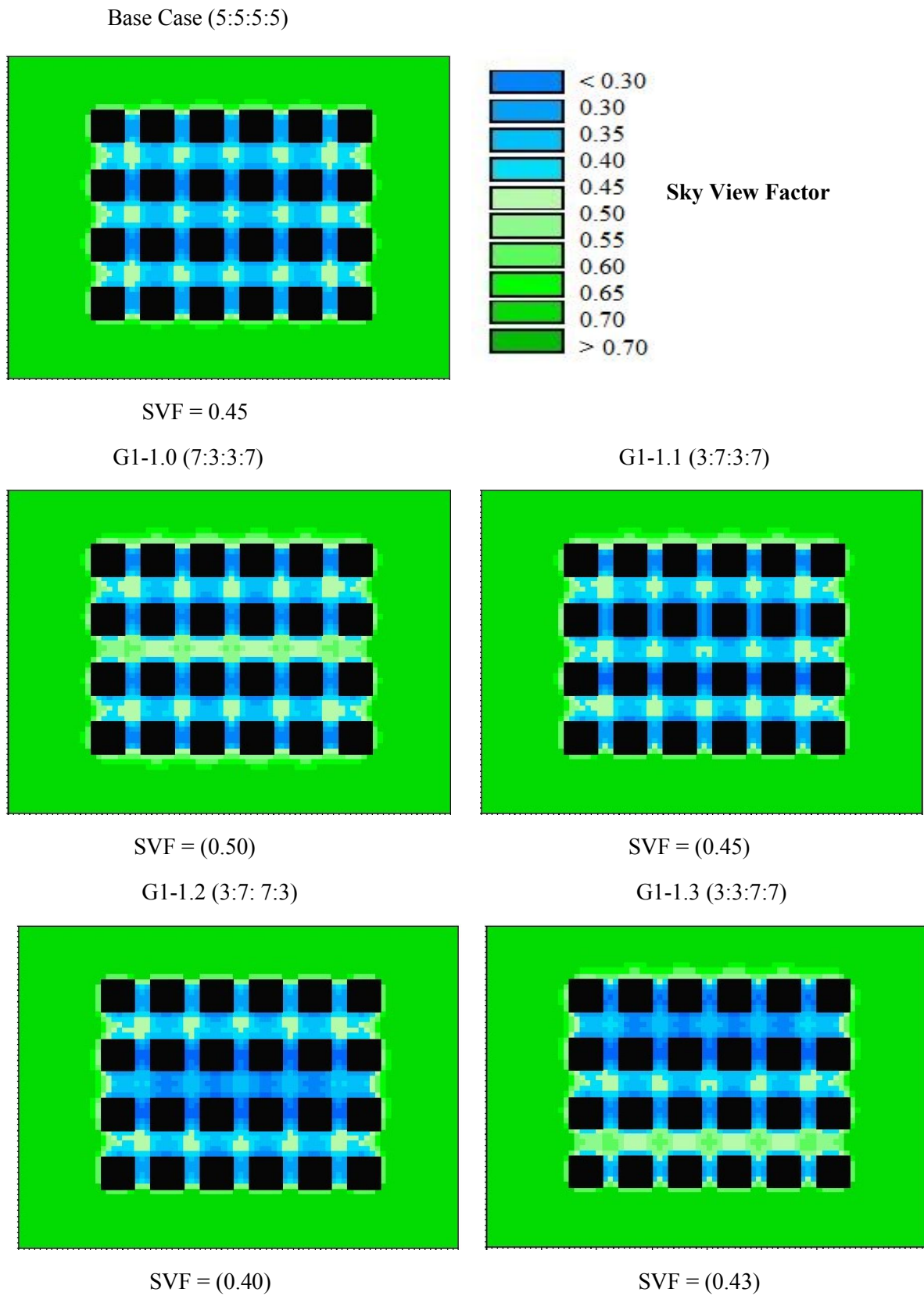
Figure 5.9: The Sky View Factor (SVF) of the base case and the four proposed configurations in the first group; G 1-1.0 (7:3:3:7), G 1-1.1 (3:7:3:7), G 1-1.2 (3:7:7:3), and G1-1.3 (3:3:7:7)

178

5.2.2 Air temperature

The average outdoor air temperature of all configurations of this group was simulated on 21 June in the four mentioned orientations; N-S, E-W, NE-SW, and NW-SE. The results of the simulation in each orientation are presented in figure 5.10.The air temperature results of the configurations in group one according to the four orientations shows the following:

- For the four different configurations in the first group, the average maximum air temperature is recorded at 15:00 pm in all orientations.

- The highest maximum air temperature for all configurations is recorded in two orientations NE-SW and NW-SE respectively, while the N-S and the E-W orientations recorded lower maximum air temperature in all configurations. Therefore, the N-S and the E-W are the preferred orientations for the block in all configurations.

- The first configuration G1-1.0 (7:3:37) recorded the highest maximum air temperature with a value of 37.5^{o}C in NE-SW orientation, while the lowest maximum air temperature in the same orientation is recorded in the configuration G1-1.2 (3:7:7:3) with a value of 36.8^{o}C. This shows that the G1-1.2 (3:7:7:3)configuration perform better than the other configurations when the block has to be oriented to NE-SW direction according to the planning requirements.

- The lowest maximum air temperature in E-W orientation is recorded in the configuration G1-1.1 (3:7:3:7) with a value of 35.4^{o}C. Therefore, this configuration records the best performance in this group for the E-W orientation.

For the N-S orientation all the configurations show a close averages of air temperature varied slightly with the lowest value of 35.5^{o}C for G1-1.2 (3:7:7:3) configuration.

- The first configuration G1-1.0 (7:3:3:7) shows the worst performance with regards to air temperature in NW-SE orientation with a value of 37.3°C, while the best performance in this orientation is for the G1-1.2 (3:7:7:3) configuration with air temperature of 35.6°C.

- From the above, the G1-1.2 (3:7:7:3) configuration records the best performance in the three directions NE-SW and NW-SE, while the G1-1.1 (3:7:3:7) configuration is the best in the E-W and N-S orientations (Figure 5.10)
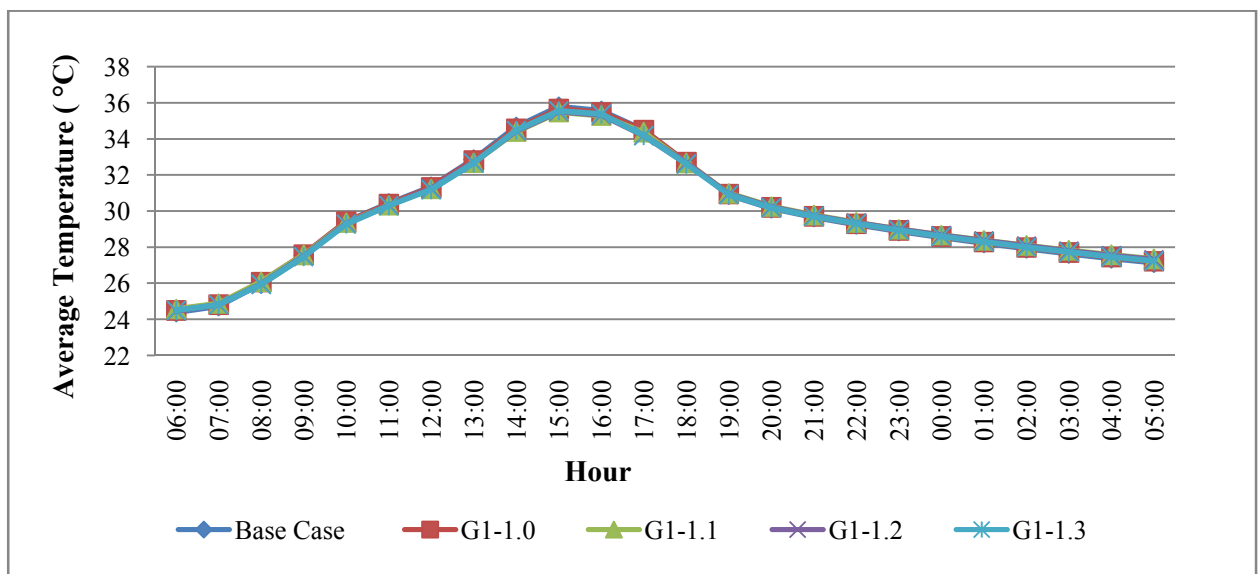
a) N-S orientation
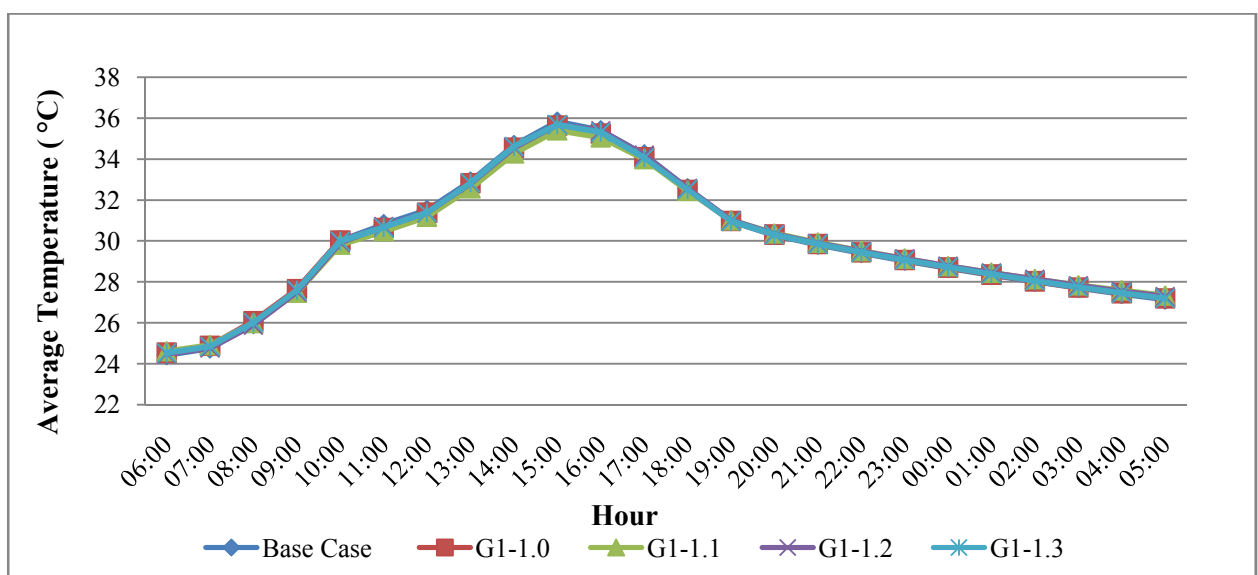
b) E-W orientation
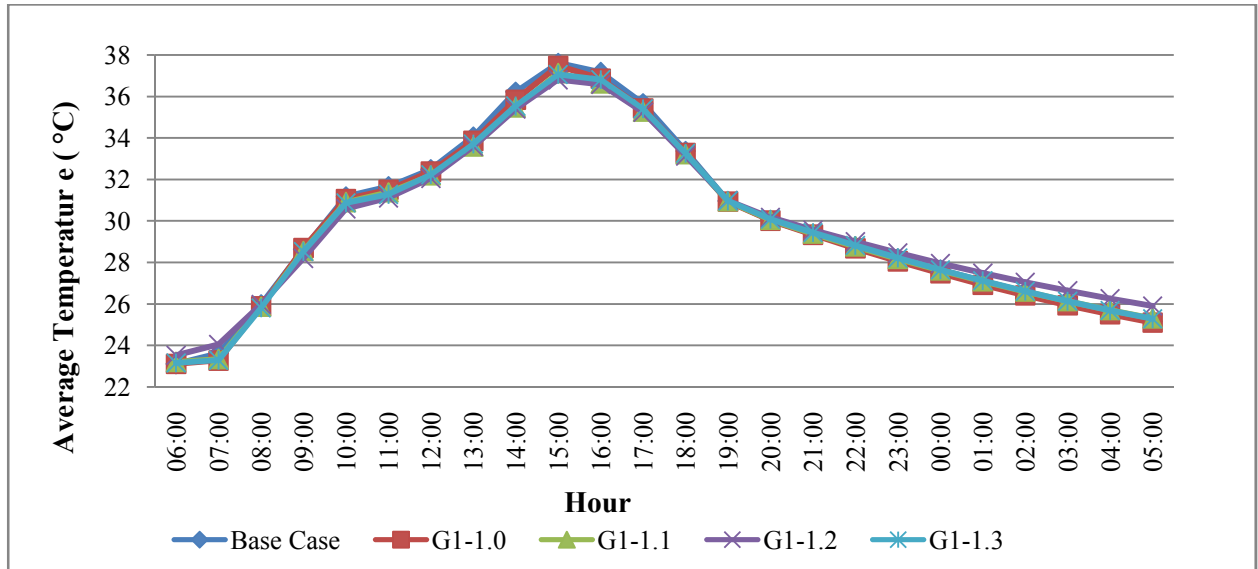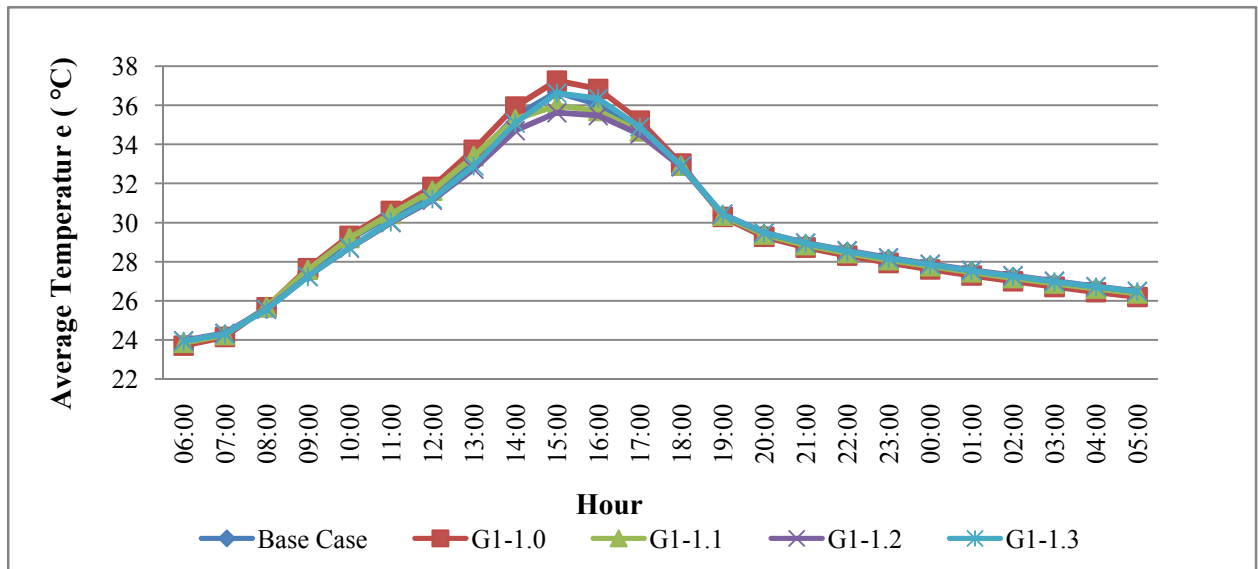
c) NE-SW orientation

d) NW-SE orientation

Figure 5.10: Hourly profile of the average air temperature on 21 June for the base case and the first group proposed configurations in the four orientations: N-S, E-W, NE-SW, and NW-SE

- The two configurations G1-1.1 (3:7:3:7) and G1-1.2 (3:7:7:3) in this group provide the lower percentages of points exposed to the sun with SVF of 0.42 and 0.45 respectively. In this configuration the effect of compactness element and the increase of the H/W ration is adopted to reduce the block surfaced that is exposed to the sun.

- While the other two configurations of this group; G1-1.0 (7:3:3:7) and G1-1.3 (3:3:7:7) recorded higher SVF compared to the base case with values of 0.50 and 0.46 respectively. The hourly profile of the average air temperature in the four orientations is illustrated in figure 5.10. Figure 5.10 d shows the clear variation in the averages of maximum air temperature attitude in the NW-SE orientation.

5.2.3 Wind Speed

The trend of the wind speed and air flow of the four configurations in the first group is simulated using the ENVI-Met software. The results of wind data are collected at a height of 1.4m from the ground level with reference to the initial simulated wind of 4 m/s at 10m. Figure 5.11 shows the averages of wind velocity obtained from the indicated receptors points in the three canyons. However, wind speed statistics and simulation results generated from running the simulation process show that:

- The wind speed in the first group is varied according to the buildings configuration and canyons orientation.

- For all configurations the wind velocity in N-S and E-W canyon orientations shows very close behaviour and values. The daily maximum wind velocity is varied around 2.7 m/s in the G1.1 (3:7:3:7) configuration, but this velocity decreases during the day to reach the minimum around 2.3m/sin these orientations (Figure 5.11 a and b).

- The wind flow attitude of the four configurations shows that the north-west prevailing wind is the dominated wind in the four configurations of the first group. The effect of this wind is obvious in the high wind velocity values in the NE-SW and NW-SE orientations. However, the values of the wind velocity have been changed according to the changes in the buildings height of each configuration.

- The drop in wind attitude for all configurations can be seen at 10:00, and it is clear in the E-W and NW-SE orientations that facing the prevailing wind.

- This drop related to the slight changes in north- south wind direction of early morning to the N-W direction after 10:00 am. The wind behaviour of the UAE was illustrated in the methodology chapter, section 3.7.1.
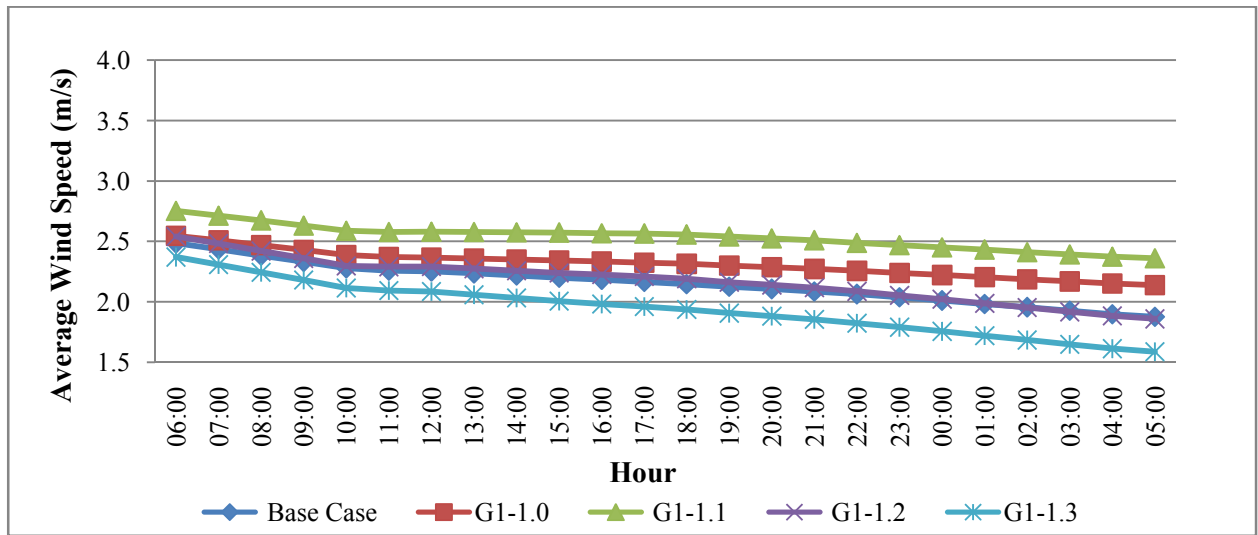
a) N-S orientation
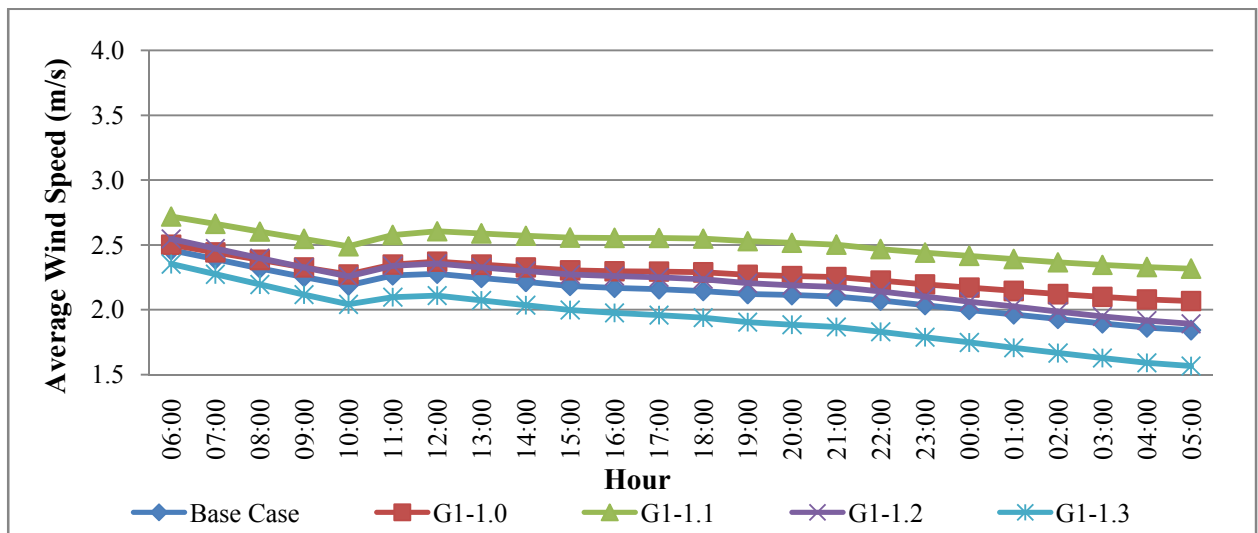
b) E-W orientation
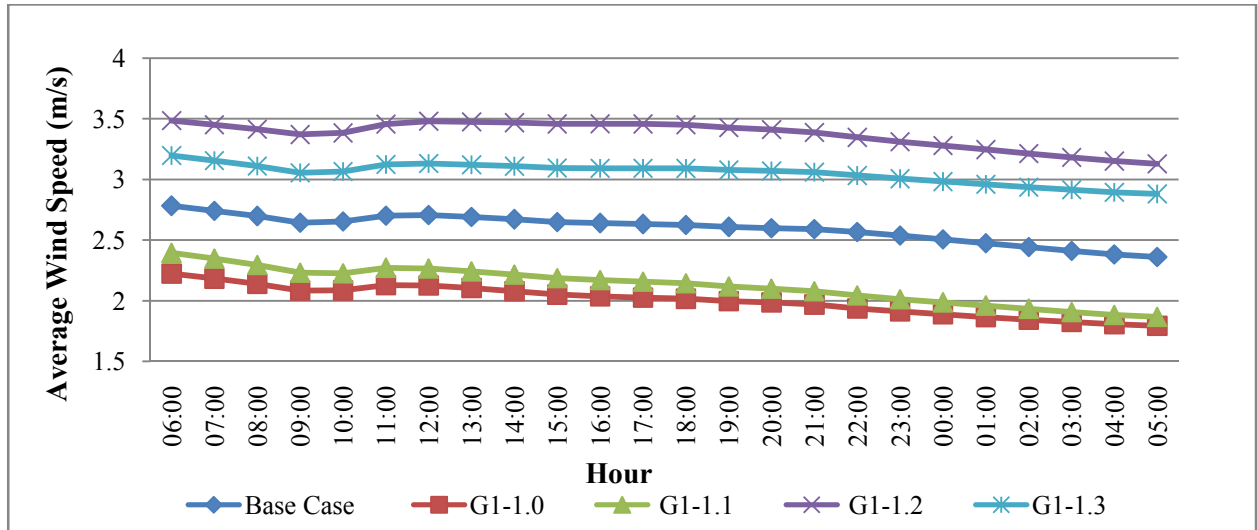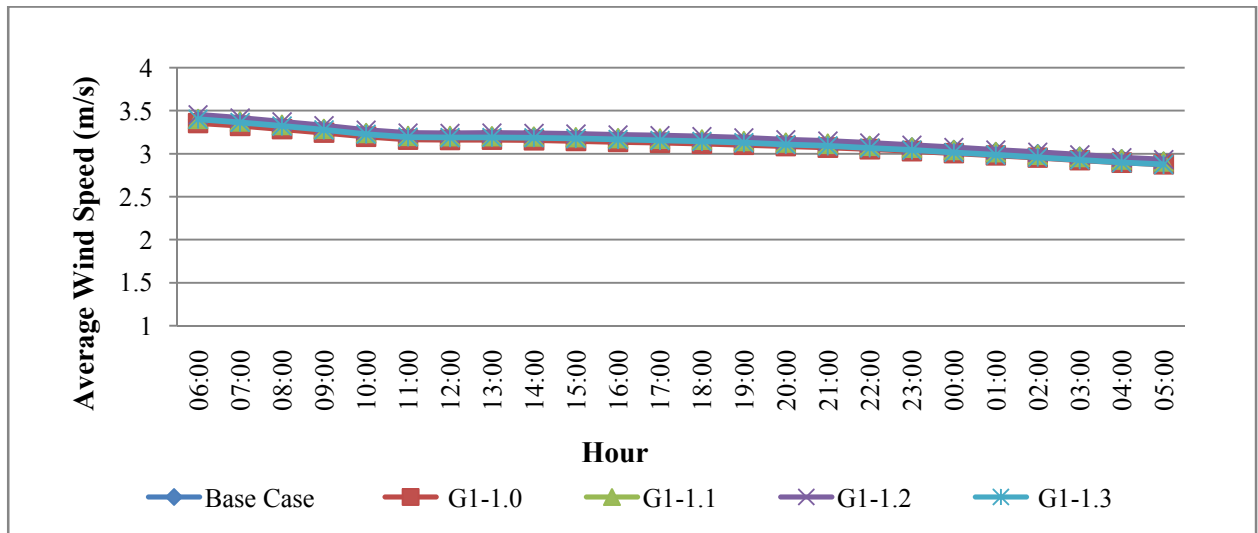
c) NE-SW orientation

d) NW-SE orientation

Figure 5.11: Hourly profile of the average wind speed on 21 June for the base case and the first group proposed configurations in the four orientations: N-S, E-W, NE-SW, and NW-SE

- The NE-SW orientation recorded the most significant variation of wind behaviour in the first group configurations. The highest wind velocity is recorded in the two configurations; G1-1.2 (3:7:7:3) and G1-1.3 (3:3:7:7) with a maximum velocity of 3.5m/s and 3.2 m/s respectively. While the configurations G1-1.0 (7:3:3:7) and G1-1.1 (3:7:3:7) recorded the lowest maximum wind velocity of 2.2 m/s and 2.4 m/s respectively (Figure 5.11 c).

The significant effect of the diversity in buildings height on wind flow can be observed in the G1-1.2 (3:7:7:3) configuration and specifically in the NE-SW and NW-SE orientations. For the first four hours the NW-SE and NE-SW orientations record maximum values of approximately 3.5 m/s. Starting from 10:00 the G1-1.2 (3:7:7:3) configuration recorded higher wind speeds in the NE-SW orientation compared to the NW-SE with a slight variation of 0.2 m/s recorded at 11:00 between the two orientations (Figure 5.11 c). The maximum and minimum wind velocity for the first group configurations is presented in figure 5.12. The figure shows;

- For the first configuration G1-1.0 (7:3:3:7), the NW-SE wind records the highest maximum averages of 3.4 m/s. On the other hand, the lowest maximum recorded in NE-SW direction with 2.2 m/s. The N-S and E-W orientations recorded close values of maximum and minimum wind speed varied between 2.5 m/s and 2.1 m/s respectively (Figure 5.12).

- Similar to the first configuration, the maximum wind speed recorded for the second configuration G1-1.1(3:7:3:7) is in the prevailing wind direction NW-SE. Furthermore, the N-S and E-W record almost similar values, and the lowest maximum for the G1-1.1 (3:7:3:7) recorded in NE-SW direction with value of 2.4 m/s (Figure 5.12).

- The third configuration 1-1.2 (3:7:7:3) performs better with regard to enhancing the wind speed to reach the highest speed in the NE-SW direction the with 3.5 m/s compared to all configuration (Figure 5.12 c).

The wind flow with respect to block orientation in the fourth configuration G1-1.3 (3:3:7:7) shows that the highest maximum speed value recorded in the NW-SE orientation with 3.4 m/s followed by 3.2 m/s in the NE-SW orientation. The two orientations record very close values staring from 11:00 as the wind in NW-SE direction slightly decreases and the wind in NE-SW direction slightly increases. Other than that, and similar to the previous configurations in this group, the N-S and E-W orientations record approximate values for wind velocity (Figure 5.12).

On the other hand, comparing the wind behaviour of the four configurations in the first group with the base case showing that the NW-SE prevailing wind is the dominate wind in four configurations in addition to the base case with a maximum velocity of 3.6 m/s for the third configuration G1-1.2 (3:7:7:3). The same configuration records the highest wind speed in NE-SW orientation with velocity of 3.5 m/s. Hence, in the NE-SW orientation, the velocity of the two blocks of configurations G1-1.2 (3:7:7:3) andG1-1.3 (3:3:7:7:) records a velocity higher by around 0.4m/s to 0.7m/s respectively compared to the base case in the same orientation. Compared to the base case, in both orientations N-S and E-W shows that the wind speed of the G1-1.0 (7:3:3:7) and G1-1.1 (3:7:3:7) is higher than the wind velocity of the base case in the same orientations. In the N-S and E-W orientations the maximum wind speed is around 2.8m/s and can be observed in configuration G1-1.1 (3:7:3:7) (5.12 a and b). This proves the effect of the height diversity on accelerating air flow within the block in all configurations G1-1.0 (7:3:3:7), G1-1.1(3:7:3:7), G1-1.2 (3:7:7:3) and G1-1.3 (3:3:7:7:) configurations compared to the base case and with respect to the canyon orientation.
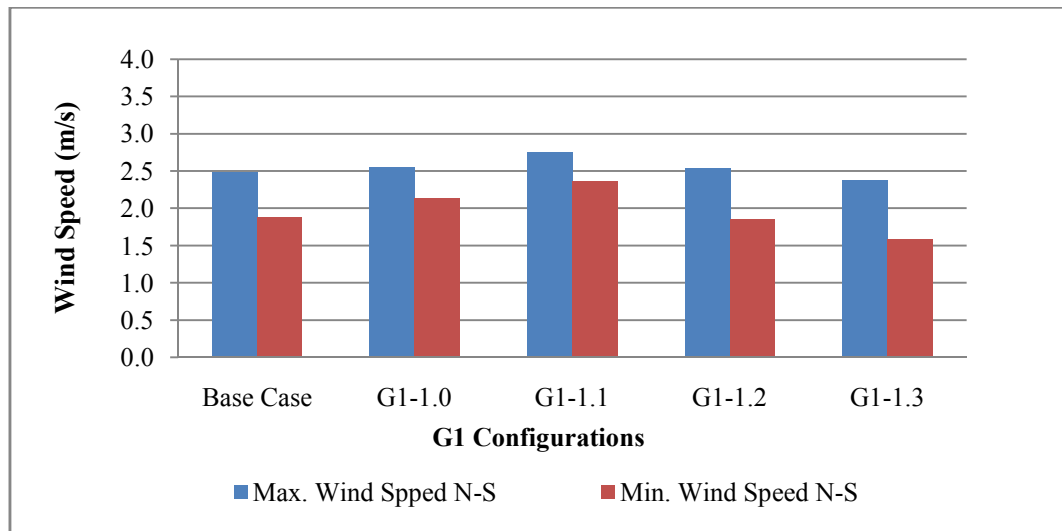
a) N-S orientation
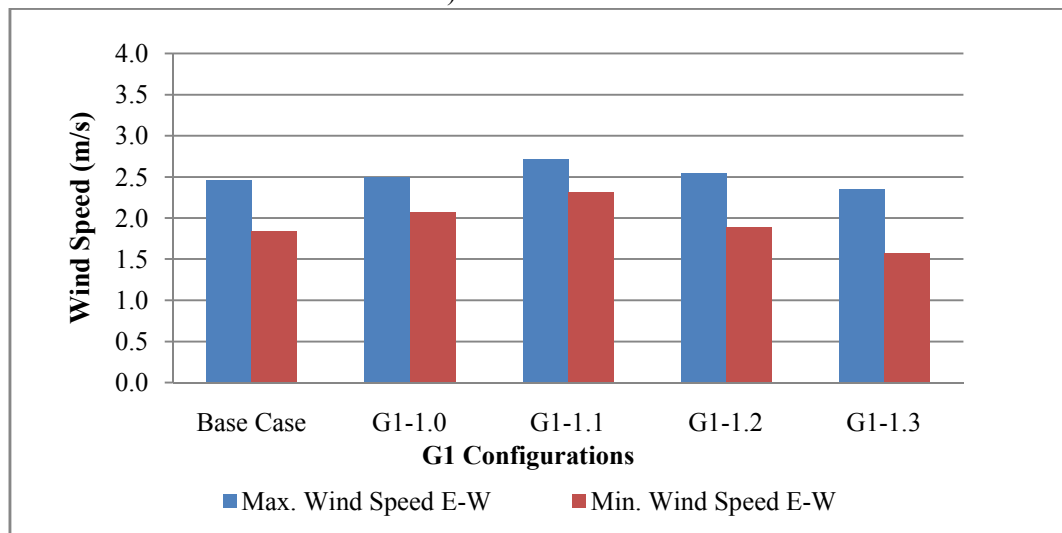
b) E-W orientation
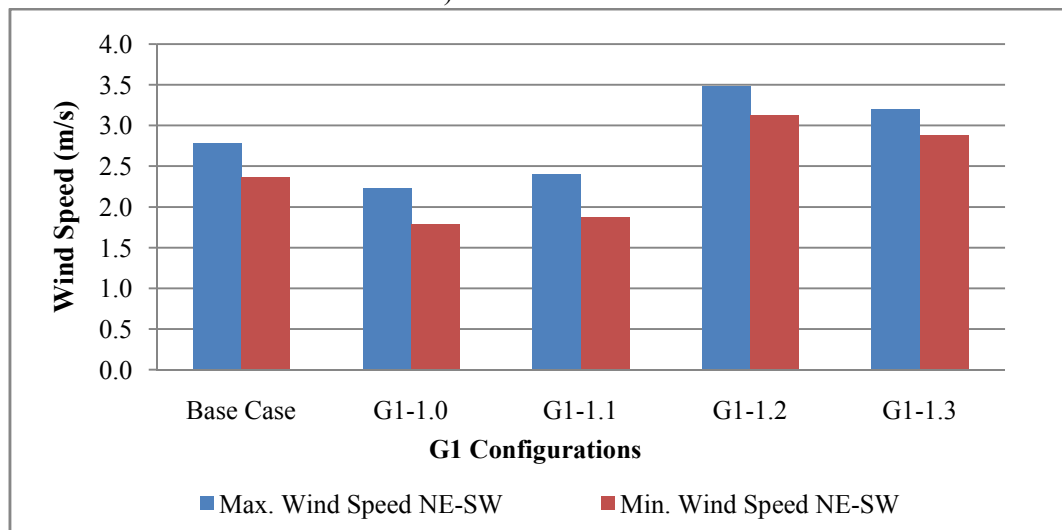
c) NE-SW orientation
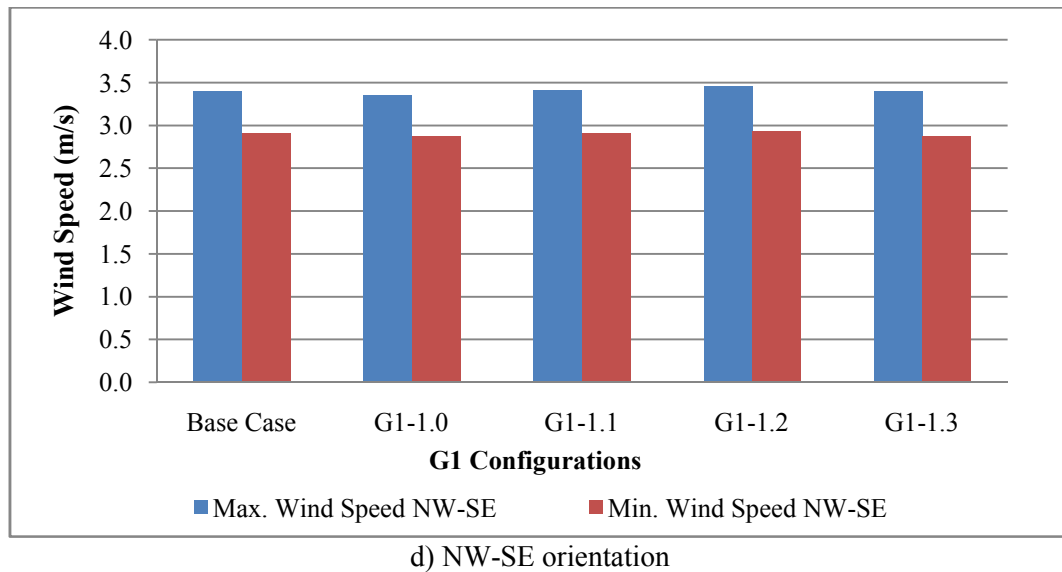
d) NW-SE orientation

Figure 5.12: The variation between the maximum and minimum wind velocity of the first group proposed configurations in the four orientations; a) N-S and b) E-W, b) NE-SW, and d) NW-SE

5.2.4 Relative Humidity

Evaluation of the average relative humidity in the canyons of the first group blocks is collected at the same level from the ground of the air temperature data1.4m using the micro climate data generated from the ENVI-Met software. The daily profile of the outdoor relative humidity of the four configurations in the first group is in the four simulated orientations illustrated in figure 5.13. Generally, the relative humidity starts by recording high values varied between 87 % and 80 % at early morning for all configurations. Then the relative humidity starts on decrease to reach the minimum values at 16:00 in all configuration and for all orientations with values varied between 38% and 40%. This is followed by another increase to reach a percentages between 45% and 55% during the evening time. However, for early morning and afternoon hours the least relative humidity values were recorded in the E-W and N-S directions. It has been observed that the decrease in relative humidity averages connected with the increase in air temperature averages. Therefore, the relative humidity averages show an opposite attitude to the air temperature averages with respect to the minimum and maximum values.

188

Moreover, comparing the relative humidity of the first group configurations with each other and with the base case is illustrated in figure 5.13.TheNW-SE orientation shows an approximate value with a slight variation in each configuration averages by about 4 %, the lowest minimum value recorded in the first configuration G1-1.0 (7:3:3:7) with 37.2 % compared to 39.0 % for the base case. Furthermore, in the E-W and N-S orientations the minimum relative humidity is stable around 40 % for the base case and the configurations of the first group.
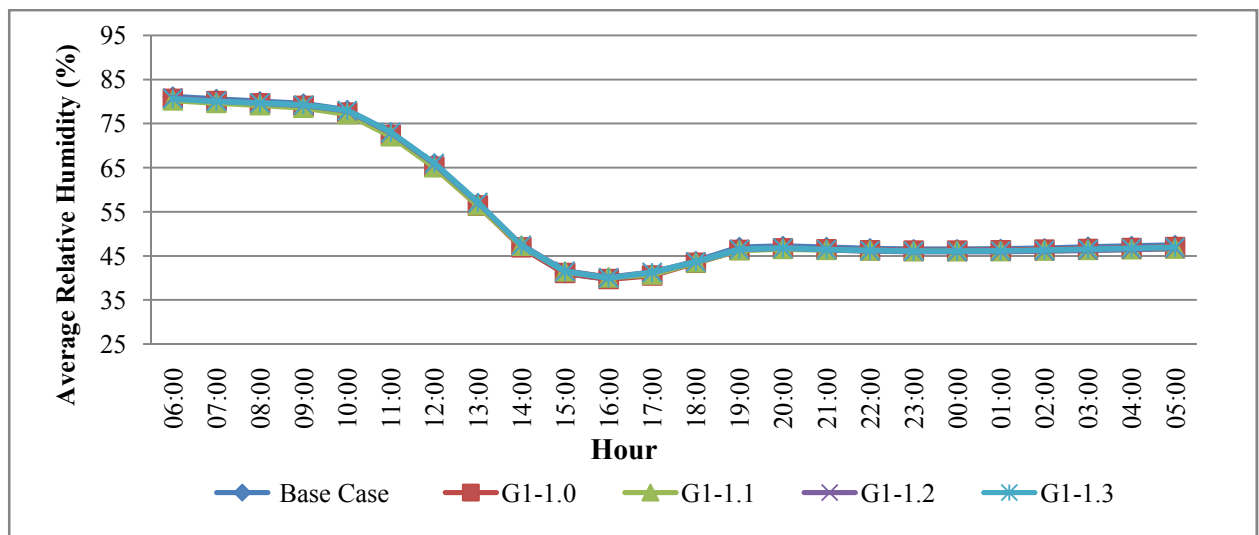
a) N-S orientation
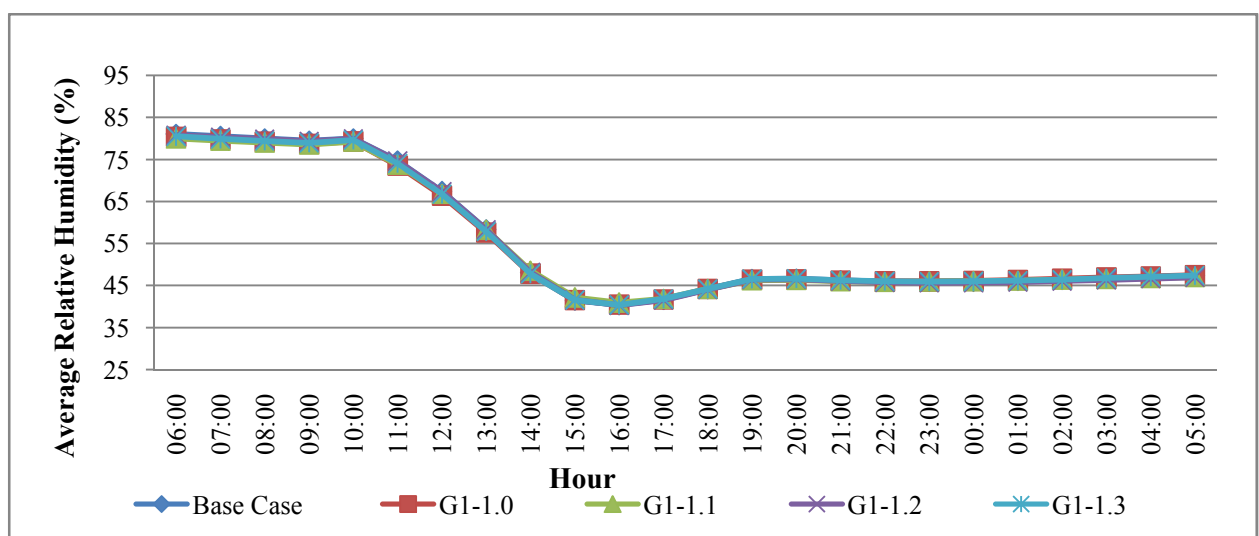
b) E-W orientation
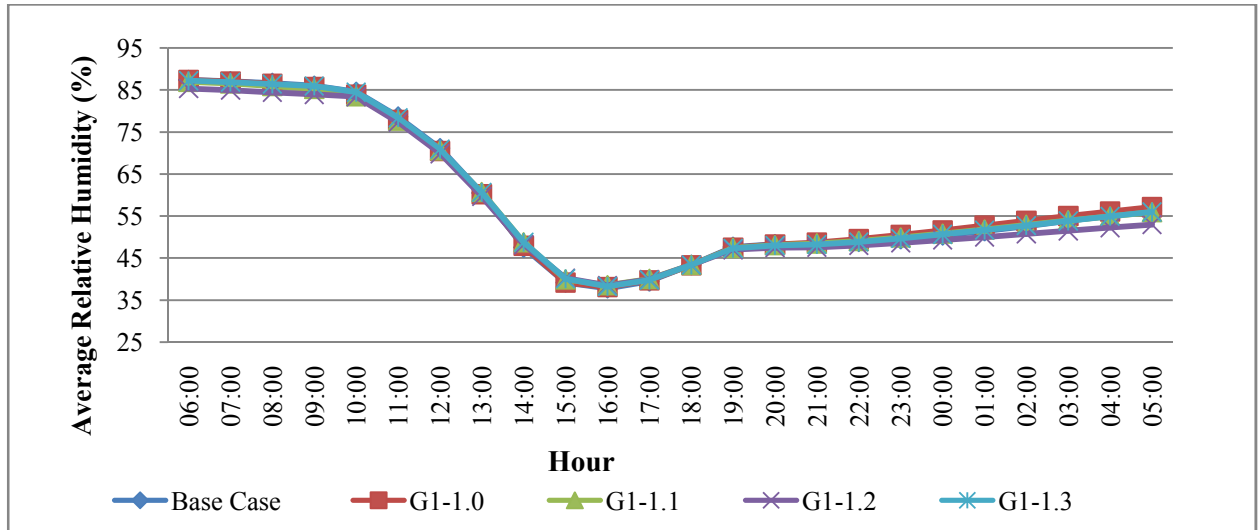
c) NE-SW orientation

d) NW-SE orientation

Figure 5.13: Hourly profile of the average relative humidity on 21 June for the base case and the first group proposed configurations in the four orientations: N-S, E-W, NE-SW, and NW-SE

However, the humidity in the E-W orientation is slightly higher than the N-S orientation for all configurations. The NE-SW orientation recorded the minimum relative humidity values while the maximum air temperature averages is recorded in the orientation as presented in the previous section.

Furthermore, the most notable fluctuation in relative humidity minimum averages are observed in NW-SE orientation comparing with the other three orientations (Figure 5.13 d). The variation in relative humidity in this orientation is related to the N-W prevailing wind effect.

Moreover, the fluctuated and minimum values of the relative humidity recorded in this orientation for all configurations proves the effect of wind speed on reducing the relative humidity averages.

5.3 The Second Group of the Proposed Configurations

The second group of proposed scenarios consists of six configurations, the variation in buildings between these configurations based on implementing gradual height variation in the long axis of the block. The general gradual proportion of this configurations is (3:5:7), and the buildings floor number: G+3,G+5, and G+7 with a total height of 16m, 24m, and 32m, respectively. The second group has six configurations with the following proportions: G 2-2.0 (7:5:3:3:5:7), G 2-2.1 (3:5:7:7:5:3), G 2-2.2 (5:7:3:3:7:5), G 2-2.3 (7:3:5:5:3:7), G 2-2.4 (3:7:5:5:7:3), and G 2-2.5 (5:3:7:7:3:5) (Figure 5.14). The impact of these configurations on the urban block's microclimate parameters will be explored.

Furthermore, a comparison between these developed topologies and the base case will be illustrated. The micro climate output results of simulating the second group will be presented and compared according to the block orientations and group proposed configurations. In the previous section the results of the first group with respect to the studied microclimate parameters is illustrated in detail. The same sequence of data illustration will be followed for the six configurations of the second group.
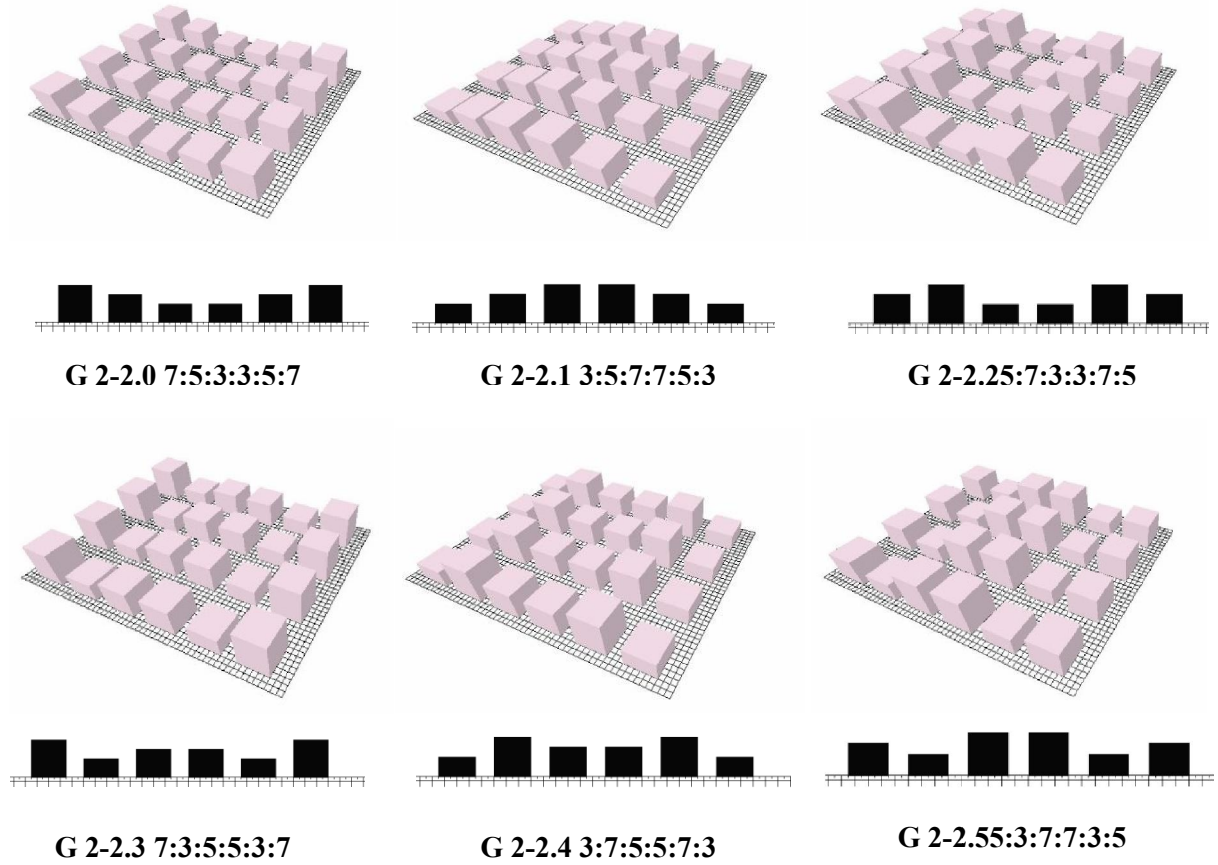
Figure 5.14: Isometric view of the second group of proposed configurations with buildings height proportion (3:5:7): G2-2.0 (7:5:3:3:5:7),G2-2.1 (3:5;7:7:5:3),G2-2.2 (5:7:3:3:7:5),G2-2.3 (7:3:5:5:3:7),G2-2.4 (3:7:5:5:7:3), and G2-2.5 (5:3:7:7:3:5)

5.3.1 Sky View Factor (SVF)

The SVF profile of the second group's configurations is illustrated in figure 5.15. The figure shows the variation in the SVF between the six configurations from one side, and with the base case from the other side. The G2-2.5 (5:3:7:7:3:5) configurations recorded the lowest average of 0.41, whereas the G2-2.0 (7:5:3:3:5:7) configuration has the highest SVF average of 0.47 with an increase of 4 % compared to the base case. Furthermore, the G2-2.1 (3:5:7:7:5:3) configuration with the highest buildings placed in the middle of the block shows a SVF similar to the best configuration with a value of 0.41.

However, the G-2.2 (5:7:3:3:7:5) and G-2.3 (7:3:5:5:3:7) configuration have very close values of SVF equal to 0.43 and 0.44, respectively. The G2-2.4 (3:7:5:5:7:3) configuration has a close performance to the best configuration G2-2.5 (5:3:7:7:3:5) with respect to exposure to the sun access, and the SVF of the G2-2.4 (3:7:5:5:7:3) configuration is 0.42 (Figure 5.15).

Base Case (5:5:5:5)

SVF = 0.45

G 2-2.0 (7:5:3:3:5:7)

SVF = 0.47

G2-2.1 (3:5:7:7:5:3)

SVF = 0.41

G2-2.2 (5:7:3:3:7:5)   G2-2.3 (7:3:5:5:3:7)

SVF = 0.43   SVF = 0.44

G2-2.4 (3:7:5:5:7:3)   G2-2.5 (5:3:7:7:3:5)

SVF = 0.42   SVF = 0.41
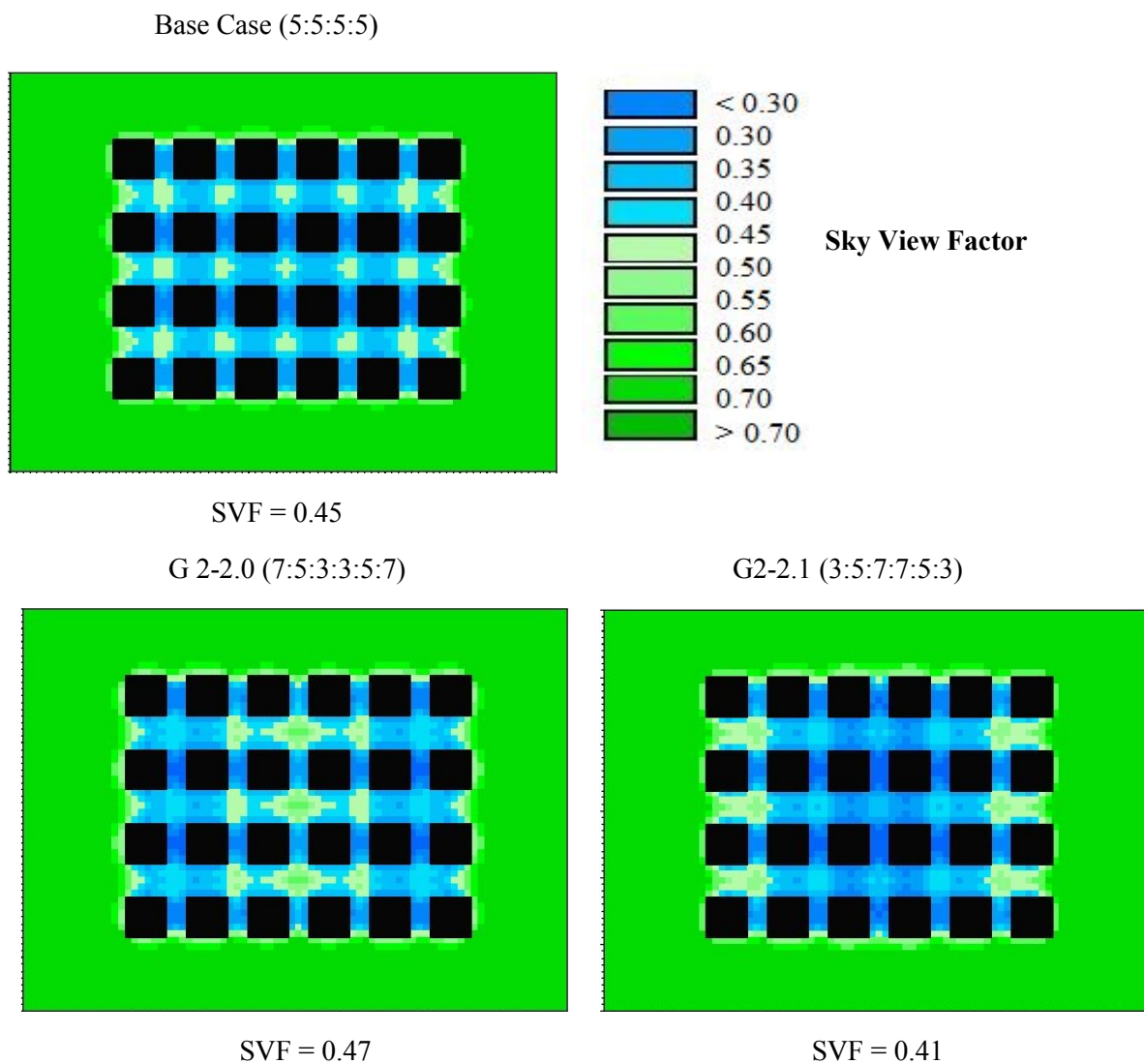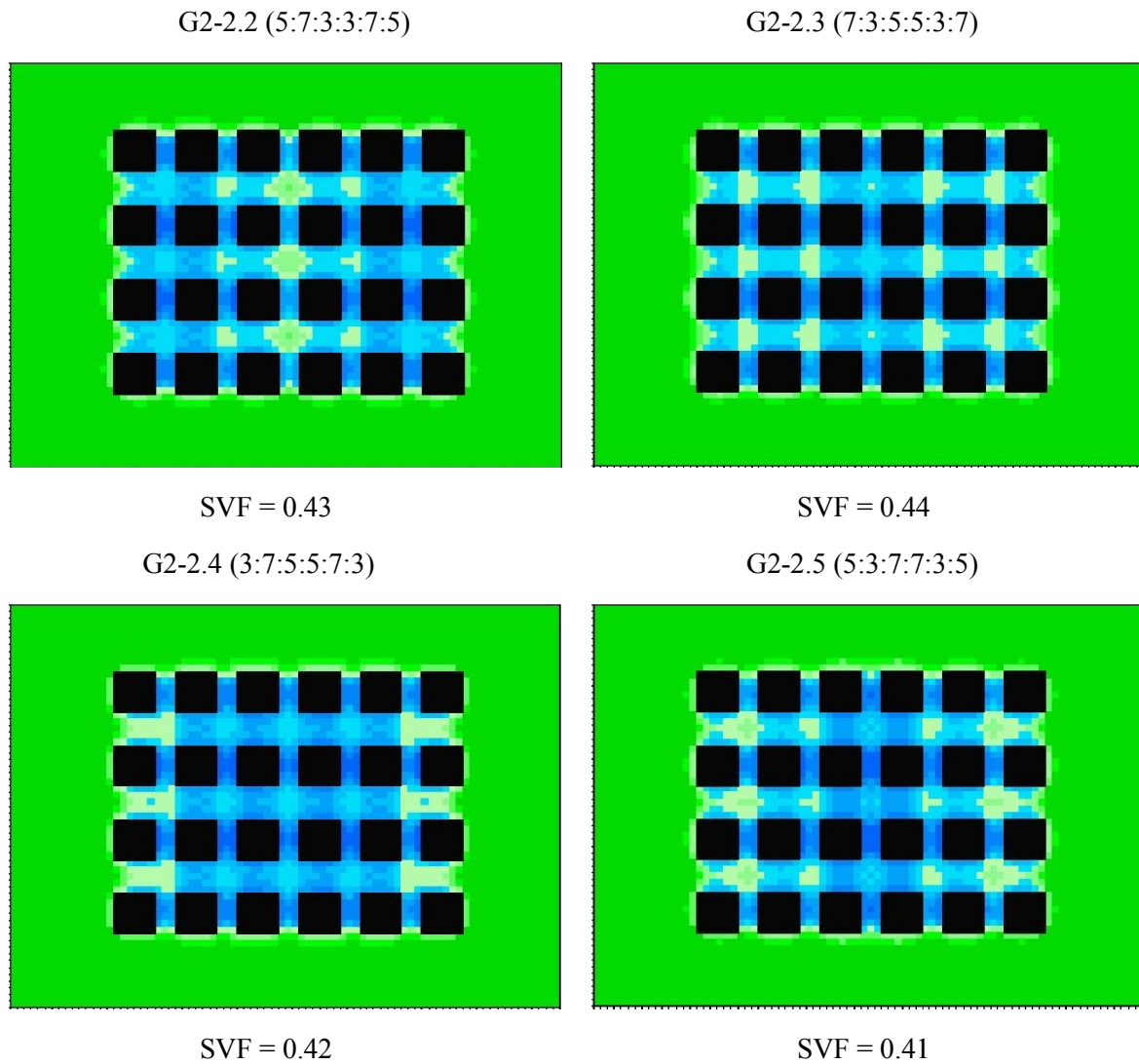
Figure 5.15: The Sky View Factor (SVF) of the base case and the six proposed configurations in the second group; G 2-2.0 (7:5:3:3:5:7), G 2-2.1 (3:5:7:7:5:3), G 2-2.2 (5:7:3:3:7:5), G 2-2.3 (7:3:5:5:3:7), G 2-2.4 (3:7:5:5:7:3), and G 2-2.5 (5:3:7:7:3:5)

5.3.2 Air Temperature

The air temperature averages of the urban block recorded on the simulated day 21st June in the four mentioned orientations; N-S, E-W, NE-SW, and NW-SE. The averages of the air temperature are collected from the nine receptor points presented in the general layout of the base case configuration. The simulation results of the six configurations in the second group shows the following:

- The maximum air temperature recorded at 15:00 for all configurations and in the four simulated orientations. Air temperature averages of the N-S and E-W orientations varied around 35.5°C with no significant variation between all configurations.

- The highest maximum air temperature is recorded in the G 2-2.1 (3:5:7:7:5:3) and G 2-2.2 (5:7:3:3:7:5) with 35.8°C and 35.7°C in the N-S and E-W directions, respectively.

- The lowest maximum air temperatures recorded in the same orientations are; 35.5°C and 35.6°C for the configurations G 2-2.0 (7:5:3:3:5:7), and G 2-2.5 (5:3:7:7:3:5), respectively. The air temperature averages of the N-S and E-W orientations are illustrated in Figure 5.16 a and b.

- From the above, no significant variation between the highest and lowest maximum temperature at 15:00 but the lowest maximum value recorded in N-S orientation for the configuration G2-2.0 (7:5:3:3:5:7) with 35.5°C. Compared to the base case to base case with maximum average air temperature of 35.8°C in N-S orientation with a slight reduction of 0.3°C (Figure 5.16 a and b).

- On the other hand, a significant variation in canyons air temperature averages is observed in the NE-SW block orientation (Figure 5.16 c). The highest maximum temperature is recorded in the third configuration G 2-2.2 (5:7:3:3:7:5) with 38.4 ° C ,followed by 38.35°C for configuration G 2-2.0 (7:5:3:3:5:7) in the same orientation.

- The configuration G 2-2.1 (3:5:7:7:5:3) records the second lowest maximum temperature is for with 36.8°C,while the least maximum air temperature at 15:00 pm recorded by configuration G 2-2.5 (5:3:7:7:3:5) is 36.7°C with a reduction of 1.7°C between the highest and lowest maximum air temperature in this orientation (Figure 5.16 c).
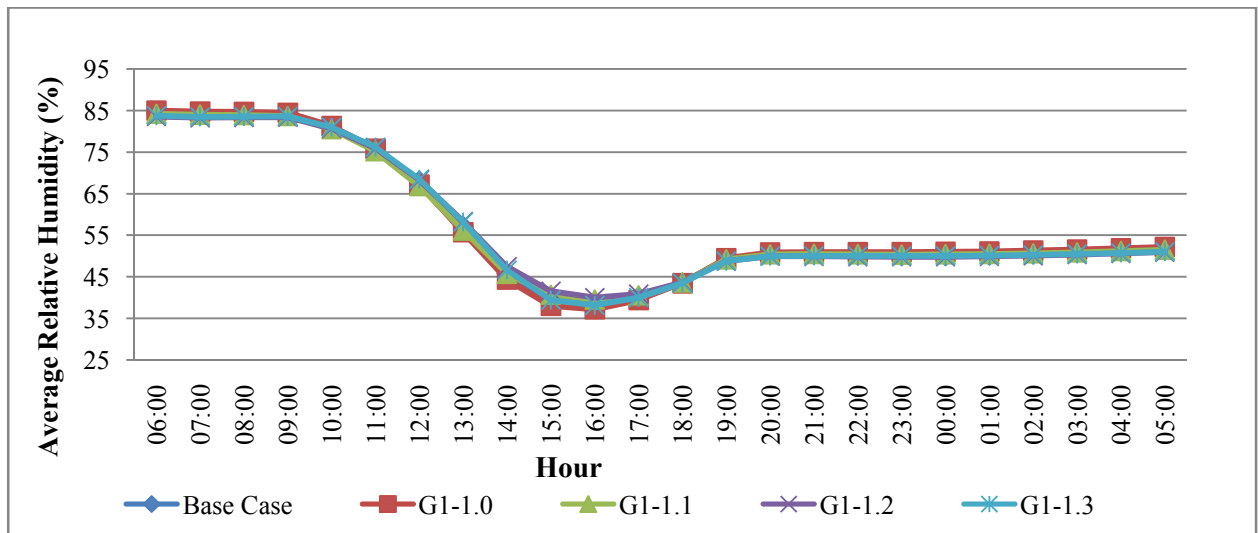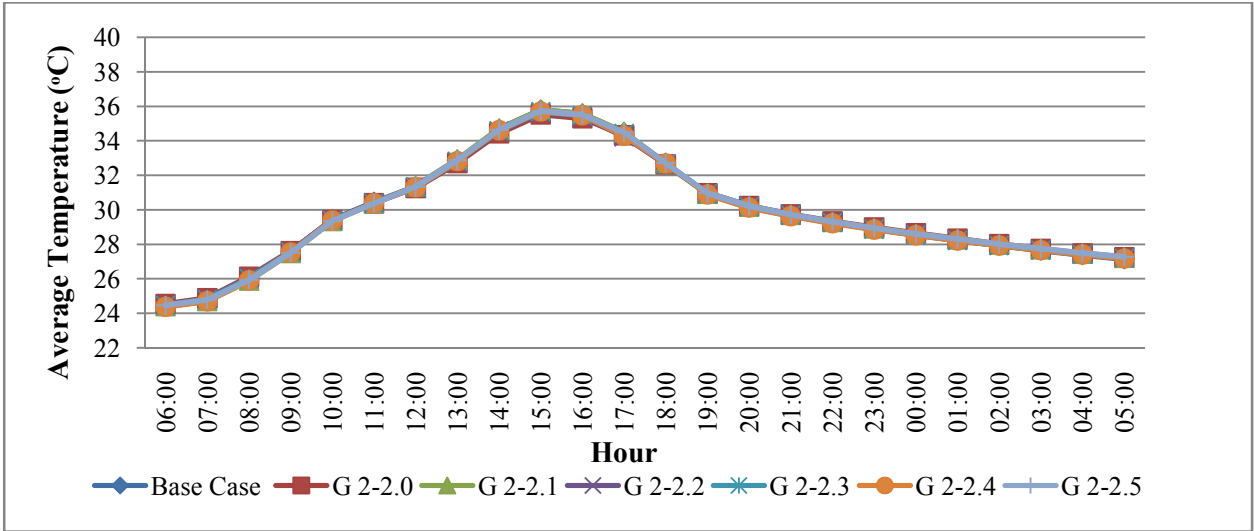
a) N-S orientation
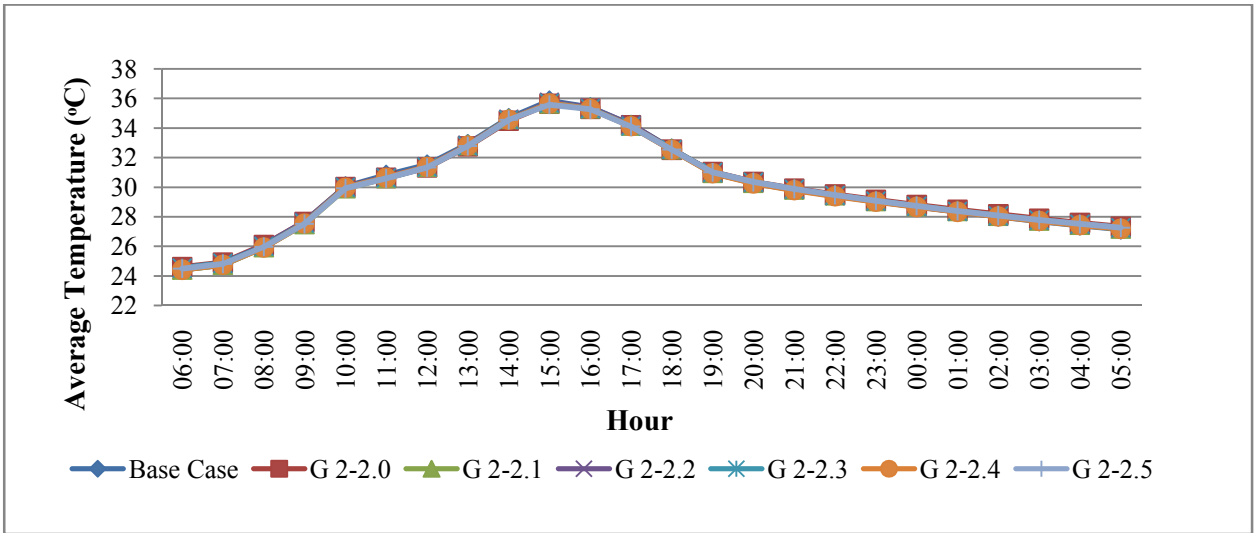
b) E-W orientation
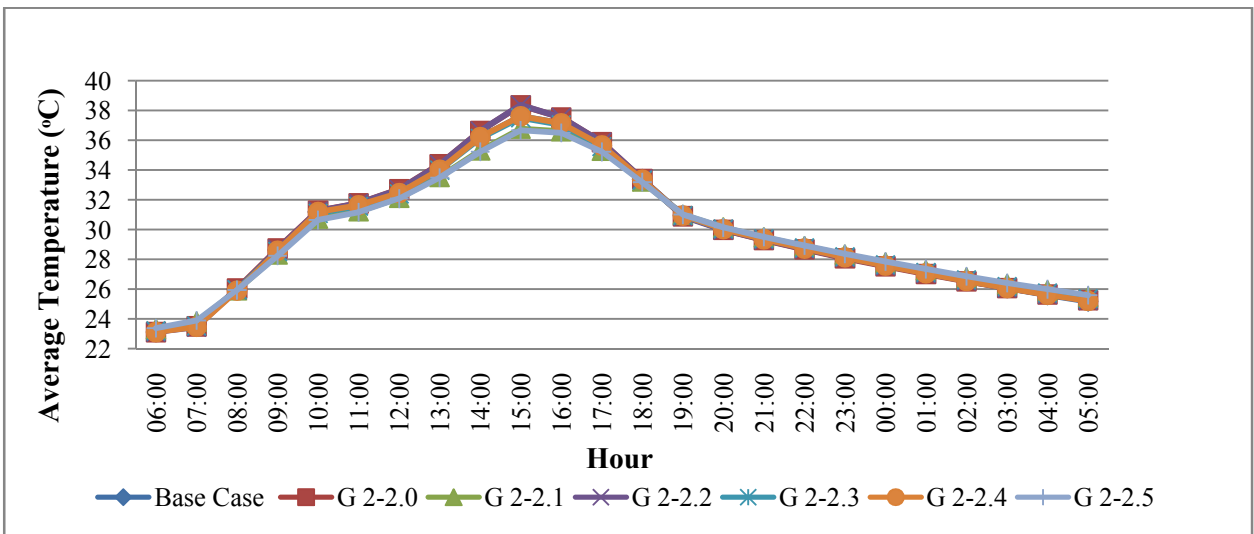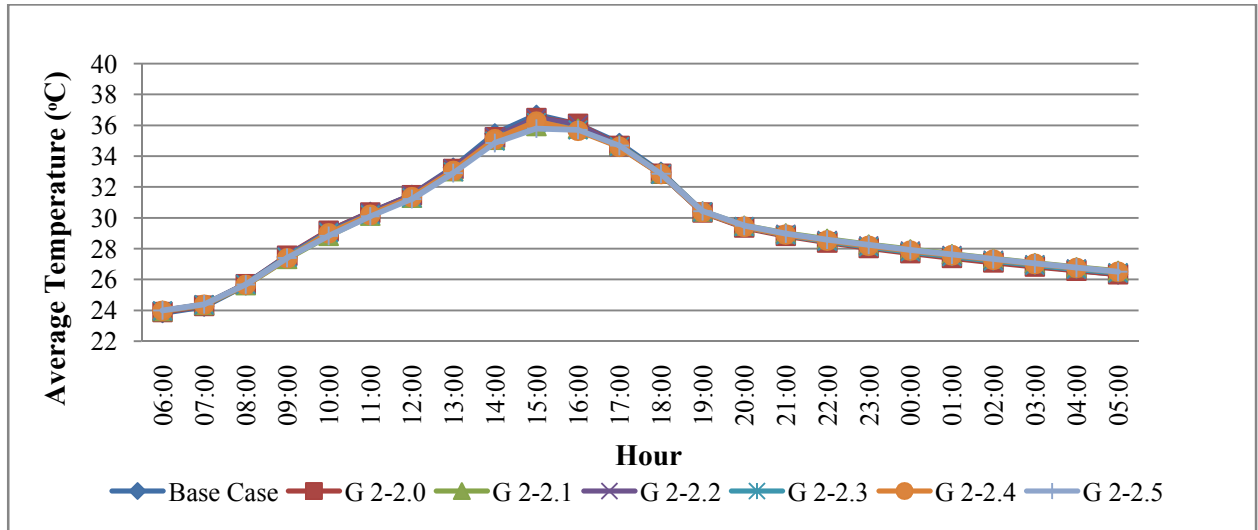
c) NE-SW orientation

b) NW-SE orientation

Figure 5.16: Hourly profile of the average air temperature on 21 June for the base case and the second group six proposed configurations in the four orientations: N-S, E-W, NE-SW, and NW-SE

- Compared to the base case with maximum air temperature of 37.6°C in NE-SW orientation, the G 2-2.5 (5:3:7:7:3:5) configuration records a decrease of 0.95°C. On the other hand, the configuration 2.4 (3:7:5:5:7:3), is the closest configuration to the base case with air temperature of 37.6°C (Figure 5.16c)

- Figure 5.16 d illustrates the second group maximum air temperature averages in the NW-SE orientation.

- All configurations show the same air temperature behaviour in the NW-SE orientation, but the G 2-2.5 (5:3:7:7:3:5) configuration records the lowest maximum air temperature of 35.8°C compared to the other configurations including the base case of 36.7°C temperature, with a reduction of 0.9°C between the G 2-2.5 (5:3:7:7:3:5) and the base case (Figure 5.16 d).

- Furthermore, the reduction between the highest maximum temperature recorded by G2-2.0 (7:5:3:3:5:7) and lowest maximum air temperature of the G2-2.5 (5:3:7:7:3:5) configuration is 0.7°C.

197

- However, the maximum air temperature recorded at 15:00 for all configurations in the four simulated orientations. The figures show a clear variation in maximum air temperature between the NE-SW, NW-SE and the two other orientations N-S and E-W. Moreover, the figures show that the lowest maximum air temperature averages recorded by the G2-2.5 (5:3:7:7:3:5) configuration in the three orientations; E-W, NE-SW, and NW-SE.

  On the other hand, the G2-2.0 (7:5:3:3:5:7) configuration recorded the highest maximum air temperature in the NW-SE orientation, and recorded the lowest maximum air temperature in the N-S orientation. The variation between the highest maximum air temperature for this configuration in the two mentioned orientations is 1.0 ^{o}C.

- In the second group six configurations and for all orientations the minimum air temperature averages recorded by G 2-2.0 (7:5:3:3:5:7) configuration in the N-S orientation. While the maximum recorded in G 2-2.2 (5:7:3:3:7:5) configuration in the NE-SW orientation with a variation of 2.8^{o}C between the minimum and the maximum.

5.3.3 Wind Speed

The wind profiles of the second group configurations in the four simulated orientations are illustrated in figure 5.17. The wind behaviour in N-S and E-W orientations have a close profile for all configurations. The effect of the prevailing NW-SE wind is clear by recording the highest maximum wind velocity by all configurations in this orientation. However, the G 2-2.5 (5:3:7:7:3:5) configuration recorded the highest wind velocity compared to other configurations and in the three orientations. While the G 2-2.1 (3:5:7:7:5:3) recorded the highest maximum velocity in NE-SW orientation and the second maximum wind velocity in the other three orientations. Further to this, in the NE-SW orientation all configurations show

a very close wind velocity values. Figure 5.17 shows that the base case configuration has a lower maximum wind velocity compared to the maximum wind velocity in all orientations. The variation observed in E-W orientation is the steep drop in wind speed at 10:00 am compared to the other orientations which has a steady drop in the wind velocity profile at the same time of the day. This steady drop is the least in the NW-SE orientation as the prevailing wind has the dominated influence in this orientation.
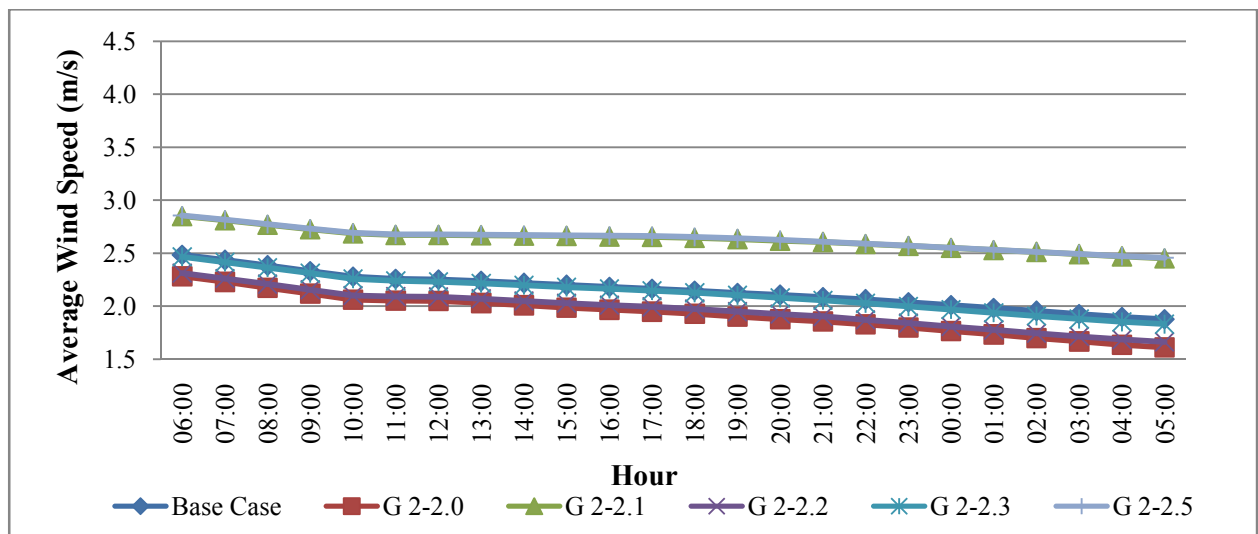
a) N-S orientation
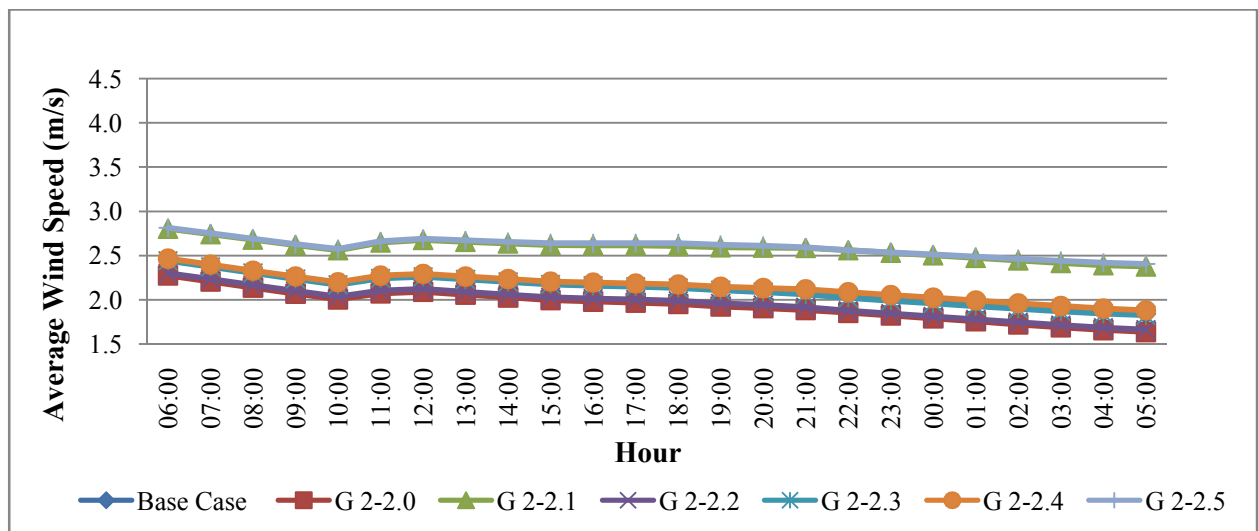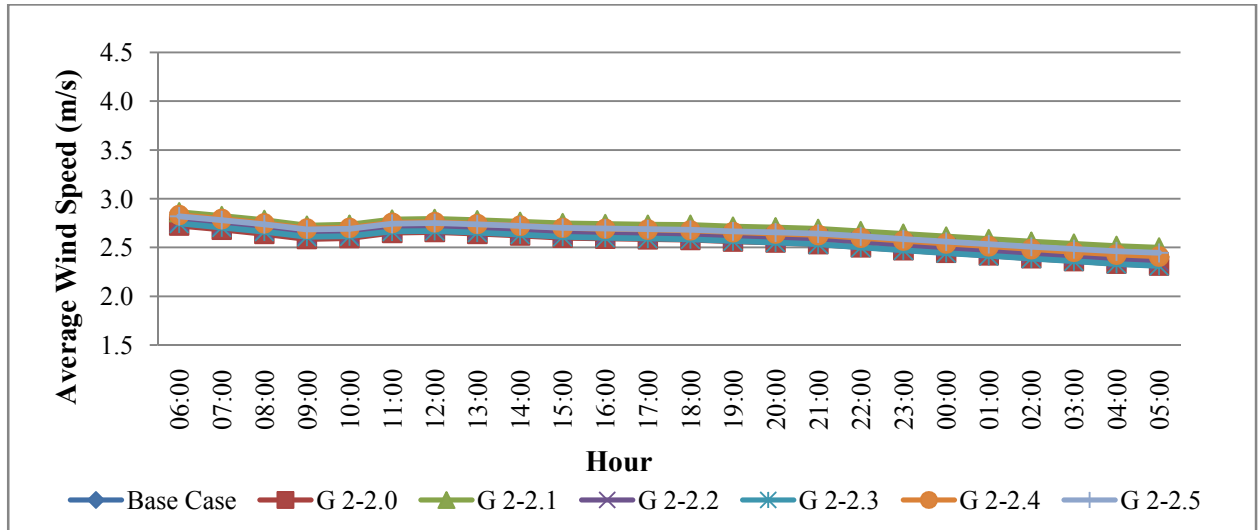
b) E-W orientation
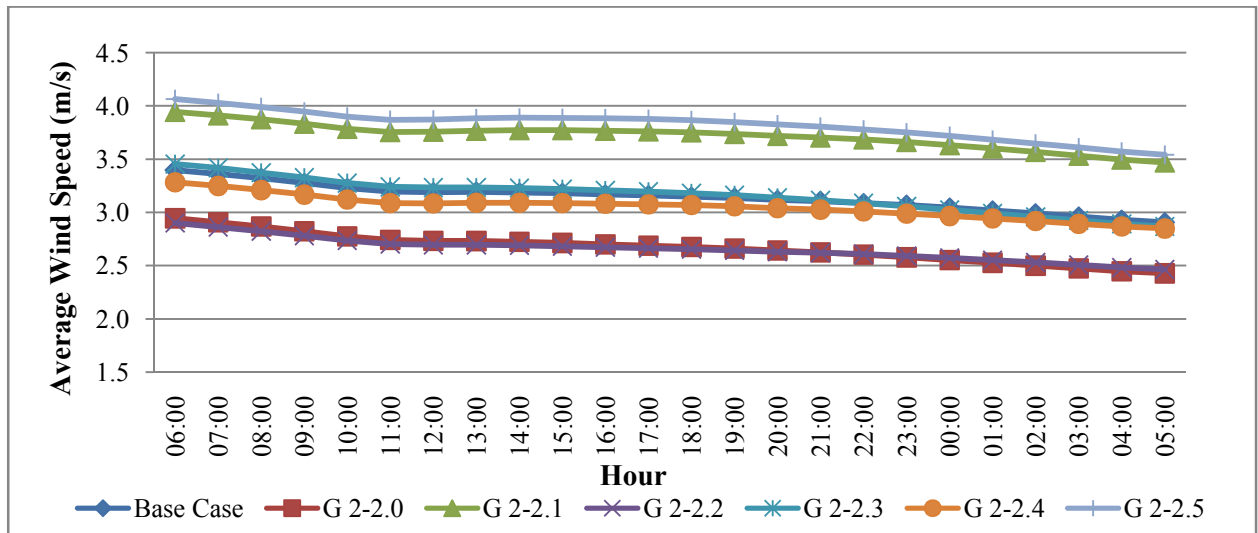
c) NE-SW orientation

d) NW-SE orientation

Figure 5.17: Hourly profile of the average wind speed on 21 June for the base case and the second group six proposed configurations in the four orientations: N-S, E-W, NE-SW, and NW-SE

Furthermore, figure 5.18 shows the maximum and minimum wind velocity in the four orientations. In the N-S and E-W orientation the maximum values of wind velocity varied between 2.2 m/s and 2.8 m/s for all configurations (Figure 5. 18 a and b).

This variation is less in the NE-SW orientation, and the NE-SW orientation shows a very close profile of wind velocity in all orientations, and the maximum wind velocity in all six configurations varied slightly between 2.7 m/s and 2.8 m/s (Figure 5. 18 c and d). The significant variation is observed in the NW-SE orientation and the maximum wind velocity

recorded is 4.1m/s in G 2-2.5 (5:3:7:7:3:5) configuration, while the minimum in this orientation is 2.4 m/s recorded in G2-2.0(7:5:3:3:5:7) configuration. The effect of the maximum wind speed in G 2-2.5 (5:3:7:7:3:5) and G 2-2.1 (3:5:7:7:5:3) configurations is reflected on the lower maximum air temperature recorded in these two configurations as illustrated in air temperature results in the previous section. On the other hand, the minimum wind velocity recorded in N-S and E-W orientation with velocity of 1.6 m/s in the first configuration G2-2.0 (7:5:3:3:5:7) shows that this configuration does not promote the wind flow.
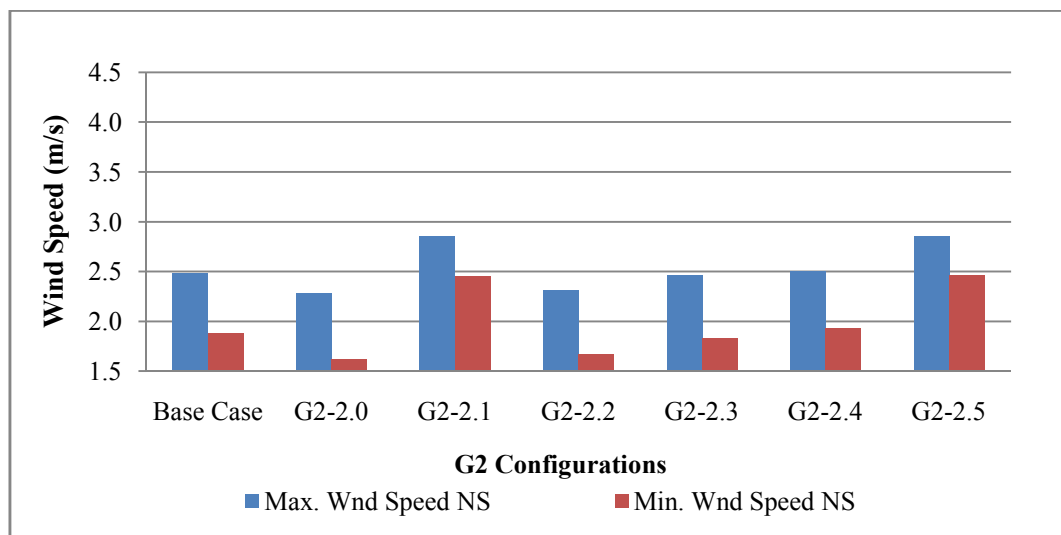
a) N-S orientation
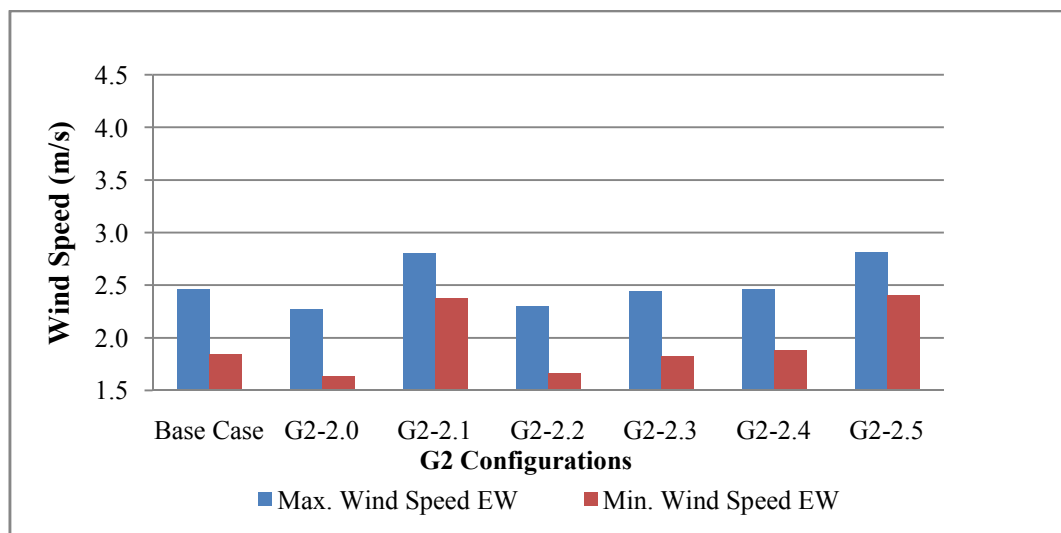
b) E-W orientation
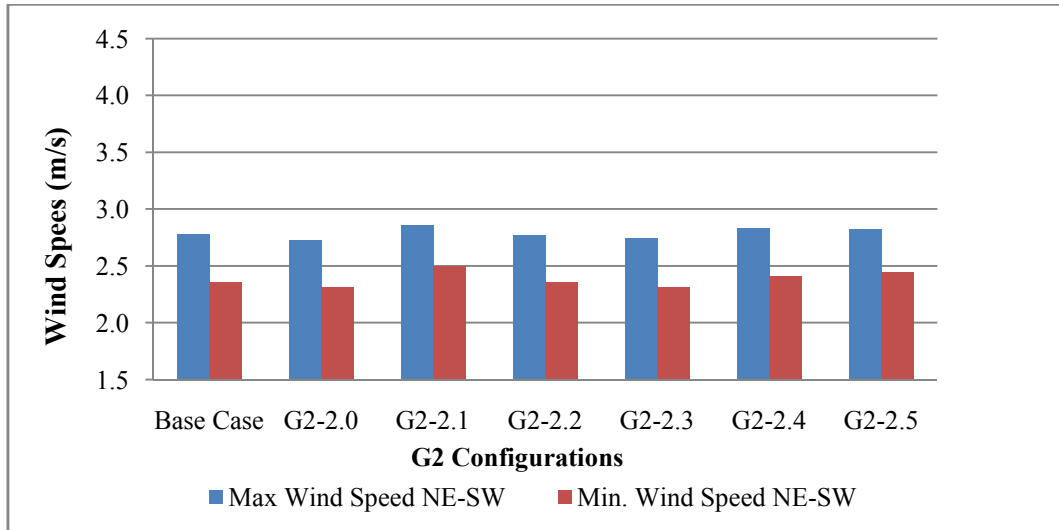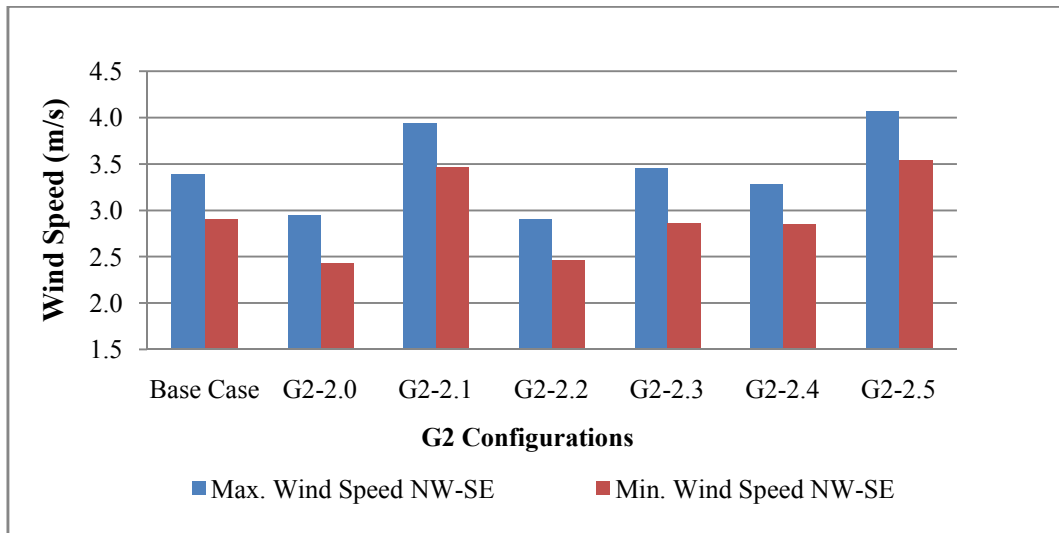
c) NE-SW orientation

d) NW-SE orientation

Figure 5.18.: The variation between the maximum and minimum wind velocity of the second group proposed configurations in the four orientations; a) N-S and b) E-W, b) NE-SW, and d) NW-SE

5.3.4 Relative Humidity

The relative humidity profiles for all configurations in the second group have very close trend profiles. The relative humidity of the second group configurations in the four orientations is presented in figure 5.19.

In general, the relative humidity averages show an opposite behaviour compared to the maximum air temperature averages, and the minimum relative humidity recorded at 16:00 for all configurations in the four orientations.

The maximum relative humidity varied around 80 % and was recorded in the N-S and E-W orientations. The E-W orientation had a slightly higher relative humidity compared to the N-S orientation.
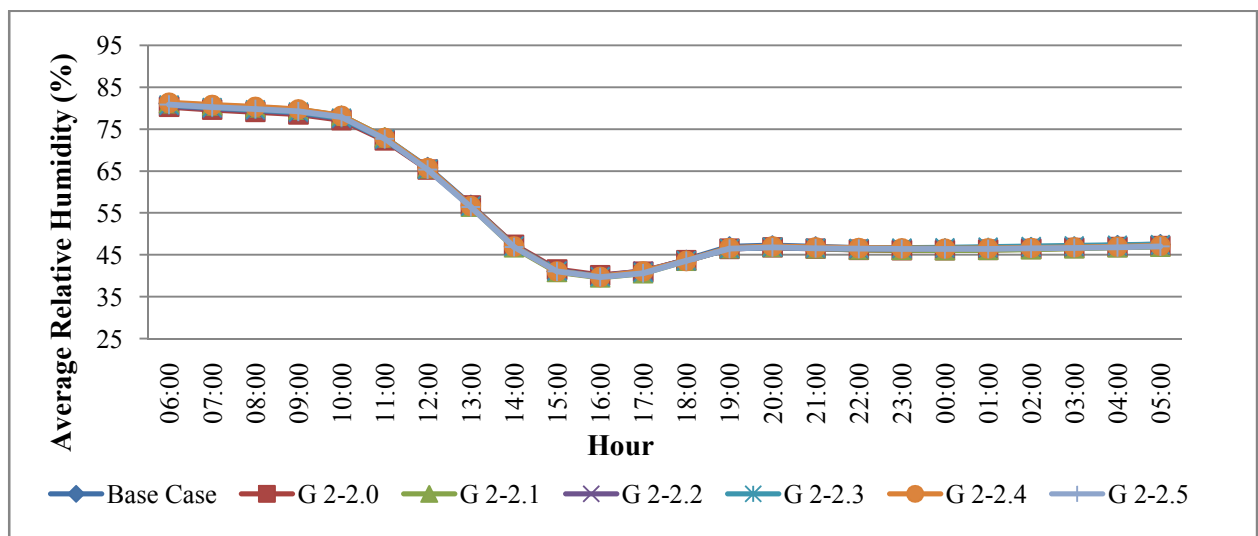
a) N-S orientation
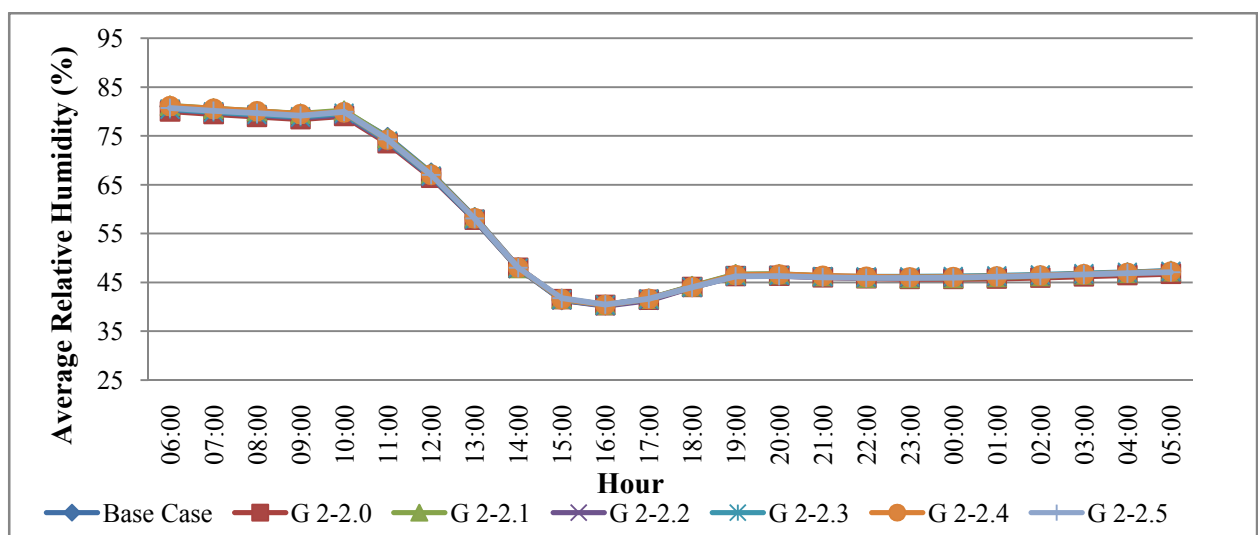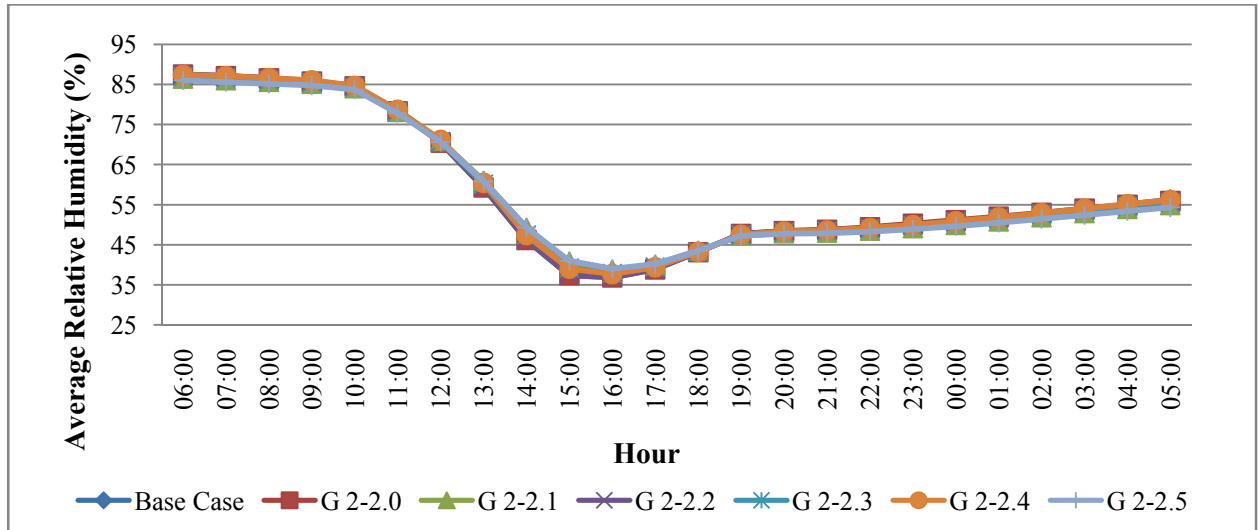
b) E-W orientation
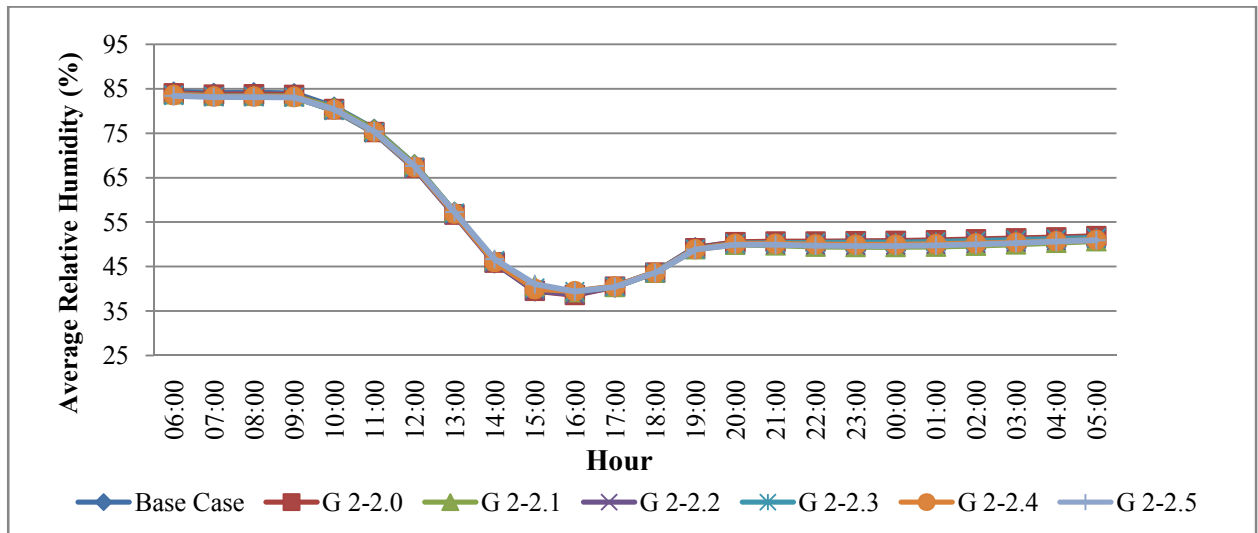
c) NE-SW orientation

d) NW-SE orientation

Figure 5.19: Hourly profile of the average relative humidity on 21 June for the base case and the second group six proposed configurations in the four orientations: N-S, E-W, NE-SW, and NW-SE

The maximum relative humidity averages recorded in the NE-SW with maximum average of 87.5% for the G 2-2.2 (5:7:3:3:7:5) configuration. Moreover, the same configuration G 2-2.2 (5:7:3:3:7:5) recorded the minimum relative humidity compared to all configurations including the base case at 16:00 pm is in the NE-SW direction with value of 36.9 %, and a reduction of 2.4 % compared to the base case.

In the NW-SE orientation, the relative humidity recorded lower maximum values varied around 83 % with a slight variation between all configurations, and the maximum recorded by G2-2.0 (7:5:3:3:5:7) with 83.9 % with a reduction of 1 % compared to the base case.

5.4 The Third Group of the Proposed Configurations

The third group consist of three configurations that represent the alternative or staggered buildings arrangement with uniform height, and the effect of arranging buildings in alternative arrangement is explored in the third group.

The three configurations included in this group are namely G 3-3.0, G 3-3.1, and G 3-3.2. Buildings' height in all configurations is G+5 with a uniform height of 24m. Placing buildings in staggered arrangement requires a change to the canyon or alley dimensions. The first configuration (canyons: alleys)width is G 3-3.0 (25m:20m), the variation implemented along the long direction to revise the alley width which became 20m, and the main canyons stay with width of 25m. In the second configuration G 3-3.1 (20m:20m), the canyons and the alleys are fixed with the same width of 20m for each. The third configuration G 3-3.2 (20m:15m), the variation implemented in the short direction and the canyons width became 20m and the alleys width stay with 15m.

The isometric view of each configuration is presented in figure 5.20. The effect of the three configurations in the third group will be illustrated with respect to the studied microclimatic parameters; air temperature, wind speed, and relative humidity. The presentation of the result will be through the comparison between the three configurations from one side, and with base case from the other side.

| G 3-3.0 (20:25) | G 3-3.1 (20:20) | G 3-3.2(15:20) |
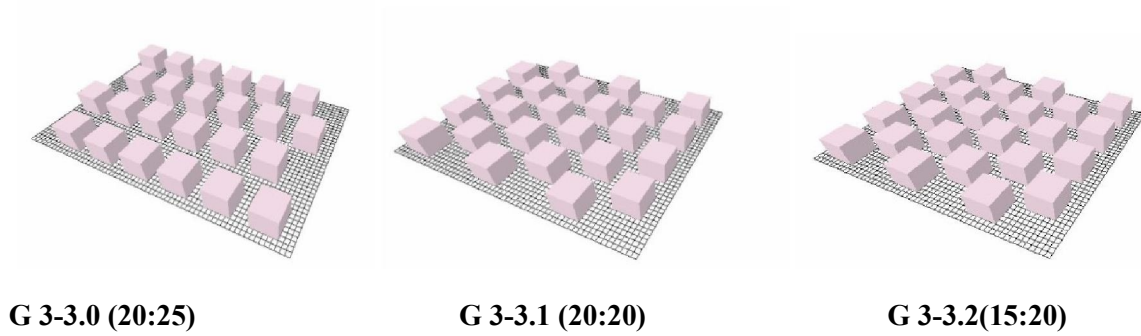
Figure 5.20 : Isometric view of the third set of proposed staggered configurations; G3-3.0 (20:25), G3-3.1 (20:20), and G3-3.2 (15:20)

5.4.1 Sky View Factor (SVF)

The SVF of the three configurations in the third group is illustrated in figure 5.21. The figure shows clearly the effect of the staggered arrangement of the buildings within the block on the SVF of the canyons between the buildings. Moreover, the figure presents the SVF for the base case and each configuration. The third configuration G 3-3.2 (20:15) recorded the lowest SVF of 0.33, and it is followed by the second and the first configurations with SVF equals to 0.39 and 0.46 respectively. In the third configuration the main canyon width was reduced from 25m to 20 in order to achieve the staggered arrangement, while the alleys were kept at the same width of 15m. Hence, and compared to the other configurations the SVF of the canyons between the buildings in this configuration is lower than the other two configurations as the H/ W ratio is higher.

Therefore, the points with high exposure to the sun access is less in this configuration compared to the two first configurations G 3-3.0 (25:20) and the second configuration G 3-3.1 (20:20), respectively. However, the buildings height over the canyon width ratio has a significant effect on the variation in the SVF as presented in the variation between this group's three configurations (Figure 5.21).

Base Case (5:5:5:5)

SVF = 0.45

G3-3.0 (20:25)

SVF = 0.47

G3-3.1 (20:20)

SVF = 0.39

G3-3.2 (15:20)

SVF = 0.33
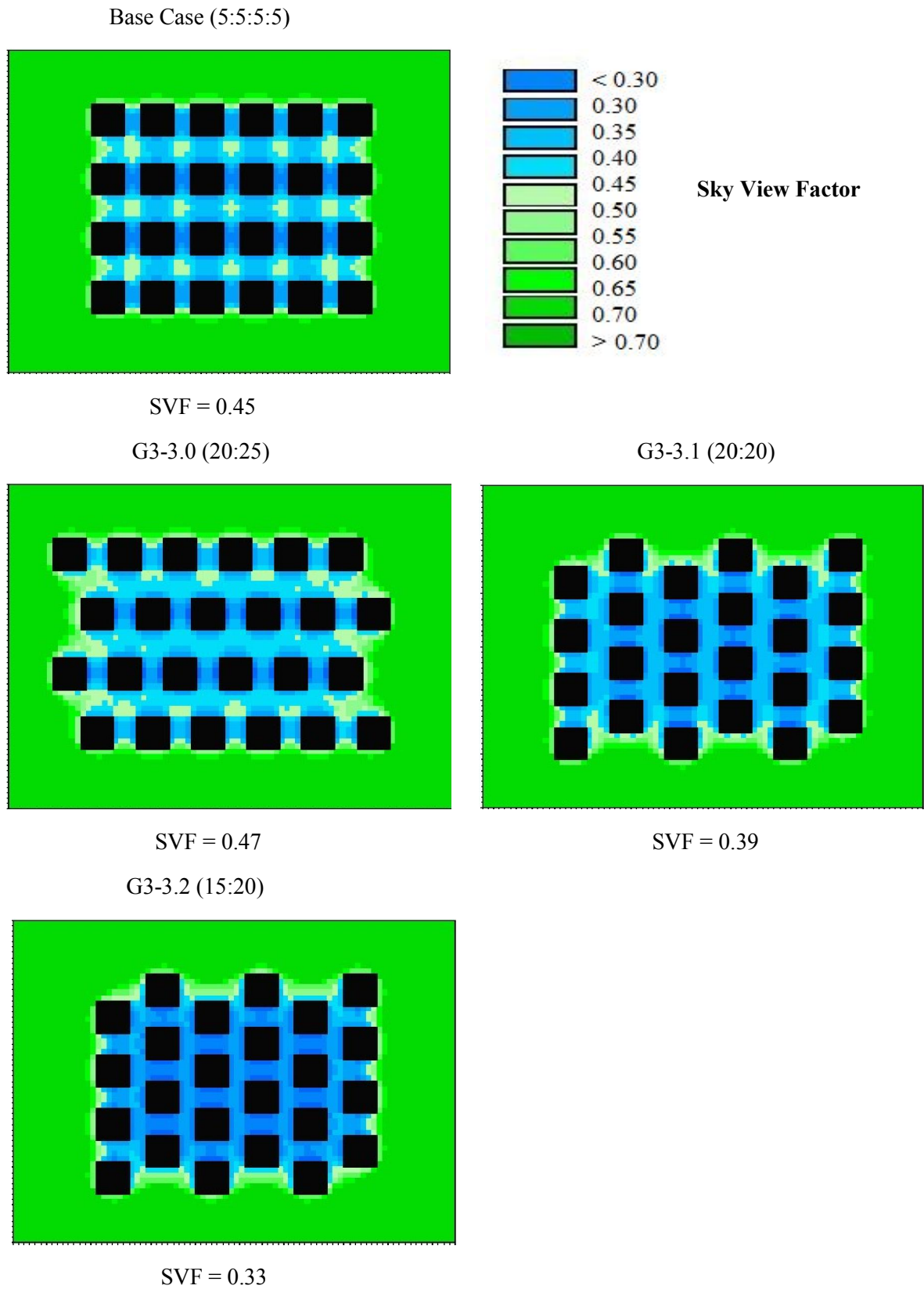
Figure 5.21: The Sky View Factor (SVF) of the base case and the three configurations of the third group; G 3-3.0 (20:25), G3-3.1 (20:20), and G3-3.2 (15:20)

5.4.2 Air Temperature

The air temperature of the three configurations in the third group is generated through simulating the configurations in four orientations; N-S, E-W, NE-SW, and NW-SE using the ENVI-Met software. The results illustrated in the figures below show the following:

- In the N-S highest maximum air temperature recorded is 35.9 °C in G 3-3.0 (25:20) configuration, while the lowest maximum air temperature is 35.2°C in G 3-3.2 (20:15) configuration with a variation of 0.8 °C between highest and lowest maximum (Figure 5.22).

- The E-W simulation recorded close values to the N-S orientation with highest maximum of 36.1°C in G3-3.1 (20:20), and lowest maximum temperature is 35.6°C in the G 3-3.2 (20:15) configuration with a decrease of 0.47°C between the highest and lowest maximum (Figure 5.22).

- However, the highest maximum air temperature at 15:00 pm recoded in the E-W orientation compared to the N-S orientation in the configuration G3-3.1 (20:20).

- Simulating the three configurations in the NE-SW orientation shows less variation in air temperature averages. The highest maximum temperature recorded in G3-3.1 (20:20) configuration with value 37.5°C, with a slight increase of 0.24°C compared to the lowest maximum of 37.2°C in configuration G3-3.0 (25:20) (Figure 5.22)

- The NW-SE orientation shows the most significant variation in air temperature averages for all configuration. The highest maximum temperature recorded in the G3-3.0 (25:20) with value of 37.4°C, and the lowest maximum temperature is 34.7°Crecorded in configuration G3-3.2 (20:15). Hence, the variation between the highest and lowest maximum outdoor air temperature averages is 2.6°C in the NW-SE orientation (Figure5.22).
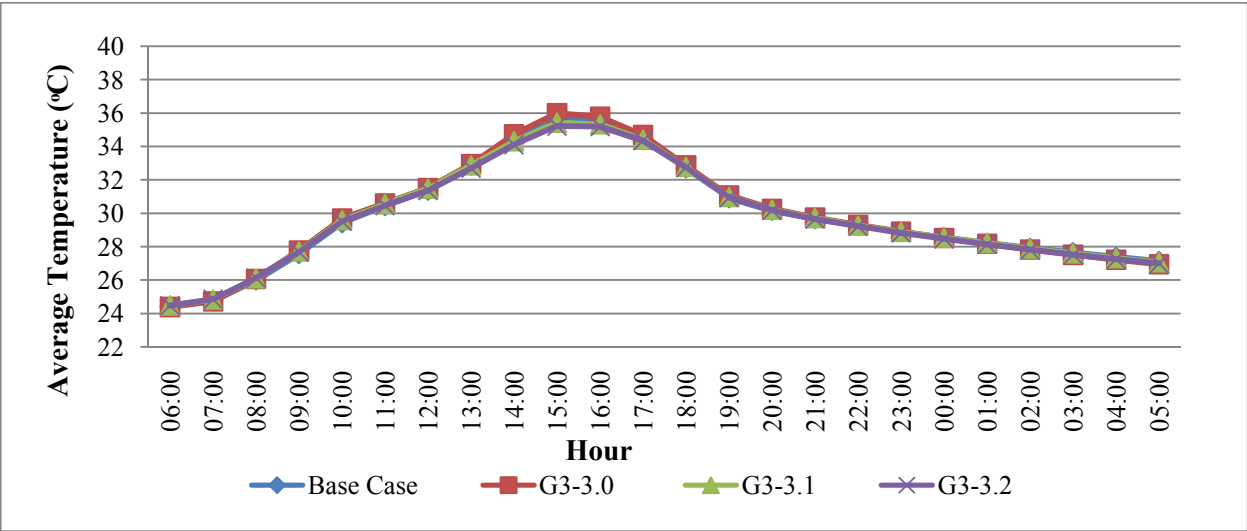
a) N-S orientation
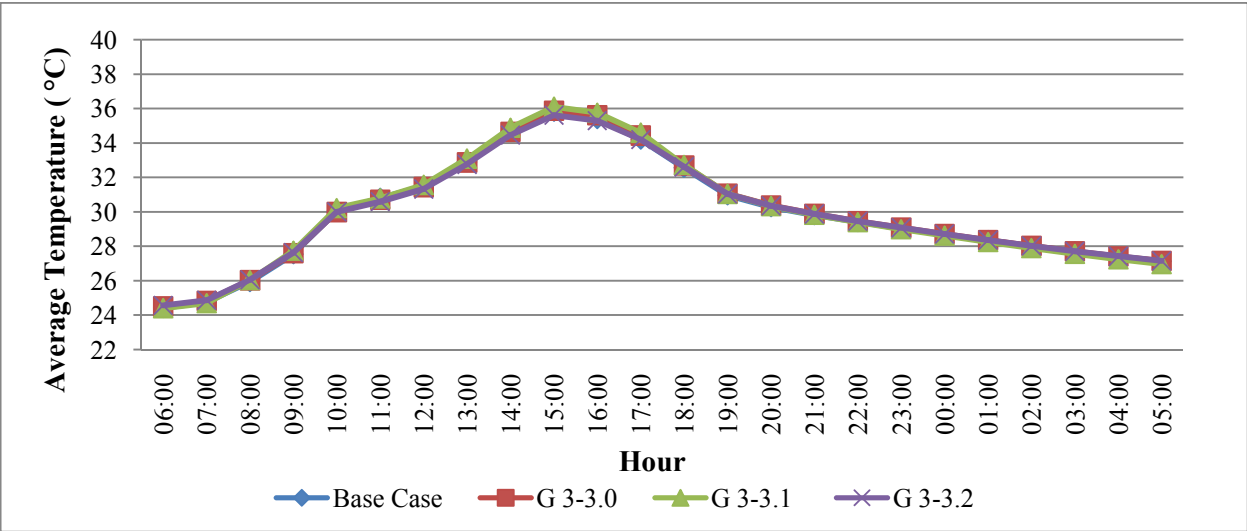
b) E-W orientation
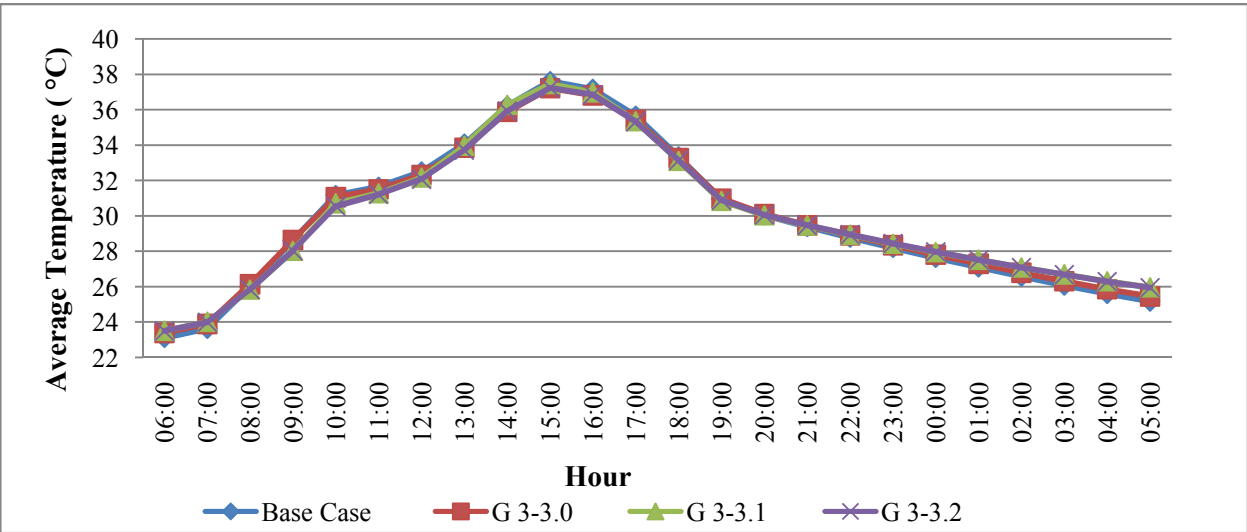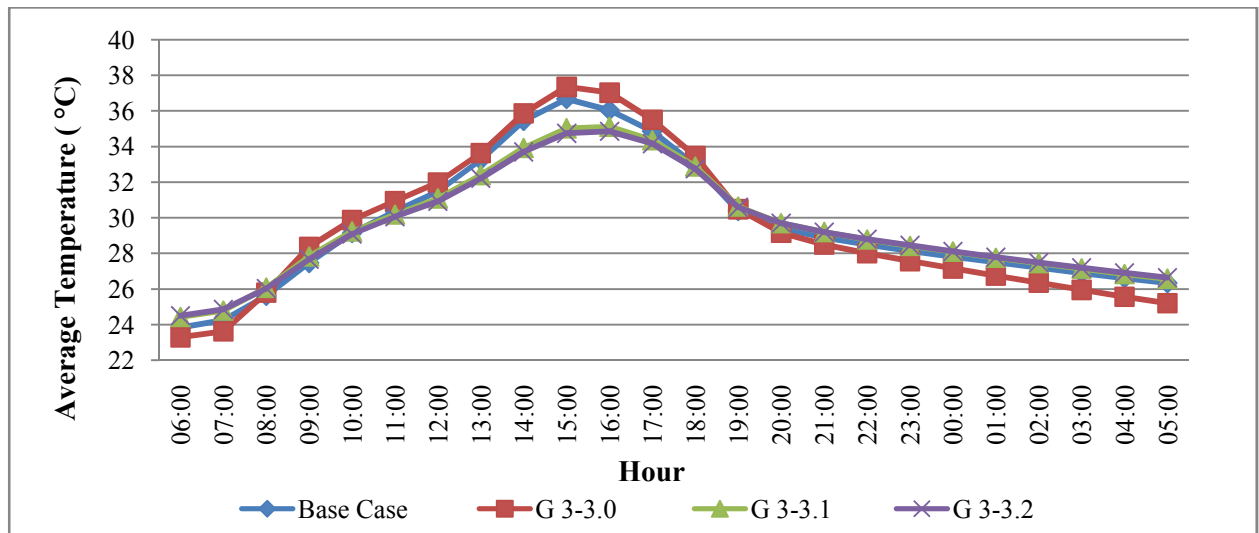
c) NE-SW orientation

d) NW-SE orientation

Figure 5.22: Hourly profile of the average air temperature on 21 June for the base case and the third group three proposed configurations in the four orientations: N-S, E-W, NE-SW, and NW-SE

- However, the base case recorded higher maximum air temperature at 15:00 compared to the three configurations, and the increase is varied according to the orientation and the configuration. The base case is higher than G3-3.2 (15:20), G3-3.2 (15:20), and G3-3.0 (20:25)in the orientations N-S, E-W, and NE-SW with increase of 0.6,°C 0.2°C and 0.4°C respectively.

- The most significant variation observed in the NW-SE orientation as the base case is higher than G3-3.2 (15:20) by 1.9°C. Therefore, all configurations perform better than the base case in term of the maximum air temperature at 15:00, and the G3-3.2 (15:20) configuration records the lowest maximum air temperature compared to the base case and other two configurations of this group.

- The G3-3.1 (20:20) configuration recorded a decrease of $1.7\,^{\circ}\text{C}$ compared to the base case. Therefore, the NW-SE orientation recorded the best orientation performance by recording the lowest maximum air temperature in the configurations G3-3.1 (20:20)

and G3-3.2 (15:20), respectively. The N-S orientation recorded a notable variation in air temperature averages between the first and the two other configurations.

- On the other hand, the NW-SE orientation recorded the most significant variation between the highest and the lowest air temperature of 2.6 °C in the configurations G3-3.0 (25:20) and G3-3.2(15:20), respectively.

5.4.3 Wind Speed

The wind flow behaviour and wind velocity averages obtained from simulating the third group configurations using ENVI-Met software in the four orientations.

Figure 5.23 illustrates the wind profile during the simulated day 21st, June of the base case and the three configurations in four orientation N-S, E-W, NE-SW, and NW-SE. The variation in wind speed between the four orientations is very obvious. In the N-S orientation the base case shows the highest wind speed recorded in the base case in addition to the first configuration G 3-3.0 (20:25), while the G3-3.1(20:20) configuration records the highest wind velocity in E-W orientation In the NE-SW orientation, the two configurations in addition to the base case record higher wind speed than the G 3-3.0 (20:25) configuration.

The opposite situation observed in the NW-SE orientation as the G 3-3.0 (20:25) configuration records the highest wind velocity with a significant variation compared to the base case and two other configurations (Figure 5.23). The maximum and minimum wind speeds for the three configurations in this group with respect to canyon orientation and compared to the base case illustrated in figure 5.24. In the N-S orientation the maximum wind speed recorded in the configuration G3-3.0 (20:25),while the minimum recorded in configuration G3-3.1 (20:20) with speed of 1.8 m/s and 1.1 m/s, respectively.
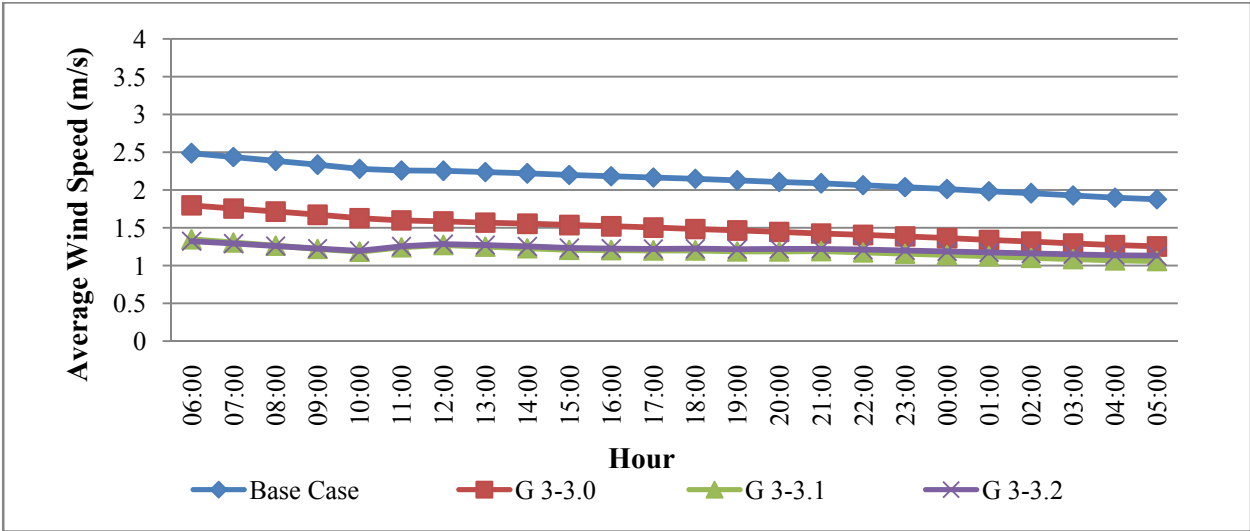
a) N-S orientation
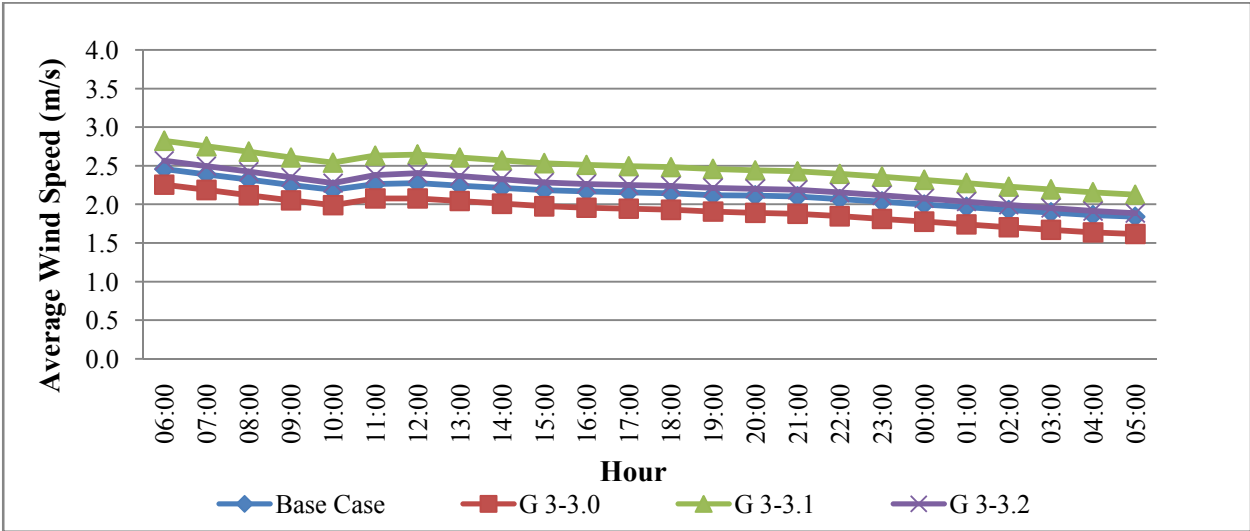
b) E-W orientation
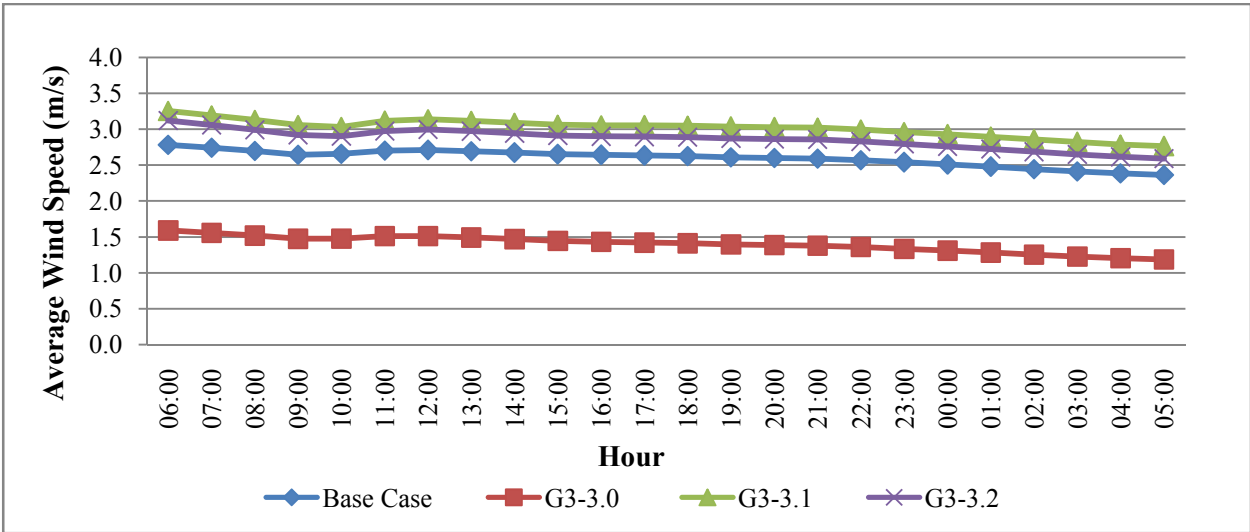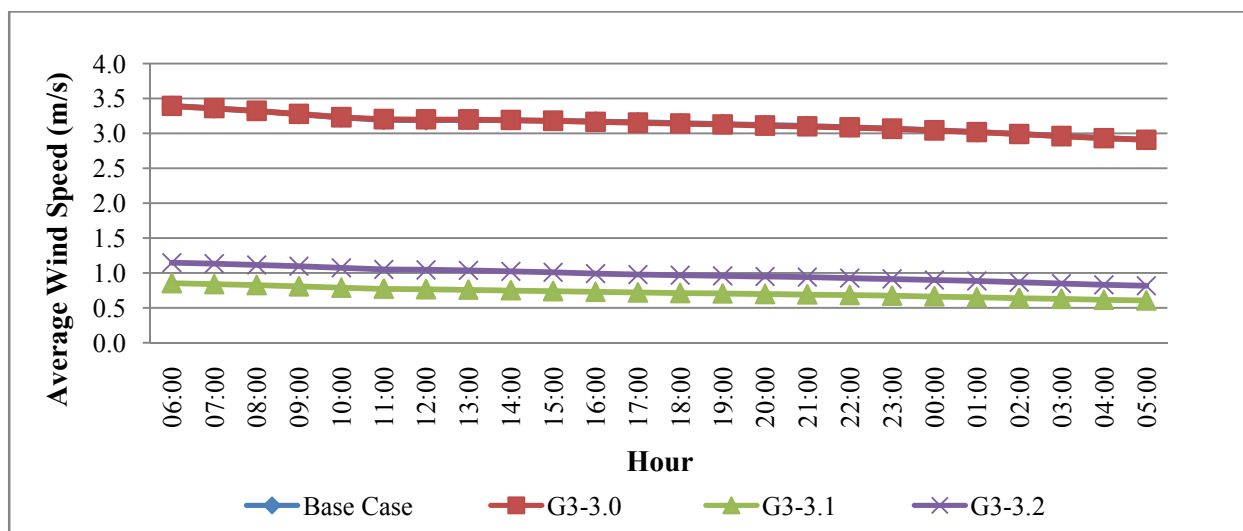
c) NE-SW orientation

d) NW-SE orientation

Figure 5.23: Hourly profile of the average wind speed on 21 June for the base case and the third group three proposed configurations in the four orientations: N-S, E-W, NE-SW, and NW-SE

However, the base case records higher wind speed than the three configurations in this orientation with maximum velocity of 2.5 m/s. In the E-W orientation, the G3-3.1(20:20) configuration records highest wind speed compared to the other configuration including the base case with maximum velocity of 2.8 m/s. Moreover, the G3-3.2 (15:20) configuration records the second higher wind speed compared to the base case with a speed of 2.8.2m/s.

Similar attitude observe in the NE-SW orientation, the G3-3.1(20:20) and G3-3.2 (15:20) configurations both recoded wind speed higher than the base case with maximum values 3.3 m/s and 3.1 m/s, respectively.

The NW-SE orientation recorded the most significant variation as the highest wind speed recorded in the G3-3.0 (25:20) configuration and the base case with 3.4 m/s and 3.4 m/s, respectively. On the other hand, the minimum wind speed recorded in the configurations G3-3.1 (20:20) and G3-3.2 (20:25) with values of 0.61 m/s and 0.8 m/s, respectively. Therefore, the minimum wind velocity recorded in the NW-SE orientation in the G3-3.1 (20:20) configuration, and the maximum velocity recorded in the base case in the same orientations with velocities of 0.6 m/s and 3.4 m/s, respectively (Figure 5.24).

To summarise, the NW-SE recorded the highest maximum wind speed compared to the other orientations. The base case performs as the best configuration in the NW-SE orientation with maximum velocity of 3.4 m/s followed by the G3-3.0 (25:20) configuration with a negligible reduction of 0.01m/s.
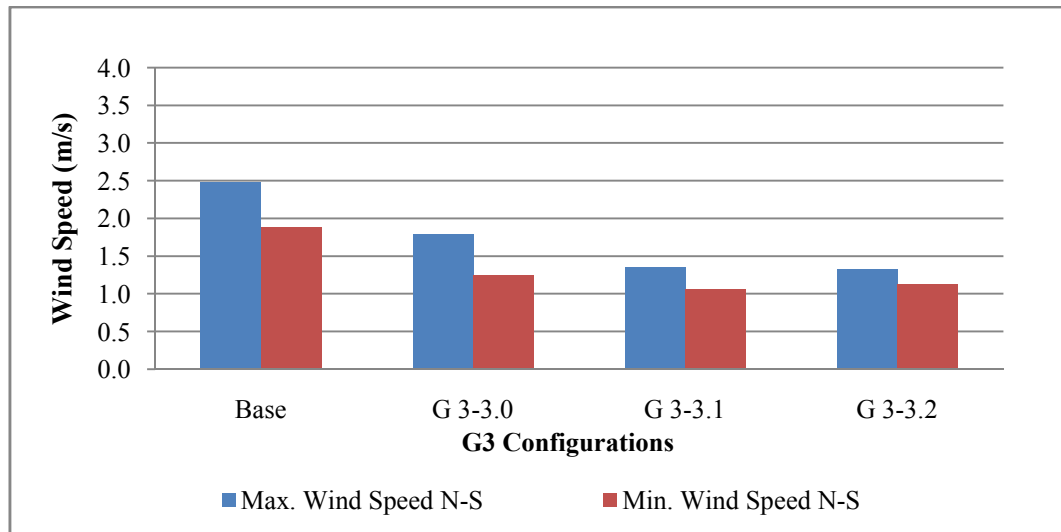
a) N-S orientation
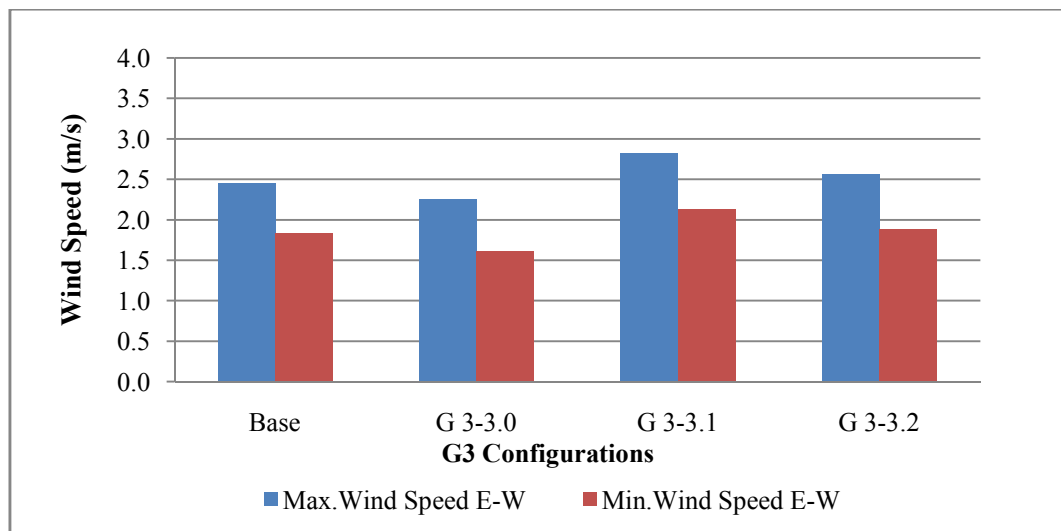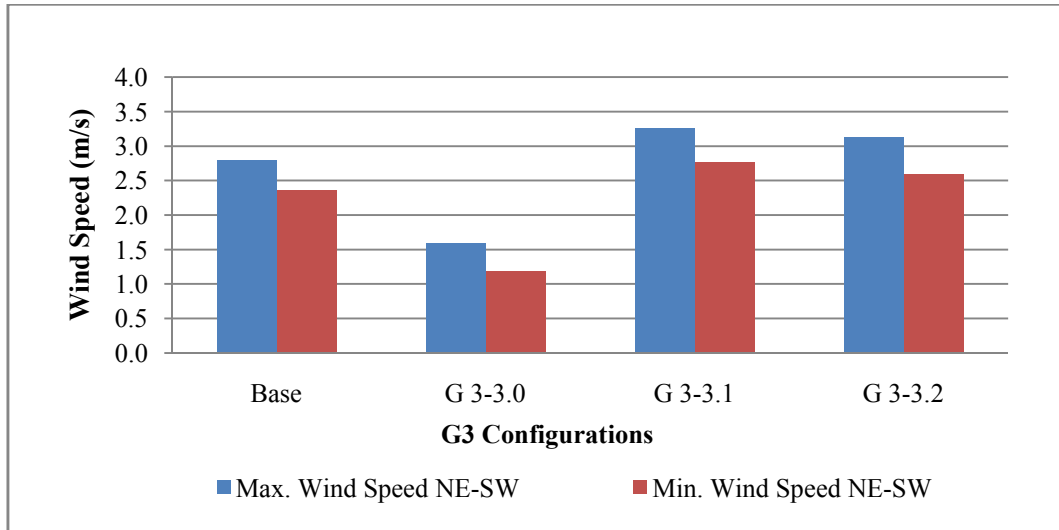
b) E-W orientation
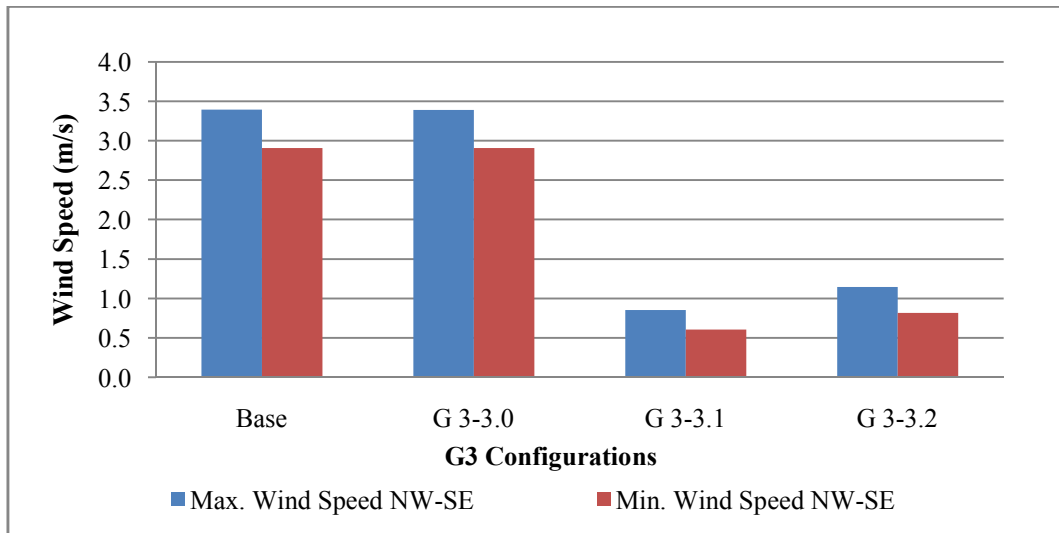
c) NE-SW orientation

d) NW-SE orientation

Figure 5.24: The variation between the maximum and minimum wind velocity of the third group proposed configurations in the four orientations; a) N-S and b) E-W, b) NE-SW, and d) NW-SE

On the other hand, the configurations G3-3.1 (20:20) and G3-3.2 (20:15) recorded the minimum velocity in the same orientation. Opposite to that, the mentioned configurations G3-3.1 (20:20) and G3-3.2 (20:15) recorded the highest velocities in the E-W and NE-SW canyons orientations compared to all configurations, including the base case, while the base case and G3-3.0 (25:20) recorded the highest wind velocity in the two other orientations N-S and NW-SE.

5.4.4 Relative Humidity

The relative humidity performance of the third group of configurations shows more significant variation compared to the two previous groups. This variation is more significant in the NE-SW and NW-SE orientation. In general, the G3-3.0 (20:25) configuration recorded higher relative humidity compared to the two other configurations and the base case in the N-S orientation in the morning and evening time.

On the other hand, the G3-3.1 (20:20) and G3-3.2 (15:20) recorded higher relative humidity averages in the afternoon time. However, this attitude reflects the maximum air temperature attitude for theses configurations. The same trend of the first configuration G3-3.0 (20:25) is observed in the NW-SE orientation with more significant variation compared to the base case and other configuration. The maximum relative humidity recorded for this configuration is 86.9% with an increase of 3%compared to the base case, while the minimum receded is in the same configuration with 4% reduction compared to the base case.

The opposite attitude for this configuration is observed in the NE-SW orientation as the maximum recorded in the base case, while the minimum is for the G3-3.1 (20:20) configuration. Figure 5.25 presents the performance relative humidity of the base case and the three configurations of the third group in the four orientations.
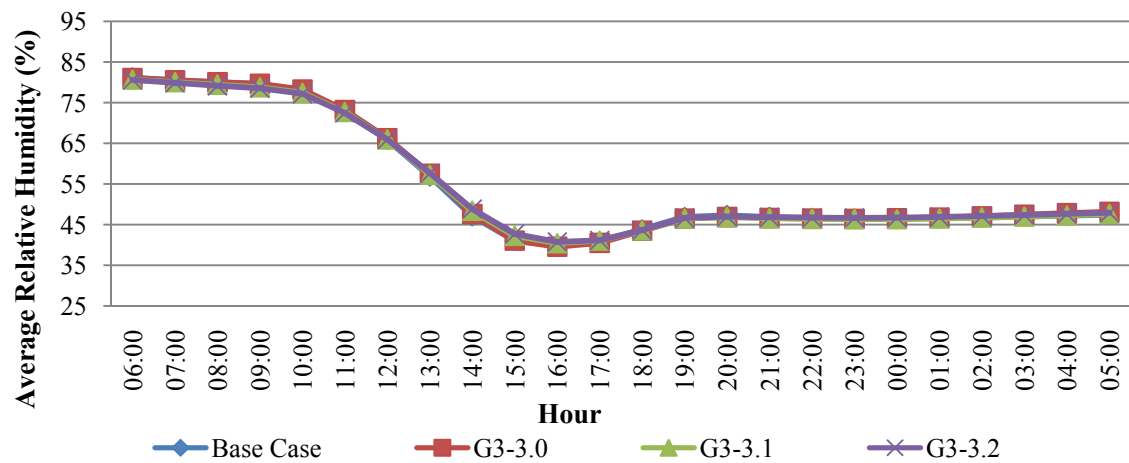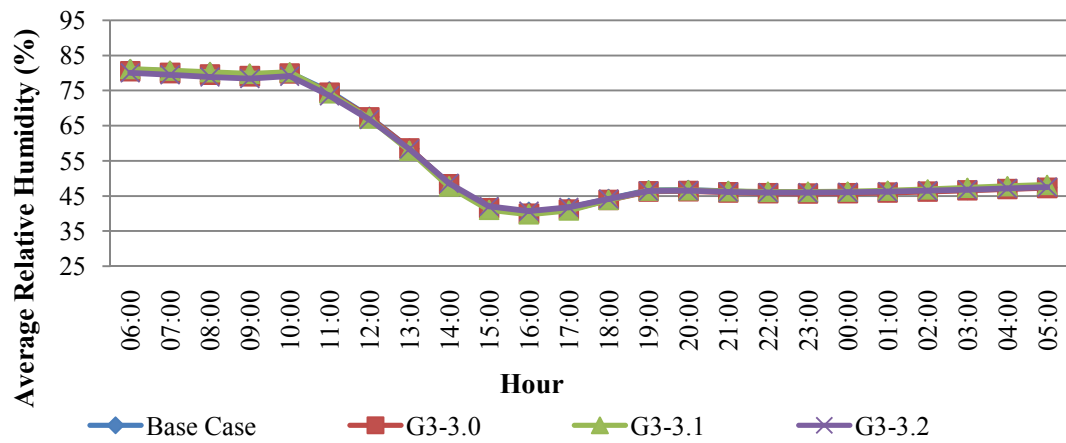
a) N-S orientation
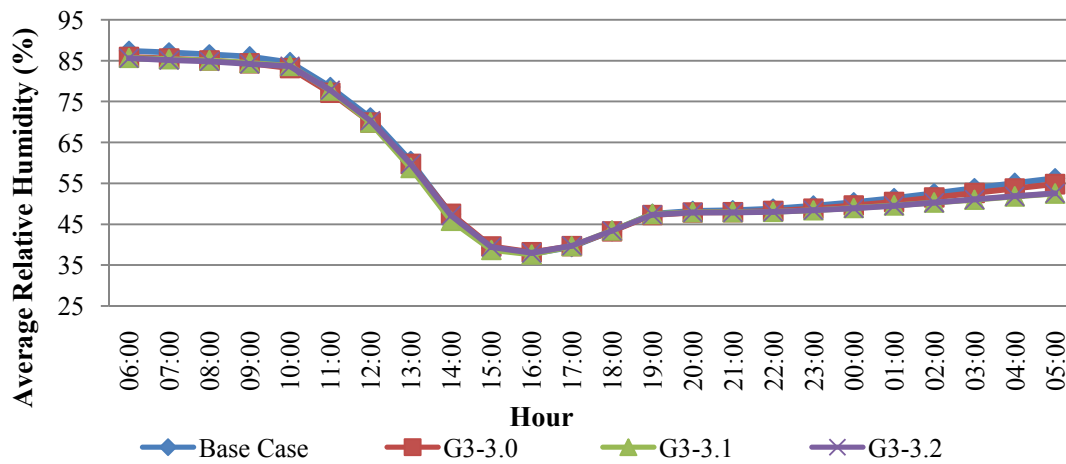
b) E-W orientation
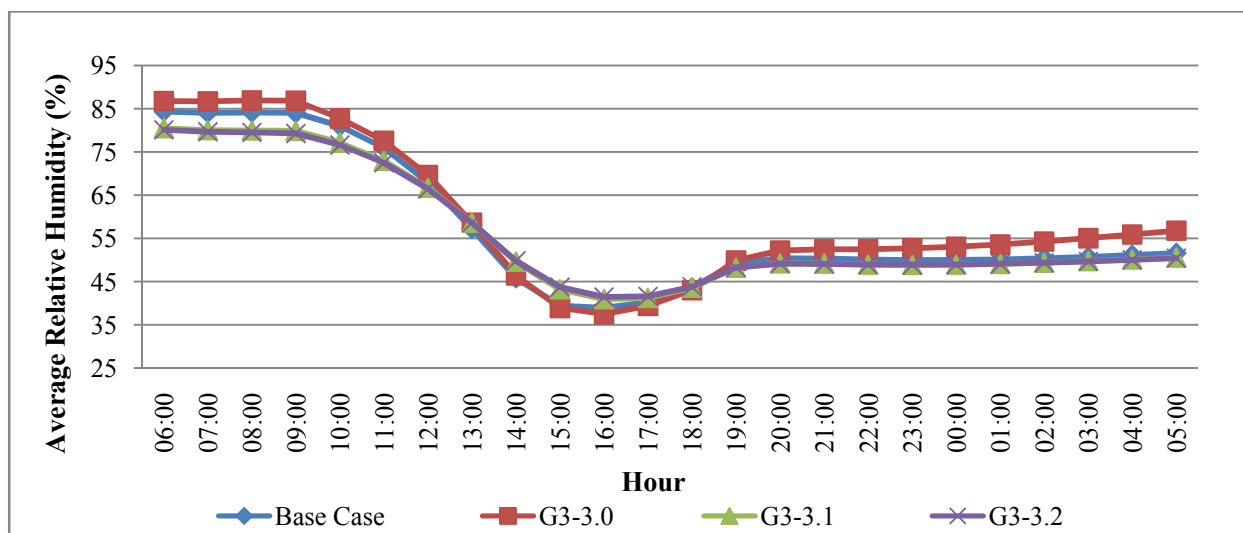
c) NE-SW orientation

d) NW-SE orientation

Figure 5.25: Hourly profile of the average relative humidity on 21June for the base case and the third group three proposed configurations in the four orientations: N-S, E-W, NE-SW, and NW-SE

5.5 Summary of the Outdoor Thermal Performance for the Three Groups Configurations

To summarise, the configurations of the three groups show a different outdoor thermal performance in terms of the studied microclimate parameters. Table 5.1 presents the name, description, proportion, SVF, and the variation in the microclimate parameters for each group configurations in the four orientations.

The tables cover the values of the maximum air temperature average at 15:00, wind velocity and relative humidity of the of each configuration at air maximum temperature.

It is clear from the table that there is direct relation between the SVF and the maximum air temperature, and it has been observed that the lowest maximum temperature is recorded in the configurations with the lowest SVF average. However, the orientation is also plays a role in indicating the configuration with the lowest outdoor maximum air temperature. In general, the highest maximum air temperature recorded in the NE-SW orientation, while the lowest maximum air temperature is varied between the N-S and E-W orientations.

The third group configuration shows a little different attitude according to the variation in buildings arrangement.

For the first group the G1-1.2 (3:7:7:3) configuration with the lowest SVF of 0.40 recorded the lowest maximum air temperature in two orientations NE-SW and NW-SE. In the second group the G2-2.1 (3:5:7:7:5:3) and the G2-2.5 (5:3:7:7:3:5) configurations has the lowest SVF of 0.41, and the lowest maximum air temperature is recorded in configuration G2-2.5 (5:3:7:7:3:5) in three orientations E-W, NE-SW, and NW-SE.

The effect of the SVF on the air temperature averages is more obvious in the third group configurations as the third configuration G3-3.2 (15:20) has the lowest SVF in the three groups, and the lowest maximum air temperature in the three orientations N-S, NE-SW and NW-SE. Moreover, the G3-3.2 (15:20) recorded the lowest maximum air temperature of 34.7°C compared to all configurations of the three groups. Further to that the table illustrates the wind velocity and relative humidity at the maximum air temperature of each configuration. In general, it has been observed that the wind velocity increases with the diversity in buildings height, and the maximum wind velocity averages recorded in the NW-SE orientation.

However, the relative humidity is directly related to the maximum air temperature, and the minimum relative humidity recorded at the maximum air temperature averages.

The next chapter demonstrates the best configuration in each of the three groups with respect to the lowest maximum air temperature compared to the base case. Furthermore, the variation in the outdoor microclimate parameters will be adopted in calculating the cooling load using the IES-VE indoor thermal performance simulation software.

Table 5.1: Description of the three groups configurations and summery for the microclimate parameters at maximum air temperature

Group No.	Name	Proportion	Floor Number	Description	Total height (m)	Total BUA (m²)	SVF (Average)	Max. Air Temperature (°C) (15:00) N-S	E-W	NE-SW	NW-SE
Base Case		5									
			G+5	5:5:5:5	24	129600	0.45	35.78	35.83	37.62	36.68
G 1		03:07									
	G 1-1.0		G+3, G+7	7:3:3:7	16, 32	129600	0.50	35.67	35.65	37.48	37.26
	G 1-1.1		G+3, G+7	3:7:3:7	16, 32	129600	0.45	35.48	35.40	37.11	35.98
	G 1-1.2		G+3, G+7	3:7:7:3	16, 32	129600	0.40	35.51	35.69	36.80	35.62
	G 1-1.3		G+3, G+7	3:3:7:7	16, 32	129600	0.46	35.56	35.68	37.06	36.62
G 2		03:05:07									
	G 2-2.0		G+3, G+5, G+7	7:5:3:3:5:7	16, 24, 32	129600	0.47	35.52	35.64	38.35	36.48
	G 2-2.1		G+3, G+5, G+7	3:5:7:7:5:3	16, 24, 32	129600	0.41	35.79	35.65	36.78	35.96
	G 2-2.2		G+3, G+5, G+7	5:7:3:3:7:5	16, 24, 32	129600	0.43	35.64	35.74	38.37	36.45
	G 2-2.3		G+3, G+5, G+7	7:5:3:3:5:7	16, 24, 32	129600	0.44	35.69	35.69	37.51	36.19
	G 2-2.4		G+3, G+5, G+7	3:7:5:5:7:3	16, 24, 32	129600	0.42	35.70	35.67	37.63	36.24
	G 2-2.5		G+3, G+5, G+7	5:3:7:7:3:5	16, 24, 32	129600	0.41	35.72	35.57	36.67	35.78
G3		5									
	G 3-3.0		G+5	15:25	24	129600	0.47	35.99	35.88	37.23	37.35
	G 3-3.1		G+5	20:20	24	129600	0.39	35.41	36.09	37.46	35.01
	G 3-3.2		G+5	15:20	24	129600	0.33	35.22	35.63	37.24	34.74

Group No.	Name	Proportion	Floor Number	Description	Total height (m)	Total BUA (m²)	SVF (Average)	Wind Speed (m/s) at (15:00)			
								N-S	E-W	NE-SW	NW-SE
Base Case		5									
			G+5	5:5:5:5	24	129600	0.45	2.20	2.18	2.65	3.18
G 1		03:07									
	G 1-1.0		G+3, G+7	7:3:3:7	16, 32	129600	0.50	2.34	2.30	2.05	3.15
	G 1-1.1		G+3, G+7	3:7:3:7	16, 32	129600	0.45	2.57	2.56	2.19	3.19
	G 1-1.2		G+3, G+7	3:7:7:3	16, 32	129600	0.40	2.24	2.27	3.46	3.23
	G 1-1.3		G+3, G+7	3:3:7:7	16, 32	129600	0.46	2.01	2.00	3.10	3.18
G 2		03:05:07									
	G 2-2.0		G+3, G+5, G+7	7:5:3:3:5:7	16, 24, 32	129600	0.47	1.99	2.00	2.60	2.71
	G 2-2.1		G+3, G+5, G+7	3:5:7:7:5:3	16, 24, 32	129600	0.41	2.66	2.62	2.75	3.77
	G 2-2.2		G+3, G+5, G+7	5:7:3:3:7:5	16, 24, 32	129600	0.43	2.03	2.03	2.64	2.68
	G 2-2.3		G+3, G+5, G+7	7:5:3:3:5:7	16, 24, 32	129600	0.44	2.18	2.17	2.61	3.22
	G 2-2.4		G+3, G+5, G+7	3:7:5:5:7:3	16, 24, 32	129600	0.42	2.23	2.21	2.70	3.09
	G 2-2.5		G+3, G+5, G+7	5:3:7:7:3:5	16, 24, 32	129600	0.41	2.67	2.64	2.70	3.89
G3		5									
	G 3-3.0		G+5	15:25	24	129600	0.47	1.54	1.98	1.44	3.18
	G 3-3.1		G+5	20:20	24	129600	0.39	1.21	2.53	3.06	0.74
	G 3-3.2		G+5	15:20	24	129600	0.33	1.23	2.28	2.91	1.01

Group No.	Name	Proportion	Floor Number	Description	Total height (m)	Total BUA (m²)	SVF (Average)	Relative Humidity (%) at (15:00)			
								N-S	E-W	NE-SW	NW-SE
Base Case		5									
			G+5	5:5:5:5	24	129600	0.45	41.08	41.44	39.19	39.45
G 1		03:07									
	G 1-1.0		G+3, G+7	7:3:3:7	16, 32	129600	0.50	41.13	41.57	39.15	38.05
	G 1-1.1		G+3, G+7	3:7:3:7	16, 32	129600	0.45	41.50	42.12	39.91	40.76
	G 1-1.2		G+3, G+7	3:7:7:3	16, 32	129600	0.40	41.58	41.60	40.26	41.61
	G 1-1.3		G+3, G+7	3:3:7:7	16, 32	129600	0.46	41.47	41.54	40.10	39.44
G 2		03:05:07									
	G 2-2.0		G+3, G+5, G+7	7:5:3:3:5:7	16, 24, 32	129600	0.47	41.49	41.60	37.44	39.57
	G 2-2.1		G+3, G+5, G+7	3:5:7:7:5:3	16, 24, 32	129600	0.41	40.92	41.68	40.77	40.72
	G 2-2.2		G+3, G+5, G+7	5:7:3:3:7:5	16, 24, 32	129600	0.43	41.22	41.40	37.43	39.58
	G 2-2.3		G+3, G+5, G+7	7:5:3:3:5:7	16, 24, 32	129600	0.44	41.14	41.50	39.28	40.16
	G 2-2.4		G+3, G+5, G+7	3:7:5:5:7:3	16, 24, 32	129600	0.42	41.10	41.58	39.04	39.96
	G 2-2.5		G+3, G+5, G+7	5:3:7:7:3:5	16, 24, 32	129600	0.41	41.04	41.79	41.01	41.07
G3		5									
	G 3-3.0		G+5	15:25	24	129600	0.47	41.05	41.46	39.61	38.92
	G 3-3.1		G+5	20:20	24	129600	0.39	42.22	41.01	38.76	43.23
	G 3-3.2		G+5	15:20	24	129600	0.33	42.71	42.04	39.44	43.76
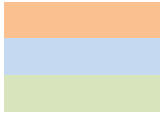
The highest maximum air temperature

The lowest maximum air temperature

The lowest Sky View Factor

Chapter 6

The Configurations of the Best Outdoor Thermal Performance

6.0 The Configurations of the Best Outdoor Thermal Performance

The developed models of the urban block in this research have been examined and simulated to explore the effect of different configurations on the outdoor thermal performance. The microclimate parameter results of each group' configurations has been illustrated in detail in the previous chapter. In this chapter the best configuration of each group with respect to the lowest maximum air temperature averages will be presented and discussed.

The discussion of the outdoor microclimate parameters of the best configurations will cover air temperature, wind speed and relative humidity.

The numerical simulation results of each group will be compared to each other, and the configuration with the best performance with respect to reducing the maximum averages of outdoor air temperature will be presented. The effect of the best configuration will be compared to the base case in order to find the variation and the improvement in outdoor thermal performance. Further to this, the results of the best configurations in each orientation will be discussed and analysed at the end of this chapter. The discussion will include the effect of the block orientation, height diversity and buildings configuration on the studied microclimate parameters. The data of the best configurations in terms of outdoor thermal performance will be presented for the base case and the configurations of the three proposed groups as blow:

Base Case

- The average of the maximum air temperature at 15:00 in °C in the four orientations; N-S, E-W, NE-SW, and NW-SE

- The average of maximum wind speed in m/s in the four orientations; N-S, E-W, NE-SW, and NW-SE.

- The average of relative humidity in percentage at maximum air temperature of all configurations in each group in the four orientations; N-S, E-W, NE-SW, and NW-SE.

Base Case and the configurations of the three groups

- The average of the maximum air temperature at 15:00 in (°C) for all configurations in each group in the four orientations; N-S, E-W, NE-SW, and NW-SE.

- The configurations with the highest and lowest reduction in maximum air temperature (°C) that can be achieved in each group.

- The average of the maximum and minimum wind speed in (m/s) for all configurations in each group in the four orientations; N-S, E-W, NE-SW, and NW-SE

- The variation in wind velocity (m/s) at maximum air temperature of the best configurations in each group compared to the base case in two orientations; (NW-SE) and (NE-SW).

- The average of relative humidity in percentage at maximum air temperature of all configurations in each group in the four orientations; N-S, E-W, NE-SW, and NW-SE.

6.1 Outdoor Thermal Performance and the Best Configurations

6.1.1 The Best Performance of the Base Case with Respect to the Block Orientation

The results of the base case simulation in the four orientations shows that the lowest maximum air temperature recorded in the N-S orientation when the block extended along the E-W orientation (Figure 6.1). On the other hand, the wind velocity in the N-S and E-W orientations are less than the two other orientations NE-SE and NW-SE (Figure 6.1).

The reduction in air temperature between the best orientation N-S and the worst orientation NE-SW is 5%.

Furthermore, figure 6.2 shows that the N-W prevailing wind is the dominated wind in the block canyons when the main canyons oriented with wind direction NW-SE, followed by the NE-SW orientation. The significant increase in wind velocity is observed between the NW-SE orientation compared to the E-W orientation with an increase of 28 %. However, the effect of the solar radiation on the air temperature of the block canyons is more than the cooling effect of the wind speed. Therefore, and in general, for the grid configuration block the best orientation of the block is the N-S followed by the E-W orientation.

Figure 6.1: The average of maximum air temperature for the base case configuration in the four orientations; N-S, E-W, NE-SW, and NW-SE
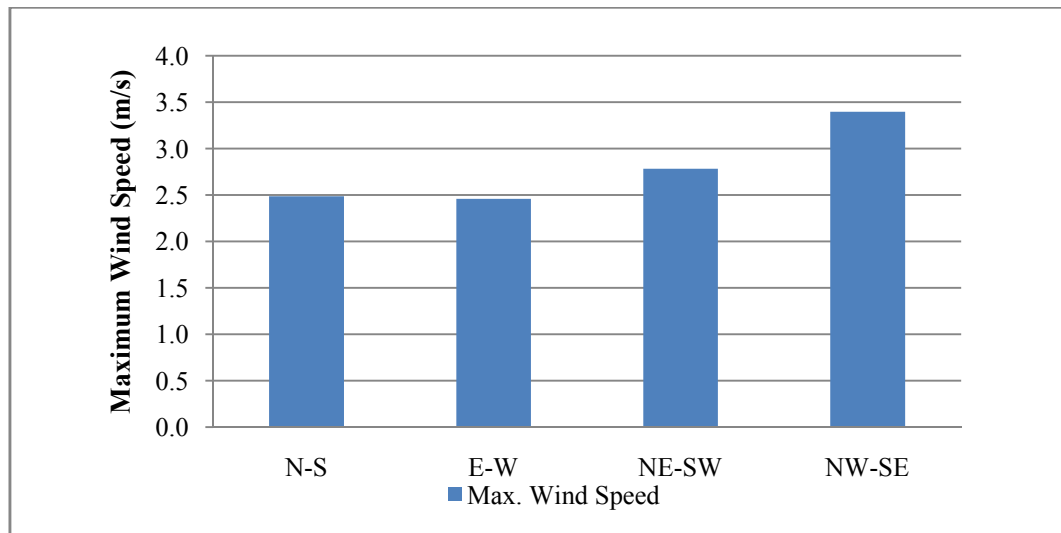
Figure 6.2: The average of maximum wind speed for the base case configuration in the four orientations; N-S, E-W, NE-SW, and NW-SE

Figure 6.3 shows the average of the relative humidity at the maximum air temperature of the base case in the four simulated orientations. However, and as illustrated in the previous chapter, the relative humidity shows an inversely attitude compared to maximum air temperature, and the minimum relative humidity for the base case recorded at 16:00 for all orientation. The minimum relative humidity recorded is in the NE-SW orientation, and the same orientation records the maximum air temperature averages. In spite of the fact that the minimum air temperature averages recorded in the N-S orientation, the maximum relative humidity recorded in the E-W orientation as the wind velocity in this orientation is lower than the N-S orientation. This proves the effect of the wind velocity on relative humidity, the increase between the maximum relative humidity in the E-W orientation and the minimum in the NE-SW orientation reaches 5.4 %.
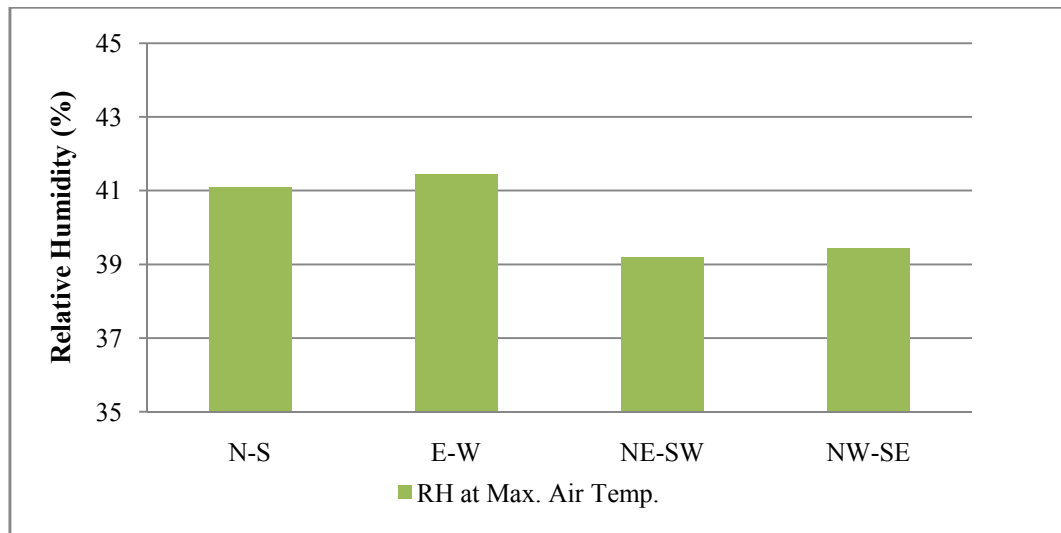
Figure 6.3: The average relative humidity at maximum air temperature for the base case configuration in the four orientations; N-S, E-W, NE-SW, and NW-SE

6.1.2 The Best Performance of the First Group Configurations

In the previous chapter the numerical results of the microclimate parameters for the first group configurations were presented in detail. Figure 6.4shows the maximum air temperature averages of the first group configurations in the four simulated orientations; N-S, E-W, NE-SW, and NW-SE. In general, the N-S and E-W orientations recorded the best orientations with respect to outdoor thermal performance for all configurations by recording a maximum air temperature averages lower than the two other orientations.
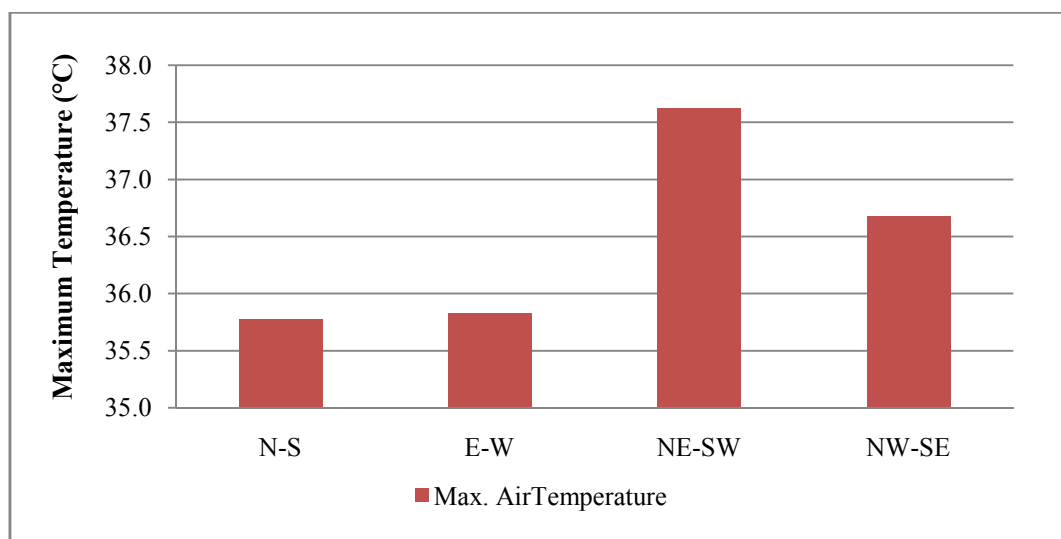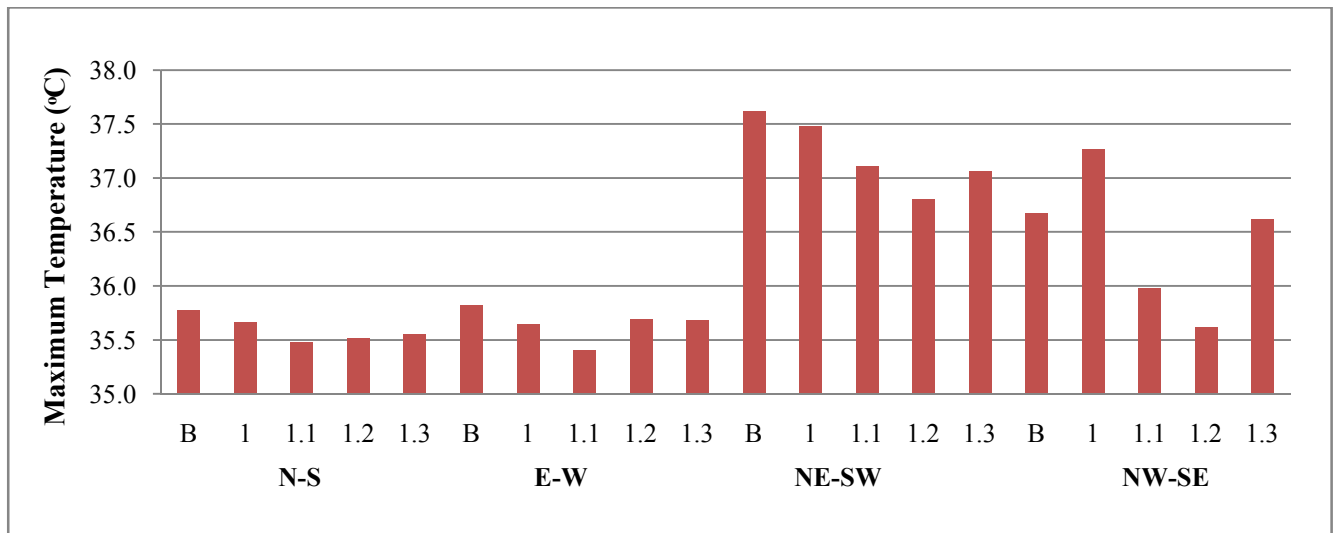
Figure 6.4: The average of maximum air temperature for the first group configurations in the four orientations; N-S, E-W, NE-SW, and NW-SE

The results of the maximum air temperature averages at 15:00 shows that for the four orientations, G1-1.2 (3:7:7:3) and G1-1.1 (3:7:3:7) are the best configurations. However, the variation in maximum outdoor air temperature averages in the N-S and E-W orientation is very small.

Therefore, the comparison between the first group's four configurations will be conducted on the two orientations, NE-SW and NW-SE, where the variation is most significant. The comparison of the N-S and E-W data is presented in appendix C.1.

Compared to the base case, the G1-1.2 (3:7:7:3) configuration recorded a reduction of $1.1\,^{\circ}$C in maximum air temperature averages at 15:00 in the NW-SE orientation (Figure 6.5 a). The heights maximum temperature in the same orientation is recorded by the G1-1.0 (7:3:3:7) configuration with a variation between the maximum and minimum outdoor air temperature of $1.6\,^{\circ}$C. On the other hand, in the NE-SW orientation recorded a lower variation with a difference of $0.7\,^{\circ}$C between the best configuration G1-1.2 (3:7:7:3) and the base case (Figure 6.4 b). However, the best configuration shows an opposite attitude in the early morning and evening time by recording an outdoor air temperature averages higher than the base case with a slight variation. This is related to the over shading effect provided by the

229

G1-1.2 (3:7:7:3) best configuration increasing during the day time. On the other hand, the buildings start releasing the heat at evening and increases the canyons air temperature averages. Furthermore, the effect of the sun set time on the best configuration block is higher in the NE-SW orientation as the main canyons are facing the NW-SE orientation and receiving more radiation (Figure 6.5 b).
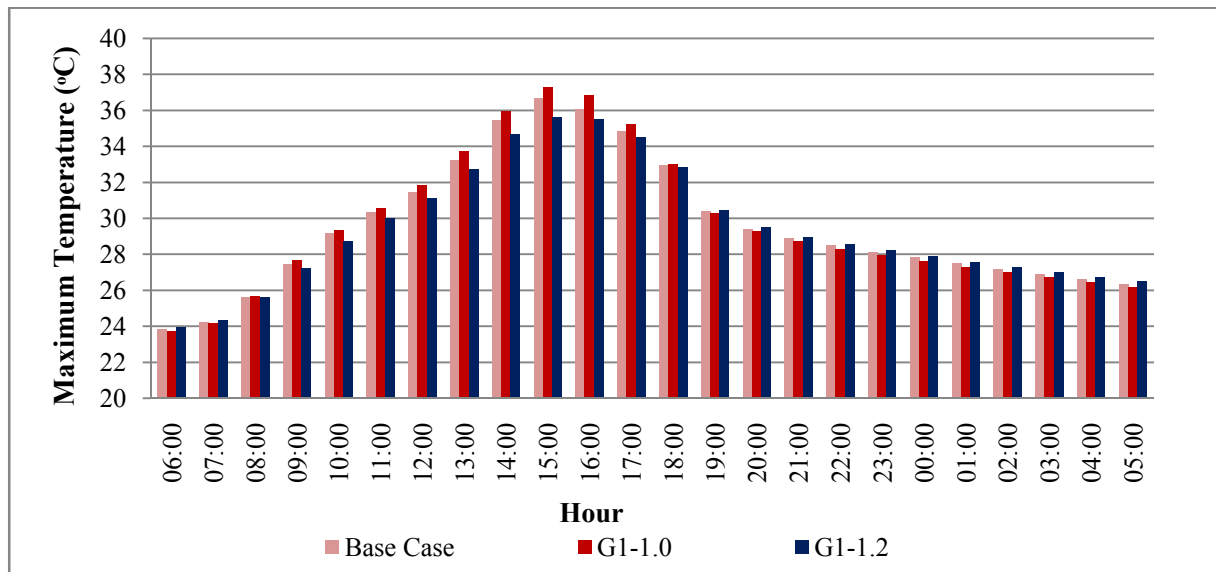
a) NW-SE orientation
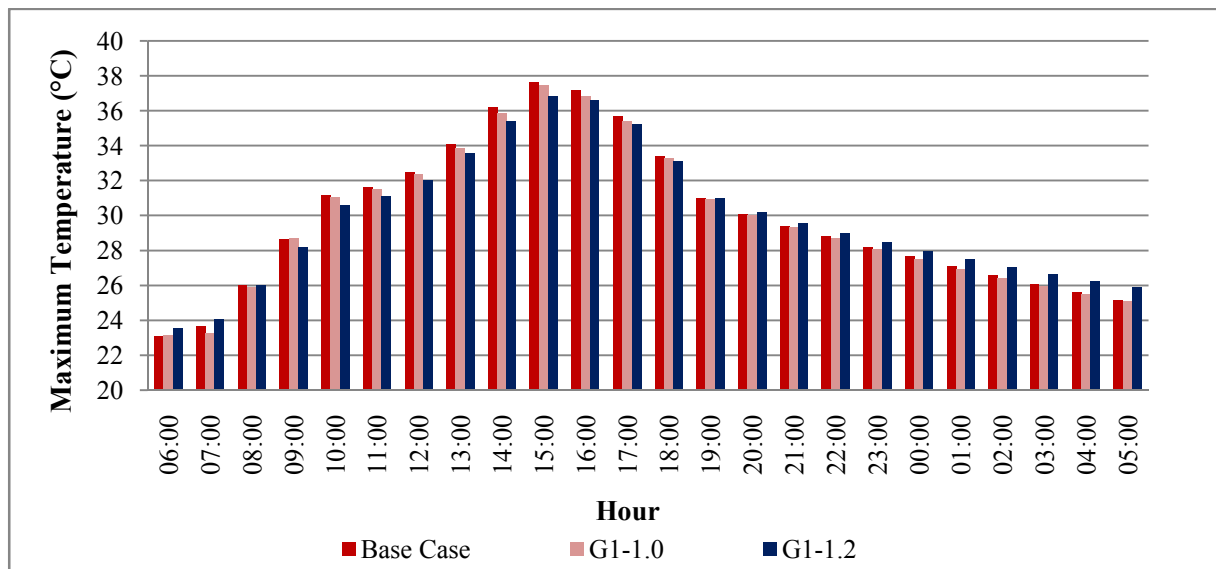
b) NE-SW orientation

Figure 6.5: The configurations with the maximum and minimum reduction in air temperature of the first group compared to the base case in: a) NW-SE and b) NE-SW orientations

The effect of the height variation on the wind speed of the first group configurations in all orientations is presented in figure 6.6. The influence of the NW-SE prevailing wind is observed clearly on the maximum and minimum wind speed averages of all configurations in this orientation. The figure shows that the there is a clear variation between the maximum and minimum wind velocity average in the four orientations, and this variation is less in the NW-SE.

This result shows the effect of the height diversity on wind flow, in the first group the height diversity of the buildings is in the short direction of the block and it is aligned with the prevailing wind in the NW-SE orientation. The inversely attitude can be clearly noticed in the second group configurations wind velocity as the NE-SW orientation has the low variation between the maximum and minimum wind speed.


Figure 6.6: The average of maximum and minimum wind speed for the first group configurations in the four orientations; N-S, E-W, NE-SW, and NW-SE

Figure 6.7 illustrates the improvement in wind speed of the best configuration at maximum air temperature in NW-SE and NE-SW orientations compared to the base case.

The enhancement in wind speed of the best configuration G1-1.2 (3:7:7:3) in the NW-SE orientation is 1.6 % compared to the base case.

On the other hand, the G1-1.0 (7:3:3:7) recorded a reduction in wind speed by 1 % compared to the base case, and this configuration recorded the lowest reduction in air temperature compared to the base case as shown earlier in figure (6.5 a).The improvement in wind velocity is higher in the NE-SW orientation and it reaches 23.3 % and 22.5 % for the best configuration G1-1.2 (3:7:7:3) and the G1-1.0 (7:3:3:7) configuration compared to the base case, respectively.

a) wind speed NW-SE
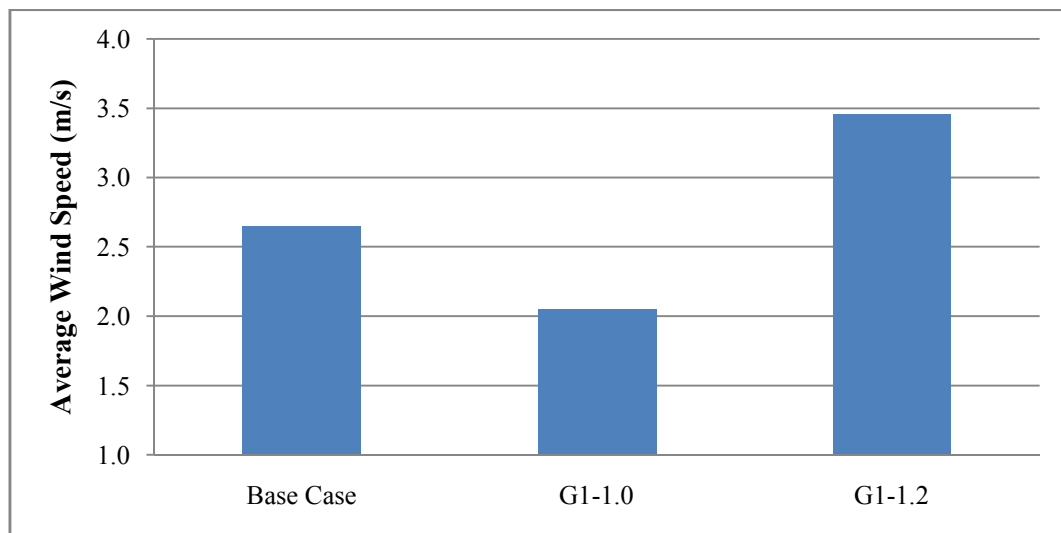
b) wind speed NE-SW

Figure 6.7: The variation in wind speed at maximum air temperature of the first group configurations compared to the base case in two orientations; a) NW-SE and b) NE-SW

The relative humidity averages at the maximum average air temperature is shown in figure 6.8. In general, it has been observed that a minimum relative humidity averages recorded at the maximum air temperature at 15:00 for all configurations in all orientations. The maximum relative humidity recorded in the N-S and E-W orientation to show an opposite attitude to air temperature records, and the variation in NE-SW and NW-SE is higher similar to air temperature behaviour in these orientations. The best configuration G1-1.2 (3:7:7:3) with lowest maximum air temperature in NW-SE orientation has the maximum relative humidity in the same orientation with an increase of 5 % compared to the base case, while the G1-1.0 (7:3:3:7) rerecorded the lowest relative humidity percentage.
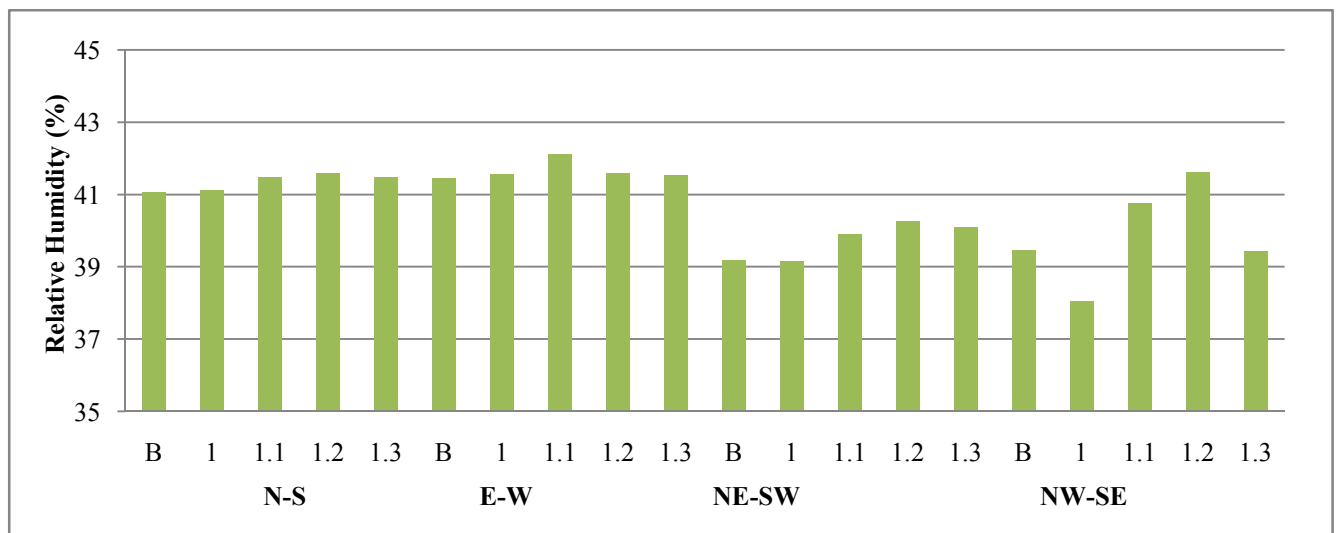
Figure 6.8: The average of the relative humidity at maximum temperature for the first group configurations in the four orientations; N-S, E-W, NE-SW, and NW-SE

6.1.3 The Best Performance of the Second Group Configurations

Similar to the first group configurations results, the N-S and E-W orientations recorded the best orientation performance for all configurations of the second group by recording a maximum air temperature averages lower than the two other orientations (Figure 6.9).
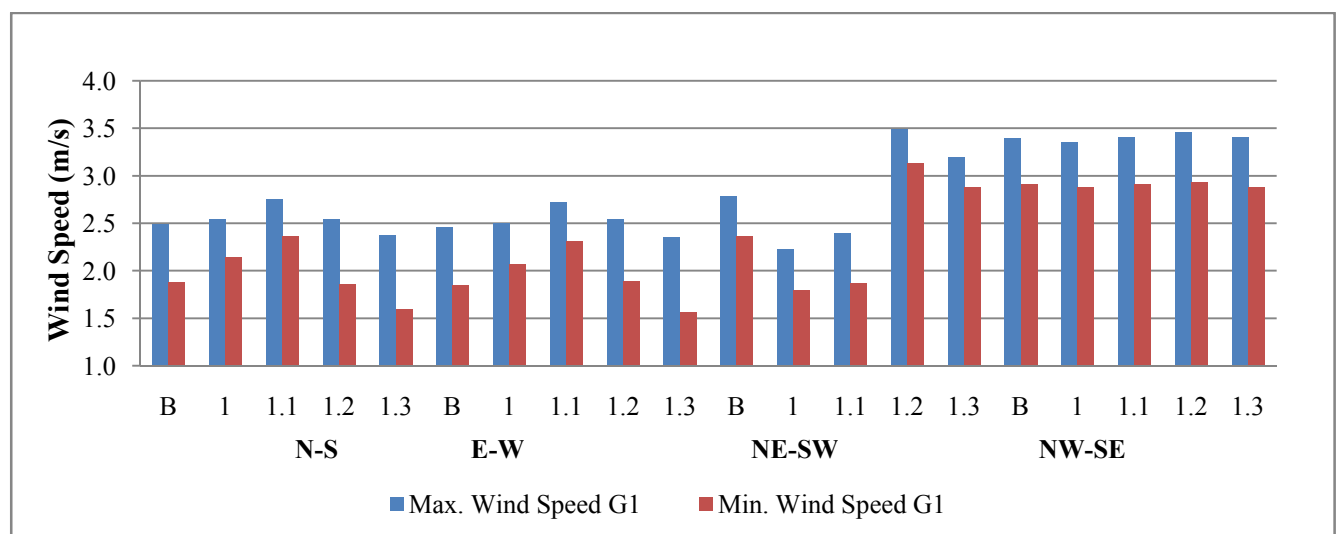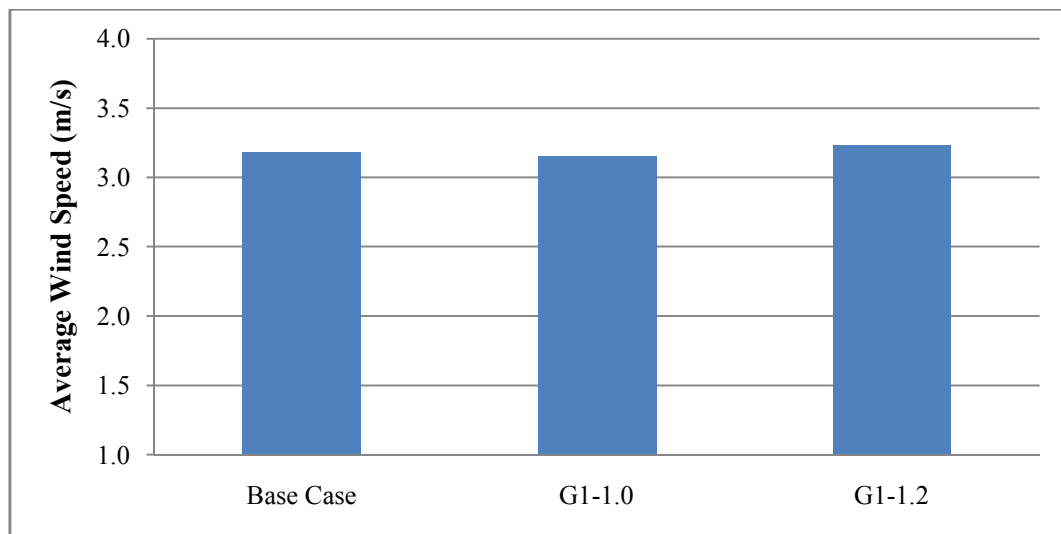
Figure 6.9: The average of maximum air temperature for the second group configurations in the four orientations; N-S, E-W, NE-SW, and NW-SE

However, the variation in maximum outdoor air temperature averages in the N-S and E-W orientation is very small. Therefore, the comparison between the second group six configurations for the best configuration will be conducted in the two orientations NE-SW and NW-SE, the N-S and E-W orientations comparison figures are presented in appendix C.2.

In the NW-SE orientation, the best configuration with respect to the lowest maximum outdoor air temperature averages is G2-2.5 (5:3:7:7:3:5) followed by the G2-2.1 (3:5:7:7:5:3) configuration with a slight difference of 0.18°C between the two configurations.

The variation in air temperature between the best configuration G2-2.5 (5:3:7:7:3:5) and the base case is 0.9 °C in the NW-SE orientation. On the other hand, the G2-2.0 (7:5:3:3:5:7) recorded the least reduction of 0.2 °C compared to the base case in the NW-SE orientation (Figure 6.10 a).

However, the same daily performance of the best configuration has been observed in the first and second group. The best configuration shows an opposite attitude in the evening and early morning time by recording an outdoor air temperature averages higher than the base case with a non-notable variation.

Around the midnight 12:00, the G2-2.5 (5:3:7:7:3:5) best configuration started to show a slight increase of $0.1\,^{\circ}$C. This is related to the effect of the direct solar radiation and the over shading effect provided in the G2-2.5 (5:3:7:7:3:5) configuration during the day time compared to the other configurations.

During the day time the direct radiation increases the outdoor air temperature of the other two configurations, at the evening time the buildings start releasing the absorbed heat and the air temperature of the block canyons decreases and becomes more balanced at the night period of the day. On the other hand, in the NE-SW orientation, a significant variation in maximum air temperature averages is recorded with a difference of $1.7\,^{\circ}$C between the best configuration G2-2.5 (5:3:7:7:3:5) and the G2-2.2 (5:7:3:3:7:5) configuration (Figure 6.10 b).

In this orientation the G2-2.2 (5:7:3:3:7:5) recorded the highest maximum temperature with a an increase of $0.75\,^{\circ}$C compared to the base case, while the lowest maximum air temperature recorded in configuration G2-2.5 (5:3:7:7:3:5) with a reduction of 0.95°C compared to the base case (Figure 6.10 b).
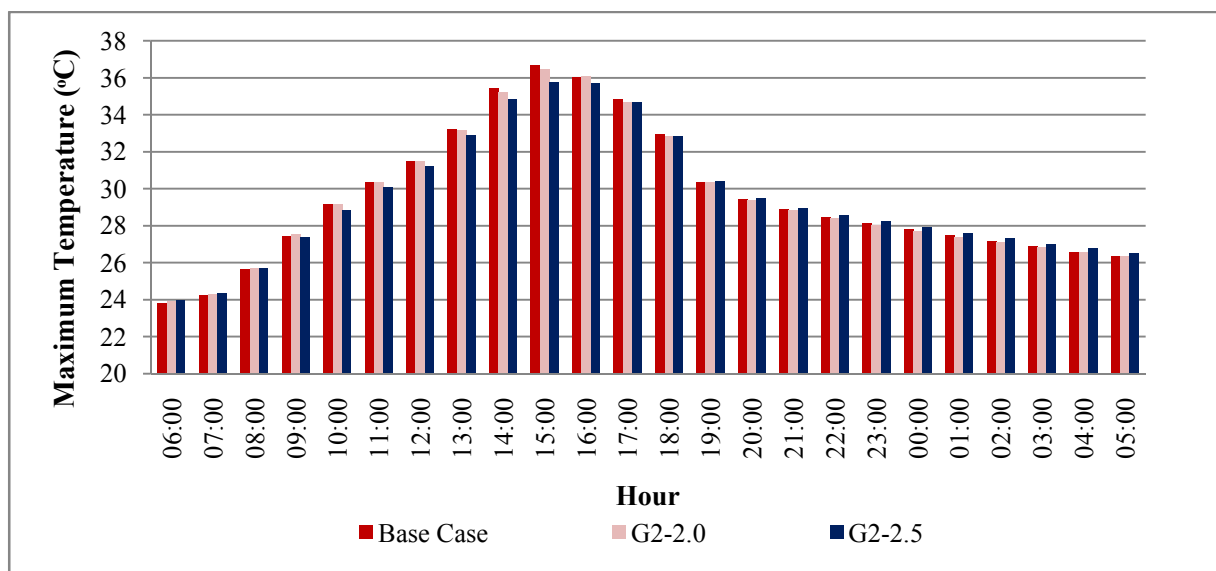
a) NW-SE orientation
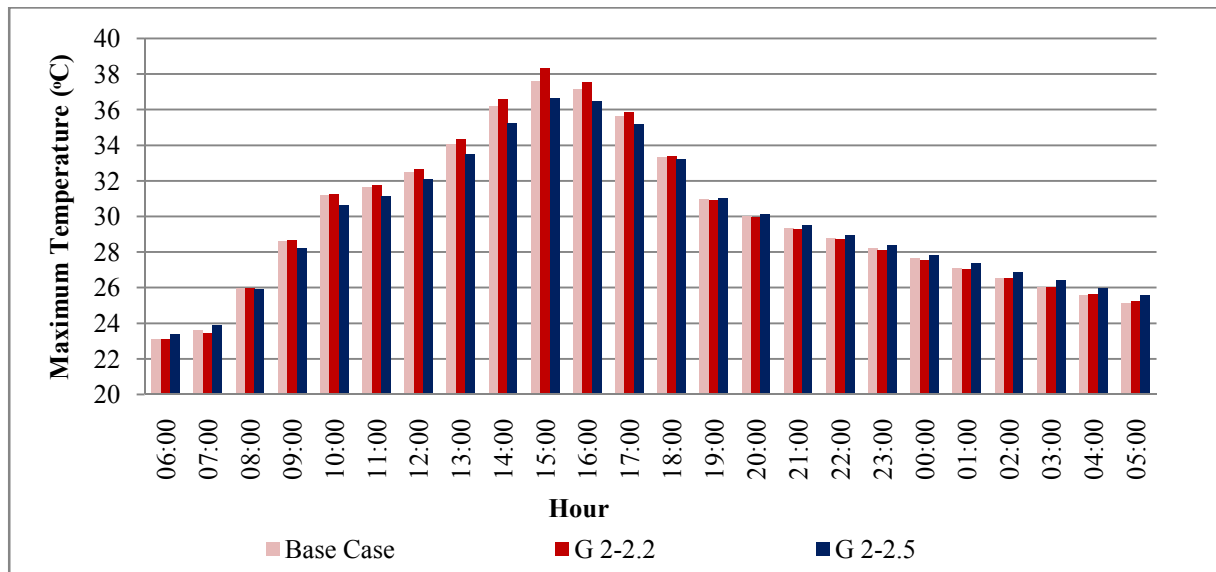
b) NE-SW orientation

Figure 6.10: The configurations with the maximum and minimum reduction in air temperature of the second group compared to the base case in; a) NW-SE and b) NE-SW orientations

The effect of the height variation on the wind speed of the second group configurations in all orientations is presented in figure 6.11. From the figure, there is a clear variation between all configurations of the second group, and the effect of the NW-SE prevailing wind is observed clearly on the maximum wind speed averages for all configurations in this orientation.

The figure shows that the there is a clear variation between the maximum and minimum wind velocity average in the four orientations, as the height diversity created the obstruction that influence the prevailing wind speed for all configurations.
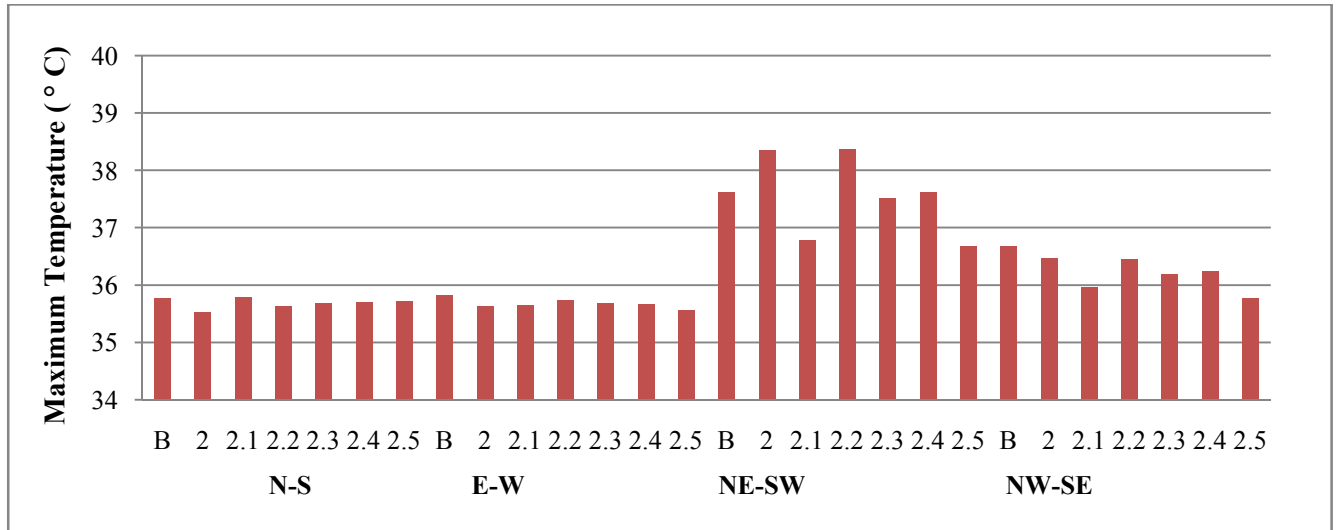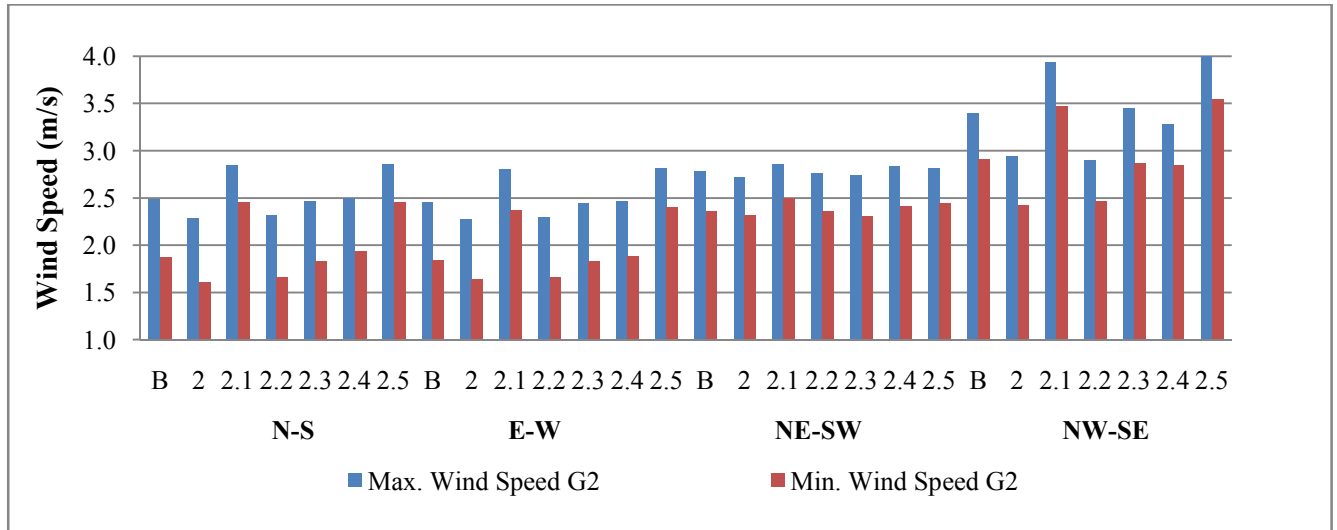
Figure 6.11: The average of maximum and minimum wind speed for the second group configurations in the four orientations; N-S, E-W, NE-SW, and NW-SE

However, the variation is less in the NE-SW orientation, as the variation in buildings height of the second group is implemented in the long axis of the block, and it is aligned with prevailing wind when the block oriented towards the NE-SW orientation. Furthermore, there is a clear variation in the NW-SE orientation related to the height diversity that is implemented in the same direction.

In general, the maximum velocity varied between the sixth configuration and the best configuration that records the maximum wind speed is G2-2.5 (5:3:7:7:3:5) followed by G2-2.1 (3:5:7:7:5:3)configuration. However, the NW-SE orientation recorded higher wind velocity averages compared to the other orientation and as a result of the effect of the north-west prevailing wind in the Dubai, UAE reported by the Dubai weather section. The maximum wind velocity recorded by G2-2.5 (5:3:7:7:3:5) configuration in the NW-SE orientation followed by G2-2.1(3:5:7:7:5:3) configuration. Compared to the base case, the increase in wind velocity values and averages in these two configuration proves the effect of the height variation in accelerating wind velocity in the canyons between the buildings.

The enhancement in the best configuration wind velocity in the NE-SW and NW-SE orientations at maximum air temperature averages for the best configuration is shown in

figure 6.11. The figure shows the effect of the height variation on increasing and accelerating wind velocity of the best configuration compared to the base case. On the other hand, the minimum wind velocity is recorded by the first configuration G2-2.0 (7:5:3:3:5:7).

This result shows that gradual variation towards the inner axis of the block and placing the highest buildings at the boundary of the block blocking the wind and reducing the wind velocity within the canyons. On the other hand, placing the highest building in the middle of the block accelerating the air velocity within the block (Figure 6.12). In the NW-SE the G2-2.5 (5:3:7:7:3:5) best configuration increases the wind velocity by 18%compared to the base case and the G2-2.0 (7:5:3:3:5:7) configuration records a decrease of 15 % compared to the base case (Figure 6.12a).

However, the increase in the wind velocity is less in the NE-SW orientation between the best configuration G2-2.5(5:3:7:7:3:5) and the base case and reaches 1.9 %, while the G2-2.2 has almost the same wind velocity of the base case with non-notable variation.
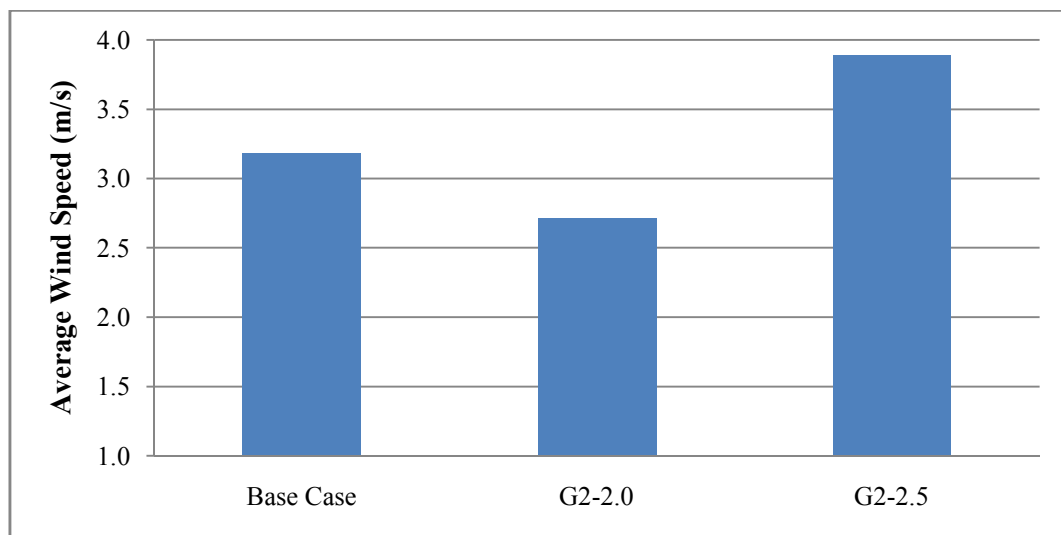
a) wind speed NW-SE
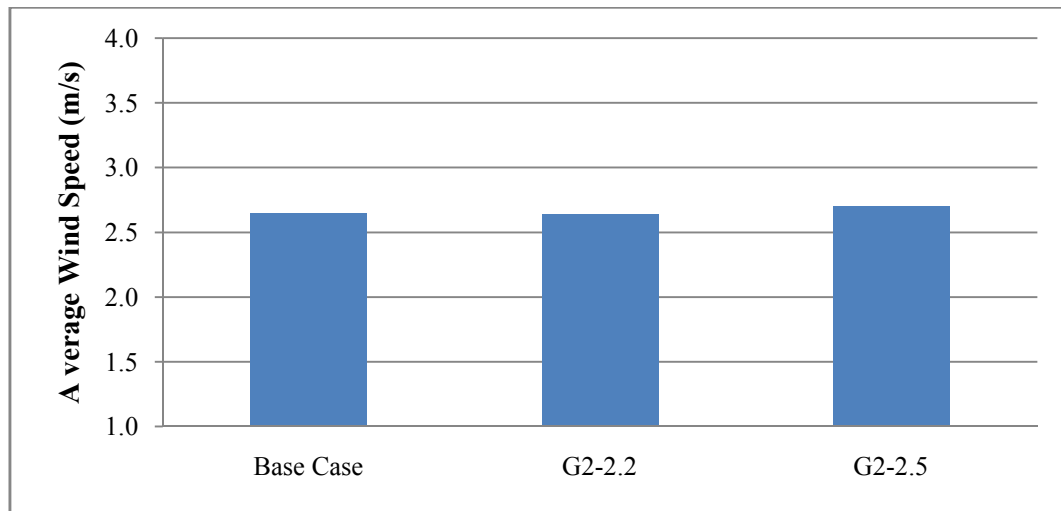
b) wind speed NE-SW

Figure 6.12: The variation in wind velocity at maximum air temperature of the second group configurations compared to the base case in two orientations; a) NW-SE and b) NE-SW

The relative humidity of the second group configurations is shown in Figure 6.13. The second group's configurations show an attitude similar to the first group with respect to the relation between the relative humidity and air temperature averages. The best configuration in the NW-SE orientation is G2-2.5 (5:3:7:7:3:5) in this group, ant it recorded the highest relative humidity in this orientation with an increase of 3.6 % compared to the base case. The minimum relative humidity in this orientation is recorded in the base case configuration as the base case has the highest maximum air temperature in the same orientation (Figure 6.13).
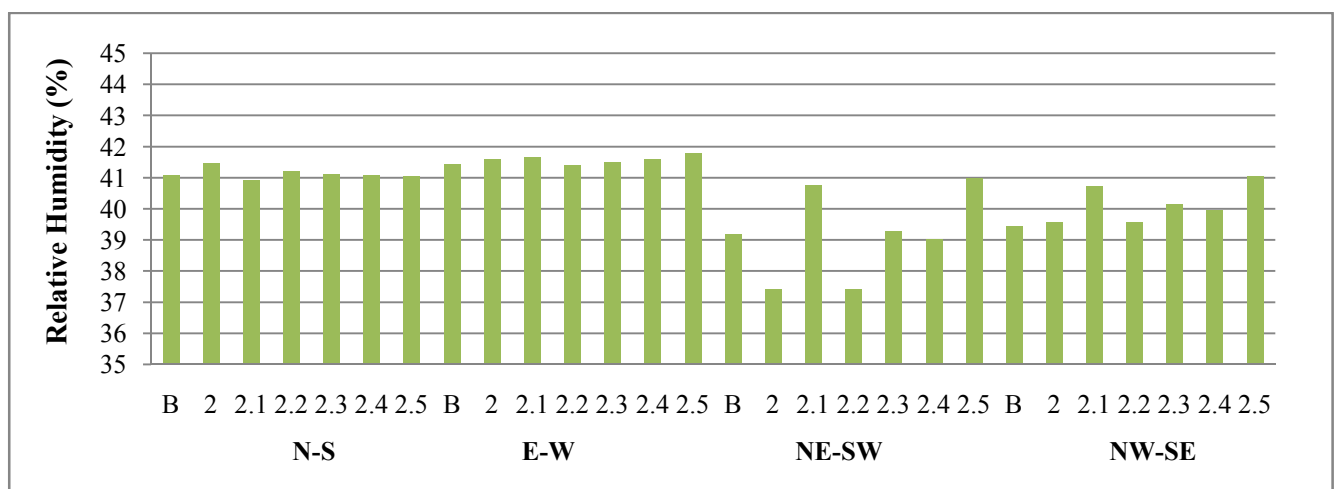
Figure 6.13: The average of the relative humidity at maximum temperature for the second group configurations in the four orientations; N-S, E-W, NE-SW, and NW-SE

6.1.4 The Best Performance of the Third Group Configurations

Figure 6.14 shows the maximum air temperature averages in the three configurations of the third group in the four orientations. It clear that there is a variation in maximum air temperature averages between the three configurations in all orientations.

Figure 6.14: The average of maximum air temperature for the third group configurations in the four orientations; N-S, E-W, NE-SW, and NW-SE

This variation is less in the NE-SW orientations and it is significant in the NW-SE orientation. The NE-SW orientation recorded the highest air temperature averages compared to the other orientations, and opposite to the other two groups, the N-S and E-W shows a variation in maximum air temperature between the three configurations.

The best performance in the third group with respect to the lowest maximum air temperature is the third configuration G3-3.2 (15:20) with a reduction of 1.9 °C compared to the base in the NW-SE (Figure 6.15 a). In the NE-SW orientation there is no significant variation between the third group configurations, but the best performance recorded by G3-3.0 (20:25) configuration with a reduction of 0.4°C compared to the base case (Figure 6.15 b).

However, the best configuration G 3-3.0 in the NE-SW orientation shows an opposite attitude to in the NW-SE orientation to record the highest maximum air temperature (Figure 6.15 a). Furthermore, and according to the same sequence of data illustration, the N-S and E-W orientations comparison figures of the third group configurations are presented in appendix C.3.
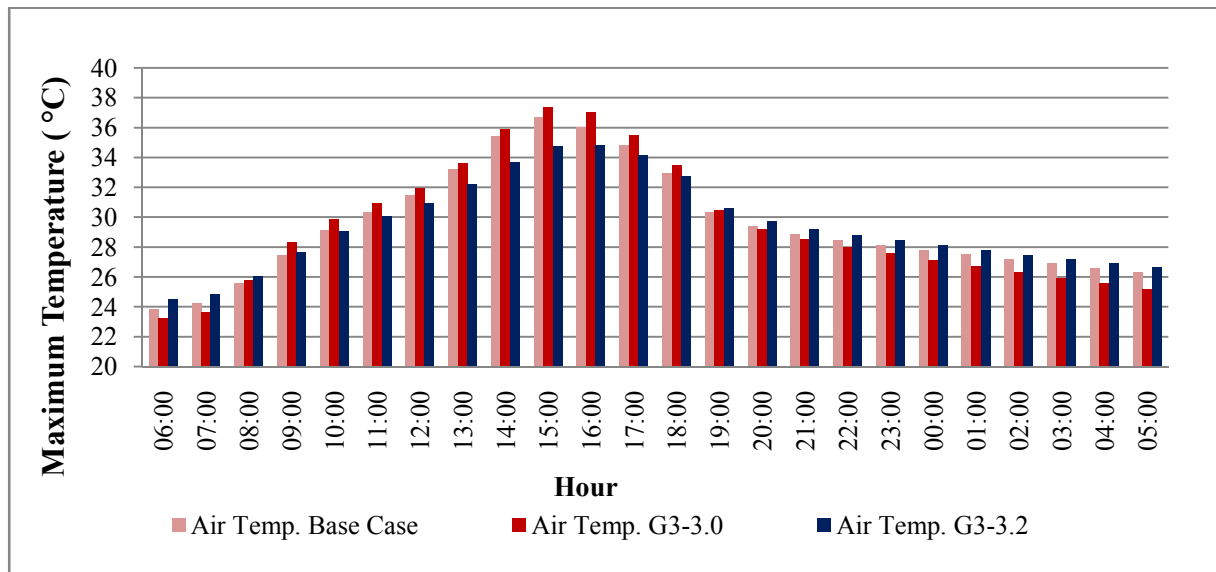
a) NW-SE orientation
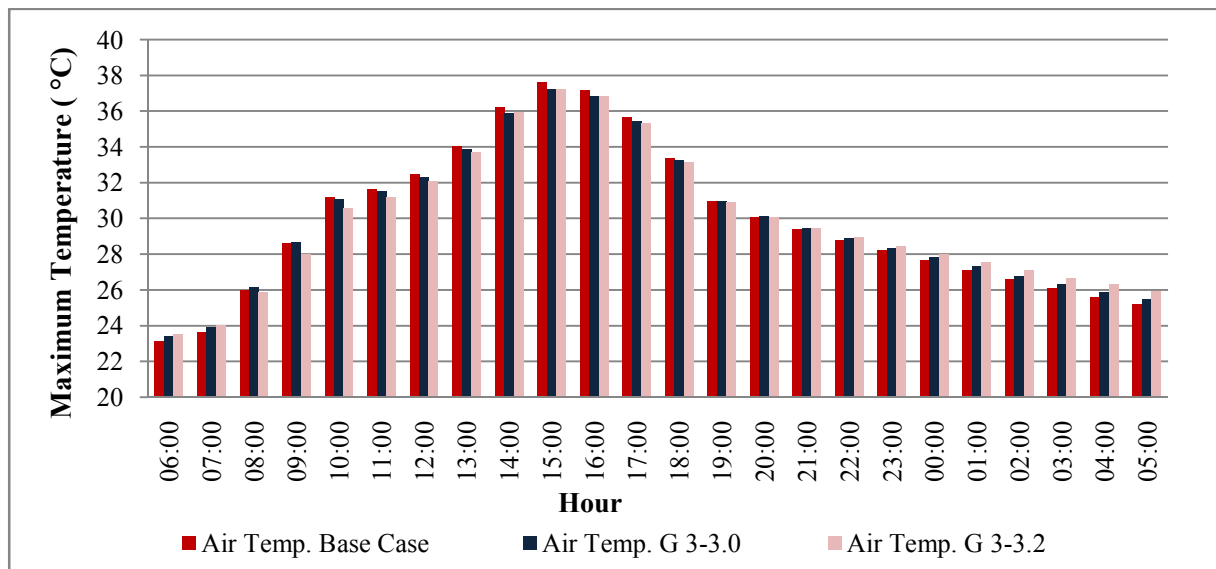
b) NE-SW orientation

Figure 6.15 The configurations with the maximum and minimum reduction in air temperature of the third group compared to the base case in; a) NW-SE and b) NE-SW orientations

The wind velocity of the third group shows clearly the significant effect of the different configurations on wind behaviour (Figure 6.16). It is obvious that the NW-SE orientation recorded the lowest velocity compared to the other orientations.
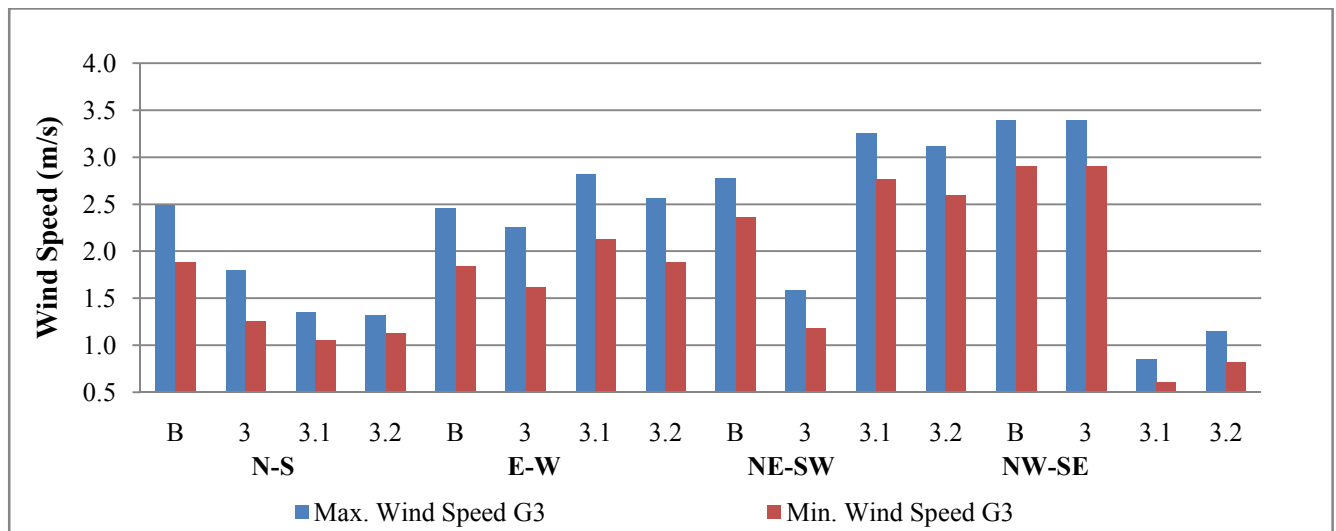
Figure 6.16: The average of maximum and minimum wind speed for the third group configurations in the four orientations; N-S, E-W, NE-SW, and NW-SE

However, the best thermal performance configuration G3-3.2 (15:20) in the NW-SE orientation did not show the same behaviour with respect to enhancing the wind velocity, and the G3-3.0 (20:25) configuration recorded the best performance in this orientation. This result proves that the effect of the wind velocity is less than the shading effect on air temperature averages.

In the NW-SE orientation the best configuration G3-3.2 (15:20) that recorded the lowest maximum air temperature averages reduce wind velocity by 68 % compared to the base case (Figure 6.17 a). On the other hand, the G3-3.0 configuration increases the wind velocity slightly compared to the base case. The same configurations show an opposite attitude in the NE-SW orientation. The best configuration in this orientation G3-3.2 (15:20) increasing the wind velocity by 8.9 % compared to the base case, while the G3-3.0 configuration decreasing the wind speed by 4.6 % compared to the base case (Figure 6.17b).
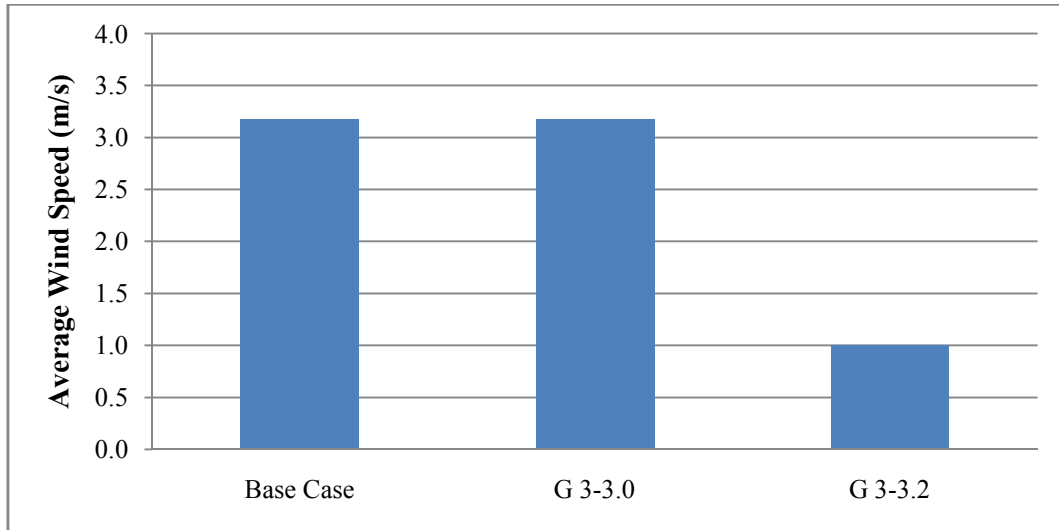
a) NW-SE orientation
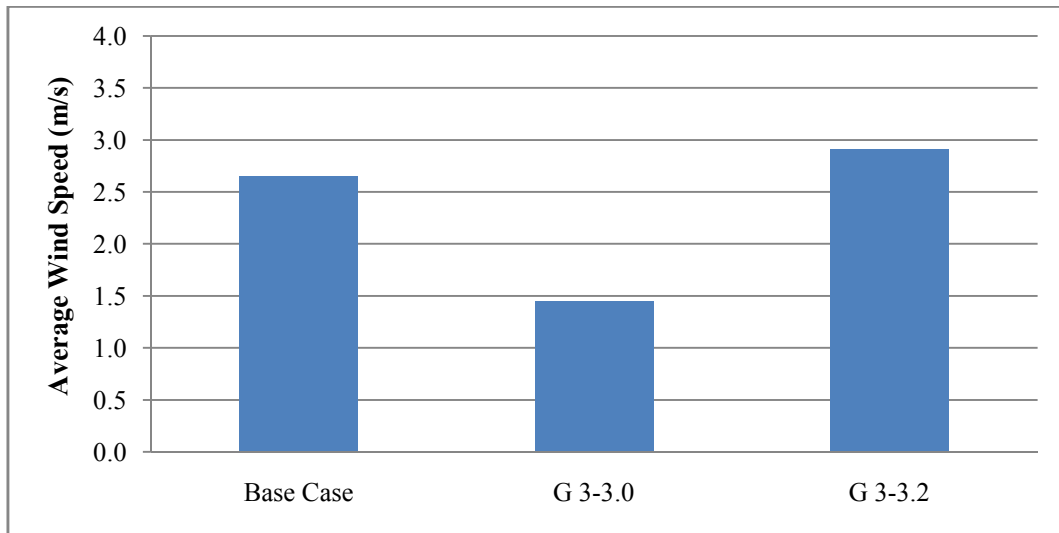
b) NE-SW orientation

Figure 6.17: The variation in wind velocity at maximum air temperature of the third group configurations compared to the base case in two orientations; a) NW-SE and b) NE-SW

Furthermore, the G3-3.2 (15:20) configuration recorded the highest relative humidity compared to all configurations in all orientations as it has the lowest maximum air temperature. The increase in relative humidity of this configuration compared to the base case in NW-SE orientations reaches 9.8 % (Figure 6.18).
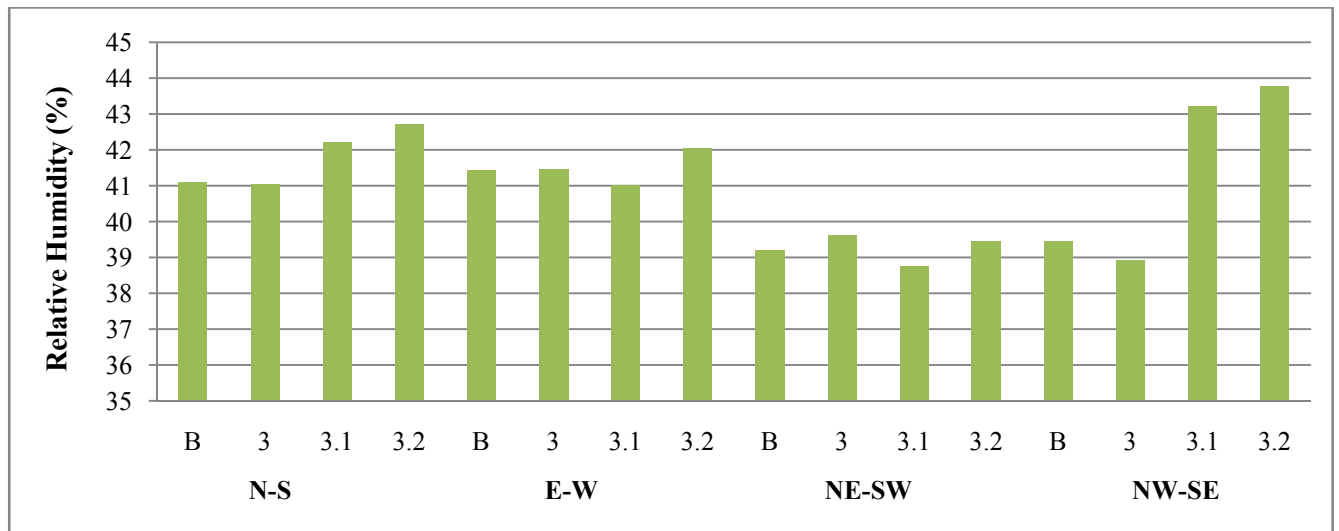
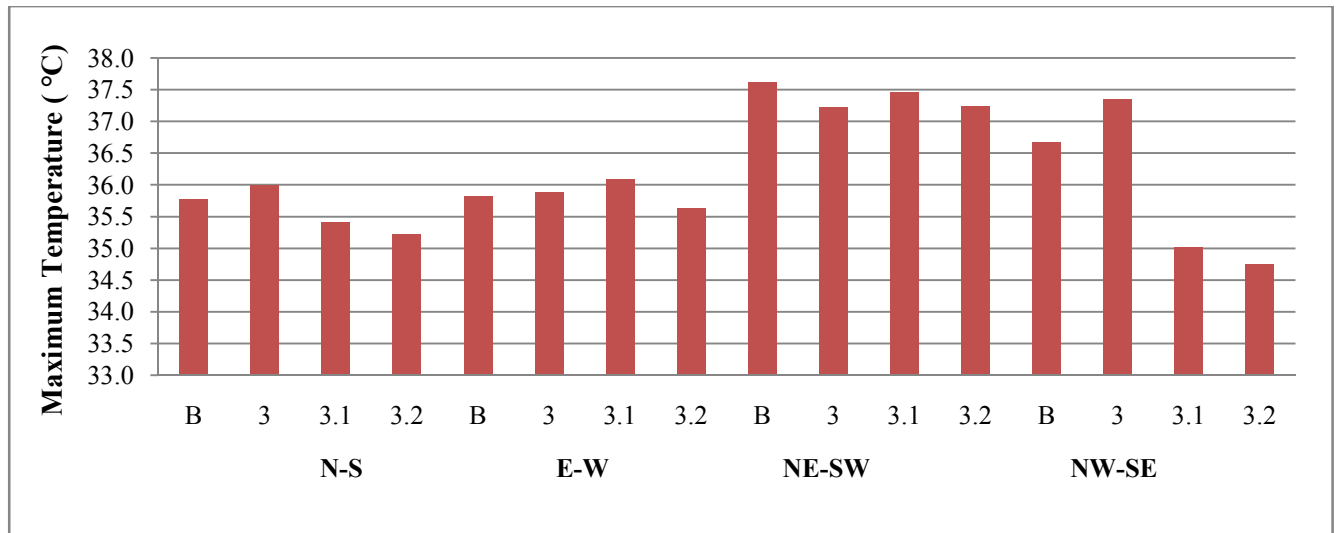Figure 6.18: The average of the relative humidity at maximum temperature for the third group configurations in the four orientations; N-S, E-W, NE-SW, and NW-SE

6.2 The Effect of the Urban Block' Geometry and Orientation on the Outdoor Microclimate Parameters

In the first section of this chapter (6.1), the best configuration of each group with respect to the lowest maximum outdoor air temperature was presented. The evaluation was done according to the effect of the studied variables; block orientation, height diversity and building configurations. In this section the presented results will be discussed and analysed. The discussion of the results will cover the spatial and temporal distribution of the covered microclimate parameters.

The effect of the studied variables of the urban geometry on the outdoor microclimate parameters will be discussed, the outdoor microclimate parameters that will be covered are; air temperature, wind speed and relative humidity. This analysing will adopt the SVF as an indicator to evaluate the studied urban geometry variables on the mentioned microclimate parameters. The effect of the urban geometry and block configurations on the outdoor microclimate parameters will be discussed by comparing the best configurations of the three developed groups in each orientation with the base case configuration.

The outdoor thermal performance results show that the block / canyon orientation plays a significant role in the outdoor thermal performance and air temperature averages. The orientation's effect on outdoor air temperature averages has been observed in the base case and the three groups configurations, specifically at the maximum air temperature and the peak cooling load consumption during the day time between 3:00 pm - 4:00 pm. In the base case configuration with uniform buildings height, and due to the grid buildings configuration, the N-S and E-W block orientations show an approximate attitude with respect to the maximum outdoor air temperature averages. However, the N-S direction represents the best orientation for reducing the outdoor maximum air temperature during the daytime in the studied area and the hot climate zone.

Similar results have been reported by Shashua and Hoffman (2003) and Andreou (2014). Furthermore, this result proves that extending the block along the E-W to face the N-S direction would avoid the long axis and the largest area of the block from facing the E-W orientation. This orientation consequently reduces the area that is exposed to the sun shine and sun set. The same preferred orientation for the urban block is highlighted in LEED Neighbourhood Development (v.4 2014) in order to provide the sustainable performance for the urban block with respect to solar access and thermal performance. Furthermore, LEED Neighbourhood Development (v.4 2014) provides credits to the block that is extended ±15 degree along the E-W orientation depending on the geographical location. However, the NE-SW and the NW-SE orientation recorded higher averages of air temperature compared to the N-S and E-W orientations.

The maximum air temperature recorded was in the NE-SW orientation, and the increase of the maximum air temperature averages in this orientation compared to the best orientation N-S reached to 1.8 °C.

Furthermore, a decrease of 0.9 °C in maximum air temperature averages was recorded in the NW-SE orientation compared to the NE-SW block orientation. The top view section at 1.4 m and the variation in maximum air temperature at 3:00 pm of the base case configuration in the four orientations is illustrated in figure 6.19. The figure shows the distribution of the outdoor air temperature extracted from the ENVI-Met software.

The images illustrate the average of maximum air temperature of the base case, and it reflect the same results of the receptors' statistics data presented in chapter 5, section 5.1 with respect to the block orientation and outdoor maximum air temperature performance .

a) N-S orientation

b) E-W orientation

c) NE-SW orientation

d) NW-SE orientation

Air Temperature (°C)

< 33.5   34.5   36.0   > 37.5

Figure 6.19: The top view of the maximum air temperature at 1.4m for the base case configuration in the four orientations; a) N-S, b) E-W, c) NE-SW, and d) NW-SE

Figure 6.20 shows a cross (vertical) section in the middle of the base case configuration and the maximum air temperature at 3:00 pm in the four orientations. The sections reflect the same result of each orientation and show that the NE-SW orientation has the highest maximum air temperature. Further to this, the variation in air temperature of 2°C reported by Oke (1988) between the bottom and the top of the uniform canyon can be observed clearly in the all orientations (Figure 6.20).

a) The base case in the N-S orientation

b) The base case in the E-W orientation

c) The base case in the NE-SW orientation

d) The base case in the NW-SE orientation

Air Temperature (°C)

< 33.5   34.5   36.0   > 37.5

Figure 6.20: The cross section in the middle of the block for the maximum air temperature of the base case in the four orientations; a) N-S, b) E-W, c) NE-SW, and d) NW-SE

On the other hand, the wind performance in the four orientations of the urban block with uniform height is shown in figure 6.21. The figure represents the top view of the wind performance at 1.4 m. The figure shows that the wind velocity averages in the N-S orientation is higher than the wind averages in the E-W due to the effect of the prevailing wind. In spite of the high average wind speed that can be observed in the alleys in the NE-SW orientation, this orientation is the highest in maximum air temperature compared to the other orientations. The increase in average air temperature in the NE-SW orientation is related to the effect of the narrow alleys exposure to the NW-SE sun direction.

The high exposure to the sun solar radiation, and the trapped heat in the narrow alleys with H/W ratio of 1.6 increases the air temperature in this orientation. This proves that the effect of the solar radiation is dominated compared to the wind effect. The same result of solar effect and the high air temperature caused by the trapped heat in the canyon of H/W ratio more than 1 was presented by Littlefair et al. (2000).

Furthermore, it has been found that the NW-SE orientation has the highest wind speed averages as the main canyons are parallel to the prevailing wind orientation. On the other hand, the NE-SW orientation recorded the lowest averages of the wind speed as the main canyon are in the opposite direction of the prevailing wind orientation. The effect of the canyon width on the amount of the air mass that flows within the canyon space is reported by Littlefair et al. (2000).

In additional to the prevailing wind in the N-S and NW-SE orientations, the reduction in air temperature is related to the block type of grid, pavilion configuration. This urban block configuration forms strait canyons which promotes the air speed within the canyons specially in the direction of the prevailing wind. This result agrees well with other study reported the acceleration of the air velocity in the strait canyons (Santamouris,1999). The base case represents the pavilion grid arrangement with uniform buildings height, the H/W ratio of the main and side canyons is 0.96 and the alleys H/W ratio is 1.6. The two types of canyons in the simulated block represent the uniform and deep canyon, respectively, according to Johansson's (2006) canyon classification. Therefore, the effect of the weak influence flow and skimming flow reported by (Oke 1988) is occurred in the main canyons and alleys respectively. This explain the high wind speed averages in the NW-SE main canyon orientation as the weak influence flow in wider canyon of H/W ratio less than 1 is more effective in reducing the air temperature than the skimming flow in the narrow canyons or alleys.

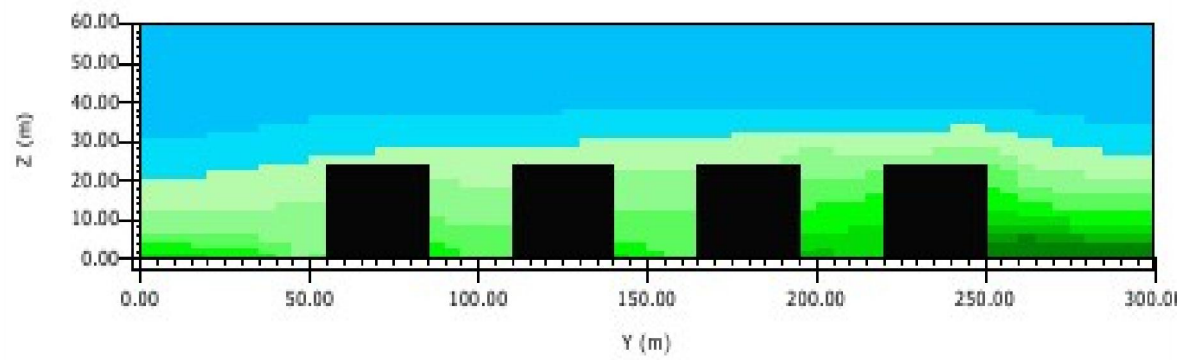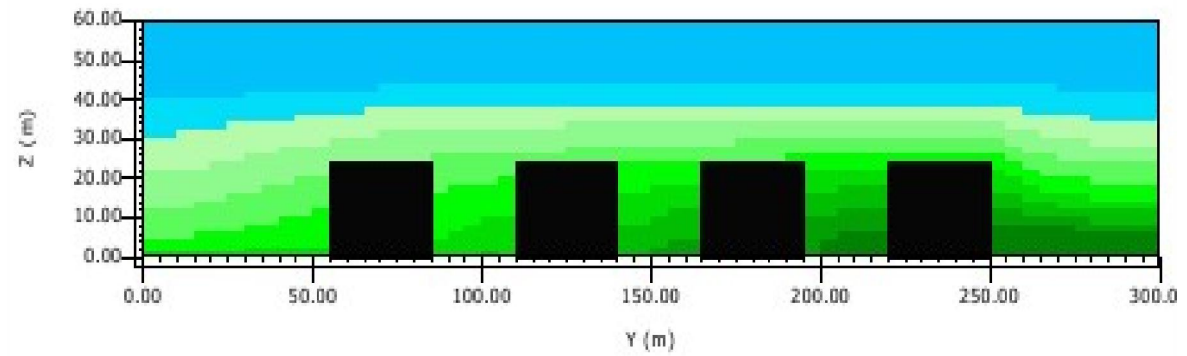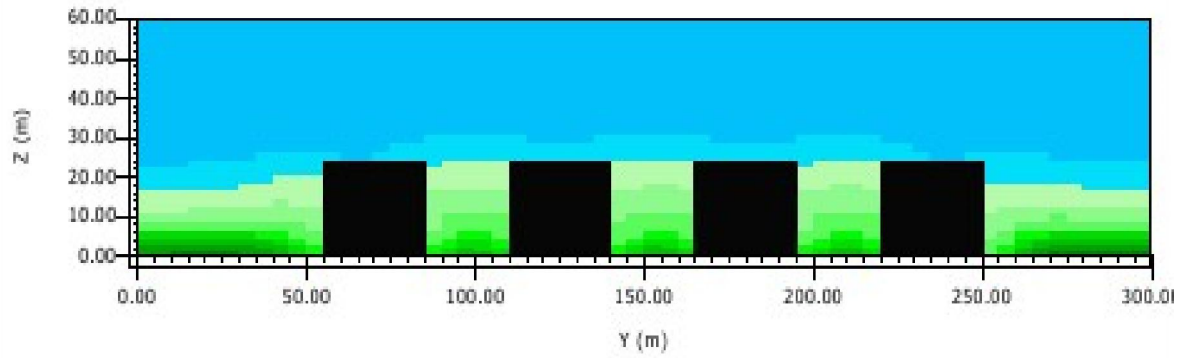a) The base case in the N-S orientation
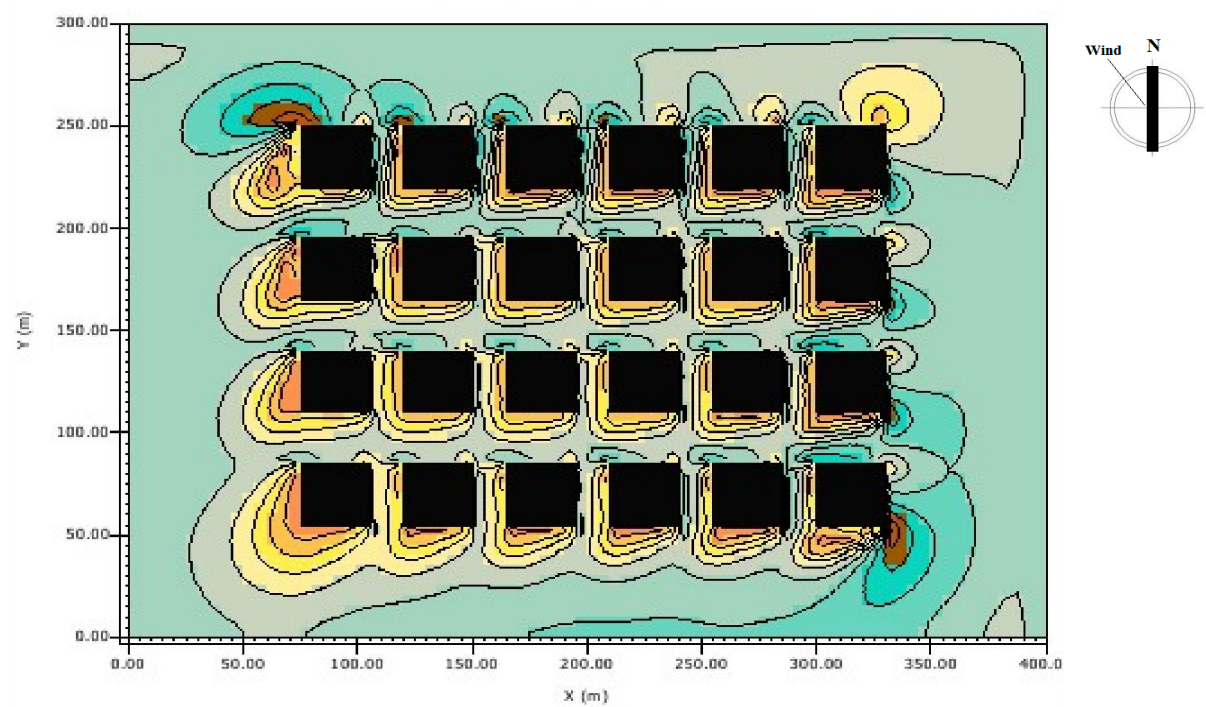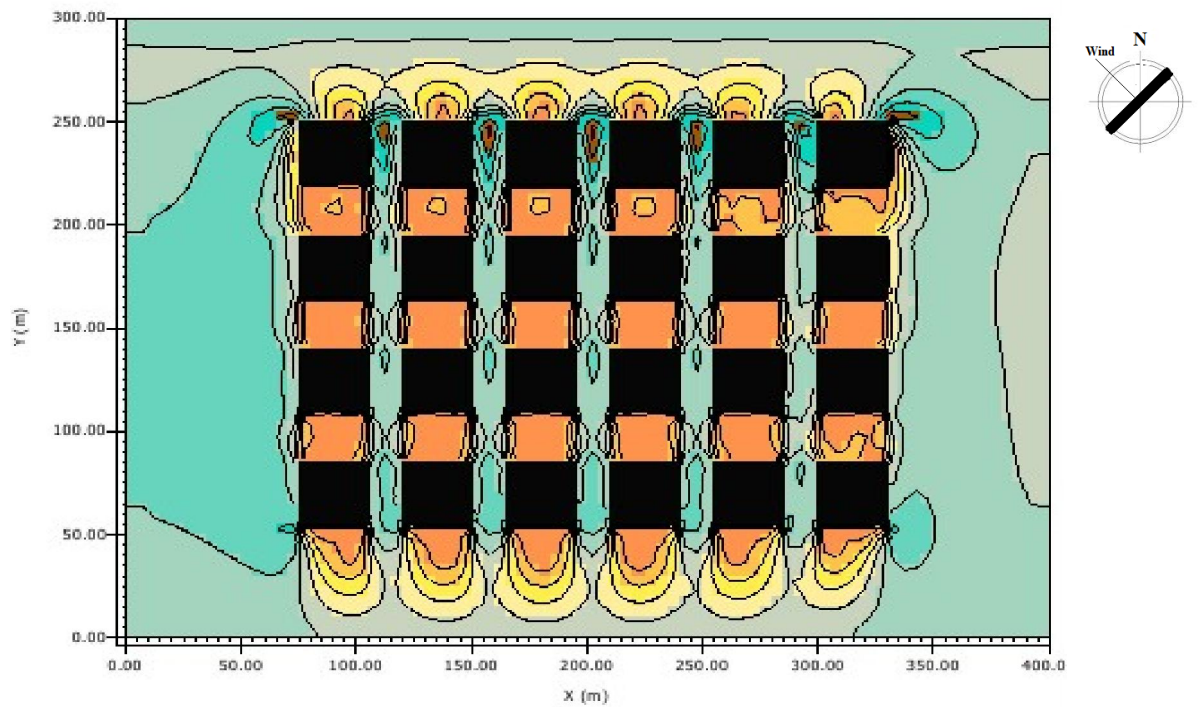
b) The base case in the E-W orientation

c) The base case in the NE-SW orientation
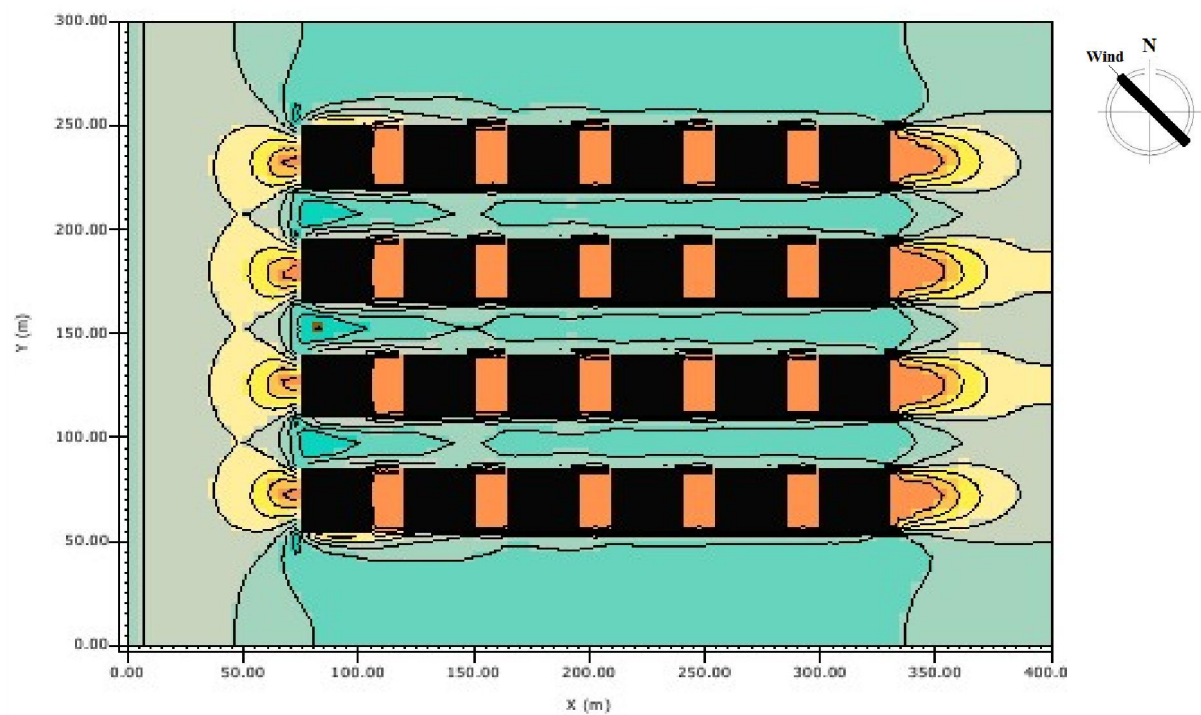
d) The base case in the NW-SE orientation
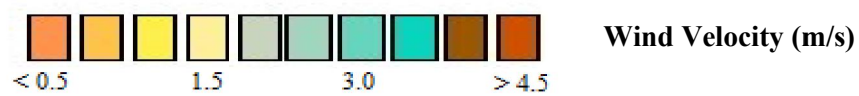
Wind Velocity (m/s)

Figure 6.21: The top view of the wind velocity for the base case in the four orientations; a) N-S, b) E-W, c) NE-SW, and d) NW-SE

Figure 6.22 presents a cross section in the middle of the block, the figure does not show the overall average, but it reflects the same attitude of the wind velocity averages compared to the base case in each orientation.
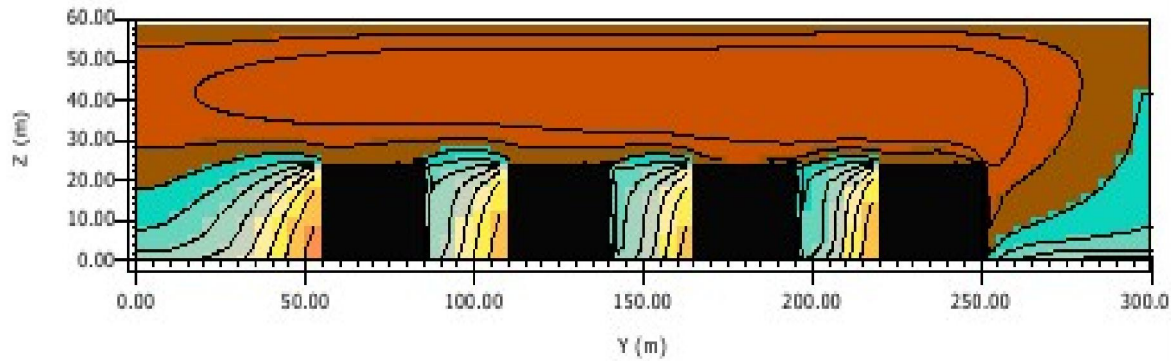
a) The base case in the N-S orientation
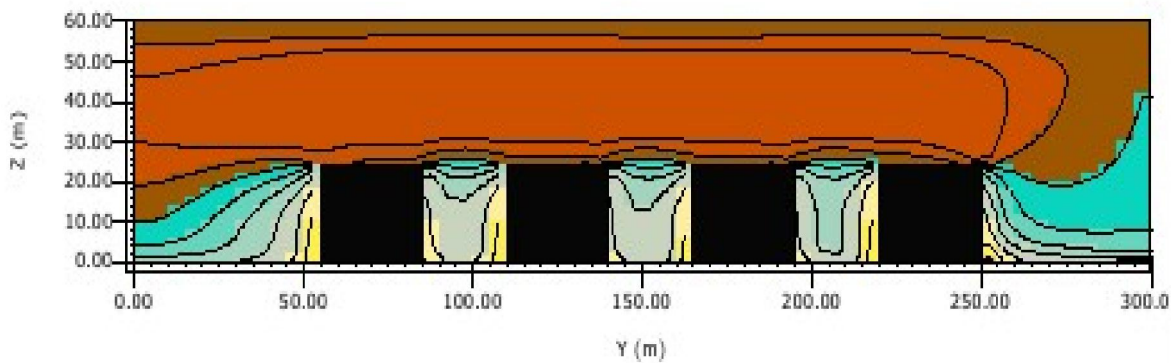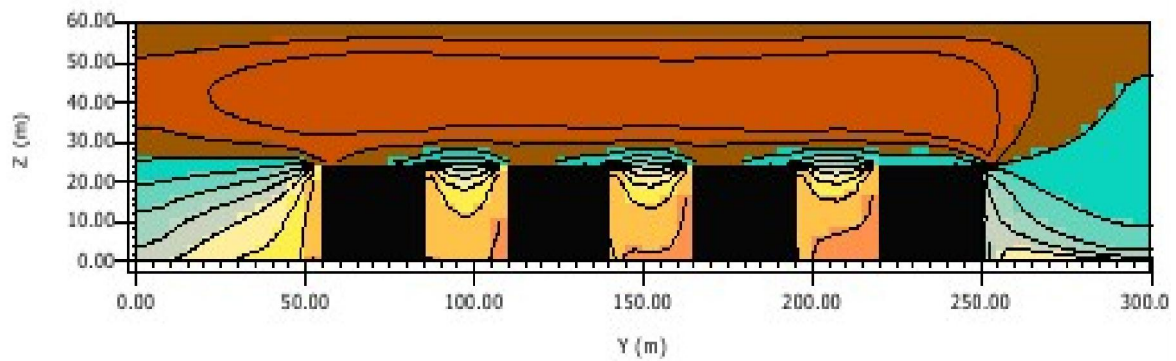
b) The base case in the E-W orientation

c) The base case in the NE-SW orientation
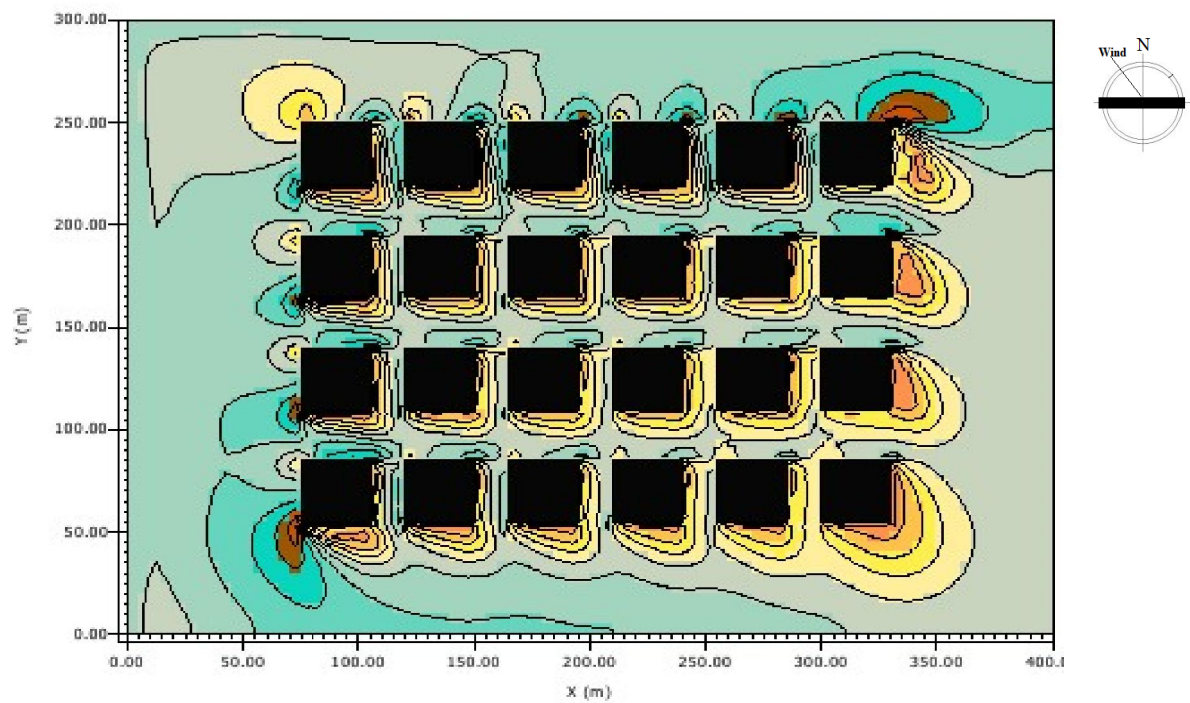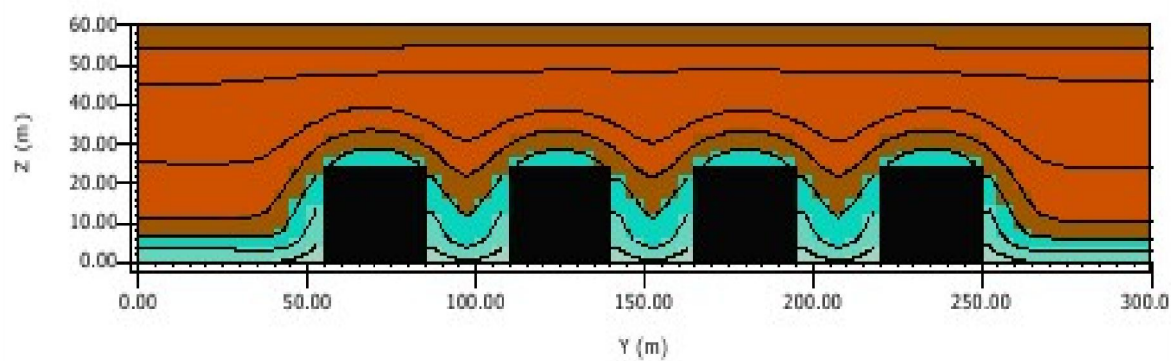

d) The base case in the NW-SE orientation
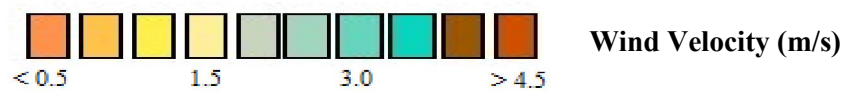
Wind Velocity (m/s)

Figure 6.22: The cross section of the wind velocity for the base case in the four orientations;
a) N-S, b) E-W, c) NE-SW, and d) NW-SE

The relative humidity averages are inversely related to the maximum air temperature averages as presented in Figure 6.3 of this chapter. In spite of the fact that the minimum air temperature was recorded in the N-S orientation, the maximum relative humidity was recorded in the E-W orientation. This can be related to the effect of the wind velocity. The wind velocity in the E-W orientation is lower than the wind velocity in the N-S orientation, this result proves the effect of the wind velocity on reducing the relative humidity in the N-S orientation.

Nevertheless, the variation in buildings' height of the developed configurations do not provide a fixed H/W ratio for evaluation, therefore, evaluation of the best configuration compared to the base case will be based on the. The averages SVF of the base case is 0.45, and it will be used to compare the base case with the other configurations.

The base case represents the pavilion configuration with uniform buildings height and the pavilion configuration are adopted in all of the three groups' configurations. The first and the second group configurations examined the effect of height variation on the outdoor microclimate parameters.

In the first group configuration, the diversity in buildings height is implemented in the short axis of the block by adopting the (3:7) ratio for buildings height. From the simulation results, the G1-1.1 (3:7:3:7) configuration with the fluctuated diversity in buildings heights performs as the best configuration in the N-S and E-W orientations with respect to lowest maximum air temperature averages.

On the other hand, in the NE-SW and NW-SE orientations, the G1-1.2 (3:7:7:3) performs as the best configuration in reducing the maximum outdoor air temperature averages. This result shows the significant effect of the height diversity compared to the uniform height in reducing the outdoor air temperature in different orientations.

Compared to the base case's SVF value of 0.45, the diversity in buildings' height reduces the SVF of the best configuration G1-1.2 (3:7:7:3) by 11%, while the G1-1.1 (3:7:3:7) has the same SFV of the base case. The reduction in outdoor air temperature of the best configuration G1-1.2 (3:7:7:3) compared to the base case in the NW-SE orientation is 1.1 $^{\circ}$C. Figure 6.23 presents the cross section of the best configurations in the first group, it reflects the best configuration in each of the four orientations compared to the base case.

However, the top view section at 1.4 m of maximum air temperature for the best configurations of the first group in four orientations is presented in appendix D.1. Further to that, the G1-1.0 (7:3:3:7) configuration with SVF of 0.50 recorded the second highest air temperature after the base case in three orientations. In the NW-SE orientation the G1-1.0 (7:3:3:7) recorded an air temperature higher than the base case by 0.6°C. This performance of the G1-1.0 (7:3:3:7) configuration in the NW-SE orientation is related to high SVF, and high exposure to the sun and less shading effect in this orientation. These findings agrees with a number of studies that reported the relation between the high SVF and the increase in outdoor air temperature averages in the same climatic conditions (Arnfield, 1990; Andreou, 2014).
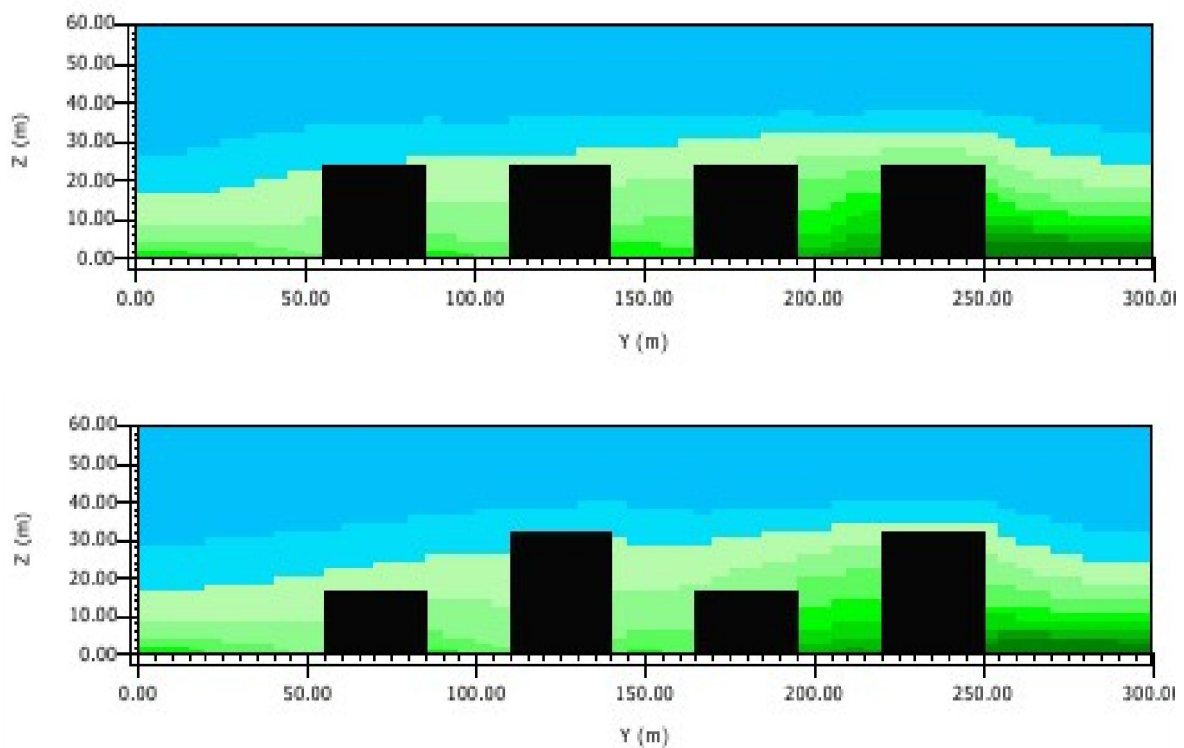
a) The base case and best configuration G1-1.1 (3:7:3:7) in the N-S orientation
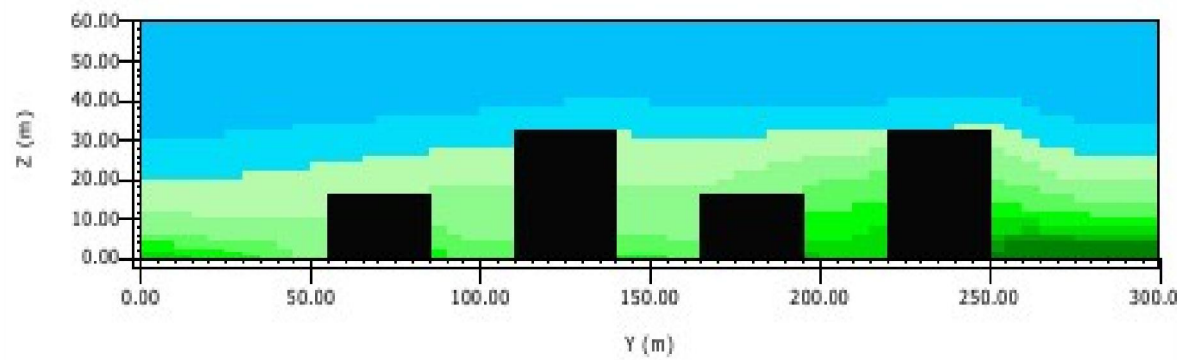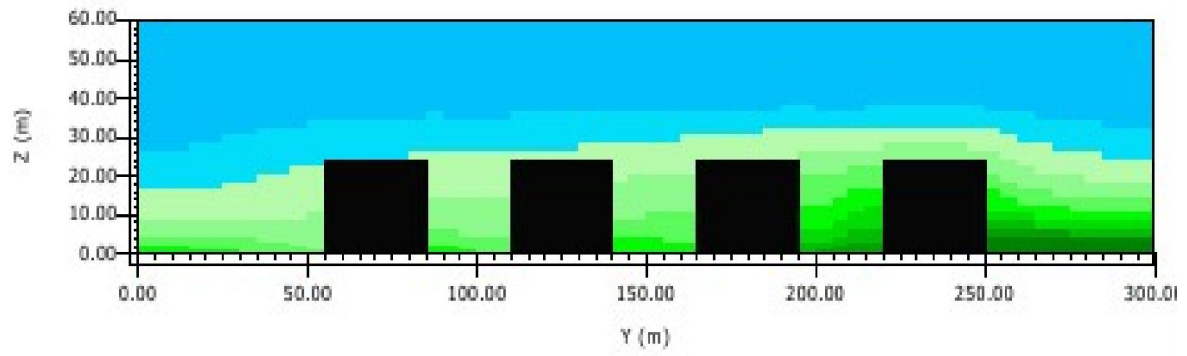
b) The base case and best configuration G1-1.1(3:7:3:7) in the E-W orientation
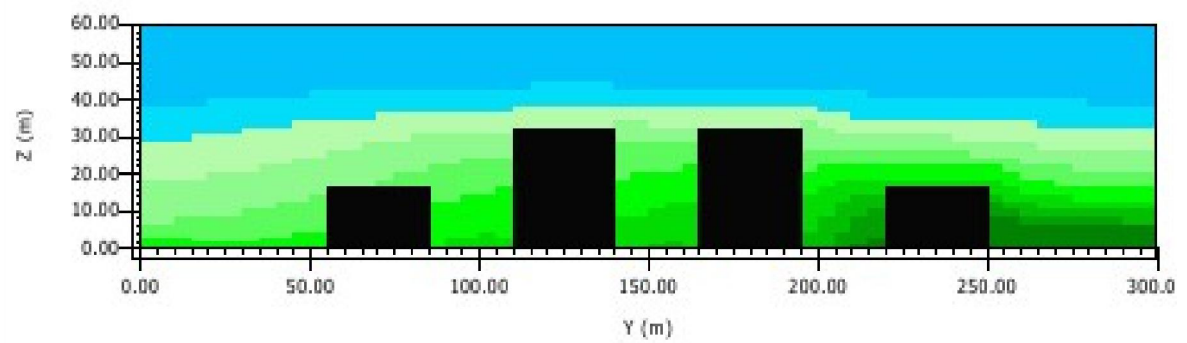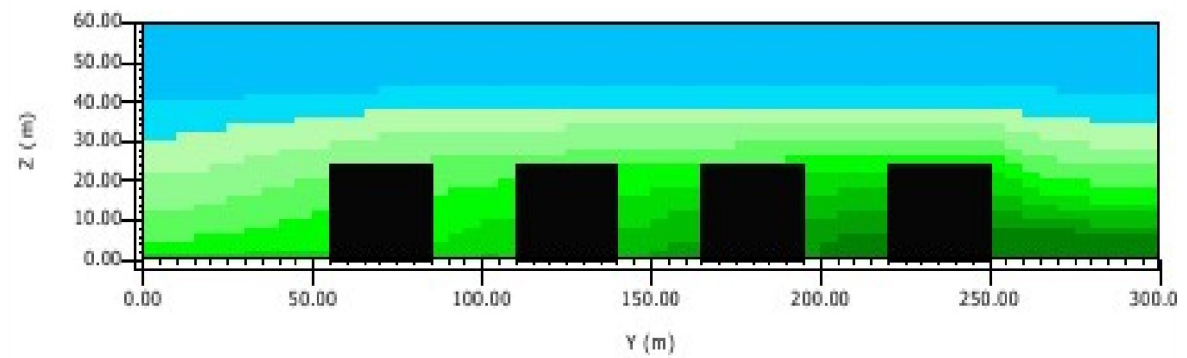
c) The base case and best configuration G1-1.2 (3:7:7:3) in the NE-SW orientation

d) The base case and best configuration G1-1.2 (3:7:7:3) in the NW-SE orientation

    Air Temperature (°C)

Figure 6.23: The cross section of the maximum air temperature for the base case and the best

configurations of the first group in the four orientations; a)N-S, b) E-W, c) NE-SW and d) NW-SE

Regardless of the SVF values, the orientation a more significant in the urban block thermal performance. In spite of the high SVF value of the G1-1.0 (7:3:3:7) configuration, the performance of this configuration with respect to air temperature values is varied according to the block orientation. It recorded an air temperature values slightly lower than the base case in three orientations, but it has a higher temperature compared to the base case in the NW-SE orientation as illustrated in figure 6.4 in this chapter. This study shows the advantages of the significant height diversity on enhancing the urban block thermal performance with respect to the orientation.

In general, and similar to the base case results, the air temperature in the NE-SW orientation is higher than the air temperature in the NW-SE orientation. This variation is due to the effect of the alleys' exposure to the solar gain from the NW-SE direction. The maximum reduction in air temperature of best configuration was recorded in the NW-SE with a reduction of 1.1 º C compared to the base case. This decrease is related to the lower SVF of the best configuration G1-1.2 (3:7:7:3) compared to the base case. Furthermore, the diversity in buildings' height and placing the tallest buildings in the middle of the block promotes the wind velocity in the canyons. The top view at 1.4 m of wind velocity at maximum air temperature for the best configurations of the first group in four orientations is presented in appendix D.2. Figure 6.24 shows a cross section in the middle of the block for the wind velocity for the best configurations of the first group in the four orientations compared to the base case. Generally, and similar to the base case, the E-W orientation recorded higher wind velocity averages than the N-S orientation due to the effect of the prevailing north wind in the main canyons. However, a clear increase in air flow is observed in the best configuration G1-1.1 (3:7:3:7) compared to the base case specifically in the main canyon in these orientations. The increase in the wind speed of the best configuration G1-1.2 (3:7:7:3) compared to the base case in NW-SE orientation reaches 16% due to the effect of the prevailing wind in the main long, straight canyons. This increase is higher and reaches 23% in the NE-SW orientation due to the fluctuated diversity in building height that face the prevailing wind. This result agrees well with the same fact stated by Chan et al. (2001) of enhancing the canyon ventilation by placing a high building among the midrise complex. However, the shading effect created by the lower SVF of 0.40 of the G1-1.2 (3:7:7:3) configuration in this group, in additional to the effect of the prevailing wind in the NW-SE orientation lead to the best performance of this configuration.

The vortex in the middle canyon of H/W equals to 1.3 appears at the top of the canyon, the same result highlighted by Littlefair et al. (2000) for the canyon with the H/W ratio more than 1. Furthermore, the reduction in the air temperature of the best configuration G1-1.1 (3:7:3:7) in the N-S and E-W orientations is less and reaches only 0.5 °C compared to the base case as the SVF is similar to the base case SVF. The fluctuated height diversity of this configuration provides more shading compared to the base case in these specific orientations, further to the increase in wind velocity which reaches 14% compared to the base case in these two orientations.

The effect of the height diversity and the changes in the arrangement pattern with respect to the buildings height can be observed by the change in the wind daily profile illustrated in the results section 6.1.2 of this chapter.

a) The base case and the best configuration G1-1.1 (3:7:3:7) in the N-S orientation
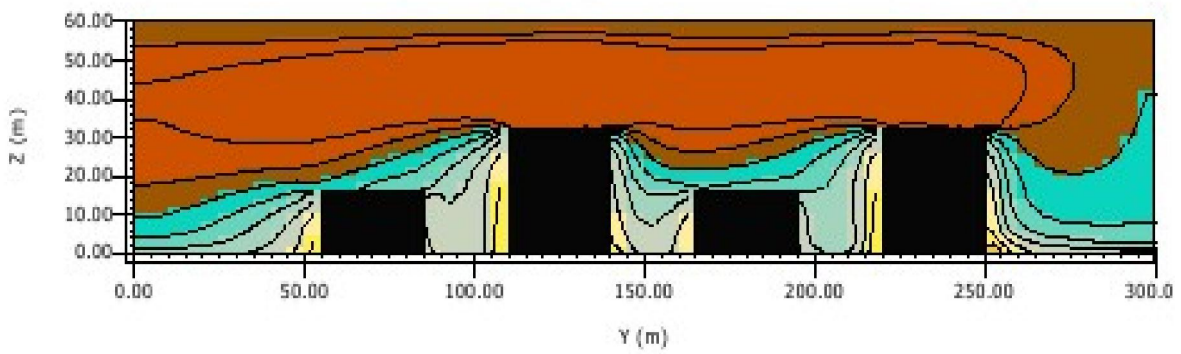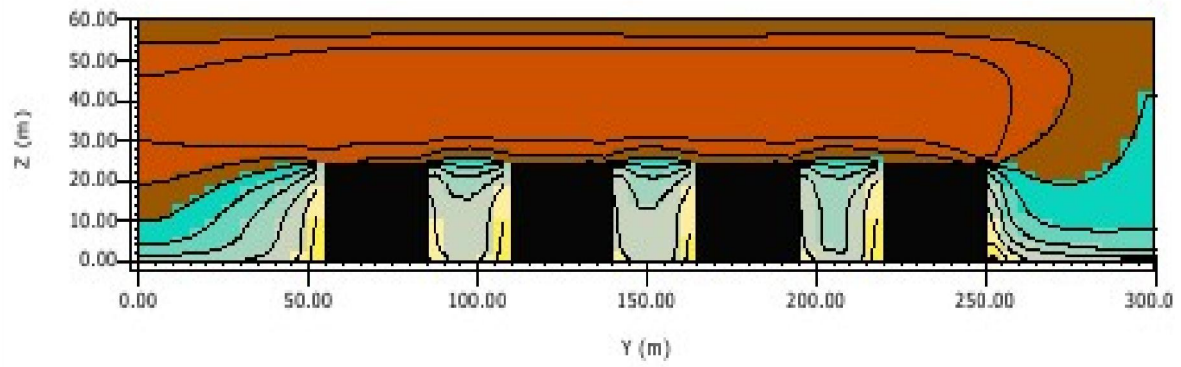
261

b) The base case and the best configuration G1-1.1 (3:7:3:7) in the E-W orientation
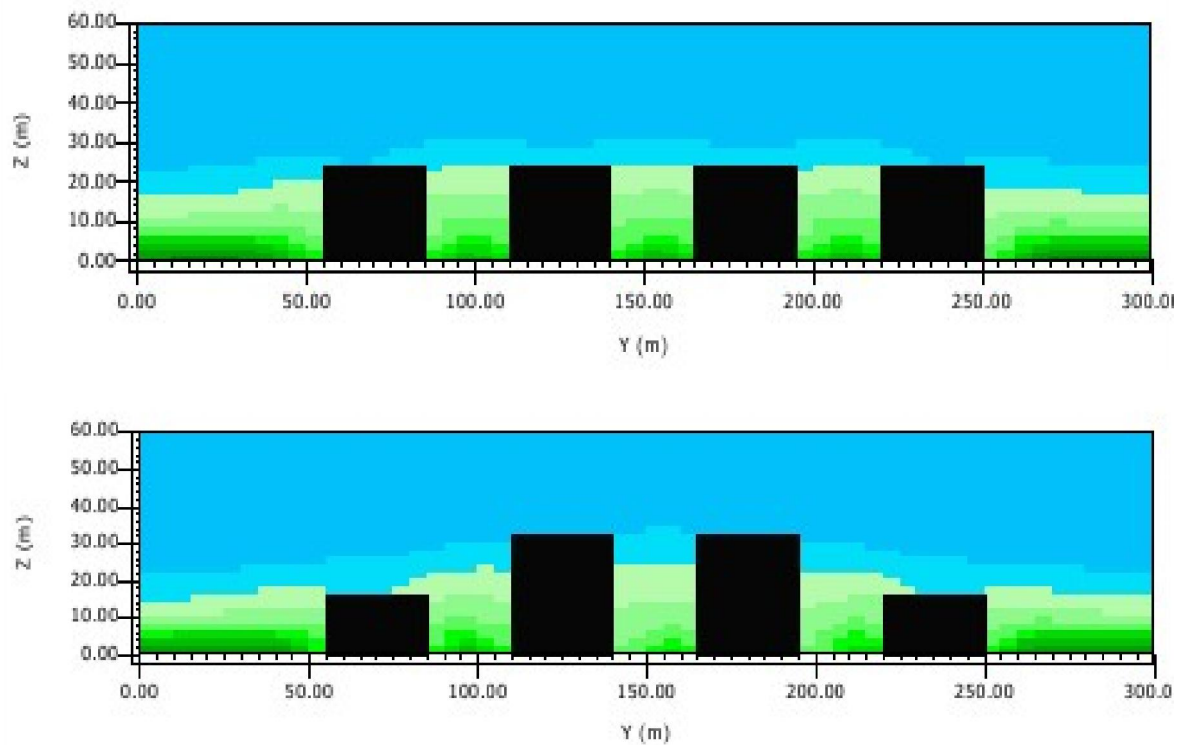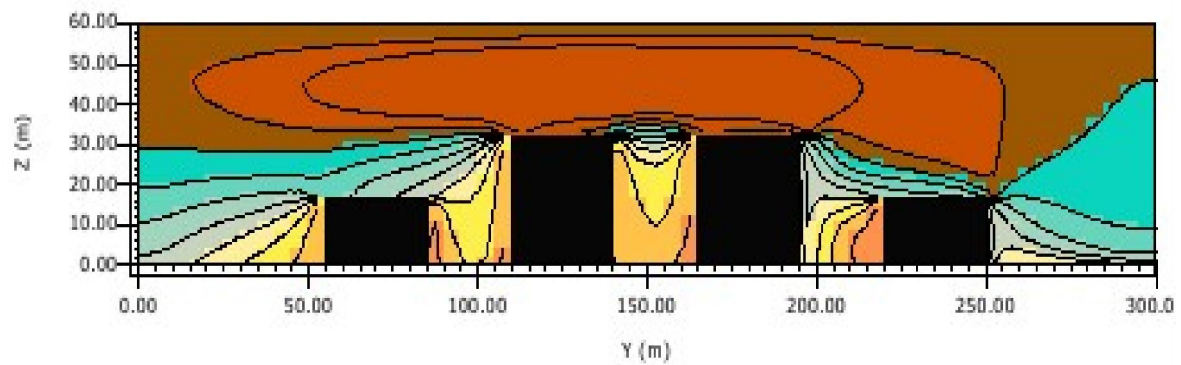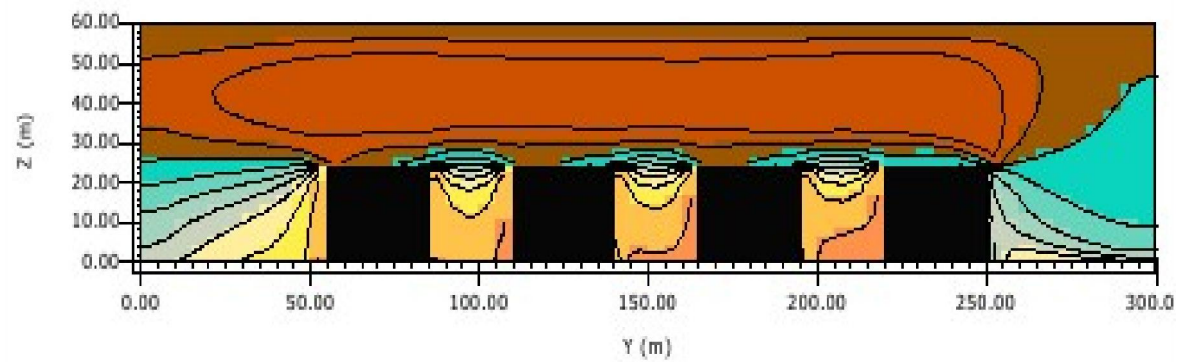

c) The base case and the best configuration G1-1.2 (3:7:7:3) in the NE-SW orientation

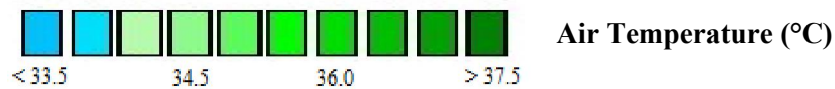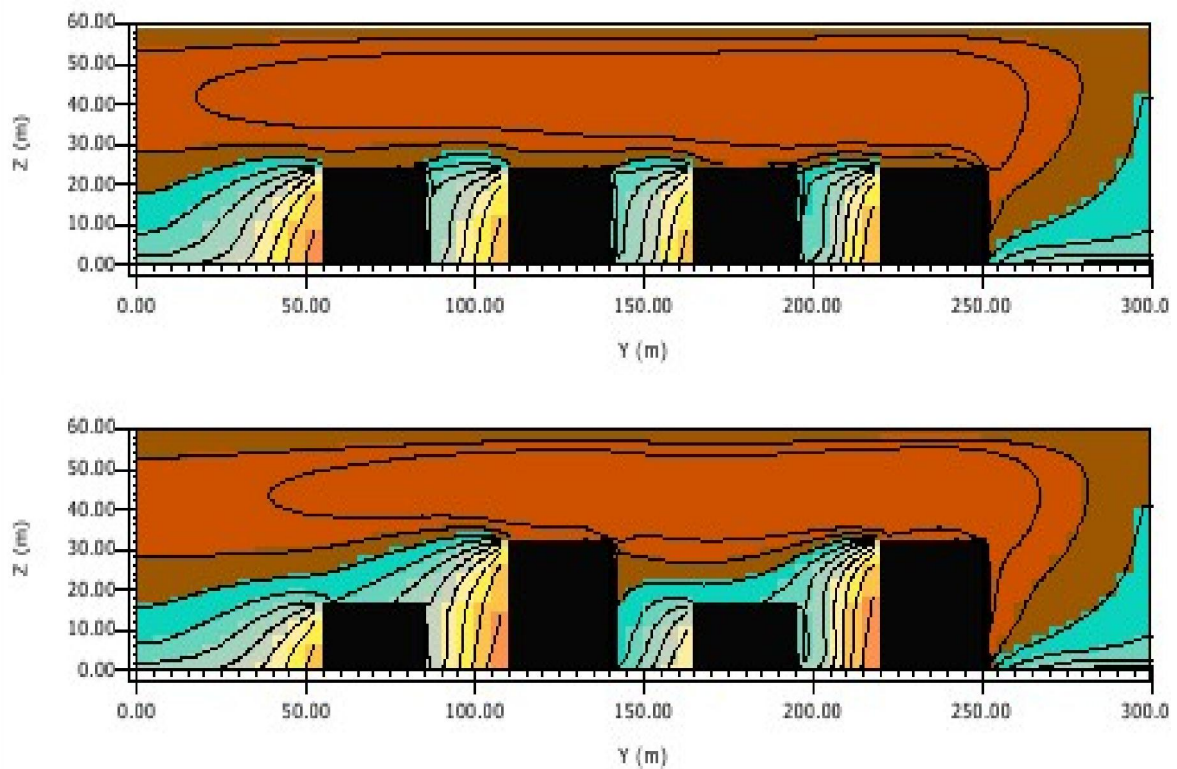d) The base case and the best configuration G1-1.2 (3:7:7:3) in the NW-SE orientation

Wind Velocity (m/s)

Figure 6.24: The cross section of the wind velocity for the base case and the best configurations of the first group in the four orientations; a)N-S, b) E-W, c) NE-SW and d) NW-SE

This change in wind behaviour can be observed clearly in the wind speed of the third and fourth configurations of this group that represent a sudden and significant variation in buildings height without transition. In the NW-SE block orientation, the prevailing wind is the dominated wind in the main canyons parallel to this orientation.

The G1-1.2 (3:7:7:3) configuration recorded the best performance with respect to the lowest maximum air temperature, and the highest maximum wind speed in NW-SE and NE-SW orientations. The close performance of the wind speed in these orientations is related to the effect of grid, orthogonal configuration of the urban block.

On the other hand, the base case shows the least performance with respect to wind velocity averages in all orientations and compared to the four configurations to prove the effect of the height diversity on wind speed averages. Therefore, the reduction in air temperature in the best configurations is mainly related to the shading effect created by the height diversity with respect to the orientation, in additional to the enhancement in wind velocity created by the diversity in buildings' height.

The relative humidity averages show a similar trend for all configurations including the base case, and in all simulated orientations. Generally, the relative humidity shows an inverse performance when compared to the maximum air temperature averages. The relative humidity is at the minimum when the air temperature is at the maximum values. This is observed clearly in relative humidity averages as the maximum air temperature recorded by all group configurations, the relative humidity was at the minimum averages with a slight differences between the configurations. The minimum relative humidity was recorded at 16:00 for all configurations. The maximum relative humidity averages in the NE-SW block orientation for all configuration proves the effect of the high air temperature on holding more water vapour than the cooler air, and the inverse relation between the air temperature and the relative humidity has been reported by Giannopoulou et al. (2014) and Irulegi, Serra and Hernandez (2017).

In additional to the maximum air temperature effect, the relative humidity is affected by wind velocity and behaviour, as the increase in wind speed reduces the relative humidity through reducing the air temperature.. The most notable fluctuation in relative humidity minimum averages was observed in NW-SE orientation compared to the other three orientations. This variation in relative humidity in this orientation is related to the prevailing wind effect.

Moreover, the fluctuated and minimum values of the relative humidity recorded in this orientation for all configurations proves the effect of wind speed on lowering the relative humidity averages. The same finding and the inverse relation between the wind velocity and the relative humidity reported by Lee and Lau (2016).

In the second group's configuration, the height diversity is implemented along the long axis of the block, and the ratio of (3:5:7) is adopted to form six configurations. Similar to the base case and the first group, the maximum air temperature averages in the N-S and E-W were lower than the other two orientations but the variation in the air temperature averages in these two orientations were less.

Table 6.1: The maximum and minimum relative humidity averages of the base case and first group configurations

Relative Humidity			
Orientation	Configuration	Maximum	Minimum
RH. N-S	B	81.13	39.77
	G1-.01	80.64	39.75
	G1-1.1	80.23	40.08
	G1-1.2	80.82	40.12
	G1-1.3	80.63	39.99
RH. E-W	B	81.06	40.36
	G1-.01	80.39	40.49
	G1-1.1	80.00	40.89
	G1-1.2	80.79	40.29
	G1-1.3	80.50	40.42
RH. NE-SW	B	87.41	37.79
	G1-.01	87.38	38.13
	G1-1.1	86.91	38.55
	G1-1.2	85.33	38.50
	G1-1.3	87.19	38.27
RH. NW-SE	B	84.32	38.95
	G1-.01	84.98	37.22
	G1-1.1	84.21	39.58
	G1-1.2	83.53	40.05
	G1-1.3	83.73	38.16

The top view at 1.4 m of maximum air temperature at 3:00 pm for the best configurations of the second group in four orientations is illustrated in appendix E.1. In the N-S orientation the G2-2.0 (7:5:3:3:5:7) configuration recorded the best performance with a slight reduction of 0.3 °C compared to the base case. However, the variation between all of the second group's configuration in this orientation is not noticeable. On the other hand, the best configuration in this group in the three other orientations is the G2-2.5 (5:3:7:7:3:5) configuration followed by G2-2.1 (3:5:7:7:5:3) with a slight difference in maximum air temperature averages. However, these two configurations recorded the lowest SVF of 0.41 with a reduction of 9 % compared to the base case. In both configurations the reduction in SVF and placing the highest buildings in the middle of the block reduces the air temperature averages, due to the shading effect and the enhancement in air movement effect. Figure 6.25 below presents a longitudinal section in the middle of the urban block and it reflects the variation of the maximum air temperature of the best configurations in the second group compared to the base case in the four orientations.
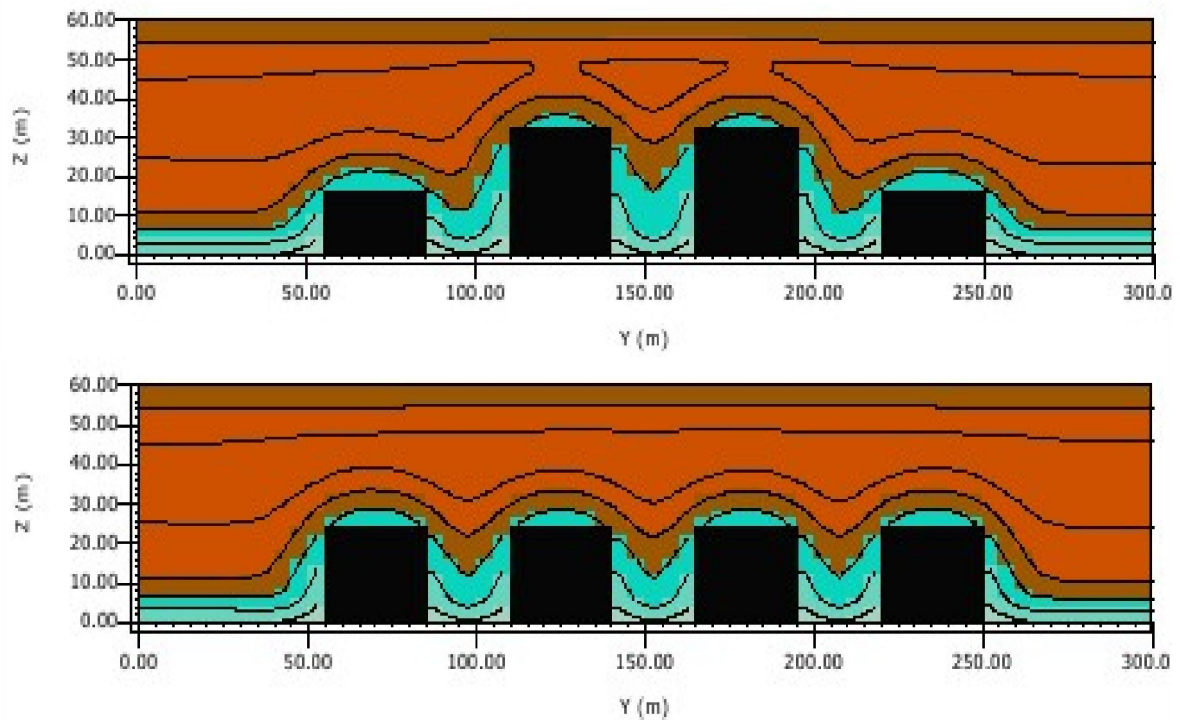

a) The base case and the best configuration G2-2.0 (7:5:3:3:5:7) in the N-S orientation
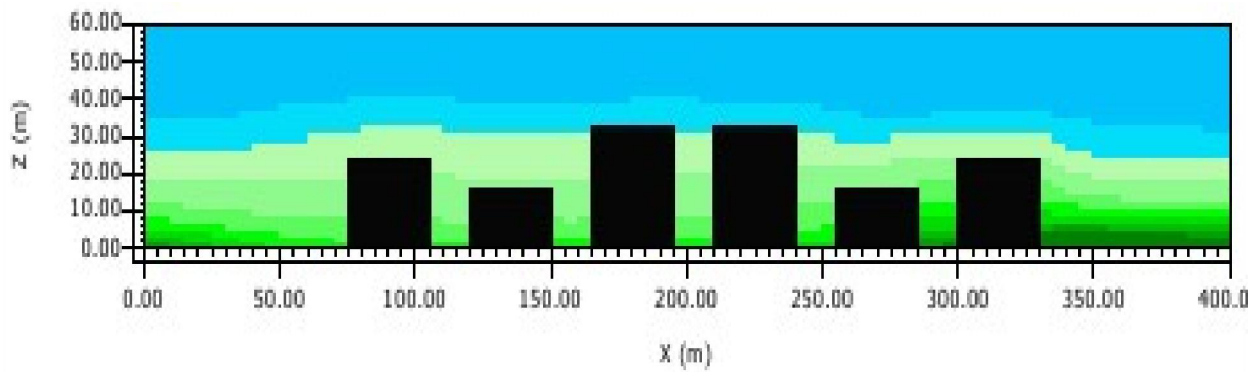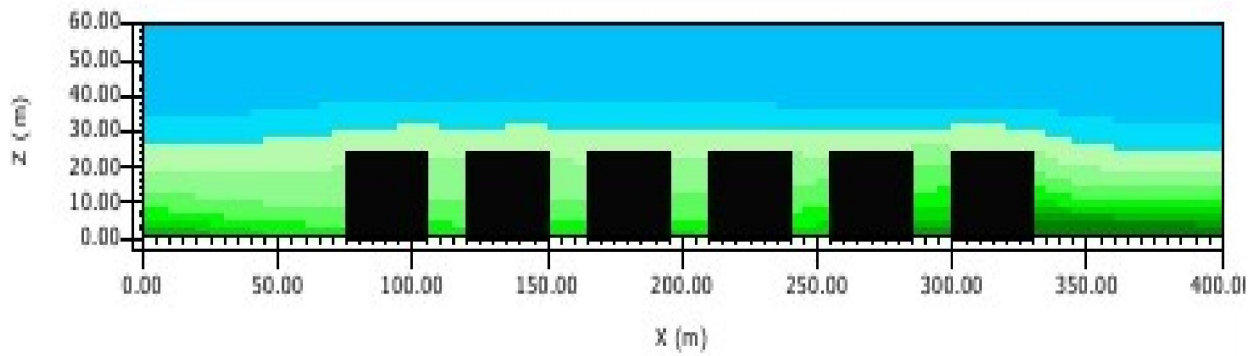
b) The base case and the best configuration G2-2.5 (5:3:7:7:3:5) in the E-W orientation
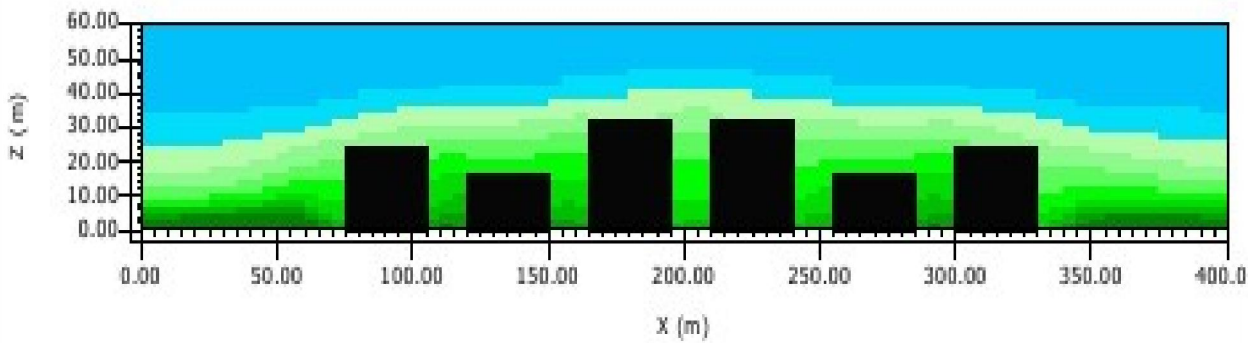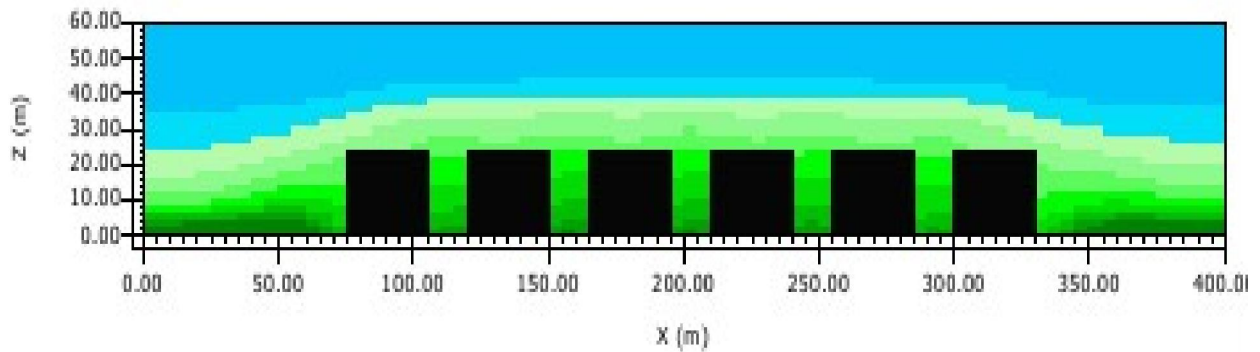
c) The base case and the best configuration G2-2.5 (5:3:7:7:3:5) in the NE-SW orientation

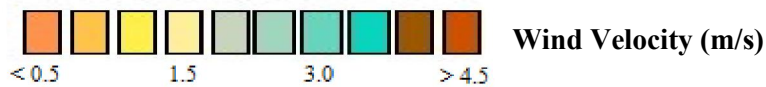d) The base case and the best configuration G2-2.5 (5:3:7:7:3:5) in the NW-SE orientation

Air Temperature (°C)

Figure 6.25: The longitudinal section of the maximum air temperature for the base case and the best configurations of the second group in the; a)N-S, b) E-W, c) NE-SW and d) NW-SE orientations

In spite of the fact that the SVFs of the G2-2.1 (3:5:7:7:5:3) and the G2-2.5 (5:3:7:7:3:5) configurations are equal, the best configuration G2-2.5 (5:3:7:7:3:5) with the tallest buildings placed in the middle of the block and fluctuated height performs better with respect to the lowest maximum air temperature.

In the NE-SW and NW-SE orientations, the G 2-2.5 (5:3:7:7:3:5) configuration shows the best performance compared to the base case with reductions in air temperature of 0.95 ° C and 0.9 ° C in these two orientations, respectively. These reductions were due to the effect of the wind velocity caused by the fluctuated diversity in buildings height. Placing the highest buildings in the middle of the block accelerated the wind velocity, this acceleration reaches 18 % in the best configuration compared to the base case in the NW-SE orientation.

The effect of the wind velocity on reducing the outdoor air temperature and enhancing the outdoor thermal comfort was reported by Al-Sallal and Al-Rais (2010) as well as Li and Meng (2015). The average wind speed in the in the best configuration G2-2.5 (5:3:7:7:3:5) reached to 3.9 m/s compared to 3.0 m/s for the base case at maximum air temperature. This speed can be described as a light to gentle breeze according to Beaufort scale, and it can provide the required outdoor comfort cooling. The same result reported by Sallal and Al-Rais (2011) in the study conducted in a case study area in Dubai. The researchers in their field measurement study found that the wind speed in a wide canyon with H/W ratio between 0.63-1.56 is between 2.02 m/s - 4.55 m/s, and they stated that the convective cooling of a body required a wind with a range of 0.5 m/s -1.0 m/s. However, the researchers presented the wind velocity data according to the H/W for different types of canyon, and their study was more concentrated on the outdoor climate comfort zone.

In the current research the average wind velocity is considered in order to find the integrated effect of the block configuration on outdoor microclimate parameters. This increase in wind speed in addition to the reduction in SVF reduces the air temperature of the best configuration G2-2.5 (5:3:7:7:3:5) in the NE-SW and NW-SE orientations. However, the increase in wind speed of the best configuration G-2-2.5 (5:3:7:7:3:5) in the E-W orientation was 17 % but the reduction in the air temperature was only 0.3 ^{o} C. This proves that the exposure to the solar radiation in this orientation is more significant than the wind speed effect. In the N-S orientation, the best configuration G2-2.0 (7:5:3:3:5:7) has almost the same wind velocity averages compared to the base case. However, the air velocity averages became lower in the canopy layer above the building of the main canyon. Hence, the gradual variation in buildings height towards the inner axis of the block does not increase nor affect the wind speed positively (Figure 7.6 a).

On the other hand, the figure shows the increase in wind speed of the best configuration G2-2.5 (5:3:7:7:3:5) by 17 % in the E-W orientation compared to the base case. This increase in wind velocity of the best configuration G2-2.5 (5:3:7:7:3:5) were 1.9 % and 18 % compared to the base case in the NE-SW and NW-SE orientations, respectively. Figure 6.26 presents the longitudinal section of the wind velocity in the middle of the block and reflects the variation in the wind velocity at the maximum air temperature of the best configurations compared to the base case in the four orientations. The top view at 1.4 m of wind velocity at maximum air temperature for the best configurations of the second group in four orientations is presented in appendix E.2. The examination of these results proves the effect of the diversity in buildings height on enhancing the outdoor air flow patterns and wind velocity compared to the uniform height configurations. The fact that placing a high-rise building among the lower buildings enhancing the air velocity was reported by Priyadarsini and Wong (2005) and Chan et al. (2001).
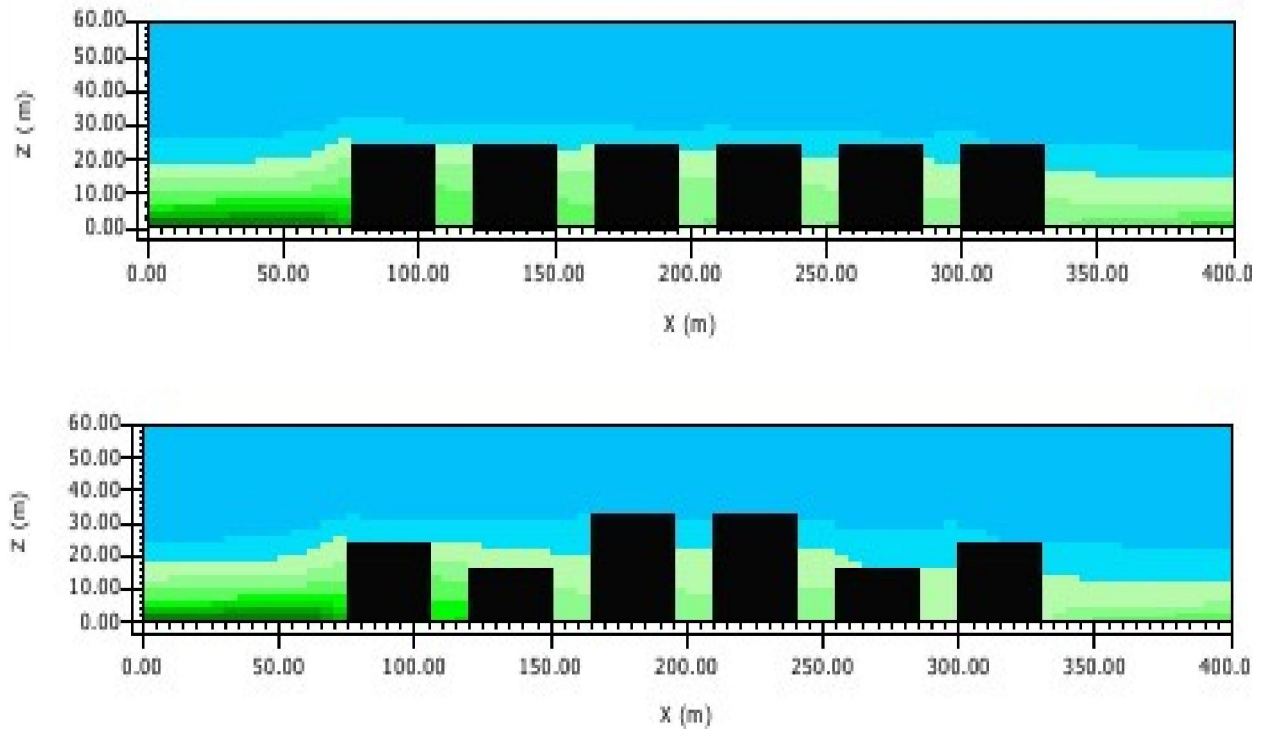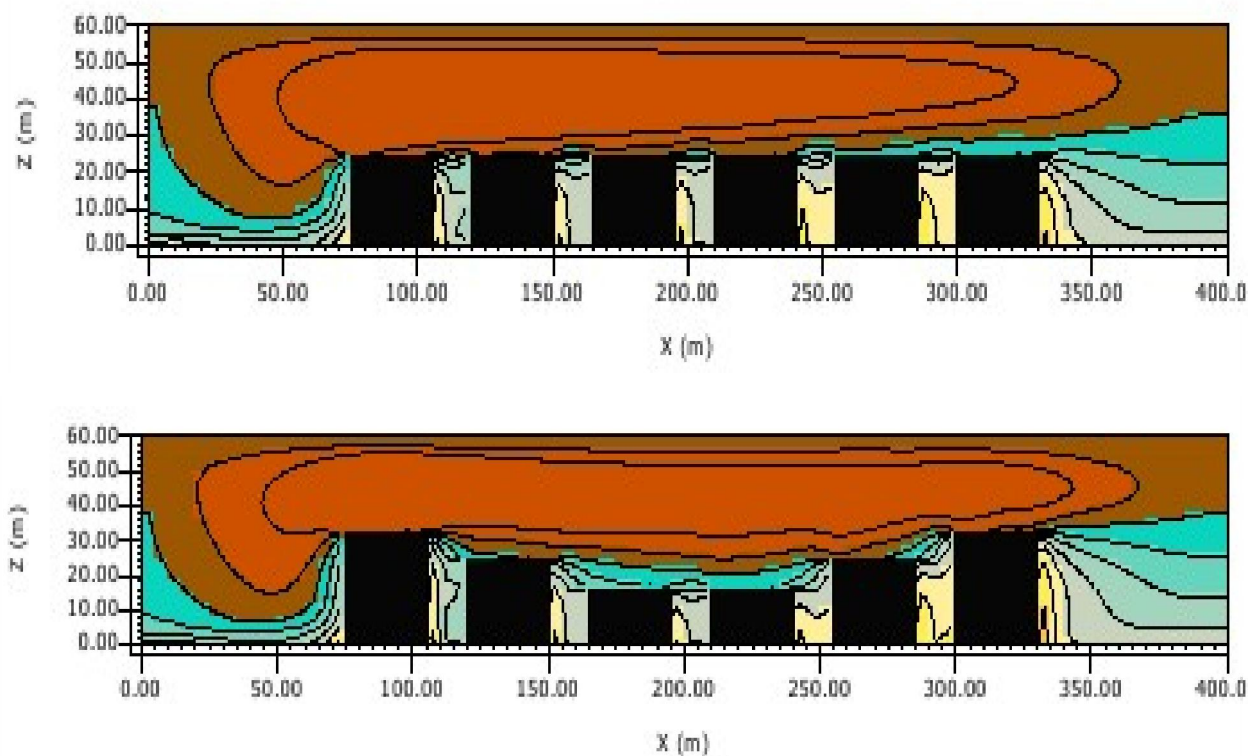

a) The base case and the best configuration G2-2.0 (7:5:3:3:5:7) in the N-S orientation
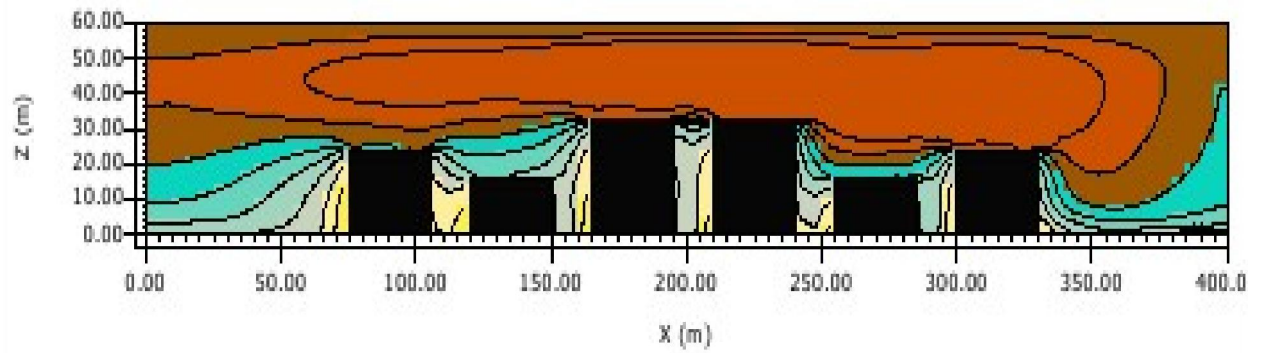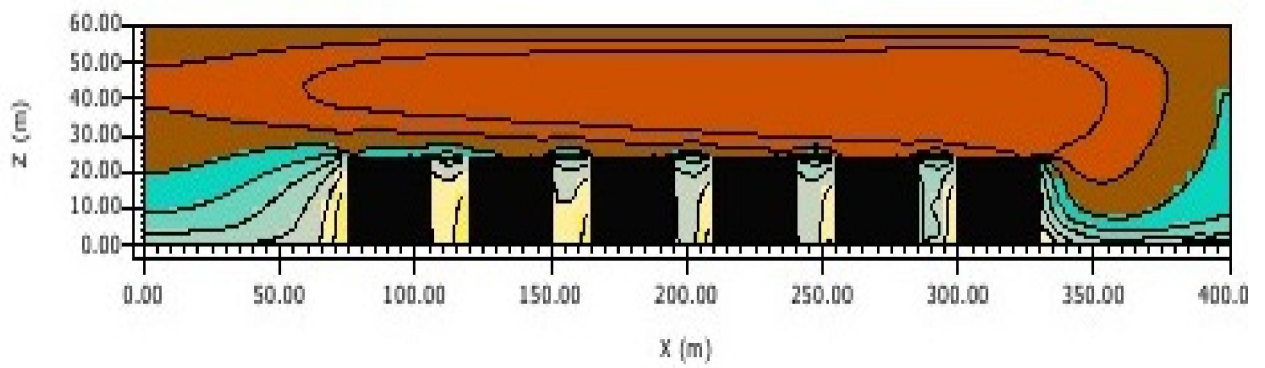
b) The base case and the best configuration G2-2.5 (5:3:7:7:3:5) in the E-W orientation

c) The base case and the best configuration G2-2.5 (5:3:7:7:3:5) in the NE-SW orientation

d) The base case and the best configuration G2-2.5 (5:3:7:7:3:5) in the NW-SE orientation

Wind Velocity (m/s)

< 0.5   1.5   3.0   > 4.5
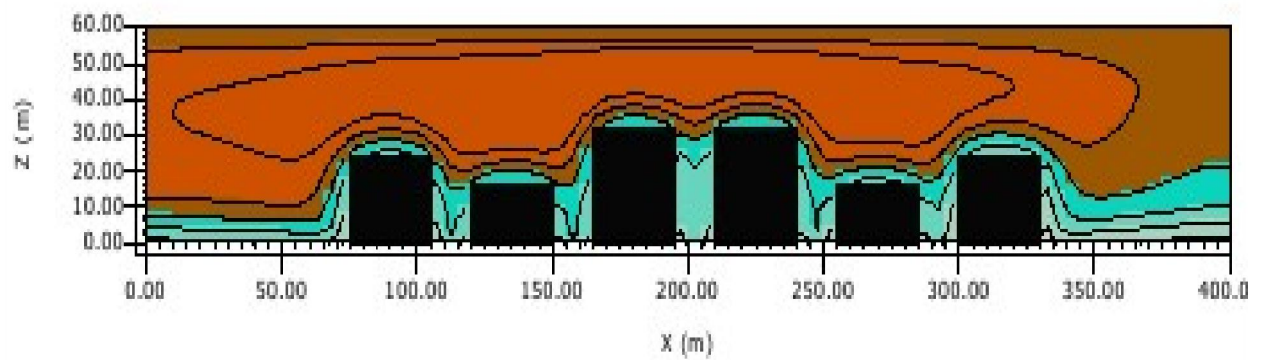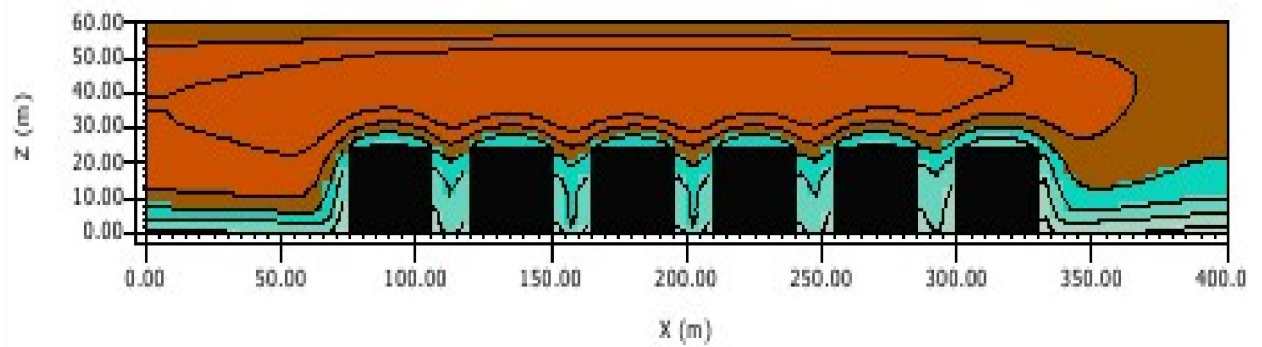
Figure 6.26 : The longitudinal section of the wind velocity for the base case and the best
configurations of the second group in the four orientations ; a)N-S, b) E-W, c) NE-SW and d) NW-SE

The relative humidity averages of the second group show that the maximum relative humidity
was recorded in the NE-SW orientation in the G 2-2.2 (5:7:3:3:7:5) configuration with
a value of 87.5 %. This value is higher than the relative humidity in the NW-SE by 3.5 %.
The minimum humidity in the NE-SW block orientation related to the maximum air
temperature averages in the same orientation, the same observations of high relative humidity
values in the western orientation reported by Giannopoulou et al. (2014). The N-S and
E-W orientations recorded humidity around 81 % lower by 6.5 % compared to the maximum
value in the NE-SW orientation.

The base case recorded lower humidity than the maximum values in all orientations by compared to all configurations except the NW-SE the base case recorded the highest maximum relative humidity averages with respect to the six configurations of this group.

Table 6.2: The maximum and minimum relative humidity averages of the base case and second group configurations

| Orientation | Relative Humidity | | |
	Configuration	Maximum	Minimum
RH. N-S	B	81.13	39.77
	2.00	80.32	40.13
	2.10	81.19	39.62
	2.20	80.59	39.91
	2.30	80.76	39.80
	2.40	81.31	39.75
	2.50	80.86	39.72
RH. E-W	B	81.06	40.36
	2.00	80.06	40.40
	2.10	81.16	40.46
	2.20	80.43	40.23
	2.30	80.51	40.40
	2.40	81.14	40.42
	2.50	80.74	40.51
RH. NE-SW	B	87.41	37.79
	2.00	87.50	36.89
	2.10	86.44	38.77
	2.20	87.53	36.88
	2.30	86.97	37.92
	2.40	87.43	37.71
	2.50	86.06	38.97
RH. NW-SE	B	84.32	38.95
	2.00	83.96	38.61
	2.10	83.75	39.27
	2.20	83.61	38.73
	2.30	83.52	39.42
	2.40	83.57	39.48
	2.50	83.41	39.43

This is observed in the effect of the wind speed on the performance of the best configuration G2-2.5 (5:3:7:7:3:5) that represents the configuration with gradual and fluctuate height variation in the long axis of the block.

This fact is supported by the same finding of the positive effect of the first group configuration G1-1.1(3:7:3:7), as the fluctuated diversity in buildings height increases the wind velocity and enhance the air flow of this configuration compared to the base case.

In addition to investigating the effect of block orientation and height diversity on outdoor microclimate parameters, the third group explored the effect of different building arrangement on the studied microclimate parameters. The three configurations of the third group have the same height with different H/W ratios which can also be represented by the SVF. Figure 2.27 presents the maximum air temperature averages of the best configurations of the third group in the four orientations. In general, and similar to the first two groups' configurations, the highest air temperature averages were recorded in the NE-SW orientations. The best performance was recorded by the third configuration G3-3.2 (15:20) in three orientations due to the low SVF and high shading effect provided.

This configuration reduced the SVF by 27% compared to the base case and reduced the maximum reduction in air temperature by 1.9 $^\circ$C in NW-SE orientation. On the other hand, this configuration shows the lowest wind velocity compared to the base case and other configurations.

The base case has a H/W ratio of0.96 and 1.6 for canyons and alleys, respectively. In the third group, the best configuration G3-3.2 (15:20) has a H/W ratio of 1.2 for the main canyons, and the alleys are with H/W value of 1.6, while the H/W ratio for the first configuration G3-3.0 (20:25) were 1.2 and 0.96 for main canyon and alleys, respectively. The second configuration G3-3.1 (20:20) H/W is 1.2 for both main canyons and alleys.

Hence, both the canyons and the alleys of the best configuration G3-3.2 (15:20) have higher H/W ratios to represent the uniform to deep canyon and reduced the SVF compared to the base case and other configurations. This explains the reason behind the reduction in air temperature of the best configuration.

This result agrees well with a field measurements study in uniform and deep canyons conducted by Johansson (2006) in the similar outdoor climate conditions. However, the results show that the air velocity at the maximum air temperature has been reduced in the best configuration G3-3.2 (15:20) by 68 % compared to the base case.

The reduction in air temperature averages is mainly related to the reduction in the SVF values compared to the base case, and the reduction in air temperature of this configuration is higher than the two other groups' best configurations. This reduction in maximum air temperature is related to the reduction in SVF and consequently the exposure to solar access is less.

Therefore, and in the third group specifically the effect of the prevailing wind on reducing the outdoor air temperature in the NW-SE orientation is uncountable compared to the best configurations in the first two groups.

Furthermore, this result proves that the shading effect is more significant than the wind speed effect on reducing the outdoor air temperature averages, the same result and the effect of the shading created by the low SVF is reported by Al Znafer (2014).
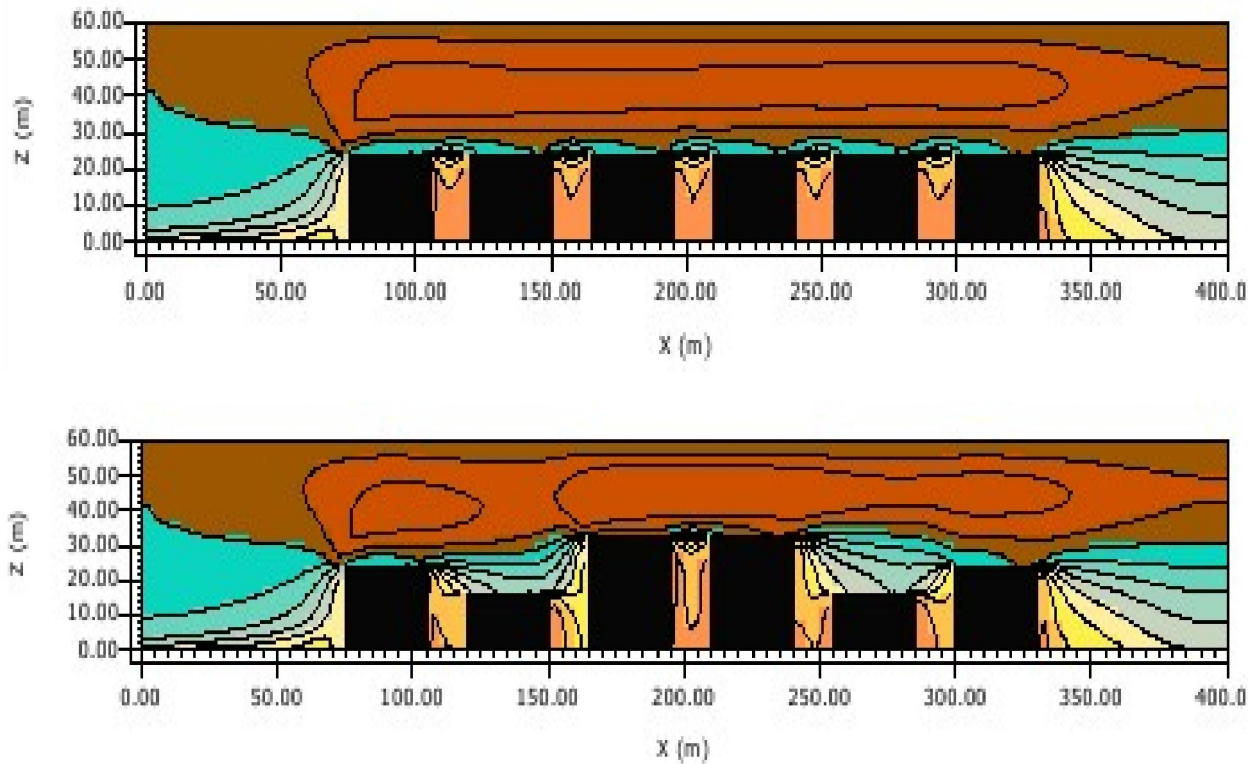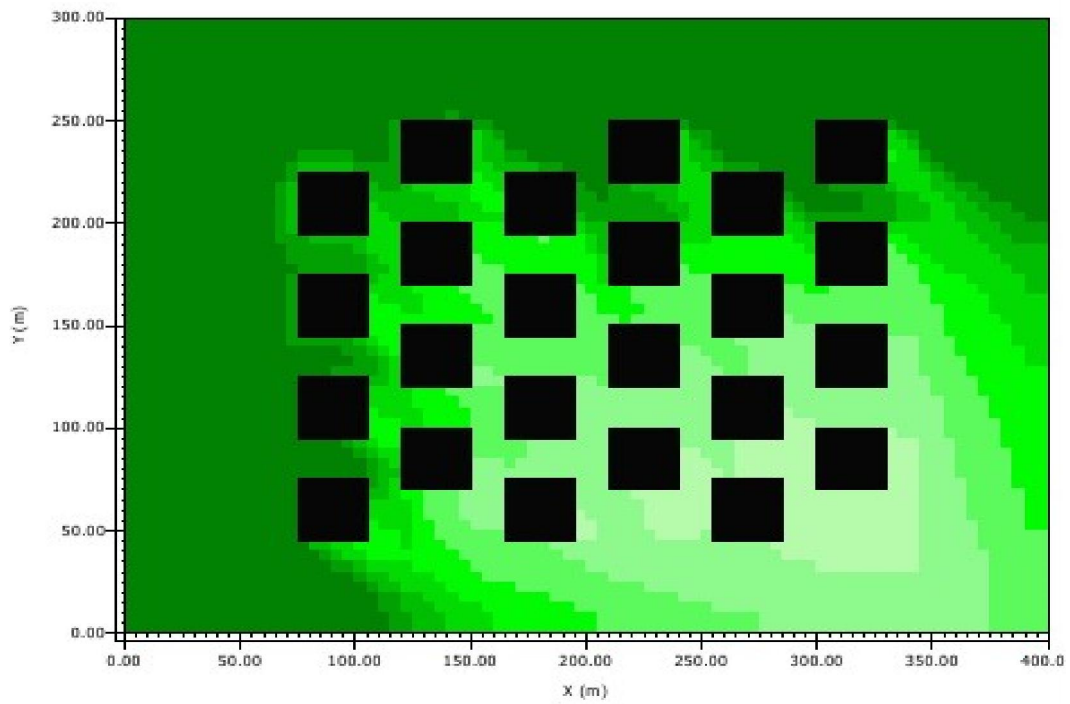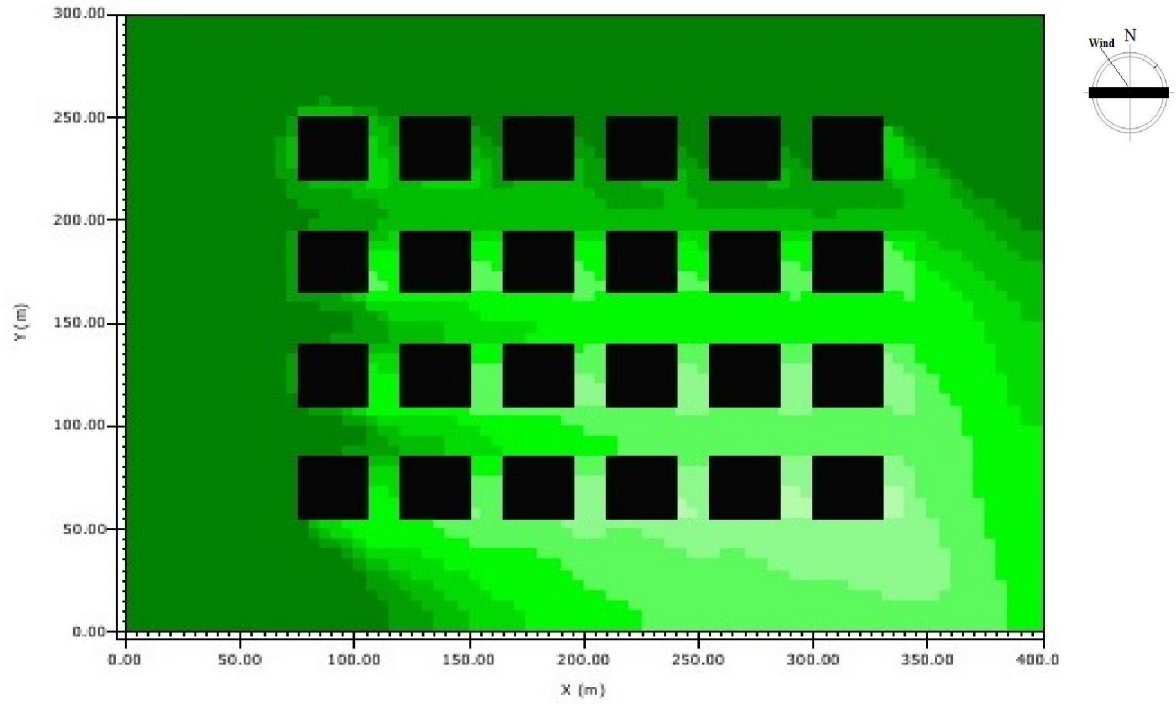
a) The base case and the best configuration G3-3.2 (15:20) in the N-S orientation
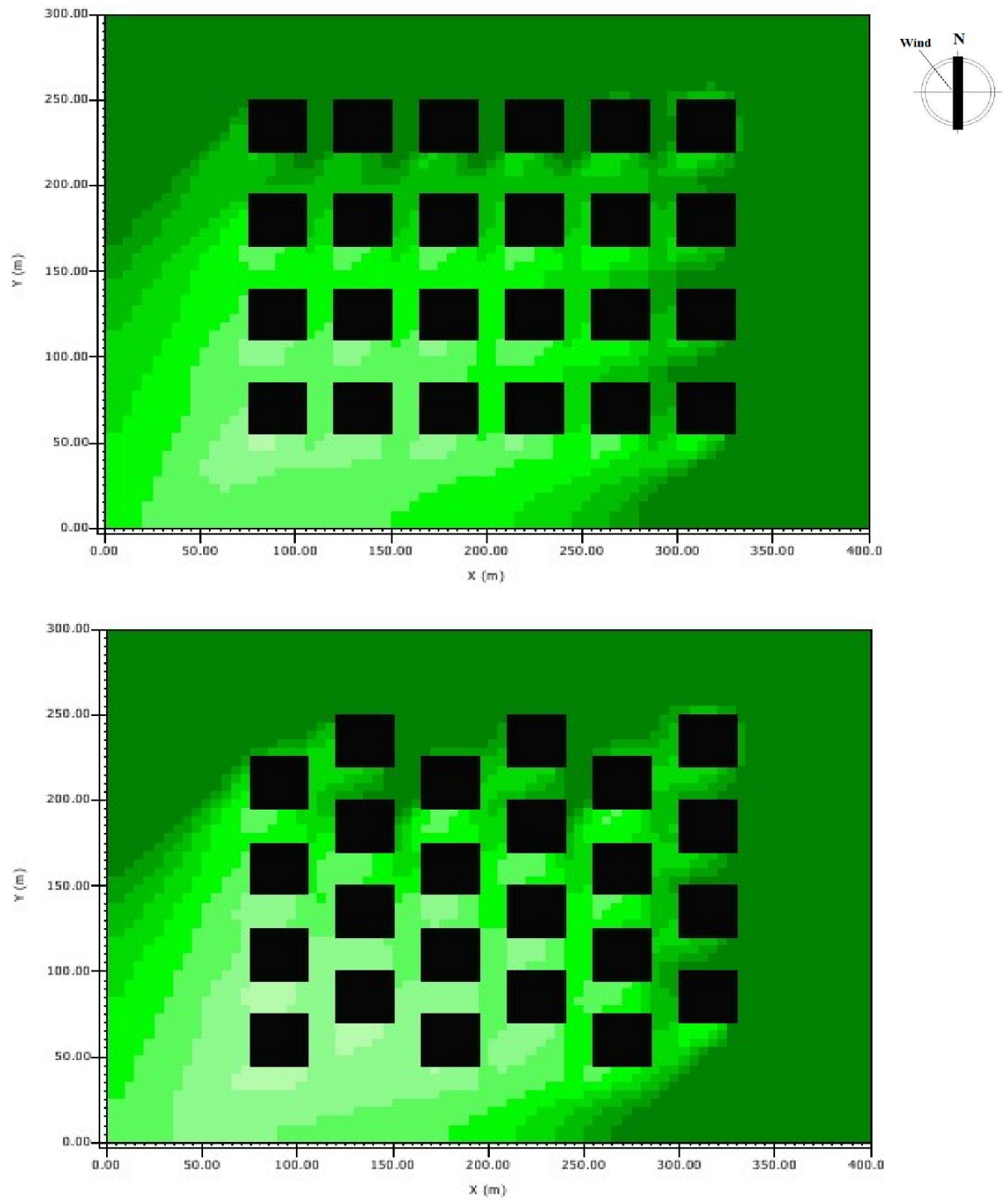
b) The base case and the best configuration G3-3.2 (15:20) in the E-W orientation

c) The base case and the best configuration G3-3.0 (20:25) in the NE-SW orientation

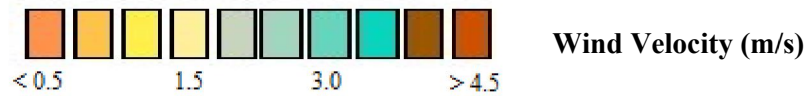d) The base case and the best configuration G3-3.2 (15:20) in the NW-SE orientation

Air Temperature (°C)

< 33.5   34.5   36.0   > 37.5
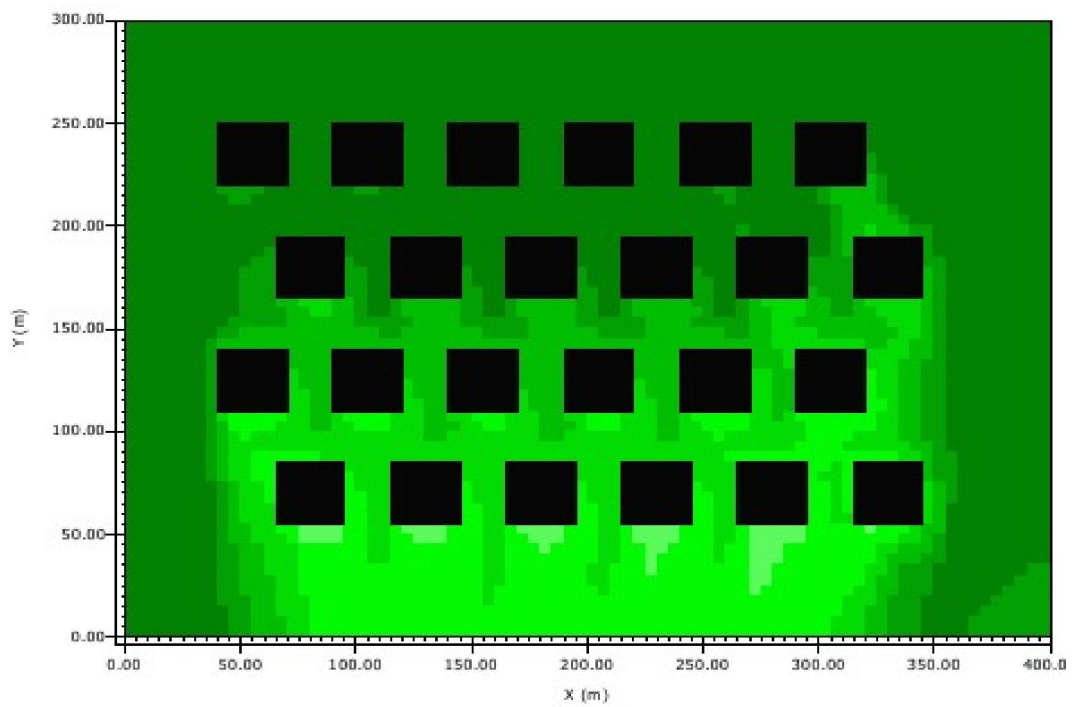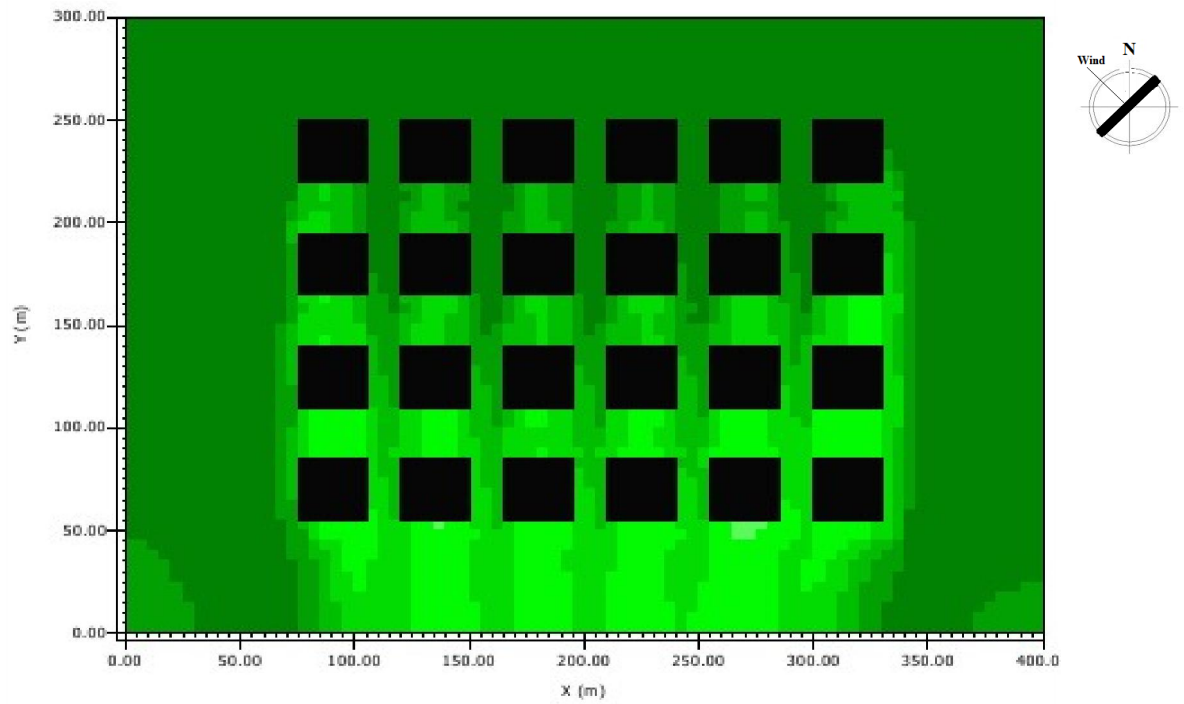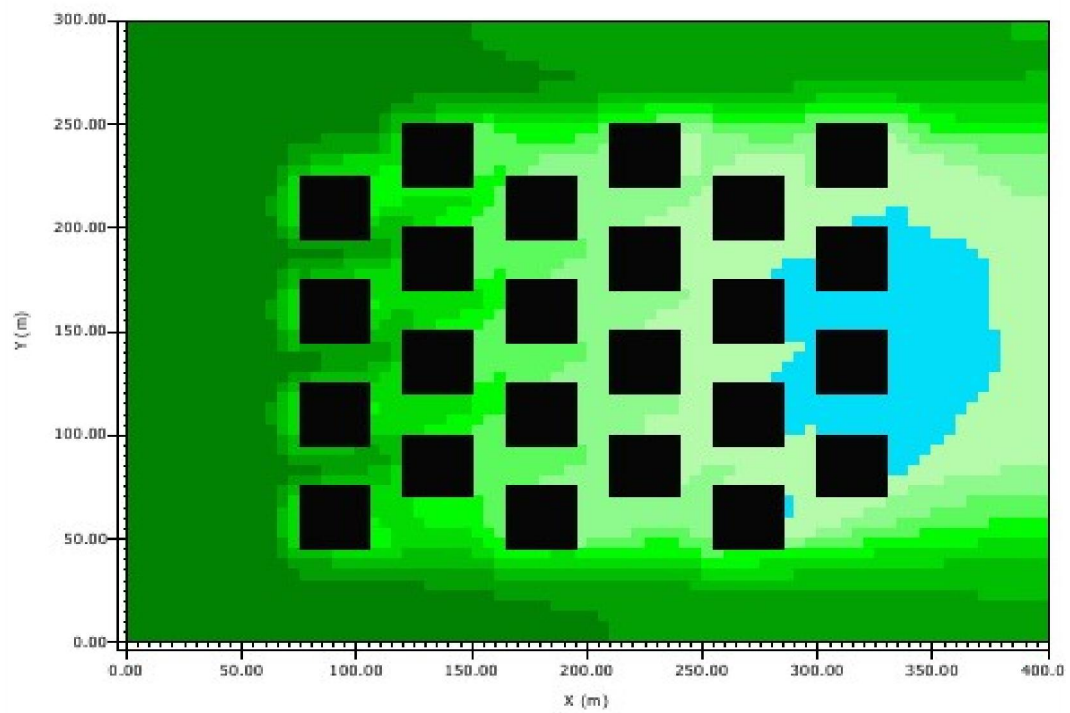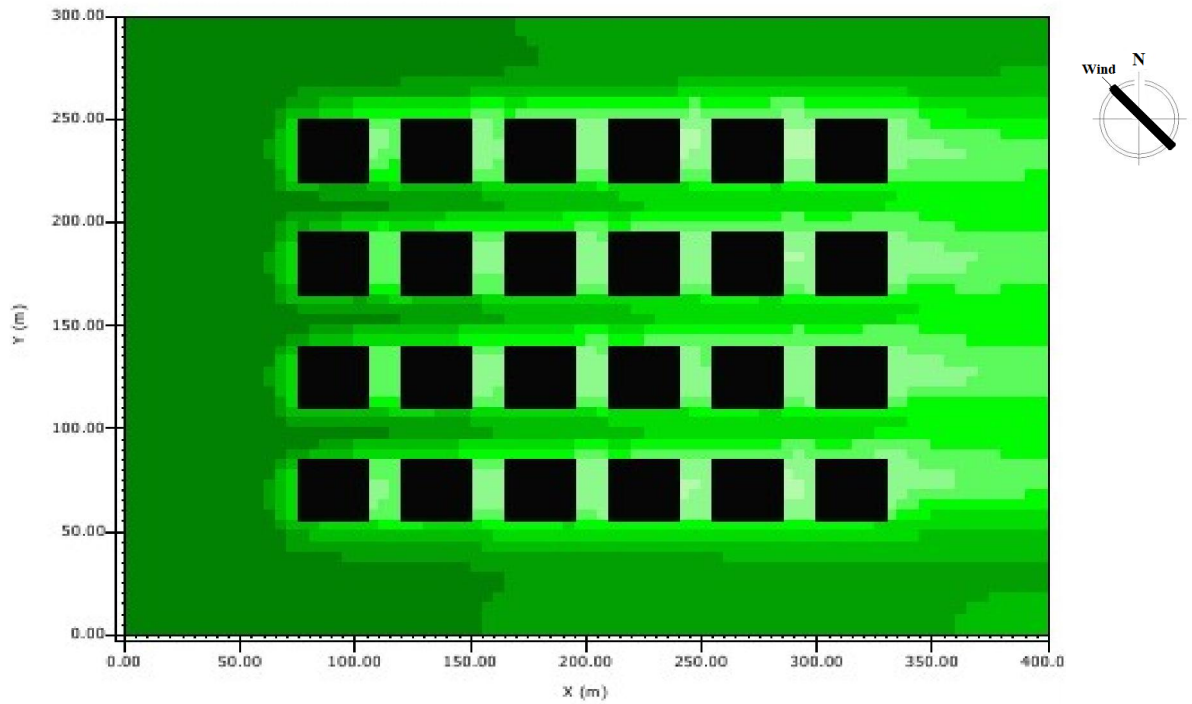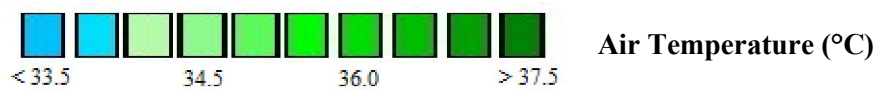
Figure 6.27: The top view of the maximum air temperature averages for the base case and the best configurations of the third group in the four orientations; a)N-S, b) E-W, c) NE-SW, and d) NW-SE

Figure 6.28 illustrates the cross section in the middle of the urban block and reflects the best configuration thermal performance compared to the base case in the four orientations.

On the other hand, and with respect to the alternative arrangement of buildings, the block and canyon orientation plays a significant role in wind velocity and air movement for each configuration. Generally, in the N-S and E-W orientations no notable variation in wind velocity has been observed. The significant variation has been recorded in NE-SW and NW-SE depending on the block orientation and the width of the canyon that is facing the prevailing wind direction.
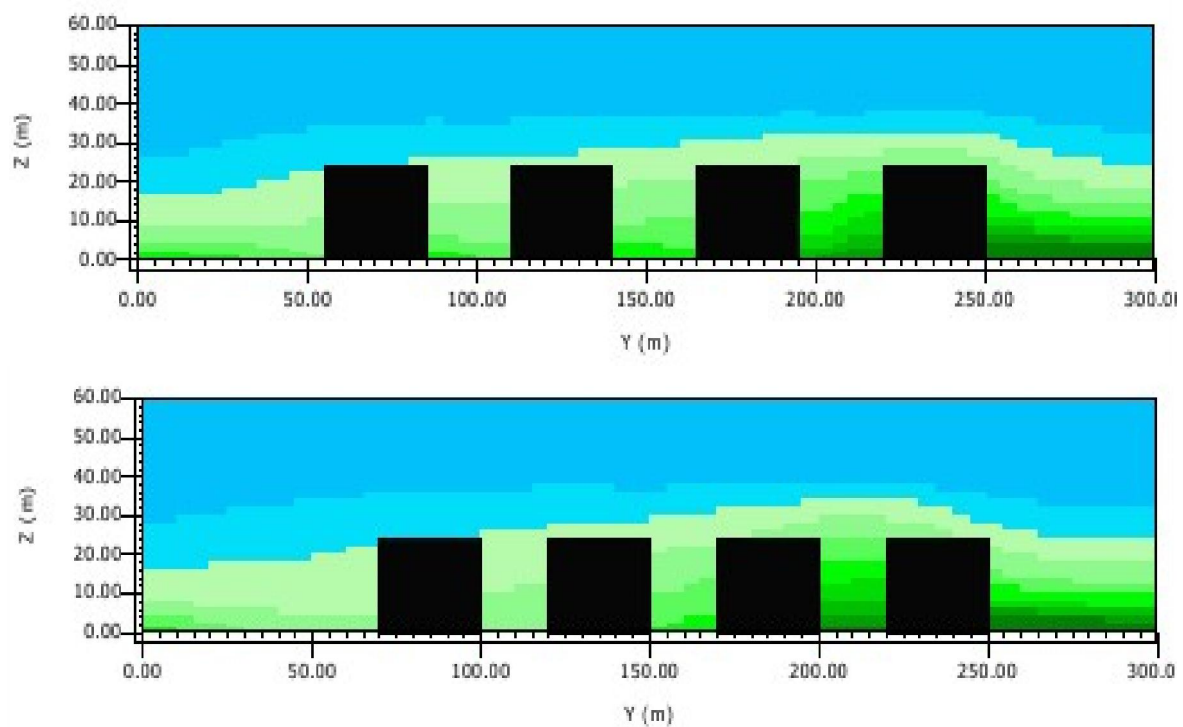
a) The base case and the best configuration G3-3.2 (15:20) in the N-S orientation
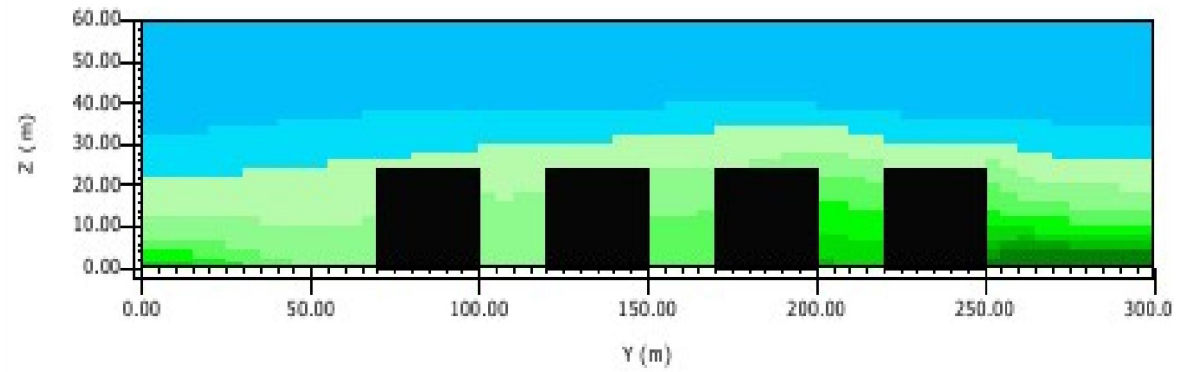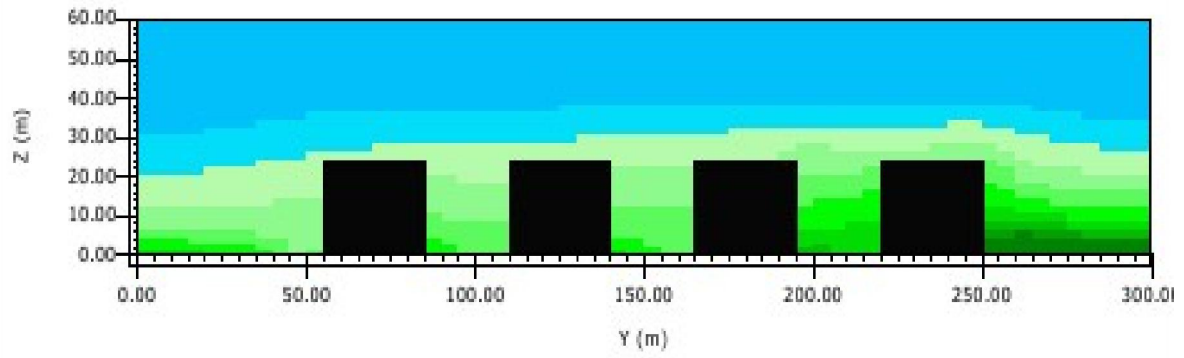
b) The base case and the best configuration G3-3.2 (15:20) in the E-W orientation
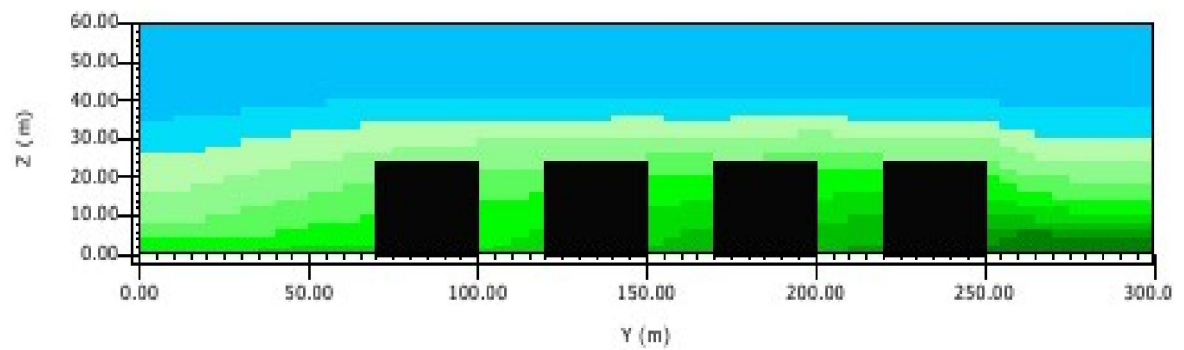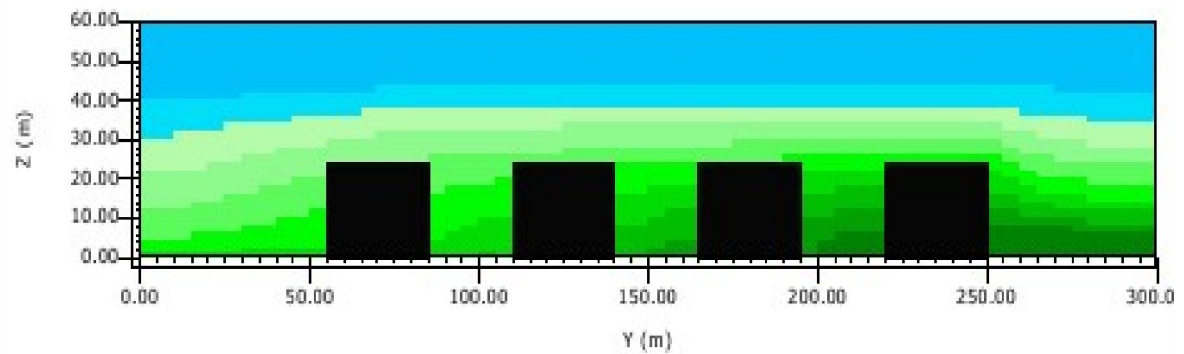
c) The base case and the best configuration G3-3.0 (20:25) in the NE-SW orientation
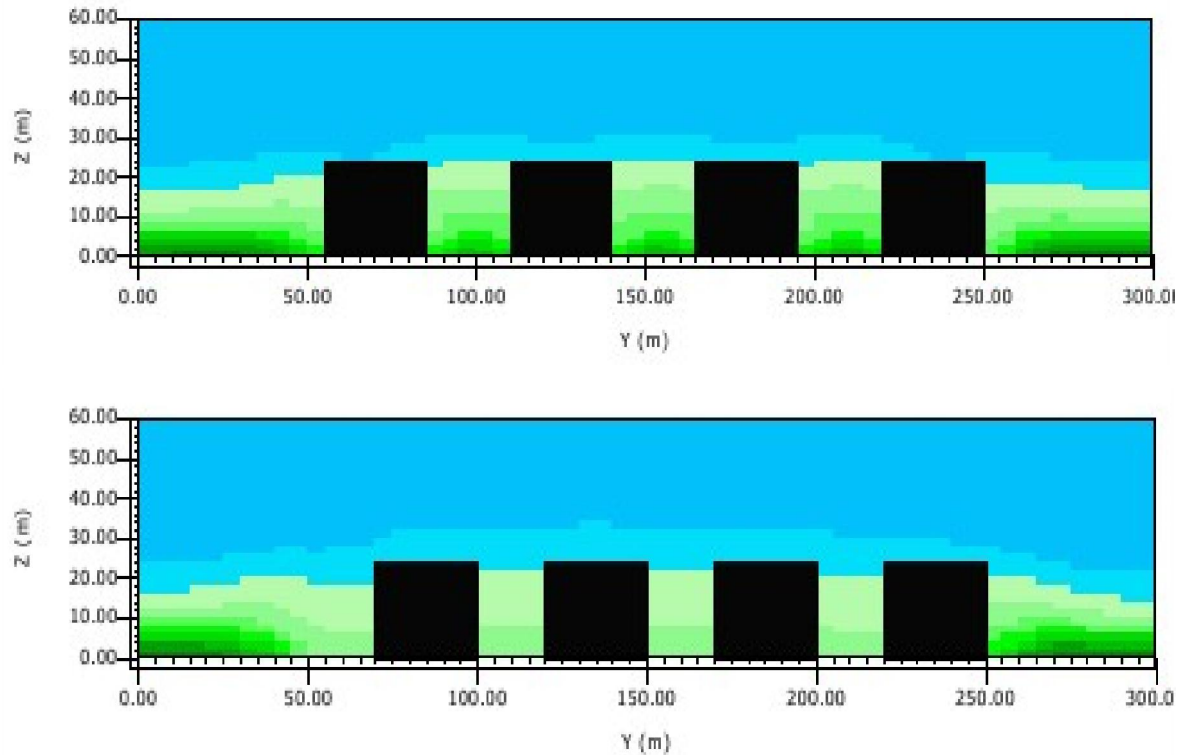
d) The base case and the best configuration G3-3.2 (15:20) in the NW-SE orientation
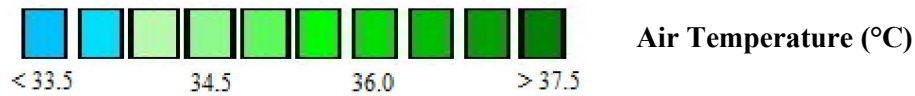
Air Temperature (°C)

Figure 6.28: The cross section in the middle of the block of the maximum air temperature for the base case in the four orientations; a)N-S, b) E-W, c) NE-SW, and d) NW-SE

The G3-3.2 (15:20) configuration performed as the best configuration in the NW-SE with respect to reducing the maximum air temperature averages, the wind profile shows a different attitude in each orientation as illustrated in chapter 6, figure 6.16. The alternative or the stagger arrangement of this configuration obstructs the wind in the NW-SE and reduces the wind velocity. The wind velocity in the main canyon has been reduced from 3 m/s - 3.5 m/s to 0.5 m/s to1.0 m/s. Figure 6.29 illustrates the wind velocity averages at maximum air temperature for the base case and the best configurations G3-3.2 (15:20) in the NW-SE orientations.

282
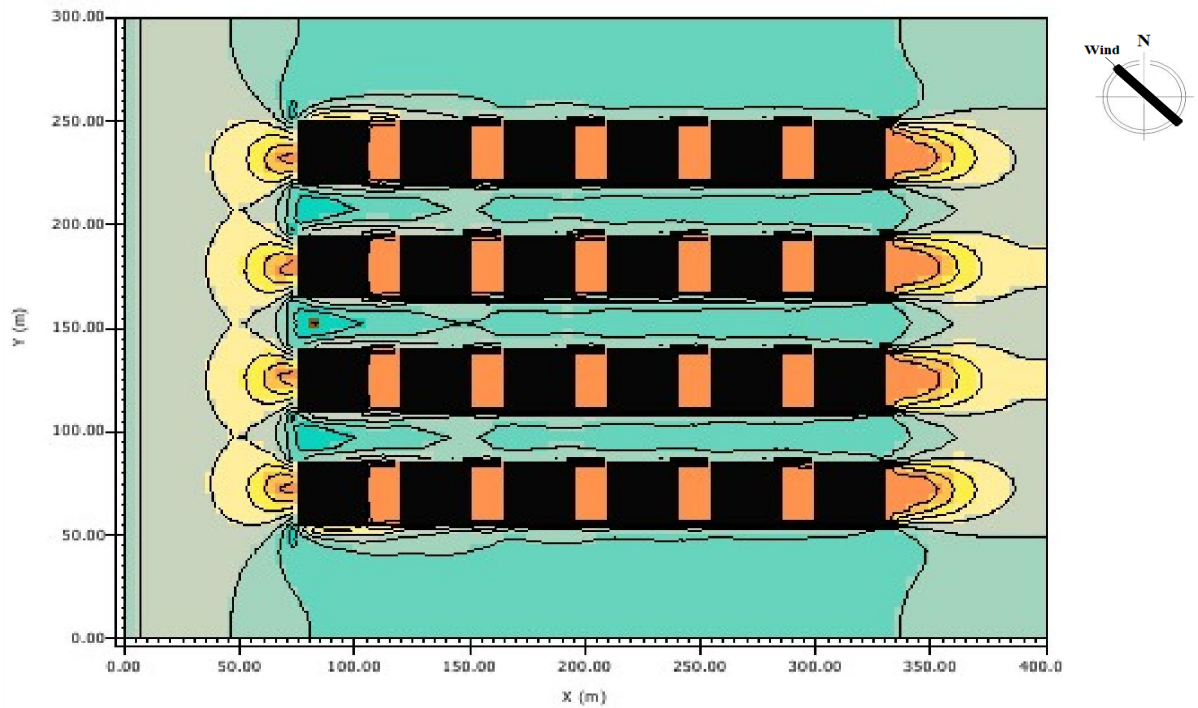
a) The base case configuration in the NW-SE orientation

b) best configurations G3-3.2 (15:20) in the NW-SE orientation

Wind Velocity (m/s)

< 0.5   1.5   3.0   > 4.5
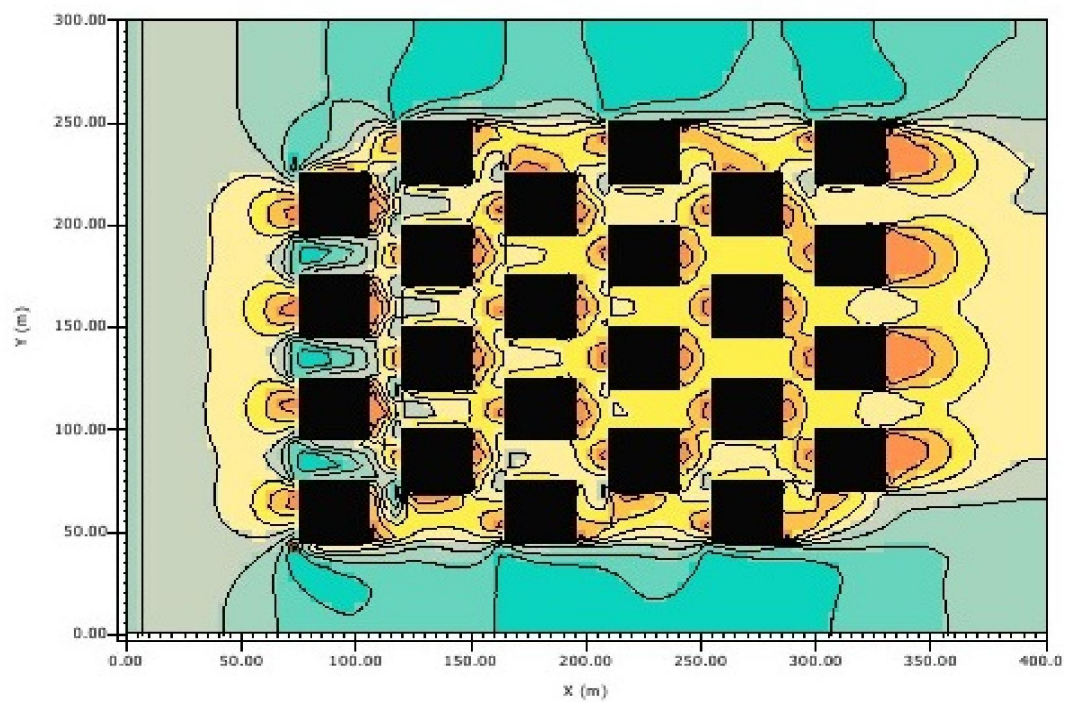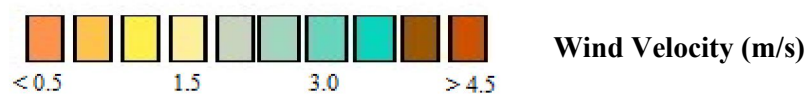
Figure 6.29: The wind velocity average of; a) the base case, and b) the best configurations G3-3.2 (15:20) of the third group in the NW-SE orientation

On the other hand, the air flow has been enhanced in the alleys and increased from an average of less than 0.5 m/s to more than 1 m/s. The same result of the enhancement in air flow around the buildings in the alternative configuration of the buildings is reported by Boutet (1987). The effect of the staggered arrangement on the wind flow can be interpreted by the 'Bernoulli effect' . The buildings in this arrangement perform as an obstacle in windward direction to create a positive pressure area in front of the buildings and a negative pressure area on the sides and behind the buildings , the air speed increase and move from the positive pressure area to negative pressure area. Bernoulli equation for kinetic energy conservation explain the effect of the increase in wind speed in the negative air pressure areas. In the staggered arrangement, the flashing air between the buildings helps to reduce the maximum air temperature around the surfaces of most of the block' buildings. Furthermore, the increase in wind velocity around the surface of most of the urban block buildings enhance the surfaces heat flux and increase the convective heat transfer coefficient CHTC, this increase will reduce the building surfaces temperature, and consequently reduce the conduction heat gain.

In the same concept, the two other configurations of the third group; G3-3.0 (20:25) and G3-3.1 (20:20) show a different attitude according to the block orientation. The configuration G3-3.0 (20:25) in the NE-SW block orientation obstruct the prevailing and reduces the wind velocity, but generally it redistributed the air and enhance the air movement in the canyons around most of the building (Figure 2.30).

The reduction in wind velocity in the alternative arrangement of the urban block is reported by Santamouris (1999). On the other hand, Boutet (1987) mentioned the enhancement in air movement around the buildings of the alternative or stagger arrangement in the urban block.
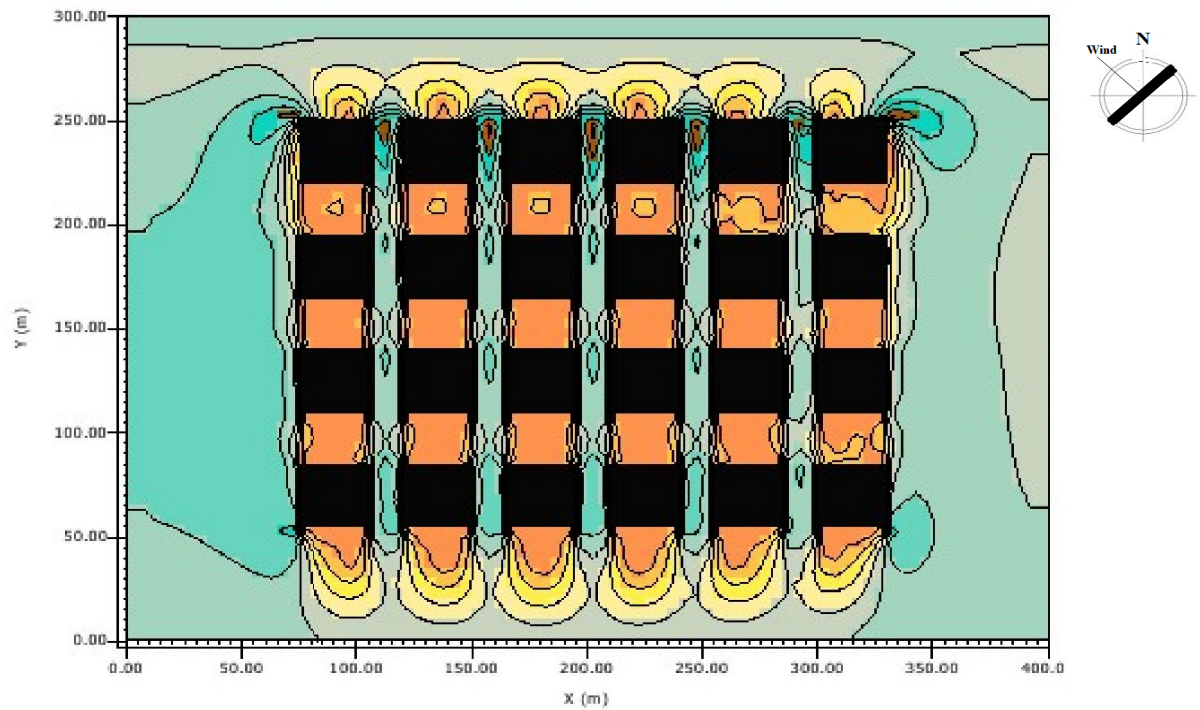
a) The base case configuration in the NE-SW orientation
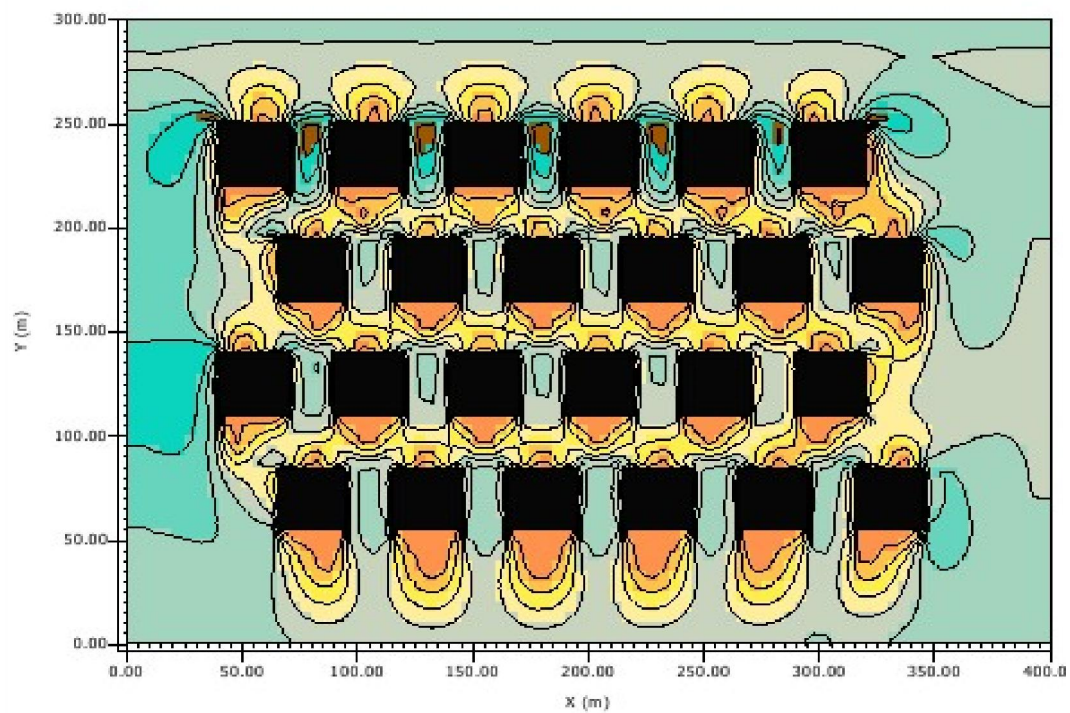
b) The best configurationG3-3.0 (20:25) in the NE-SW orientation
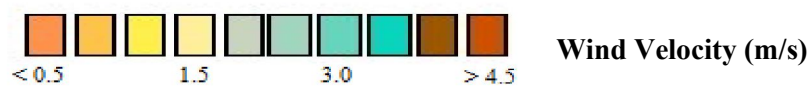
Wind Velocity (m/s)

Figure 6.30: The wind velocity average of; a)base case, and b) the best configurations G3-3.0 (20:25) of the third group in the NE-SW orientation
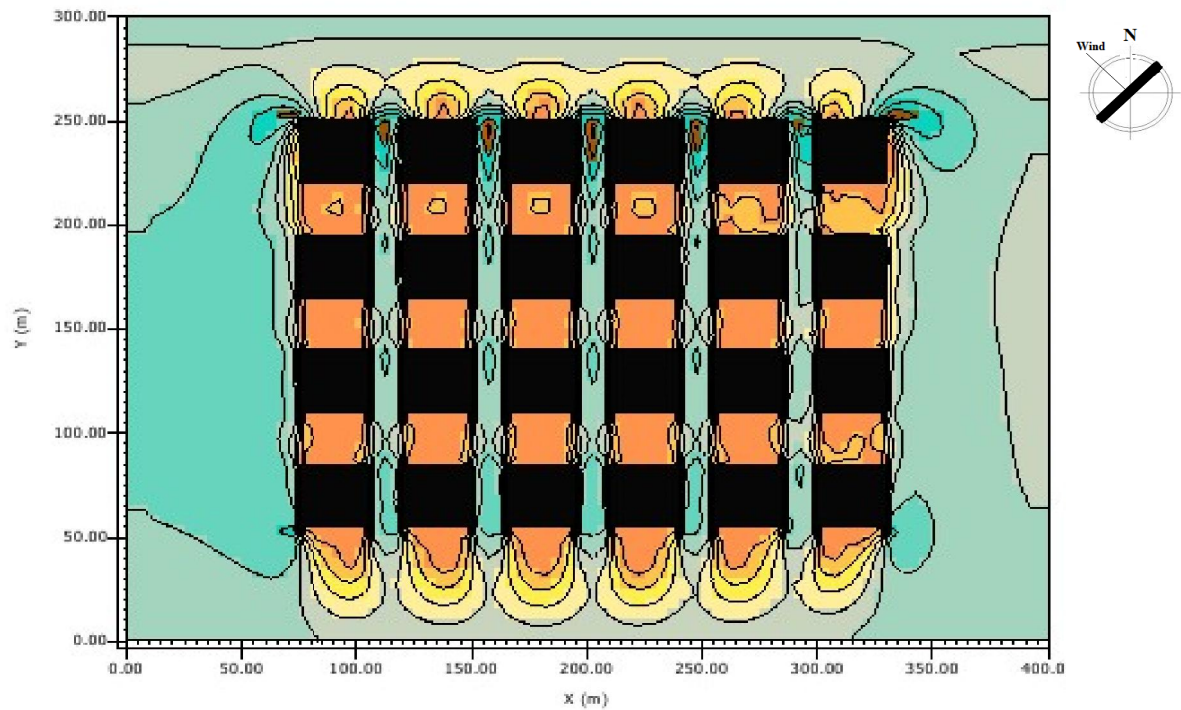
a) The base case configuration in the NE-SW orientation
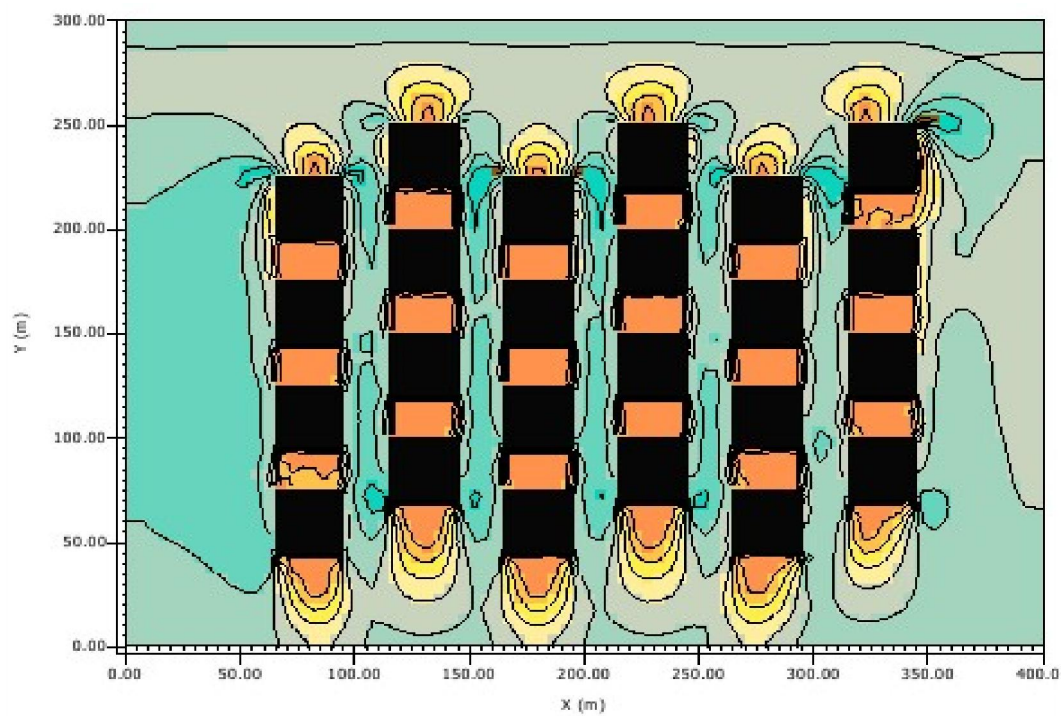
b) The best configuration G3-3.1 (20:20) in the NE-SW orientation
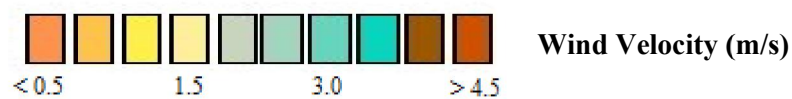
Wind Velocity (m/s)

Figure 6.31: The wind velocity average of; a) the base case, and b) the G3-3.1 (20:20) configurations of the third group in the NE-SW orientation

In the same concept, the G3-3.1 (20:20) configuration shows the same performance and recorded the highest wind velocity in the NE-SW orientation. The G3-3.1 (20:20) enhanced the wind velocity at maximum air temperature averages by 13% compared to the base case in the NE-SW, due to the effect of the NW-SE prevailing wind in the strait and wide alleys proving that when the alleys width range from 15m to 20m the air flow within the block is enhanced (Figure 6.31).

Similar findings were reported by Yang, Qian and Lau (2013) in a study carried out in China on high-rise building area. The researches proved that increasing the SVF by 10 % enhanced the wind velocity by 7 % - 8 %. The effect of the alternative arrangement of the urban block on the wind velocity has been varied according to the block arrangement and orientation, and it has been observed clearly in this group all configurations. In general, the alternative arrangement in the direction of the prevailing wind will obstruct the wind flow and reduce the wind velocity.

However, the increase in wind speed can be archived in the main, strait canyons facing the prevailing wind direction. This finding is strongly supports the results reported by Santamouris et al. (1999) of arranging buildings in a grid configuration and creating parallel, strait canyons, would promote the airflow within the canyon. On the other hand, rearranging the buildings with a staggered configuration will decrease wind velocity within the canyon and enhance the air flow around all buildings as Boutet (1987) stated.

However, the alternative arrangement can provide more shading by reducing the SVF, but it reduces the wind velocity and affects the outdoor thermal comfort. Moreover, it can be suitable for hot or cold stressful climate to reduce the stormy or high-speed wind and create more comfortable environment.

Chapter 7

The Heat Gain and Cooling Load of the Urban Block

7.0 The Heat Gain and Cooling Load of the Urban Block

In this chapter, the effect of the building geometry on the outdoor microclimate parameters will be included in the heat gain and cooling load calculations of the urban block. This integration will reflect the impact of urban geometry on the indoor cooling energy consumption. The outdoor microclimate data resulted from outdoor thermal simulation software will be used to calculate the heat gain and cooling plant load for all configurations of the three groups.

The indoor energy consumption will be presented in terms of the cooling load, moreover, the contribution of the direct solar gain and the transferred conduction heat gain in buildings' heat gain will be presented. The cooling load of the developed models will be calculated using the IES-VE software, and according to the microclimatic data extracted from simulating the models using ENVI- Met software. As mentioned in the methodology chapter 3, the outdoor air temperature and relative humidity are the new variables that will be used in the IES-VE indoor thermal performance simulation software. These variables will be used to explore the effect of the variation in urban morphology on indoor thermal performance represented by the total heat gain and cooling load.

The maximum and minimum dry bulb air temperature were edited in the IES-VE weather file, further to the wet bulb temperature at the maximum dry bulb temperature to reflect the outdoor relative humidity effect on the cooling energy consumption. The wet bulb temperature was extracted from the dry bulb temperature and the relative humidity using the 'Air Lite Psychrometric Calculation' software. The values of the wet bulb temperature for the three groups' configurations are presented in appendix G.

In the base case configuration, the simulation will cover the four orientations mentioned previously in order to find the effect of each block orientation on the block heat gain and cooling load of the 24 buildings.

For the other three groups, all configurations result in the four orientations will be illustrated and compared with each other, and the best configuration will be evaluated against the base case. For the heat gain and cooling load best performance the data will be presented as follows:

Base Case

- Hourly profile of the total direct solar gain on 21 June in kW June for the base case configuration in the four orientations; N-S, E-W, NE-SW and NW-SE.

- Daily average of the total solar gain on 21 June in kWh for the base case configuration in the four orientations; N-S, E-W, NE-SW and NW-SE.

- Hourly profile of cooling plant load on 21June in kW/m² for the base case in the four orientations; N-S, E-W, NE-SW and NW-SE.

- Daily average of cooling plant load on 21 June in kWh/m² for the base case configuration in the four orientations; N-S, E-W, NE-SW and NW-SE.

- Daily average of the conduction heat gain and direct solar gain in kWh for the base case configuration in the block four orientations; N-S, E-W, NE-SW and NW-SE.

Base Case and the configurations of the three groups

- Daily average of cooling plant load on 21 June in kWh/m² for the first group configurations in the four orientations; N-S, E-W, NE-SW and NW-SE.

- Hourly profile of cooling plant load on 21 June in kW/m² of all configurations in each group in; a) NE-SW and b) NW-SE orientations.

- The average cooling load performance kWh/m²of the configurations in each group in; a) NE-SW and b) NW-SE orientations.

- Daily average of direct solar gain on 21st June in kWh for all configurations in each group in the four orientations; N-S, E-W, NE-SW, and NW-SE.

- Daily average of conduction heat gain on 21 June in kWh for all configurations in each group in the four orientations; N-S, E-W, NE-SW, and NW-SE.

- The contribution of conduction heat gain and direct solar gain in kWh of all configurations in each group in; a) NE-SW and b) NW-SE orientations.

7.1 The Indoor Heat Gain and Cooling Plant Load

7.1.1 Heat Gain and Cooling Plant Load of the Base Case

Simulating the base case and the developed block configurations using the IES-VE software generated a set of indoor thermal performance data covers number of parameters. In this section, the heat gain and the plant cooling load for each configuration will be explored, further to the contribution of the direct solar gain and conduction gain to the total heat gain of the urban block. Figure7.1 shows the total solar gain for the 24 buildings of the base case in the four simulated orientations namely; N-S, E-W, NE-SW, and NW-SE. The figure shows the daily solar gain profile of the simulated day (21 June). The direct solar effect on the urban block starts with sunrise at around 5:30 to reach the maximum gain during the day time at 9:30. The decreases in solar gain is observed in the middle of the day to reach the minimum during the day time around 12:30 when the sun is vertical in the sky, and all orientation recorded the almost the same solar gain. The maximum solar gain recorded is in the NE-SW orientation at 15:30.On the other hand, the minimum average direct solar gain of the base case configuration with respect to the orientation is recorded in the N-S with a reduction of 13 % compared to the NE-SW orientation (Figure 7.2).

However, the NE-SW and the NW-SE orientations recorded approximate values of the solar gain due to the orthogonal configuration of the base case.
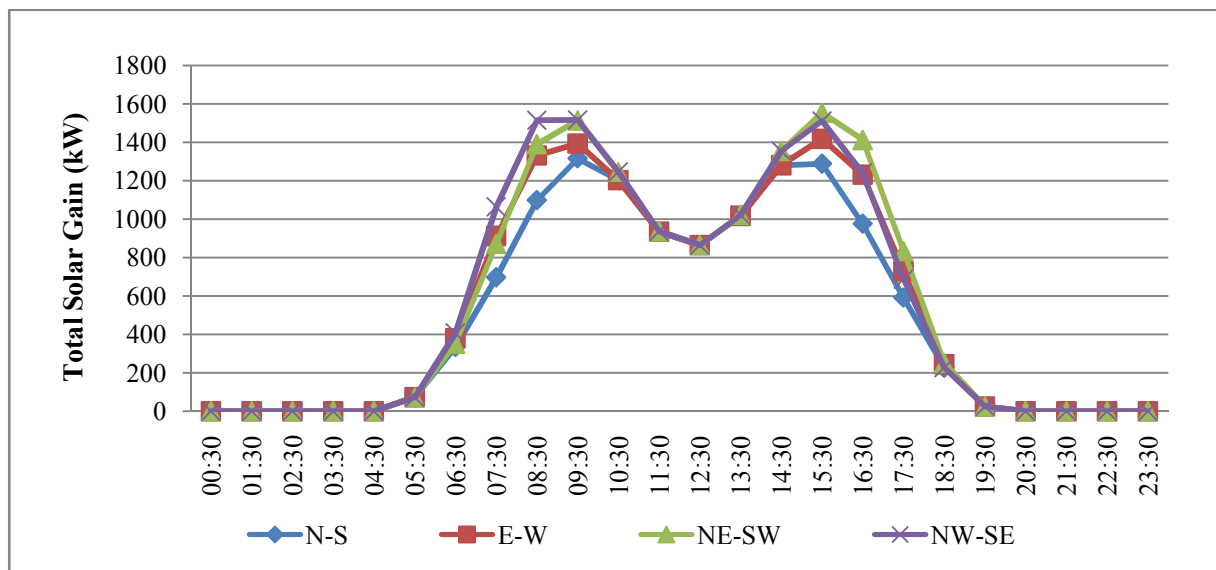
Figure 7.1: Hourly profile of the total direct solar gain on 21 June for the base case configuration in the four orientations; N-S, E-W, NE-SW and NW-SE
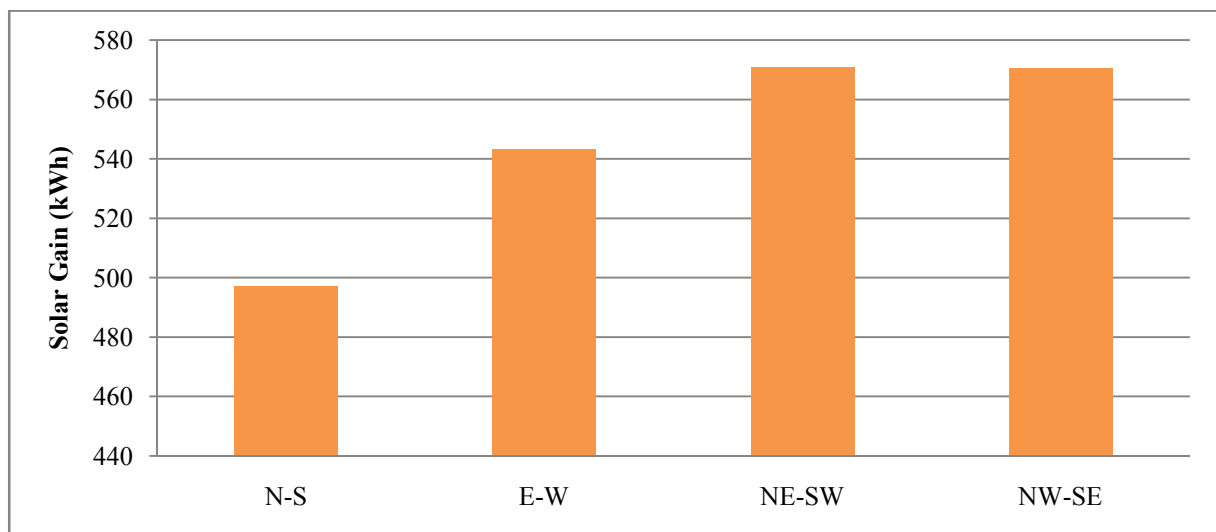
Figure 7.2: Daily average of the total solar gain on 21 June for the base case configuration in the four orientations; N-S, E-W, NE-SW and NW-SE

The cooling plant load of the base case configuration in the four simulated orientations is illustrated in figure 7.3. It is clear from figure that the cooling load is directly affected by the solar gain of the urban block, and accordingly, the sunrise and sunset timing.

Furthermore, the daily profile of the cooling load shows that the cooling load in the fourth orientations starts with low values at the early morning around 5:30 and increases to reach the peak at 15:30. The load keeps on decreasing during the afternoon time until the next day sunrise. Furthermore, the figure shows that the cooling plant load of the block is varied significantly according to the block orientation which reflects the effect of the direct solar gain and the variation on outdoor air temperature on indoor cooling energy consumption.

As mentioned in the air temperature of the base case results illustration, the average of the highest maximum outdoor air temperature recorded in the NE-SW block orientation with 37.62 $^{\circ}$ C. The reflection of this temperature has been observed in the highest cooling load consumption recorded in the same block orientation at 15:30 with a peak value of 0.0718 kW/m². On the other hand, the lowest maximum outdoor air temperature recorded in the N-S block orientation is 35.78 $^{\circ}$ C, accordingly, the lowest peak load consumption is recorded in this orientation with a value of 0.06707 kW/m². The decrease in the peak load of the N-S orientation is 6.6 % compared to the NE-SW orientation (Figure 7.3). The daily average of cooling plant load in the fourth orientations illustrated in figure 7.3. The figure shows that the reduction in average cooling load between the worst and the best orientations reaches 6.4 % (Figure 7.4). Therefore, the best orientation for the base case block configuration and lowest cooling energy consumption can be achieved is the N-S block orientation (Figure 7.4).

Furthermore, the contribution of the conduction heat gain and the direct solar gain in cooling load of the base case configuration in the block four orientations are presented in figure 7.5. The effect of the conduction gain is higher than the effect of the direct solar gain in total heat gain in the two orientations; N-S and NE-SW.
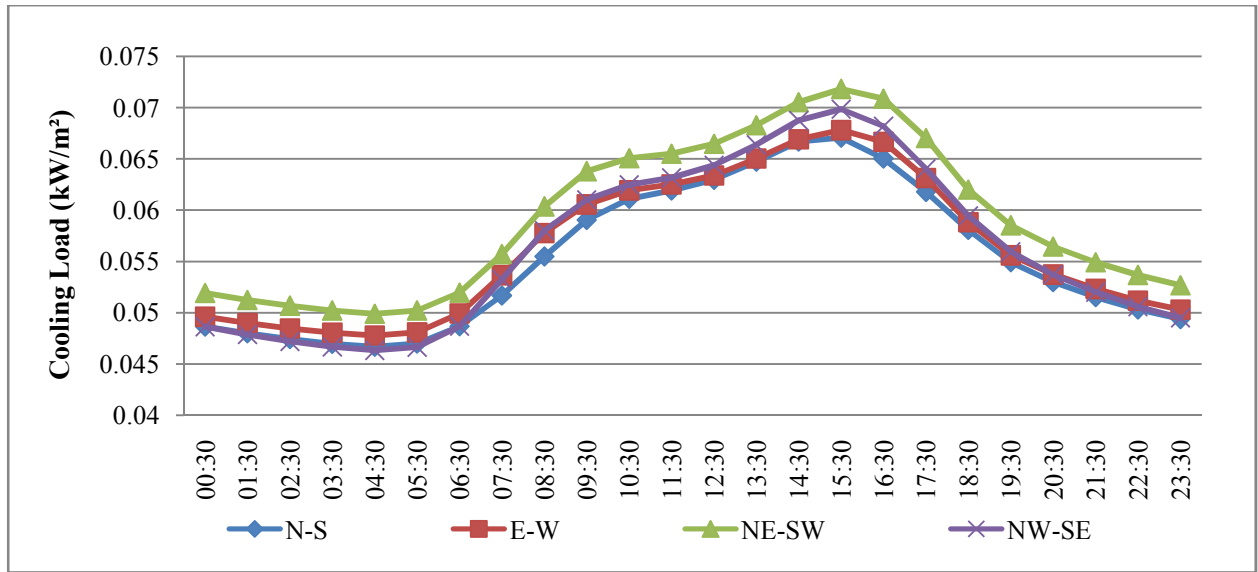
Figure 7.3: Hourly profile of cooling plant load on 21June for the base case in the four orientations; N-S, E-W, NE-SW and NW-SE
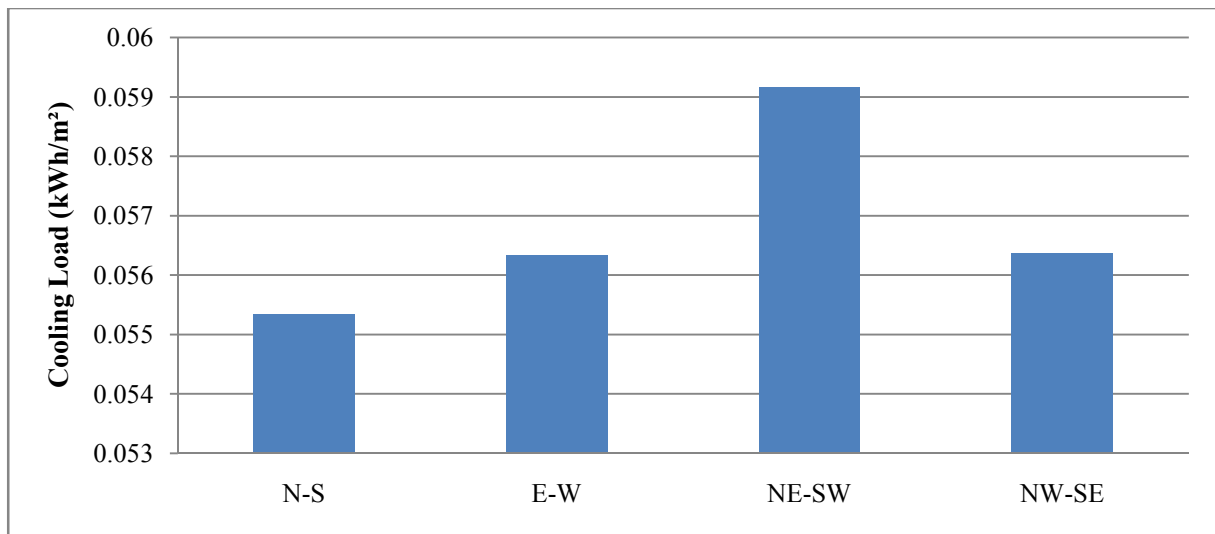
Figure 7.4: Dailyaverage of cooling plant load on 21 June for the base case configuration in the four orientations; N-S, E-W, NE-SW and NW-SE

On the other hand, in the NW-SE block orientation the direct solar gain has more contribution in total heat gain compared to the conduction gain, and it is slightly higher in the E-W orientation due to the exposure of the long axis of the block to the west orientation.
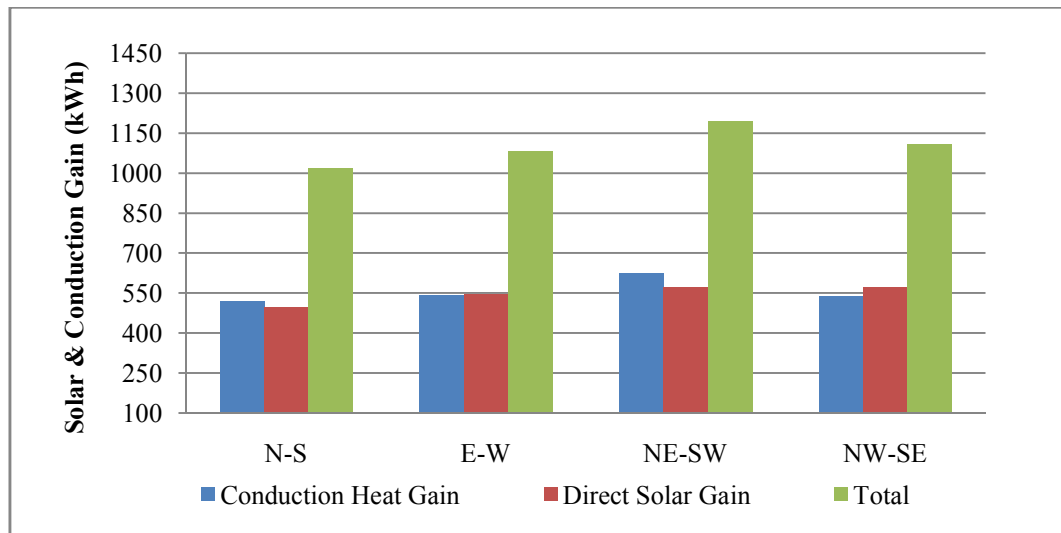
Figure 7.5: Daily average of the conduction heat gain and direct solar gain for the base case configuration in the block four orientations; N-S, E-W, NE-SW and NW-SE

7.1.2 Heat Gain and Cooling Plant Load of the First Group Configurations

The variation in energy consumed for the cooling load of the first group configurations is illustrated in figure 7.6. In general, the cooling load averages in the N-S and E-W orientations is less than the other two orientations. Furthermore, the variation between the first group configurations in these two orientations is smaller compared to the two other orientations. However, in the N-S orientation, the minimum load recorded is for the G1-1.2 (3:7:7:3) configuration with a reduction of 1.8 % compared to the base case. On the other hand, the G1-1.1 (3:7:3:7) configuration shows the best performance in the E-W orientation with a reduction of 2 % compared to the base case. The minimum saving in these two orientations is recorded in the G1-1.0 (7:3:3:7) configuration with negligible variation compared to the base case. The comparison between the first group configurations and the base case in the N-S and E-W orientations daily cooling load profiles are presented in appendix F.1.
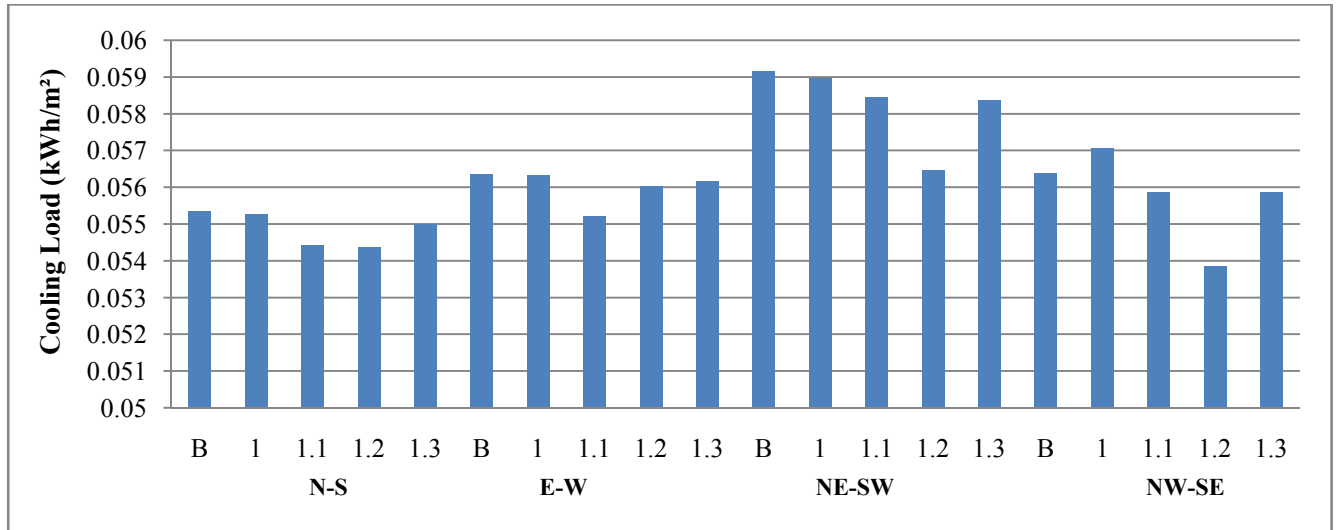
Figure 7.6: Daily average of cooling plant load on 21 June for the first group configurations in the four orientations; N-S, E-W, NE-SW and NW-SE

In the NE-SW and NW-SE orientations more significant reduction in cooling load compared to the base case is observed. The cooling load and the daily profile of the 21st June in these two orientations is presented in figure 7.7. Similar to the base case the cooling load starts on increase from the sunrise after 5:30 am to reach the maximum at 15:30 pm.
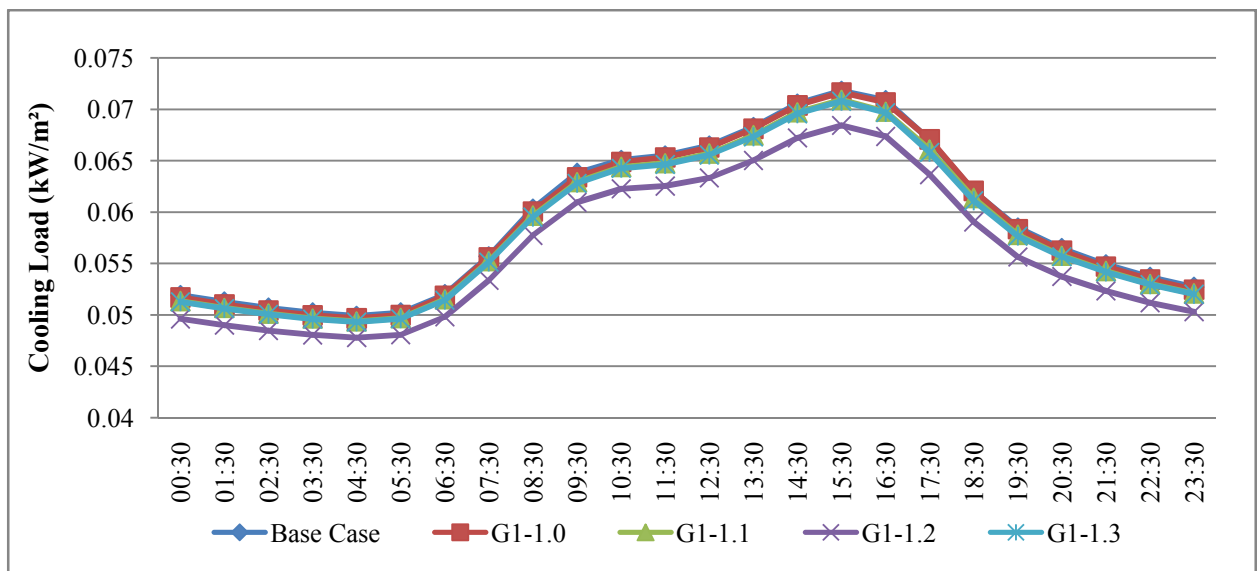
a) NE-SW orientation

b) NW-SE orientation

Figure 7.7: Hourly profile of cooling plant load on 21June for the first group configurations in; a) NE-SW and b) NW-SE orientations

The variation in cooling load between the first group configurations is higher in the NW-SE compared to the NE-SW orientation.

However, the G1-1.2 (3:7:7:3) configuration recorded the best performance in these orientations with a reduction of 4.6 % and 4.5 % compared to base case in the NE-SW and NW-SE, respectively (Figure 7.8). On the other hand, the G1-1.0 (7:3:3:7) configuration shows an approximate cooling load values compared to the base case in the NE-SW orientation, but in the NW-SE the G1-1.0 (7:3:3:7) recorded a higher cooling load with an increase of 1.2 % compared to the base case (Figure 7.8 b).

b) NE-SW orientation

b) NW-SE orientations

Figure 7.8: The average cooling load performance of the first group configurations compared to the base case in; a) NE-SW and b) NW-SE orientations

The cooling load of the indoor space is affected by the direct solar radiation on the building surfaces and the heat conduction gain of the buildings envelop from the surrounding environment. Figure 7.9 shows the direct solar gain attitude of the first group configurations in all orientations. The daily profile of the first group configurations shows clearly the effect of each orientation on the variation in solar gain between the different configurations, and the variation is higher in the E-W orientation compared to the other configurations.

The daily profiles of the solar gain for the first group's configurations in each orientation are presented in appendix E. In general, the N-S and E-W orientation records lower solar gain than the other two orientations. This trend is reflected clearly on the cooling load performance in these two orientations. The figure shows that the best configuration with respect to the least solar gain and highest shading effect is the G1-1.2 (3:7:7:3) configuration in the four orientations.

Figure7.9: Daily average of direct solar gain on 21 June for the first group configurations in the four orientations; N-S, E-W, NE-SW, and NW-SE

The other urban block heat gain resource is the external transferred heat from outdoor space to the indoor space, or the conduction heat gain through the buildings envelope. Figure 7.10 shows the effect of the conduction heat on cooling load of each configuration in all orientations. The figure shows that the conduction gain is the highest in the NE-SW orientation compared to the other three simulated orientations. This result is due to the highest outdoor air temperature recorded in this orientation. However, the best configuration G1-1.2 (3:7:7:3) recorded the lowest conduction heat gain compared to the other configurations in all orientations.

Figure 7.10: The daily average conduction heat gain on 21 June for the first group configurations in the four orientations; N-S, E-W, NE-SW, and NW-SE

Figure 7.11 presented the direct solar and conduction heat gain contribution to the total heat gain for each configuration of the first group in the NE-SW and NW-SE orientations. In the NE-SW orientation, the effect of the conduction gain is higher than the solar gain due to the higher outdoor air temperature recorded. The reduction in conduction heat gain and solar gain between the best configuration G1-1.2 (3:7:7:3) and the base case is 6.2 % and 1.5 %, respectively (Figure 7.11 a).

In the NW-SE orientation, the first configuration G1-1.0 (7:3:3:7) recorded the highest conduction gain according to the highest air temperature recorded in this configuration, and the best configuration G1-1.2 (3:7:7:3) recorded the lowest conduction gain compared to all other configurations including the base case (Figure 7.11 b). In the NW-SE orientation the best configuration G1-1.2 (3:7:7:3) recorded lower solar gain and provided higher shading effect by 1.5 % compared to the base case. On the other hand, the conduction gain in the best configuration G1-1.2 (3:7:7:3) is reduced by 7.2 % compared to the base case in this orientation (Figure 7.11 b).
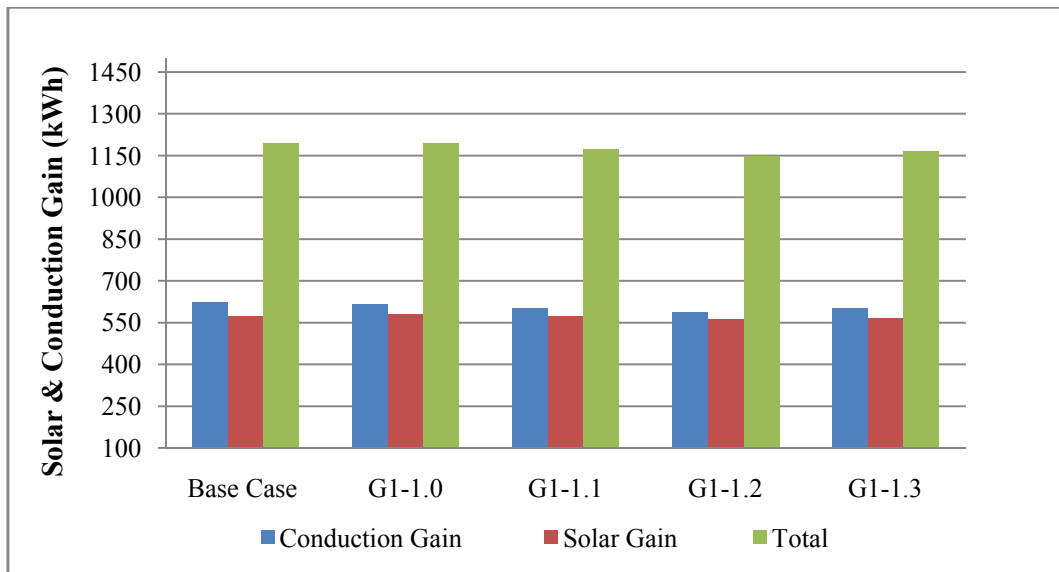
a) NE-SW orientation
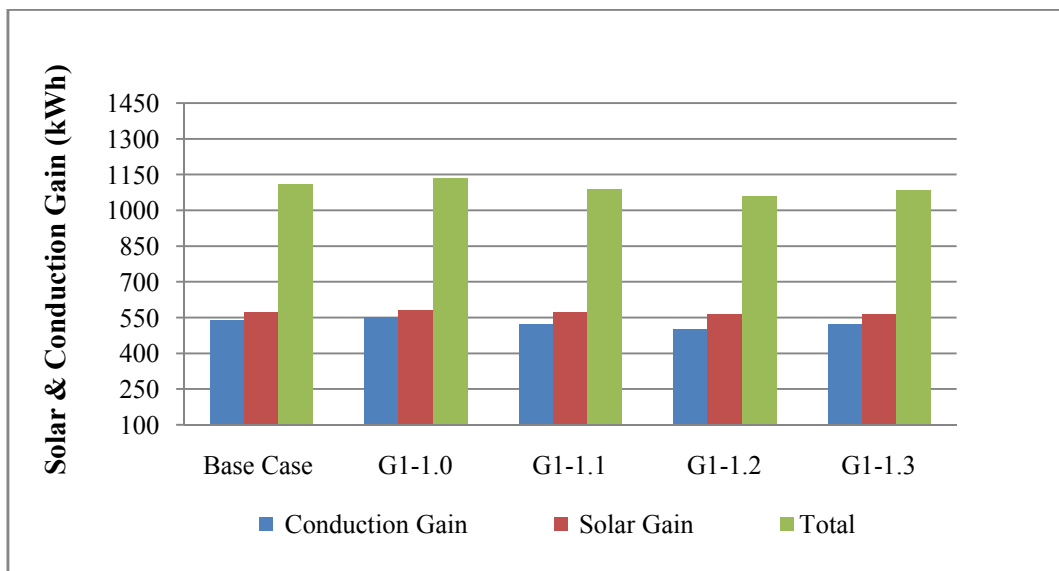
b) NW-SE orientation

Figure 7.11: The contribution of conduction heat gain and direct solar gain for the first group configurations in; a) NE-SW, and b) NW-SE orientations

7.1.3 Heat Gain and Cooling Plant Load of the Second Group Configurations

The effect of the height variation towards the long axis of the urban block on load required for cooling consumption and energy saving will be illustrated in this section. Figure 7.12 shows the cooling plant load of the second group configurations in the four simulated orientations. It is clear from the figure that the cooling load averages is the highest in the block oriented towards NE-SW direction.

Other than that, the three simulated orientations show an approximated performance with respect to the averages and variations in cooling load between the second group configurations.

The N-S and E-W orientation recorded a less variation in cooling load between the group configurations compared to the two other configurations. The variation in the N-S orientation between the best configuration G2-2.1 (3:5:7:7:5:3) and the base case is 1.3 %. However, the E-W recorded slightly higher averages than the N-S orientation and the variation in cooling load between the best configuration G2-2.5 (5:3:7:7:3:5) and the base case reaches 1.7 %. Hence, the illustration of the detailed cooling load data will be concentrated on the NE-SW and NW-SE orientations.

The comparison in cooling load figures in the N-S and E-W orientations are presented in appendix F.2. Figure 7.13 shows the daily profile of the cooling load for the second group configurations in these two orientations.

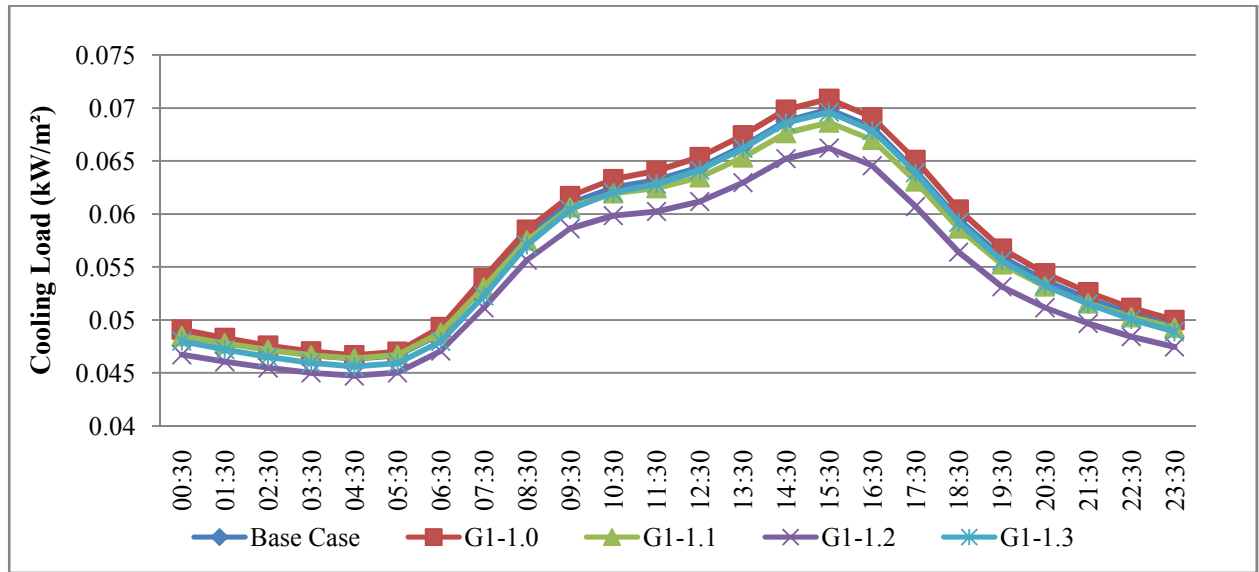

Figure 7.12: Daily average of cooling plant load on 21 June for the second group configurations in the four orientations; N-S, E-W, NE-SW and NW-SE
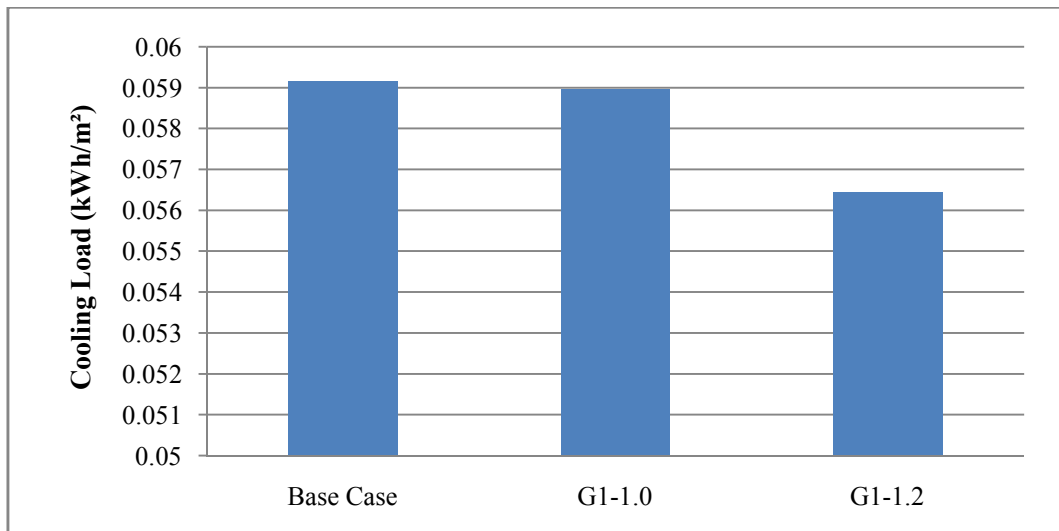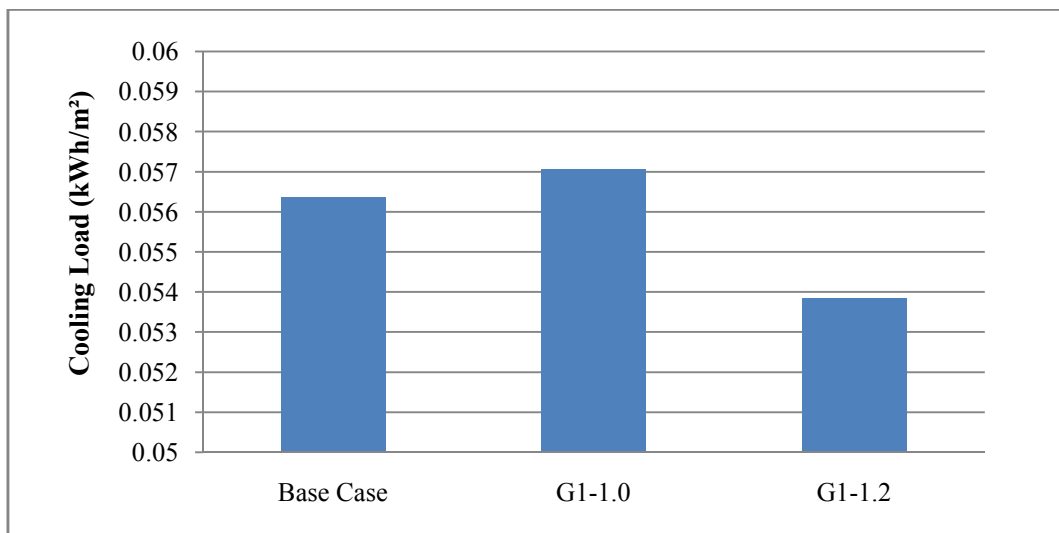
a) NE-SW orientation

b) NW-SE orientation

Figure 7.13: Hourly profile of the cooling plant load on 21st. June for the second group configurations; a) NE-SW and b) NW-SE orientations

The NE-SW orientation recorded the highest cooling load averages, and the G2-2.0 (7:5:3:3:5:7) configuration shows the highest load averages compared to the base case and other group configurations. The G2-2.0 (7:5:3:3:5:7) recorded an increase of 1.2 % compared to the base case. On the other hand, the G2-2.5 (5:3:7:7:3:5) configuration shows the best performance with a reduction of 4.5 % compared to the base case in this orientation (Figure 7.14 a).

In the NW-SE orientation the same configuration G2-2.5 (5:3:7:7:3:5) recorded the best cooling load performance and the reduction reaches 3.9 % compared to the base case, while the first configuration G2-2.0 (7:5:3:3:5:7) recorded the least cooling load saving compared to the base case as it approximately has the same cooling load of the base case (Figure 7.14 b).

a) NE-SW orientation

b) NW-SE orientation

Figure 7.14: The average cooling load performance of the second group configurations compared to the base case in; a) NE-SW and b) NW-SE orientations

On the other hand, the best configuration with respect to the lowest solar gain and highest shading provided is the G2-2.1 (3:5:7:7:5:3) configuration in all orientations (Figure 7.15). The block oriented in the N-S direction recorded the lowest direct solar gained by the buildings surfaces. The highest reduction in the solar gain is recorded in the N-S with a percentage of 1.6 % between the best configuration G2-2.1 (3:5:7:7:5:3)and the base case (Figure 7.15). On the other hand, the daily profile of the solar gain shows the effect of the height variation with respect to the orientation. In the N-S the variation in daily solar gain between the second group configurations is more significant, as the diversity in buildings height facing the E-W orientation. The solar gain daily profile and the heat conduction gain of the second group configurations in all orientations are presented in appendix F.
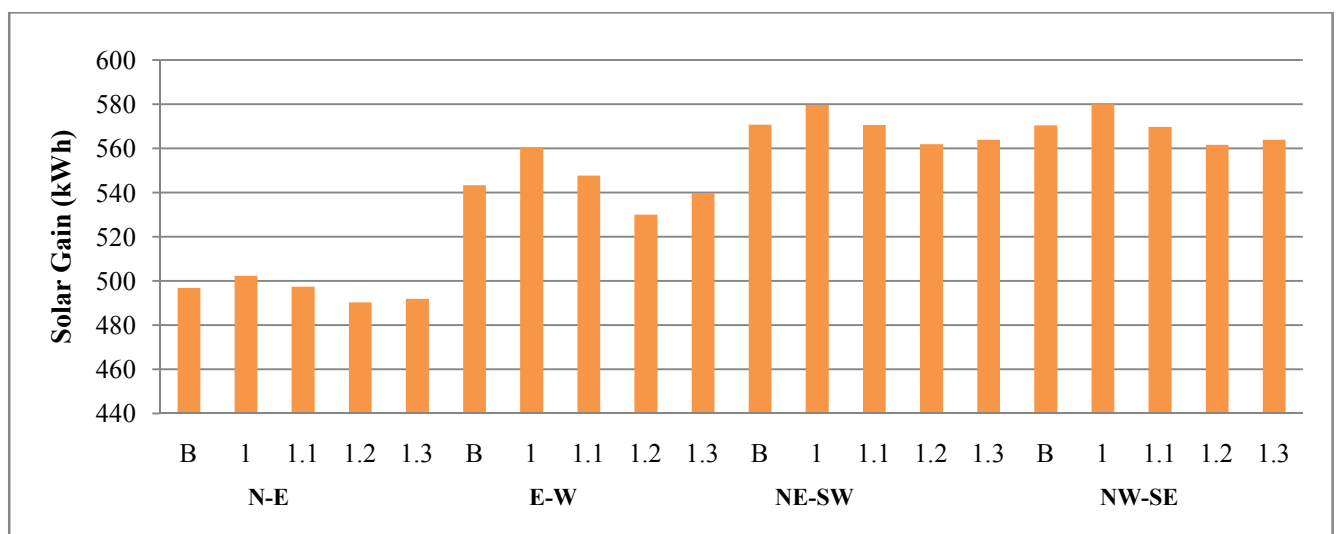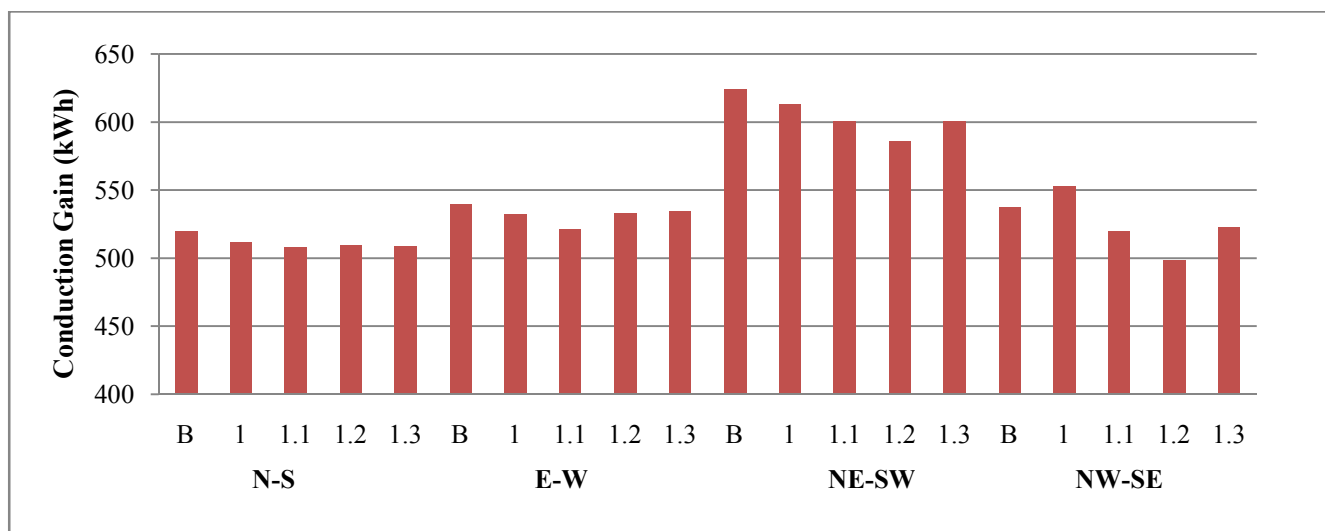

Figure 7.15: The daily average of direct solar gain on 21 June for the second group configurations in the four orientations; N-S, E-W, NE-SW, and NW-SE

The conduction heat gain of the second group configuration is presented in figure7.16. The simulated results show an approximate performance between the second group configurations in the three orientations; N-S, E-W, and NW-SE. The highest variation is observed is in the NE-SW orientation, in this orientation the conduction gain is reduced by 6.7 % between the best configuration G2-2.5 (5:3:7:7:3:5) and the base case (Figure 7.17 a).

On the other hand, the reduction in the conduction gain between the best configuration G2-2.5 (5:3:7:7:3:5) and the base case in the NW-SE orientation is 6.3 % (Figure 7.17 b).
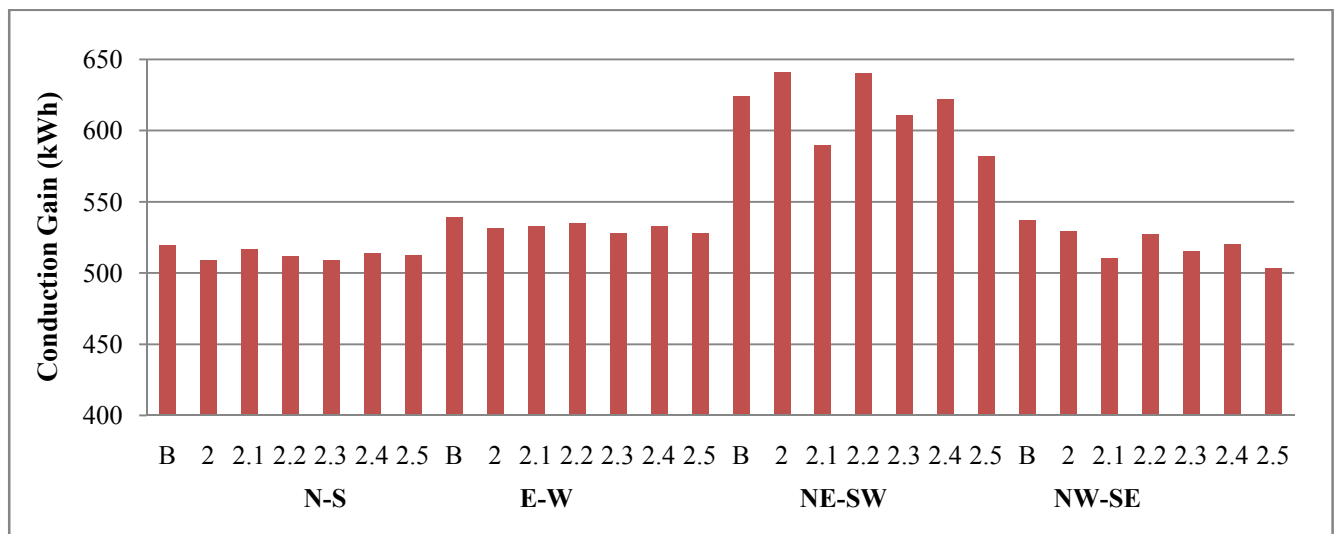

Figure 7.16: The daily average of conduction heat gain on 21 June for the second group configurations in the four orientations; N-S, E-W, NE-SW, and NW-SE

Furthermore, it has been observed that the conduction heat gain is higher in the NE-SW orientation compared to the solar gain due to the higher temperature recorded in this orientation for all configurations. The NW-SE shows an opposite attitude as the solar gain averages in the NW-SE orientation is higher than the conduction heat gain (Figure 7.17).
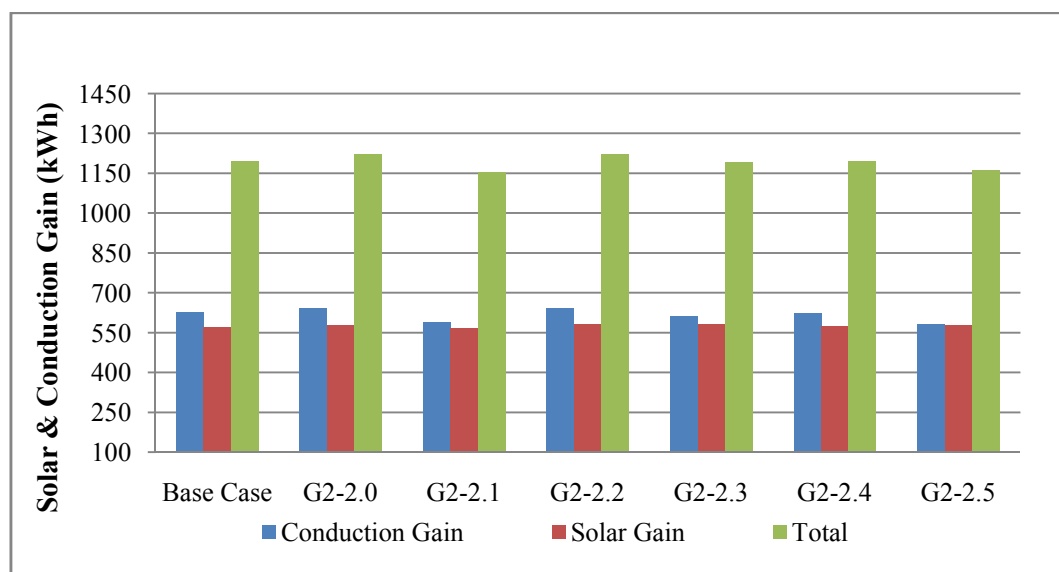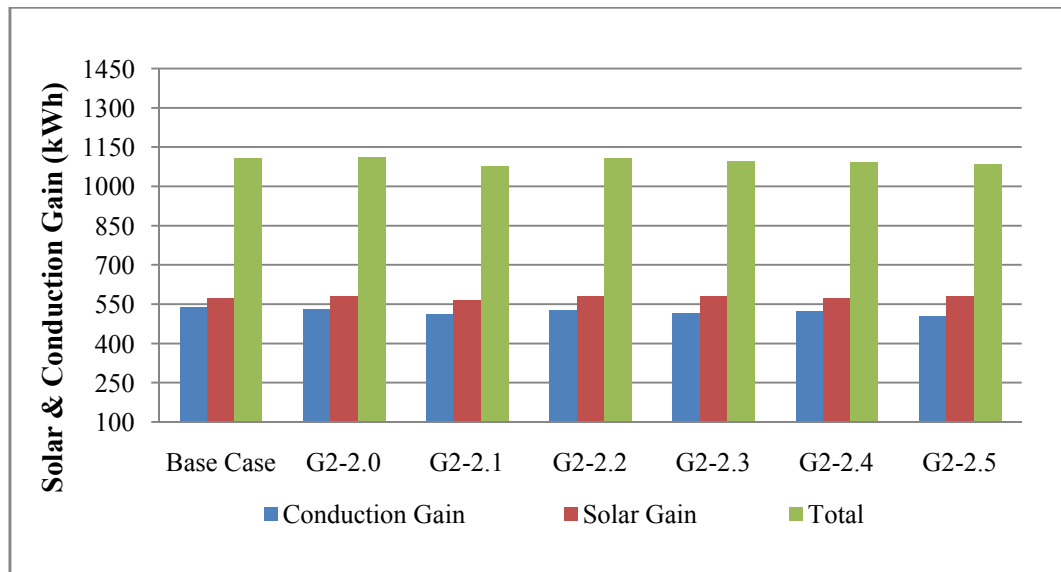
a) NE-SW orientation

Figure 7.17: The contribution of conduction heat gain and direct solar gain for the second group configurations in; a) NE-SW, and b) NW-SE orientations

7.1.4 Heat Gain and Cooling Plant Load of the Third Group Configurations

The indoor energy performance of the third group three configurations were simulated in the four orientations and the results is illustrated in Figure 7.18. The variation in cooling load between the three configurations is obvious in all orientations. The figure shows that the third configuration G3-3.2 (15:20) recorded the lowest load required for cooling in two orientations; E-W, and NW-SE. In the N-S orientation, the base case has the best performance. However, in the NE-SW orientation, the first configuration G3-3.0 (20:25) recorded the best performance with respect to the reduction of energy consumption for cooling purpose.
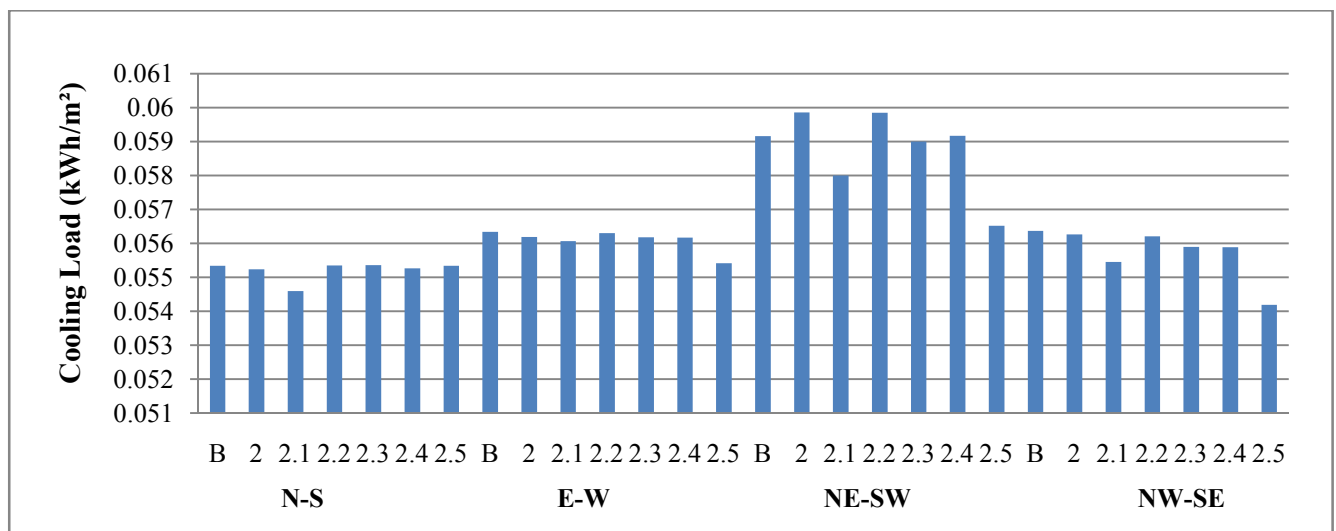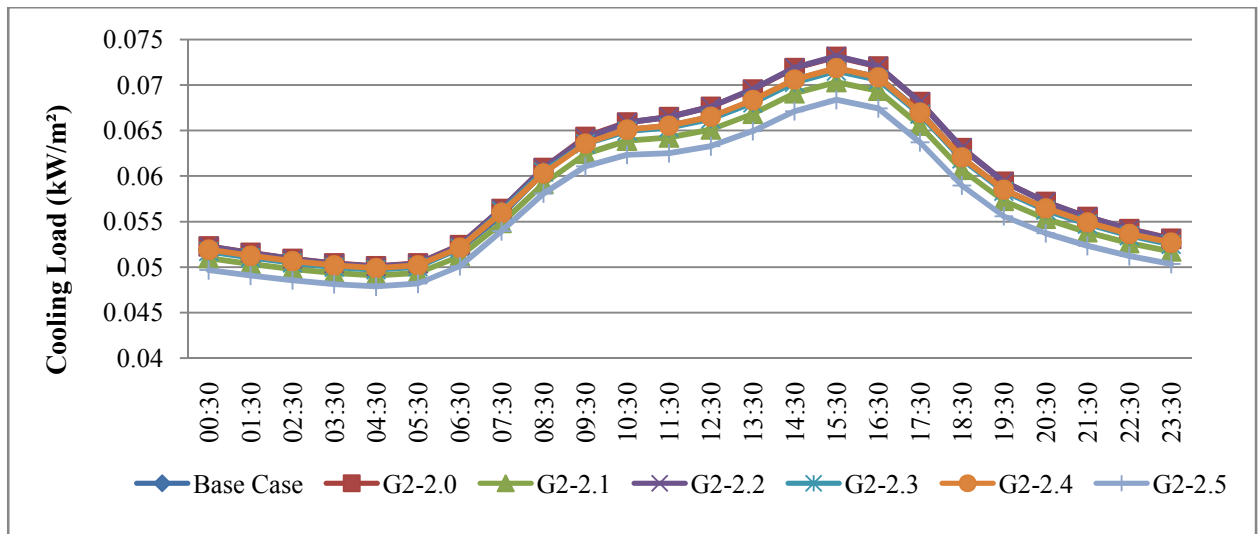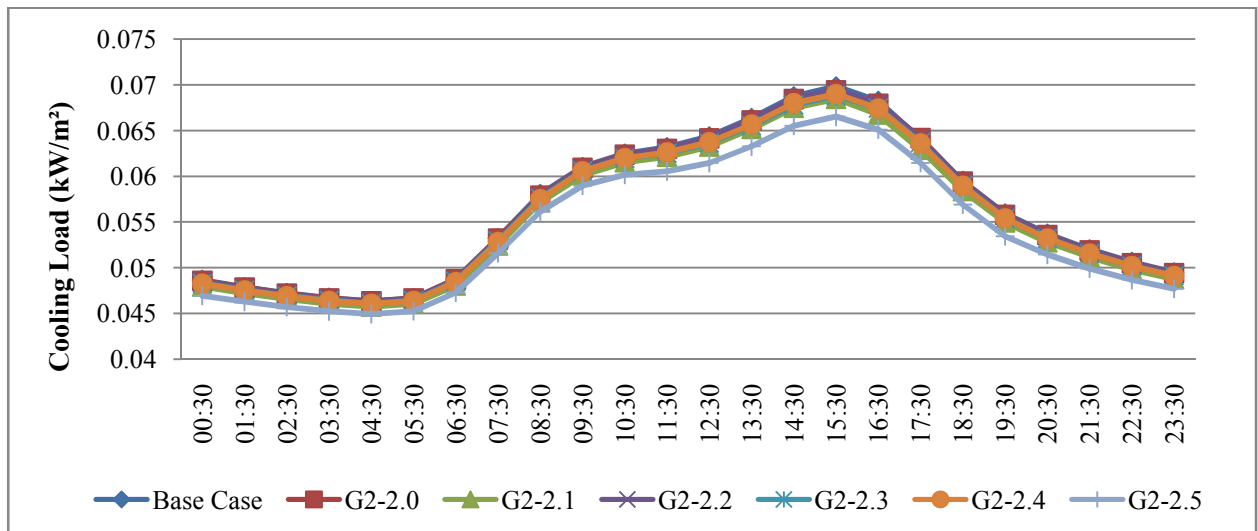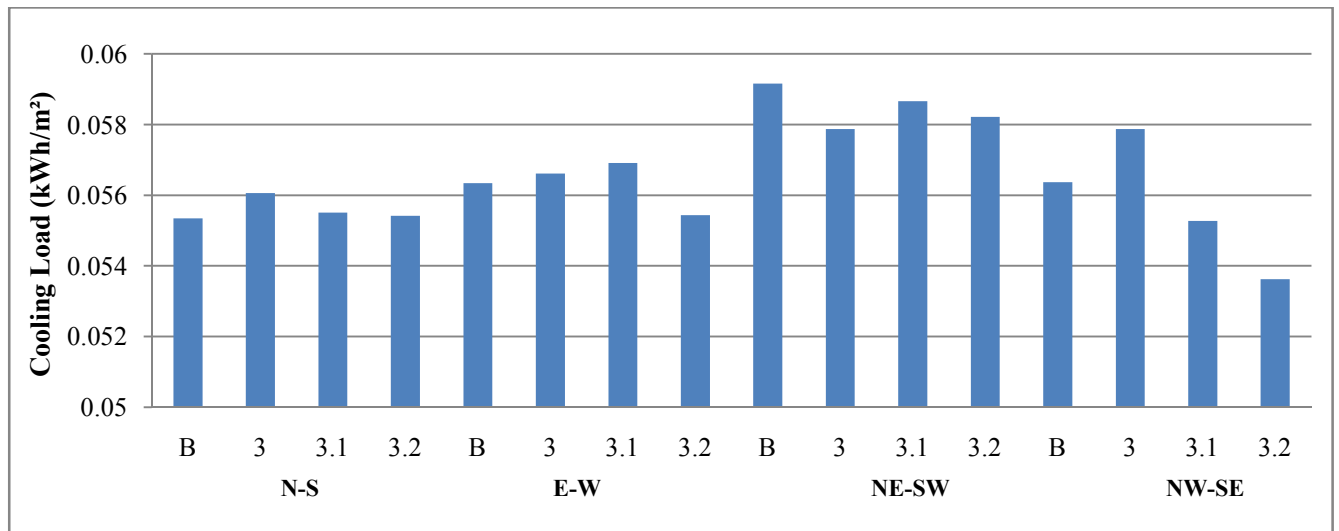
Figure 7.18: Daily average of cooling plant load on 21 June for the third group configurations in the four orientations; N-S, E-W, NE-SW, and NW-SE

The daily cooling plant load of the third group configurations in the NE-SW and NW-SE orientations is illustrated in figure 7.19. From the figure, the variation between the best configuration and the other configurations including the base case in the NW-SW orientation is obvious and it is more than the variation in NE-SW orientation, however, the cooling load figures show the same attitude in both orientations. In the NE-SW orientation the best configuration G3-3.0 (20:25) recorded the lowest cooling load, and the reduction in the average cooling load between the best configuration G3-3.0 (20:25) and the base case is 2.2 % (Figure 7.20 a).

On the other hand, the third group configurations show different performance in the NW-SE orientation (Figure 7.20 b). The best performance in this orientation is recorded by G3-3.2 (15:20) configuration with a significant reduction reaches 4.9 % compared to the base case. However, the best performance in the NE-SW orientation G3-3.0 (20:25) shows an opposite attitude in the N-S and NW-SE orientations and recorded a cooling load higher than the base case by 1.3 % and 2.6 % respectively.
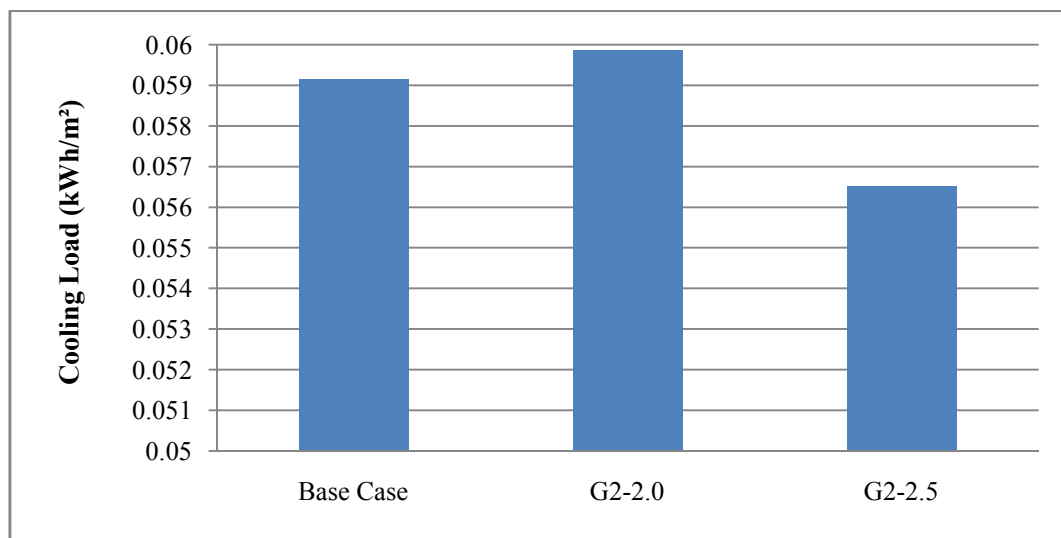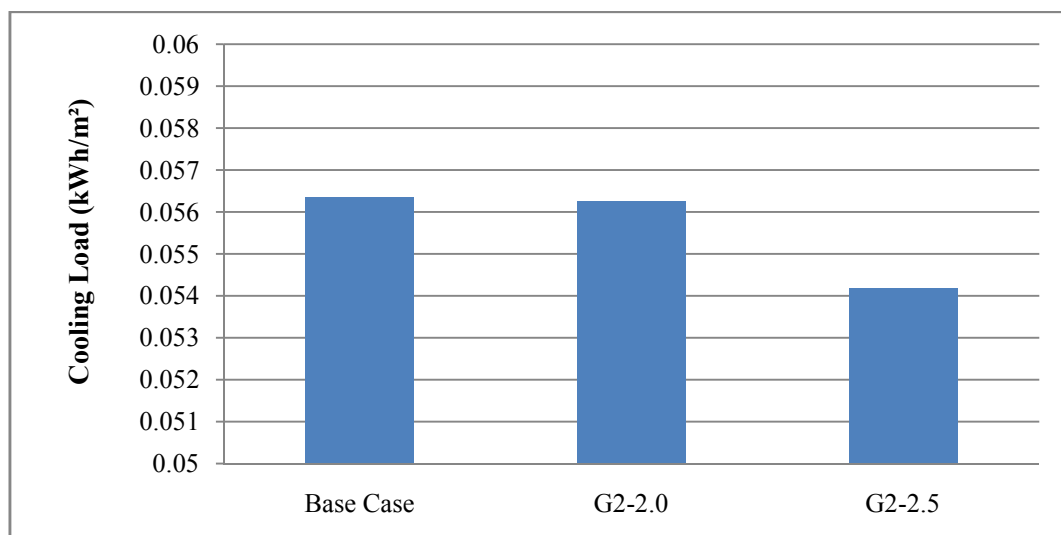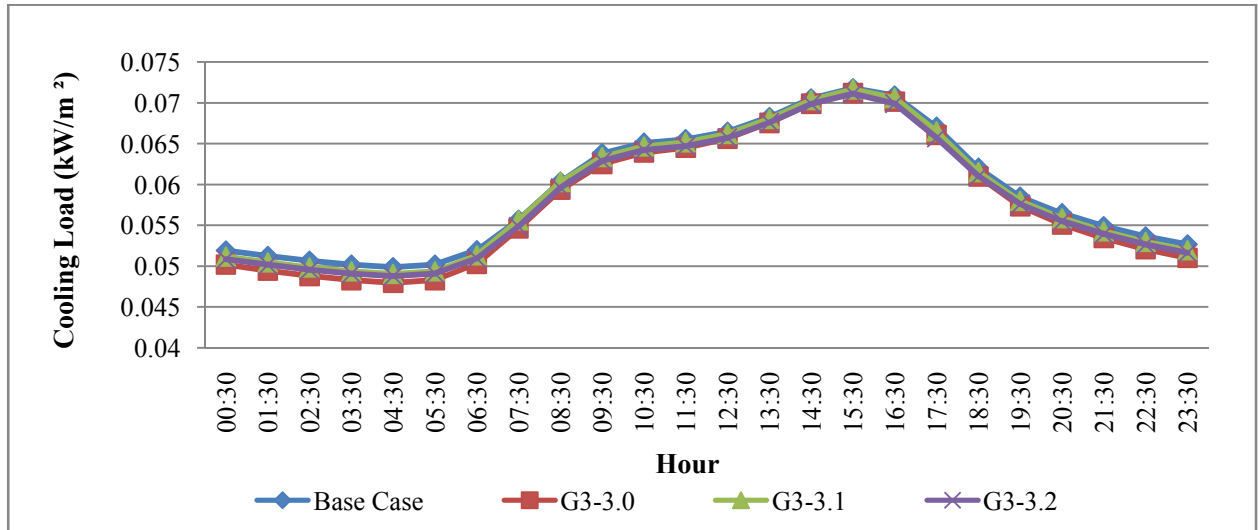
a) NE-SW orientation
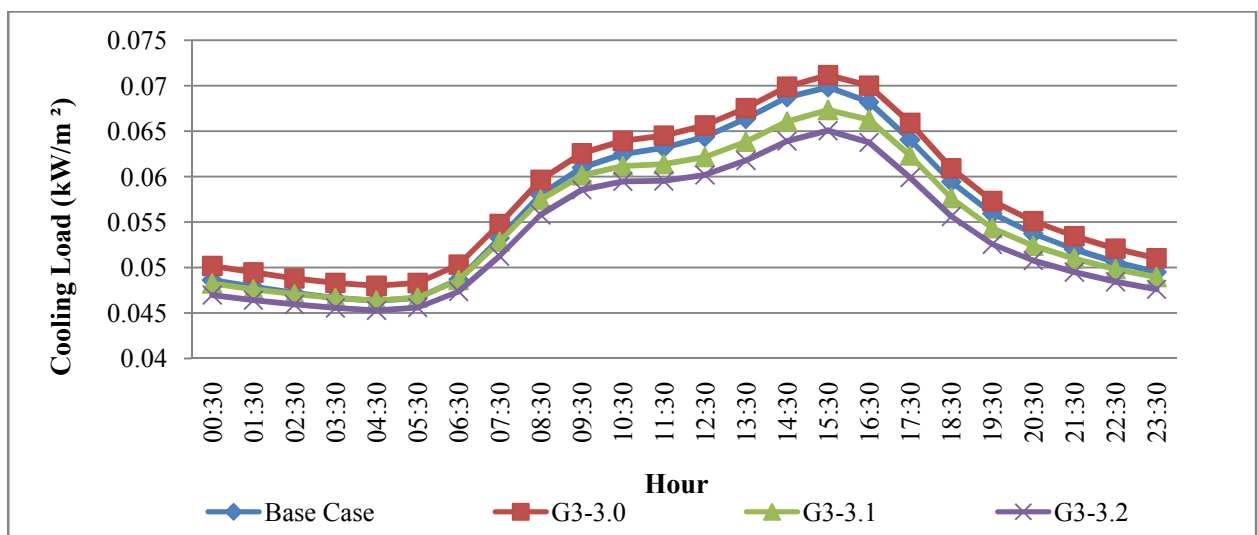
b) NW-SE orientation

Figure 7.19: Hourly profile of the cooling plant load on 21 June for the third group configurations in the; a) NE-SW and NW-SE orientations
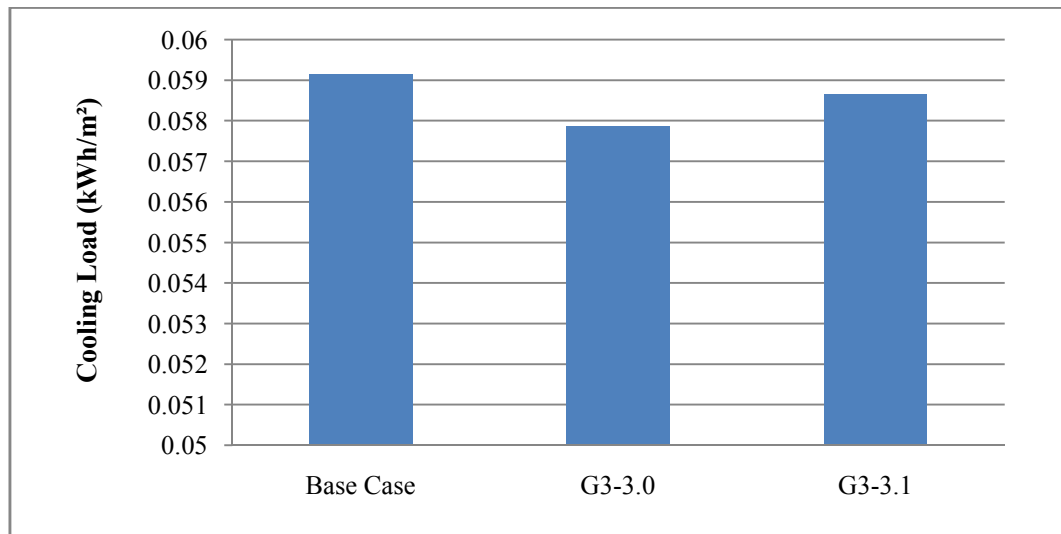
a) NE-SW orientation
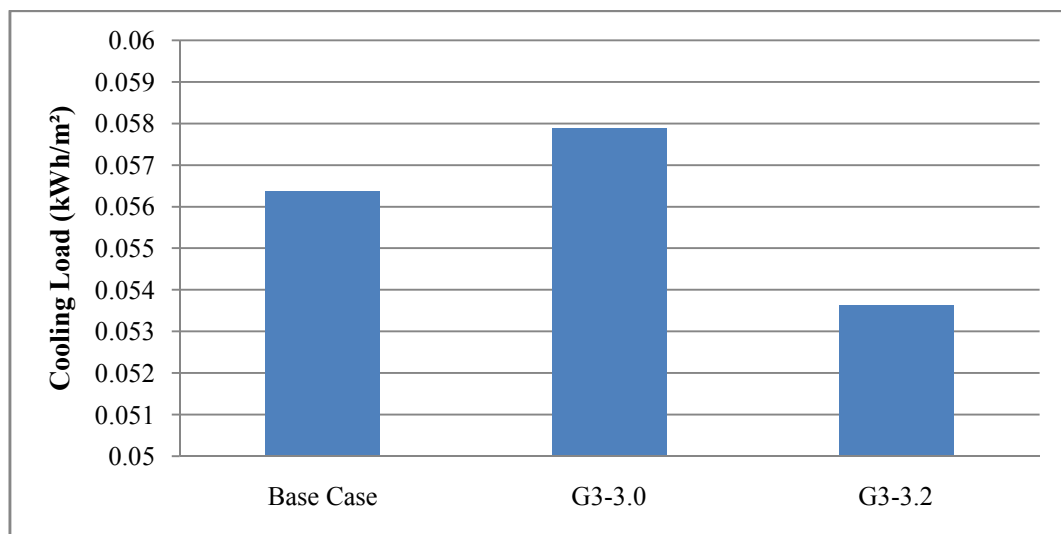
b) NW-SE orientation

Figure 7.20: The average cooling load performance of the third group configurations compared to the base case in; a) NE-SW and b) NW-SE orientations

The solar gain figure 7.21 shows that the base case in the N-S orientation recorded the lowest solar gain compared to all configurations in all orientations.

The solar gain daily profile and the heat conduction gain of the third group configurations in all orientations are presented in appendix F.3. The reduction in solar gain in the base case compared to the best configuration in this orientation G3-3.1 (20:20) reaches to 7 % (Figure 6.38).

Furthermore, in the NE-SW and NW-SE orientations the best configuration G3-3.2 (15:20) recorded the lowest solar gain with a very slight reduction of 0.1 % and 0.2 % compared to the base case in these two orientations respectively (Figure 7.21).
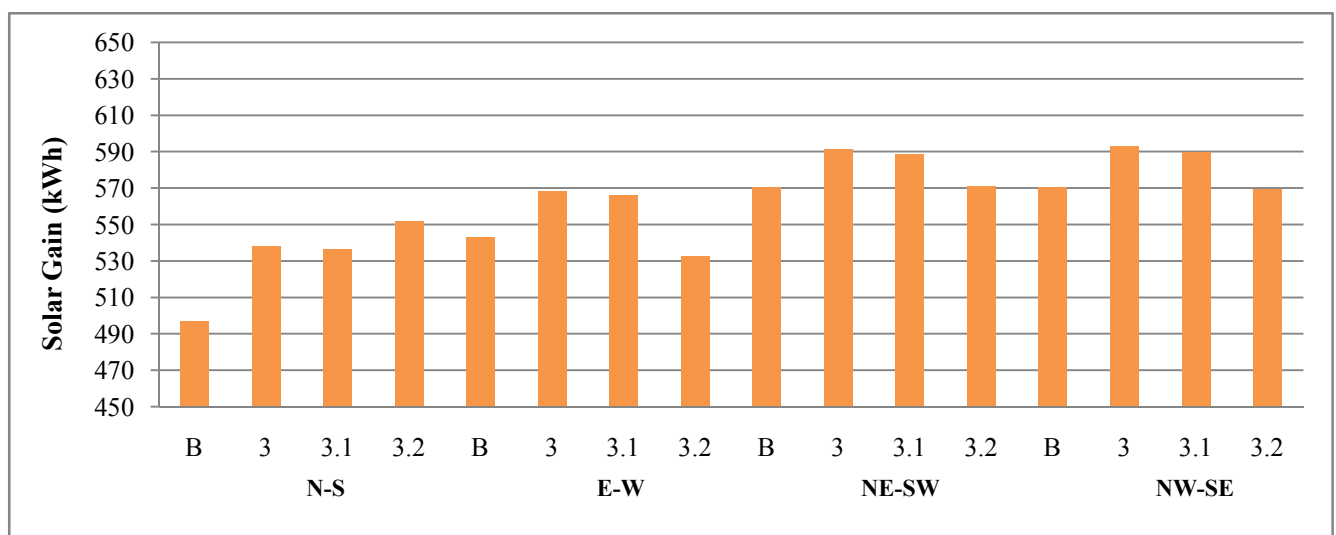
Figure7.21: The daily average of direct solar gain on 21 June for the third group configurations in the four orientations; N-S, E-W, NE-SW, and NW-SE

Figure 7.22 shows the conduction heat gain performance of the third group configurations and the base case. The conduction heat gain in the NE-SW orientation is the highest in the base case configuration compared to the other configurations and in all orientations.
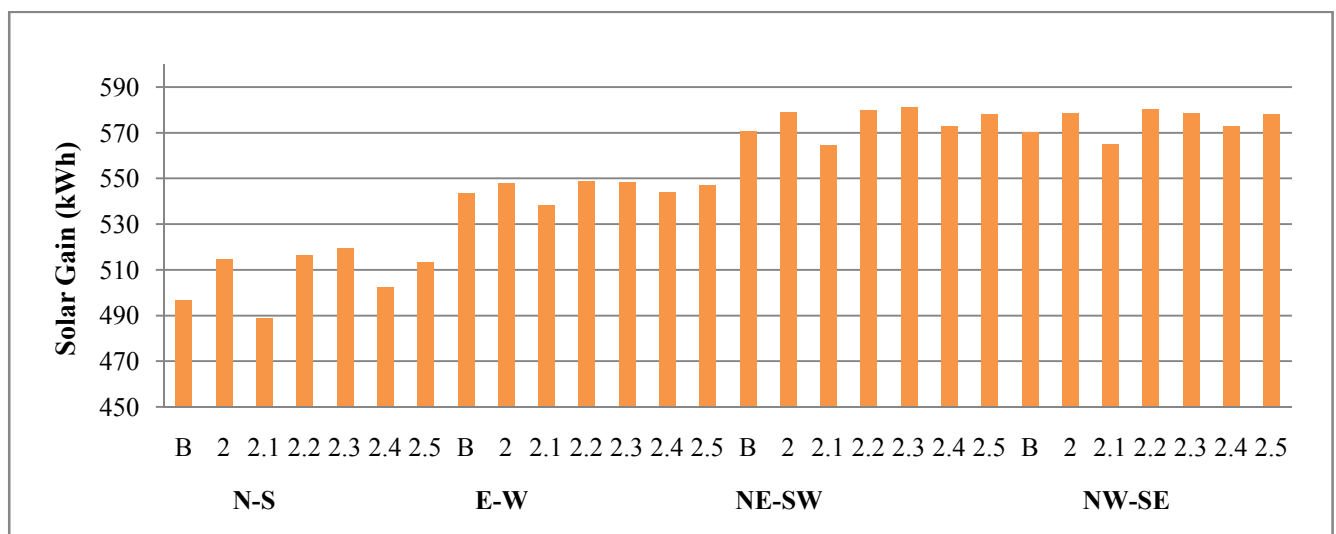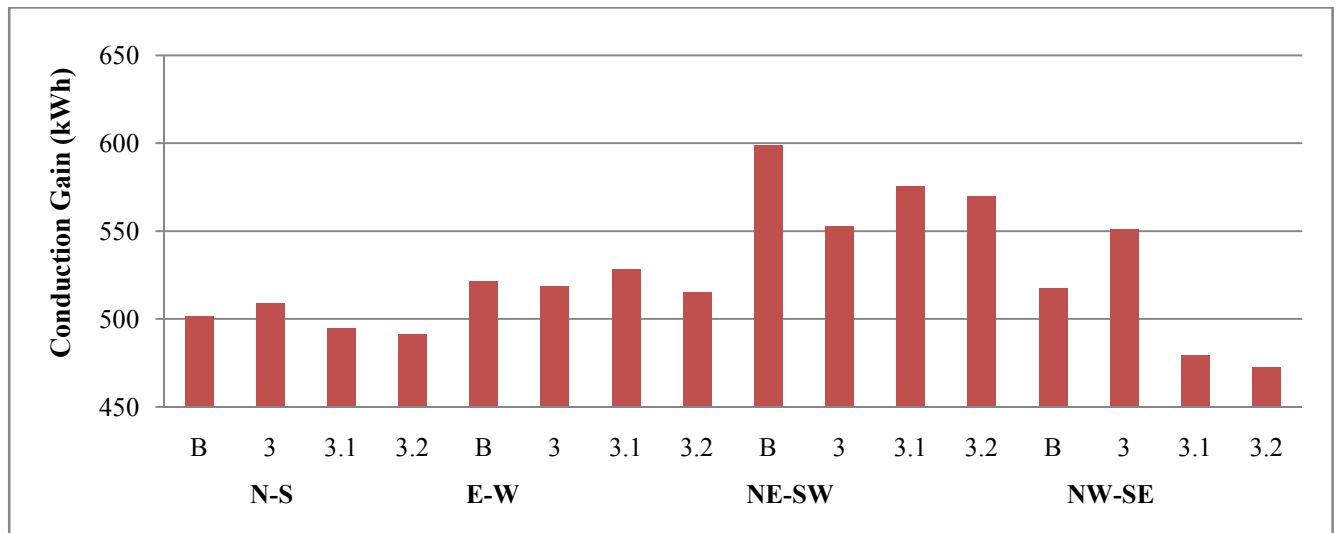
Figure 7.22: The daily average of conduction heat gain on 21 June for the third group configurations in the four orientations; N-S, E-W, NE-SW, and NW-SE

For the third group the highest reduction in conduction gain is recorded between the best performance configurations and base case. This reduction is 7.6 % in the NE-SW orientation between the best configuration G3-3.0 (20:25) and the base case. In the NW-SE orientation it is higher and reaches 9.3 % between the best configuration G3-3.2 (15:20) and the base case in this orientation. Furthermore, in the NE-SW orientation the contribution of the conduction heat gain is higher compared to the solar gain in all configurations except the G3-3.0 (20:25) configuration (Figure 67.23 a).

On the other hand, in the NW-SE orientation the effect of the direct solar gain is higher than the effect of the conduction gain in all configurations including the base case (Figure 7.23 b). The G3-3.0 (20:25) has wider alleys compared to the base case and other configuration, and it is more exposed to the NW-SE sun radiation compared to the other configurations.
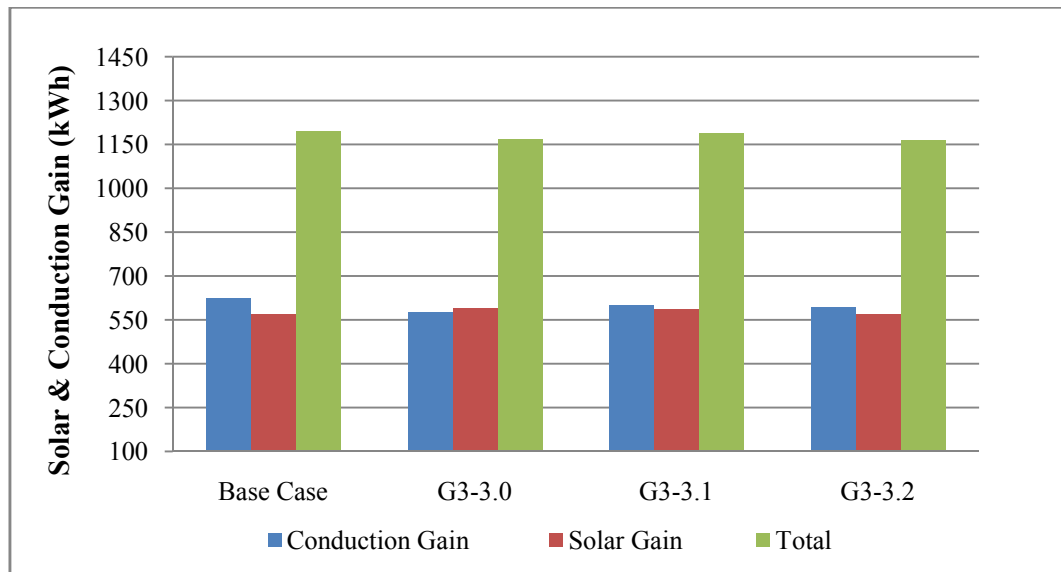
a) NE-SW orientation
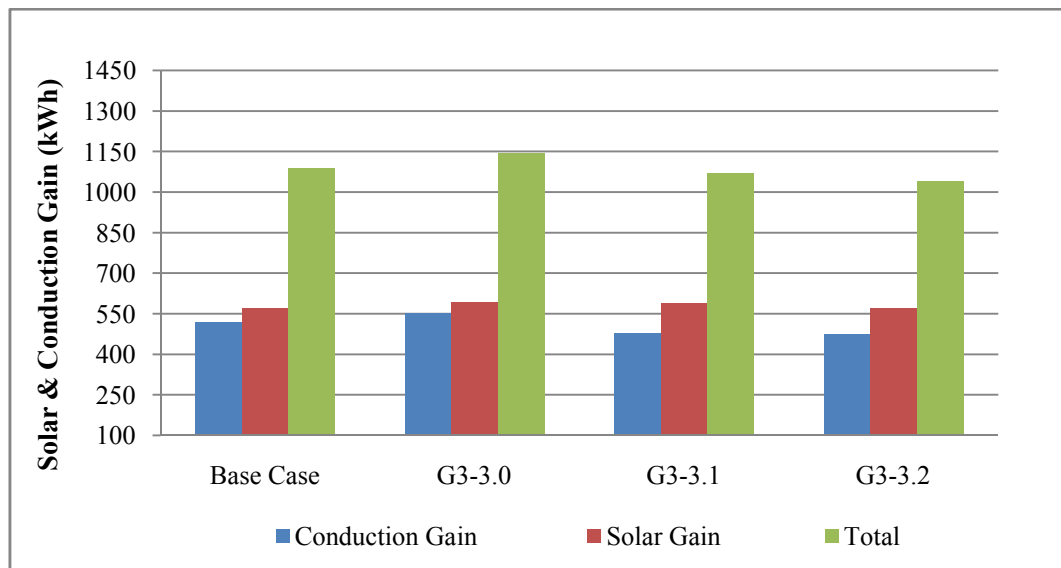
b) NW-SE orientation

Figure 7.23: The contribution of conduction heat gain and direct solar gain for the third group configurations in; a) NE-SW, and b) NW-SE orientations

7.2 The Effect of Urban Geometry and Outdoor Microclimate Parameters on Cooling Load and Energy Saving

The effect of urban geometry on the studied microclimate parameters; air temperature, wind flow and relative humidity of the building configurations was illustrated in detail in the previous chapter 6.

Further to this, the best configuration of each group with respect to minimizing the outdoor air temperature were presented and discussed. In the first section of this chapter, section (7.1), the heat gain and the cooling plant load results of the three groups configurations were presented. In this section, the best configuration of each group that optimise the cooling load and save more energy will be discussed and analysed. The discussion will cover the shading effect or the direct solar radiation, further to the conduction gain through the buildings envelope. These two parameters in additional to the internal heat gain affect the total heat gain of the indoor space for each building and, consequently the total heat gain and cooling load of the urban block.

From the results of the urban block heat gain illustrated in this chapter, it has been observed that the block and canyon orientation plays a significant role in the direct solar access and shading effect. In general, and with respect to the urban block orientation, the N-S orientation shows the best performance in reducing the cooling load. The N-S orientation recorded the lowest outdoor air temperature averages as presented, and this has a positive effect in terms of reducing the heat gain and the cooling demand of the urban block. This finding agrees well with previous studies that reported the capability of the N-S orientation to provide the highest protection from solar exposure in hot climates (Arnfield, 1990). The E-W orientation shows an approximate attitude to the N-S, but it records slightly higher averages of cooling load compared with the N-S orientation due to the higher block area exposed to the solar sun. Further to the N-S and E-W cooling load performance, the NW-SE block orientation was also observed to performs better than the NE-SW in reducing the cooling load in all groups. In general, for the NW-SE canyon orientation with of the block's long axis is facing the NE-SW direction which allows a solar exposure in the morning before the afternoon time.

The NW-SE orientation performs as a best orientation for some configurations in terms of energy saving by minimizing the indoor heat gain and, consequently, the energy required for cooling demand. On the other hand, the NE-SW canyon orientation recorded the worst performance according to the high averages of heat gain and cooling load required for the base case and all configurations. The dramatic increase of the cooling load of the NE-SW orientation is related to the highest air temperature recorded in this orientation, in addition to the high exposure to the solar sun. The NE-SW canyon orientation represents the long axis of the block facing the NW-SE orientation.

In this orientation the long facade of the block is affected by direct solar exposure in the afternoon time and implies the solar radiation on the buildings walls for longer duration. Similar findings of the high solar exposure by facing the NW-SE orientation has been reported by Ali-Toudert and Mayer (2004).

The cooling demand depends on heat gain of the buildings, and the direct solar gain is one of the heat gain resources of the buildings. The best performance of the N-S orientation in reducing the solar gain of the urban block is due to extending the long axis of the urban block along the E-W direction and the minimum duration recorded for the exposure to the sun. The N-S and the E-W orientations show similar performance according to the block and canyon orthogonal configuration. However, the E-W orientation of the block shows higher averages of solar gain and cooling loads than the N-S orientation due to the exposure of the long axis of the block to the E-W direction and higher duration of the exposure to the sun radiation.

In the same concept, the NW-SE canyon orientation reduced the direct solar exposure and recorded less solar gain. In this direction, the long axis of the block receives the solar radiation at morning before noon time, and the exposure is less duration in the afternoon time.

These results and the significant role of the orientation on the cooling load and energy saving of the urban block are in line with the findings reported by Van Esch et al. (2012). However, the outdoor microclimatic conditions affect the indoor thermal performance which in turn affects the cooling load requirements and contribute to total energy saving as reported by Arnfield (1990).

In the first group, the G1-1.2 (3:7:7:3) configuration performs as the best configuration with respect to the cooling load consumption in the three orientations N-S, NE-SW and NW-SE. The best performance of this configuration is in the NW-SE canyon orientation with a reduction in cooling load of 4.5 % compared to the base case.

This result supports the results of a previous study conducted by Ali-Toudert and Mayer (2004). The researcher claimed that the NE-SW and NW-SE orientation might provide more shading effect compared to the N-S and E-W orientation in the hot climate in summer season. The reduction in the G1-1.2 (7:3:3:7) configuration is related to the lowest maximum air temperature in the NW-SE canyon orientation. In addition to the reduction in the direct solar gain compared to the base case in the same orientation. This reduction in cooling load of the best configuration compared to the base case is a result of a reduction in the outdoor air temperature by $1.1\,^{\circ}C$ and the conduction gain by 7.5 %. Further to the reduction in the direct solar radiation of this configuration by 1.5 % compared to the base case. The reduction in cooling load is achieved by adopting the height diversity and providing more shading which reduces the direct solar access to the canyons and buildings as well. This result supports the importance of the Environmental Diversity Map presented by Edward (2010) for enhancing the outdoor and indoor thermal performance.

Furthermore, in the second group, and similar to the first group, the minimum cooling load recorded for all configuration is in the N-S followed by E-W with small variation. The cooling load best performance is in the N-S orientation for the G2-2.1 (3:5:7:7:5:3) configuration with a reduction of 1.3 % compared to the base case. On the other hand, and in the E-W, NE-SW and NW-SE orientations the best cooling load performance recorded by the G2-2.5 (5:3:7:7:3:5) configuration in these three orientations. The minimum cooling load was recorded in the NW-SE canyon orientation by the best configuration G2-2.5 (5:3:7:7:3:5) with a reduction in cooling load of 3.9 % compared to the base case.

The lowest maximum outdoor air temperature recorded for this configuration in the same orientation with a reduction of 0.9 $^\circ$C compared to the base case, and a reduction of 6.7 % in conduction gain is recorded between the best configuration and the base case.

On the other hand, the solar radiation of the G 2-2.5 (5:3:7:7:3:5) configuration in this orientation is higher by 1.3 % compared to the base case due to the diversity in buildings height and the building surfaces exposure to the solar sun. The increase of solar gain in this orientation shows that the effect of the height diversity in the long axis does not provide the required protection to the block buildings compared to the best configuration in the first group with the same orientation.

Therefore, adopting the height diversity along the short access provides more shading to the urban block and higher percentage of cooling load reduction and energy saving. From the other side, the reduction in cooling load in the G2-2.5 (5:3:7:7:3:5) configuration proves the major effect of the decrease in outdoor air temperature and the conduction gain on the indoor thermal performance and, consequently, the reduction in cooling load.

The best configurations for cooling load reduction and energy saving in the third group were recorded in the E-W and NW-SE orientations by G3-3.2 (15:20) configuration. The savings in cooling load was the highest in the NW-SE orientation with a reduction in cooling plant load of 4.9 % compared to the base case. This reduction is related to the reduction in outdoor air temperature of this configuration in the same orientation by 1.9°C compared to the base case.

The reduction in outdoor air temperature is due to the decrease in SVF by 27 % compared to the base case, and the shading effect provided for the block' canyons. However, the solar gain of the best configuration is slightly less than the base case. The NW-SE block orientation provides more shading effect as the main facade of the block is facing the NE-SW orientation and the block is extended along the NW-SE axis. This shading plays the significant role in reducing the outdoor air temperature in addition to the impact of the air flashing role in reducing the outdoor air temperature around most of the buildings' surfaces.

The reduction in cooling load with respect to the SFV reported by Al Znafer (2014). The author stated that a reduction in cooling load by 9.5 % can be achieved by a reduction of 52 % in SVF from 0.71 to 0.34. However, Al Znafer's research based on the cooling load calculation of individual building within the urban complex, while the results of the current research reflect the integrated effect of the 24 buildings of the urban block on cooling load per square meter. The shading effect at 15:00 , 21 June of the best configurations compared to the base case for the three groups in the NE-SW and NW-SE orientations are illustrated in figures 7.24, 7.25, and 7.26.
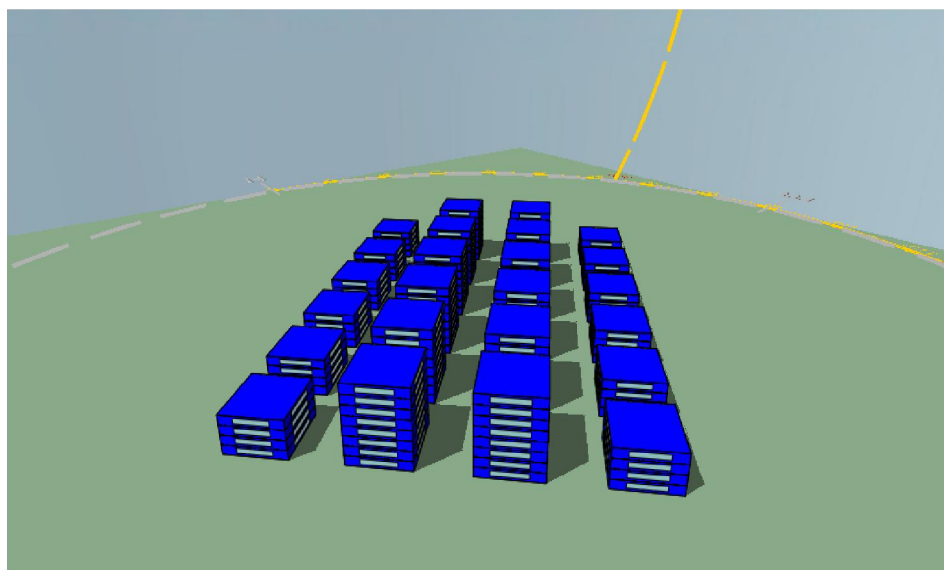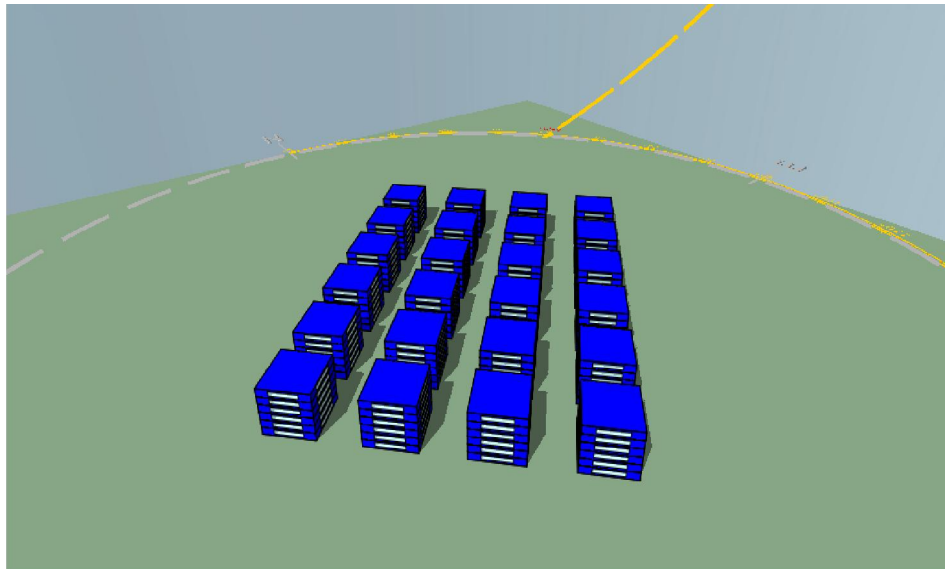
a) NE-SE orientation
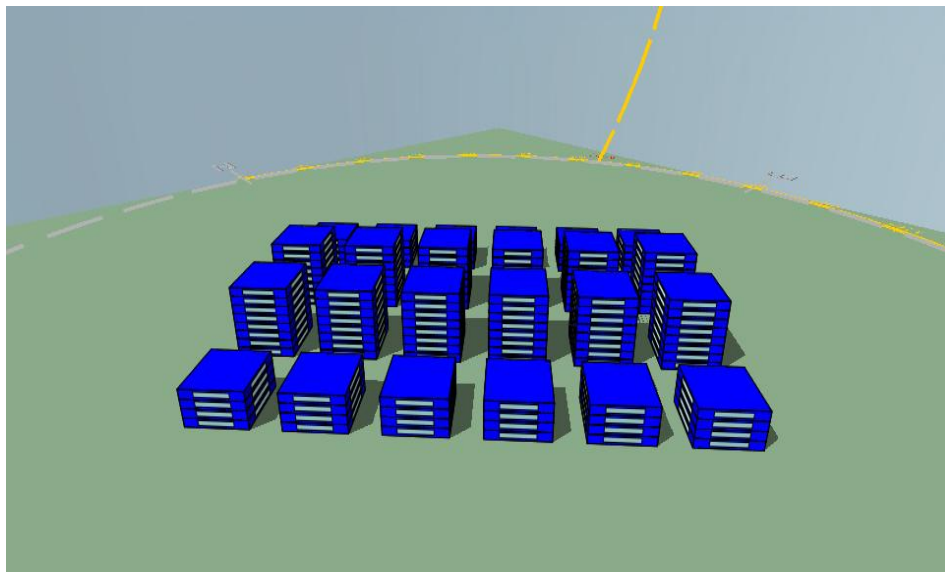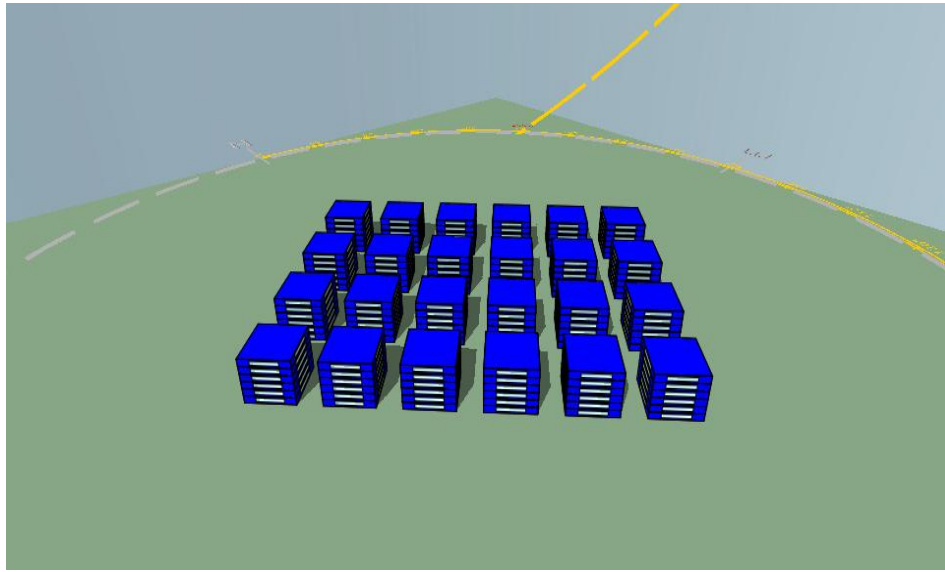
b) NW-SE orientation

Figure 7.24: The shading effect of the best configuration in the first group G1-1.2 (3:7:7:3)
compared to the base case in the; a) NE-SW and b) NW-SE orientations
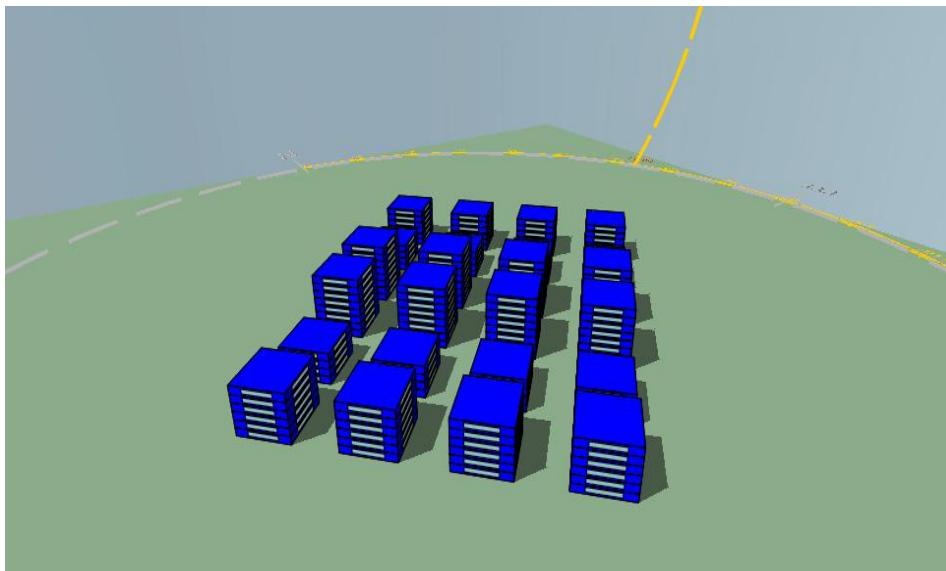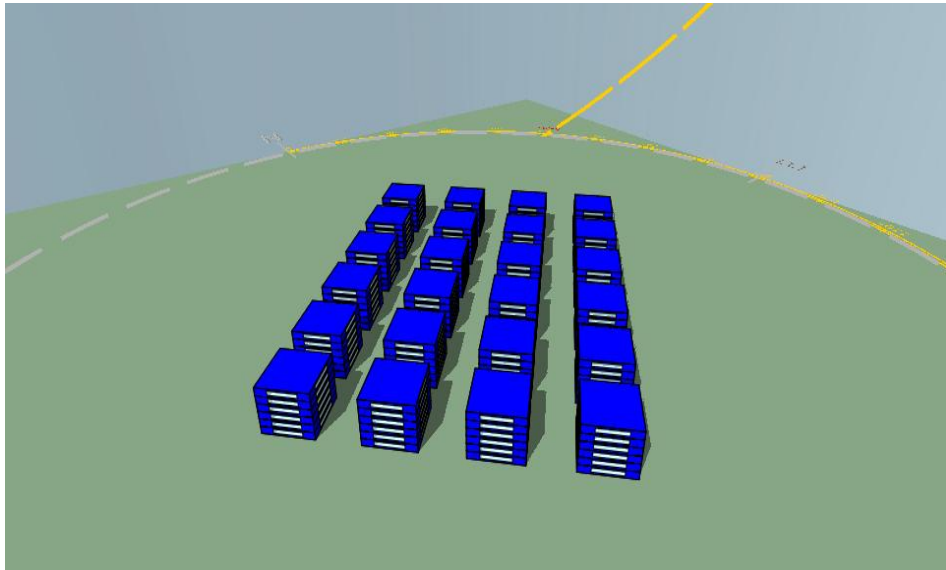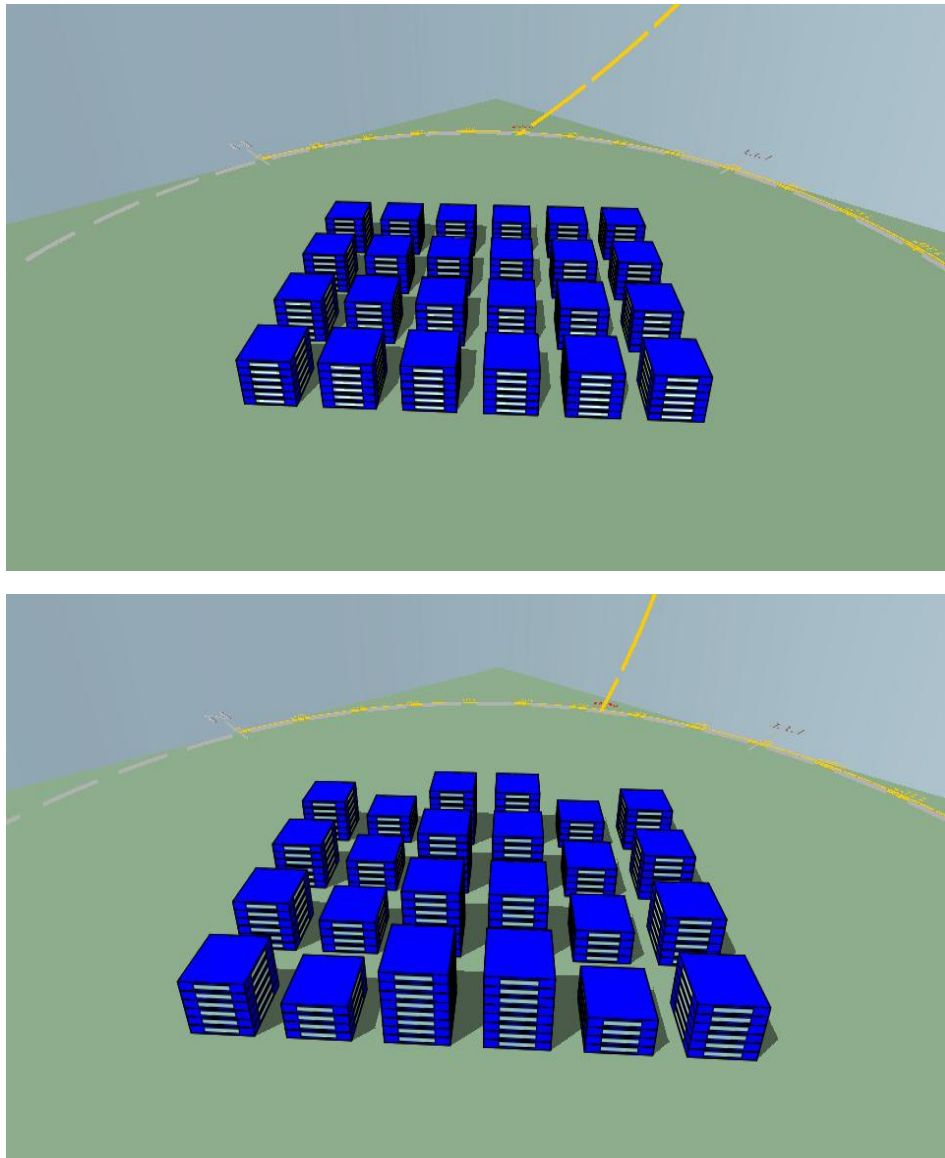
a) NE-SE orientation

b) NW-SE orientation

Figure 7.25: The shading effect of the best configuration in the second group G2 -2.5 (5:3:7:7:3:5) compared to the base case in the; a) NE-SW and b) NW-SE orientations
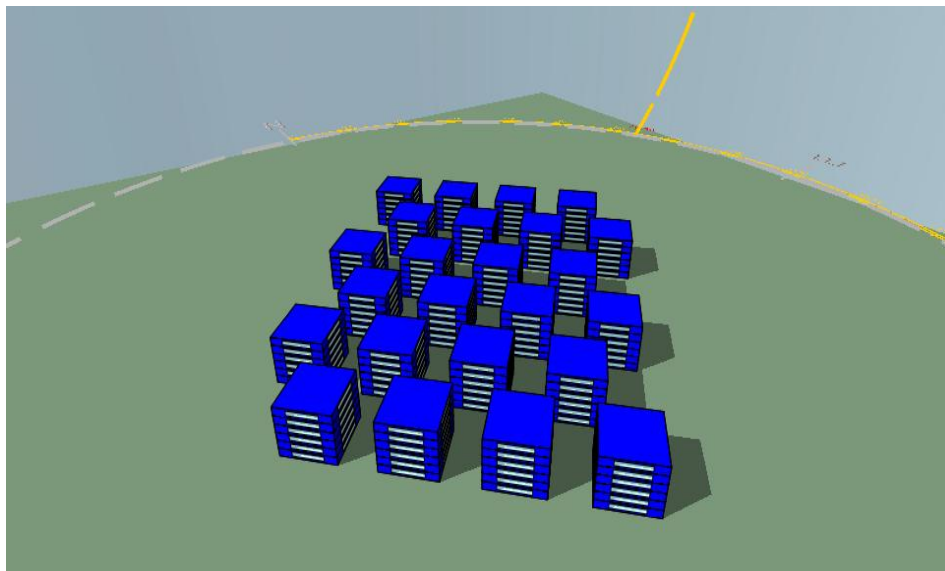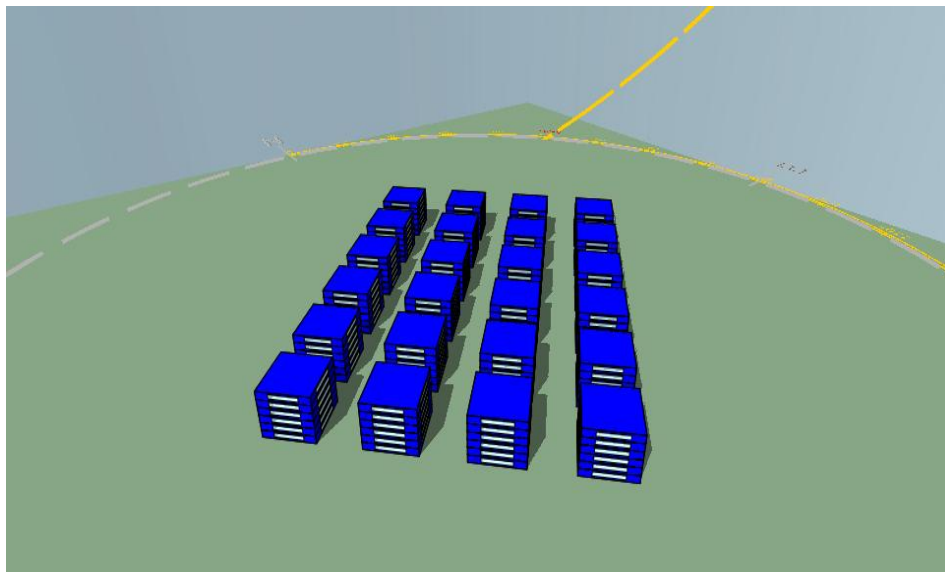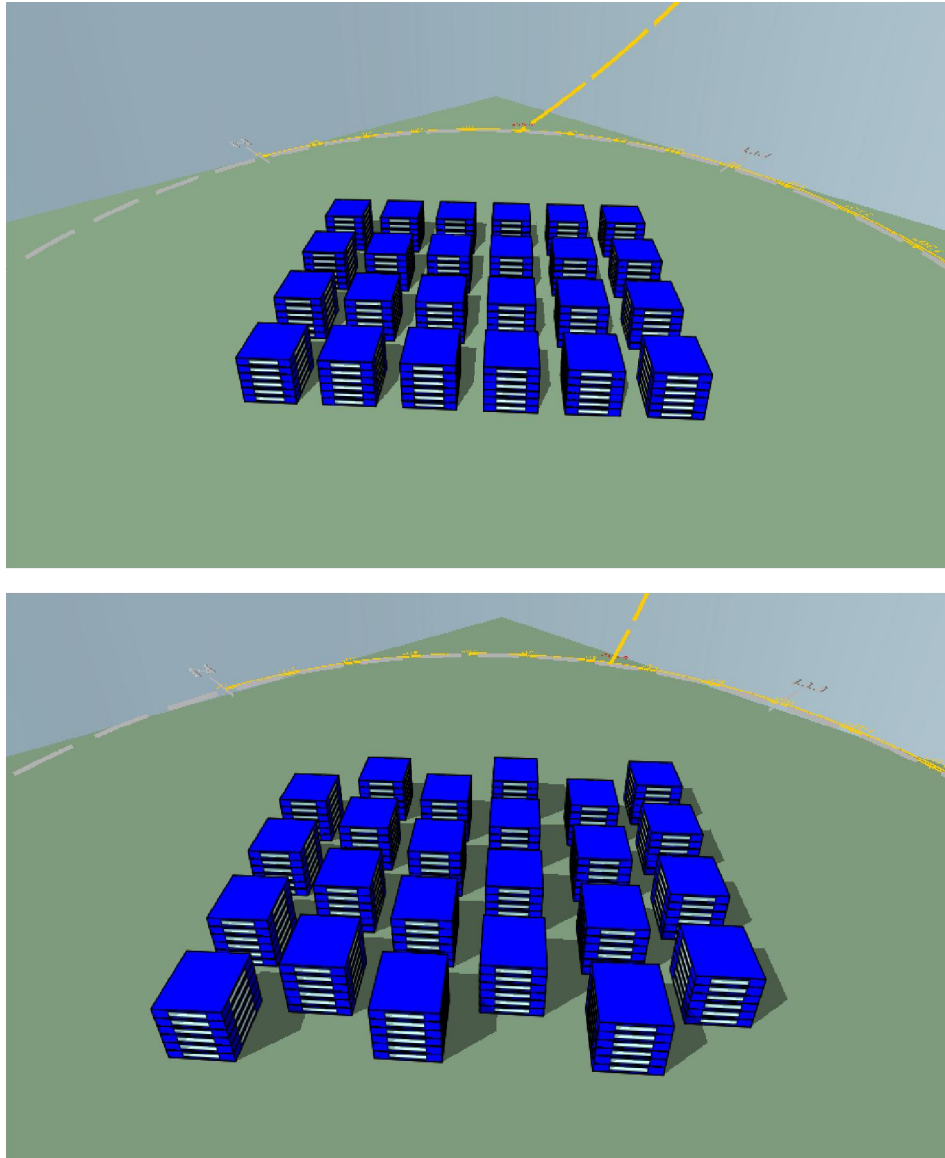
a) NE-SE orientation

b) NW-SE orientation

Figure 7.26: The shading effect of the best configuration in the third group G3-3.2 (15:20) compared to the base case in the; a) NE-SW and b) NW-SE orientations

Furthermore , in spite of the focus of this research on the cooling load calculations , it should be mentioned that the reduction in cooling load and energy consumption will be reflected positively on reducing the CO_2 emission and carbon footprint. According to DEWA (2017) , a reduction of 500 gm CO_2 emission can be achieved through 1 kWh decrease in energy consumption.

On the other hand, the wind speed profile of best performance G3-3.2 (15:20) configuration in the NW-SE shows a different outdoor thermal attitude compared to the other configurations in the same orientation as illustrated in chapter 6, section 6.1.4. The significant reduction in the wind velocity of the alternative configuration proves that the main effect of the reduction cooling load is related to the shading effect, and the reduction in SVF compared to the base case.

In the NE-SW orientation the G3-3.0 (20:25) configuration shows the best performance with a reduction in cooling load by 2.2 % compared to the base case. The performance of this configuration resulted in a reduction of 0.4 $^{\circ}$C in outdoor air temperature averages compared to the base case in the same orientation. Therefore, the variation in air temperature and the effect of the conduction gain reduced the indoor heat gain and, consequently, the energy required for cooling for the best configuration compared to the base case. However, and regardless of the SVF or the H/W ratio, the G3-3.0 (20:25) configuration, that have slightly higher SVF compared to the base case and other configurations in the third group, this configuration recorded the best performance in the NE-SW orientation with respect to minimum load required for cooling, but it shows a different attitude in the other orientations.

Therefore, the SVF is not the only indicator that reflects the thermal performance of the urban block configuration, the orientation is the crucial factor in predicting and assessing the thermal statue of the built environment. Figure 7.27 shows a matrix of the best configurations with respect to the lowest maximum air temperature and minimum cooling load recorded for the three groups compared to the base case in the four orientations. In general, it has been observed that the reduction in the SFV and the H/W ratio values for both canyons and alleys of the third configuration have major contributions towards reducing the cooling load. The average of maximum and minimum wind velocity profile for the three groups shows a clear variation in wind velocity for all of the groups configurations.

This result proves the effect of the variation in buildings height on the wind velocity profile of the urban block. The variation was observed in three orientations depending on the configuration and block orientation. The variation is higher when the height diversity facing the prevailing wind direction. For the first group configurations the variation maximum and minimum wind speed is higher in the NE-SW orientation compared to the NW-SE orientation . In the first group configurations the variation in buildings height applied to the short axis of the block, and there is no variation in building height in the direction of the prevailing wind (Figure 6.6). On the other side, this variation is higher in the NW-SE orientation compared to the NE-SW orientation for the second group configurations as the variation in buildings' height is facing the NW-SE prevailing wind direction (Figure 6.11).

This result proves the effect of the diversity in buildings height on enhancing the wind flow , especially in the direction of the prevailing wind.

Finally, this research proves that the outdoor air temperature is the major parameter that has a direct effect on indoor cooling load consumption, the reduction in outdoor air temperature reduced the conduction gain and the transferred heat from outer to inner space. Similar findings were reported by Afshari, Nikolopoulou and Martin (2013), as the researchers stated that the outdoor air temperature is the most influenced microclimate parameter on the cooling load consumption compared to the solar gain and the relative humidity. The shading effect created by the height diversity of the best configurations in the first two groups, and the stagger configurations in the third group turn in to a positive effect by reducing the outdoor air temperature and, consequently, the indoor cooling demand.

The Best Configurations of the Lowest Maximum Air Temperature

The First Group Configurations

N-S	E-W	NE-SW	NW-SE
G1-1.1 (3:7:3:7)	G1-1.1 (3:7:3:7)	G1-1.2 (3:7:7:3)	G1-1.2 (3:7:7:3)

The Second Group Configurations

N-S	E-W	NE-SW	NW-SE
G2-2.0 (7:5:3:3:5:7)	G2-2.5 (5:3:7:7:3:5)	G2-2.5 (5:3:7:7:3:5)	G2-2.5 (5:3:7:7:3:5)

The Third Group Configurations

N-S	E-W	NE-SW	NW-SE
G3-3.2 (15:20)	G3-3.2 (15:20)	G3-3.0 (20:25)	G3-3.2 (15:20)

The Best Configurations of the Minimum Cooling Load

The First Group Configurations

N-S	E-W	NE-SW	NW-SE
G1-1.2 (3:7:7:3)	G1-1.1 (3:7:3:7)	G1-1.2 (3:7:7:3)	G1-1.2 (3:7:7:3)

The Second Group Configurations

N-S	E-W	NE-SW	NW-SE
G2-2.1 (3:5:7:7:5:3)	G2-2.5 (5:3:7:7:3:5)	G2-2.5 (5:3:7:7:3:5)	G2-2.5 (5:3:7:7:3:5)

The Third Group Configurations

N-S	E-W	NE-SW	NW-SE
G3-3.2 (15:20)	G3-3.2 (15:20)	G3-3.0 (20:25)	G3-3.2 (15:20)

Figure 7.27: The matrix of the best configurations of the lowest maximum air temperature and minimum cooling load for the three groups compared to the base case in the four orientations

Chapter 8

Conclusion and Recommendations

8.0 Conclusion and Recommendations

The aim of this research is find the effect of the urban geometry on indoor cooling load energy consumption. To achieve this aim a number of objectives were identified. The literature review as a method of study was conducted and the significant urban geometry variables were indicated. The selected variables of the urban geometry explored covered; urban block orientation, height diversity and block configuration. The impacts of the mentioned geometry variables were investigated on both indoor and outdoor thermal and energy performance of the urban block. The software simulation methodology was implemented to explore fifty six proposed scenarios, and the result covered the effects of the studied variables on the outdoor microclimate parameters and indoor energy savings. The outdoor thermal performance results covered: shading effect, air temperature, wind speed, and relative humidity. The indoor thermal performance and energy savings were assessed in terms of the buildings' heat gain and cooling load. This research investigated the effect of integrating the changes occurred on outdoor microclimate parameters due to the variation in urban geometry variables to the indoor cooling load of the urban block. It explored the amount of the energy that can be saved from the interactive performance of the buildings within the same block or complex. In general, it has been found that the changes in the urban geometry variables have a notable effect on cooling load.

The outdoor air temperature and the conduction heat gain have more significant impact on the indoor cooling load compared to solar radiation effect. The 21 of June has been selected for running the simulation process as it is the longest day in the year , and the variation in urban geometry variables addressed the solar radiation effect on indoor cooling load.

Selecting another day for running the simulation process such as the warmest day of the year in August, different impact on indoor cooling load will be expected. The increase in outdoor air temperature will increase the conduction heat gain, and consequently the indoor cooling load. Further to that the average microclimate data of the urban block was extracted from the nine receptor points mentioned in the chapter 4. The sensitivity analysis was conducted to find out the receptors' location impact on the results, and no significant variation has been observed between the receptors data and the average data in the (x,y) plain at height of 1.4 m. The outdoor air temperature in the middle of the canyons and the air temperature near the buildings surface is very close, and a strong correlation between the data of the selected points for the receptors in the middle of the canyons and the data of the points close to the buildings' surfaces, therefore, the receptors data reflects properly the average of the maximum air temperature for the proposed block.

The correlation between the receptors data and the data of the points close to the buildings' surfaces on (x,y) plain is illustrated in appendix A.3. However, the effect of the buildings surfaces' temperature on indoor thermal performance and cooling load is calculated by the IES-VE software. The IES-VE calculated the effect of conduction heat gain on indoor cooling load of the base case and the proposed configurations.

In order to find the sensitivity of the receptors selection in Z direction, a sensitivity analysis was carried out and the maximum air temperature data at different heights cover; 1.4 m, 5 m, 11 m, and 17 m was extracted. It has been found that by increasing the height of the receptors or moving upward in (z) direction towards the top of the buildings , the air temperature will decrease. The decrease in maximum air temperature should affect the cooling load positively by reducing the conduction heat gain, and consequently the indoor heat gain and the cooling load. In this research the peak cooling load is targeted and the highest maximum temperature from the receptors were recorded is at 1.4 m , this temperature

was adopted to evaluate the cooling load of the urban block using the IES-VE software. The table of the air temperature receptors and the selected points data in (z) direction is presented in appendix A.3.

8.1 The Effect Urban Geometry on Outdoor and Indoor Thermal Performance

8.1.1 The Effect of the Block Orientation

The urban block orientation has the major influence on both outdoor microclimate parameters and indoor energy consumption. Conducting the simulation process for the developed urban block in four orientations showed that the N-S orientation was the best orientation for minimizing the outdoor air temperature and indoor energy consumption. This is mainly related to the least duration of exposure to the solar sun in this orientation during the simulated day 21 of June. The E-W orientation showed a similar trend with slightly higher averages compared to the N-S. The similarity in the trends of the E-W to the N-S was due to the rectangular shape of the grid configuration and the orthogonal type of the developed urban block. However, the slight increase in air temperature averages and cooling load of the E-W orientation compared to the N-S orientation is related to the longer axis of the block that is facing the E-W afternoon solar radiation. However, the NW-SE orientation shows a better performance than the NE-SW in terms of the lowest maximum air temperature averages and solar gain. The better performance for this orientation is related to the direction of the longer facade of the block as the main facade facing the NE-SW orientation and exposed to the morning sun and less duration of the solar gain before the noon afternoon time.

On the other hand, the NE-SW orientation exposure had the maximum solar radiation in the afternoon time. This orientation affects both outdoor and indoor thermal performance. In addition to that, the N-S and NW-SE orientations utilise the advantages of the prevailing wind to enhance the airflow in the main canyons and reduce the outdoor air temperature.

The maximum reduction in air temperature achieved by the base case between the N-S and NE-SW orientations reached to 1.8 $^{\circ}$ C and 5 %, the reduction in solar gain reached to 13 %.

This reduction in outdoor air temperature and solar gain translated to a reduction in the cooling load of the base case by 6.4 % between the N-S and NE-SW orientations, and this reduction reached 6.6 % at the peak time of cooling load consumption at 15:30.

8.1.2 The Effect of the Height Diversity

This study added new findings which is related to the height diversity effect of the urban block on outdoor and indoor thermal and energy performance. Implementing the height diversity on both short and long axis of the developed block with different ratios or proportions shows some interesting facts.

Firstly, the effect of the height variation in the short axis of the block is more significant than the effect of the variation in the long axis of the block. Furthermore, adopting the significant variation is more effective than the gradual variation with respect to the enhancement in outdoor thermal performance and indoor energy saving.

In general, and as mentioned in the effect of the block orientation, implementing the height diversity shows the same performance for the N-S and E-W orientations. These orientations perform as the best for all developed configurations for both outdoor and indoor thermal performance.

The notable variation in the block's thermal characteristics was observed in the NE-SW and NW-SE orientations between the base case and the developed scenarios. The NE-SW orientation shows the worst performance with respect to the outdoor and indoor thermal performance compared to the three other orientations. Placing the highest buildings in the middle of the block enhanced the outdoor thermal performance, which reflected positively in terms of a lower indoor cooling load.

In this research two height proportions' groups were explored (3:7) and (3:5:7). The first group had four configurations, while the second one had six configurations. Each of the ten configurations were simulated in four orientations. This resulted in forty combinations of outdoor and indoor thermal performance parameters.

For the first group, the G1-1.2 (3:7:7:3) configuration performed the best configuration in the two orientations NE-SW and NW-SE, while the G1-1.1 (3:7:3:7) performed the best in the N-S and E-W orientation. These findings prove that the significant height performs better in the NE-SW and NW-SE orientations. The fluctuated variation in buildings' height performs better than the uniform and the significant variation in the two other orientations; N-S and E-W. The maximum reduction in outside air temperature obtained was in the NW-SE orientation with a decrease of $1.1\,^{\circ}$C compared to the base case.

The reduction in solar gain reached 1.5 % and the reduction in the cooling load was 4.5 %. For the gradual height variation and implementing the height variation along the long axis of the urban block the G2-2.5 (5:3:7:7:3:5) configuration performed as the best configuration in the three orientations.

The maximum reduction in the outside air temperature reaches $0.9\,^{\circ}$ C. The maximum decrease in cooling load obtained from this configuration was 3.9 % in the NW-SE orientation.

Therefore, the gradual height in the long axis of the urban block of the G2-2.5 (5:3:7:7:3:5:) configuration performs better than the significant height with respect to the shading effect and wind velocity.

This performance is better when the block oriented towards the prevailing wind direction. However, the reduction in outdoor air temperature and, consequently, in cooling load was related to the shading effect created by the height diversity and the reduction in outdoor air temperature and conduction heat gain through the building envelop.

Furthermore, the research proves the effect of the height diversity on enhancing the wind velocity within the block, and the positive effect of the wind speed on decreasing the outdoor air temperature and, consequently, the indoor heat gain and cooling load.

As for the SVF effect, it was found that the SVF does not properly reflect the amount of shading that can be provided for a configuration. The SVF represents the amount of the sky that can be observed from specific point , the sun angle and location of this point with respect to the sun path are taken in to consideration in the solar radiation and shading effect calculations. Therefore, the orientation of the urban block combined with diversity in the buildings' height are more crucial factors in properly indicating the amount of area exposed to the solar radiation, and consequently the shading that can be provided by the configuration.

However, and regardless of the effect and the value of the SVF, it was found that the block orientation plays most significant role in indicating the best configuration for each direction, specifically when adopting the building height diversity to enhance the thermal performance. For configurations with comparable SVF values, the orientation and the sun path effect as well as the amount of the shading created by different configuration play the major role in determining the best configuration for each orientation.

Furthermore, this research proves that the height diversity as an urban geometry variable has a significant effect on the wind velocity. Implementing the height diversity with significant variation in the direction align with the prevailing wind enhance the wind velocity within the urban' canyons and alleys. This enhancement in wind speed reaches the maximum in the NW-SE prevailing wind orientation. Therefore, the significant variation in buildings' height and placing the highest buildings in the middle of the block provided more energy saving by reducing the outdoor air temperature and, consequently, the cooling load.

On the other hand, placing the highest buildings in the middle of the block and adopting the gradual height variation on the long axis of the block improved the air flow in the canyons. This increase in wind speed reached 16 % in the G2-2.1 (3:5:7:7:5:3) configuration, and 18 % in the fluctuated configuration G2-2.5 (5:3:7:7:3:5).These two configurations have the same SVF of 0.41, and a slight variation of 0.2°C in maximum air temperature averages in the NW-SE orientation.

This research proves the effect of the enhancement in wind velocity on reducing the outdoor air temperature. This reduction results in a reduction of indoor energy required for cooling and thus enhanced energy savings.

Therefore, and in additional to the shading effect that can be increased by implementing the building height diversity on the urban block, the effect of the prevailing wind can play an effective role in decreasing the outdoor air temperature and indoor cooling load. Thus, this research proves the capability of adopting the buildings height as an urban geometry variable to benefit from the potential of the prevailing wind in energy saving.

8.1.3 The Effect of the Block Configuration

The effect of the urban block alternative configuration on outdoor and indoor thermal performance represents one of this research's main objectives. The staggered or the alternative arrangement of the buildings in urban block was implemented in both the long and short axis of the urban block. The staggered arrangement generated different H/W ratios for the block canyons. The main and significant finding of this type of configurations shows that the alternative arrangement reduces the wind velocity in the direction of the prevailing wind.

The wind profile of the stagger configurations show a clear variation for all configurations in the four orientation (Figure 6.16). The stager arrangement created an obstruction to the wind flow and reduced the wind velocity. This finding proves the significant impact of buildings arrangement on the wind velocity within the urban block. However, the wind movement and air distribution have been enhanced in main strait canyon specifically in the NW-SE prevailing wind direction.

The best performance with respect to the lowest maximum air temperature averages was the G-3.2 (15:20) configuration in which the air temperature average was reduced by 1.9 °C and cooling load reduced by 4.9 %.

These reductions are mainly related to the reduction in the SVF due to the reduction of the main canyon width to achieve the alternative configuration. However, a significant reduction in wind velocity recorded as this type of configuration reduces the wind velocity in the direction of the alternative arrangement. This arrangement obstructs the wind flow and reduces its speed. Therefore, the best configuration provides more shading effect and reduces the outdoor air temperature and consequently the cooling load.

On the other hand, it decreases the wind velocity, whereas the air movement has been enhanced around most of the buildings. Therefore, designing the urban block in a pavilion grid buildings' arrangement with strait canyons performs better than the block with staggered arrangement with respect to the enhancement of the air velocity. The obstruction created by arranging the buildings attentively results in decreasing the wind speed. On the other hand, it provides a general enhancement in wind flow. Therefore, the staggered arrangement enhances the canyons' ventilation but doesn't affect the air temperature averages significantly compared to the shading effect.

Furthermore, the G3-3.0 (20:25) configuration has H/W ratios higher than that of the base case and the other staggered configurations the same group. The results show that increasing the H/W ratio in the G3-3.0 (20:25) configuration increases the total block solar gain slightly.

However, this configuration shows the best cooling load performance in the NE-SW orientation compared to the base case. The G3-3.0 (20:25) configuration recorded lower cooling load due to the effect of the lower outdoor air temperature and conduction heat gain recorded in the NE-SW orientation.

This result proves the significant effect of the conduction heat gain compared to the direct solar gain on the urban block cooling load reduction and energy saving.

On the other hand, the same configuration G3-3.0 (20:25) shows different outdoor thermal behaviour and in door cooling load performance. This prove the significant role of the orientation on outdoor and indoor thermal performance of the urban block.

8.2 Urban Block Design and the Consideration for Climatic Design

Urban block orientation and the relation between the buildings and the streets of an urban block have a major impact on the micro outdoor thermal performance and consequently indoor energy consumption.

Urban planning roles and regulations are the crucial tool that control the urban design in order to achieve the optimised plan of the best environmental performance. However, the best performance with respect to the outdoor and indoor thermal comfort and energy saving varies according to the location of the proposed urban development. This study is conducted to find the urban geometry effect on energy consumption in the hot climatic conditions represented by the case study area, Dubai, UAE climate. Therefore, all the recommendation obtained from this research is advised to be implemented in the same climate conditions.

In general, the urban block with a length of the long axis higher by 75 % than the short axis is recommended. This block preferred alignment is along the E-W or NW-SE orientations. Extending the urban block along the E-W and NW-SE orientations to face the N-S and NE-SW orientations enhances the micro outdoor thermal performance and provides the maximum energy saving as well. Furthermore, orienting the block towards the NW-SE captures the maximum effect of the prevailing wind to enhance the canyon ventilation and reduce the air temperature.

The N-S and E-W orientations of the grid urban block configurations are the best orientations that reduces the heat gain and energy required for internal cooling load. In addition to the positive effect of these orientations on enhancing the micro outdoor thermal comfort in the grid block configuration. The grid, orthogonal arrangement for the buildings results in a straight canyon that promotes the wind speed specifically in the prevailing wind direction. The findings of this study show that in the N-S and E-W orientations, the significant fluctuated height diversity of the buildings within the urban block is recommended. This diversity is preferred to be significant in the short direction of the urban block in order to achieve the maximum reduction in cooling load and save the energy required for this

purpose. Furthermore, significant variation in buildings' height is preferred in the prevailing wind direction, and this direction represented by the N-S and NW-SE orientations according to the climatic conditions of the case study area.

On the other hand, the gradual fluctuated diversity in buildings height is preferred to be implemented in the long axis of the urban block in three orientations: E-W, NE-SW, and NW-SE. This configuration enhances the outdoor thermal performance and reduces the indoor cooling load. Further to that , the height diversity will increase the potential of implementing 'Building Integrated Photovoltaic BIPV' system on the building's facade with higher exposure to the solar radiation , this opportunity could not be a achieved by adopting the uniform height or increasing the H/W ratio. Also the height diversity has a positive effect on increasing the viewshed factor compared to the uniform height, and this will be reflected positively on the occupants wellbeing and buildings' natural ventilation.

However, the best performance of the three types of proposed block; suggested configurations or diversity in short and long directions of the block is recommended, the height diversity can provide more shading compared to the base case configuration while keeping the canyon width with same averages. Furthermore, the height diversity improves the wind velocity, which positively affects the micro outdoor air temperature and reduce the maximum air temperature averages. This enhances the micro outdoor thermal comfort by reducing the relative humidity averages. Furthermore, the alternative option of urban block configuration for reducing the maximum outdoor air temperature is the stagger or alternative arrangement for buildings within the complex. This configuration can provide low SVF and more shading can be achieved.

This type of building configuration reduces the wind velocity within the block canyons, but it enhances the air movement and redistributed the air around most of the buildings. It can be a preferred configuration in locations or areas with a stormy wind of an averages to reduce the

wind speed and enhance the air flow and distribution around the buildings. However, the orientation plays a significant role in this configuration as well. The staggered arrangement can be implemented in the E-W and NE-SW orientations of high exposure to the sun to create the shading required from solar radiation. However, the reduction in wind speed may have a negative effect on the outdoor relative humidity.

In humid locations, it is preferred to increase the wind velocity to adopt the potential of the prevailing wind on reducing the humidity averages and enhance the outdoor air quality. Furthermore, the reduction in relative humidity affects the indoor energy consumption positively. It reduces the cooling load and the energy required for dehumidification. Therefore, the grid, pavilion configuration that form straight canyons are more preferred for high humidity locations compared to the staggered arrangement.

Recommendation for Future Studies

This research explored the impact of the urban geometry on the outdoor microclimate parameters and consequently on the indoor energy consumption. Three major urban geometry variables were explored: building height diversity, building configurations, and the urban block orientation. In additional to different H/W ratios or SVF values of that represents the variation in the developed configurations. The height diversity was implemented with specific ratios (3:7) and (3:5:7), in the future studies more proportions can be investigated with a significant or gradual variation in buildings height. Investigating more proportions, specifically in the significant diversity of buildings height may results with more increase in shading effect or wind velocity. Moreover, the building configuration or stagger arrangement covers a number of H/W ratio varied between 0.96 and 1.6, and more H/W ratio for buildings configurations can be explored.

Other than that, a future study may explore the effect of integrating the stagger arrangement with the diversity in buildings height to find this influence on outdoor and indoor thermal parameters.

Furthermore, the effect of the buildings height diversity on the viewshed factor can be explored. The enhancement of the buildings height diversity on the viewshed can be investigated to find the economic advantages that can be added to the building compared to the uniform height of the urban block buildings.

Further to that, the effect of the mentioned variables on the outdoor thermal performance has been investigated. For future studies, more urban geometry variables can be included to find their effect on the outdoor microclimate parameters, such as urban surfaces material and building cladding materials.

Furthermore, the effect of a number of urban design elements can be studied such as vegetation, green areas and water features. The effect of these variables can be studied on canyon level as well as on buildings level. The green roofs can be investigated to find it is influence on both indoor and outdoor thermal performance, in additional of providing better view from the adjacent buildings and increasing the liveability factor.

However, this research studied the major outdoor micro climate parameters covers; solar gain that reflects the shading effect, air temperature, wind speed and relative humidity. The solar gain included direct solar radiation and the conduction heat gain. The direct solar radiation represented by the short-wave radiation, more specific parameters can be included in the total solar gain such as the effect of the diffused and long wave radiation. The aim of this study is to investigate the effect of the variation in urban geometry variables on indoor energy consumption. The indoor energy consumption is expressed by the cooling load, another parameter of energy consumption can be included, such as lighting consumption.

Moreover, the total heat gain of the block is a summation of the internal and external gain, and this research concentrated on the external gain. Future research can be conducted to find the effect of the internal gain variables such as total block occupancy and buildings equipment on the total gain, and consequently the cooling load and energy consumption. Furthermore, the indoor cooling load or energy consumption is influenced by the insulation and building envelop materials, different types of insulation materials can be investigated to find their effect on reducing cooling load and optimising the energy consumption.

Furthermore, the glazing implemented on the buildings of the urban block configuration is with a percentage of 30 % , reducing this percentage can be investigated to find out the reduction in the buildings heat gain, and consequently the reduction that can be achieved in cooling load of the urban block.

References

Abohela, I., Hamza, N. & Dudek, S. (2013). Effect of roof shape, wind direction, building height and urban configuration on the energy yield and positioning of roof mounted wind turbines. *Renewable Energy*, vol. 50, pp.1106-1118.

Afshari, A., C. Nikolopoulou, M. & Martin (2013). Development of a Demand-Side Marginal Cost of Carbon Abatement Curve for the Emirate of Abu Dhabi. *International Conference on Green Energy for Sustainable Development.*

Ai, Z. & Mak, C. (2015). From street canyon microclimate to indoor environmental quality in naturally ventilated urban buildings: Issues and possibilities for improvement. *Building and Environment*, vol. 94, pp.489-503.

Aida, M., (1982). Urban albedo as a function of the urban structure – a model experiment (Part I). *Boundary-Layer Meteor*, vol. 23, pp.405-413.

Al-ajmi, F. & Loveday, D. (2010). Indoor thermal conditions and thermal comfort in air-conditioned domestic buildings in the dry-desert climate of Kuwait. *Building and Environment*, vol.45(3), pp.704-710.

Al-Masri, N. & Abu-Hijleh, B. (2012). Courtyard housing in midrise buildings: An environmental assessment in hot-arid climate. *Renewable and Sustainable Energy Reviews*, vol. 16 (4), pp.1892-1898.

AL SA'FAT, Dubai Green Building Evaluation System, version 1.0 (2016).

Al-Sallal, A. & Al-Rais, L. (2012). Outdoor airflow analysis and potential for passive cooling in the modern urban context of Dubai. *Renewable Energy,* vol.38, pp. 40-49.

Ali-Toudert, F. & Mayer, H. (2004).Planning-oriented assessment of street thermal comfort in arid regions. *The 21th Conference on Passive and Low Energy Architecture.* Eindhoven, Netherlands, Sep.19 - 22.

Ali-Toudert, F. & Mayer, H. (2006). Numerical study on the effects of aspect ratio and orientation of an urban street canyon on outdoor thermal comfort in hot and dry climate. *Building and Environment*, vol. 41 (2), pp. 94-108.

Ali-Toudert, F. & Mayer, H. (2007). Effects of asymmetry, galleries, overhanging façades and vegetation on thermal comfort in urban street canyons. *Solar Energy*, vol. 81 (6), pp. 742-754

Alsema, E., Anink, D., Meijer, A., Straub, A. and Donze, G. (2016). Integration of Energy and Material Performance of Buildings: I=E+M. *Energy Procedia*, vol.96, pp.517-528.

Al Znafer, B. (2014) The Impact of Neighbourhood Geometries on Outdoor Thermal Comfort and Energy Consumption from Urban Dwellings. PhD Thesis. Cardiff University, UK.

Andreou, E. & Axarli, K. (2012). Investigation of urban canyon microclimate in traditional and contemporary environment. Experimental investigation and parametric analysis. *Renewable Energy*, vol. 43, pp.354-363.

Andreou, E. (2013). Thermal comfort in outdoor spaces and urban canyon microclimate. *Renewable Energy*, vol. 55, pp.182-188.

Andreou, E. (2014). The effect of urban layout, street geometry and orientation on shading conditions in urban canyons in the Mediterranean. *Renewable Energy*, vol. 63, pp.587-596.

Arnfield, A. J. (1990). Street design and urban canyon solar access. *Energy and Buildings*, vol. 14(2), 117–131.

Arnfield, A. & Grimmond, C. (1998). An urban canyon energy budget model and its application to urban storage heat flux modelling. Energy and Buildings, vol. 27 (1), pp. 61-68.

ASHRAE. (2009) . *Handbook - Fundamentals (2009) c*. American Society of Heating,

Refrigerating and Air-Conditioning Engineers, Inc.

Badland, H., Whitzman, C., Lowe, M., Davern, M., Aye, L., Butterworth, I., Hes, D. and Giles-Corti, B. (2014). Urban liveability: Emerging lessons from Australia for exploring the potential for indicators to measure the social determinants of health. *Social Science and Medicine*, vol.111, pp.64-73.

Bady, M., Kato, S. & Huang, H. (2008). Towards the application of indoor ventilation efficiency indices to evaluate the air quality of urban areas. *Building and Environment*, vol. 43(12), pp.1991-2004.

Bassett, T. et al. (2012). Solar potential of the urban fabric with Sketch Up and HTB2. *In:*

Solar Building Skins Conference. Bressanone, Italy, Dec. 6-7.

BBC Weather. (2018). [online]. [Accessed 16 Jan. 2018]. Available at: http://www.bbc.com/weather

Berardi, U. (2016). The outdoor microclimate benefits and energy saving resulting from green roofs retrofits. *Energy and Buildings*, vol.121, pp.217-229.

Berger, T., Amann, C., Formayer, H., Korjenic, A., Pospichal, B. & Neururer, C. et al. (2014). Impacts of urban location and climate change upon energy demand of office buildings in Vienna, Austria. *Build Environment* , vol. 81, pp.258.

Beaufort (1805). [online]. [Accessed 16 Jan. 2018]. Available at: http://Beaufort Wind Scale Developed in 1805 by Sir Francis Beaufort, U.K. Royal Navy

Boutet, T. (1987).*Controlling air movement*. New York: McGraw-Hill.

Brown, R. (2012). Book Review: Urban Microclimate: Designing the Spaces Between Buildings. *Urban Studies*, vol. 49(5), pp.1157-1159.

Brown, R., Vanos, J., Kenny, N. & Lenzholzer, S. (2015). Designing urban parks that ameliorate the effects of climate change. *Landscape and Urban Planning*, vol. 138, pp.118-131.

Bruse, M. & Fleer, H. (1998). Simulating surface plant air interactions inside urban environments with a three dimensional numerical model. *Environmental Modeling and Software*, vol. 13(3-4), pp.373-384.

Bruse, M. (1999). *The Influences of Local Environmental Design on Microclimate*. PhD. Thesis. University of Bochum, Bochum.

Business Bay Development Code, (2005). Dubai Properties (DP), Dubai, UAE.

Cao, A., Li, Q. and Meng, Q. (2015). Effects of Orientation of Urban Roads on the Local Thermal Environment in Guangzhou City. *Procedia Engineering*, vol.121, pp.2075-2082.

City forms.(2015). [online]. [Accessed 21 Nov. 2016].Available at: http://www.slideshare.net/vjspa/city-forms.

Chan, A.T. , So, E. S. P. & Samad, S. (2001). Strategic guidelines for street canyon geometry to achieve sustainable street air quality. *Atmospheric Environment*, vol. 35(24), pp.4089-4098.

Chen, L. & Ng, E. (2011). Quantitative urban climate mapping based on a geographical database: A simulation approach using Hong Kong as a case study. *International Journal of Applied Earth Observation and Geoinformation*, vol. 13(4), pp.586-594.

Cheng, V. (2010). *Understanding density and high density*. London and Sterling, VA: Earthscan.

Che-Ani, A. I., Shahmohamadi, P., Sairi, A., Mohd-Nor, M. F. I., Zain, M. F. M., Surat, M., (2009). Mitigating the urban heat island effect: some points without altering existing city planning. *European Journal of Scientific Research*, vol.35 (2), 204- 216.

Crook, J. & Forster, P. (2014). Comparison of surface albedo feedback in climate models and observations. *Geophys. Res. Lett.*, vol. 41(5), pp.1717-1723.

Danielson, Levin, & Abrams, (2003). *Meteorology*, McGraw Hill.

De Lieto Vollaro, A., de Simone, G., Romagnoli, R., Vallati, A. & Botillo, S. (2014). Numerical Study of Urban Canyon Microclimate Related to Geometrical Parameters. *Sustainability*, vol. 6 (11), pp. 7894-7905.

Dempsey, N., Brown, C,. & Bramley, G. (2012). The key to sustainable urban development in UK cities? The influence of density on social sustainability. *Progress in Planning,* vol. 77, pp. 89–141.

Depecker, P., Menezo, C., Virgone, J. & Lepers, S. (2001). Design of buildings shape and energetic consumption. *Building and Environment*, vol. 36(5), pp.627-635.

Dewa.gov.ae. (2016). HE Saeed Mohammed Al Tayer highlights DEWA's contribution to transformation of Dubai into the smartest and happiest city in the world. [online]. [Accessed 21 Nov. 2016]. Available at: https://www.dewa.gov.ae/en/about-dewa/news-and-media/press-and-news/latest-news/2016/10/he-saeed-mohammed-al-tayer-highlights

Dias, N., Curwell, S. & Bichard, E. (2014). The Current Approach of Urban Design, its Implications for Sustainable Urban Development. *Procedia Economics and Finance*, vol. 18, pp.497-504.

Djukic, A., Vukmirovic, M. & Stankovic, S. (2015). Principles of climate sensitive urban design analysis in identification of suitable urban design proposals. Case study: Central zone of Leskovac competition. *Energy and Buildings*, vol. 115, pp.23-35.

Droege, P. (2008). *Urban energy transition*. 1st ed. Amsterdam: Elsevier.

Dubai Municipality, DM. (2015).*Dubai Urban Master Plan (2020)*.

Ebrahimabadi, S., Nilsson, K. & Johansson, C. (2015). The problems of addressing microclimate factors in urban planning of the subarctic regions. *Environment and Planning B: Planning and Design*, vol. 42(3), pp.415-430.

Eco Who. (2015). [online]. [Accessed 20 Dec. 2016].Available at: http://Eco Who (2015)

Economic, social, and environmental sustainability in development theory and urban planning practice (2012). [online]. [Accessed 20 Dec. 2016].Available at: https://www.bing.com/cr

Edward, Ng (2010). *Designing high-density cities for social and environmental sustainability*. London: Earthscan.

El-Darwish, I., Ragheb, A. & Ahmed, S. (2016). Microclimate and human comfort considerations in planning a historic urban quarter. *International Journal of Sustainable Built Environment*.

Emmanuel, R. & Fernand, H. J. S. 2007. Urban heat islands in humid and arid climates: role of urban form and thermal properties in Colombo, Sri Lanka and Phoenix, USA. *Climate Research*, vol. 34(3), pp. 241-251.

ENVI-MET. Simulating Environments Building Comfort.(2016) Available at: http://www.envi-met.com/

ENVI_MET. (2018). ENVI_MET - Decoding urban nature. [online]. [Accessed 16 Jan. 2018]. Available at: http://www.envi-met.com/

Environmental Design of Urban Buildings – An Integrated Approach. (2006). *International Journal of Sustainability in Higher Education*, vol.6 (3).

EPA. Energy Protection Agency.(USEPA).(2012). *Urban Heat Island Basics, Reducing Urban Heat Islands: Compendium of Strategies*. U.S. EPA, p. 4.

EPA. Energy Protection Agency.(US EPA).(2008). *Sustainability*.[online].[Accessed 20 Dec. 2016]. Available at: https://www.epa.gov/sustainability/learn-about-sustainability#what About

Erell, E. et al. (2011). *Urban Microclimate: Designing the Spaces Between Buildings*. 1st ed. Earthscan.

ESDAC (2006). Climatic Zones (European Soil Data Centre). [online]. Available at: http://esdac.jrc.ec.europa.eu/

Fahmy, M. & Sharples, S. (2009). On the development of an urban passive thermal comfort system in Cairo, Egypt. *Building and Environment*, vol. 44 (9), pp. 1907-1916.

Fahmy, M. & S. Sharples (2009). Urban form adaptation towards minimizing climate change effects in Cairo, Egypt. *Building Services Engineering Research and Technology*. In Press

Fang, C., Wang, S. & Li, G. (2015). Changing urban forms and carbon dioxide emissions in China: A case study of 30 provincial capital cities. *Applied Energy*, vol. 158, pp.519-531.

Forsyth, L. (1987). *Marcus, Clare Cooper and Sarkissian, Wendy, 'Housing as if People Mattered: Guidelines for Medium-Density Family Housing*. (Book Review). Town Planning Review, vol. 58 (2), p. 217.

Garratt, J. R. (1994). *The Atmospheric Boundary Layer*. Cambridge University Press.

Gash, J. (1994). The atmospheric boundary layer, J. R. Garratt, Cambridge University Press (Cambridge), 1992. No. of pages: xviii + 316. Price: £50.00, US$79.95 (hardback) ISBN 0521380529. *International Journal of Climatology*, 14(1), pp.112-113.

Gal, T., Lindberg, F. & Unger, J. (2009). Computing continuous sky view factors using 3D urban raster and vector databases: comparison and application to urban climate. *Theoretical and Applied Climatology,* vol. 95, 111–123.

Giannopoulou, K., Livada, I., Santamouris, M., Saliari, M., Assimakopoulos, M. & Caouris, Y. (2014). The influence of air temperature and humidity on human thermal comfort over the greater Athens area. *Sustainable Cities and Society*, vol. 10, pp.184-194.

Gill, L., Hathway, E., Lange, E., Morgan, E. & Romano, D. (2013). Coupling Real-Time 3D Landscape Models with Microclimate Simulations. *International Journal of E-Planning Research,* vol. 2 (1), pp.1-19.

Givoni, B. (1998). *Climate Considerations in Building and Urban Design*. Van Nostr and Reinhold, New York.

Golany, G. (1996). Urban design morphology and thermal performance. *Atmospheric Environment*, vol. 30 (3), pp. 455-465.

Goodland, R. (1995). *Environmental Assessment (ea) in Africa - a World Bank Commitment.* 1st ed. WORLD BANK.

Guhathakurta, S. & Williams, E. (2015). Impact of Urban Form on Energy Use in Central City and Suburban Neighborhoods: Lessons from the Phoenix Metropolitan Region. *Energy Procedia*, vol. 75, pp.2928-2933.

Guzman, S. & Harrell, R. (2014). Increasing Community Livability for People of All Ages. *Public Policy & Aging Report*, vol. 25(1), pp.28-29.

Hammad, F. & Abu-Hijleh, B. (2010). The energy savings potential of using dynamic external louvers in an office building. *Energy and Buildings*, vol. 42(10), pp.1888-1895.

Han, Y., Taylor, J. & Pisello, A. (2015). Toward mitigating urban heat island effects: Investigating the thermal-energy impact of bio-inspired retro-reflective building envelopes in dense urban settings. *Energy and Buildings*, vol. 102, pp.380-389.

Heathcott, J. (2005). Modeling the urban future: planning, slums and the seduction of growth in St Louis, 1940–1950. *Planning Perspectives*, vol. 20 (4), pp. 369-387.

Helicon Publishing is a division of RM. (2011). [online]. [Accessed 16 Jan. 2018]. Available at: Average Conditions data © Copyright RM.. All rights reserved. http://www.bbc.com/weather/6300096

Hemsath, T. & Alagheband Bandhosseini, K. (2015). Sensitivity analysis evaluating basic building geometry's effect on energy use. *Renewable Energy*, vol. 76, pp.526-538.

Hicks, J. (1946). *Economic perspectives*. Oxford University Press, Clarendon, Oxford.

Ichinose, T., Matsumoto, F., & Kataoka K. (2008).Counteracting urban heat islands in Japan. In: Droege P, editor. Urban energy transition e from fossil fuels to renewable power. *Energy and Buildings*. Elsevier. pp. 365-380.

Ignatiusa, M., Wonga, N. & Jusuf, S. (2015). Urban microclimate analysis with consideration of local ambient temperature, external heat gain, urban ventilation, and outdoor thermal comfort in the tropics. *Sustainable Cities and Society*, vol. 19, pp.121–135.

Irulegi, O., Serra, A. & Hernández, R. (2017). Data on records of indoor temperature and relative humidity in a University building. *Data in Brief*, vol.13, pp.248-252.

Integrated Environmental Solution- Virtual Environment (IESVE). (2016). [Online]. Available at: http://www.iesve.com/software

International Energy Agency (IEA). (2012) [online]. [Accessed 20 Dec. 2016].Available at: http://International Energy Agency (IEA) (2012), World Energy Outlook.

Jansson, C. (2006). *Urban microclimate and surface hydro meteorological processes*. KTH.

Jones, P. & Alexander, D. K. eds. (1999). Modeling Building Performance. *The 3rd international Symposium on Heating, Ventilation and Air Conditioning*. Shenzhen, China.

Jones, P. J., Lannon, S., & Williams, J. (2001). Modeling Building Energy Use at Urban Scale. *In Paper Presented at the Seventh International IBPSA Conference*. Rio deJaneiro, Brazil.

Johansson, E. (2006). Influence of urban geometry on outdoor thermal comfort in a hot dry climate: a study in Fez, Morocco. *Building and Environment,* vol. 41, pp. 1326_1338.

Jumeriah Village Development Code (2006). Nakheel Properties, Dubai, UAE.

Jusuf, S. K., Wong, N. H., Hagen, E., Anggoro, R., & Yan, H. (2007). The influence of land use on the urban heat island in Singapore. *Habitat International*, vol. 31, pp. 232–242.

Kaimal, J. C. & Finnigan, J. J. (1994). *Atmospheric boundary layer flows: their structure and measurement. Oxford University Press on Demand.*

Karl, T. (2003). Modern Global Climate Change. *Science*, 302(5651), pp.1719-1723.

Kavgic, M., Mavrogianni, A., Mumovic, D., Summerfield, A., Stevanovic, Z. & Djurovic-Petrovic, M. (2010). A review of bottom-up building stock models for energy consumption in the residential sector. *Building and Environment*, vol. 45(7), pp.1683-1697.

Kearns, A. & Parkinson, M. (2001).The Significance of Neighborhood. *Urban Study*, vol.38 (12), pp.2103-2110.

Kent, J. and Thompson, S. (2014). The Three Domains of Urban Planning for Health and Well-being. *Journal of Planning Literature*, vol.29 (3), pp.239-256.

Kolokotroni, M., Zhang, Y. and Watkins, R. (2007). The London Heat Island and building cooling design. *Solar Energy*, vol.81(1), pp.102-110.

Kruger, E., Minella, F. & Rasia, F. (2011).Impact of urban geometry on outdoor thermal comfort and air quality from field measurements in Curitiba, Brazil. *Building and Environment*, vol. 46(3), pp.621-634.

Ku, C. (2003) . *A Study on Energy Conservation Design of Residential Buildings through Multiple Objective.* Master Thesis. Chaoyang University of Technology, China.

Kwak, K., Baik, J., Ryu, Y. & Lee, S. (2015). Urban air quality simulation in a high-rise building area using a CFD model coupled with mesoscale meteorological and chemistry-transport models. *Atmospheric Environment*, vol.100, pp.167-177.

Lahme, E., Bruse, M. (2003). Microclimatic effects of a small urban park in densely built-up areas: measurements and model simulations. ICUC5, Lodz, pp. 1–5.

Lawrence Berkeley National Libratory . (2015) [online]. [Accessed 20 Dec. 2016]. Available at: http://Construction materials albedo.

Learnqse.wordpress.com. (2018). *Built Up Area « QUANTITY SURVEYING AND ESTIMATION*. [online]. [Accessed 16 Jan. 2018]. Available at: https://learnqse.wordpress.com/tag/built-up-area

Lee, J. and Lau, E. (2017). Effects of relative humidity in the convective heat transfer over flat surface using ionic wind. *Applied Thermal Engineering*, vol.114, pp.554-560.

Lee, R. X., Jusuf, S. K., & Wong, N. H. (2013). The study of height variation on outdoor ventilation for Singapore's high-rise residential housing estates. *International Journal of Low-Carbon Technologies,* vol. 0, pp. 1–19.

LEED 'Leadership in Energy and Environmental Design' v4. (2014) *NEIGHBORHOOD DEVELOPMENT* . Updated version, October (2014).

Lehmann,S. (2010). *The principles of Green Urbanism*. UK, Earthscan.
Letcher, T. (2009). *Climate change*. 1st ed. Amsterdam: Elsevier.

Li, L., Yang, L., Zhang, L. & Jiang, Y. (2012). Numerical study on the impact of ground heating and ambient wind speed on flow fields in street canyons. *Advances in Atmospheric Sciences*, vol. 29 (6), pp. 1227-1237.

Li, X., Li, C., Parriaux, A., Wu, W., Li, H., Sun, L. & Liu, C. (2016). Multiple resources and their sustainable development in Urban Underground Space. *Tunneling and Underground Space Technology*.

Li, Z., Quan, S. & Yang, P. (2016). Energy performance simulation for planning a low carbon neighborhood urban district: A case study in the city of Macau. *Habitat International*, vol. 53, pp.206-214.

Liu, K., Su, H., Zhang, L., Yang, H., Zhang, R. & Li, X. (2015). Analysis of the Urban Heat Island Effect in Shijiazhuang, China Using Satellite and Airborne Data. Remote Sensing, vol.7(4), pp.4804-4833.

Limitless Regulation Code (2008). Dubai, UAE.

Littlefair, P. J. (2002.) *Environmental site layout planning : solar access, microclimate and passive cooling in urban areas*. IHS, BRE Press.

Lo, A. (2016). Small is green? Urban form and sustainable consumption in selected OECD metropolitan areas. *Land Use Policy*, vol. 54, pp.212-220.

McGrath, B. (2013). *Urban design ecologies*. Chichester, West Sussex: Wiley.

Magli, S., Lodi, C., Lombroso, L., Muscio, A. and Teggi, S. (2014). Analysis of the urban heat island effects on building energy consumption. *International Journal of Energy and Environmental Engineering*, vol. 6(1), pp.91-99.

Mahboob, M., I- Tsaia, T., Bacaa, E.S.& Afshari, A.(2014). Effects of Building Density on Energy Demand for Indoor Cooling Under Extreme Hot Weather. *The 5th International Conference on Environmental Science and Technology.* IPCBEE, vol(.69). IACSIT Press, Singapore, DOI: 10.7763/IPCBEE. vol. (26).

Maleki, S., Bell, S., Hosseini, S. & Faizi, M. (2015). Developing and testing a framework for the assessment of neighborhood liveability in two contrasting countries: Iran and Estonia. *Ecological Indicators*, vol.(48), pp.263-271.

Marciotto, E., Oliveira, A. & Hanna, S. (2010). Modeling study of the aspect ratio influence on urban canopy energy fluxes with a modified wall-canyon energy budget scheme. *Building and Environment*, vol. 45 (11), pp. 2497-2505.

March, L. and Martin, L. (1972). *Urban space and structures*. Cambridge: The University Press.

Marcus, C. C. & W. Sarkissian (1986). *Housing as if People Mattered: Site Design Guidelines for Medium Density Family Housing*. Los Angeles University of California Press.

Mirzaei, P.A. & Haghighat, F.(2010). Approaches to study Urban Heat Island – abilities and limitations. *Build Environment*, vol. 45(10), pp. 2192-2201.

Mirzaei Ahranjani, P. (2011). Systematic Simulation Method to Quantify and Control Pedestrian Comfort and Exposure during Urban Heat Island. 1st ed. [Montreal, Quebec]: Concordia University Press.

Middel, A., Habb, K., Brazel, A., Martin, C. & Guhathakurta, S. (2014). Impact of urban form and design on mid-afternoon microclimate in Phoenix Local Climate Zones. *Landscape and Urban Planning*, vol. 122, pp.16-28.

Montazeri, H., Blocken, B., Derome, D., Carmeliet, J., Hensen, J. (2015). CFD analysis of forced convective heat transfer coefficients at windward building facades: Influence of building geometry. *Journal of Wind Engineering and Industrial Aerodynamics,* vol. 146, pp.102-116.

Mostafavi, M. and Doherty, G. (2010). *Ecological urbanism*. Baden, Switzerland: Lars Muller Publishers.

Muhaisen, A. & Gadi, M. (2006). Effect of courtyard proportions on solar heat gain and energy requirement in the temperate climate of Rome. *Building and Environment*, vol. 41(3), pp.245-253.

Nakamura, Y. and Oke, T. (1988). Wind, temperature and stability conditions in an east-west oriented urban canyon. *Atmospheric Environment*, vol. 22, pp. 2691-2700.

National Aeronautics and Space Administration (NASA). (1998). [online] [Accessed 20 Dec. 2016].Available at: http://'NASA GISS: Science Briefs: Greenhouse Gases: Refining the Role of Carbon Dioxide 1998'. www.giss.nasa.gov. Retrieved 2016-04-26.

National Aeronautics and Space Administration (NASA). (2013). [online]. [Accessed 20 Dec. 2016]. Available at: National Aeronautics and Space Administration (NASA), Global Climate change and Pollution. http://climate.nasa.gov/news/860

Nazarian, N. & Kleissl, J. (2015). CFD simulation of an idealized urban environment: Thermal effects of geometrical characteristics and surface materials. *Urban Climate*, vol. 12, pp.141-159.

Negendahl, K. & Nielsen, T. (2015). Building energy optimization in the early design stages: A simplified method. *Energy and Buildings*, vol. 105, pp.88-99.

Neuman, M. (2005). The Compact City Fallacy. *Journal of Planning Education and Research*, 25(1), pp.11-26.

Ng, E. (2010). *Designing high-density cities for social and environmental sustainability*. London: Earthscan.

Ng, E., Yuan, C., Chen, L., Ren, C. & Fung, J. (2011). Quantitative urban climate mapping based on a geographical database: A simulation approach using Hong Kong as a case study. *International Journal of Applied Earth Observation and Geoinformation*, vol. 13, pp. 586–594.

Ng, W. & Chau, C. (2013).A modeling investigation of the impact of street and building configurations on personal air pollutant exposure in isolated deep urban canyons. *Science of The Total Environment*, vol. 468-469, pp.429-448.

Ng, W. & Chau, C. (2014). A modeling investigation of the impact of street and building configurations on personal air pollutant exposure in isolated deep urban canyons. *Science of The Total Environment*, vol. 468-469, pp.429-448.

Niachou, K. et al. (2008). Experimental study of temperature and airflow distribution inside an urban street canyon during hot summer weather conditions—Part I: Air and surface temperatures. *Building and Environment* 43(8), pp. 1383-1392.

Nunez, M. & Oke, T. (1977). The Energy Balance of an Urban Canyon. *Journal of Applied Meteorology*, vol. 16 (1), pp. 11-19.

Oke, T. (1973). City size and the urban heat island. *Atmospheric Environment (1967)*, vol. 7(8), pp.769-779.

Oke, T. (1987). *Boundary layer climates*. London [u.a.]: Methuen.

Oke, T. (1988). Street design and urban canopy layer climate. *Energy and Buildings*, 11(1-3), pp.103-113.

Oke, T. R. (2002). *Boundary layer climates*. Second edition ed. Taylor & Francis.

Offerle, B., Eliasson, I., Grimmond, C. and Holmer, B. (2006). Surface heating in relation to air temperature, wind and turbulence in an urban street canyon. *Boundary-Layer Meteorology*, vol.122 (2), pp.273-292.

Pampanga, D., Majid, M. & Johar, F. (2015). Appropriate Urban Livability Indicators for Metropolitan Johor, Malaysia via Expert-Stakeholder Approach: a Delphi technique. *International Journal of BES*, vol. 2(4).

Park, C. (2007). *A dictionary of environment and conservation.* 1st ed. Oxford: Oxford University Press.

Patton, M. (2001). *Qualitative Research and Evaluation Methods.* Thousand Oaks, Calif.: Sage Publications.

Pearlmutter, D., Bitan, A. & Berliner, P. (1999). Microclimatic analysis of 'compact' urban canyons in an arid zone. *Atmospheric Environment*, vol. 33 (24-25), pp. 4143-4150.

Pearlmutter, D., Berliner, P. & Shaviv, E. (2005). Evaluation of Urban Surface Energy Fluxes Using an Open-Air Scale Model. *Journal of Applied Meteorology*, vol. 44 (4), pp. 532-545.

Peng, S., Piao, S., Ciais, P., Friedlingstein, P., Ottle, C., Bréon, F., Nan, H., Zhou, L. and Myneni, R. (2012). Surface Urban Heat Island Across 419 Global Big Cities. *Environmental Science & Technology*, vol. 46 (2), pp.696-703.

Peng, L. and Jim, C. (2013). Green-Roof Effects on Neighborhood Microclimate and Human Thermal Sensation. *Energies*, vol. 6 (2), pp.598-618.

Peren, J., Hooff, T., Ramponi, R., Blocken, B. & Leite, B. (2015). Impact of roof geometry of an isolated leeward southwest roof building on cross-ventilation: Straight, concave, hybrid or convex?. *Journal of Wind Engineering and Industrial Aerodynamics*, vol. 145, pp.102-114.

Pew Center. U.S. (2013) .[online].[Accessed 15 May. 2015]. Available at:http://www.people-press.org/2014/12/18/as-u-s-energy-production-grows-public-policy-views-show-little-change/

Pichierri, M., Bonafoni, S. and Biondi, R. (2012). Satellite air temperature estimation for monitoring the canopy layer heat island of Milan. *Remote Sensing of Environment*, vol. 127, pp.130-138.

Pont, M. B., & Haupt, P. (2004). *Space mate: The spatial logic of urban density.* Delft: Delft University Press.

Porter, M.E. (1990). *The Competitive Advantage of Nations*. Free Press, New York, 1990.

Priyadarsini, R.& Wong, N. (2005). Parametric studies on urban geometry, airflow and temperature. *International journal on architectural science*, vol. 6, (3) , pp. 114-132.

Quora (2017). [online]. [Accessed 16 Jan. 2018].Available at: https://www.quora.com/The-relationship-between-temperature-and-humidity-Directly-proportional-or-inversely-proportional-if-temperature-increases-decreases-does-humidity-decrease-increase

Rahman, M.M., Rasul, M.G. & Khan, M.M.K. (2008). Energy conservation measures in a nine situational building by dynamic simulation using Design Builder. *The Third International Conference on Energy and Cambridge Environment*, 23–25 Feb.

Ritchie, A. & Thomas, R. (2009). *Sustainable urban Design*. London & New York: Taylor & Francis.

Rizwan, A., Dennis, L. and Liu, C. (2008). A review on the generation, determination and mitigation of Urban Heat Island. *Journal of Environmental Sciences*, 20(1), pp.120-128.

Rlsenergy: Gradient wind speed velocity (2012) [online]. [Accessed 16 Jan. 2018]. Available at http://Rlsenergy.com/

Robati, M., Kokogiannakis, G. and McCarthy, T. (2017). Impact of structural design solutions on the energy and thermal performance of an Australian office building. *Building and Environment*, vol.124, pp.258-282.

Rodrigues, E., Amaral, A., Gaspar, A. & Gomes, A. (2015). How reliable are geometry-based building indices as thermal performance indicators?. *Energy Conversion and Management*, vol. 101, pp.561-578.

Ruiza Arias, J., Tovara Pescador, J., PozoaVa¡zquez, D. & Alsamamra, H. (2009). A comparative analysis of DEM based models to estimate the solar radiation in mountainous terrain. *International Journal of Geographical Information Science*, vol. 23(8), pp.1049-1076.

Sabzi, D., Haseli, P., Jafarian, M., Karimi, G. & Taheri, M. (2015). Investigation of cooling load reduction in buildings by passive cooling options applied on roof. *Energy and Buildings*, vol. 109, pp. 135-142.

Saitoh, T., Shimada, T. and Hoshi, H. (1996). Modeling and simulation of the Tokyo urban heat island. *Atmospheric Environment*, vol.30(20), pp.3431-3442.

Salat, S., Labbei, F., Nowacki, C. and Walker, G. (2011). *Cities and forms*. [Paris]: CSTB Urban Morphology Laboratory.

Sander, H. & Manson, S. (2007). Heights and locations of artificial structures in viewshed calculation: How close is close enough?. *Landscape and Urban Planning*, vol. 82(4), pp.257-270.

Santamouris, M., Papanikolaou, N., Koronakis, I., Livada, I. and Asimakopoulos, D. (1999). Thermal and air flow characteristics in a deep pedestrian canyon under hot weather conditions. *Atmospheric Environment,* vol. 33 (27), pp.4503-4521.

Schulte, N., Tan, S. & Venkatram, A. (2015). The ratio of effective building height to street width governs dispersion of local vehicle emissions. *Atmospheric Environment*, vol. 112, pp.54-63.

Sensible and Latent Cooling Load Control Using Centrally-Ducted, Variable-Capacity Space Conditioning Systems in Low Sensible Load Environments James Cummings BA-PIRC. (2012). *Solar Energy Center, Presented at BA Summer Meeting*. Florida, July 26.

Shashua-Bar, L. and Hoffman, M. (2003). Geometry and orientation aspects in passive cooling of canyon streets with trees. *Energy and Buildings*, vol.35(1), pp.61-68.

Shimoda, Y., Fujii, T., Morikawa, T. & Mizuno, M. (2004). Residential end-use energy simulation at city scale. *Building and Environment*, vol. 39(8), pp.959-967.

Shishegar, N. (2013). Street Design and Urban Microclimate: Analyzing the Effects of Street Geometry and Orientation on Airflow and Solar Access in Urban Canyons. *Journal of Clean Energy Technologies*, pp.52-56.

Steemers, K. (2006). *Integrated Building Design. Environmental Design of Urban Buildings; An Integrated Approach*. M. Santamouris. London, Earthscan**:** 310-318.

Stromann-Andersen, J. & Sattrup, P. (2011). The urban canyon and building energy use: Urban density versus daylight and passive solar gains. *Energy and Buildings*, vol. 43(8), pp.2011-2020.

Sun, Y. and Augenbroe, G. (2014). Urban heat island effect on energy application studies of office buildings. *Energy and Buildings*, 77, pp.171-179.

Swaid, H. (1992). Intelligent urban forms (IUF) a new climate-concerned, urban planning strategy. *Theoretical and Applied Climatology*, vol. 46 (2-3), pp. 179-191.

Swan, L. & Ugursal, V. (2009). Modeling of end-use energy consumption in the residential sector: A review of modeling techniques. *Renewable and Sustainable Energy Reviews*, vol. 13(8), pp.1819-1835.

Syrios, K. & Hunt, G. R. (2008). 'Passive air exchanges between building and urban canyon via openings in a single façade. *International Journal of Heat and Fluid Flow*, vol.29, pp. 364–373.

Szokolay, S. V. (2008). Introduction to Architectural Science: *The Basis of Sustainable*

Design. Second edition ed. Elsevier/Architectural Press.

Taha, H. (2013). Meteorological, emissions and air-quality modeling of heat-island mitigation: recent findings for California, USA. *International Journal of Low-Carbon Technologies*, vol.10 (1), pp.3-14.

Takebayashi, H. & Moriyama, M. (2012). Relationships between the properties of an urban street canyon and its radiant environment introduction of appropriate urban heat island mitigation technologies. *Solar Energy,* vol. 86(9), pp. 2255-2262.

Taleghani, M., Kleerekoper, L., Tenpierik, M. & van den Dobbelsteen, A. (2015). Outdoor thermal comfort within five different urban forms in the Netherlands. *Building and Environment*, vol. 83, pp.65-78.

Taleghani, M., Tenpierik, M., van den Dobbelsteen, A. and de Dear, R. (2013). Energy use impact of and thermal comfort in different urban block types in the Netherlands. *Energy and Buildings*, vol. 67, pp.166-175.

Taleb, H. (2014). Using passive cooling strategies to improve thermal performance and reduce energy consumption of residential buildings in U.A.E. buildings. *Frontiers of Architectural Research*, vol. 3(2), pp.154-165.

Taleb, D. & Abu-Hijleh, B. (2013). Urban heat islands: Potential effect of organic and structured urban configurations on temperature variations in Dubai, UAE. *Renewable Energy*, vol. 50, pp.747-762.

Taleb, H. & Musleh, M. (2015). Applying urban parametric design optimization processes to a hot climate: Case study of the UAE. *Sustainable Cities and Society*, vol. 14, pp.236-253.

Tarekegn, T., Haile, A., Rientjes, T., Reggiani, P. & Alkema, D. (2010). Assessment of an ASTER-generated DEM for 2D hydrodynamic flood modeling. *International Journal of Applied Earth Observation and Geoinformation*, vol. 12(6), pp.457-465.

Todhunter, P. E. (1990). Microclimatic Variations Attributable to Urban Canyon Asymmetry and Orientation. *Physics and Geography,* vol.11, pp.131-141.

Todhunter, P. and Terjung, W. (1990). The response of urban canyon energy budgets to variable synoptic weather types— A simulation approach. Atmospheric Environment. Part B. *Urban Atmosphere*, vol.24 (1), pp.35-42.

Toja-Silva, F., Lopez-Garcia, O., Peralta, C., Navarro, J. & Cruz, I. (2016). An empirical heuristic optimization of the building-roof geometry for urban wind energy exploitation on high-rise buildings. *Applied Energy*, vol. 164, pp.769-794.

Tooming, H. (1996). *Changes in surface albedo and air temperature at Tartu, Estonia*. TELLUSA.

Trancik, R. (1986). *Finding lost space*. New York: Van Nostr and Reinhold.

Tseliou, A. & Tsiros, I. (2016). Modeling urban microclimate to ameliorate thermal sensation conditions in outdoor areas in Athens (Greece). *Building Simulation*, vol. 9 (3), pp. 251-267.

Tuhus-Dubrow, D. & Krarti, M. (2010). Genetic-algorithm based approach to optimize building envelope design for residential buildings. *Building and Environment*, vol. 45(7), pp.1574-1581.

Unger, J. (2004). Intra-urban relationship between surface geometry and urban heat island: review and new approach. *Climate Research*, vol. 27, pp.253-264.

Unger, J., Sümeghy, Z., Szegedi, S., Kiss, A. & Géczi, R. (2010). Comparison and generalization of spatial patterns of the urban heat island based on normalized values. *Physics and Chemistry of the Earth*, Parts A/B/C, vol.35(1-2), pp.107-114.

United Nation Climate Change Conference, Paris (2015).[online] Available at:
https://www.un.org/sustainabledevelopment/cop21/ [Accessed 2 Dec. 2016].

United Nation Framework on Climate Change (UNFCC). (1992). [online] Available at:
http://United Nation Framework on Climate Change (UNFCC) (1992), Kyoto/Japan.
[Accessed 2 Dec. 2016].

United Nations (UN) General Assembly. *The World summit*.(2005). A/RES/60/1.[Online].
Available at: http://unpan1.un.org/intradoc/groups/public/documents/un/unpan1752.pdf

University Corporation for Atmospheric Research (UCAR). (2016). Atmospheric Layers
[online]. Available at : http://scied.ucar.edu/atmosphere-layers [Accessed 20 Dec.
2016].

Van Esch, M., Looman, R. & de Bruin-Hordijk, G. (2012). The effects of urban and building
design parameters on solar access to the urban canyon and the potential for direct passive
solar heating strategies. *Energy and Buildings*, vol.47, pp.189-200.

Walter Gropius Papers. Houghton Library , Harvard Library. (1925-1969) (MS Ger 208).
Harvard University.

WAM. The Emirates News Agency, (Wekalat Anba'a al Emarat).(2016). [online].
[Accessed2 Dec. 2016]. Available
at:http://faculty.uaeu.ac.ae/k_sallal/ibpsauae/green%20buildings/Dubai%20as%20a%20
Green%20City.html

Wang, M. & Kexin, L. (2013). Transportation Model Application for the Planning of Low
Carbon City--Take Xining City in China as Example. *Procedia Computer Science*, vol.
19, pp.835--840.

Wanphen, S. and Nagano, K. (2009). Experimental study of the performance of porous
materials to moderate the roof surface temperature by its evaporative cooling
effect. *Building and Environment,* 44(2), pp.338-351.

Whang, S. & Kim, S. (2014). Determining sustainable design management using passive
design elements for a zero emission house during the schematic design. *Energy and
Buildings*, vol. 77, pp.304-312.

Weather spark (2012). [online]. [Accessed 16 Jan. 2018]. Available at: https://weatherspark.com/averages/32855/ Dubai-United-Arab-Emirates

Weng, Q., Lu, D. and Schubring, J. (2004). Estimation of land surface temperature– vegetation abundance relationship for urban heat island studies. *Remote Sensing of Environment*, vol. 89(4), pp.467-483.

Weston, K. (1988). Boundary layer climates (Second edition). By T. R. Oke. Methuen. 1987. Pp. 435 + xvi. £39.95 hardback; £14.95 paperback. *Quarterly Journal of the Royal Meteorological Society*, vol. 114 (484), pp.1568-1568.

Whang, S. & Kim, S. (2014). Determining sustainable design management using passive design elements for a zero emission house during the schematic design. *Energy and Buildings*, vol.77, pp.304-312.

Windfinder.com. (2018). *Windfinder.com - Wind and weather statistic Dubai Airport*. [online]. [Accessed 16 Jan. 2018].Available at: https://www.windfinder.com/windstatistics/dubai

Wong, N., Jusuf, S. & Tan, C. (2011). Integrated urban microclimate assessment method as a sustainable urban development and urban design tool. *Landscape and Urban Planning*, vol. 100 (4), pp.386-389.

Wong, N. H., Jusuf, S. K., Syafii, N. I., Chen, Y., Hajadi, N. & Sathyanarayanan, H., et al. (2011). Evaluation of the impact of the surrounding urban morphology on building energy consumption. *Solar Energy*, vol. 85, 57–71.

Wright R. & Boors D. (2011). *Environmental Science Toward a sustainable future.* Pearson.

Yang, L. and Li, Y. (2011). Thermal conditions and ventilation in an ideal city model of Hong Kong. *Energy and Buildings*, vol. 43(5), pp.1139-1148.

Yang, X., Zhao, L., Bruse, M. and Meng, Q. (2012). An integrated simulation method for building energy performance assessment in urban environments. *Energy and Buildings*, vol. 54, pp.243-251.

Yang Lin, K. (2013). *Investigating Reducing Building Energy Useat Urban Scale in Taipei.* PhD Thesis. University of Cardiff, UK.

Yang, F., Qian, F. & Lau, S. (2013). Urban form and density as indicators for summertime outdoor ventilation potential: A case study on high-rise housing in Shanghai. *Building and Environment,* vol. 70, pp.122-137.

Yang, X., Zhao, L., Bruse, M., & Meng, Q. (2012). An integrated simulation method for building energy performance assessment in urban environments. *Energy and Buildings,* vol.54, pp. 243–251

Yeo, I., Yoon, S. & Yee, J. (2013). Development of an urban energy demand forecasting system to support environmentally friendly urban planning. *Applied Energy*, vol. 110, pp.304--317.

Yu, L. (2014). Potentials of Passive Cooling for Passive Design of Residential Buildings in Qingyuan, Z. and China. *Energy Procedia*, vol. 57, pp.1726-1732.

Yuan, C. & Ng, E. (2014). Practical application of CFD on environmentally sensitive architectural design at high density cities: A case study in Hong Kong. *Urban Climate*, vol. 8, pp.57-77.

Yuan, C., Ng, E. & Norford, L. (2014). Improving air quality in high-density cities by understanding the relationship between air pollutant dispersion and urban morphologies. *Building and Environment*, vol. 71, pp.245-258.

Zanon, B. & Verones, S. (2013). Climate change, urban energy and planning practices: Italian experiences of innovation in land management tools. *Land Use Policy*, vol. 32, pp.343--355.

Zhang, W., Huang, B. & Luo, D. (2014). Effects of land use and transportation on carbon sources and carbon sinks: A case study in Shenzhen, China. *Landscape and Urban Planning*, vol. 122, pp.175--185.

Zhang, Y., Guindon, B. & Sun, K. (2016). Exploring the link between urban form and work related transportation using combined satellite image and census information: Case of the Great lakes region. *International Journal of Applied Earth Observation and Geoinformation*, vol. 47, pp.139-150.

Zhao (2011). *Impact of urbanization on climate change.10.000 scientific problem.* Science Press, pp843-846.

Zhao, F., Martinez-Moyano, I. J. & Augenbroe, G. (2011). Agent-based modeling of commercial building stocks for policy support. *Proceedings of Building Simulation*, pp. 2385-2392.

Appendices

Appendices

Appendix A

A.1 : Actual and simulation data for the ENVI - Met software validation

----
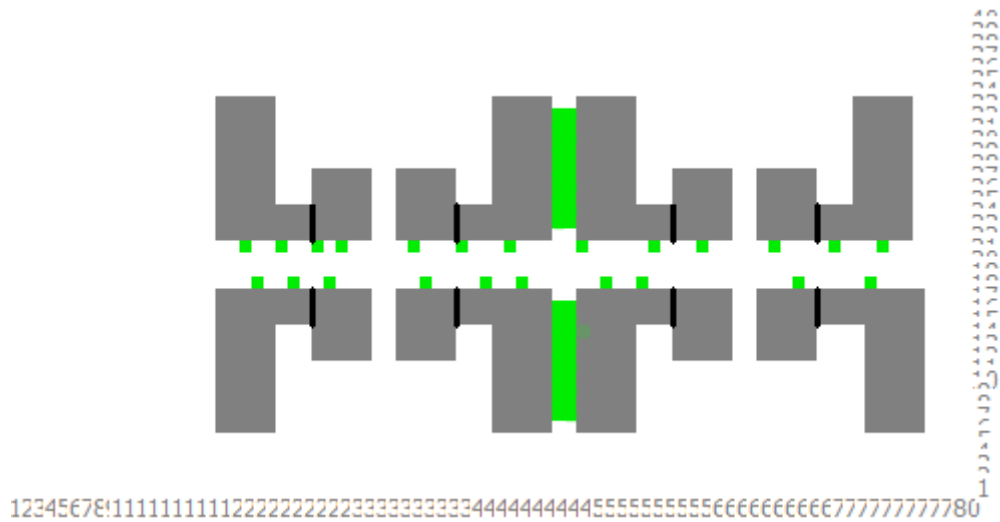
The simulated model for the ENVI-Met software validation

Time	Real Temp. °C (x)	Simulation Temp. °C (y)
07:00	21.2	21
08:00	21.4	21.2
09:00	21.5	21.3
10:00	21.7	21.5
11:00	22.1	21.9
12:00	22.5	22.1
13:00	22.6	22.2
14:00	22.9	22.5
15:00	23.5	22.9
16:00	23.6	23.2
17:00	22.9	22.7
18:00	22.6	22.5
19:00	22.2	22.1

Real and simulation data for the ENVI - Met software validation

A.2 : Comparison between the microclimate data of the simulation day 21st. June 2017 and five years data

----
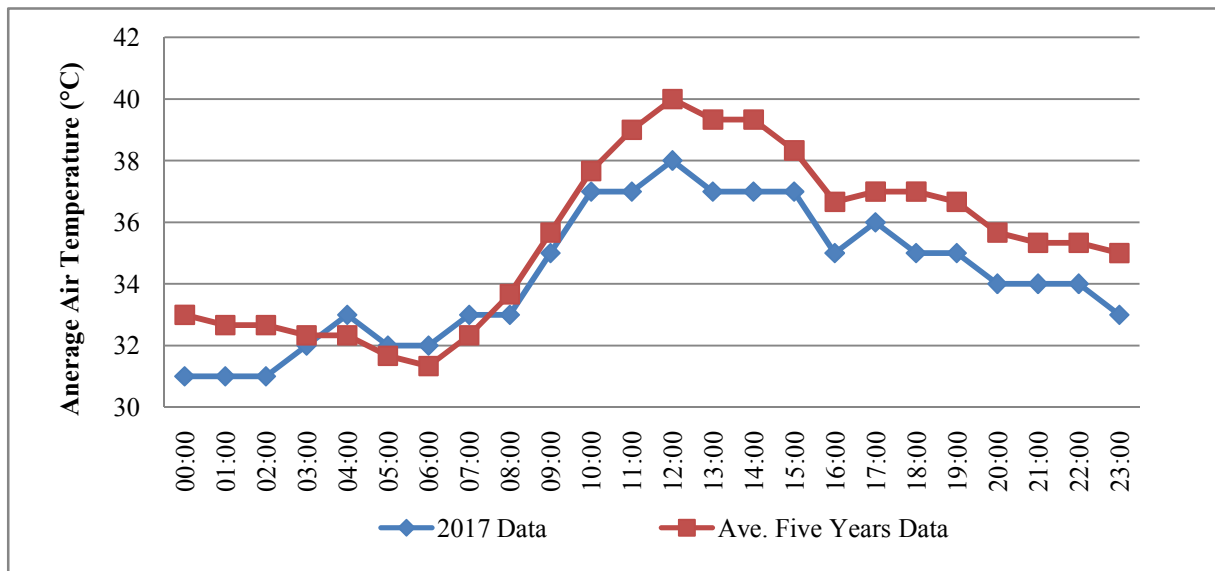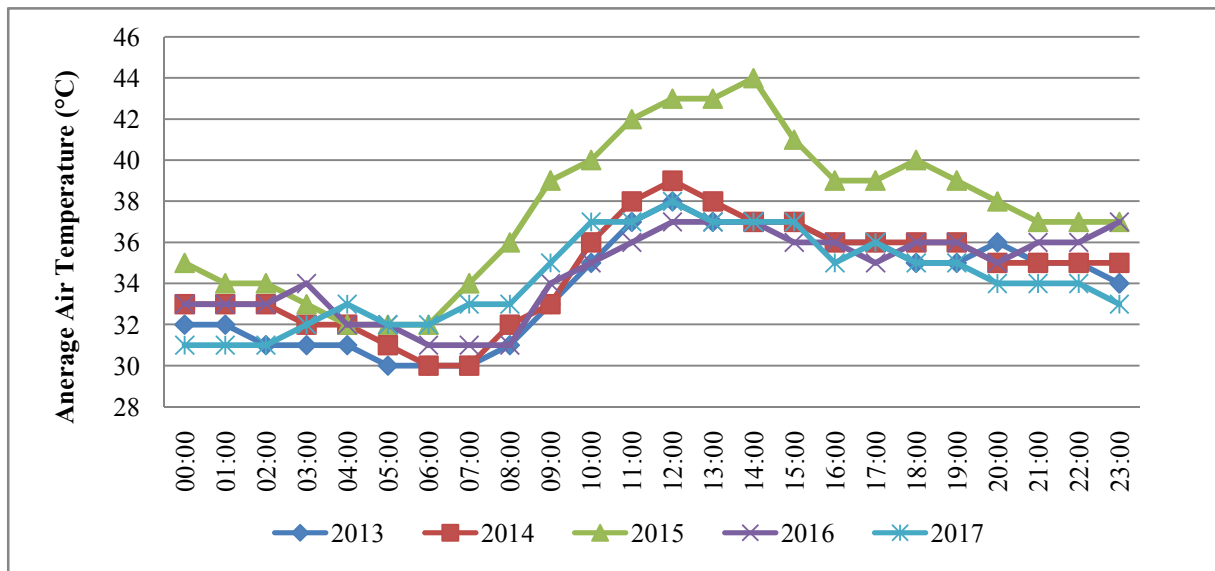
Hourly and average air temperature of 21st. June for five years; 2013,2014,2015,2016, and 2017
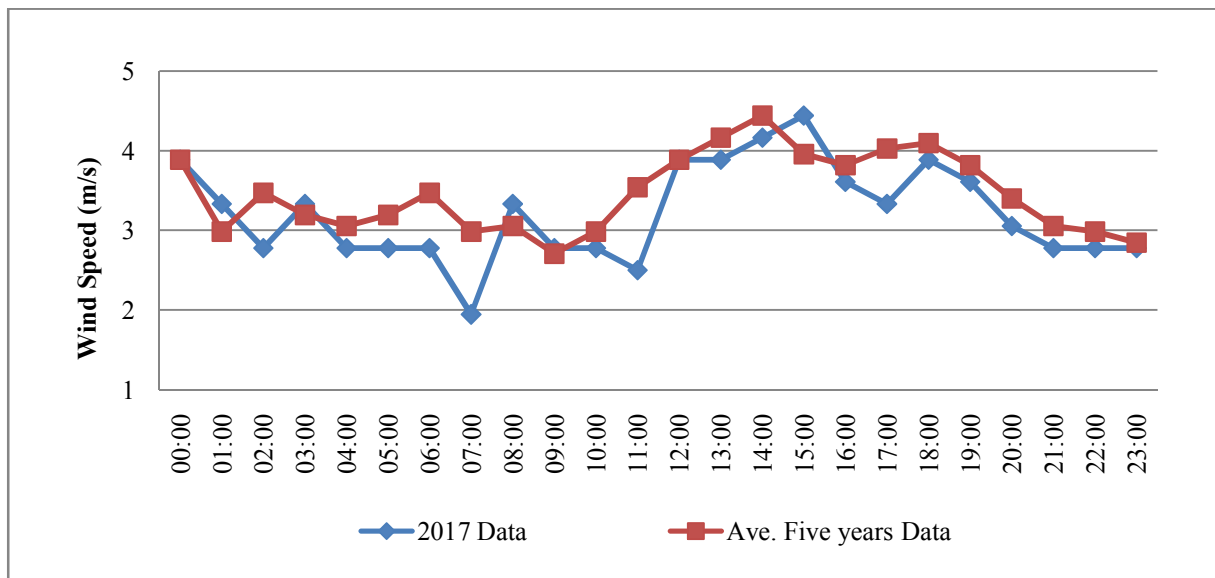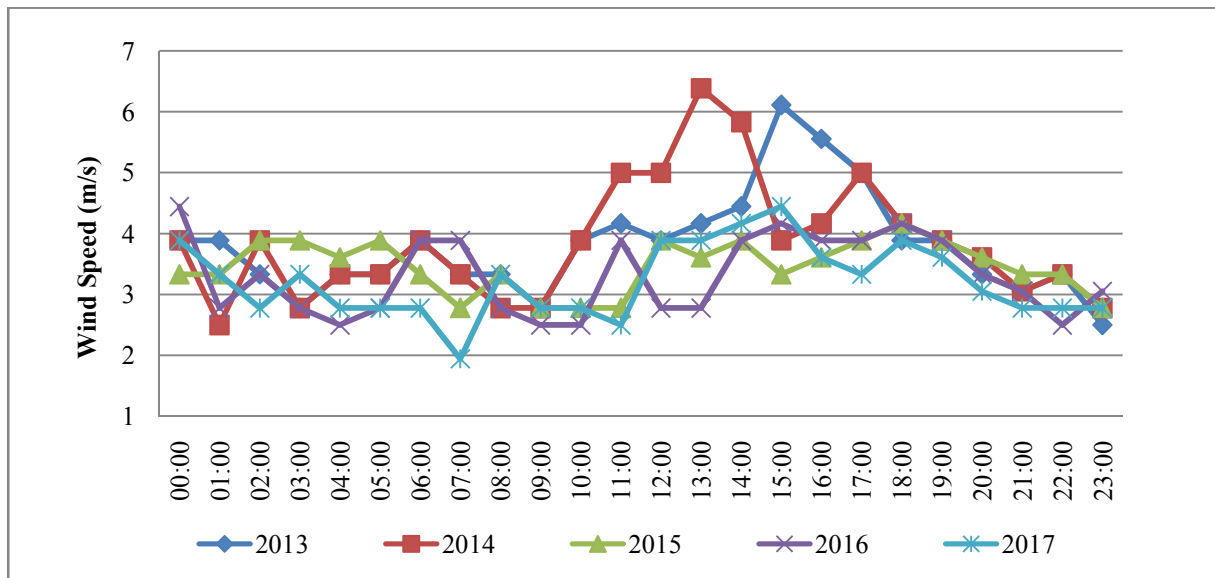
Hourly and average wind speed profile of 21st. June for five years; 2013,2014,2015,2016, and 2017
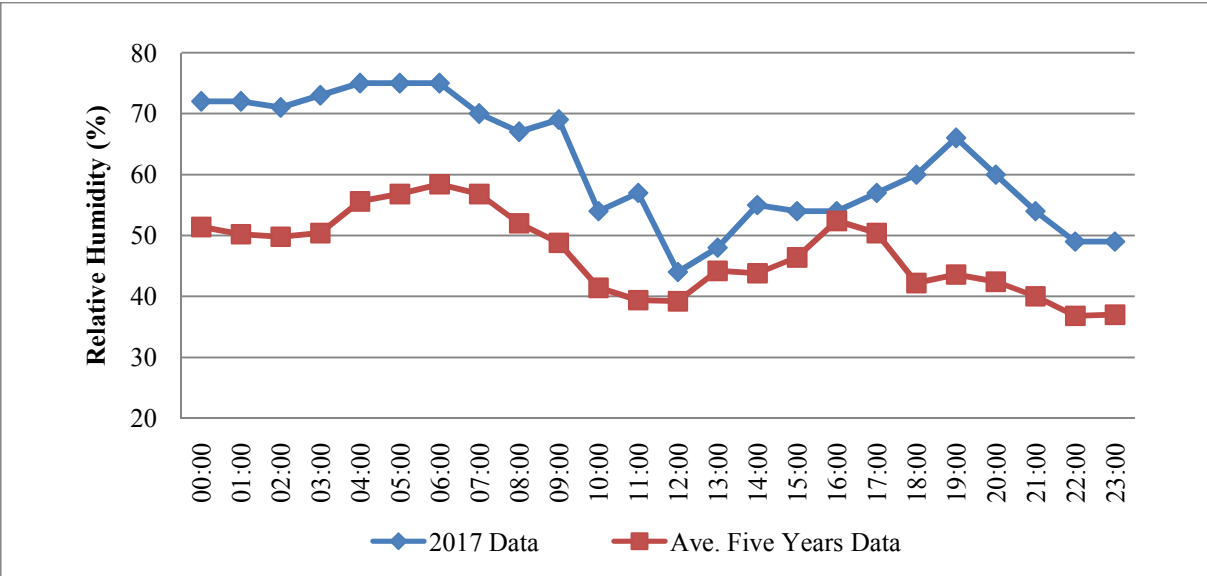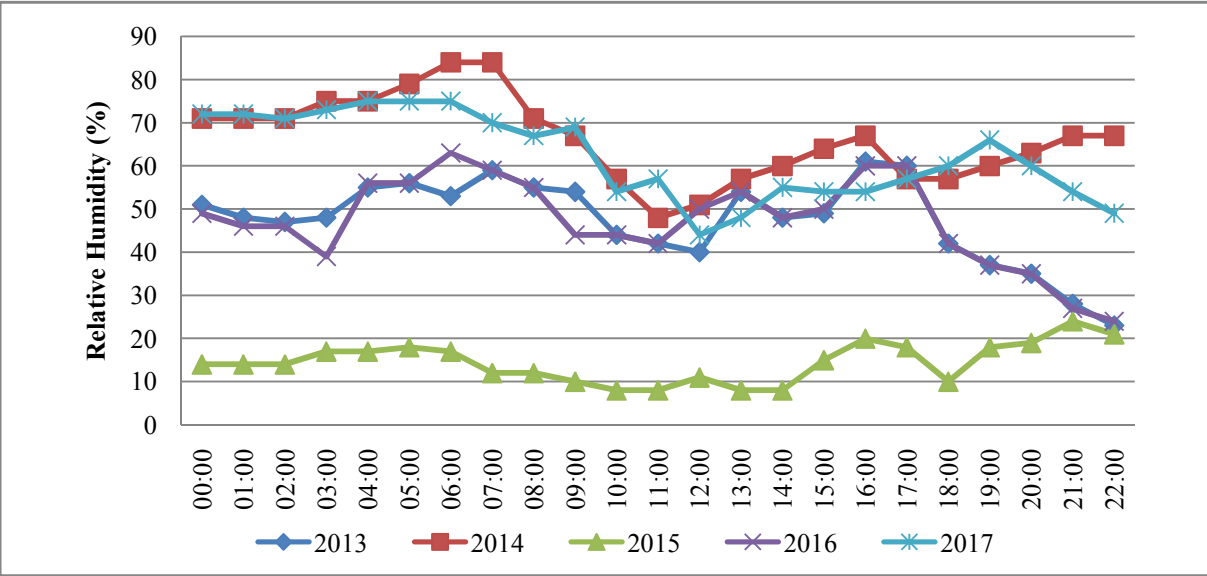
Hourly and average relative humidity profile of 21st. June for five years; 2013,2014,2015,2016, and 2017

A.3 : The sensitivity between the receptors data and the urban block microclimate data in (x,y) plain and (z) direction.

Canyon	Points (X,Y)	Beginning of Canyon	Middle of Canyon	End of Canyon
Side Canyon 1	Point 1	36.9	39	36.5
	Receptors	37	38.8	36.6
	Point 2	37	38.4	36.6
Middle Canyon	Point 1	36	37.8	36
	Receptors	36.1	37.6	36.1
	Point 2	36	37.5	36
Side Canyon 2	Point 1	35.5	36.8	35.7
	Receptors	35.5	36.8	35.7
	Point 2	35.6	36.7	35.7

The data of maximum air temperature from the receptors and the points close to the buildings' surfaces in the three canyons at the beginning , middle, and end of each canyon
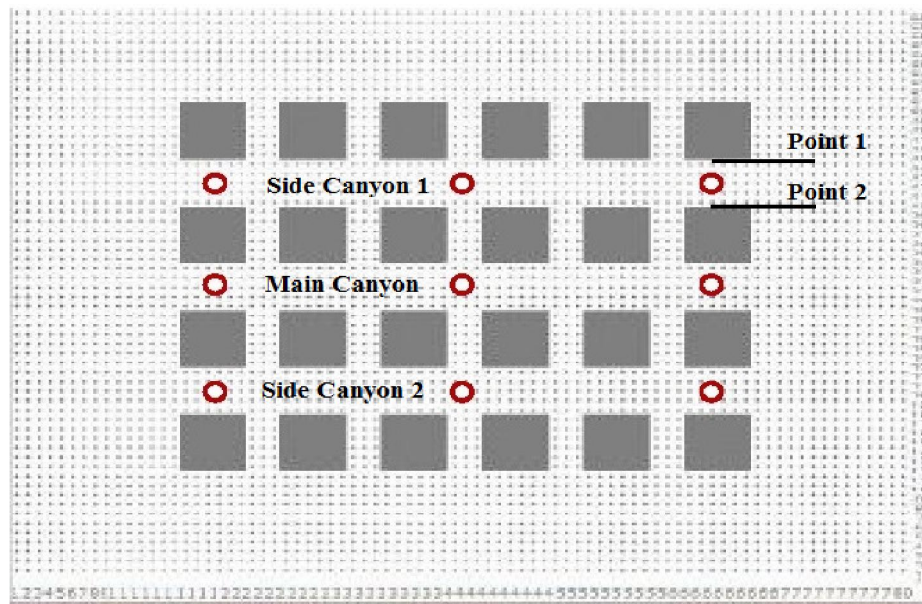
Canyon	Points (Z Direction)	Beginning of Canyon (1)	Middle of Canyon (2)	End of Canyon (3)
Side Canyon 1	Receptors (1.4 m)	37	38.8	36.6
	5 m	36.8	38.3	36.5
	11 m	36.5	37.4	36.2
	17 m	36	36.8	35.8
Main Canyon	Receptors (1.4 m)	36.1	37.6	36.1
	5 m	36	37.1	36
	11 m	35.7	36.6	35.7
	17 m	35.4	36.2	35.4
Side Canyon 2	Receptors (1.4 m)	35.5	36.8	35.7
	5 m	35.5	36.5	35.6
	11 m	35.3	36.1	35.4
	17 m	35	35.7	35.1

The data of maximum air temperature from the receptors and the selected points at height of 1.4m,7m,11m, and 17m in the three canyons at the beginning , middle, and end of each canyon

Canyon	Points (X,Y)	Beginning of Canyon	Middle of Canyon	End of Canyon
Side Canyon 1	Point 1	0.3	3.8	0.3
	Receptors	0.6	3.2	0.5
	Point 2	0.8	3	0.3
Middle Canyon	Point 1	0.2	2.9	36
	Receptors	0.4	2.7	0.2
	Point 2	0.2	3	0.4
Side Canyon 2	Point 1	0.3	2.9	0.2
	Receptors	0.4	2.7	0.4
	Point 2	0.5	3.2	0.3

Canyon	Points (Z Direction)	Beginning of Canyon (1)	Middle of Canyon (2)	End of Canyon (3)
Side Canyon 1	Receptors (1.4 m)	0.5	3.2	0.5
	5 m	0.5	3.9	0.5
	11 m	0.4	4.2	0.4
	17 m	0.2	4.3	0.3
Main Canyon	Receptors (1.4 m)	0.4	2.7	0.4
	5 m	0.4	3	0.4
	11 m	0.3	3.2	0.3
	17 m	0.3	3.5	0.3
Side Canyon 2	Receptors (1.4 m)	0.4	2.7	0.4
	5 m	0.5	3	0.5
	11 m	0.5	3.1	0.4
	17 m	0.4	3.3	0.3

The data of wind speed from the receptors and the selected points at height of 1.4m,7m,11m, and 17m in the three canyons at the beginning , middle, and end of each canyon

FLIR SYSTEMS

Declaration of Conformity

Extech Model: 45170
Description: Humidity/Temperature/Airflow/Light Level Meter
Date of Issue: 07-Nov-13

We, FLIR Commercial Systems, Inc. - Extech Brand, 9 Townsend West, Nashua, NH 03063 declare that a sample of the product listed above has been tested by a third party for CE marking according to:

EMC Directive: 89/336/EEC
Report Number: 53-11
Report Date of Issue: 1/29/2002

Standards:
CISPR Class B

The test reports show that the product fulfills the requirement in the EC EMC Directive for CE Marking. On this basis, together with the manufacturer's own documented production control, the manufacturer (or his European authorized representative) can in his EC Declaration of Conformity verify compliance with the EC EMC Directive.

Tony Campagna
Director of Quality Services

The microclimate measuring tool certificate

Appendix B

B.1: Initial thermal and construction data of the typical configuration file used in IES-VE software

----

Construction Element	Layer Order	Layer Name	Thickness (cm)	Density (w/cm²)	U-Value (w/cm²)
Roof	External	Concrete Tiles	2.5	0.0227	
		Cement Mortar	2	0.0215	
		Sand And Gravel	8	0.2857	
	To	Polymer Waterproof Sheet	1	0.0667	0.25
		Asphalt Rolling Materials	1	0.0435	
	Internal	Reinforced Concrete	20	0.0862	
		Cement Plaster	2	0.0215	
External Walls	External	Cement Plaster	2	0.0215	
		Hollow Block	7.5	0.2679	
	To	Polystyrene	5	1.667	0.43
	Internal	Hollow Block	7.5	0.2679	
		Cement Plaster	2	0.0215	
Internal Walls	Internal	Cement Plaster	2	0.0215	
		Hollow Block	10		1.07
		Cement Plaster	2	0.0215	
Ground	Top	Concrete Tiles	2.5	0.0227	
		Cement Mortar	2	0.0215	
		Sand And Gravel	8	0.2857	
	To	Reinforced Concrete	6	0.0345	
		Autoclaved Conc. Block	14	0.7778	0.54
	Bottom	Asphalt Rolling Material	3	0.013	
		Fine Aggregate Concrete	6	0.0397	
		Earth	60	0.4688	
				1.6637	
Floor and Ceiling		Concrete Tiles	2.5	0.0227	
		Cement Mortar	2	0.0215	
		Sand And Gravel	5	0.2857	1.6
		Reinforced Concrete	15	0.0862	
		Cement Plaster	2	0.0215	
Glazing	External	Glass	0.6	0.0079	
	To	Cavity	0.16	0.161	2.8
	Internal	Glass	0.6	0.0079	

Appendix C

C.1: The maximum and minimum microclimate parameters of the first group configurations comparing to the base case in ; a) N-S and b) E-W orientations

----
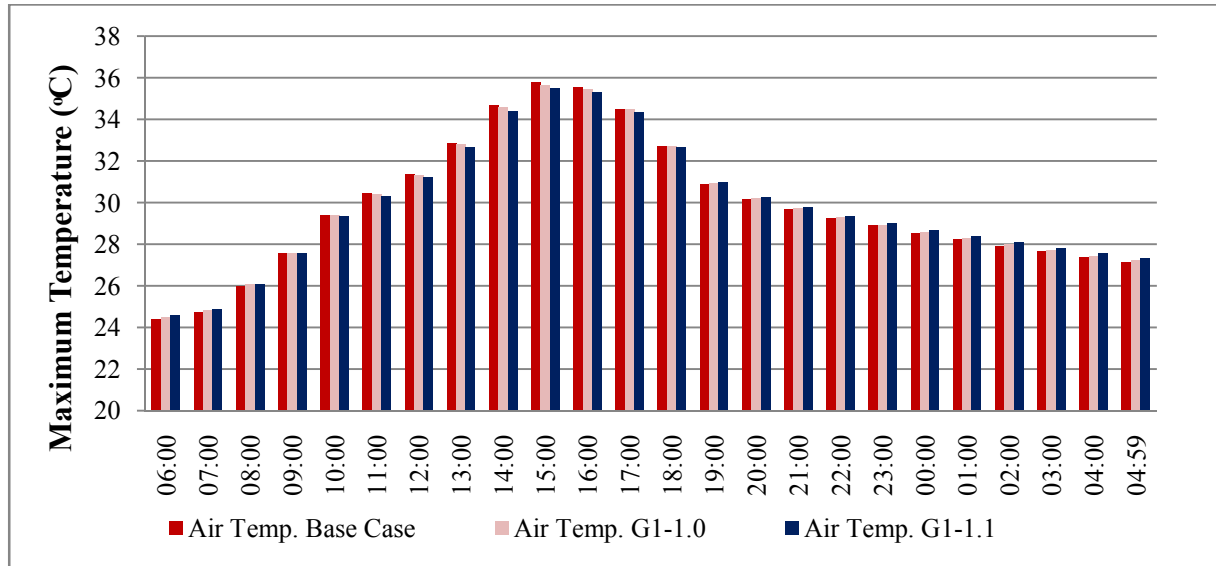
a) N-S orientations
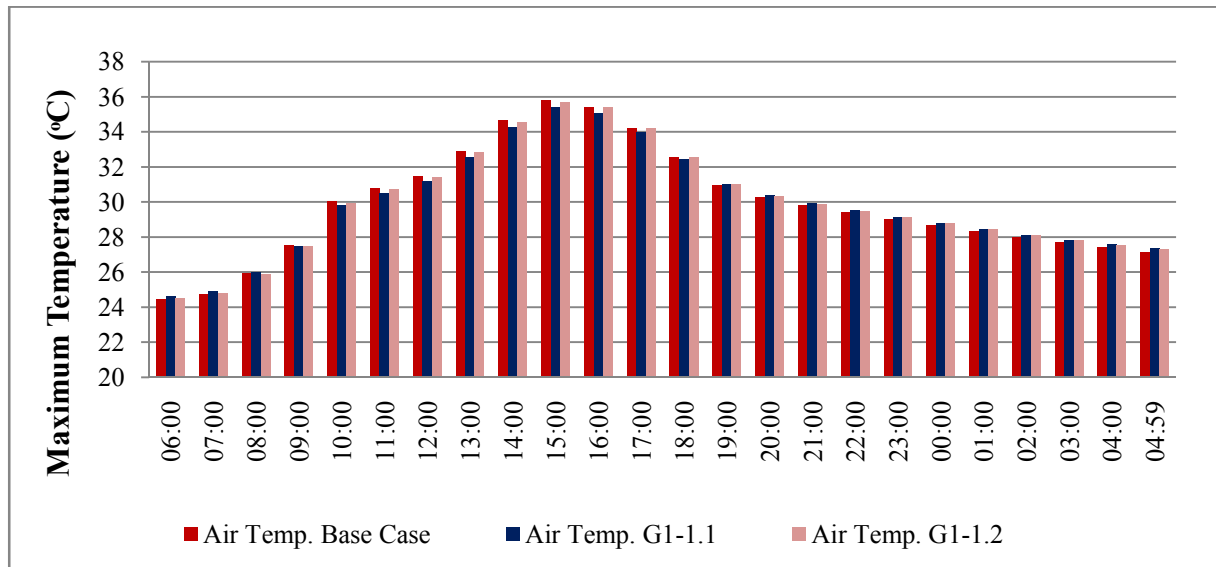
a) E-W orientations

The maximum and minimum reduction in air temperature averages of the first group comparing to the base case in ; a) N-S and b) E-W orientations
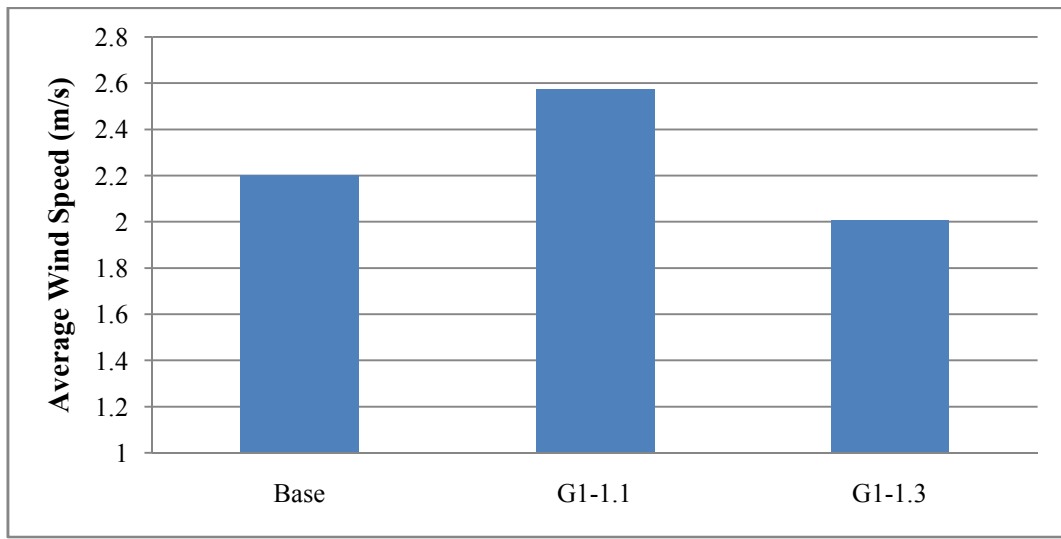
wind velocity N-S
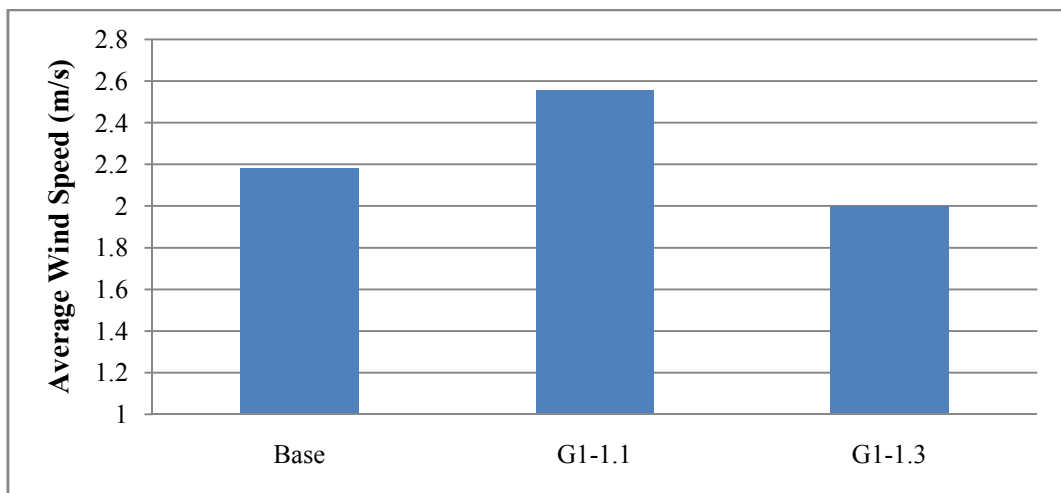
wind velocity E-W

The maximum and minimum wind velocity of the first group configurations comparing to the base case in two orientations; a) N-S and b) E-W

C. 2: The maximum and minimum microclimate parameters of the second group configurations comparing to the base case in ; a) N-S and b) E-W orientations

----
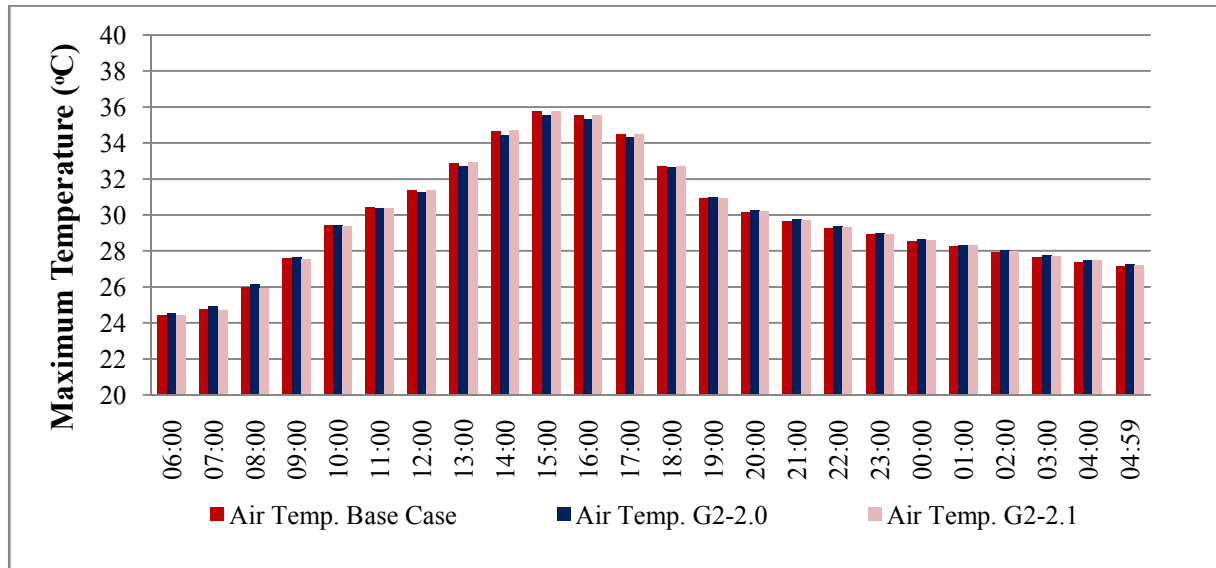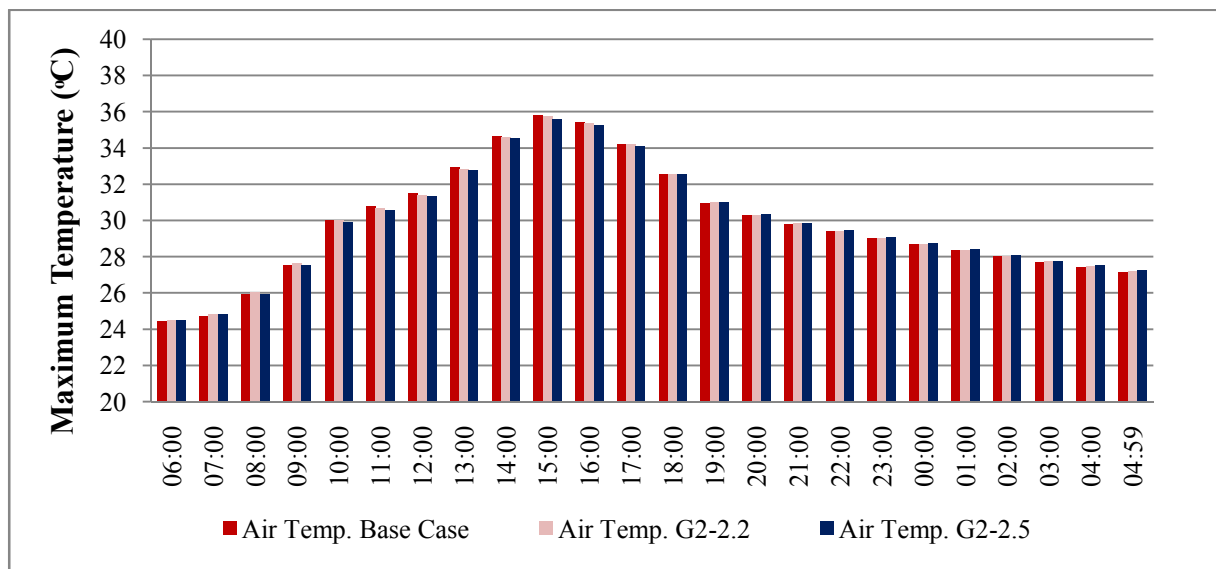
a) N-S orientation

b) E-W orientation

The maximum and minimum reduction in air temperature averages of the second group comparing to the base case in ; a) N-S and b) E-W orientations
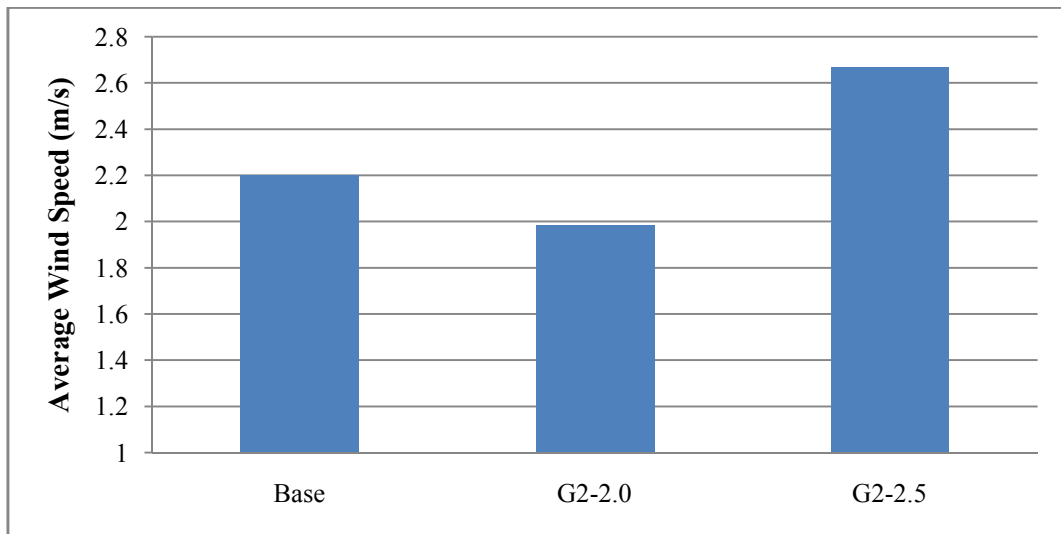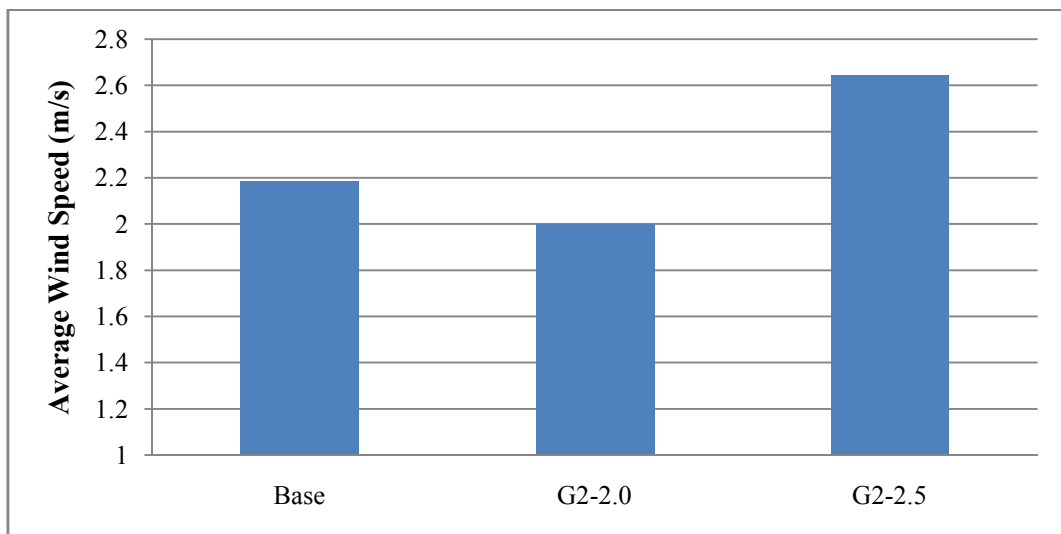
a) N-S orientation

b) E-W orientation

The maximum and minimum wind velocity of the second group configurations comparing to the base case in two orientations; a) N-S and b) E-W

C. 3: The maximum and minimum reduction in air temperature averages of the third group comparing to the base case in ; a) NW-SE and b) NE-SW orientations

----
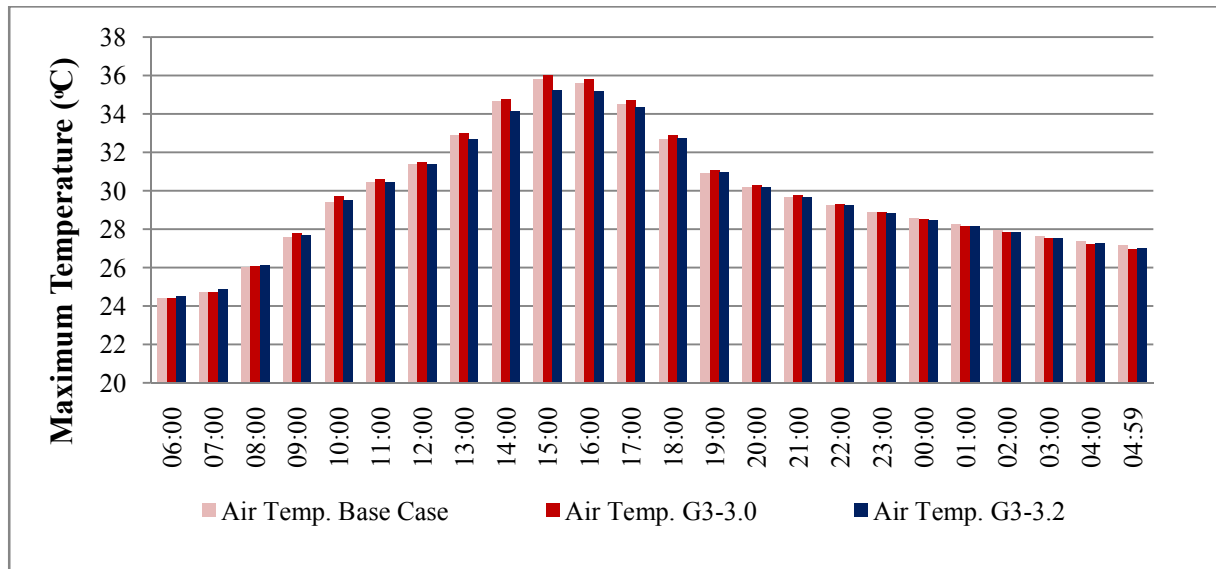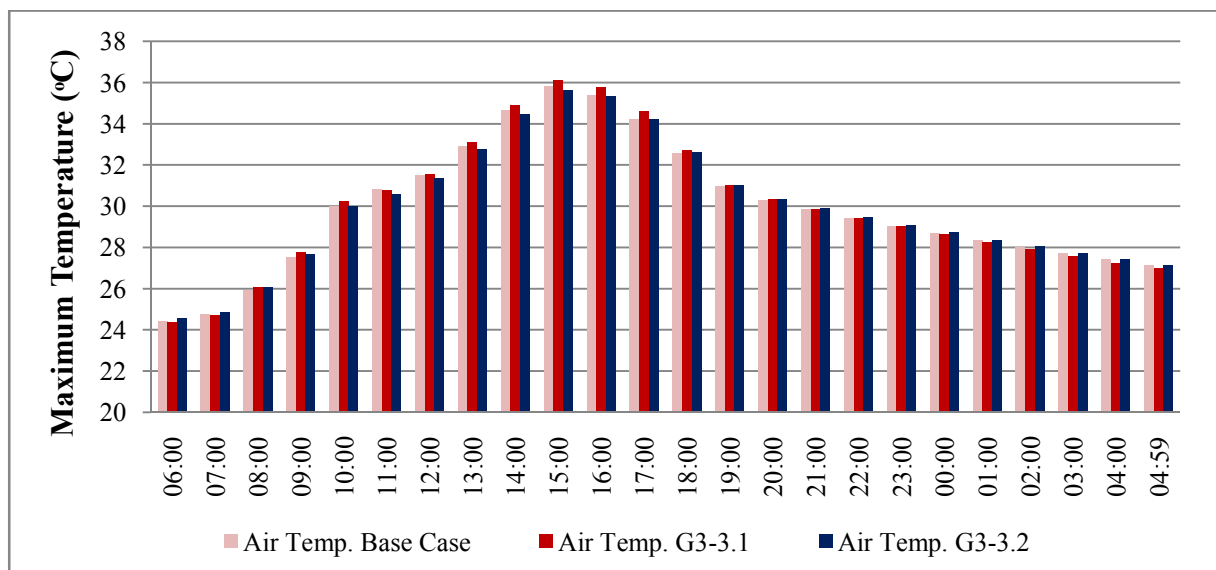
a) N-S orientation

b) E-W orientation

The maximum and minimum reduction in air temperature averages of the third group comparing to the base case in ; a) N-S and b) E-W orientations
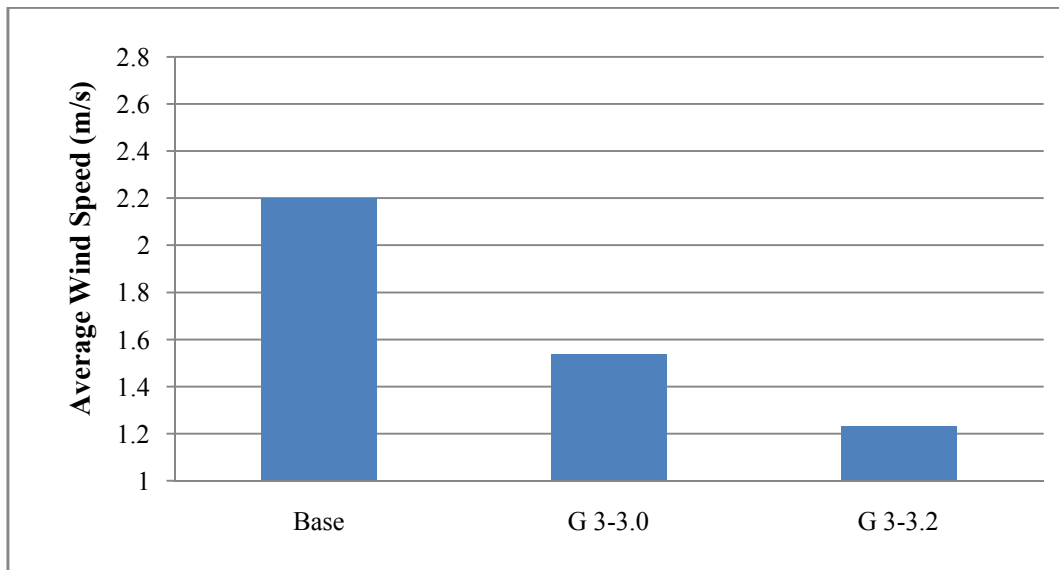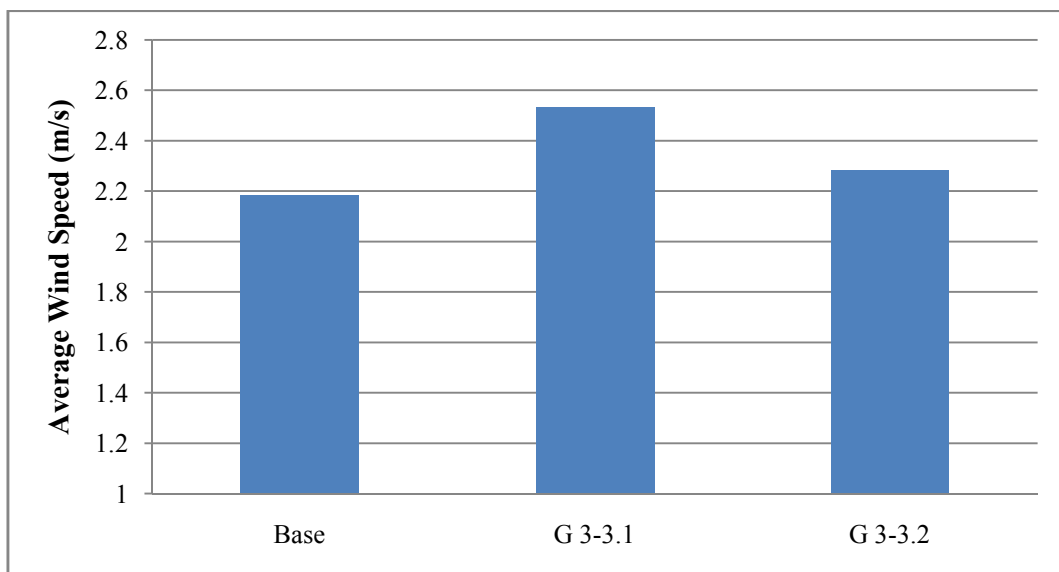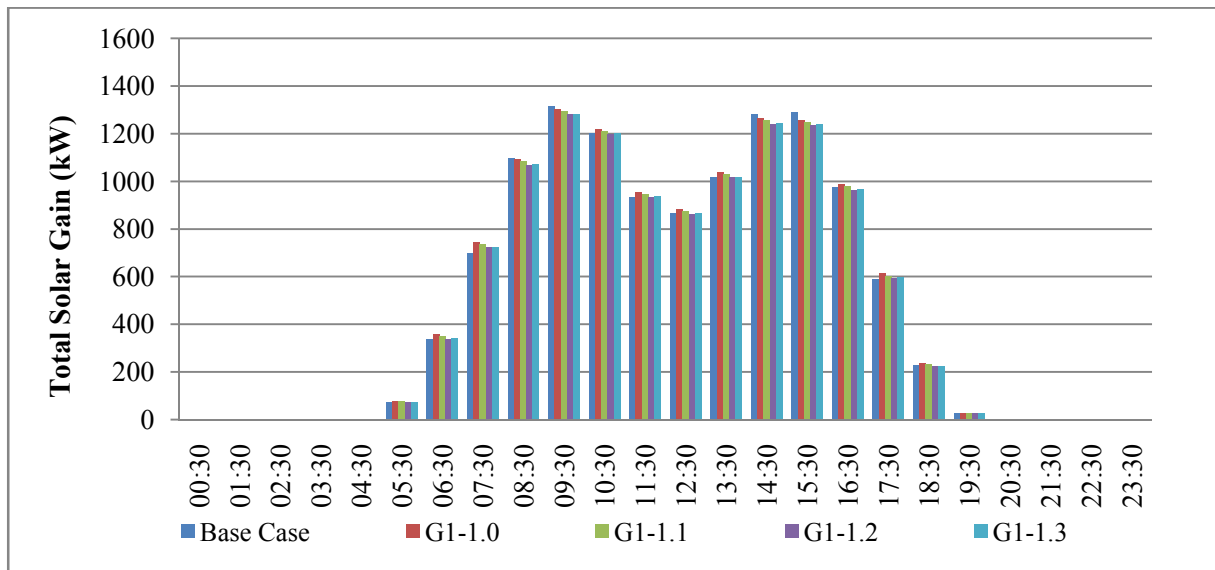
a) N-S orientation

b) E-W orientation

The maximum and minimum wind velocity of the third group configurations comparing to the base case in two orientations; a) N-S and b) E-W

Appendix D

D.1: Top veiw at 1.4 m of maximum air temperature at 3:00 pm for the best configurations of the first group in four orientations

G1-1.1 (3:7:3:7) in N-S orientation

G1-1.1 (3:7:3:7) in E-W orientation

G1-1.2 (3:7:7:3) in NE-SW orientation

G1-1.2 (3:7:7:3) in NW-SE orientation

< 33.5   34.5   36.0   > 37.5

Air Temperature ° C

D.2: Top veiw at 1.4 m of wind velocity at maximum air temperature for the best configurations of the first group in four orientations

G1-1.1 (3:7:3:7) in N-S orientation

G1-1.1 (3:7:3:7) in E-W orientation

G1-1.2 (3:7:7:3) in NE-SW orientation

G1-1.2 (3:7:7:3) in NW-SE orientation

Wind Speed m/s
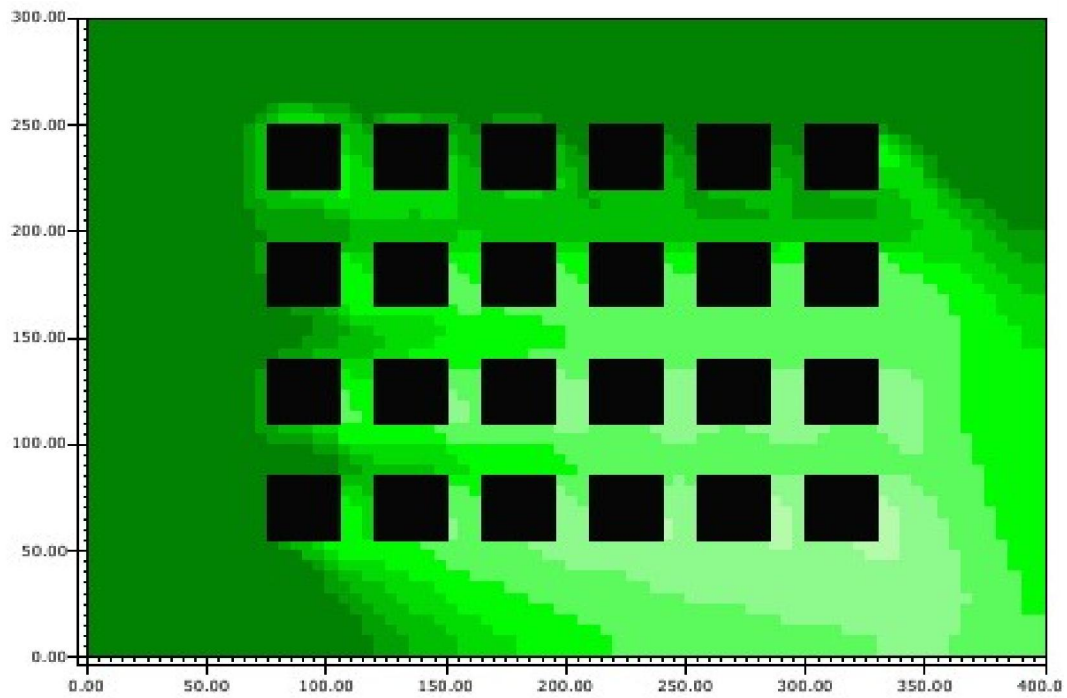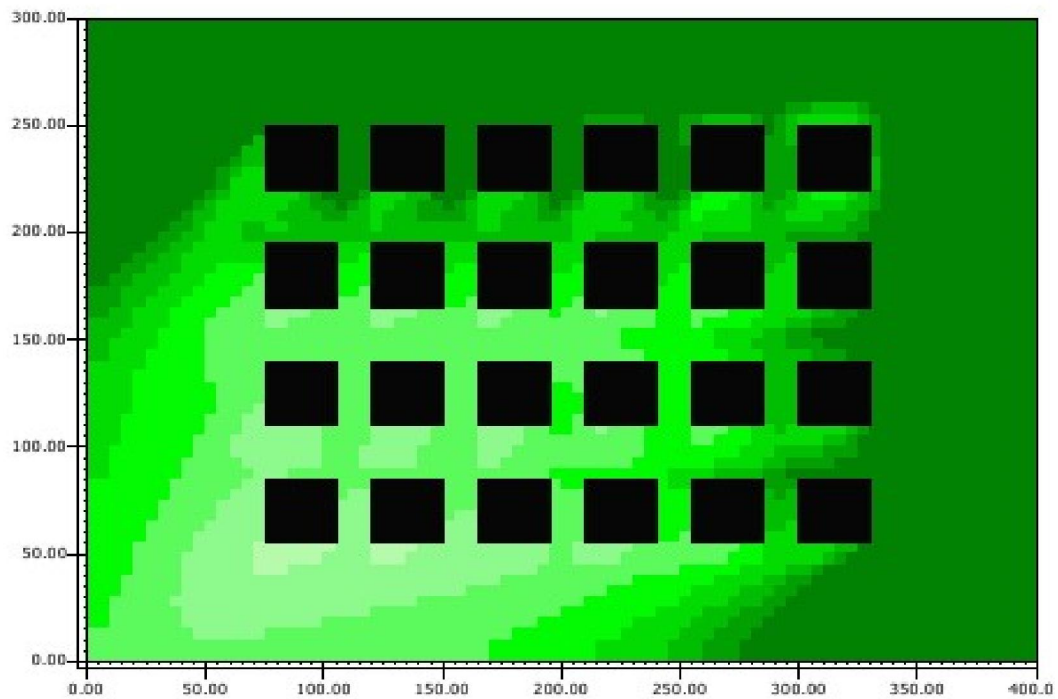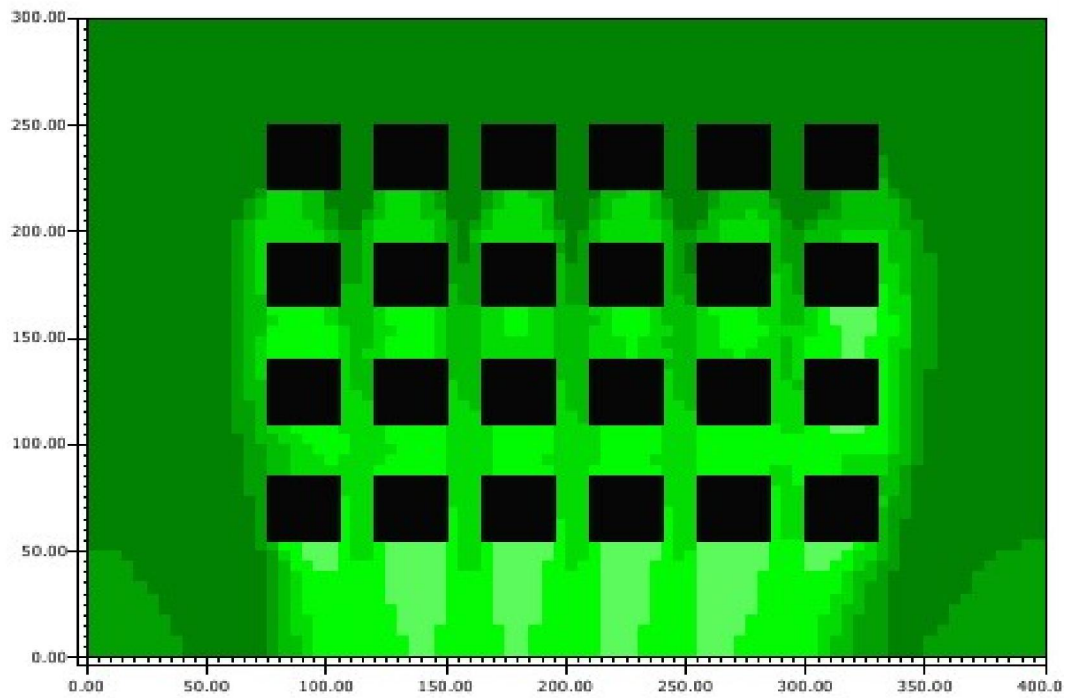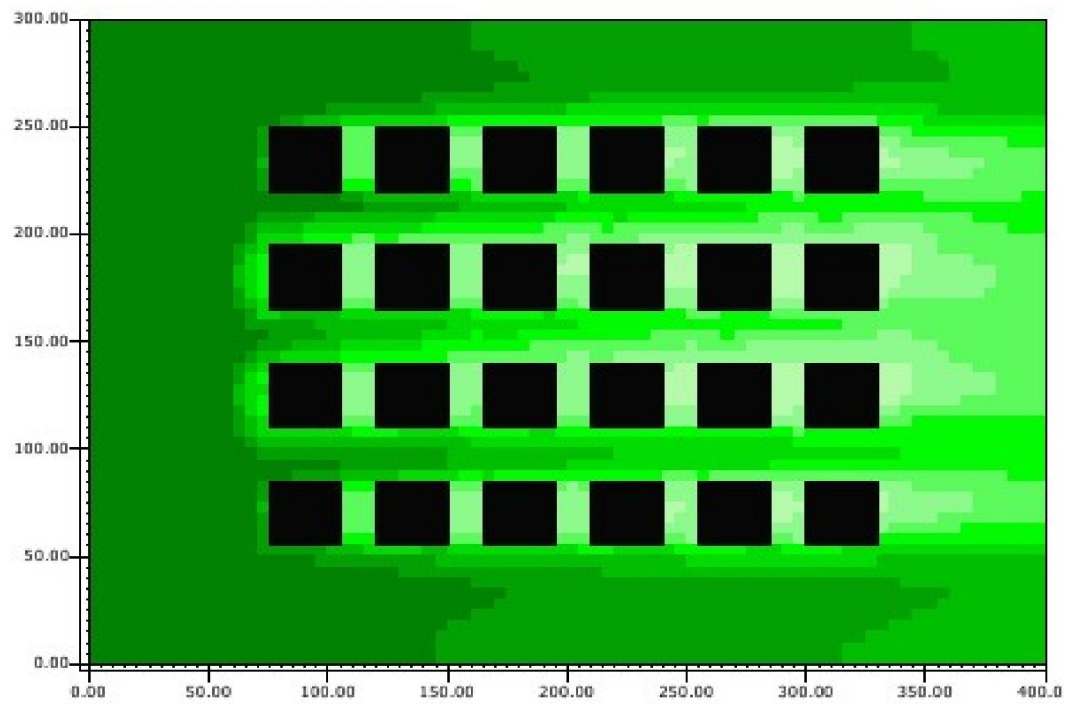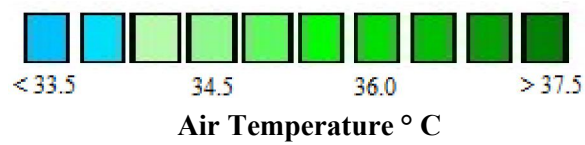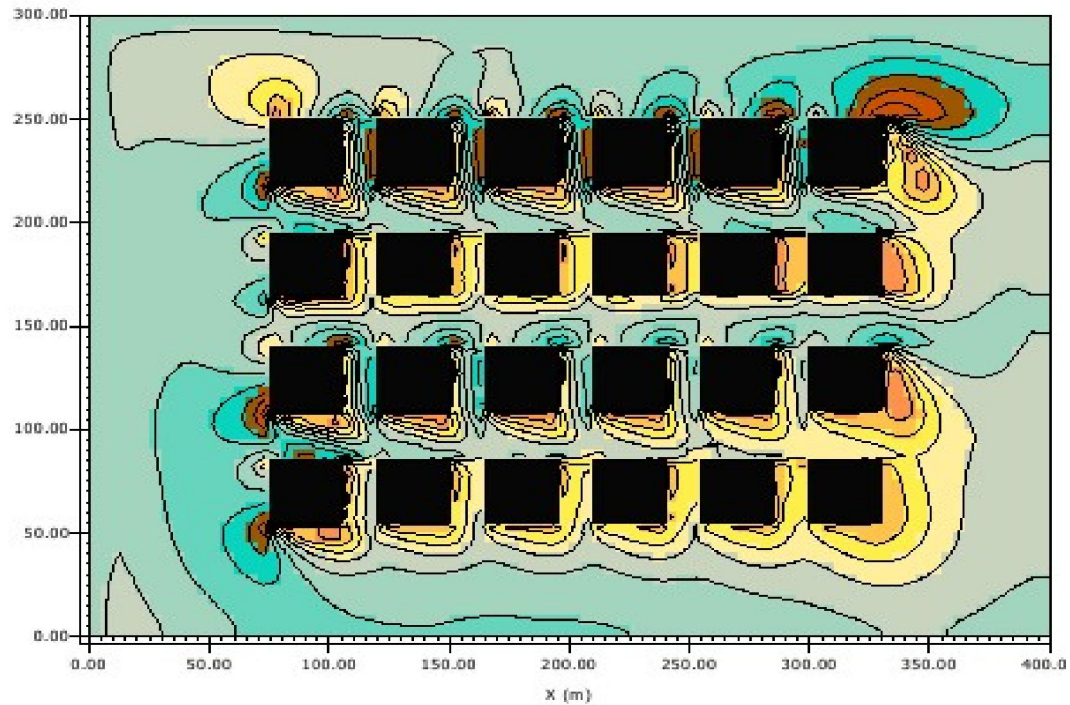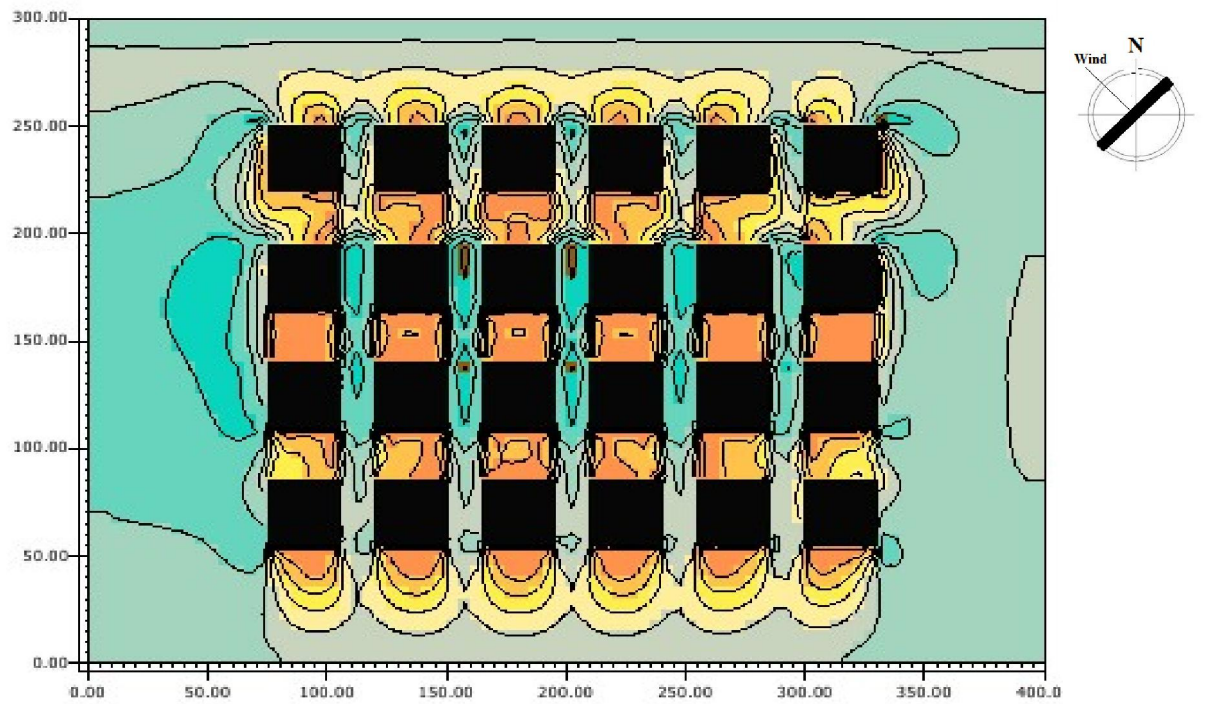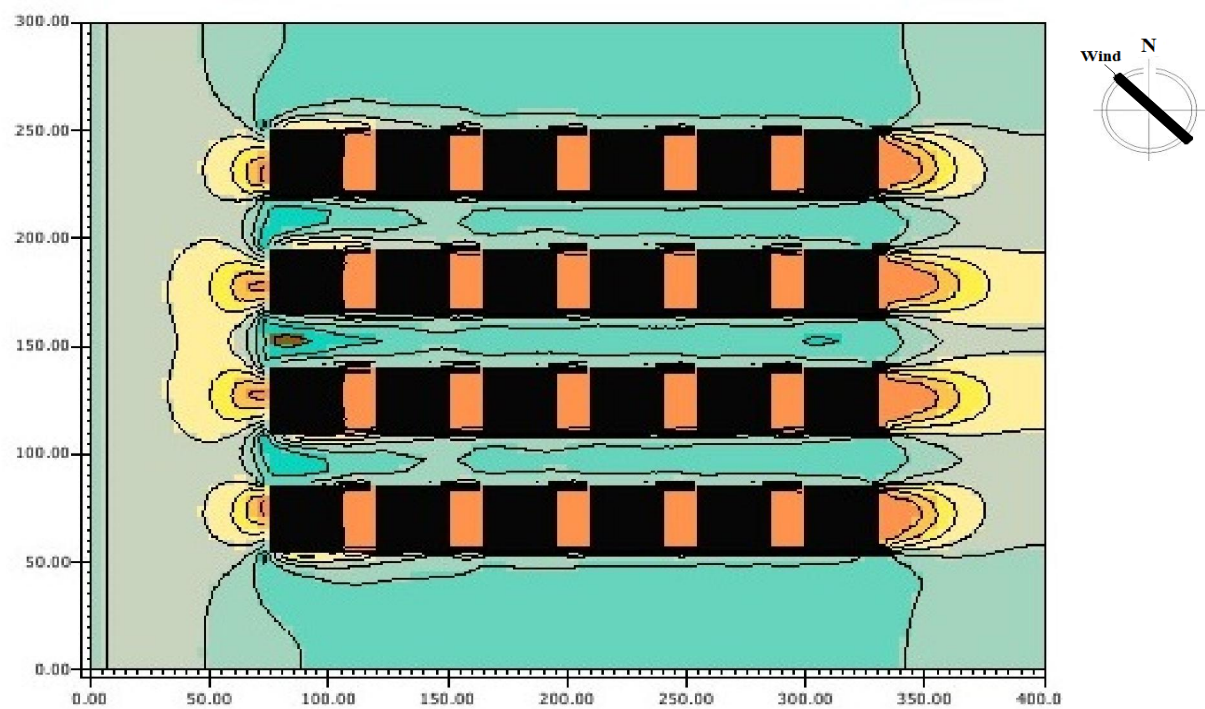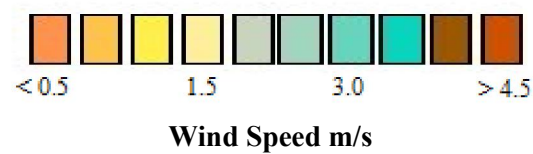
Appendix E

E. 1: Top view at 1.4 m of maximum air temperature at 3:00 pm for the best configurations of the second group in four orientations

G2-2.0 (7:5:3:3:5:7) in N-S orientation
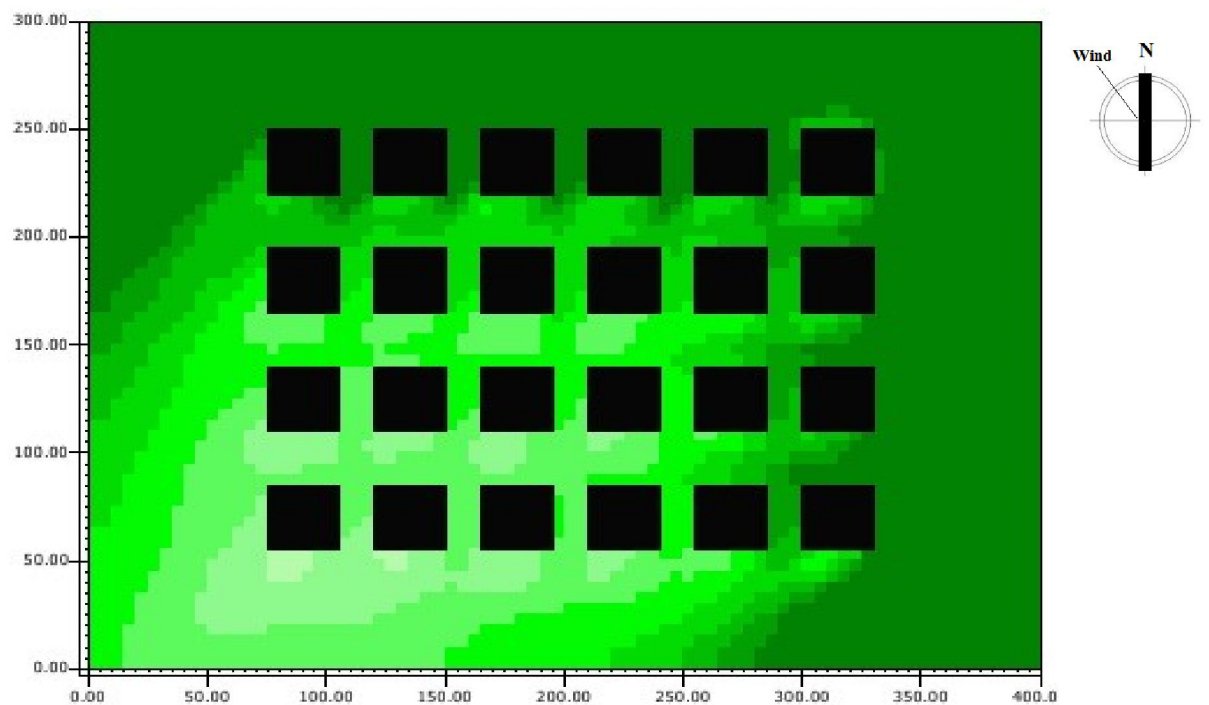
G2-2.5 (5:3:7:7:3:5) in E-W orientation
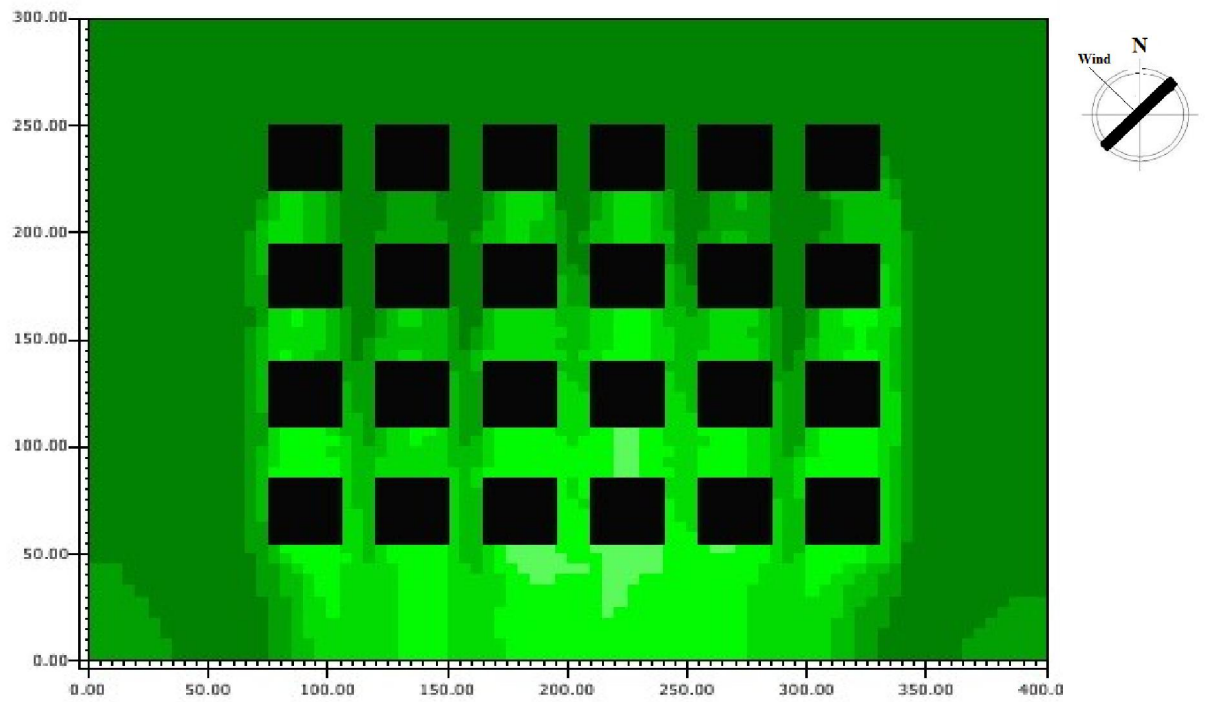
G2-2.5 (5:3:7:7:3:5) in NE-SW orientation
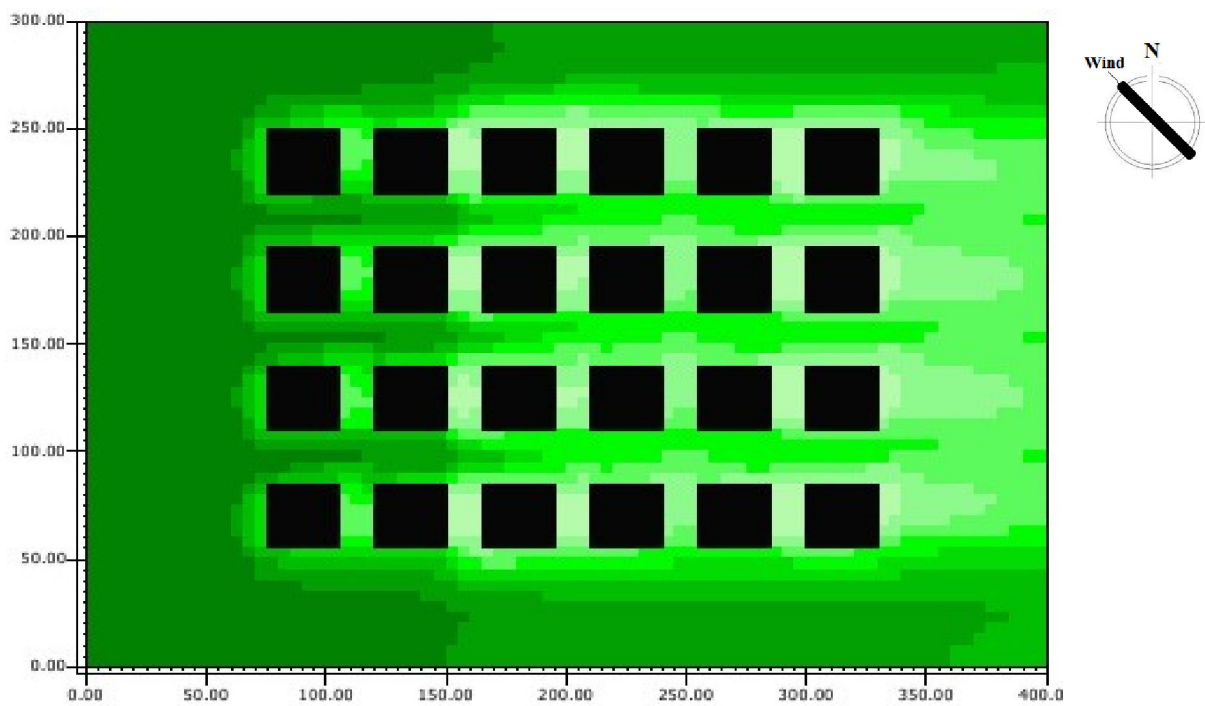
G2-2.5 (5:3:7:7:3:5) in NW-SE orientation
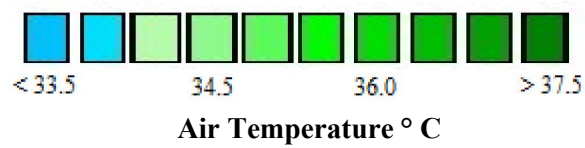
Air Temperature ° C

E.2 : Top view at 1.4 m of wind velocity at maximum air temperature for the best configurations of the second group in four orientations

G2-2.0 (7:5:3:3:5:7) in N-S orientation

G2-2.5 (5:3:7:7:3:5) in E-W orientation

G2-2.5 (5:3:7:7:3:5) in NE-SW orientation

G2-2.5 (5:3:7:7:3:5) in NW-SE orientation

Wind Speed m/s

< 0.5   1.5   3.0   > 4.5
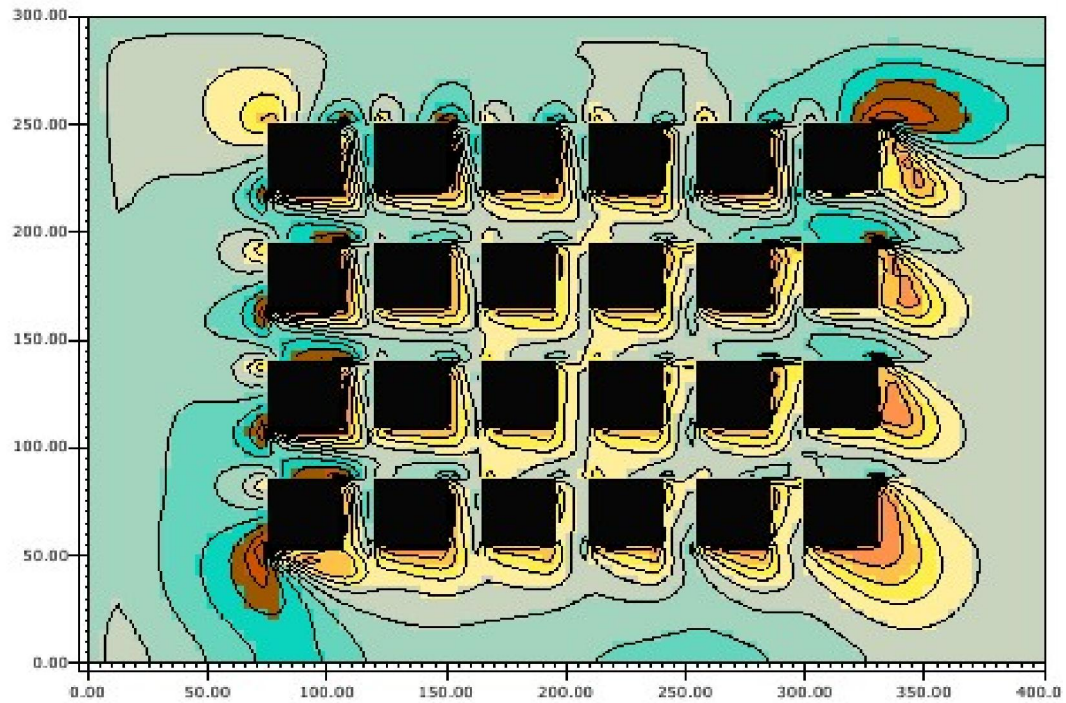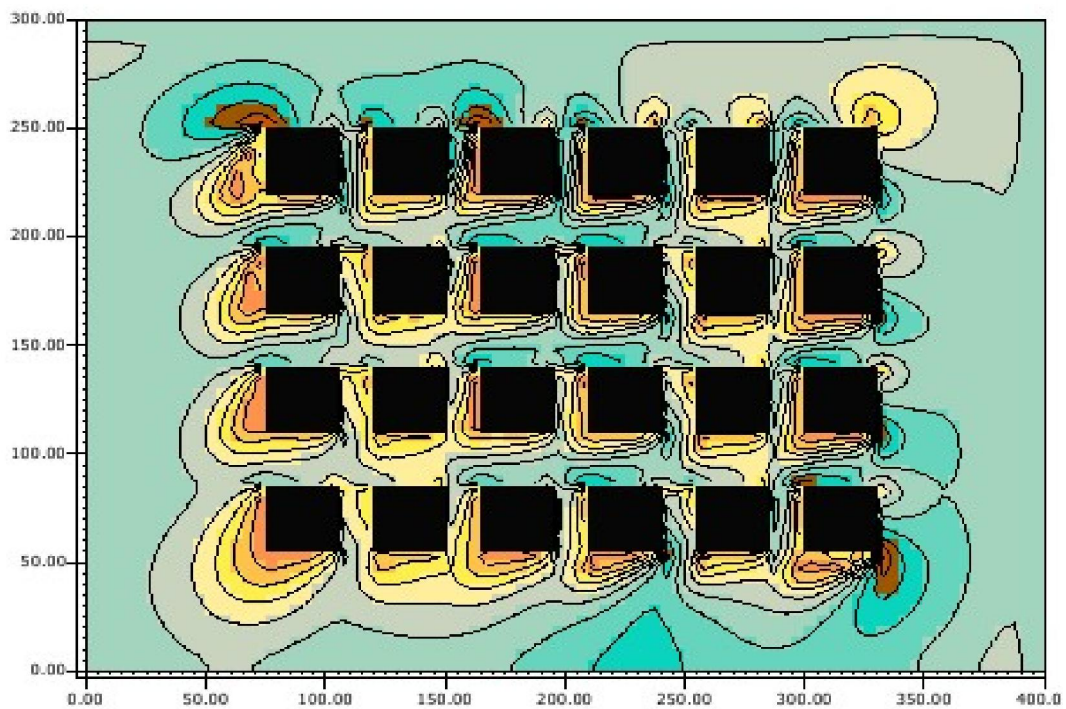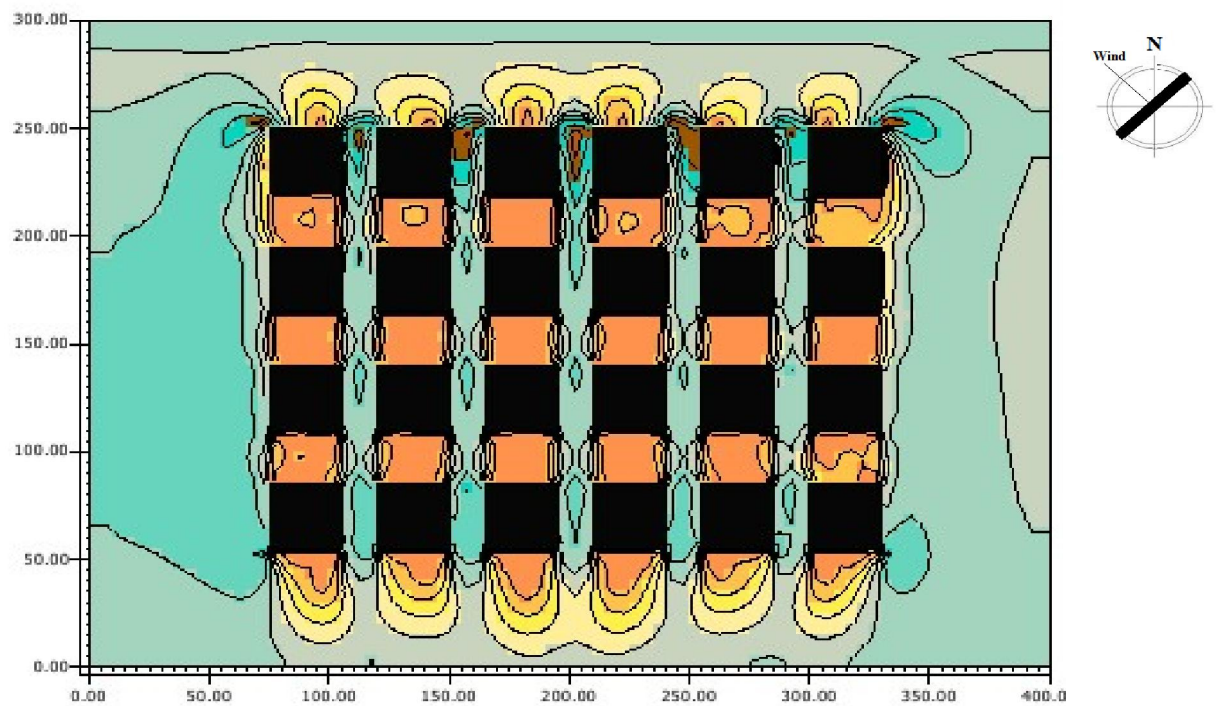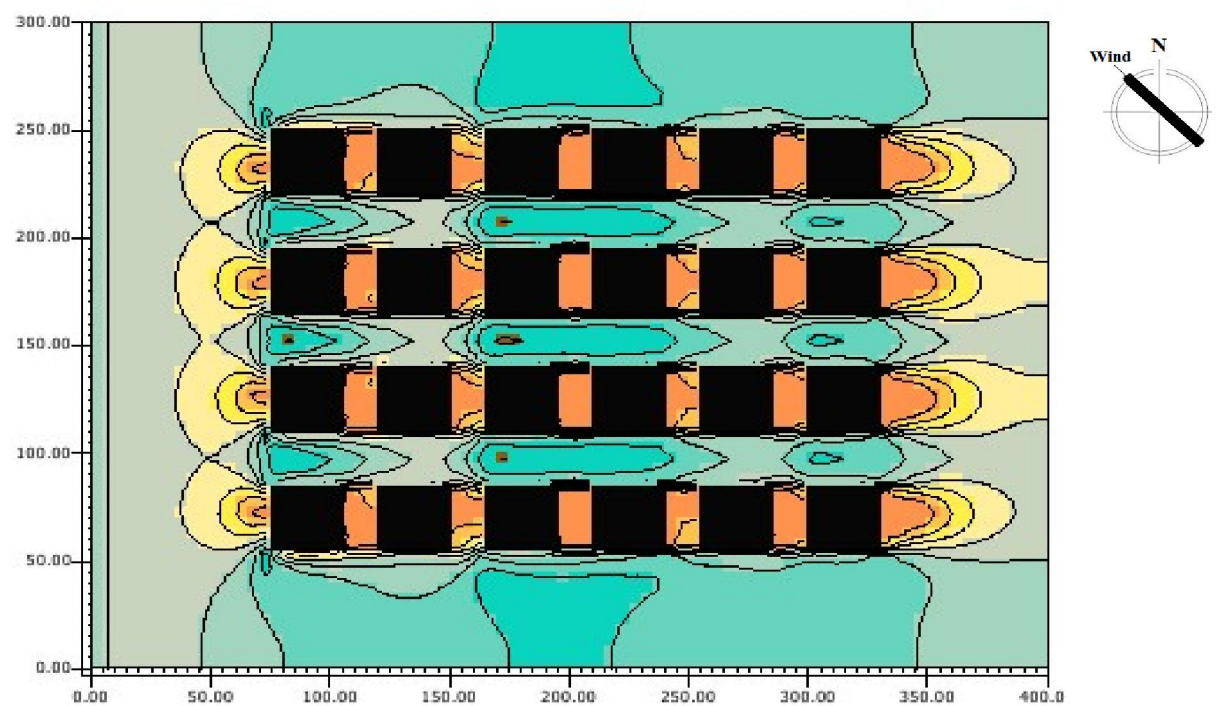
F.1 : The cooling load and the heat gain of the base case and the first group configurations

----
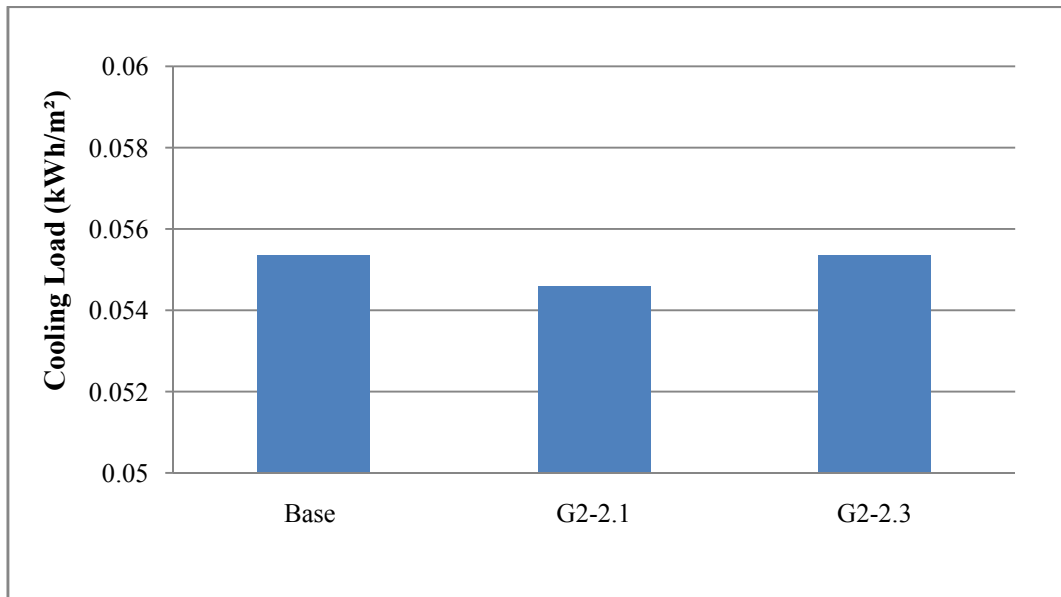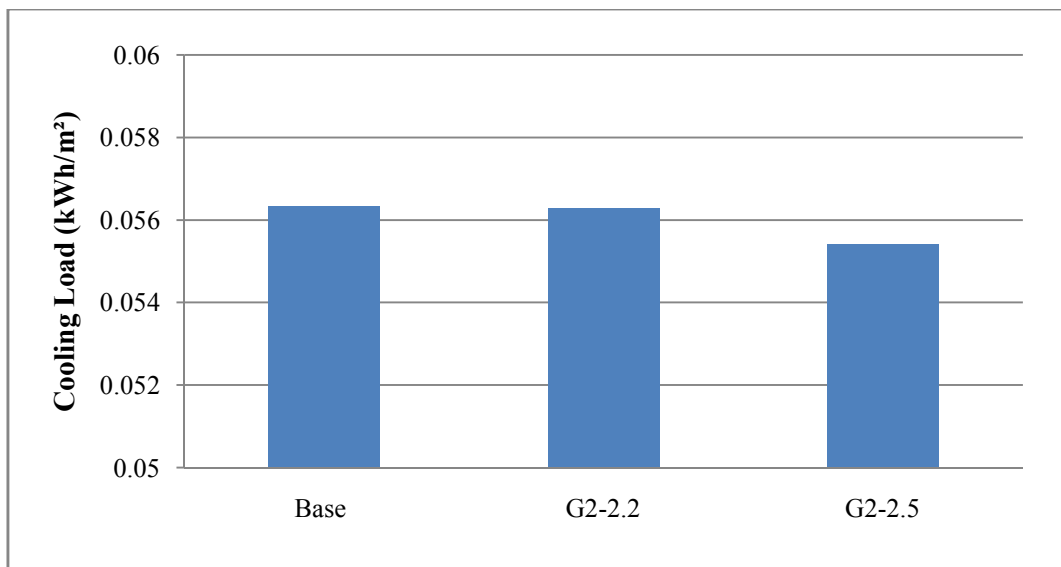

a) N-S orientation

;

b) E-W orientation

Cooling plant load daily profile on 21st. June of the first group configurations in the;
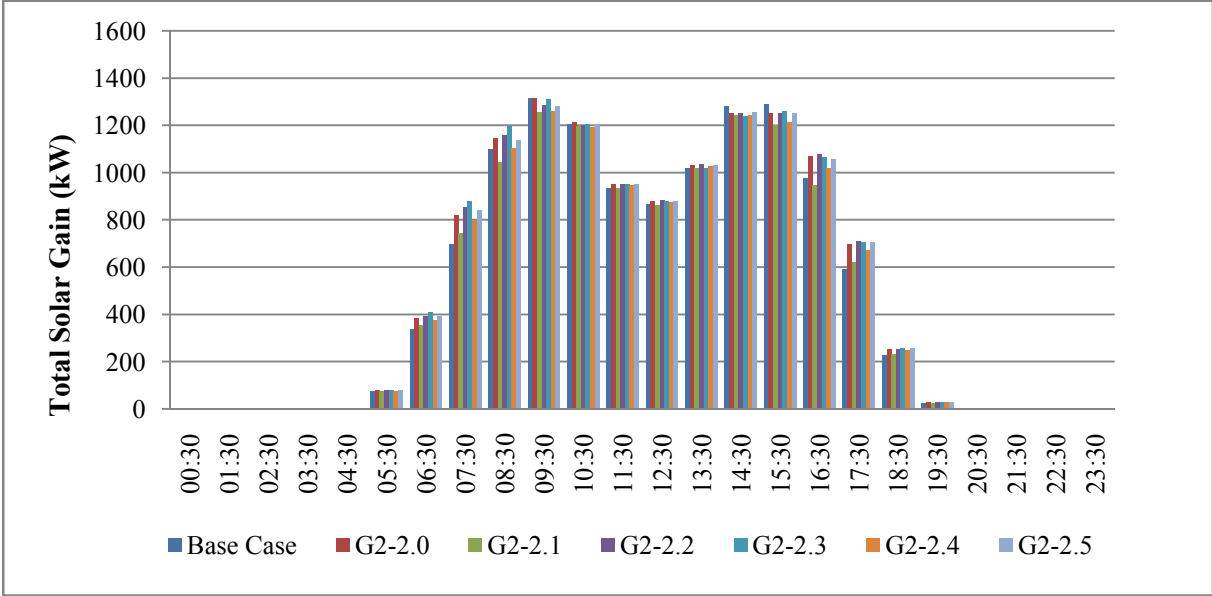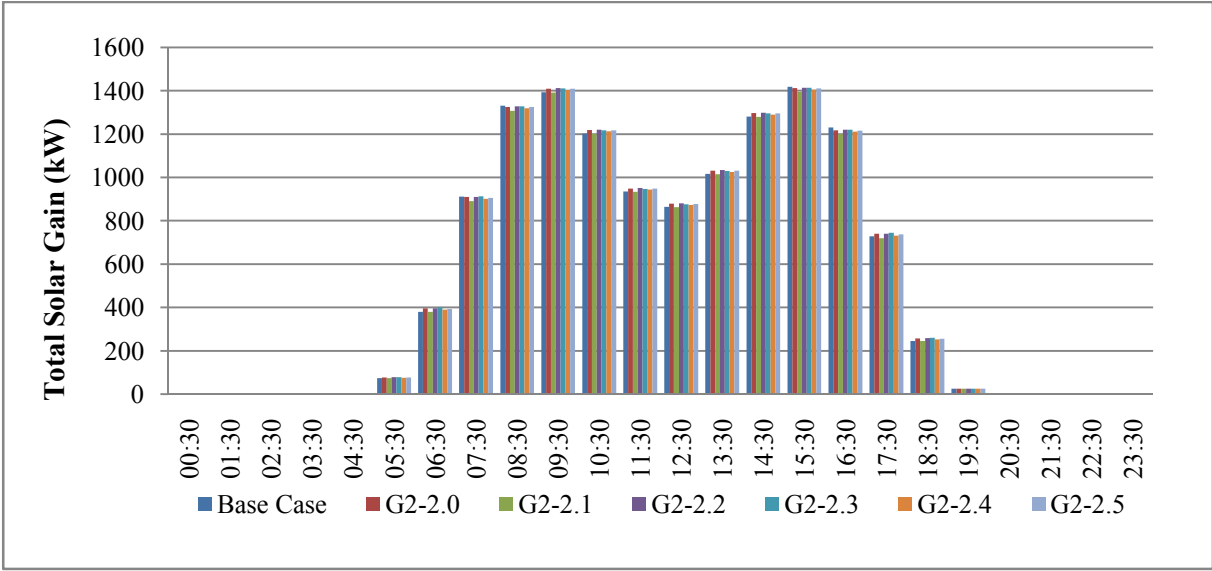a) N-S and b) E-W orientations
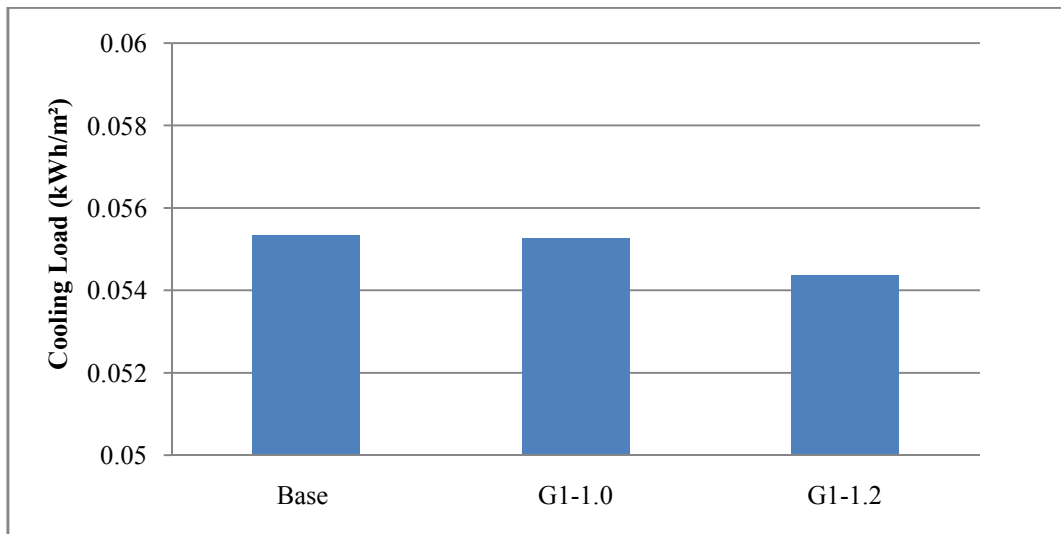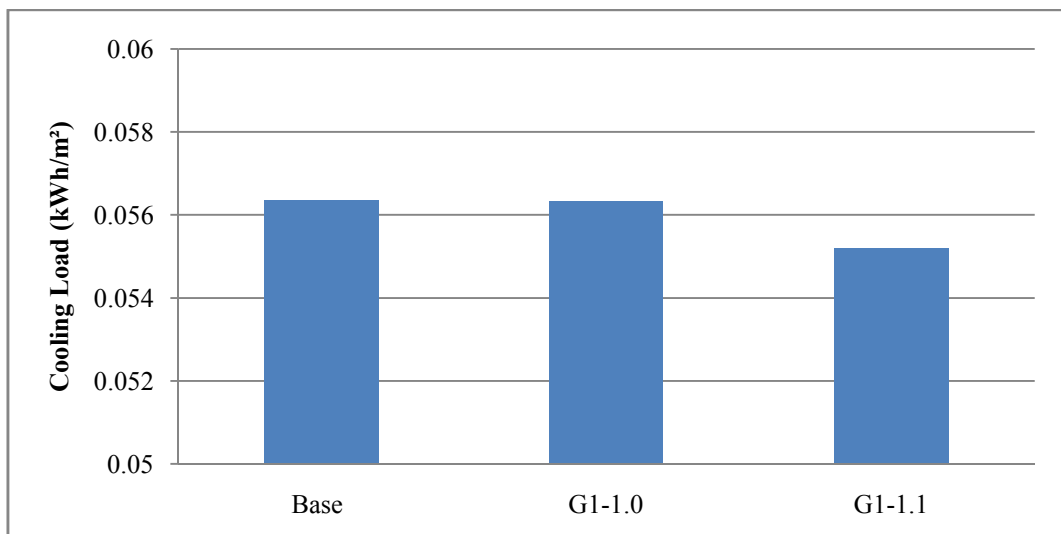
a) N-S orientation

b) E-W orientation
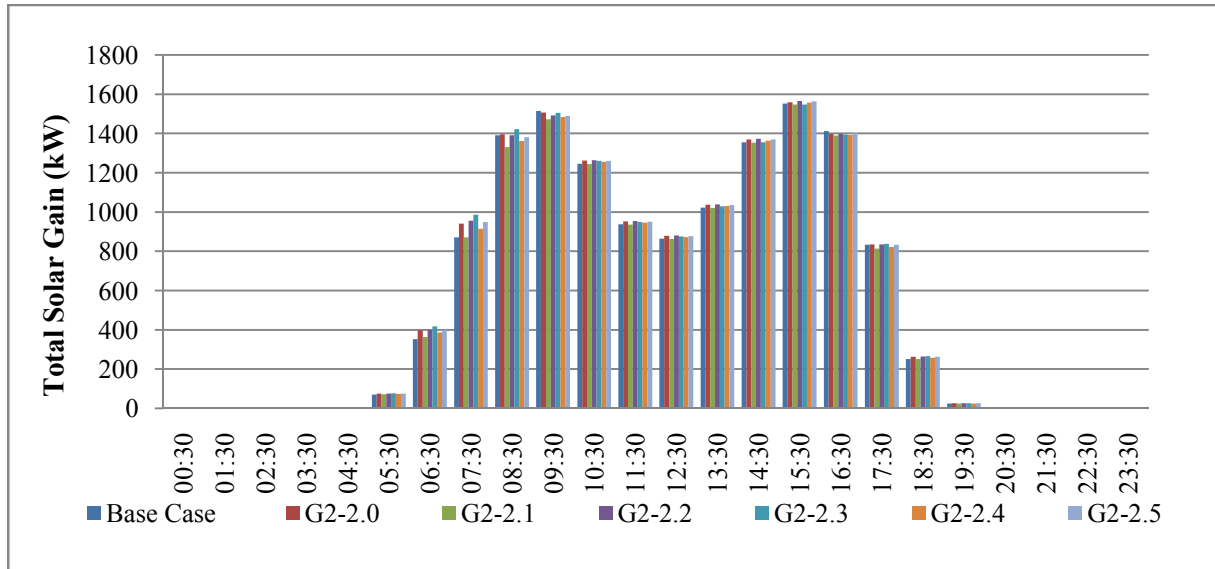
The maximum and munimum cooling load saving of the first group configurations comparing to the base case in; a) N-S and b) E-W orientations
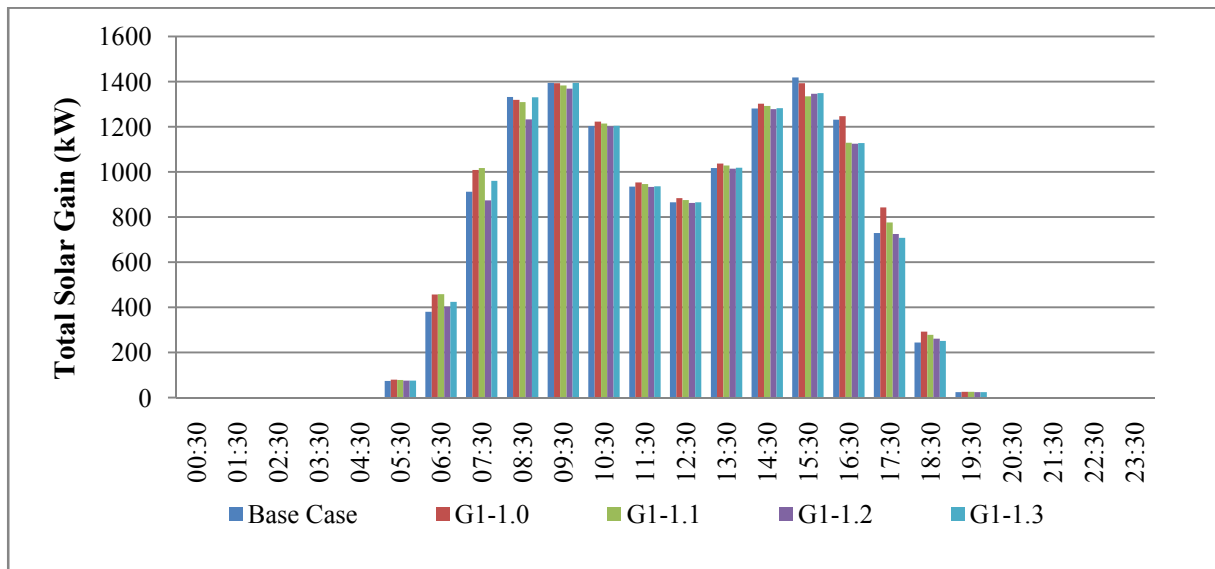
a) N-S orientation
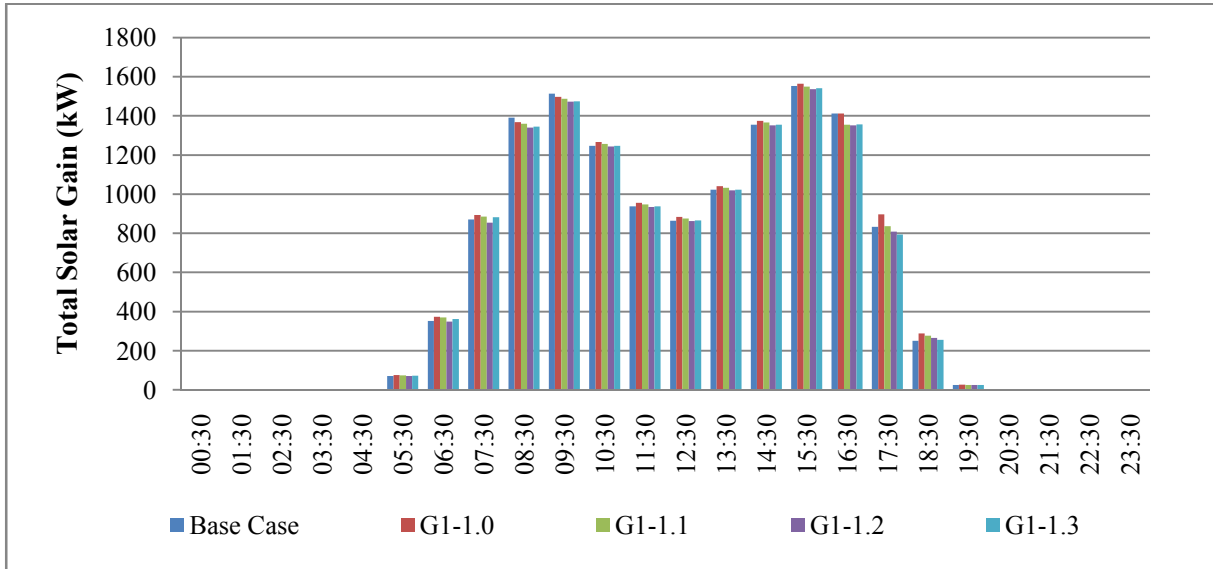
b) E-W orientation
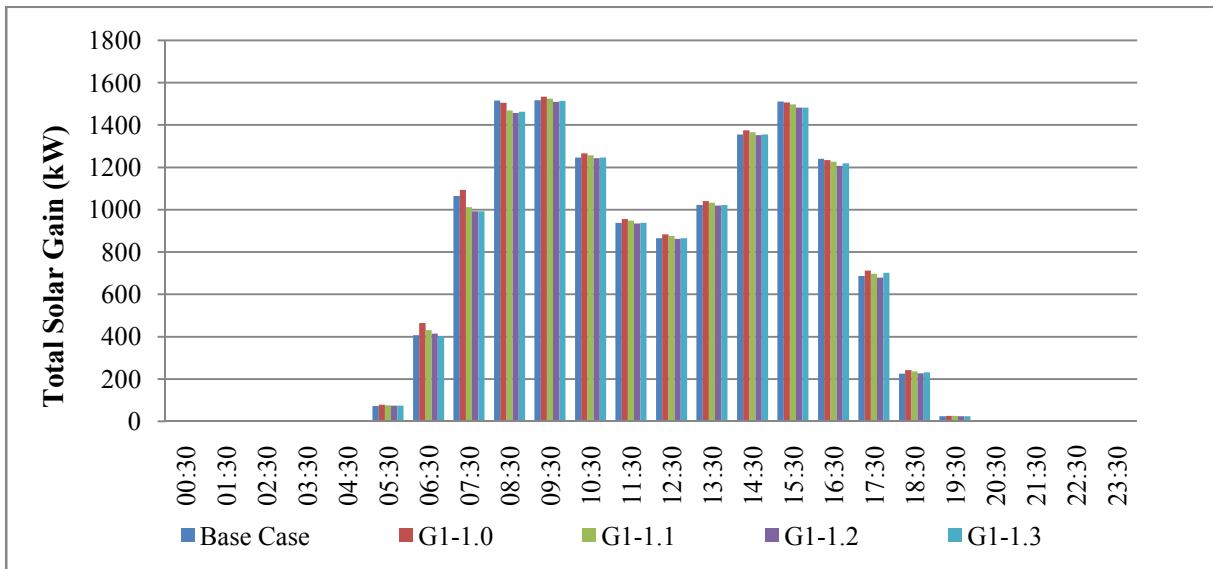
c) NE-SW orientation

d) NW-SE orientation

The direct solar gain of the base case and the first configurations in the four orientaions;
a) N-S , b) E-W, c) NE-SW and d) NW-SE
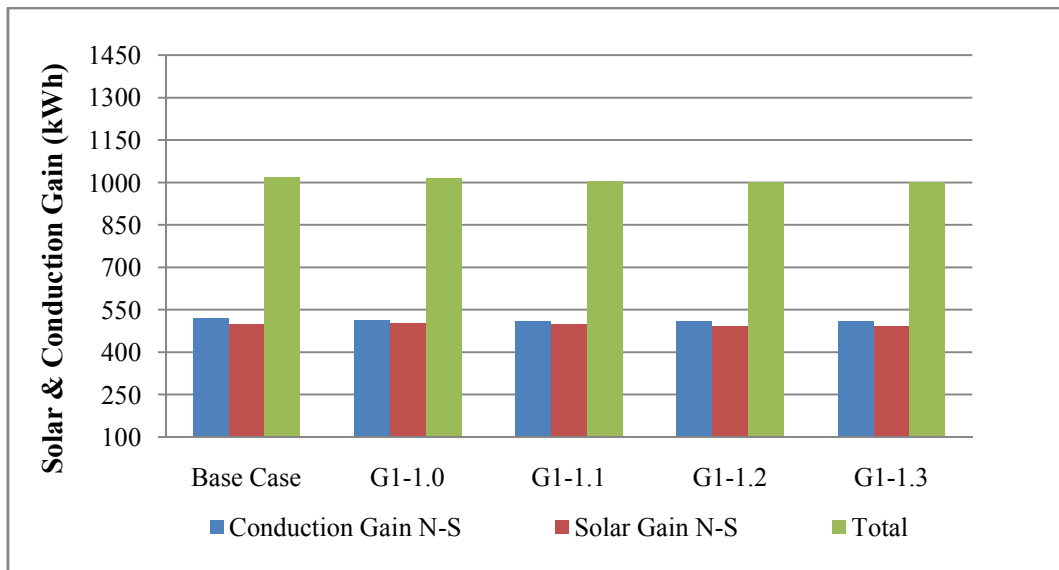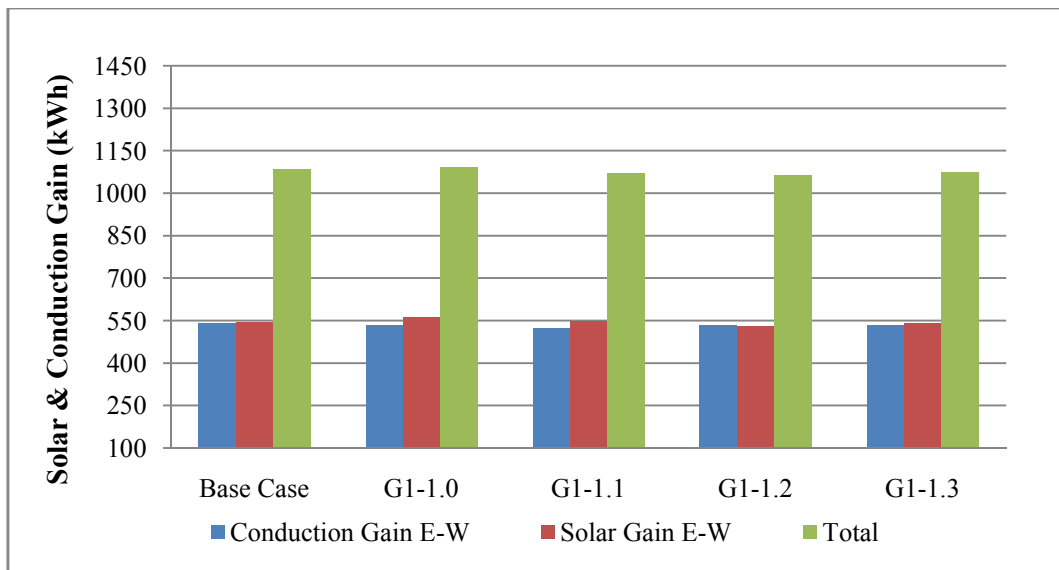
a) N-S orientation

b) E-W orientation

Solar and conduction heat gain of the first group configurations in;
a) N-S orientation, and b) E-W orientation

393

F.2 : The cooling load and the heat gain of the base case and the second group configurations

----
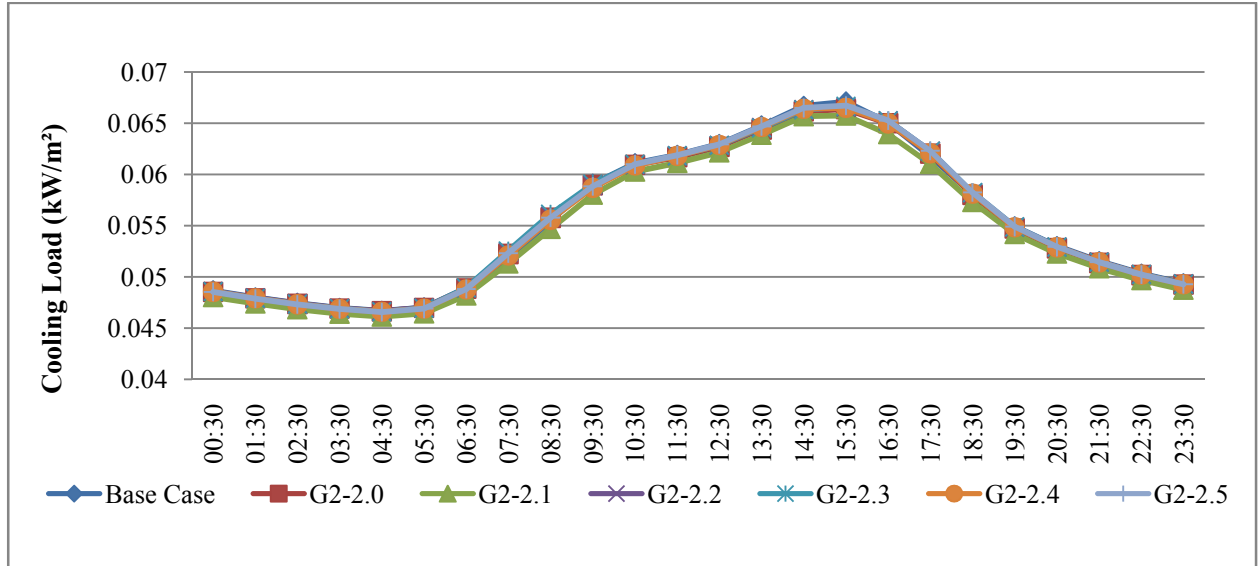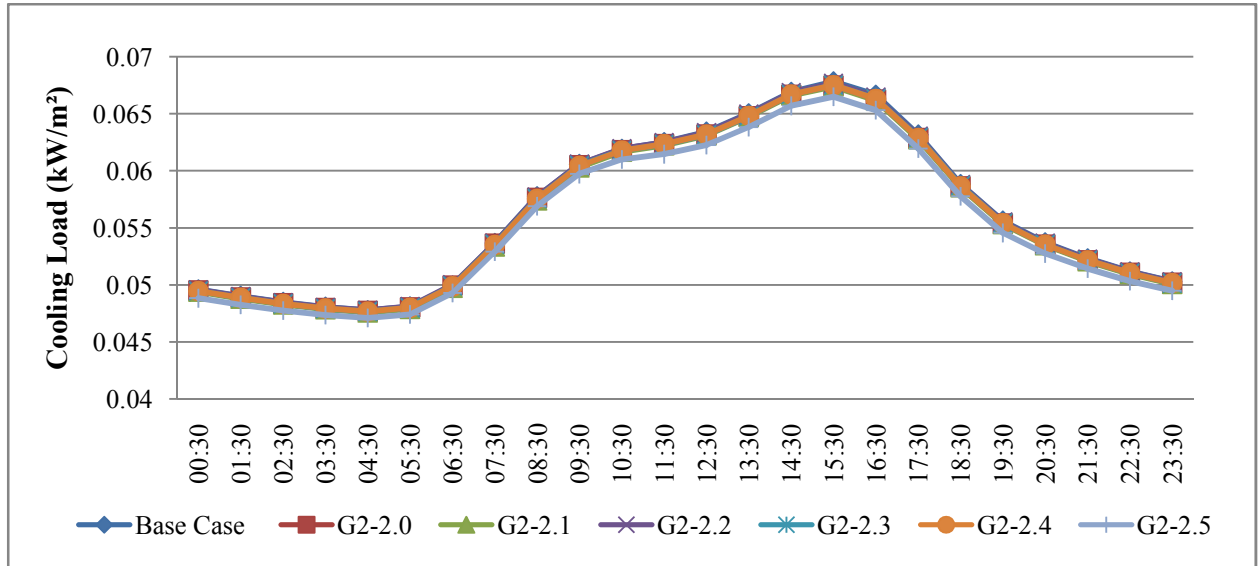
a) N-S orientation

b) E-W orientation

Cooling plant load daily profile on 21st. June of the second group configurations in the ; a) N-S and
b) E-W orientations

a) N-S orientation

b) E-W orientation

The maximum and munimum cooling load saving of the second group configurations comparing to the base case in; a) N-S and b) E-W orientations
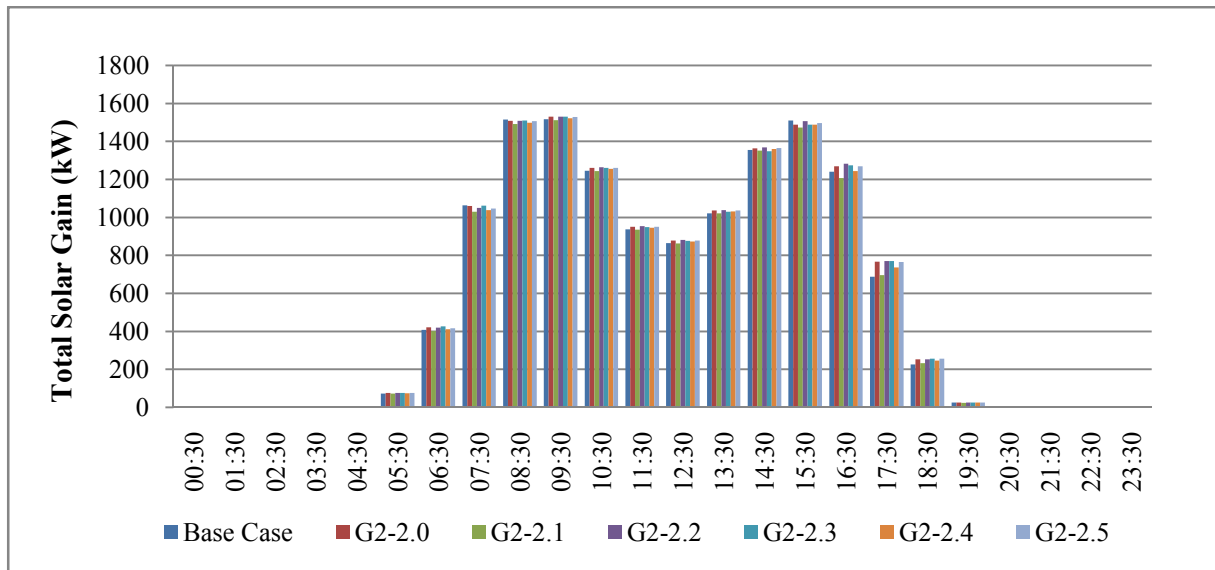
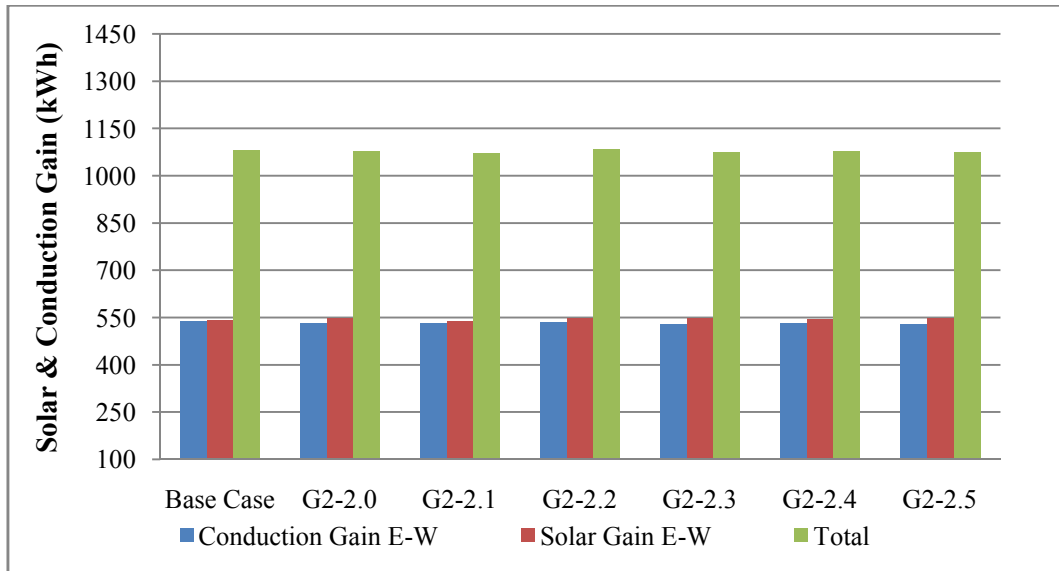a) N-S orientation
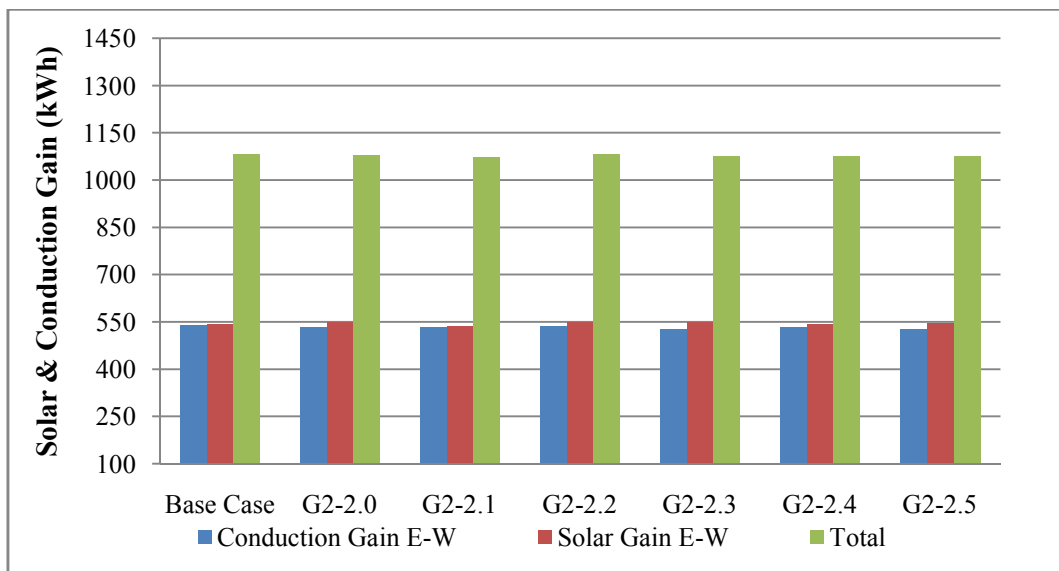

b) E-W orientation

c) NE-SW orientation

d) NW-SE orientation

Figure 6.19: The direct solar gain of thebase case and the second group configurations in the four orientaions; N-S , E-W, NE-SW and NW-SE
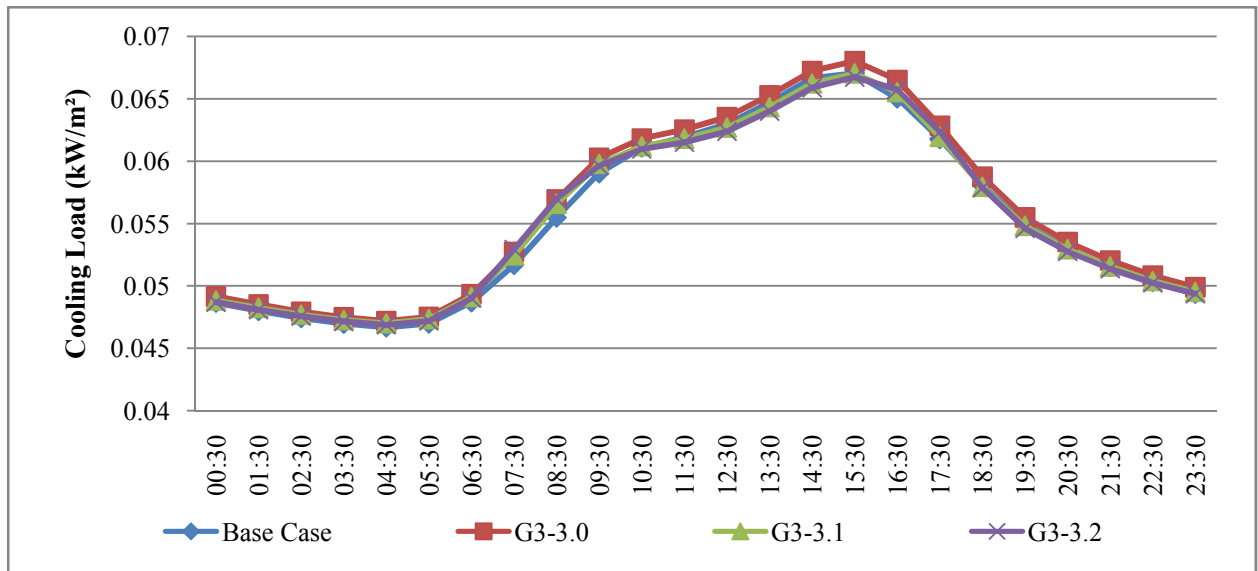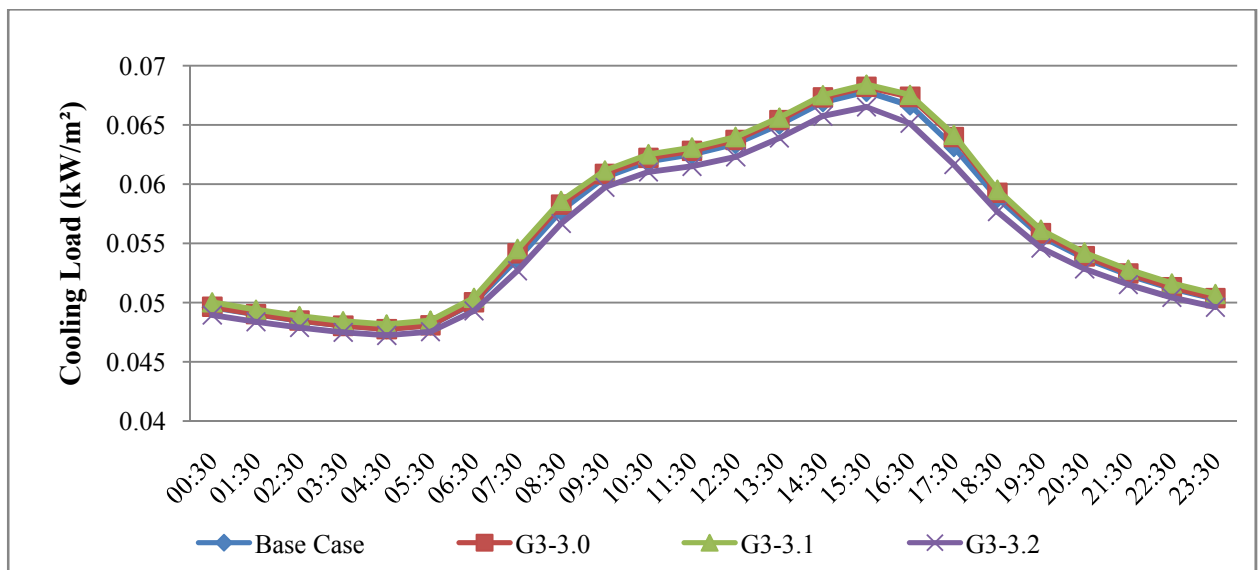
a) N-S orientation

b) E-W orientation

Solar and conduction heat gain of the second group configurations in the ; a) N-S orientation, and b) E-W orientation

F.3 : The cooling load and the heat gain of the base case and the third group configurations

----
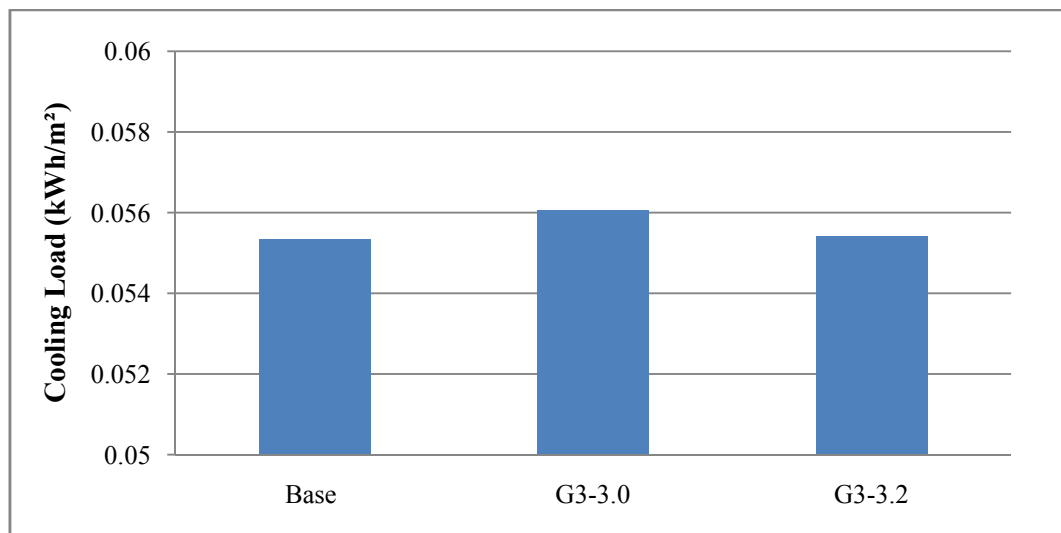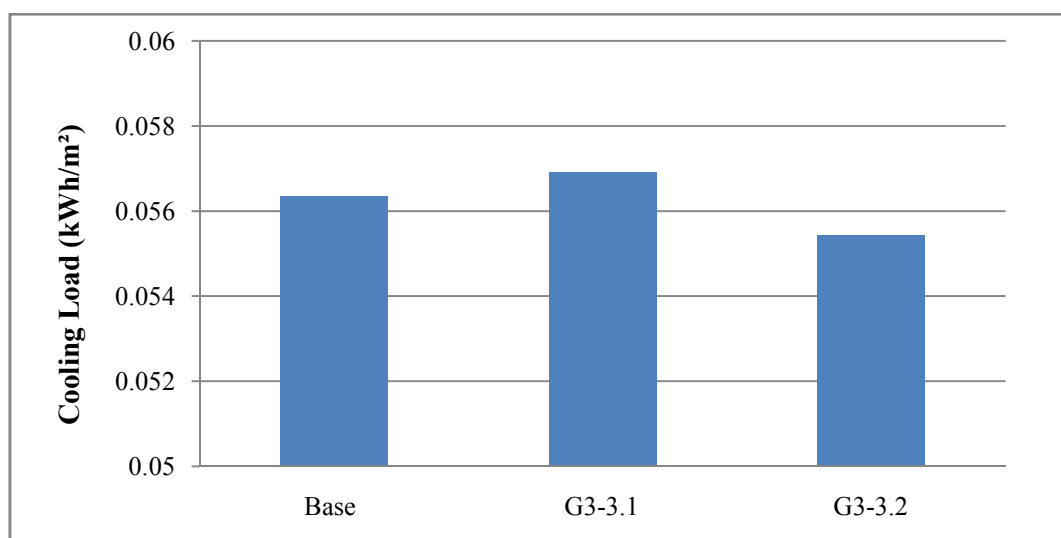

a) N-S orientation

b) E-W orientation

Cooling plant load daily profile on 21st. June of the third group configurations in the ; a) N-S
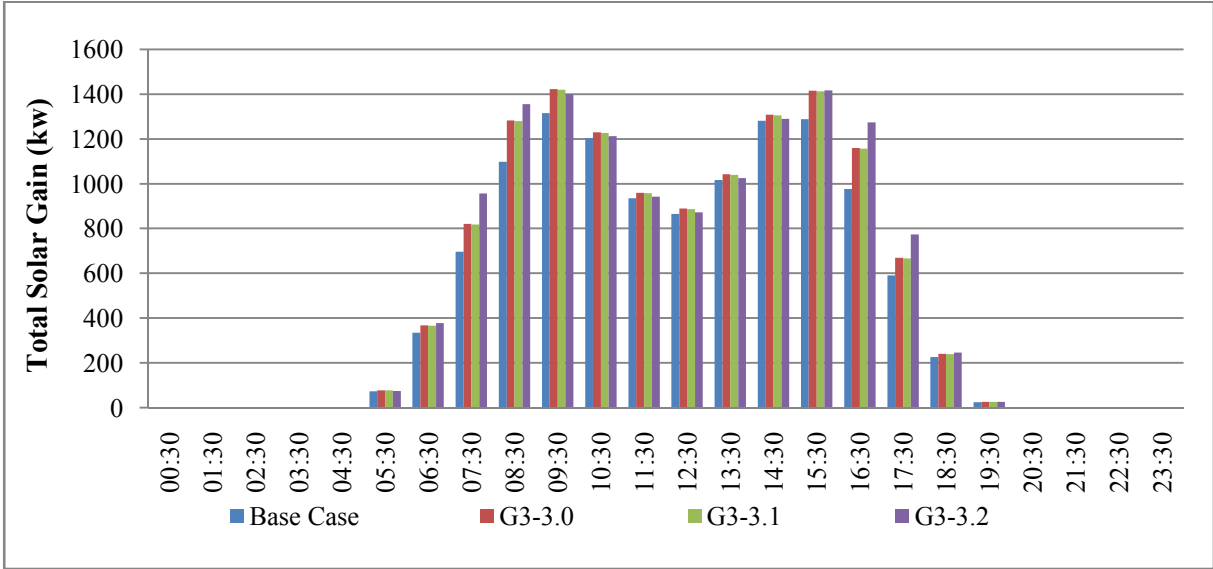and b) E-W orientations

a) N-S orientation
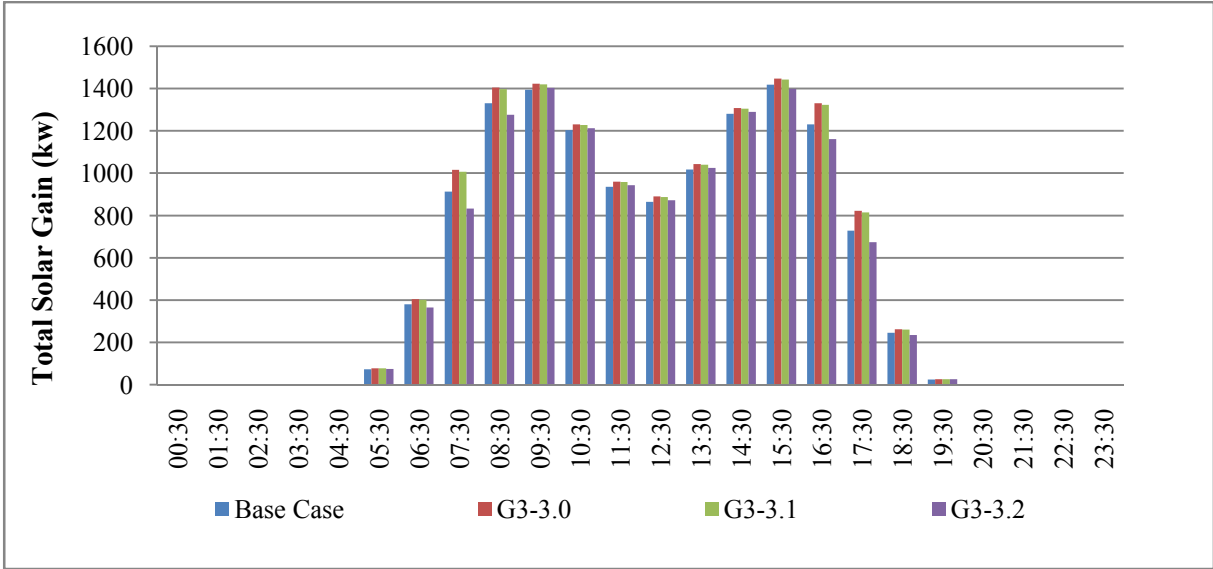

b) E-W orientation

The maximum and munimum cooling load saving of the third group configurations comparing to the base case in; a) N-S and b) E-W orientations

a) N-S orientation
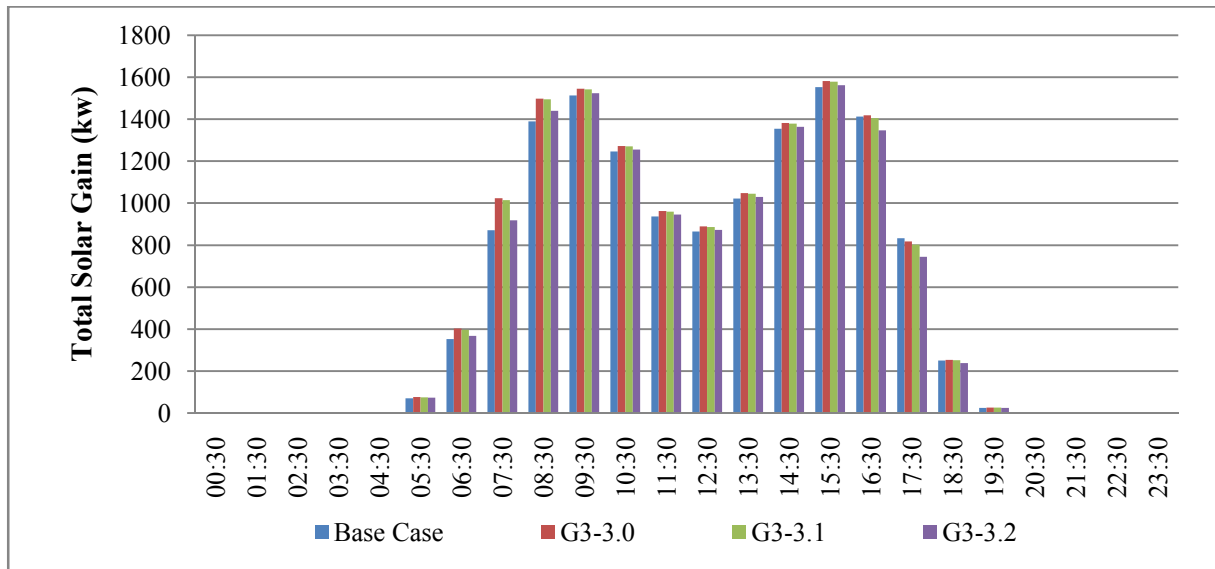
b) E-W orientation

c) NE-SW orientation

d) NW-SE orientation

The direct solar gain of the base case and the third group configurations in the four orientaions;
a) N-S , b) E-W, c) NE-SW and d) NW-SE

a) N-S orientation

b) E-W orientation

Solar and conduction heat gain of the third group configurations in; a) N-S orientation and b) E-W orientation

Appendix G

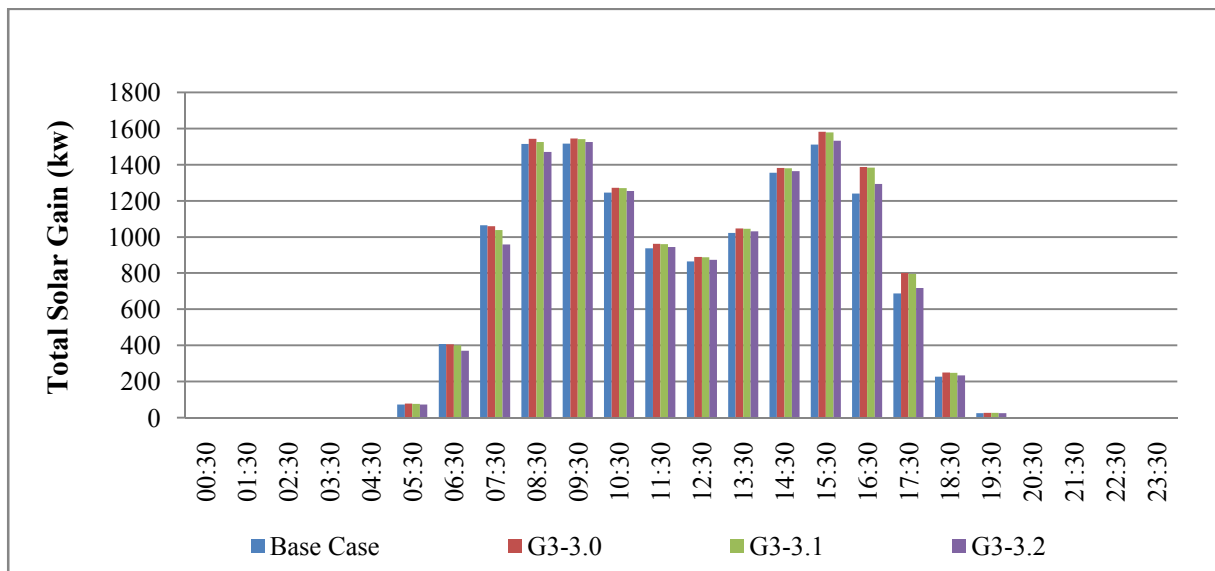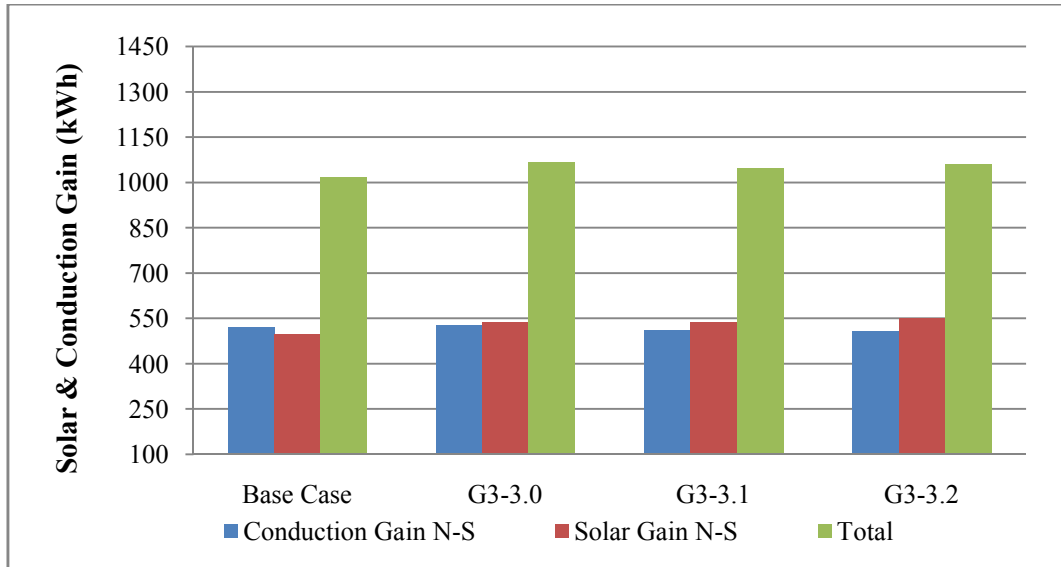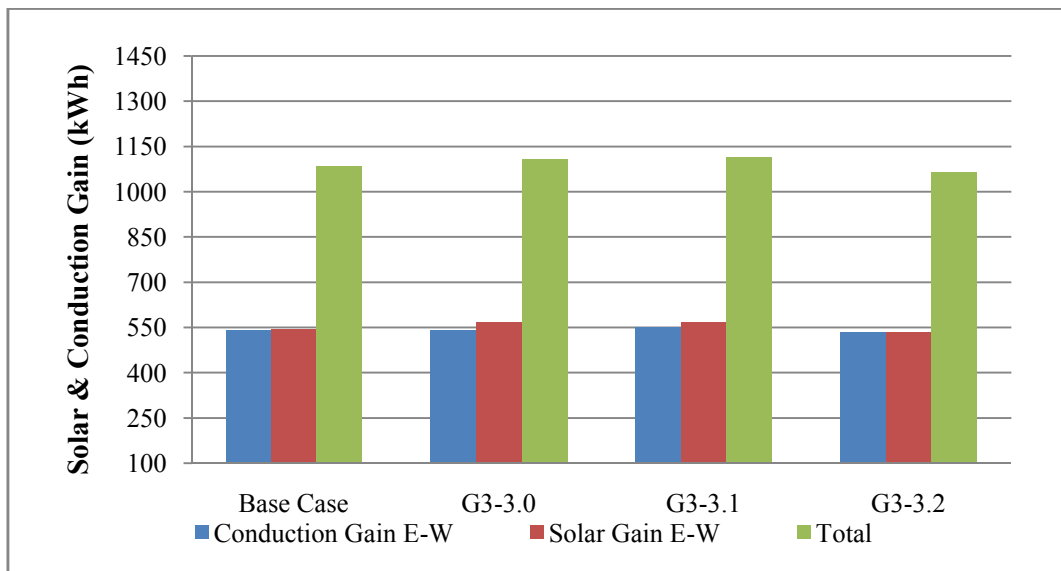**G.1 : The maximum dry bulb air temperature, relative humidity, and the wet bulb temperature at the maximum dry bulb air temperature for the three groups configurations in the four orientations**

Orientation	Configuration	Max. Dry Bulb Temp.° C	% RH at Max. Temp.	Wet Bulb Temp.° C
RH. N-S	Base	35.778	41.081	24.8
	G1-.01	35.665	41.128	24.7
	G1-1.1	35.476	41.496	24.8
	G1-1.2	35.514	41.58	24.7
	G1-1.3	35.555	41.466	24.7
RH. E-W	Base	35.825	41.437	24.9
	G1-.01	35.646	41.565	24.8
	G1-1.1	35.404	42.116	24.8
	G1-1.2	35.692	41.599	24.9
	G1-1.3	35.681	41.536	24.8
RH. NE-SW	Base	37.619	39.191	25.8
	G1-.01	37.48	39.154	25.7
	G1-1.1	37.111	39.909	25.6
	G1-1.2	36.803	40.257	25.4
	G1-1.3	37.059	40.095	25.6
RH. NW-SE	Base	36.675	39.449	25.1
	G1-.01	37.264	38.046	25.2
	G1-1.1	35.983	40.76	24.9
	G1-1.2	35.619	41.613	24.8
	G1-1.3	36.62	39.438	25.1

Orientation	Configuration	Max. Dry Bulb Temp. ° C	% RH at Max. Temp.	Wet Bulb Temp. ° C
RH. NS	Base	35.778	41.081	24.82
	G-2.2.0	35.524	41.485	24.71
	G2-2.1	35.788	40.924	24.79
	G2-2.2	35.638	41.222	24.74
	G2-2.3	35.69	41.138	24.76
	G2-2.4	35.699	41.096	24.76
	G2-2.5	35.722	41.042	24.76
RH. EW	Base	35.825	41.437	24.94
	G-2.2.0	35.637	41.603	24.83

	G2-2.1	35.651	41.677	24.85
	G2-2.2	35.736	41.4	24.86
	G2-2.3	35.686	41.501	24.84
	G2-2.4	35.665	41.583	24.85
	G2-2.5	35.569	41.791	24.82
	Base	37.619	39.191	25.8
	G-2.2.0	38.353	37.436	25.92
	G2-2.1	36.775	40.771	25.53
RH. NE-SW	**G2-2.2**	38.365	37.425	25.93
	G2-2.3	37.507	39.278	25.73
	G2-2.4	37.626	39.04	25.77
	G2-2.5	36.674	41.005	25.5
	Base	36.675	39.449	25.13
	G-2.2.0	36.475	39.574	25.01
	G2-2.1	35.957	40.719	24.87
RH. NW-SE	**G2-2.2**	36.454	39.581	24.98
	G2-2.3	36.185	40.163	24.92
	G2-2.4	36.235	39.961	24.91
	G2-2.5	35.778	41.067	24.81

Orientation	Configuration	Max. Dry Bulb Temp. °C	% RH at Max. Temp.	Wet Bulb Temp. °C
	Base	35.778	41.081	24.8
	G3-3.0	35.992	41.047	24.97
	G3-3.1	35.412	42.216	24.79
RH. NS	**G3-3.2**	35.221	42.706	24.75
	Base	35.825	41.437	24.9
	G3-3.0	35.884	41.462	24.98
	G3-3.1	36.093	41.005	25.06
RH. EW	**G3-3.2**	35.625	42.035	24.92
	Base	37.619	39.191	25.8
	G3-3.0	37.225	39.609	25.6
	G3-3.1	37.461	38.757	25.57
RH. NE-SW	**G3-3.2**	37.237	39.442	25.56
	Base	36.675	39.449	25.13
	G3-3.0	37.346	38.917	25.52
	G3-3.1	35.012	43.229	24.7
RH. NW-SE	**G3-3.2**	34.744	43.757	24.6
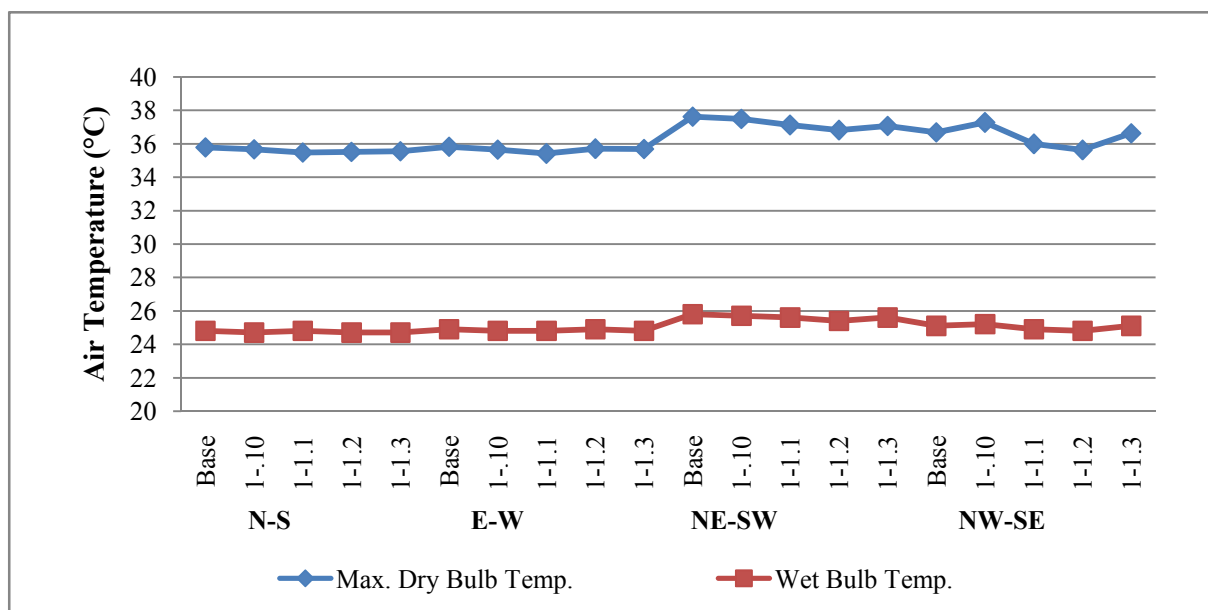
a) First Group
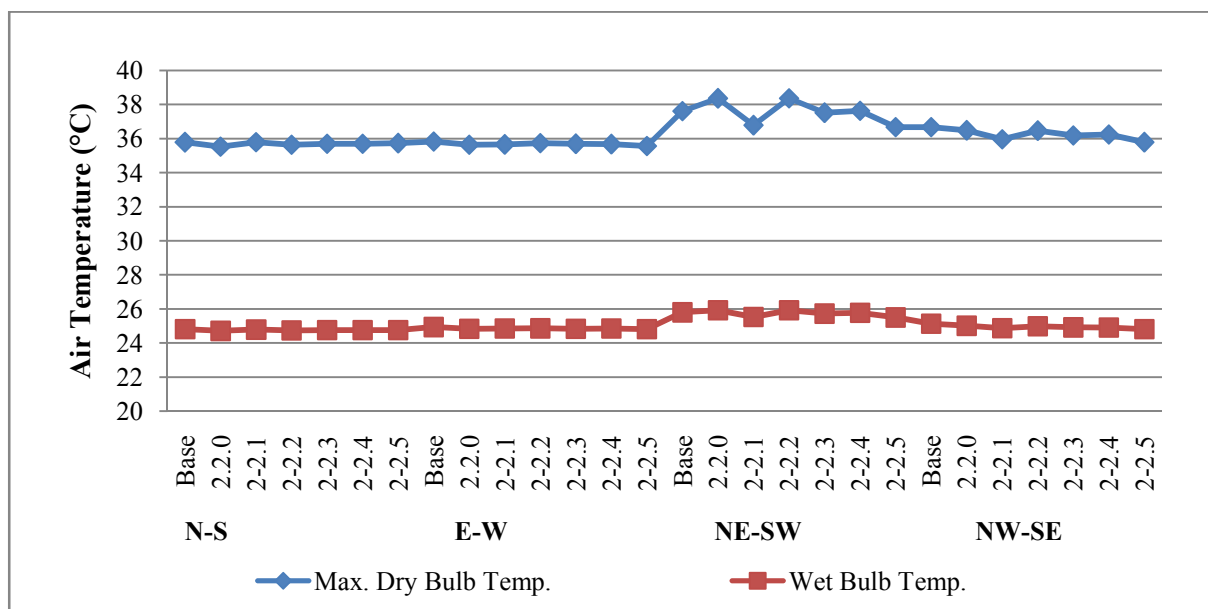
b) Second Group
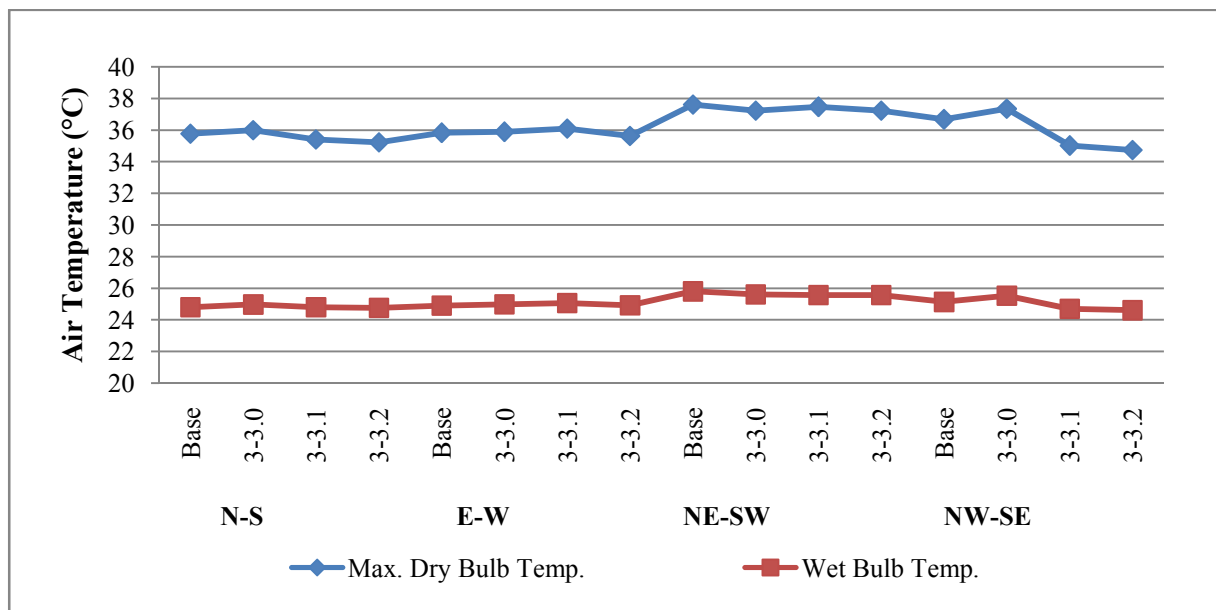
c) Third Group

Max. dry bulb and wet bulb air temperature of the three groups configurations in the four orientations;
a) First Group , b) Second Group , and c) Third Group